Macromolecular Symposia 248

M. Buback, A.M. v. Herk (Eds)

# Radical Polymerization: Kinetics and Mechanism

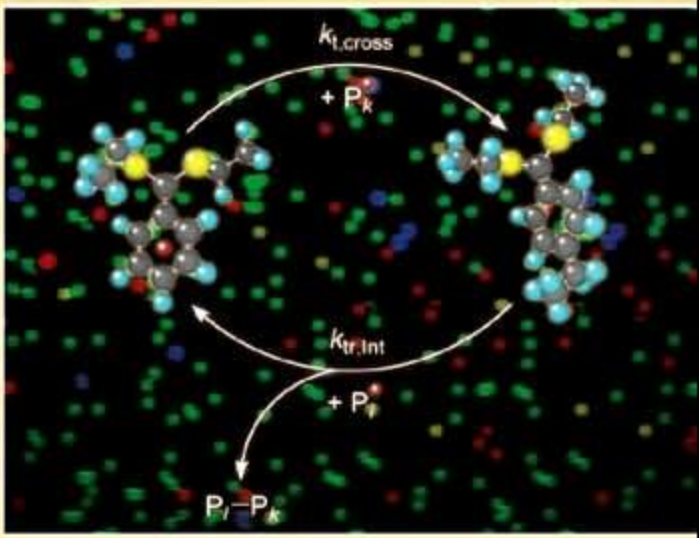


WILEY-VCH

IUPAC

**Macromolecular Symposia | 248**

# Radical Polymerization: Kinetics and Mechanism

Selected Contributions
from the conference in
Il Ciocco (Italy), September 3–8, 2006

Symposium Editors:
M. Buback (Germany),
A. M. v. Herk (The Netherlands)

M. Matsuo, K. Tashiro, Y. Bin (Eds.)

**14th Annual Polychar World Forum on Advanced Materials**

Vol. 242

J. M. Guenet, A. K. Nandi (Eds.)

**Fibrillar Networks as Advanced Materials**

Vol. 241
ISBN 3-527-31748-1

D. Baskaran, S. Sivaram (Eds.)

**Recent Trends in Ionic Polymerization**

Vol. 240
ISBN 3-527-31747-3

K. Matyjaszewski, Yves Gnanou, Ludwik Leibler

**Macromolecular Engineering**

ISBN 3-527-31446-6

M. Lazzari, G. Liu, S. Lecommandoux

**Block Copolymers in Nanoscience**

ISBN 3-527-31309-5

D. O. Hummel

**IR Hummel Defined Polymers Basic Collection**

ISBN 3-527-31628-0

Macromolecular Symposia Vol. 248

# Radical Polymerization: Kinetics and Mechanism

Selected Contributions
from the conference in
Il Ciocco (Italy), September 3–8, 2006

Symposium Editors:
M. Buback (Germany),
A. M. v. Herk (The Netherlands)


ISBN 10 3-527-32056-3
ISBN 13 978-3-527-32056-1

WILEY-VCH

**Full text and further information: www.ms-journal.de**



**Macromolecular Symposia**
is published 14 times a year

**Annual subscription rates 2007**
Macromolecular Full Package
(All seven *Macromolecular Journals*; 101 issues in total):

| | | | |
|---|---|---|---|
| Europe | Euro | 8,445 | 9,290 |
| Switzerland | Sfr | 13,995 | 15,395 |
| All other areas | US$ | 11,145 | 12,260 |
| | | print only **or** electronic only | print **and** electronic |

Postage and handling charges included.
All Wiley-VCH prices are exclusive of VAT.
Prices are subject to change.
Individual subscriptions, single issues and back copies are available.
Please ask for details at: service@wiley-vch.de

**Orders** may be placed through your bookseller or directly at the publishers:
WILEY-VCH Verlag GmbH & Co. KGaA,
P.O. Box 10 11 61, 69451 Weinheim, Germany,
Tel. +49 (0) 62 01/6 06-400,
Fax +49 (0) 62 01/60 61 84,
E-mail: service@wiley-vch.de

**Copyright Permission:**
Fax: +49 (0) 62 01/6 06-332,
E-mail: rights@wiley-vch.de

**For USA and Canada:** Macromolecular Symposia (ISSN 1022-1360) is published with 14 volumes per year by WILEY-VCH Verlag GmbH & Co. KGaA, Boschstr. 12, 69451 Weinheim, Germany. Air freight and mailing in the USA by Publications Expediting Inc., 200 Meacham Ave., Elmont, NY 11003, USA. Application to mail at Periodicals Postage rate is pending at Jamaica, NY 11431, USA. POSTMASTER please send address changes to: Macromolecular Symposia, c/o Wiley-VCH, III River Street, Hoboken, NJ 07030, USA.

Printed on acid-free paper.
Typesetting: Thomson Press (India) Ltd., India
Printing: Strauss Offsetdruck, Mörlenbach
Binding: Litges & Dopf, Heppenheim

# Macromolecular Symposia

**Articles published on the web will appear several weeks before the print edition. They are available through:**

WILEY InterScience®

**www.interscience.wiley.com**

**Cover:** The IUPAC-sponsored International Symposium on "Radical Polymerization: Kinetics and Mechanism" was held in Il Ciocco (Italia) during the week September 3-8, 2006. Attended by close to 200 people from all over the world with a good balance between attendees from industry and academia, this symposium was the fourth within the series of so-called SML conferences, which are the major scientific forum for addressing kinetic and mechanistic aspects of free-radical polymerization and of controlled radical polymerization. The present symposium comprised five major themes: Fundamentals of free-radical polymerization, Heterogeneous polymerization, Controlled radical polymerization, Polymer reaction engineering, and Polymer characterization. Most of the invited lectures covering these topics are reflected as written contributions in this issue. SML IV again marked an important step forward toward the better understanding of the kinetics and mechanism of radical polymerization, which is extremely relevant for both conventional and controlled radical polymerization and for people in academia as well as in industry.

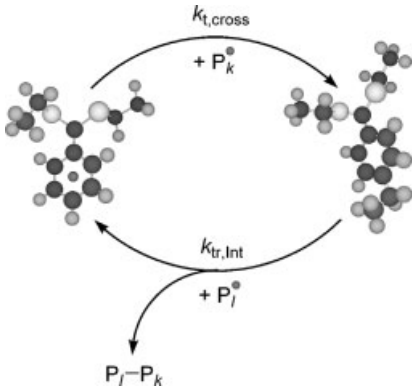


## Radical Polymerization: Kinetics and Mechanism

Il Ciocco (Italy), September 3–8, 2006



 

 

 

 

 

This volume contains articles of the invited speakers at the IUPAC-sponsored International Symposium on ''Radical Polymerization: Kinetics and Mechanism'' held in Il Ciocco (Italia) during the week September 3–8, 2006. The conference was attended by close to 200 people from all over the world with a good balance between attendees from industry and academia. About 40 per cent of the attendees were Ph.D. students, who very actively participated in the scientific program.

This symposium was the fourth within the series of so-called SML conferences, which are the major scientific forum for addressing kinetic and mechanistic aspects of free-radical polymerization and of controlled radical polymerization. The first SML meeting was organized by Ken O'Driscoll and Saverio Russo at Santa Margherita Ligure (Italy) in May 1987. The second SML meeting was held at the same location by the same organizers in 1996. The third SML meeting was organized in 2001 by Michael Buback from Göttingen University and by Ton German from the Technical University of Eindhoven. They selected the conference hotel at Il Ciocco as the new symposium site. This venue is located in the beautiful province of Lucca. Thus, the abbreviation SML, which originally referred to Santa Margherita Ligure, now stands for Scientific Meeting Lucca.

The fourth SML meeting (September 3–8, 2006) was organized by Michael Buback and by Alex van Herk from the Technical University of Eindhoven. As has been foreseen in the last meeting, the number of contributions on controlled radical polymerization (CRP) has significantly increased. Four out of the eight sessions were devoted to CRP and the organizers consequently decided to remove the word 'Free' from the conference heading. The symposium nevertheless remains the number one forum where kinetic and mechanistic issues are addressed in detail and depth for the entire field of radical polymerization. Several important aspects of radical polymerization have first been presented at SML conferences, e.g., the groundbreaking pulsed–laser polymerization – size-exclusion chromatography method for the reliable measurement of propagation rate coefficients, which has been introduced by Professor O. F. Olaj and his group at SML I.

Distinctive features of the conference are that all attendees stay in the same hotel, that no parallel sessions are presented and that the posters may be discussed throughout the entire week. A total of 35 invited lectures have been given, eight of which were selected from the submitted poster abstracts. Moreover, 114 posters were presented, mostly by research students. Most of the invited lectures are reflected as written contributions in this issue of Macromolecular Symposia. In addition, the six groups of authors, who received most of the votes during the election of the poster prize winners, were also invited to contribute to this volume. It should be noted that all conference attendees could participate in the voting procedure for the poster prizes.

The symposium comprised five major themes:

- Fundamentals of free-radical polymerization
- Heterogeneous polymerization
- Controlled radical polymerization
- Polymer reaction engineering
- Polymer characterization

We are pleased to see that SML IV again marked an important step forward toward the better understanding of the kinetics and mechanism of radical polymerization, which is extremely relevant for both conventional and controlled radical polymerization and for people in academia as well as in industry.

The organizers want to acknowledge financial support of the conference by the ''Foundation Emulsion Polymerization'' (SEP) and by the European Graduate School on ''Microstructural Control in Free-Radical Polymerization''.

*M. Buback,*
*A. M. Van Herk*

 

 DOI: 10.1002/masy.200750201 

# The Cutthroat Competition Between Termination and Transfer to Shape the Kinetics of Radical Polymerization

*Gregory B. Smith, Gregory T. Russell**

**Summary:** There is a fascinating interplay between termination and transfer that shapes the kinetics of radical polymerization (RP). In one limit all dead-chain formation is by termination, in the other by transfer. Because of chain-length-dependent termination (CLDT), the rate law for RP takes a different form in each limit. However, common behavior is observed if one instead considers how the average termination rate coefficient varies with average degree of polymerization. Examples are given of using these principles to understand trends in actual RP data, and it is also demonstrated how to extract quantitative information on CLDT from simple steady-state experiments.

**Keywords:** chain transfer; radical polymerisation; termination; kinetics (polym.)

## Some Introductory Thoughts

The steady-state rate of radical polymerization (RP) is given by

$$\frac{-\mathrm{d}c_\mathrm{M}}{\mathrm{d}t} = k_\mathrm{p} c_\mathrm{M} \left(\frac{R_\mathrm{init}}{2k_\mathrm{t}}\right)^{0.5} \quad (1)$$

Here $c_\mathrm{M}$ is monomer concentration, $t$ time, $k_\mathrm{p}$ propagation rate coefficient, $R_\mathrm{init}$ rate of initiation, and $k_\mathrm{t}$ termination rate coefficient. Measurement of initiator decomposition rates, and thus specification of $R_\mathrm{init}$, has never been a problem. However for much of the history of RP, the disentangling of $k_\mathrm{p}$ and $k_\mathrm{t}$ was a problem. This was solved in 1987 when it was shown that by relatively simple analysis of the molecular weight distribution from a pulsed-laser polymerization (PLP), the value of $k_\mathrm{p}$ could be obtained without requirement for any knowledge of $k_\mathrm{t}$ (or $R_\mathrm{init}$).[1] So enthusiastically and successfully was this method adopted by the RP community that within just a few years it was recommended by an IUPAC Working Party as the method of choice for $k_\mathrm{p}$ determination;[2] recent reviews emphasize just how widely the method has been deployed.[3,4]

With the measurement of $R_\mathrm{init}$ and $k_\mathrm{p}$ ticked off, that of the third and last fundamental rate parameter of RP, $k_\mathrm{t}$, becomes easy: it follows simply from a measurement of rate. If the experiment is carried out in a steady state, then one uses Equation (1), involving $k_\mathrm{p}^2/k_\mathrm{t}$; if it is carried out in a non-steady state, then the rate will instead yield $k_\mathrm{p}/k_\mathrm{t}$, still enabling $k_\mathrm{t}$ to be easily obtained.[5,6] This has opened up hope that many of the frustrations associated with $k_\mathrm{t}$, a centrally important parameter, will be resolved. With this in mind, an IUPAC Task-Group looking into this broad issue was created. A comprehensive analysis of the seemingly multitudinous methods for measuring $k_\mathrm{t}$ was carried out.[5] A summary of the deliberations is presented in Table 1. Of course some methods were considered to be superior to others. Most notably, the single-pulse PLP method, as proposed,[7] developed and widely exploited[4] by Buback and coworkers, was felt to be peerless "because of its exceptional precision and because of the unparalleled control over

Department of Chemistry, University of Canterbury, Private Bag 4800, Christchurch, New Zealand
Fax: (+64) 03 3642110
E-mail: greg.russell@canterbury.ac.nz

***Table 1.***
Critical evaluation of methods for measuring $k_t$.[5]

| Method | Conversion dependence | Chain-length dependence | Instrumentation | Applicability |
|---|---|---|---|---|
| Steady-state rate | Yes | No[a)] | Simple | Wide |
| Steady-state EPR | Yes (not for low $c_R$[b)]) | No | Expensive, requires expertise | Wide |
| Living RP | No (may be possible) | Yes (usually for small chain lengths only) | Simple | Wide |
| Classical post-effect (including with EPR) | Yes (difficult at low conversion) | No | Requires expertise | Wide |
| Single-pulse PLP | Yes | Yes (long chain lengths only) | Expensive, requires expertise | Wide |
| EPR with single-pulse PLP | Yes | Yes (if $k_p$ not too high) | Very expensive, requires much expertise | Limited (low and moderate $k_t$ only) |
| Rotating sector | No (may be possible) | No (may be possible) | Sophisticated analysis | Wide |
| Buback's multiple-pulse PLP | Yes | No (may be possible) | Pulsed laser required | Wide |
| Olaj's multiple-pulse PLP | No (may be possible) | Yes (long chain lengths only) | Pulsed laser required | Limited (requires $\rho$[b)]) |
| Time-resolved quenching | No | No | Simple | Limited (low $k_p$ only) |
| $DP_w$[b)] from multiple-pulse PLP | No | Yes (long chain lengths only) | Laser required | Limited (no transfer) |
| Low-frequency PLP | No | Yes (power-law only) | Laser required; sophisticated analysis | Limited (no transfer) |

[a)] This may now be revised to read ''Yes'', as demonstrated in the present work.
[b)] $c_R$: radical concentration; $\rho$: radical concentration generated by a laser pulse; $DP_w$: weight-average degree of polymerisation.

conversion which it gives: it may routinely be used to measure $k_t$ at conversion intervals of less than 1%."[5] However it was also concluded that all the methods in Table 1 potentially should provide good $k_t$ values, as long as the user is aware of particular limitations that apply (see Table 1). This finding came as something of a surprise, because the notorious problem of excessive scatter[6] in literature values of $k_t$ was commonly assumed to arise, at least in part, from some methods of measurement simply being inherently bad techniques. There is no doubt that scatter in literature data for $k_t$ is due in no small part to naive employment of measurement methods, for example allowing a large change of conversion over the course of a $k_t$ measurement, or the choice of a poor value of $k_p$ or $R_{init}$ for data analysis. However it would also seem that theoretical forces have been at work. By far the most notable of these is chain-length-dependent termination (CLDT).[6] The aim of the present work is to illuminate some of the most significant trends to which CLDT gives rise, and thus to reveal the rich impact that it has on $k_t$. Once these effects are comprehended, it becomes clear why many purportedly identical $k_t$ measurements in fact were nothing of the sort, thus explaining why different values of $k_t$ were found.

## The Competition Between Termination and Transfer

The standard reaction scheme for RP comprises of initiation, propagation, termination and chain transfer to (small-molecule) species X, whether monomer, solvent, chain-transfer agent (CTA) or initiator. The corresponding population balance equations are

$$\frac{dc_{R^1}}{dt} = R_{init} + k_{trX}c_X c_R - k_p c_M c_{R^1} - k_{trX}c_X c_{R^1} - 2c_{R^1}\sum_{j=1}^{\infty} k_t^{1,j} c_{R^j} \quad (2)$$

$$\frac{dc_{R^i}}{dt} = k_p c_M c_{R^{i-1}} - k_p c_M c_{R^i} - k_{trX}c_X c_{R^i} - 2c_{R^i}\sum_{j=1}^{\infty} k_t^{i,j} c_{R^j},\ i = 2, \infty \quad (3)$$

$$\frac{dc_{D^i}}{dt} = 2\lambda c_{R^i}\sum_{j=1}^{\infty} k_t^{i,j} c_{R^j} + k_{trX}c_X c_{R^i} + (1-\lambda)\sum_{j=1}^{i-1} k_t^{j,i-j} c_{R^j} c_{R^{i-j}},\ i = 1, \infty \quad (4)$$

Hopefully the notation here is largely self-explanatory: $k$ always denotes a rate coefficient and $c$ a concentration; the subscript of a rate coefficient denotes the particular reaction – initiation, propagation, termination, and transfer to species X; the subscript of a concentration signifies the species – (small-molecule) species X involved in transfer, Monomer, Radical and Dead chain; lastly, a superscript always denotes chain length. Thus, for example, $c_{R^i}$ signifies the concentration of radicals of degree of polymerization $i$, while $k_t^{i,j}$ represents the rate coefficient for termination between radicals of chain length $i$ and $j$. The only exceptions to these principles of notation are that the rate of initiation is written directly as $R_{init}$ rather than in terms of rate coefficients and a concentration, and the fraction of termination events occurring by disproportionation, $\lambda$, is used rather than introducing rate coefficients for disproportionation and combination explicitly into Equation (4).

While Equations (2)–(4) may look complicated, in fact they are easily derived, as they consist merely of gain and loss terms resulting from the various reactions that produce and consume, respectively, each species. Further, it is sobering to realize that these equations only become even more forbidding if further RP reactions occur, for example chain transfer to polymer. They also become more complicated if additional reactions are deemed to be chain-length dependent, most notably propagation.[8] However while this effect can be highly significant where the average degree of

 

polymerization is less than 100,[8] it seems unlikely that it is relevant where genuine polymer is made. Thus it will not be considered in the present work, where a chain-length-independent value of $k_p$ will always be used. This serves to focus attention wholly onto CLDT. This is as desired, because it is felt that this phenomenon is by far the most important driver of RP kinetics.

For homo-termination rate coefficients, the following simple model will be used in all the calculations of this work:

$$k_t^{i,i} = k_t^{1,1} i^{-e} \quad (5)$$

Here $k_t^{1,1}$ is the rate coefficient for termination between monomeric radicals and $e$ is an exponent quantifying the strength of the CLDT: the larger the value of $e$, the stronger the variation with chain length. Although recent theoretical[9] and experimental[10,11] work has shown that this two-parameter model is an oversimplification of reality, it is a nice model to use for calculations, as it clearly exposes the general effects of CLDT on RP kinetics,[12–14] and these trends are essentially the same for more complex homo-termination models.[9] The same also holds for cross-termination models,[12–14] and so the simplest one will be employed here unless otherwise stated:

$$k_t^{i,j} = (k_t^{i,i} k_t^{j,j})^{0.5} = k_t^{1,1} (ij)^{-e/2} \quad (6)$$

This is called the geometric mean model, and it is especially amenable to computational use.[9,14,15]

Most radical polymerizations are carried out with continuous initiation, which means that to excellent approximation they are in a steady state. Thus the steady-state solutions of Equations (2) and (3) will be computed in this work.[16,17] This procedure yields the full set of $c_{R^i}$ values, from which one may evaluate the overall rate coefficient for termination, $\langle k_t \rangle$:

$$\langle k_t \rangle = \sum_{i=1}^{\infty} \sum_{j=1}^{\infty} k_t^{i,j} \frac{c_{R^i} c_{R^j}}{c_R^2} \quad (7)$$

Thus defined, $\langle k_t \rangle$ replaces $k_t$ in Equation (1), which otherwise remains an exact expression for steady-state rate. For this reason $\langle k_t \rangle$ is a tremendously important quantity: its variations directly dictate, through Equation (1), variations in rate of polymerization. This is why CLDT can be said to shape RP kinetics.

To begin with we present in Figure 1 calculated results for the variation of (steady-state) $\langle k_t \rangle$ with (a) rate of initiation and (b) frequency of chain transfer. It is stressed that in these calculations the *only* quantities that are varied are $R_{init}$ (alone) in (a) and $k_{trX} c_X$ (alone) in (b). In other words, all values of $k_t^{i,j}$ are identical in all the calculations for Figure 1, and yet, remarkably, there is large variation of $\langle k_t \rangle$, the termination rate coefficient that would be measured experimentally. Further, the way in which $\langle k_t \rangle$ varies with $R_{init}$ and with $k_{trX} c_X$ varies depending on the value of these quantities.

It turns out that what Figure 1 beautifully brings to light is a competition between termination and transfer to shape RP kinetics. First considering Figure 1(a), the easiest trend to understand is, perhaps counter-intuitively, the region at high $R_{init}$ where the change of $\langle k_t \rangle$ is strongest, because this variation is due to a commonly realized effect of CLDT: as $R_{init}$ increases, the radical chain-length distribution (RCLD), i.e., the $c_{R^i}$ distribution, becomes more weighted towards small chain lengths, and thus $\langle k_t \rangle$ increases, because CLDT means that small radicals terminate relatively quickly.[18] From how this argument has just been expressed there is no reason to expect that this trend should not continue down to low values of $R_{init}$, so the puzzling result of Figure 1(a) is perhaps that $\langle k_t \rangle$ becomes independent of $R_{init}$ at low $R_{init}$, even though CLDT is still very much operative (see what is written above about $k_t^{i,j}$ values). Why is this? The explanation is that at low values of $R_{init}$, radical creation is dominated by transfer rather than by initiation, i.e., $R_{init} \ll k_{trX} c_X c_R$ in Equation (2). Thus dead-chain formation is predominantly by transfer and there is negligible

 

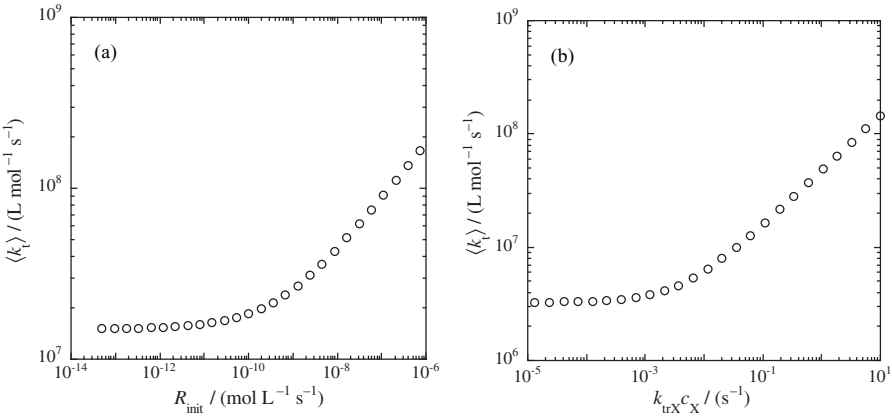


***Figure 1.***
Calculated values of overall termination rate coefficient, $\langle k_t \rangle$, using $k_t^{1,1} = 1 \times 10^9$ L mol$^{-1}$ s$^{-1}$, $e = 0.5$ and $k_p c_M = 1000$ s$^{-1}$. (a) $k_{trX}c_X = 0.1$ s$^{-1}$ with varying rate of initiation, $R_{init}$. (b) $R_{init} = 5 \times 10^{-12}$ mol L$^{-1}$ s$^{-1}$ with varying transfer frequency, $k_{trX}c_X$.

variation in the RCLD as $R_{init}$ changes, which means that $\langle k_t \rangle$ is independent of $R_{init}$ (see Equation (7)).

For obvious reasons we term the situation at low $R_{init}$ in Figure 1(a) the *transfer limit*. Physically it corresponds to a radical undergoing many, many cycles of growth and transfer before eventually undergoing termination, something that can occur at any chain length, i.e., termination does not necessarily happen at short chain length. With this grasped, we can now reach a deeper understanding of the converse situation at high $R_{init}$: this the *termination limit*, in which $k_{trX}c_X c_R \ll R_{init}$ in Equation (2), and thus there is variation of $c_{R^i}$ values as $R_{init}$ changes, meaning that there is variation of $\langle k_t \rangle$. Physically this limit corresponds to all dead-chain formation being by termination, and thus every radical that is created undergoes just one generation of growth before experiencing its ultimate fate at the hands of termination. Figure 1(a) also reveals that at intermediate $R_{init}$ there is a transition between the two limits. Physically this is the region of relatively even *competition* between transfer and termination, i.e., there is significant dead-chain formation by both these pathways, something that is specifically reflected in the $\langle k_t \rangle$ behavior: it is intermediate between those of the two limits.

Turning now to Figure 1(b), in it one sees all the same phenomena as in Figure 1(a), except that roles are now reversed. This is because it is $k_{trX}c_X$ rather than $R_{init}$ that is being varied. An increase in the transfer frequency means that the rate of production of small radicals is increased, meaning that the RCLD becomes more weighted towards small radicals, meaning that $\langle k_t \rangle$ is increased. This explains the strong variation of $\langle k_t \rangle$ that one observes at high $k_{trX}c_X$ in Figure 1(b). Because $k_{tr}X^cR$ is high it means that $R_{init} \ll k_{trX}c_X c_R$, i.e., one is in the transfer limit. Thus, paradoxically, it is now the transfer limit in which $\langle k_t \rangle$ varies strongly. Conversely, at low $k_{trX}c_X$ one is in the termination limit, in which event $\langle k_t \rangle$ is constant because $R_{init}$ is now constant: the variation of $k_{trX}c_X$ now has no effect on $\langle k_t \rangle$, because termination dominates its competition with transfer. Finally, at intermediate $k_{trX}c_X$ this competition is relatively evenly balanced, and there is a transition between the two limiting behaviors.

This discussion of Figure 1 has been long because it reveals much fascinating, subtle behavior. It is felt with conviction that these patterns are highly relevant to the study of RP kinetics, because realistic parameter values and a general kinetic model have been used to generate these results. In other

 

words, these calculations have not been specially designed to produce the trends on display; rather, any CLDT model combined with reasonable values of rate coefficients will produce results of the same form. Of course it is correct to point out that no set of experiments will have the 8-orders-of-magnitude variation of initiator concentration at first implied by Figure 1(a). However this is to ignore that one may easily change $R_{init}$ by this amount through choice of initiator. In other words, the point of Figure 1(a) is that in a set of experiments with a slowly decomposing initiator one will be at the low-$R_{init}$ end of Figure 1(a), where one will observe very different termination behavior to a set of experiments that is otherwise identical except for having a rapidly decomposing initiator. Analogous applies with Figure 1(b) and choice of CTA.

The remainder of this paper will look at some of the behaviors of Figure 1 in more detail, including giving examples of their expression in experimental data, thereby authenticating the point above that these considerations are highly relevant to understanding of RP kinetics, in fact it is contended that they are integral for this purpose.

## The Termination Limit

Making the steady-state assumption and the long-chain approximation, use of Equations (5) and (6) in Equations (2), (3) and (7) for the case of $k_t rX = 0$ (i.e., the termination limit) results in[9,14,15]

$$\langle k_t \rangle = k_t^{1,1} \left[ \Gamma\left(\frac{2}{2-e}\right) \right]^{-2} \times \left[ \frac{(2R_{init} k_t^{1,1})^{0.5}}{k_p c_M} \left(\frac{2}{2-e}\right) \right]^{2e/(2-e)} \quad (8)$$

This equation holds strictly only for the geometric mean model, the physical basis of which is dubious for RP.[14] However, the remarkable thing about Equation (8) is that it holds *qualitatively* and *semi-quantitatively* for all models of cross-termination.[12,13] This is exemplified in Figure 2, which also

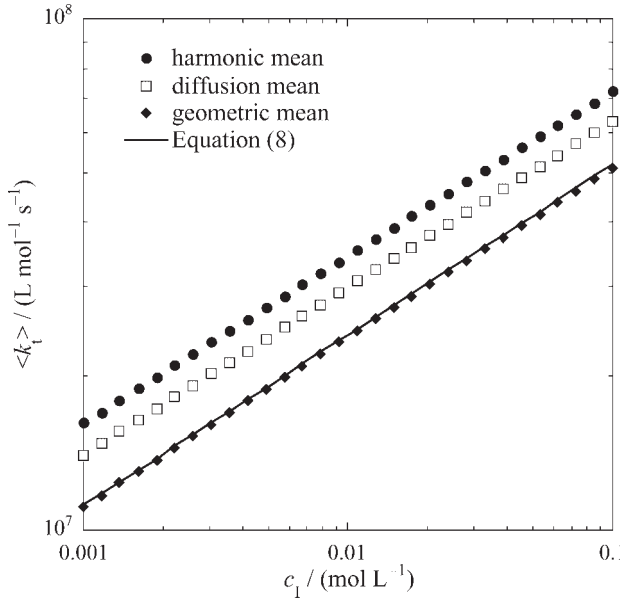


***Figure 2.***
Computed[14,19] variation of overall termination rate coefficient, $\langle k_t \rangle$, with initiator concentration, $c_I$, for three different cross-termination models, as indicated. Also shown are values calculated with Equation (8). Parameter values employed: $k_t^{1,1} = 1 \times 10^9$ L mol$^{-1}$ s$^{-1}$, $e = 0.5$, $R_{init} = c_I \times 2 \times 10^{-7}$ s$^{-1}$, $k_p c_M = 1000$ s$^{-1}$, $k_{trX} = 0$.

 

shows results[14,19] for the diffusion and harmonic mean models, Equations (9) and (10) respectively, both of which are physically plausible for RP:

$$k_t^{i,j} = \frac{1}{2}(k_t^{i,i} + k_t^{j,j}) = \frac{1}{2}k_t^{1,1}(i^{-e} + j^{-e}) \qquad (9)$$

$$k_t^{i,j} = k_t^{1,1}\left(\frac{2ij}{i+j}\right)^{-e} \qquad (10)$$

Because of the model independence of Equation (8) (providing $e$ is not too large[14,19]), one may use it to analyze data from experiments in which there is negligible dead-chain formation by transfer, regardless of the mechanism of cross-termination that actually holds (i.e., one does not even need to know how cross-termination occurs). For example, Equation (8) describes quantitatively the variation of $\langle k_t \rangle$ with $c_M$ (i.e., changing solvent concentration) and $k_t^{1,1}$ (i.e., changing solvent viscosity). Here we will illustrate the utility of Equation (8) by applying it to a set of experiments for which only initiator concentration, $c_I$, was varied. The data is from low-conversion bulk polymerization of methyl methacrylate (MMA)[20] and is presented in Figure 3. Equation (8) stipulates that

$$\text{slope of } \log\langle k_t \rangle \textit{ vs. } \log c_I = \frac{e}{(2-e)} \qquad (11)$$

$$\text{intercept of } \log\langle k_t \rangle \textit{ vs. } \log c_I \approx \log\left\{ k_t^{1,1}\left[\Gamma\left(\frac{2}{2-e}\right)\right]^{-2}\left[\frac{(4fk_dk_t^{1,1})^{0.5}}{k_pc_M}\frac{2}{2-e}\right]^{2e/(2-e)}\right\} \qquad (12)$$

The new quantities here are initiator efficiency $f$ and initiator decomposition rate coefficient $k$d, i.e., $R_{init} = 2fk_dc_I$. Firstly applying Equation (11) to the best-fit line of the data of Figure 3, one obtains $e = 0.20$. Using this value together with the known values of $fk_d$ and $k_pc_M$, one can now apply Equation (12) to the data of Figure 3 and thereby procure $k_t^{1,1} \approx 2 \times 10^8$ L mol$^{-1}$ s$^{-1}$

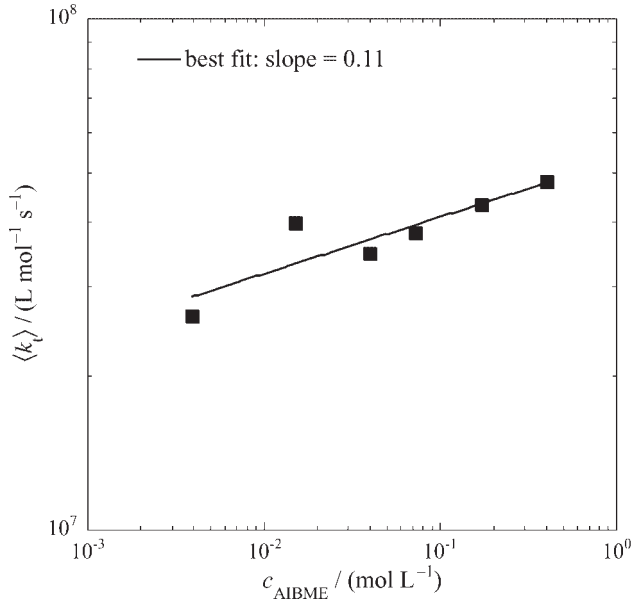


***Figure 3.***
Variation of overall termination rate coefficient, $\langle k_t \rangle$, with concentration of 2,2′-azoisobutyromethylester (AIBME), $c_{AIBME}$, for bulk RP of MMA at 40 °C.[19,20] The $\langle k_t \rangle$ measurements were made using the "steady-state rate" method of Table 1.

 

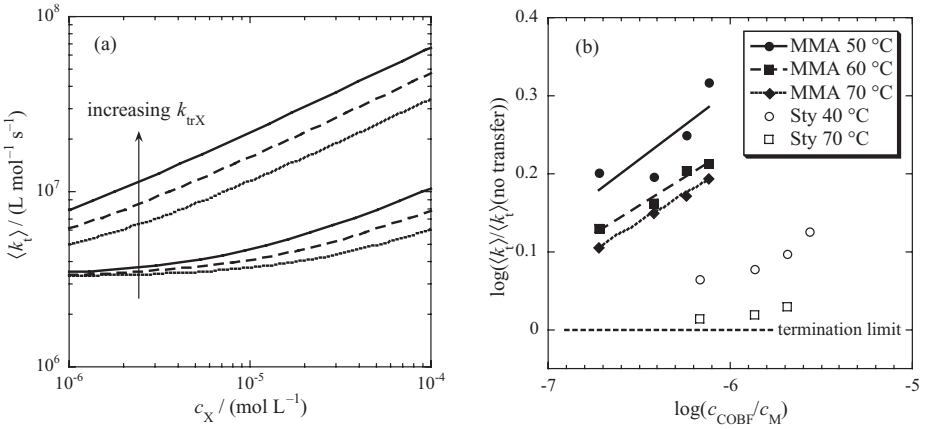


***Figure 4.***
(a) Calculated $\langle k_t \rangle$ using the parameter values of Figure 1(b). Bottom group of curves: $k_{trX} = 1$, 2 and $4 \times 10^2$ L mol$^{-1}$ s$^{-1}$; top group: $k_{trX} = 0.5$, 1 and $2 \times 10^4$ L mol$^{-1}$ s$^{-1}$. (b) Relative $\langle k_t \rangle$ for low-conversion bulk RP of MMA and Sty in the presence of COBF.[22] Linear best fits to each set of MMA data are shown, as is the termination limit value.

(this value is only an estimate because of the uncertainty introduced by not knowing the mechanism of cross-termination). Both these values are in excellent agreement with those obtained by other methods,[9] although it is stressed that these values pertain to long chains only, not to short chains, meaning that $k_t^{1,1}$ is not the true value of this quantity.[9]

We additionally point out that Equation (8) confirms that $\langle k_t \rangle$ is independent of $k_{trX}c_X$ in the termination limit, exactly as seen in Figure 1(b) (values at low $k_{trX}c_X$). Summarizing this section, it has firstly illustrated the capacity of Figure 1 and Equation (8) to explain trends in RP data. Second, it has demonstrated how Equation (8) can easily be used to extract accurate quantitative information on CLDT from simple steady-state experiments. Given all this, Equation (12) is recommended as a powerful tool for understanding RP kinetics.

## The Transfer Limit

Making the same clutch of mathematical assumptions as used in deriving Equation ((8)), except for now considering the transfer limit rather than the termination limit, one can derive[21]

$$\langle k_t \rangle(\text{geometric mean}) = k_t^{1,1}\left[\Gamma\left(1-\frac{e}{2}\right)\right]^2\left(\frac{k_{trX}c_X}{k_p c_M}\right)^e \quad (13)$$

$$\langle k_t \rangle(\text{diffusion mean}) = k_t^{1,1}\Gamma(1-e)\left(\frac{k_{trX}c_X}{k_p c_M}\right)^e \quad (14)$$

No closed result is possible with the harmonic mean, however it has been shown numerically to display the same qualitative behavior as Equations (13) and (14).[21] So exactly as with the termination limit, all cross-termination models give the same trends in the transfer limit. Thus one may confidently use the above equations to understand patterns of behavior in transfer-dominated systems. The first thing one notices is that $\langle k_t \rangle$ is independent of $R_{init}$ in this limit, as observed in Figure 1(a) (region of low $R_{init}$). The next thing one notices is that $\langle k_t \rangle$ increases with increasing transfer frequency, completely in accord with Figure 1(b) (region at high $k_{trX}c_X$). Further, the more marked is the CLDT (i.e., the higher the value of $e$), the stronger this effect. Of course this makes sense physically, but Equations (13) and (14) additionally provide a quantitative footing for analyzing this effect.

 

All the above may be illustrated by considering data for bulk, low-conversion polymerization of MMA and styrene (Sty) in the presence of the catalytic chain transfer agent known as COBF.[22] To begin with, calculations are presented in Figure 4(a) for variation of $\langle k_t \rangle$ with $c_X$ for different $k_{trX}$ (each curve in Figure 4(a) is just a version of Figure 1(b)). All parameter values used in Figure 4(a) have been chosen to reflect those of the experimental results[22] presented in Figure 4(b): relative $\langle k_t \rangle$ was measured as a function of COBF level for the two monomers at different temperatures. It should be clear why these two figures have been juxtaposed: because the model calculations explain all aspects of the experimental results, most notably: $\langle k_t \rangle$ is higher for MMA because $k_{trX}$ – actually, $k_{trX}/k_p$ is the important parameter – is higher;[22] $\langle k_t \rangle$ decreases with temperature for both monomers because $k_{trX}/k_p$ decreases with temperature;[22] the MMA results are steeper because they are in the transfer limit whereas the Sty systems have mixed transfer and termination (see Figure 1(b)), consistent with COBF being a much less efficient CTA for Sty;[22,23] and this is also why the Sty results are curved whereas the MMA results are linear (within experimental precision). All these trends defy explanation outside the current framework, and indeed this is the first time they have been explained.

Equations (13) and (14) may also be used for quantitative analysis of data: they dictate that for transfer-dominated systems, i.e., the present MMA data but not the present Sty data, a plot of $\log\langle k_t \rangle$ *vs.* $\log^c X$ has slope of $e$, providing all else is held constant, as is the case here. From the linear fits of Figure 4(b) one thus obtains $e = 0.18$, 0.14 and 0.14 for MMA at 50, 60 and 70 °C respectively. These values are consistent with those obtained by other means,[9] including the termination-limit data of Figure 3 here. Unfortunately it is not possible to estimate $k_t^{1,1}$ from the intercepts of the linear fits Figure 4(b), because only relative rather than absolute rates were reported.[22]

## Number-Average Degree of Polymerization

So far only the effect of CLDT on $\langle k_t \rangle$, and hence, via Equation (1), on rate, has been considered. CLDT also affects molecular weight (MW). Of course MW is important both in its own right and in that it is very commonly measured as part of RP studies. Properly the whole distribution of MWs should be considered, but there is no denying that it is more convenient to deal with a single index of MW; further, quite often a single parameter is adequate as a description of MW. Here we will use number-average degree of polymerization, $DP_n$, which is both commonly employed and is the most intuitive of MW indexes: it is just the arithmetic mean of the number distribution of dead chains. Thus for steady-state polymerizations it may be calculated as the arithmetic mean of $dc_{Di}/dt$ values, as delivered by Equation (4). Before presenting any such results, it is worthwhile contemplating what might be expected. Easiest are transfer-dominated systems, for which $DP_n = (k_p c_M)/(k_{trX} c_X)$. Thus one immediately obtains from Equation (13):

$$\langle k_t \rangle(\text{transfer limit}) = k_t^{1,1} G_{\text{transfer}} (DP_n)^{-e}, \text{ where } G_{\text{transfer}} = \left[\Gamma\left(1 - \frac{e}{2}\right)\right]^2 \tag{15}$$

More difficult to show, it turns out that for disproportionation-dominated systems[9,15]

$$\langle k_t \rangle(\text{disprop. limit}) = k_t^{1,1} G_{\text{disprop}} (DP_n)^{-e}, \text{ where } G_{\text{disprop}} = \left[\Gamma\left(\frac{2}{2-e}\right)\right]^{e-2} \left(\frac{2}{2-e}\right)^e \tag{16}$$

Even more remarkable here than the identical scaling behavior – i.e., variation of $\langle k_t \rangle$ with $DP_n$ – is the almost exact quantitative coincidence, e.g. $e = 0.20$ gives $G_{\text{transfer}} = 1.14$ and $G_{\text{disprop}} = 1.13$, while $e = 0.50$ gives 1.50 and 1.36 respectively.

 

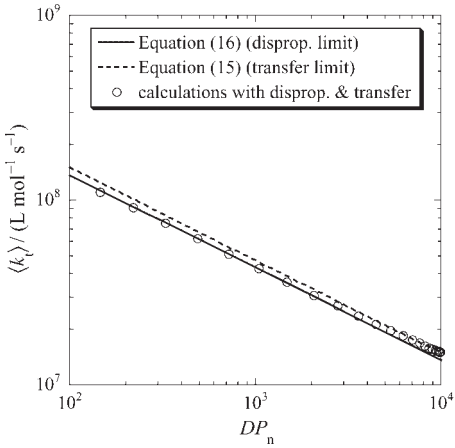


***Figure 5.***
Points: calculations of Figure 1(a), using also $\lambda = 1$, presented as $\langle k_t \rangle$ *vs.* $DP_n$. Lines: evaluations of Equations (15) and (16) using same parameter values as for calculations.

Where transfer and disproportionation both occur, points are constrained to lie between the two limits of Equations (15) and (16) respectively. Because, as explained, these limits are nearly identical, points in between must be almost exactly described by either of the above equations. This is illustrated in Figure 5, which shows $\langle k_t \rangle$ as a function of $DP_n$ from calculations in which both transfer and disproportionation are allowed to occur, as well as evaluation of Equations (15) and (16) with the same parameter values.

Figure 5 illustrates not just that $\log\langle k_t \rangle$ *vs.* $\log DP_n$ is linear regardless of the balance of the competition between termination and transfer, but it also illustrates *why* this is so. From Equations (15) and (16) one thus has the following simple, powerful, intuitively reasonable and widely applicable relationship:[9,12,13]

$$\langle k_t \rangle = k_t^{1,1} G (DP_n)^{-e} \tag{17}$$

Figure 6 shows an example of applying this to experimental data: from the slope one obtains $e = 0.24$, from the intercept $k_t^{1,1} \approx 3 \times 10^8$ L mol$^{-1}$ s$^{-1}$ (taking the lazy option of $G \approx 1$) or $k_t^{1,1} \approx 2 \times 10^8$ L mol$^{-1}$ s$^{-1}$ (the more refined option of using Equation (16) for $G$). The accuracy of these values has been established (see above). Note though that Equation (17) can break down, e.g. if $e$ is high or combination is occurring in competition with transfer.[21]

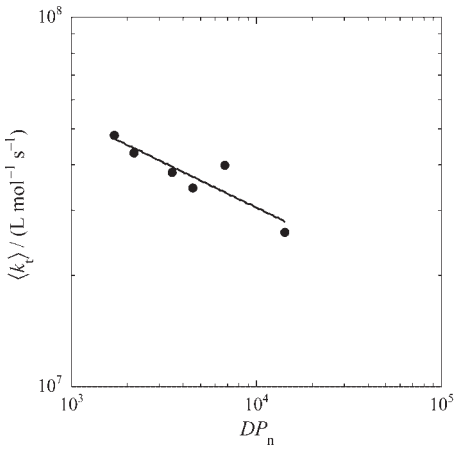


***Figure 6.***
Points: variation of $\langle k_t \rangle$ with $DP_n$ for AIBME-initiated bulk RP of MMA at 40 °C.[20] Line: linear best fit. The $\langle k_t \rangle$ measurements were made using the "steady-state rate" method of Table 1.

## Conclusion

It has been shown that the phenomenon of CLDT results in RP kinetics being writ on a rich, fascinating tableau. Hopefully this work has helped to promote understanding of these complexities. The discussed trends hold for RP in general, the presented equations for steady state only. Using the latter it has been shown that simple steady-state experiments can yield good information on CLDT, although there is no disputing that single-pulse PLP remains the method of choice for such studies[10,11] (see Table 1). In particular the transfer limit is recommended as an important but little realized phenomenon: it can have the guise of 'classical' kinetics (e.g., $\langle k_t \rangle$ invariant with $R_{init}$) where actually CLDT is occurring.

[1] O. F. Olaj, I. Bitai, F. Hinkelmann, *Makromol. Chem.* **1987**, *188*, 1689.

 

[2] M. Buback, R. G. Gilbert, R. A. Hutchinson, B. Klumperman, F.-D. Kuchta, B. G. Manders, K. F. O'Driscoll, G. T. Russell, J. Schweer, *Macromol. Chem. Phys.* **1995**, *196*, 3267.
[3] A. M. van Herk, *Macromol. Theory Simul.* **2000**, *9*, 433.
[4] S. Beuermann, M. Buback, *Prog. Polym. Sci.* **2002**, *27*, 191.
[5] C. Barner-Kowollik, M. Buback, M. Egorov, T. Fukuda, A. Goto, O. F. Olaj, G. T. Russell, P. Vana, B. Yamada, P. B. Zetterlund, *Prog. Polym. Sci.* **2005**, *30*, 605.
[6] M. Buback, M. Egorov, R. G. Gilbert, V. Kaminsky, O. F. Olaj, G. T. Russell, P. Vana, G. Zifferer, *Macromol. Chem. Phys.* **2002**, *203*, 2570.
[7] M. Buback, H. Hippler, J. Schweer, H.-P. Vögele, *Makromol. Chem., Rapid Commun.* **1986**, *7*, 261.
[8] J. P. A. Heuts, G. T. Russell, *Eur. Polym. J.* **2006**, *42*, 3.
[9] G. B. Smith, G. T. Russell, J. P. A. Heuts, *Macromol. Theory Simul.* **2003**, *12*, 299.
[10] M. Buback, M. Egorov, T. Junkers, E. Panchenko, *Macromol. Rapid Commun.* **2004**, *25*, 1004.
[11] M. Buback, E. Müller, G. T. Russell, *J. Phys. Chem. A* **2006**, *110*, 3222.
[12] O. F. Olaj, G. Zifferer, *Makromol. Chem., Macromol. Symp.* **1987**, *10/11*, 165.
[13] O. F. Olaj, G. Zifferer, *Macromolecules* **1987**, *20*, 850.
[14] G. T. Russell, *Aust. J. Chem.* **2002**, *55*, 399.
[15] O. F. Olaj, G. Zifferer, G. Gleixner, *Makromol. Chem., Rapid Commun.* **1985**, *6*, 773.
[16] O. F. Olaj, G. Zifferer, G. Gleixner, *Makromol. Chem.* **1986**, *187*, 977.
[17] G. T. Russell, *Macromol. Theory Simul.* **1994**, *3*, 439.
[18] G. T. Russell, *Macromol. Theory Simul.* **1995**, *4*, 519.
[19] G. B. Smith, J. P. A. Heuts, G. T. Russell, *Macromol. Symp.* **2005**, *226*, 133.
[20] M. Stickler, *Makromol. Chem.* **1986**, *187*, 1765.
[21] G. B. Smith, G. T. Russell, results to be published.
[22] D. Kukulj, T. P. Davis, *Macromol. Chem. Phys.* **1998**, *199*, 1697.
[23] J. P. A. Heuts, G. E. Roberts, J. D. Biasutti, *Aust. J. Chem.* **2002**, *55*, 381.

 

 DOI: 10.1002/masy.200750202

# The Importance of Chain-Length Dependent Kinetics in Free-Radical Polymerization: A Preliminary Guide

*Johan P. A. Heuts,*[*1] *Gregory T. Russell,*[2] *Gregory B. Smith,*[2] *Alex M. van Herk*[1]

**Summary:** The effect of chain-length dependent propagation at short chain lengths on the observed kinetics in low-conversion free-radical polymerization (frp) is investigated. It is shown that although the values of individual propagation rate coefficients quickly converge to the high chain length value (at chain lengths, *i*, of about 10), its effect on the average propagation rate coefficients, $\langle k_p \rangle$, in conventional frp may be noticeable in systems with an average degree of polymerization ($DP_n$) of up to 100. Furthermore it is shown that, unless the system is significantly retarded, the chain-length dependence of the average termination rate coefficient, $\langle k_t \rangle$, is not affected by the presence of chain-length dependent propagation and that there exists a simple (fairly general) scaling law between $\langle k_t \rangle$ and $DP_n$. This latter scaling law is a good reflection of the dependence of the termination rate coefficient between two *i*-meric radicals, $k_t^{i,i}$, on *i*. Although simple expressions seem to exist to describe the dependence of $\langle k_p \rangle$ on $DP_n$, the limited data available to date does not allow the generalization of these expressions.

**Keywords:** chain-length dependent propagation; chain-length dependent termination; free-radical polymerization; kinetics

## Introduction

The main process and product parameters to be controlled in free-radical polymerization are the rate of polymerization ($R_p$) and the molecular weight distribution of the formed polymer. In the latter case, one often tries to control the number average degree of polymerization ($DP_n$) and the polydispersity index (*PDI*). Although an increasing number of researchers are starting to use (complicated) computer modelling packages, most people would still use the steady-state rate equation (Eq. 1) for predicting changes in rate and the Mayo equation (Eq. 2) for predicting changes in the average degree of polymerization when changing reaction conditions.

The steady-state rate equation for a free-radical polymerization of a monomer M initiated by a thermal initiator I, with decomposition rate coefficient $k_d$ and initiator efficiency *f* (defined as the fraction of primary radicals not undergoing cage reactions), is given by Eq. 1, where $\langle k_t \rangle$ is the chain-length averaged termination rate coefficient and $\langle k_p \rangle$ is the chain-length averaged propagation rate coefficient for the given system. The use of a system-dependent $\langle k_t \rangle$ instead of an (incorrect) single chain-length independent value of $k_t$ in this equation seems to be generally accepted now,[1],[2] but as we have shown previously and will elaborate upon in this paper, in certain cases the use of $\langle k_p \rangle$ instead of the long-chain $k_p$ value is also required.[3–5]

$$R_p = \langle k_p \rangle \sqrt{\frac{f k_d [I]}{\langle k_t \rangle}} [M] \quad (1)$$

Similarly, the familiar Mayo equation, given by Eq. 2, should contain $\langle k_p \rangle$ and $\langle k_t \rangle$

[1] Laboratory for Polymer Chemistry, Department of Chemical Engineering and Chemistry, Eindhoven University of Technology, PO Box 513, 5600 MB Eindhoven, The Netherlands
E-mail: j.p.a.heuts@tue.nl
[2] Department of Chemistry, University of Canterbury, Private Bag 4800, Christchurch, New Zealand

instead of their chain-length independent equivalents.

$$\frac{1}{DP_n} = (1+\lambda)\frac{\langle k_t\rangle[R]}{\langle k_p\rangle[M]} + \sum_X \frac{k_{tr,X}[X]}{\langle k_p\rangle[M]} \quad (2)$$

In this equation, λ is the fraction of chains terminated by disproportionation, [R] is the overall radical concentration and $k_{tr,X}$ is the rate coefficient for chain transfer to any chain transfer agent X (including monomer). Note that a chain-length independent chain transfer rate coefficient has been used, which is unlikely to be the case for similar reasons as to why the propagation rate coefficient is chain-length dependent.[6] However, in order to not unnecessarily overcomplicate the discussion and to focus on the effect of chain-length dependent propagation, we have assumed $k_{tr,X}$ independent of chain length in the current study.

Both equations are, in principle, simple to use and clearly show how the rate and molecular weight change with changing reaction conditions (*i.e.*, reactant/additive concentrations and rate coefficients). The only complicating factor in using these expressions is the fact that adequate values for $\langle k_t\rangle$ (and in some cases also for $\langle k_p\rangle$) must be used and these values are not always readily available from standard reference sources such as the Polymer Handbook.[1] In the case of $\langle k_t\rangle$ this is caused by the fact that the reaction is diffusion-controlled and hence the rate coefficient for termination is chain-length dependent; therefore a chain-length averaged value, given by Eq. 3, should be used.

$$\langle k_t\rangle = \frac{\sum_{i=1}^{\infty}\sum_{j=1}^{\infty} k_t^{i,j}[R_i][R_j]}{[R]^2} \quad (3)$$

In this expression, $k_t^{i,j}$ is the rate coefficient for the termination reaction between an *i*-meric radical $R_i$ and a *j*-meric radical $R_j$. It is important to note that in this work $R_1$ refers to a truly monomeric radical, whether it has been derived from initiator, chain transfer agent or chain transfer to monomer (so it does *not* refer to the radical after the first addition to monomer – this radical would be denoted as $R_2$ here). Hence, to really determine a value for $\langle k_t\rangle$ one would need to know the individual values for the $k_t^{i,j}$ and the propagating radical distribution. It is therefore clear that a ''termination rate coefficient'' measured for a given monomer may not be applicable to the same monomer, polymerized under different reaction conditions.[1] To make things even more complicated, $\langle k_t\rangle$ also depends on conversion, as the diffusion of the chains depends highly on the viscosity of the reaction medium.[1] In order to simplify our discussion, we limit ourselves here to low-conversion polymerization, so as to eliminate this conversion/viscosity effect.

The chain-length dependence of the propagation rate coefficient is of a more ''chemical'' nature in that it is caused by differences in the activation energy and the frequency factor of the actual, intrinsic, rate coefficients of the addition reaction for different size radicals.[5] The chain-length averaged propagation rate coefficient is defined by Eq. 4,

$$\langle k_p\rangle = \frac{\sum_{i=1}^{\infty} k_p^i[R_i]}{[R]} \quad (4)$$

where $k_p^i$ is defined as the rate coefficient for the addition of an *i*-meric radical to monomer. The chain-length dependence of $k_p$ is relatively small and only noticeable for systems in which a relatively low $DP_n$ is produced (see below).[5] Hence, in contrast to reported values of $k_t$, which are only applicable to very specific situations, carefully obtained values for $k_p$ in general do represent a ''true'' physical, generally applicable, rate coefficient (be it for long-chain propagation).

So, where does this leave the experimental polymer chemist? Is detailed knowledge really required about $k_p^i$, $k_t^{i,j}$ and the distribution of $R_i$? Those familiar with the literature regarding chain-length dependent termination (and now also chain-length dependent propagation) have probably encountered unfriendly looking math-

 

ematical equations and some may have even decided to put the paper aside labelling it as only relevant to theoreticians. To some extent these readers might have been right in their thinking, were it not that chain-length dependence often causes deviations from what is expected from classical theory and ignoring it in certain instances can cause incorrect conclusions to be drawn. Hence, for those workers only interested in rough estimates for the chain-length dependence of $\langle k_p \rangle$ and $\langle k_t \rangle$ to be used in Eqs. 1 and 2, it would be very useful to have approximate scaling laws such as Eqs. 5 and 6.

$$\langle k_t \rangle \approx G \cdot DP_n^{-e} \tag{5}$$

$$\langle k_p \rangle \approx Q \cdot DP_n^{-a} \tag{6}$$

Here, $G$ and $Q$ are constant pre-exponential factors and $e$ and $a$ scaling exponents for $\langle k_t \rangle$ and $\langle k_p \rangle$, respectively.

In what follows we will investigate whether such scaling laws exist and how important chain length dependent propagation is in free-radical polymerization.

## Chain-Length Dependent Termination and Propagation Rate Coefficients

It has been known for many decades that the termination process is diffusion-controlled and therefore the rate coefficient for termination depends on the length of the reacting radical.[1] Furthermore, it has been known that the rate-determining processes for the termination of small and long radicals are center-of-mass and segmental diffusion, respectively. These processes scale with the chain length as $i^{-e}$, where $e \approx 0.5$ and 0.16 for the former and latter processes respectively. It is also known that two monomeric radicals undergo a termination reaction with a rate coefficient of about $10^9$ $dm^3mol^{-1}s^{-1}$. Although these facts have been known for quite some time, we recently presented for the first time a simple composite termination model that encompasses all these experimental facts.[7] In this model, which is schematically shown in Figure 1, the termination rate coefficient between two $i$-meric radicals is given by Eq. 7, where we assume a critical chain length $i_{crit}$ of about 100 units at which the rate determining process from center-of-mass diffusion ($i \leq i_{crit}$) changes to segmental diffusion ($i > i_{crit}$). Cross-termination is then described by $k_t^{i,j} = (k_t^{i,i} \times k_t^{j,j})^{1/2}$.

$$k_t^{i,i} = \begin{cases} k_t^{1,1} \times i^{-e_S} & \text{for } i \leq i_{crit} \\ k_t^{1,1} \times (i_{crit})^{-(e_S - e_L)} \times i^{-e_L} & \text{for } i > i_{crit} \end{cases} \tag{7}$$

The values for the parameters in Eq. 7 that we used in our modeling for MMA at 60 °C are $k_t^{1,1} = 1 \times 10^9$ $dm^3mol^{-1}s^{-1}$, $e_S = 0.50$, $e_L = 0.16$ and $i_{crit} = 100$; we will use these parameters as our defaults in all the kinetic modelling for this paper. The applicability of this model was confirmed experimentally for several different monomer systems by Buback and co-workers with parameter-values very close to those proposed by us.[8,9]

Based on an analysis of kinetic data on small radical additions and the first few propagation steps in free-radical polymerization, backed up by theoretical investigations of the propagation rate coefficient, we proposed the empirical formula given by Eq. 8 for the description of the chain-length dependence of the propagation rate coeffi-

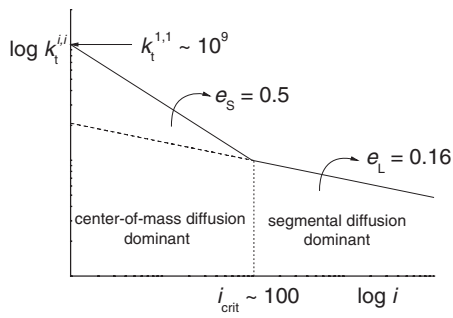


***Figure 1.***
Chain-length dependence of $k_t^{i,i}$ according to Eq. 7 indicating the regions where center-of-mass diffusion and segmental diffusion are the rate dominating processes.

 

cient:[3–5]

$$k_p^i = k_p\left[1 + C_1 \exp\left\{-\frac{\ln 2}{i_{1/2}}(i-1)\right\}\right] \quad (8)$$

In this equation, $k_p$ is the long-chain propagation rate coefficient, $C_1 = (k_p^1 - k_p)/k_p$ and $i_{1/2}$ is the chain length at which $k_p^1 - k_p$ halves in value (*i.e.*, a sort of "half-life"). Available data thus far suggest $C_1 \approx 10$–$50$ and $i_{1/2} \approx 0.5$–$1.5$;[5] for MMA polymerization we found values of $C_1 = 15.8$ and $i_{1/2} = 1.12$. These latter values were obtained by fitting pulsed laser polymerization data obtained by Van Herk and co-workers[10] and were found to describe well our (independently obtained) experimental steady state data (both rates and molecular weight distributions).[3,4]

In Figure 2, Eq. 8 is graphically displayed for $C_1 = 10$ and three different values for $i_{1/2}$, and it is clear from this figure that the chain length dependence of $k_p^i$ quickly converges to its long chain value: for the more realistic values of $i_{1/2} = 0.5$ and 1.0, this happens before $i = 10$, and even for the unrealistically high value of $i_{1/2} = 5$ this happens before $i = 50$. This behaviour is not significantly affected by the value of $C_1$. Although this effect becomes insignificant quickly for the *elemental* rate coefficients, we will see in a following section that its *macroscopic* effect may be noticeable in polymerizations with average degrees of polymerization of up to 100.

Finally, two important notes need to be made here regarding chain length dependent propagation (CLDP): (i) the equation given by Eq. 8 is purely an empirical (but physically realistic!) formula that describes the currently available experimental and theoretical data well, and (ii) there is some contention as to whether there may be an additional process happening that causes an additional chain length dependence up to much higher chain lengths[10,11] – in this work we limit ourselves to CLDP at short chain lengths.

## Kinetic Modelling Procedure

In order to determine the values of $\langle k_t \rangle$ and $\langle k_p \rangle$ for varying reaction conditions, it can be seen from Eqs. 3 and 4 that we need to know the individual rate coefficients $k_t^{i,j}$ and $k_p^i$ and the radical distribution (i.e., $[R_i]$ for all $i$). The individual rate coefficients are known from Eqs. 7 and 8, and the radical distribution can be determined using an iterative procedure for solving Eq. 9, which

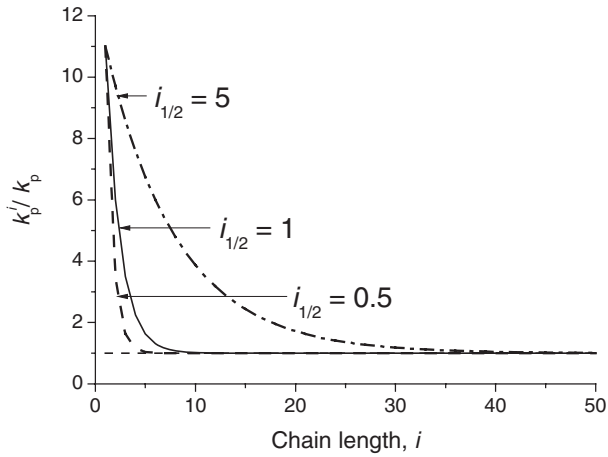


***Figure 2.***
Chain-length dependence of $k_p$ according to Eq. 8, with $C_1 = 10$ and $i_{1/2} = 0.5$, 1 and 5.

 

is easily derived after making the steady-state assumption for all radical concentrations.[7]

$$[\mathrm{R}_i] = \frac{R_{\mathrm{init}} + f_{\mathrm{trX}}[\mathrm{R}]}{f_{\mathrm{p}}^{i}} \prod_{j=1}^{i} \left( \frac{f_{\mathrm{p}}^{j}}{f_{\mathrm{p}}^{j} + f_{\mathrm{trX}} + f_{\mathrm{t}}^{j}} \right) \quad \text{for } i = 1, \infty \tag{9}$$

In this equation, $R_{\mathrm{init}}$ is the initiation rate ($= 2f k_{\mathrm{d}}[\mathrm{I}]$ for a thermal initiator), [R] is the overall radical concentration, $f_{\mathrm{trX}}$ is the transfer frequency of an $i$-meric propagating radical ($= k_{\mathrm{trX}}[\mathrm{X}]$), $f_{\mathrm{p}}^{i}$ is its propagation frequency ($= k_{\mathrm{p}}^{i}[\mathrm{M}]$) and $f_{\mathrm{t}}^{i}$ its termination frequency ($= (2k_{\mathrm{t}}^{i,i}R_{\mathrm{init}})^{1/2}$ for $k_{\mathrm{t}}^{i,j} = (k_{\mathrm{t}}^{i,i} \times k_{\mathrm{t}}^{j,j})^{1/2}$). All these parameters are known, except the overall radical concentration [R], which is at the same time an input of the calculation process and its result ($[\mathrm{R}] = \Sigma\ [\mathrm{R}_i]$). Hence, an iterative procedure is required to solve the radical balances, in which first a guess needs to be made for [R] (a reasonable starting point being a guess based on ''classical'' kinetics) after which Eq. 9 is solved up to sufficiently high $i$. Once convergence has been reached for [R], $\langle k_{\mathrm{t}} \rangle$ and $\langle k_{\mathrm{p}} \rangle$ can be calculated using Eqs. 3 and 4. To get an exact value for the corresponding $DP_{\mathrm{n}}$ in the system, one would need to evaluate the entire molecular weight distribution starting from the radical distribution. Alternatively, one could use the Mayo equation (Eq. 2) and for short chains add 1 unit to the $DP_{\mathrm{n}}$ to correct for the long-chain-approximation; although this is clearly an approximation, it is sufficiently accurate for the present purposes. This whole procedure, which we carried out using an EXCEL spreadsheet up to $i = 65519$ (i.e., the maximum number of rows that we could use), is schematically shown in Figure 3.[5] In order to effect changes in $DP_{\mathrm{n}}$, we varied $f_{\mathrm{trX}}$ and/or $R_{\mathrm{init}}$.

## The Effect of CLDP on the Observed Kinetics

Firstly we will consider the effect of CLDP on the observed termination rate coefficient $\langle k_{\mathrm{t}} \rangle$. In Figure 4, the variation of $\langle k_{\mathrm{t}} \rangle$ with $DP_{\mathrm{n}}$ is shown for both chain length independent (CLIP) and dependent propagation. Two things are immediately clear from this figure. Firstly that the $\langle k_{\mathrm{t}} \rangle$-$DP_{\mathrm{n}}$ relationship reflects that of $k_{\mathrm{t}}^{i,i}$-$i$, and

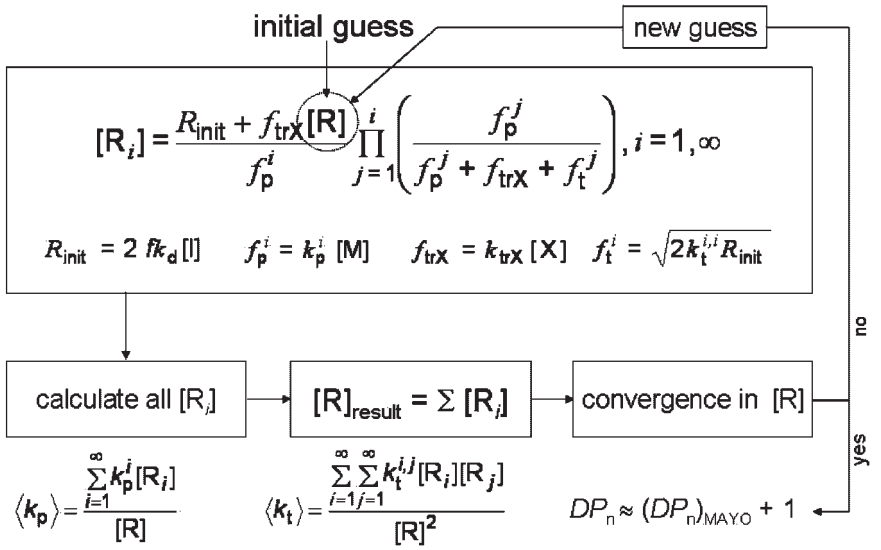


***Figure 3.***
Schematic diagram containing the steps taken to determine $\langle k_{\mathrm{p}} \rangle$ and $\langle k_{\mathrm{t}} \rangle$ for systems with a varying $DP_{\mathrm{n}}$.

 

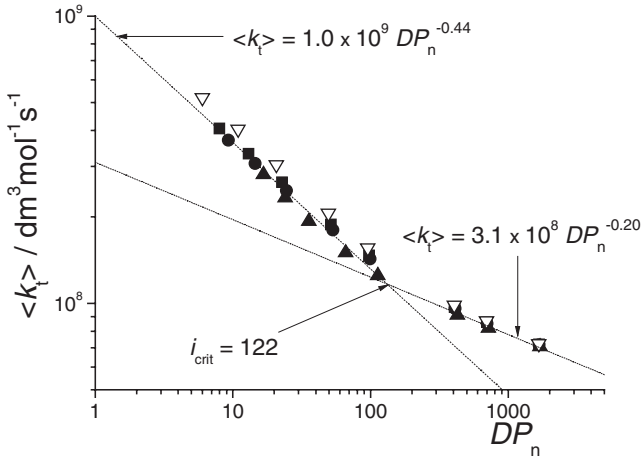


***Figure 4.***
The chain-length dependence of the average termination rate coefficient assuming a constant $k_p$ (△) and chain length dependent $k_p$ with $C_1 = 10$ and $i_{1/2} = 0.5$ (■), 1.0 (●) and 5 (▲).

secondly that the effect of chain length dependent propagation on this relationship is very small. So, we can conclude that a simple scaling law exists between $\langle k_t \rangle$ and $DP_n$. Such a scaling law, holding for Eq. 7 with the given parameter values, is shown in Figure 4.

In Figure 5, the relationship between the observed propagation rate coefficient $\langle k_p \rangle$ and $DP_n$ is shown. The first thing that draws attention is the fact that the effect of CLDP on $\langle k_p \rangle$ is noticeable up to much higher values of $DP_n$ than the value of the chain length $i$ up to which CLDP is significant in the individual rate coefficients (see Figure 2). For example, for the experimentally most likely values of $i_{1/2} = 0.5$ and 1.0, $k_p^i \approx k_p$ for $i \approx 10$, but $\langle k_p \rangle \approx k_p$ only for $DP_n \approx 100$. Hence, especially when working in systems where $DP_n < 100$, one should be aware that the observed propagation rate coefficient $\langle k_p \rangle$ may not be the same as the long chain propagation rate coefficient $k_p$ (normally determined by PLP).

In Figure 5 are also shown the first attempts to arrive at a simple scaling law for $\langle k_p \rangle$ with $DP_n$ similar to what was done earlier for $\langle k_t \rangle$. Starting from a simple

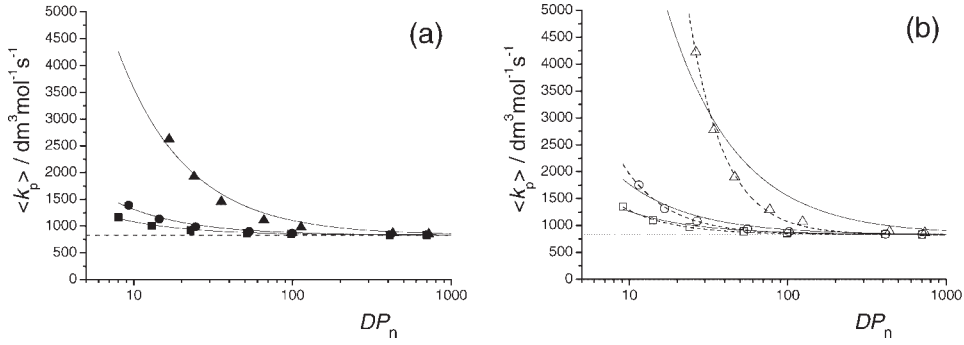


***Figure 5.***
Dependence of $\langle k_p \rangle$ on $DP_n$, with (a) $C_1 = 10$ and $i_{1/2} = 0.5$ (■), 1.0 (●) and 5 (▲); (b) with $C_1 = 50$ and $i_{1/2} = 0.5$ (□), 1.0 (○) and 5 (△). Full and dotted lines are the fits according to Eqs. 12 and 13 respectively.

 

"two-state" propagation model used by Van Herk and co-workers (Eq. 10),[10] we derived a linear relationship between $\langle k_p \rangle$ and the amount of chain transfer agent in the system (Eq. 11).[4]

$$k_p^i = \begin{cases} \infty & \text{for } i \leq i_{fast} \\ k_p & \text{for } i > i_{fast} \end{cases} \quad (10)$$

$$\langle k_p \rangle = k_{trX} \frac{[X]}{[M]} \times i_{fast} + k_p \quad (11)$$

The form of Eq. 11 suggests the possible existence of the following relationship between $\langle k_p \rangle$ and $DP_n$, where $Q$' is the only adjustable parameter.

$$\langle k_p \rangle = Q' DP_n^{-1} + k_p \quad (12)$$

The fits to the data with $C_1 = 10$ are shown in Figure 5a and the results appeared very promising, but in the case of $C_1 = 50$, the results were significantly worse as shown in Figure 5b.

Clearly, the simple propagation model (Eq. 10) on which Eq. 12 is based does not adequately describe the true CLDP behaviour and therefore we modified it to incorporate two fit parameters $Q$ and $a$ (Eq. 13). The corresponding data fits are also shown in Figure 5b and it is immediately clear that Eq. 13 performs much better in describing the data than does Eq. 12. In Table 1, all fit parameters for Eqs. 12 and 13 to all combinations of $C_1 = 10$, 20 and 50 and $i_{1/2} = 0.5$, 1.0 and 5.0 are listed.

$$\langle k_p \rangle = Q DP_n^{-a} + k_p \quad (13)$$

From Table 1 it can be seen that for the same value of $i_{1/2}$, $Q'$ and $Q$ increase with increasing $C_1$ (as expected) and that $a$ increases with increasing $i_{1/2}$ (with only a small dependence on $C_1$). It would be useful to have a simple relationship between these fit parameters and the more "fundamental" CLDP parameters $C_1$ and $i_{1/2}$, but thus far we have not been able to discover any obvious one. (NB. Although $C_1$ and $i_{1/2}$ are indeed more fundamental in that they describe the chain length dependence of $k_p^i$, one should remember that, at least at present, Eq. 8 is also an *empirical* relationship).

We conclude this section with a discussion on the effect of CLDP on the observed rate of polymerization. In Figure 6, the dependence of $\langle k_p \rangle / \langle k_t \rangle^{1/2}$ (note that $R_p \propto \langle k_p \rangle / \langle k_t \rangle^{1/2}$) on $DP_n$ is shown, where the dotted line indicates the situation of CLIP.

As expected for CLIP, the ratio $\langle k_p \rangle / \langle k_t \rangle^{1/2}$ (and hence the rate) decreases with decreasing $DP_n$: $\langle k_t \rangle$ increases with decreasing $DP_n$, while $k_p$ remains constant. For CLDP we see a positive deviation from the CLIP situation, because the effect of an increasing value of $\langle k_t \rangle$ is compensated by an increasing value of $\langle k_p \rangle$ with decreasing $DP_n$. This effect becomes more pronounced with increasing values of $i_{1/2}$ and $C_1$. It should also be noted here that this behaviour was observed experimentally for the low-conversion bulk polymerization of methyl methacrylate at 60 °C in the presence of dodecanethiol.[3]

The main message from Figure 6 is that we will see different rate behaviour with changing $DP_n$ depending on the values of $C_1$ and $i_{1/2}$; systems with a very weak dependence of $\langle k_p \rangle$ on $DP_n$ will show a decrease in rate at low $DP_n$, whereas a stronger

***Table 1.***
Summary of fit parameters for $\langle k_p \rangle$ according to eqs 12 and 13.

| $C_1$ | $i_{1/2}$ | $Q'$/dm$^3$ mol$^{-1}$ s$^{-1}$ | $Q$ / dm$^3$ mol$^{-1}$ s$^{-1}$ | $a$ |
|---|---|---|---|---|
| 10 | 0.5 | $2.8 \times 10^3$ | $6.5 \times 10^3$ | 1.34 |
| 10 | 1.0 | $5.7 \times 10^3$ | $2.1 \times 10^4$ | 1.49 |
| 10 | 5.0 | $3.9 \times 10^4$ | $6.1 \times 10^5$ | 1.79 |
| 20 | 0.5 | $3.4 \times 10^3$ | $8.4 \times 10^3$ | 1.37 |
| 20 | 1.0 | $7.2 \times 10^3$ | $2.8 \times 10^4$ | 1.51 |
| 20 | 5.0 | $5.3 \times 10^4$ | $1.1 \times 10^6$ | 1.87 |
| 50 | 0.5 | $4.3 \times 10^3$ | $1.1 \times 10^4$ | 1.37 |
| 50 | 1.0 | $9.3 \times 10^3$ | $3.9 \times 10^4$ | 1.54 |
| 50 | 5.0 | $7.2 \times 10^4$ | $2.1 \times 10^6$ | 1.97 |

 

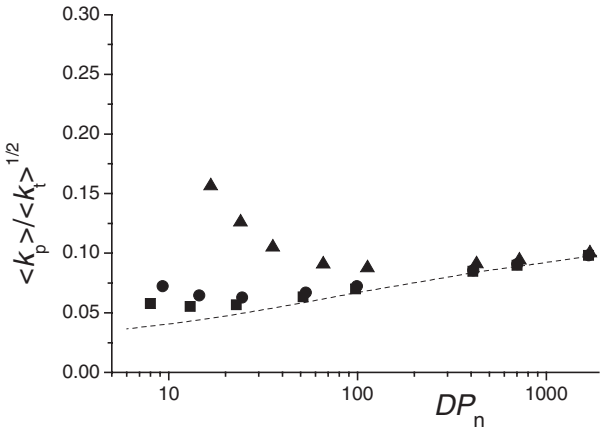


***Figure 6.***
The effect of CLDP on the observed rate of polymerization (expressed here as $\langle k_p \rangle / \langle k_t \rangle^{1/2}$) at a given average degree of polymerization in the system. Data are shown for the cases of $C_1 = 10$ and $i_{1/2} = 0.5$ (■), 1.0 (●) and 5 (▲).

dependence may lead to apparent classical (chain-length independent) kinetics or even increased rates. Hence, when predicting the rate at lower values of $DP_n$ from rate data at higher $DP_n$ we may significantly underestimate the rate if we only take into account the chain length dependence of $\langle k_t \rangle$. It is therefore important to have an idea about the chain length dependence of either $k_p$ or $\langle k_p \rangle$. However, as is clear from Figures 4–6, any possible effects from CLDP probably only manifest themselves for $DP_n < 100$ and are probably safely ignored at higher $DP_n$.

## The Effect of $k_p^1$ on the Observed Kinetics

Thus far, we have considered the chain length dependence of propagation assuming that $R_1$ has the same, or a very similar, chemical nature as the polymeric propagating radical, *i.e.*, it is a truly monomeric radical. Naturally, this need not always be the case. Initiator-derived radicals may react faster with a given monomer than the radical derived from this monomer, similar to propagating radicals that may prefer crosspropagation over homopropagation in copolymerization. The opposite can also be the case. One may have chosen a poor initiator and the primary radical reacts only slowly with monomer, *e.g.*, cyanoisopropyl radical addition to vinyl acetate monomer.[12] Additionally, chain transfer agent-derived radicals may reinitiate at different rates with different monomers, where slow additions can lead to retardation or inhibition as has recently been studied extensively in RAFT polymerization.[13] It is therefore interesting to investigate the effect of different values of $k_p^1$ on the overall reaction kinetics; preliminary results of these studies have been published earlier and it should be noted that in this previous publication a small error was made in the calculation of $DP_n$.[5] Although this does not affect any qualitative conclusions of the earlier study, it changes the quantitative trends slightly. The results presented in this paper replace those presented earlier.[5]

We consider two different primary radicals $R_A$ and $R_B$, derived from initiator decomposition and chain transfer, respectively. The addition to monomer for these two radicals occurs with different rate coefficients as indicated in Scheme 1. For simplicity we assume that the resulting radicals after the first addition steps are indistinguishable and that the rate coeffi-

 

$$\mathrm{I} \xrightarrow{fk_d} 2\,\mathrm{R_A} \qquad \left.\begin{array}{l} \mathrm{R_A} + \mathrm{M} \xrightarrow{k_p^A} \mathrm{R_2} \\ \mathrm{R_B} + \mathrm{M} \xrightarrow{k_p^B} \mathrm{R_2} \end{array}\right\} \mathrm{R_2} + \mathrm{M} \xrightarrow{k_p^2} \mathrm{R_3}$$

$$\mathrm{R}_i + \mathrm{X} \xrightarrow{k_{trX}} \mathrm{P}_i + \mathrm{R_B}$$

***Scheme 1.***

cient of the subsequent monomer addition is independent of the primary radical fragment. We realise that this assumption is unlikely to be completely correct as the existence of significant penultimate unit effects has been proven.[14] However, it is unlikely that a possible penultimate unit effect will significantly alter any observed *trends* in CLDP and if so, it is expected that it would enhance the observed effect. Hence, while lacking any reliable quantitative information on the penultimate unit effect we assume Scheme 1 to be an adequate reflection of the kinetic situation.

In the current study (using a modification of Eq. 9 to incorporate two different primary radicals as described previously),[5] $DP_n$ was varied by varying the chain transfer frequency and we examined the effect of changing $k_p^B$ ($50\times$, $10\times$, $1\times$ and $0.1\times k_p$), while maintaining $k_p^A = (15.8+1)\times k_p$ (*i.e.*, MMA at 60 °C); see Figure 7a. In Figures 7b–d, the results of these calculations are shown and it is immediately clear that only the lowest value of $k_p^B$ gives results which are very different to those discussed in Figures 4–6.

The calculated values of $\langle k_t \rangle$ at low $DP_n$ for $k_p^B = 0.1\times k_p$ are significantly higher than those for the other three cases, which are well described by the $\langle k_t \rangle$ equation derived from the data in Figure 4. This is

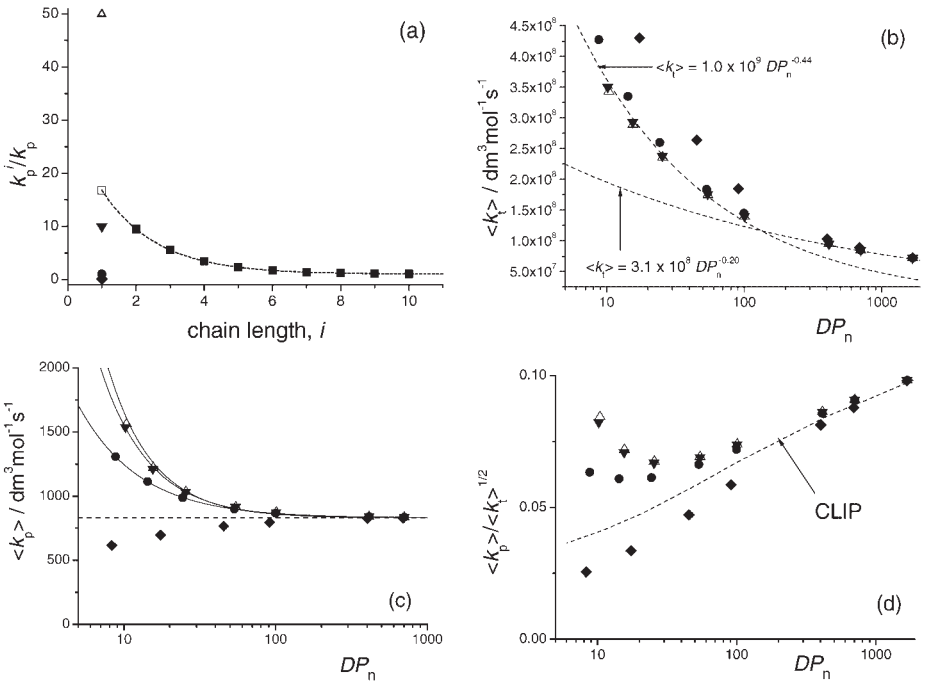


***Figure 7.***

Effect of changing $k_p^1$ on the observed kinetics. Chain length dependence of (a) $k_p^i$, (b) $\langle k_t \rangle$, (c) $\langle k_p \rangle$ with full lines fits according to Eq. 13, (d) $\langle k_p \rangle / \langle k_t \rangle^{1/2}$. For all figures: (□) $k_p^A = 16.8 \times k_p$ for all calculations, (△) $k_p^B = 50 \times k_p$, (▼) $k_p^B = 10 \times k_p$, (●) $k_p^B = k_p$, (◇) $k_p^B = 0.1 \times k_p$ and (■) $k_p^i$ according to Eq. (8) with $C_1 = 15.8$ and $i_{1/2} = 1.12$ for all $i \geq 2$, with $k_p = 831$ dm$^3$mol$^{-1}$s$^{-1}$.

 

presumably caused by an increase in primary radical termination, but more detailed simulations will be required to shed more light on this situation. In accordance with what we have seen earlier (*i.e.*, in Figures 5–6 for $i_{1/2} = 1$), the results in Figures 7c and d show that for all four values of $k_p^B$ there is a significant effect on $\langle k_p \rangle$ and the rate for $DP_n < 100$, with the results obtained for $k_p^B = 0.1 \times k_p$ showing a very strong retardation. It is conceivable that this retardation effect is underestimated here, as a possible penultimate unit effect is likely to lower $k_p^2$ and hence further reduce $\langle k_p \rangle$ and the rate at lower values of $DP_n$. The data obtained for the other three cases were fitted by Eq. 13 with the resulting fit parameters listed in Table 2.

It can be seen from Figure 7c that Eq. 13 provides a reasonable description of the found $\langle k_p \rangle$ data, with the situations in which $k_p^B > k_p$ having values for $Q$ and $a$ in the same range as those shown in Table 1 for $i_{1/2} = 0.5 - 1$. Although it is too early to draw any general conclusions at this stage, the current results suggest that it is likely that in the future (with more explicit experimental data available) it may be possible to simply estimate the $\langle k_p \rangle$-$DP_n$ behaviour from a known value of $k_p^1$ and a generally assumed chain-length dependence of $k_p^i$.

In the light of the results discussed above, the rate data shown in Figure 7d do not show any surprises. The case of $k_p^B = 0.1 \times k_p$ shows a significant retardation at low $DP_n$, whereas the other three cases show a faster rate as compared to the case of CLIP; in the cases where $k_p^B > k_p$ we observe a significant rate increase at low $DP_n$.

## Conclusion

In this paper we examined the effect of CLDP on kinetics in low-conversion free-radical polymerization. We have shown that although the chain length dependence of the individual $k_p^i$ does not extend beyond $i \approx 10$ for common systems, a significant macroscopic effect may be observed in systems with $DP_n$ up to $\sim$100. This observation leads us to draw some preliminary conclusions regarding CLDP: (a) it should probably not be ignored in living radical polymerizations with low $DP_n$ ($\approx i$), (b) one should be aware of it in conventional frp in systems with $DP_n < 100$, and (c) it is probably safe to ignore at higher $DP_n$. It has to be stressed here, however, that (although physically sensible!) these conclusions are only based on a limited amount of available data and that a possible additional mechanism of CLDP at higher chain lengths may complicate matters further. The situation for termination seems to be much clearer. Our recently proposed composite-termination model has independently been shown to present a good representation for the termination process in several different monomers. A generally applicable scaling law, reflecting the chain-length dependence of the individual rate coefficients, seems to apply to the dependence of $\langle k_t \rangle$ on $DP_n$ and is fairly insensitive to CLDP. For propagation, we have not yet succeeded in deriving a generally applicable scaling law for the variation of $\langle k_p \rangle$ with $DP_n$.

***Table 2.***
Fit parameters according to Eq. (13) for the $\langle k_p \rangle$ data in Figure 7c.

| $k_p^B/k_p$ | $Q$/dm$^3$mol$^{-1}$s$^{-1}$ | $a$ |
|---|---|---|
| 0.1 | no fit possible | no fit possible |
| 1.0 | $5.0 \times 10^3$ | 1.08 |
| 10 | $1.7 \times 10^4$ | 1.34 |
| 50 | $2.4 \times 10^4$ | 1.46 |

[1] M. Buback, M. Egorov, R. G. Gilbert, V. Kaminsky, O. F. Olaj, G. T. Russell, P. Vana, G. Zifferer, *Macromol. Chem. Phys.* **2002**, *203*, 2570.
[2] C. Barner-Kowollik, M. Buback, M. Egorov, T. Fukuda, A. Goto, O. F. Olaj, G. T. Russell, P. Vana, B. Yamada, P. B. Zetterlund, *Prog. Polym. Sci.* **2005**, *30*, 605.
[3] G. B. Smith, G. T. Russell, M. Yin, J. P. A. Heuts, *Eur. Polym. J.* **2005**, *41*, 225.

 

[4] G. B. Smith, J. P. A. Heuts, G. T. Russell, *Macromol. Symp.* **2005**, *226*, 133.
[5] J. P. A. Heuts, G. T. Russell, *Eur. Polym. J.* **2006**, *42*, 3.
[6] J. P. A. Heuts in *Handbook of Radical Polymerization*, K. Matyjaszewski, T. P. Davis, Eds., *John Wiley & Sons* **2002**, 1.
[7] G. B. Smith, G. T. Russell, J. P. A. Heuts, *Macromol. Theory Simul.* **2003**, *12*, 299.
[8] M. Buback, M. Egorov, T. Junkers, E. Panchencko, *Macromol. Rapid Commun.* **2004**, 1004.
[9] M. Buback, E. Muller, G. T. Russell, *J. Phys. Chem. A* **2006**, *110*, 3222.
[10] R. X. E. Willemse, B. B. P. Staal, A. M. van Herk, S. C. J. Pierik, B. Klumperman, *Macromolecules* **2003**, *36*, 9797.
[11] O. F. Olaj, M. Zoder, P. Vana, A. Kornherr, I. Schnöll- Bitai, G. Zifferer, *Macromolecules* **2005**, *38*, 1944.
[12] H. Fischer, L. Radom, *Angew. Chem. Int. Ed.* **2001**, *40*, 1349.
[13] See, for example, S. Perrier, C. Barner-Kowollik, J. F. Quinn, P. Vana, T. P. Davis, *Macromolecules* **2002**, *35*, 8300.
[14] M. L. Coote, T. P. Davis, *Prog. Polym. Sci.* **1999**, *24*, 1217.

 

# Propagation Kinetics of Free-Radical Methacrylic Acid Polymerization in Aqueous Solution. The Effect of Concentration and Degree of Ionization

*Sabine Beuermann,*[1,2] *Michael Buback,*[1] *Pascal Hesse,*[1] *Silvia Kukučková,*[1,3] *Igor Lacík**[3]

**Summary:** Propagation rate coefficients, $k_p$, of free-radical methacrylic acid (MAA) polymerization in aqueous solution are presented and discussed. The data has been obtained via the pulsed laser polymerization – size-exclusion chromatography (PLP-SEC) technique within extended ranges of both monomer concentration, from dilute solution up to bulk MAA polymerization, and of degree of ionic dissociation, from non-ionized to fully ionized MAA. A significant decrease of $k_p$, by about one order of magnitude, has been observed upon increasing monomer concentration in the polymerization of non-ionized MAA. Approximately the same decrease of $k_p$ occurs upon varying the degree of MAA ionization, $\alpha$, at low MAA concentration from $\alpha = 0$ to $\alpha = 1$. With partially ionized MAA, the decrease of $k_p$ upon increasing MAA concentration is distinctly weaker. For fully ionized MAA, the propagation rate coefficient even increases toward higher MAA concentration. The changes of $k_p$ measured as a function of monomer concentration and degree of ionization may be consistently interpreted via transition state theory. The effects on $k_p$ are essentially changes of the Arrhenius pre-exponential factor, which reflects internal rotational mobility of the transition state (TS) structure for propagation. Friction of internal rotation of the TS structure is induced by ionic and/or hydrogen-bonded intermolecular interaction of the activated state with the molecular environment.

**Keywords:** aqueous-phase polymerization; free-radical polymerization; methacrylic acid; PLP-SEC; propagation rate coefficients; pulsed-laser initiation; water-soluble monomers

## Introduction

Water-soluble homopolymers and copolymers are of high technical importance because of their wide-spread application in hydrogels, thickeners, viscosifiers, flocculants, membranes, coatings, etc.[1] Mostly, these polymers are obtained from free-radical polymerization in aqueous solution. Water-soluble monomers of particular technical relevance are acrylic acid, acrylamide, 2-acrylamido-2-methylpropane sulfonic acid, *N-iso*-propyl acrylamide, *N*,*N*′-dimethylacrylamide, methacrylic acid, dimethylamino-ethyl methacrylate, *N*-vinyl amides, *N*-vinyl pyrrolidone, *N*-vinyl formamide, *N*-vinyl imidazole, *N*-methyl-*N*-vinyl imidazolinium chloride. Investigations into the free-radical rate coefficients for polymerizations of these monomers in aqueous as well as organic solutions are scarce.[2] Significant changes of the rate coefficients are expected as a consequence of the action of hydrogen bonds between monomer, polymer, growing radicals, and water. The complexity may be further

[1] Institute of Physical Chemistry, Georg-August-University Göttingen, Tammannstrasse 6, D-37077 Göttingen, Germany
[2] Present address: University of Potsdam, Institute of Chemistry, Polymer Chemistry, Karl-Liebknecht-Str. 24-25, D-14476 Golm/Potsdam, Germany
[3] Polymer Institute of the Slovak Academy of Sciences, Dúbravská cesta 9, 842 36 Bratislava, Slovakia
FAX: (+421) 2 5477 2467
E-mail: igor.lacik@savba.sk

enhanced in case that ionic interactions come into play which requires to additionally consider the degree of ionization for monomer, polymer, and free-radical species and the associated ionic interactions.

The first studies into the kinetics of free-radical polymerization in aqueous phase date back to the work of Katchalsky and coworkers in the early 1950s.[3] In the 1970s and 1980s, polymerizations in aqueous solution were investigated by the Russian school, as reviewed by Gromov et al.[4,5] Generally, polymerizations in aqueous solution are characterized by strongly enhanced polymerization rates as compared to reactions in organic phase. The higher rates were assigned to the increased reactivity of monomer with a radical upon solvation by water. Also association of species, conformation of polymer coils, and hydrophobic interactions were assumed to govern free-radical polymerization rates in aqueous solutions.[5] The arguments were mostly based on measured overall rates of polymerization. A few individual rate coefficients have been determined by combining stationary methods with the instationary rotating sector technique. The quality of so-obtained data may however be rather insufficient, in particular in cases where the radical concentrations and radical size distributions are clearly different for the underlying two experiments.[6] Reported data thus exhibit an enormous scatter. The propagation rate coefficients for non-ionized acrylic acid (AA) in aqueous solution at ambient temperature that were available in the year 2000, differed by orders of magnitude. A value of $4\,000\ \mathrm{L \cdot mol^{-1} \cdot s^{-1}}$ has been deduced from post-polymerization experiments,[7] whereas $k_p = 27\,000\ \mathrm{L \cdot mol^{-1} \cdot s^{-1}}$ has been obtained via the rotating sector technique,[8,9] and $k_p = 92\,000\ \mathrm{L \cdot mol^{-1} \cdot s^{-1}}$ was determined by pulsed-laser polymerization in conjunction with size-exclusion chromatography (PLP-SEC).[10] Obviously, such a large spread in reported $k_p$ values is undesirable and poses problems for modeling acrylic acid polymerization processes in aqueous solution. The situation for most of the other water-soluble monomers was even worse at that time as no individual free-radical polymerization rate coefficients were available at all.

During recent years, the PLP-SEC technique has been used extensively for $k_p$ measurements in aqueous phase and reliable $k_p$ values[11] became available for AA,[10,12–14] methacrylic acid (MAA),[10,15,16] *N-iso*-propyl acrylamide (NIPAm)[17] and acrylamide (AAm).[18] The implementation of aqueous-phase SEC into PLP-SEC studies on water-soluble monomers[12] brought a significant improvement of $k_p$ determination, as molecular weight distributions of polymer samples from PLP could be measured directly without the need for carrying out polymer modification reactions to produce samples which may be subjected to SEC analysis in organic phase.[10] Such polymer modification may give rise to changes of the size distribution and thus may result in unreliable $k_p$ values.[12] Such an effect is more likely to occur with acrylates than with methacrylates. Recent PLP-SEC studies into $k_p$ of non-ionized MAA in aqueous solution demonstrated that the $k_p$ data deduced from aqueous-phase SEC[15] are in close agreement with the ones obtained from SEC in tetrahydrofuran on poly(methyl methacrylate) samples produced by methylation of poly(MAA) samples from PLP of MAA.[10] The data sets have been combined to form the first set of benchmark $k_p$ values for a polymerization in aqueous solution.[16]

The PLP-SEC investigations into $k_p$ of free-radical polymerization in aqueous phase suggest that $k_p$ varies strongly with monomer concentration. For MAA,[10] NIPAm[17] and AAm[18] a strong decrease in $k_p$ was found upon increasing monomer concentration. The same trend is seen for AA[13] from monomer concentrations of 3 wt.-% on, whereas at very low AA contents $k_p$ increases with acrylic acid concentration. Attempts to assign the strong solvent effects to associated structures,[10] to dimerization,[17,18] or to local monomer concentrations at the radical site

 

being different from overall monomer concentration[13] were unable to provide a consistent physical picture of the propagation kinetics.

In order to provide a comprehensive understanding of the effects of the solvent environment on $k_p$ in aqueous-phase polymerization, it is highly recommendable to have reliable rate coefficient data for extended ranges of experimental conditions, in particular of temperature, monomer concentration, and degree of ionization. With acrylate-type monomers, PLP-SEC experiments are limited to lower temperatures because of the formation of mid-chain radicals, which disfavor $k_p$ studies at temperatures well above ambient temperature.[19,20] No such restrictions occur with MAA, which appears to be a perfect monomer for fundamental studies into $k_p$ for the following reasons: (*i*) The so-called backbiting reaction, by which mid-chain radicals are produced, does not occur. (*ii*) The $k_p$ values of methacrylate-type monomers are such that suitable laser repetition rates for reliable PLP-SEC experiments are easily available. (*iii*) The poly(MAA) quantities produced during the PLP experiment are soluble within a wide range of MAA concentrations in water, from very dilute MAA solution up to the situation of MAA bulk polymerization. The first PLP-SEC studies into the temperature dependence of $k_p$ for non-ionized MAA dissolved in water[10] were carried out at a single monomer concentration, of 15 wt.-% MAA, and the concentration dependence was mapped out only at 25 °C. Within our earlier work on $k_p$ of non-ionized MAA in aqueous phase, monomer concentration was varied from 1 to 100 wt.-% MAA and the polymerization temperatures covered the range from 15 to 80 °C.[15] The present contribution extends this work to PLP-SEC studies in which, in addition to temperature and MAA concentration, the degree of ionic dissociation of MAA is varied. The experimental details and the extended body of individual $k_p$ data measured under conditions of partial and full ionization will be presented elsewhere.[21]

## Propagation Rate Coefficients for Aqueous-phase Polymerizations of Non-ionized Methacrylic Acid

Investigations into $k_p$ of non-ionized MAA were carried out over the entire concentration range, between 1 wt.-% MAA in aqueous solution up to bulk MAA polymerization, at temperatures ranging from 15 to 80 °C.[15] Presented in Figure 1 is the variation of $k_p$ with methacrylic acid concentration, $c_{MAA}$, at 60 °C. In going from the bulk system to 5 wt.-% MAA, $k_p$ increases by one order of magnitude, from 1 200 to 12 300 $L \cdot mol^{-1} \cdot s^{-1}$. Corresponding changes of $k_p$ with MAA concentration are observed for 25, 40 and 80 °C, where $k_p$ data for several monomer concentrations was collected.[15] Similar trends have been seen with AA, where in experiments at and slightly below ambient temperature,[13] a decrease in $k_p$ by a factor of three was found upon increasing the acrylic acid concentration in aqueous solution, $c_{AA}$, from 3 wt.-% to the highest experimentally accessible concentration of 40 wt.-%. Within these earlier experiments that were carried out within a narrower monomer concentration range, it appeared justified to assign the observed concentration dependence of $k_p$ to a local monomer concentration at the free-radical site to be different from overall acrylic acid concentration.[13] In case of MAA, $k_p$ could be measured over the entire concentration range from very dilute aqueous solution up to the bulk system. The data convincingly shows that local monomer concentration effects can not be made responsible for the observed order of magnitude change of $k_p$ with MAA concentration.[15]

The extended temperature range of the experiments reported in Ref.[15] allows for reliably deducing Arrhenius factors, $A(k_p)$, and activation energies, $E_A(k_p)$, for a wide range of MAA concentrations. A single (mean) value of $E_A(k_p) = (15.6 \pm 1.1)$ $kJ \cdot mol^{-1}$ affords for a very satisfactory representation of the temperature dependence of $k_p$ for the entire range from dilute aqueous solution (5 wt.-% MAA) to the bulk polymerization system.[15] Replacing

 

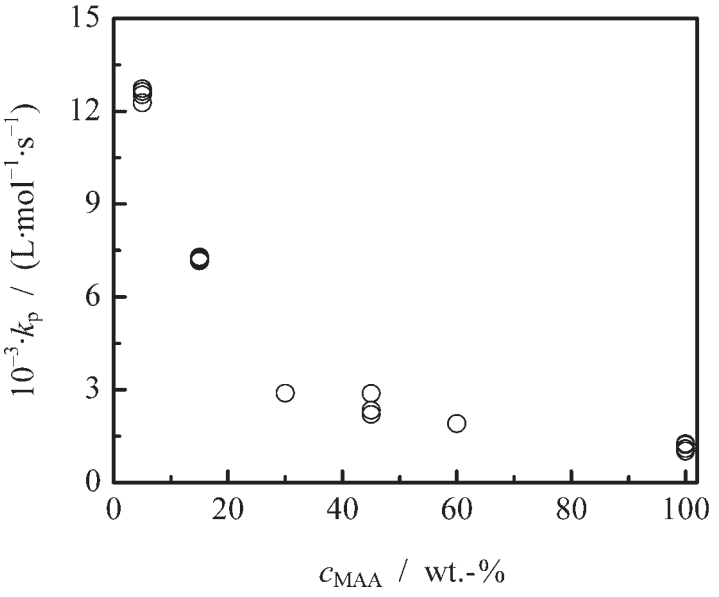


***Figure 1.***
Variation of $k_p$ for methacrylic acid in aqueous solution as a function of monomer concentration, $c_{MAA}$. The data is from aqueous-phase PLP-SEC experiments at 60 °C tabulated in Ref. [15]

water molecules by MAA and vice versa thus does not affect the energy barrier for propagation. The large variation of $k_p$ with $c_{MAA}$ may be unambiguously assigned to effects on the pre-exponential factor.

Although $E_A(k_p)$ and $A(k_p)$ are determined as correlated parameters from Arrhenius fitting of experimental rate coefficient data, both parameters constitute independent physical quantities and may be separately deduced from transition state theory. The pre-exponential factor is determined by the geometry of the rotating groups and by the rotational potentials of the relevant internal motions of the transition state structure.[22,23] These internal motions of the transition state structure are schematically represented by the arrows in Figure 2. There is an internal rotational motion around the terminal C–C bond of the macroradical, a rotation around the C–C bond that is formed during the propagation step, and a bending motion associated with this new C–C bond. The shaded area represents the environment consisting of varying amounts of MAA and water molecules which may interact with the internal motions of the TS structure via hydrogen bonds. The pre-exponential factor, $A(k_p)$, of MAA free-radical propagation in dilute aqueous solution is significantly higher than in MAA bulk polymerization, e.g., is $4.62 \cdot 10^6$ L·mol$^{-1}$·s$^{-1}$ for 5 wt.-% MAA as compared to $0.38 \cdot 10^6$ L·mol$^{-1}$·s$^{-1}$ in case of bulk MAA polymerization

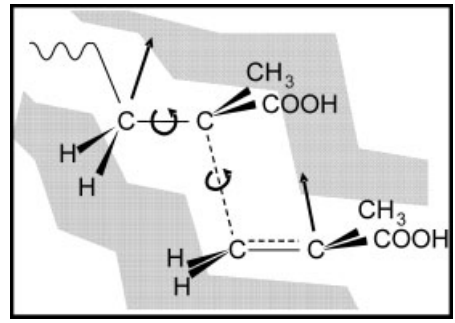


***Figure 2.***
Illustration of the transition state (TS) structure for the propagation step in MAA polymerization. The arrows indicate rotational and bending motions of the TS structure. The internal rotational motions of the TS structure are affected by hydrogen bonded interactions with the molecular environment (shaded area).

 

**Table 1.**
Arrhenius parameters, $A(k_p)$ and $E_A(k_p)$, for bulk polymerizations of methacrylic acid (MAA), methyl methacrylate (MMA) and methyl acrylate (MA) and for polymerizations of MAA and AA in aqueous solution. Bulk polymerizations are indicated by monomer concentrations of $c_M = 100$ wt.-%.

| | $c_M$/wt.-% | $E_A(k_p)$/kJ · mol$^{-1}$ | $A(k_p) \cdot 10^{-6}$/L · mol$^{-1}$ · s$^{-1}$ | Ref. |
|---|---|---|---|---|
| MAA | 5 | 16.5 | 4.62 | [15] |
| MAA | 15 | 14.5 | 1.33 | [15] |
| MAA | 100 | 16.1 | 0.38 | [15] |
| MMA | 100 | 22.4 | 2.67 | [24] |
| AA | 20 | 11.9 | 12.0 | [12] |
| AA | 40 | 12.2 | 8.9 | [12] |
| MA | 100 | 17.7 | 16.6 | [25] |

(see Table 1). This comparison indicates that the internal rotational mobility of the transition state for propagation is higher at larger water contents. The lower rotational mobility in case of bulk polymerization is indicative of stronger hydrogen bonding interactions of the transition state structure with an environment that essentially consists of MAA molecules.

It is instructive to compare the Arrhenius parameters for $k_p$ of MAA in bulk and in aqueous solution with the corresponding parameters for methyl methacrylate (MMA) and methyl acrylate (MA) bulk polymerizations as well as for AA polymerizations in aqueous solution. Listed in the upper part of Table 1 are the numbers for the methacrylic monomers, MAA and MMA, whereas the values for AA and MA are given in the lower part.

The first three entries in Table 1 illustrate that the activation energy for MAA propagation, $E_A(k_{p,MAA})$, is almost insensitive toward the molecular environment, whether the solvent is pure MAA (entry 3) or whether it is mostly water (entry 1). The pre-exponential factor, $A(k_{p,MAA})$, on the other hand, is enhanced by about one order of magnitude in passing from pure MAA to an environment essentially consisting of water. The pre-exponential, $A(k_{p,MAA})$, at low MAA concentrations, in between 5 and 15 wt.-% is close to the pre-exponential reported for methyl methacrylate bulk polymerization, $A(k_{p,MMA})$, listed as entry 4 in Table 1. Taking MAA bulk polymerization as a reference, this finding indicates that the pre-exponential factor and thus internal rotational motion are enhanced to similar extents by either changing the environment of the TS structure from pure MAA to an $H_2O$/MAA mixture containing about 10 wt.-% MAA or by methyl esterifying all carboxylic acid groups and thus transfer an MAA bulk polymerization into an MMA bulk polymerization in which hydrogen bonds will be absent. Despite the similarity in pre-exponential factor, the latter two systems, bulk MMA and aqueous solution MAA (10 wt.-%) polymerization clearly differ in activation energy, which is by about 6 kJ · mol$^{-1}$ lower with the MAA system(s).

For AA, bulk polymerization parameters are not accessible because of the insolubility of poly(AA) in its own monomer. The $E_A(k_{p,AA})$ values for polymerization in aqueous solution containing 20 and 40 wt.-% AA (entries 5 and 6 in Table 1), respectively, are both close to 12 kJ · mol$^{-1}$. It appears reasonable to assume that a value of this size should also apply to bulk AA polymerization. Thus, also with the acrylic systems, the value of the acid monomer, $E_A(k_{p,AA})$, would be by about 6 kJ · mol$^{-1}$ below the methyl ester value, $E_A(k_{p,MA})$, which indicates a similar effect of the hydrogen bonded interactions on the activation barrier for the propagation reaction upon passing from MAA to MMA and from AA to MA. It should be noted that the quantum-chemical calculations in Ref.[26] predicted a lowering of $E_A(k_{p,AA})$ upon introducing a water solvent field as compared to $E_A(k_{p,AA})$ in the gas phase. These calculations, however, did not

 

consider the influence of the monomer solvent field nor of mixed water/monomer solvent fields. Our experimental data indicates that the acid monomer is capable of lowering the reaction barrier by approximately the same extent as do water molecules. Also for the AA polymerizations in aqueous solution, the pre-exponential largely increases toward lower monomer concentration (see entries 5 and 6 in Table 1). At AA concentrations below 20 wt.-%, the pre-exponential factor may approach the value reported for bulk methyl acrylate polymerization, in close agreement with the observation for $A(k_p)$ of bulk MMA polymerization and polymerization of MAA in aqueous solution at MAA contents of about 10 wt.-%. The similarity seen with the propagation rate coefficients of the two carboxylic acid monomers in aqueous solution provides further support for assigning the change in $k_p$ to the internal rotational mobility of the TS structure due to friction induced by hydrogen bonding interactions with the molecular environment.

In MMA and MA no such hydrogen bonds are operative. The distinct difference in the pre-exponential for bulk polymerization of these two monomers (see entries 4 and 7 in Table 1), however also originates from effects on internal rotational mobility. The lower value of $A(k_{p,MMA})$ is due to enhanced *intramolecular* friction induced by the α-methyl groups on the polymer backbone.

The studies into $k_p$ of non-ionized MAA suggest that the strong dependence of $k_p$ values on monomer concentration that has been observed for other water-soluble monomers in aqueous-phase polymerization [10,13,17,18] is most likely also a genuine kinetic effect. The measured propagation rate coefficients should be regarded as ''true'' $k_p$ values rather than as ''apparent'' rate coefficients which are associated with local monomer concentrations being largely different from the easily accessible overall monomer concentrations. It goes without saying that no firm conclusions about the $k_p$ behavior of other water-soluble monomers can be drawn on the basis of the MAA data. For example, the observed insensitivity of $E_A(k_{p,MAA})$ toward the MAA to water ratio of the polymerizing system must not hold for other water-soluble monomers, as the interactions of the TS structure with monomer molecules and with water molecules may be rather different. The variation of $E_A(k_p)$ and $A(k_p)$ thus needs to be separately investigated for each monomer system by careful PLP-SEC measurements within extended temperature and concentration intervals.

Having realized that $k_p$ varies with the MAA to $H_2O$ ratio, immediately raises the question whether and to which extent the change in monomer concentration during polymerization to higher degrees of monomer conversion may affect $k_p$. As PLP-SEC experiments have to be carried out at low degrees of monomer conversion, the situation of high conversion has to be simulated by adding polymer to the PLP system prior to laser pulsing. The data from such experiments on methacrylic acid polymerization in aqueous solution are presented and discussed in another paper contained in this volume.[27]

The following section addresses the impact of ionic dissociation of MAA on the propagation kinetics in aqueous solution at different monomer concentrations. The primary intention of these studies is to find out whether the preceding kinetic analysis, which assumes *intramolecular* rotational mobility of the TS structure and thus the pre-exponential factor being affected by strong *intermolecular* interactions, is also suitable for interpreting free-radical propagation of ionized MAA in aqueous solution.

### Propagation Rate Coefficient in Aqueous Solution of Partially and Fully Ionized Methacrylic Acid

Methacrylic acid in aqueous solution is a weak acid with a $pK_a$ value of ~4.36.[3] Thus, the degree of ionization, $\alpha$, is below 1 mol.% within the entire range of MAA concentrations. Adding a base, e.g., sodium

 

hydroxide, to the system enhances the p*H* and produces anionic carboxylate groups. Thus, MAA is an excellent candidate for studying radical propagation rate coefficients at different extents of ionic dissociation. Charged carboxylate groups may occur with the monomer, the polymer, and the growing radicals. In addition, the system contains counter-ions, e.g., sodium cations, in case of using NaOH for partial or complete neutralization. Depending on the molar ratio of the base and the monomeric acid, PLP-SEC experiments may be carried out over an extended range of degrees of ionization, from $\alpha = 0$ to $\alpha = 1$. Neutralization appears to be a rather simple procedure, but it needs to be taken into account that the p$K_a$ values of MAA and poly(MAA) are different. Thus, full ionization of the monomer does not necessarily mean that also poly(MAA) is fully ionized. Moreover, the effects of counter-ions are difficult to be adequately described for the high molecular weight polymer. In addition, the structure and the dynamics of charged macroradical species may significantly affect the polymerization kinetics.

Until recently, the knowledge about the polymerization kinetics and mechanism of ionized (meth)acrylic acid was based on a very limited set of rate coefficients from the pioneering studies,[3,28] in which the rate of polymerization was measured for various p*H* values. Only recently, the first PLP-SEC study was carried out for 5 wt.-% acrylic acid at 6 °C over the full range from $\alpha = 0$ to $\alpha = 1$.[14] In going from non-ionized to fully ionized AA, an approximately ten-fold decrease in $k_p$, from 111 000 to 13 000 $L \cdot mol^{-1} \cdot s^{-1}$, was observed. The lowering in $k_p$ was explained by repulsive interactions between negatively charged macroradicals and monomer molecules, following the line of arguments put forward earlier.[3,28] It was, however, clear[14] that this limited set of PLP-SEC data will not be sufficient to answer the various questions concerning the effects on $k_p$ due to ionic speciation, to counter-ions, to electrochemical equilibria, to acid-base properties of monomer, macroradical, and polymer, to the ionic strength, and perhaps to local monomer concentration.

Obviously, more experimental data for wider ranges of temperatures and monomer concentrations are required to arrive at a better understanding of the mechanism of free-radical polymerization in partially and fully ionized systems. Acrylic acid is no perfect monomer for kinetic studies in wide ranges of experimental conditions. As in the case of PLP-SEC studies into $k_p$ of non-ionized monomers, methacrylic acid is a better choice also for investigations into ionized systems within extended temperature and monomer concentration ranges. For MAA, $k_p$ values were measured at monomer concentrations, $c_{MAA}$, between 5 and 40 wt.-% and at temperatures from 6 to 80 °C over the entire range of MAA ionization, between $\alpha = 0$ and $\alpha = 1$.[21] The experimental procedure is similar to the one used in the experiments on aqueous solutions of AA at different degrees of ionic dissociation.[14]

For polymerizations at 40 °C, the dependence of $k_p$ on monomer concentration, between 5 and 40 wt.-% MAA, is illustrated for different degrees of monomer ionization ($\alpha = 0$, 0.7, and 1.0) in Figure 3. The concentration dependence of $k_p$ for non-ionized MAA (that is moving along line 1 in Figure 3) has been discussed in the preceding section. At $\alpha = 0.7$, the decrease of $k_p$ with $c_{MAA}$ is much weaker than at $\alpha = 0$. For $\alpha = 1.0$ (that is along line 3 in Figure 3), the situation is reversed in that $k_p$ even increases with $c_{MAA}$. This effect is weak but can be safely established. The approximately ten-fold decrease in $k_p$ from $\alpha = 0$ to $\alpha = 1$ at $c_{MAA}$ of 5 wt.-% is indicated by the arrow (2) in Figure 3. An analogous order-of-magnitude change of $k_p$ upon passing from the non-ionized to the fully ionized acid monomer has been observed for acrylic acid polymerization in aqueous solution at 5 wt.-% AA.[14] The lowering of $k_p$ with $\alpha$ becomes less pronounced toward higher $c_{MAA}$, and $k_p$ is insensitive toward the degree of ionic dissociation at 40 wt.-% MAA, as is indicated by point (4) in Figure 3. In view of the strong variations

 

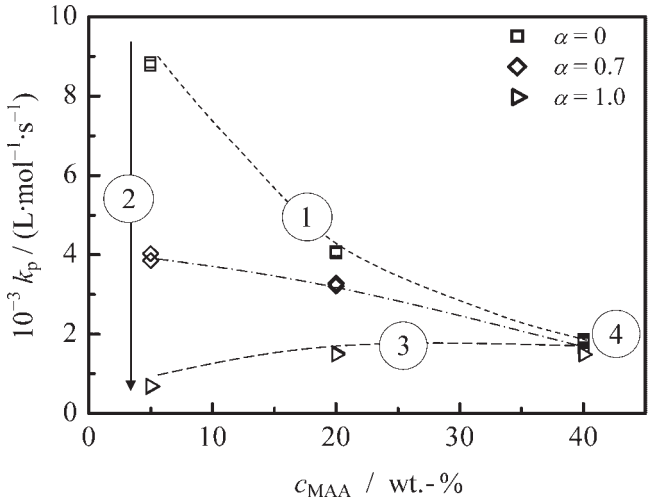


***Figure 3.***
Dependence of the free-radical propagation rate coefficient, $k_p$, of methacrylic acid polymerization in aqueous solution on monomer concentration, $c_{MAA}$, between 5 and 40 wt.-%. Data are presented for three degrees of monomer dissociation, $\alpha = 0$, 0.7, and 1. The polymerization temperature was 40 °C. The numbers 1, 2, 3 and 4 in the figure are referred to in the text.

of aqueous-phase $k_p$ as a function of both $\alpha$ and $c_{MAA}$ monomer concentration, this latter observation appears to be particularly noteworthy. It says that introducing negative charges on the monomer and on the growing radicals does not lower $k_p$ due to increasing repulsive interactions, what one would intuitively assume.

Attempts to quantitatively determine the extent of ionic dissociation of all relevant species including macroradicals and polymer molecules and to correlate such speciation with the variations observed for $k_p$ is difficult, if not impossible, in view of the complex acid-base properties and polyelectrolyte behavior as well as the coupled electrochemical equilibria.[21] Studies into polyelectrolyte behavior in aqueous solution carried out so far,[1,29] have been performed at conditions precisely defined with respect to solvent composition, ionic strength, concentration regime, and molecular weight. These conditions differ from the ones met in the actual free-radical polymerization experiments presented in Figure 3 and in Reference [21]. Despite this complexity, it has been realized[21] that with all the aqueous solutions of partially and fully ionized MAA under investigation the concentration of ionized monomer providing the ionic strength is above 0.1 mol · L$^{-1}$. According to the existing knowledge about polyelectrolytes in aqueous solution, such an ionic strength is sufficient to effectively screen ionic interactions.[30] As a consequence, repulsive interactions should not result in a distinct decrease of $k_p$ toward higher degrees of ionization. This conclusion is supported by the experimental observation that an increase of ionic strength, by adding sodium chloride to an aqueous solution of 5 wt.-% MAA, does not affect the $k_p$.[21]

Rather than trying to assign the measured changes in $k_p$ to the complex polyelectrolyte behavior and in particular to repulsive interactions, it seems recommendable to follow the line of arguments presented in the section on $k_p$ of non-ionized MAA. In the preceding section, variations by one order of magnitude of $k_p$ have been assigned to different extents of attractive intermolecular interactions between the TS structure for propagation and

 

the molecular environment. These changes essentially affect the pre-exponential factor, whereas the activation energy within the limits of experimental accuracy remains constant. It appears reasonable to assign the variations induced by ionizing MAA, which at low $c_{MAA}$ also extend over one order of magnitude, to the same genuine kinetic effect. This strategy is supported by the fact that, at least up to $\alpha = 0.7$, the activation energy, $E_A(k_p)$, is not significantly changed by the degree of MAA ionic dissociation and stays close to the value obtained for non-ionized MAA.[21]

Within the framework of the kinetic analysis applied to non-ionized MAA, which assigns the change in $k_p$ essentially to an effect on the pre-exponential, $A(k_p)$, the significant drop in $k_p$ upon increasing $\alpha$ at 5 wt.-% MAA (see Figure 3), is attributed to an increased friction to internal rotation of the relevant degrees of rotation in the TS structure for MAA due to attractive interactions of the anionic carboxyl groups with the counter-ions in the molecular environment. Toward increasing $c_{MAA}$, this effect becomes less pronounced because of increasing ionic strength (at identical $\alpha$). The slight increase with MAA concentration of $k_p$ for $\alpha = 1$ (along line 3 in Figure 3) may be understood as resulting from an increased flexibility of polymer chains upon increasing the ionic strength in passing from 5 to 40 wt.-%, which reduces friction of internal rotational motion. The interesting situation met at 40 wt.-% MAA, where $k_p$ is more or less independent of the degree of ionization (point 4 in Figure 3) suggests that, with reference to propagation of non-ionized MAA in dilute aqueous solution, an aqueous-phase environment containing 40 wt.-% fully ionized MAA has the same effect on the (ionized) TS structure for propagation as has an environment of 40 wt.-% non-ionized MAA on the associated non-ionized TS structure.

Because of solubility restrictions, PLP-SEC experiments on aqueous solutions of MAA at concentrations above 40 wt.-% and $\alpha$ approaching unity were not successful so far. Within further experiments attempts will be made to extend the $c_{MAA}$ – $\alpha$ range for PLP-SEC experiments. Of particular interest are polymerization conditions under which an increase of ionic dissociation of MAA, at constant overall $c_{MAA}$, may enhance $k_p$. Such kind of investigations should help to provide a general understanding of the $k_p$ behavior of water-soluble monomers in aqueous solution.

## Conclusions

PLP-SEC studies into the propagation rate coefficient of MAA in aqueous solution at 40 °C reveal that starting from a dilute solution of non-ionized MAA ($\alpha = 0$) both an increase of MAA concentration up to MAA bulk polymerization, at $\alpha = 0$, as well as an increase of the degree of ionic dissociation up to $\alpha = 1$, at 5 wt.-% MAA, result in a significant drop of $k_p$, by about one order of magnitude. Under conditions of full ionization of MAA, $\alpha = 1$, $k_p$ slightly increases upon enhancing MAA concentration. At an MAA concentration of 40 wt.-%, within experimental accuracy, $k_p$ is insensitive toward the degree of ionic dissociation of MAA. The experimental findings on the influence of $c_{MAA}$ and $\alpha$ on $k_p$ of MAA may be consistently interpreted within the framework of transition state theory. The effects are primarily assigned to interactions of the transition state structure for propagation with the molecular environment. Ionic interactions as well as hydrogen-bonded interactions significantly affect the pre-exponential factor, $A(k_p)$, whereas the activation energy, $E_A(k_p)$, remains almost constant. The availability of reliable $k_p$ values for MAA in aqueous solution at widely differing concentrations and degrees of ionization allows for estimating additional rate coefficients from coupled kinetic parameters (such as termination and transfer coefficients), for describing and optimizing polymerization kinetics, and for predicting polymer properties. Studies into the free-radical polymerization of other water-soluble monomers,

 

which are currently underway, will reveal whether and to which extent the variations of $k_p$ measured for MAA generally apply for free-radical polymerization of water-soluble monomers in aqueous solution.

*Acknowledgements:* The authors wish to acknowledge financial support by the *Deutsche Forschungsgemeinschaft* within the framework of the European Graduate School "Microstructural Control in Radical Polymerization", a fellowship (to P.H.) from the *Fonds der Chemischen Industrie*, support from BASF AG and from the Slovak Research and Development Support Agency under the contract No. APVV-51-037905.

[1] "*Handbook of polyelectrolytes and their applications*", S. K. Tripathy, J. Kumar, H. S. Nalva. (Eds.), American Scientific Publishers, Stevenson Ranch, California, 2002.
[2] S. Beuermann, M. Buback, *Prog. Polym. Sci.* **2002**, *27*, 191.
[3] A. Katchalsky, G. Blauer, *Faraday Soc. Trans.* **1951**, *47*, 1360.
[4] V. F. Gromov, N. I. Galperina, T. O. Osmanov, P. M. Khomikovskij, A. D. Abkin, *Eur. Polym. J.* **1980**, *16*, 529.
[5] V. F. Gromov, E. V. Bune, E. N. Teleshov, *Russ. Chem. Rev.* **1994**, *63*, 507.
[6] M. Buback, R. G. Gilbert, G. T. Russell, D. J. T. Hill, G. Moad, K. F. O'Driscoll, J. Shen, M. A. Winnik, *J. Polym. Sci., Polym. Chem. Ed.* **30**, 851 (1992).
[7] K. S. Anseth, R. A. Scott, N. A. Peppas, *Macromolecules* **1996**, *29*, 8308.
[8] N. I. Galperina, T. A. Gugunava, V. F. Gromov, P. M. Khomikovskij, A. D. Abkin, *Vysokomol. Soed.* **1975**, *A17*, 1455.
[9] "*Polymer Handbook*", J. Brandrup, E. H. Immergut, E. A. Grulke, Eds., 4th edition, John Wiley & Sons, Inc. New York, 1999.
[10] F.-D. Kuchta, A. M. van Herk, A. L. German, *Macromolecules* **2000**, *33*, 3641.
[11] M. Buback, R. G. Gilbert, R. A. Hutchinson, B. Klumperman, F.-D. Kuchta, B. G. Manders, K. F. O'Driscoll, G. T. Russell, J. Schweer, *Macromol. Chem. Phys.* **1995**, *196*, 3267.
[12] I. Lacík, S. Beuermann, M. Buback, *Macromolecules* **2001**, *34*, 6224.
[13] I. Lacík, S. Beuermann, M. Buback, *Macromolecules* **2003**, *36*, 9355.
[14] I. Lacík, S. Beuermann, M. Buback, *Macromol. Chem. Phys.* **2004**, *205*, 1080.
[15] S. Beuermann, M. Buback, P. Hesse, I. Lacík, *Macromolecules* **2006**, *39*, 184.
[16] S. Beuermann, M. Buback, P. Hesse, F.-D. Kuchta, I. Lacík, A. M. van Herk, *Pure Appl. Chem.* **2006**, accepted
[17] F. Ganachaud, R. Balic, M. J. Monteiro, R. G. Gilbert, *Macromolecules* **2000**, *33*, 8589.
[18] S. A. Seabrook, M. P. Tonge, R. G. Gilbert, *J. Polym. Sci. Part A: Polym. Chem.* **2005**, *43*, 1357.
[19] R. X. E. Willemse, A. M. van Herk, E. Panchenko, T. Junkers, M. Buback, *Macromolecules* **2005**, *38*, 5098.
[20] J. M. Asua, S. Beuermann, M. Buback, P. Castignolles, B. Charleaux, R. G. Gilbert, R. A. Hutchinson, J. R. Leiza, A. N. Nikitin, J.-P. Vairon, A. M. van Herk, *Macromol. Chem. Phys.* **2004**, *205*, 2151.
[21] S. Beuermann, M. Buback, P. Hesse, S. Kukuckova, I. Lacík, in preparation
[22] J. P. A. Heuts, R. G. Gilbert, L. Radom, *Macromolecules* **1995**, *28*, 8771.
[23] J. P. A. Heuts, Theory of radical reactions, In: "*Handbook of radical polymerization*", K. Matyjaszewski, T. P. Davis (Eds.), John Wiley & Sons, New York 2002, p. 1–76.
[24] S. Beuermann, M. Buback, T. P. Davis, R. G. Gilbert, R. A. Hutchinson, O. F. Olaj, G. T. Russell, J. Schweer, A. M. van Herk. *Macromol. Chem. Phys.* **1997**, *198*, 1545.
[25] B. Manders, TU Eindhoven, PhD thesis **1997**.
[26] S. C. Thickett, R. G. Gilbert, *Polymer* **2004**, *45*, 6993.
[27] S. Beuermann, M. Buback, P. Hesse, S. Kukuckova, I. Lacík, *Macromol. Symp.* this issue.
[28] V. A. Kabanov, *J. Polym. Sci. Symp.* **1973**, *42*, 173.
[29] H. Dautzenberg, W. Jaeger, J. Kötz, B. Philipp, C. Seidel, D. Stscherbina, "*Polyelectrolytes: Formation, Characterization and Application*", Hauser Publishers, Munich, Vienna, New York, 1994.
[30] M. Sedlák, Polyelectrolytes in solution, In: "*Light scattering: Principles and development*", W. Brown, Ed. Clarendon Press, Oxford, 1996, Chapter 4, 120–163.

 

# Investigation of the Chain Length Dependence of $k_p$: New Results Obtained with Homogeneous and Heterogeneous Polymerization

*Irene Schnöll-Bitai,*[*1] *Christoph Mader*[2]

**Summary:** New experimental results were collected for the free radical polymerization of styrene by pulsed laser polymerization in solution or in microemulsion. The location of the point of inflection (on the low molecular weight side) and the maximum of the first peak in the chromatograms (measured by size-exclusion chromatography) was used to extract $k_p$ data. The extent of band broadening was determined with narrow polystyrene standards with an assumed Poisson chain length distribution. For a given experiment both $k_p$ values (obtained via the point of inflection and the maximum) were corrected and thus became identical in most cases. Even after the correction, the effect of chain length dependence persists to a higher chain length.

**Keywords:** gel permeation chromatography; kinetics (polym.); polystyrene; radical polymerization

## Introduction

About six years ago Olaj et al.[1] presented their result that chain propagation in radical polymerization is a chain length dependent (CLD) process. This they deduced from the observation that the rate coefficient determined by the PLP-SEC method (pulsed laser polymerization and subsequent analyses of the chromatograms measured by size-exclusion chromatography) decreased with increasing chain length. Shortly afterwards van Herk and co-worker[2] also presented experimental evidence of this phenomenon. They also included results deduced from chain length distributions measured by matrix assisted laser desorption ionization time of flight mass spectrometry (MALDI-ToF). In the latter case they chose the location of the peak maximum as being the proper quantity to yield $k_p$ from the respective chain length $L$ according to[3]

$$k_p = \frac{L}{[M]t_0} \quad (1)$$

$[M]$ signifies the monomer concentration and $t_0$ the time interval between two subsequent laser pulses. When the results for the polymerization of methyl methacrylate at 25 °C were compared it became obvious that the $k_p$ values deduced via the points of inflection showed almost the same general trend whereas the function describing the CLD seemed to be completely different when deduced from the location of the peak maxima from the MALDI-ToF spectra. As a consequence it was concluded by these authors that the observed discrepancies with respect to the considerable chain length dependence at higher chain lengths is a result of the influence of band broadening (BB) on the location of the points of inflection.

[1] Institute of physical chemistry, University of Vienna, Währinger Straße 42, A-1090 Vienna, Austria
Fax: (+43) 01 4277 9524
E-mail: Irene.Schnoell-Bitai@univie.ac.at
[2] Isovolta AG, Industriezentrum NÖ Süd, Straße 3, A-2355 Wiener Neudorf, Austria

Still, it is not clear whether such a comparison is legitimate because of the following reasons:

a) As a justification for the use of the peak maximum instead of the point of inflection it was claimed that all experiments were carried out in the high termination rate limit.[4] Under such conditions it was shown that the peak maximum yielded the more accurate $k_p$ value. Therefore, this should not only be true for the MALDI-ToF spectra but also for the molecular weight distributions (MWD) determined by SEC.
b) For a comparison the data derived from the points of inflection from the MALDI-ToF spectra and those derived from the maxima from the SEC chromatograms are missing. Such a comparison would have revealed in a more direct way how strong the differences were due to the influence of BB on the location of the inflection point. Although it could, in principle, be speculated whether MALDI measurements are biased by some kind of experimental difficulty it is far more vital to know whether the results obtained with SEC will display a systematic adulteration due to the phenomenon of BB as this is the standard method for the measurement of MWDs. Besides this, it is necessary to be able to determine the extent of BB and furthermore to know how to correct for the deterioriating influence of BB – at least pointwise.

## Phenomenon of BB in SEC

Whenever a uniform sample is measured by SEC a continuous spectrum instead the ideally single line is detected. For such samples it is obvious that BB leads to a broadening of the signal. Synthesis of polymers does not lead to uniform samples but will display a certain chain length or molecular weight distribution in most cases. The narrowest distribution that can be achieved by synthesis alone is a Poisson distribution. Simulations of the effect of BB on the distribution by applying the so called Tung equation[5] revealed that these narrow peaks are also broadened under the influence of BB.

## Determination of BB in SEC

Although the extent of BB could be determined with a variety of methods, a newly developed approach based on the use of samples with Poisson distribution[6,7] was employed. Poisson (number chain length) distributions are characterized by one quantity, namely the location of the peak maximum, $L_{max}$, which is easily accessible from experiment. Furthermore, it was shown by Chang and coworker[8] that anionically prepared polystyrenes approach Poisson distributions.

The peak width is acquired from chromatograms via the location of the points of inflection ($V_{low}$, $V_{high}$). Due to the logarithmic dependence of the molecular weight $M$ on the retention volume $V$ ($\log M = a\text{-}bV$, $a,b$ constants) the difference $V_{low}$-$V_{high}$ transforms to the ratio of the two corresponding chain lengths according to

$$\begin{aligned} 2\sigma_{SEC} &= V_{low} - V_{high} \\ &= \frac{1}{b}\{\log M_{high} - \log M_{low}\} \\ &= \frac{1}{b}\log\frac{L_{high}}{L_{low}} \end{aligned} \tag{2}$$

When BB can be described by a Gaussian (or exponentially modified Gaussian) function characterized by the variance $\sigma_{BB}$ (and the exponential decay term $\tau_{BB}$) then the rearrangement of the experimental peak width ($\sigma^2_{SEC} = \sigma^2_{BB} + 0.5 \cdot \tau^2_{BB} + \sigma^2_{Poisson}$)[9] leads to a simple algebraic equation with which the extent of BB can be calculated.

$$\begin{aligned} &\sigma^2_{BB} + 0.5 \cdot \tau^2_{BB} \\ &\quad = \sigma^2_{SEC} - \frac{1}{4b^2}\log^2\frac{L_{max} + L_{max}^{1/2}}{L_{max} - L_{max}^{1/2}} \end{aligned} \tag{3}$$

The second term on the r.h.s. of Equation (3) represents the theoretical peak width of a Poisson distribution.[10]

 

If we recall the necessary ''ingredients'' that lead to Poisson distributions, the following prerequisites must be mastered experimentally: First, all propagating chains must be generated at the same instant. Second, any type of chain termination process must be absent during propagation. Third, all active chains must be deactivated at the same time. Besides ideal anionic polymerization there exist several other possibilities to accomplish these conditions. Pulsed laser polymerization in microemulsion can be regarded to fulffill these necessities too, due to the following reasons. The propagating chains are generated during an extremely short laser pulse. The validity of the zero-one condition ensures that the radicals are separated from each other thus inhibiting chain termination events in between two laser pulses. With the arrival of the subsequent laser pulse a certain percentage of the present polymer radicals are terminated within an extremely short period. This means that the accumulated chain length distribution is composed of several Poisson peaks which locations are governed by $k_p[M]t_0$. Overlays of molecular weight distributions[11] of polystyrenes prepared this way and commercially available polystyrene standards revealed an excellent agreement for individual peaks thus demonstrating that both synthetic routes lead to almost identical narrow distributions. Lee and coworker[8] demonstrated that anionically prepared polystyrenes with a peak maximum located between $2 \cdot 10^4$ and $10^6$ gmol$^{-1}$ can be described by Poisson distributions.

## Determined Extent of BB

The investigation of BB carried out with commercially available polystyrene standards as well as polystyrene samples prepared by pulsed laser polymerization in microecmulsion revealed that the extent of BB is not constant over the entire separation range.[11] The function decreases continually from the maximum value at low retention volume. Such a behaviour was already found as early as 1987[12] and later.[13,14] Different column combinations were tested and all results could be described by a somewhat more elaborate van Deemter equation[15]

$$\sigma^2_{BB} = \lambda \frac{2d_p}{l} V^2 + \gamma \frac{2D_m}{l} \frac{1}{u} V^2 + q \frac{V_0}{l} \times \frac{d_p^2}{D_s} u(V - V_0) \quad (4)$$

$d_p$ signifies the particle diameter of the separating material, $l$ is the length of the columns, $D_m$ and $D_s$ are the respective diffusion coefficients of the dissolved polymer in the mobile (m) and the stationary (s) phase. $V_0$ correspond to the interstitial volume, $u$ is the linear flow velocity and $q$ is equal to 1/30[16]. The diffusion coefficient for polystyrene in THF at 25 °C ($D_m = KM^\alpha$) can be found in literature.[13] $\lambda$ is a parameter describing the quality of column packing and lies usually in the range of 1 to 10. All experimental result could be described with $\lambda = 1$ and $\gamma = 1$. The diffusion coefficient of the solute in the stationary phase is not known and the ratio of $D_m$ over $D_s$ is sometimes described by an exponential function[17] of the form $D_m/D_s = \exp\{-\beta(R_s/R_{1/2}\}$ depending on the aspect ratio of the Stokes radius $R_s$ over the average pore size $R_{1/2}$. Columns with different pore sizes were combined, but no information exists how to incorporate the influence of different pore sizes. Therefore, the ratio of diffusion coefficients was treated as being constant as an approximation.

## Influence of BB on the Location of the Points of Inflection

BB will always increase the peak width of narrow peaks and therefore it is important to know how strong the location of the points of inflection is shifted due to the influence of BB. Although the extent of BB varied by at least 100% for different column combinations only moderate differences were found with respect to the shift in the location of the points of inflection. The deviations ranged from 2 to 20% when the

 

points of inflection relative to the ideal values for Poisson distributions ($L_{max} - L_{max}^{1/2}$) were compared for different column combinations.[18]

In order to understand these results it is necessary to recall that the actual quantity describing the deteriorating effect of BB is not the variance alone but rather the product of the variance and the square of the slope of the calibration curve.[13,19] This dimensionless efficiency parameter is at least one order of magnitude smaller than the variance and the considerable differences reduced to moderate ones. A correction factor *cf* can be constructed to describe the shift[7] of the points of inflection due to BB

$$\log(cf) = \log\frac{L_{corr}}{L_{exp}} = b \cdot \text{shift} = b(\sigma_{SEC} - \sqrt{\sigma_{SEC}^2 - (\sigma_{BB}^2 + 0.5 \cdot \tau_{BB})}) \quad (5)$$

In order to obtain the true location of the point of inflection on the low molecular weight side the experimental one must be multiplied with this correction factor whereas that at the high molecular weight side must be divided accordingly. The correction factor is highest for uniform samples and Poisson distributions with very high $L_{max}$ values. For a Poisson distribution with $L_{max} = 100$ the correction factor is smaller and for distributions centred around still lower values the necessary corrections become even smaller. Thus, evidence is given of the already observed phenomenon that in the case of broad distributions almost no shift in the location of the points of inflection can be observed.

### Correction Procedure for More Accurate $k_p$ Values

With respect to molecular weight distributions obtained when polymers are prepared with pulsed laser polymerization the situation is somewhat more complicated. From

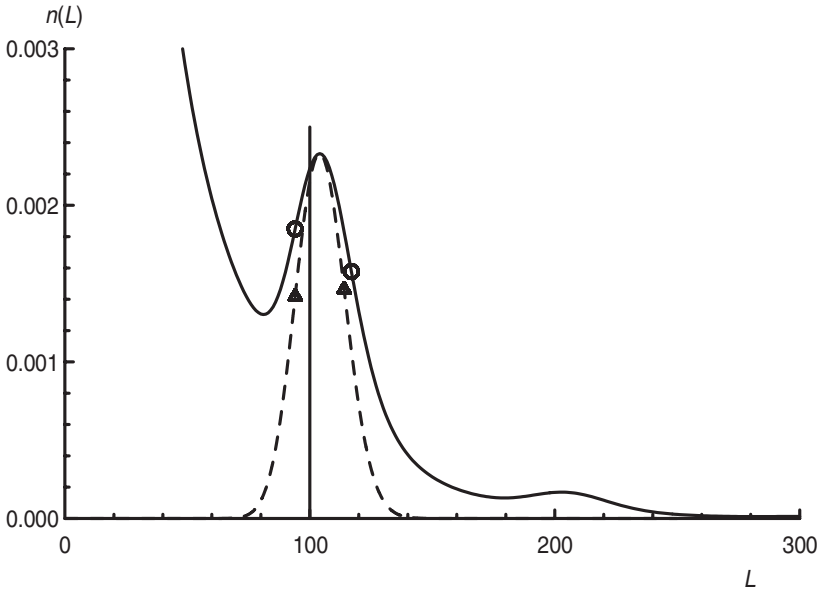


***Figure 1.***
Number chain length distribution, *n(L)*, calculated for homogeneous pulsed laser polymerization and $L_o = 100$. An ideal Poisson distribution centred at the same $L_{max}$ value is included and the positions of the points of inflection are presented by circles and triangles.

 

simulations it can be seen[20] that neither the point of inflection nor the maximum is the ideal value to yield $k_p$ via equation 1 (c.f. Figure 1). Furthermore, the simulations revealed that the peak width is broader than the peak width of an ideal Poisson distribution in most cases[20,21] and that this ''kinetic'' peak width is gouverned by the experimental conditions. Only in the limit of the high termination rate range[4] will the width of the distribution be close to that of a Poisson distribution. The peak width of narrow peaks increases under the influence of BB (not shown in the diagram). Therefore an auxiliary function $X$ is defined as the difference between the experimental peak width and the theoretical one (the peak width of a Poisson distribution broadened by BB):

$$X = \log^2 \frac{L_{high}}{L_{low}} - \log^2 \left( \frac{L_{high}}{L_{low}} \right)_{theory} = \log^2 \frac{L_{high}}{L_{low}} - \log^2 \left( \frac{L_{high}}{L_{low}} \right)_{Poisson} - 4\sigma_{BB}^2 \quad (6)$$

From several number chain length distributions simulated for pulsed laser polymerization for a great variety of experimental parameters[21] which were converted to chromatographic dimensions and subsequently submitted to the influence of BB by applying the Tung equation[5] correction functions were deduced. The comparison of the input values for the point of inflection and the maximum lead to the following correction functions:

$$f_X^{LPI} = \frac{L_0}{L_{LPI}} = (I_I + S_I\sigma^2) - (I_S + S_S\sigma^2)X \quad (7a)$$

$$f_X^{MAX} = \frac{L_0}{L_{MAX}} = (I_I + S_I\sigma^2) - (I_S + S_S\sigma^2)X \quad (7b)$$

where $I$ and $S$ signify the respective intercepts and slopes. It was already demonstrated that without a correction the under estimation of $k_p$ (when deduced from the point of inflection) can be as high as 15% whereas the maximum can lead to an over estimation of almost 40%. Whenever these corrections are applied the true $L_0$ value should be obtained by both approaches with a higher accuracy. Thus, the question of whether the maximum or the point of inflection is the better means to obtain correct $k_p$ values is of no importance as the correction should lead to identical values when carried out properly. The extent of BB is an essential quantity and must be known or determined beforehand in order to be able to apply this correction.

## Experimental Part

### Pulsed Laser Polymerization in Microemulsion

Polymerization was either carried out in solution (50 wt.-% toluene and styrene, each) or in microemulstion. In the latter case the polymerization mixture was prepared according to the recipe of Gan and coworker.[22] The oil phase consisted again of 50 wt.-% toluene and styrene, each. For all experiments 2,2′-azoisobutyronitrile (AIBN) was used as a photoinitiator at a concentration of $5 \cdot 10^{-3}$ moll$^{-1}$ for the polymerization in solution and $44 \cdot 10^{-3}$ moll$^{-1}$ with respect to the oil phase. The polymerization mixture was purged with Argon (15 min) prior to polymerization. For the intermittant illumination a Nd:Yag laser (Quanta Ray GCR-130-20) was used at different pulse frequencies. All polymerizations were carried out at $T = 25\,^{\circ}C$ to low conversions only (in order to avoid phase separation). Immediately after irradiation all radicals were deactivated by injecting a solution of 2,2,6,6-tetramethylpiperidine-N-oxyl (TEMPO) in toluene. The polymers were precipitated in pure methanol and filtered. Detergent was removed by carefully washing with water and methanol several times.

### Size-exclusion Chromatography

A combination of four SDV columns ($10^6$, $10^5$, $10^4$, $10^3$; 8 mm × 300 mm, particle

 

diameter = 10 μ) from Polymer Standard Service (PSS) were used. THF was the solvent for the polymer and the eluent at a flow rate of 1 ml $min^{-1}$. A differential refractive index detector (Waters 2412) was employed. With the aid of narrow polystyrene standards from PSS and scientific products a third order polynomial calibration curve was constructed. The molar mass distributions were exported and numerical differentiation was carried out with a home made software[23] in order to determine the location of the points of inflection and the peak maximum. From the analysis of the polymer standards the extent of BB was determined following the procedure outlined in the preceding paragraph.

## Results and Discussion

With respect to the polymerization in microemulsion there is the question about the actual monomer concentration which seems to be smaller than the nominal one.[22] For a comparison of the $k_p$ values obtained from homogeneous and heterogeneous polymerization it would be necessary to know this quantity with certainty. As this is not the case comparison of the natural logarithm of $k_p[M]$ values for the two different systems is shown in Figure 2 as the concentration will only contribute additively in this case and the results are shifted along the ordinate. Thus the chain length dependence of the $k_p$ values can not only be compared directly for the two polymerization systems but can also be compared with the data published by Willemse et al.[2]

The filled diamonds (triangles) represent the results for the polymerization in microemulsion (solution) as deduced from the location of the point of inflection on the low molecular weight side; the full squares (inverted triangles) represent the data obtained from the peak maximum. All four data sets show the same general trend of a chain length dependence persisting to higher chain lengths as was already shown by Olaj et al.[1,24]

In order to make sure that BB can be excluded as a possible source for discre-

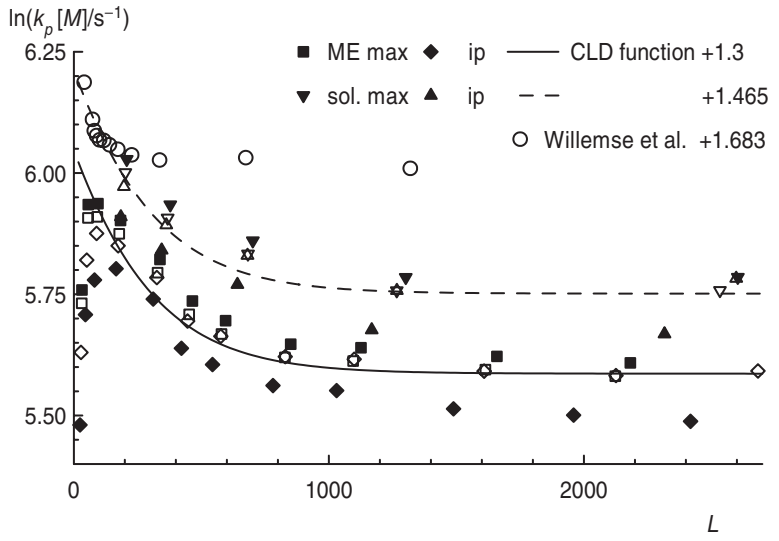


***Figure 2.***
Comparison of uncorrected $k_p$ values (full symbols) for the polymerization a) in microemulsion: diamonds (inflection points, ip) and squares (maximum, max) and b) in solution: triangles (ip) and inverted triangles (max). The corresponding open symbols represent the results after application of the correction (Equations (7a) and (7b)). The CLD function calculated according to Equation (8) is included as full and broken curve, respectively, which are only shifted by the constant value as indicated.

 

pancies the correction procedure presented above was applied to the data sets. The investigated peak widths (determined via the points of inflection) were very close or identical to those of the corresponding Poisson distributions broadened by BB. Therefore, the auxiliary function was zero and the second term in the Equations (7a) and (7b) did not contribute to the correction; the values for the slope $S$ and the intercept $I$ were taken from literature.[20] The corrected values are depicted as open quadrangles (triangles) in Figure 2. The correction lead to identical values deduced from the maximum and the points of inflection and did not change the type of the CLD. The corrected data can be described by the exponential model

$$\ln k_p(L) = \ln kLk_p - \ln\left\{\ln\left[1+\frac{k_p(\infty)}{k_p(0)}(e^{kL}-1)\right]\right\} \quad (8)$$

with the coefficients as given in reference [21]. In all, the results from heterogeneous (full curve) and homogeneous (broken curve) polymerization can be described by one function which is merely shifted along the ordinate as indicated in the diagram.

For comparison the data deduced from the peak maxima of MALDI spectra[2] (open circles) were converted to 25 °C by applying the Arrhenius equation (parameters from ref.[2]]) and were shifted by a constant value so that the high frequency values lay on the broken curve. Thus, a completely different CLD behaviour becomes obvious as the effect levels off at a chain length of approximately 300 where it converges towards a constant value. When the data obtained via MALDI is compared with that deduced by the same group from SEC measurements[2] a similar CLD behaviour becomes obvious which clearly does not support the idea that BB can be made responsible for the observed differences.

Agreement with the Willemse data[2] is only given at higher frequencies whereas the decrease in the $k_p$ values at lower frequences was less pronounced. The maximum difference corresponds to about 0.3 on the logarithmic scale which means that the peak maxima are about 40% higher in comparison.[21] This is of a comparable dimension as the error introduced by (wrongly) using the location of the peak maximum in the low termination rate limit.[25] This leads to the question whether polymerization was really carried out in the high termination rate limit in all cases as was claimed by the authors. Usually, laser intensities decrease dramatically with increasing pulse separation times what would lead to the generation of lower concentrations of initiating radicals. Unfortunately, information about laser intensities are missing in most publications and one is thus left to decide what limit applies without an impartial criterion.

## Conclusion

Homogeneous and heterogeneous pulsed laser polymerization of styrene was carried out at 25 °C. For the extraction of the $k_p$ values as a function of the chain length from measured SEC curves it was necessary to determine the extent of BB. The analyses of narrow Poisson-like polystyrene standards revealed a non constant extent of BB over the complete separation range which could be described by a somewhat more elaborate van Deemter equation.[11,13,14] The shift of the points of inflection and as a consequence the introduced error correlates directly to the extent of BB.[18]

The application of the correction procedure[21] lead to identical results when both options (point of inflection and maximum) were used. The type of the chain length dependence deduced from polymers prepared by homogeneous and heterogeneous polymerization was the same which is demonstrated in Figure 2 as they simply differ by a constant term. The persistence of the chain length dependence to higher degrees of polymerization is not in agreement with the results from

 

Willemse et al.[2] and deviates also from theoretical expectations.[26] This leads to the ultimate questions: a) What is the reason for the differences of the deduced $k_p$ values? b) Can we influence the experimental parameters in such a way to switch from one experimental result to the other? And c) Are there only two distinct possibilities – like switching from one state to the other – or is it possible to change continuously from one type of functionality to the other?

The collection of data and critical evaluation of possible influences of parameters on the CLD (as was carried out by Heuts et al.[26]) might help to elucidate the current question of the true nature of chain length dependence of the rate constant of propagation in free radical polymerization. Therefore, the investigation of the polymerization behaviour of monomers other than styrene and methyl methacrylate is necessary[27] and the use of the correction procedures[20,21] should eliminate the error introduced by the effect of BB. Thus, comparison of data obtained from either different research groups and/or with the aid of different techniques[2,28] (MALDI, SEC) should be better feasible.

[1] O. F. Olaj, P. Vana, M. Zoder, A. Kornherr, G. Zifferer, *Macromolecular Rapid Commun.* **2000**, *21*(*13*), 913; O. F. Olaj, P. Vana, M. Zoder, A. Kornherr, G. Zifferer, *Macromolecules* **2002**, *35*, 1214.
[2] R. X. E. Willemse, B. B. P. Staal, A. M. van Herk, S. C. J. Pierik, B. Klumperman, *Macromolecules* **2003**, *36*, 9797.
[3] O. F. Olaj, F. Hinkelmann, I. Bitai, *Makromol. Chem.* **1987**, *188*, 1689.
[4] J. Sarnecki, J. Schweer, *Macromolecules* **1995**, *28*, 4080.
[5] L. H. Tung, *J. Appl. Polym. Sci.* **1966**, *10*, 1271.
[6] I. Schnöll-Bitai, *Chromatographia* **2003**, *58*, 375.
[7] I. Schnöll-Bitai, *Macromol. Symp.* **2004**, *217*, 357.
[8] W. Lee, H. Lee, J. Cha, T. Chang, K. J. Hanley, T. P. Lodge, *Macromolecules* **2000**, *33*, 5111.
[9] J. R. Vega, I. Schnöll-Bitai, *J. Chromatogr. A* **2005**, *1095*, 102.
[10] I. Schnöll-Bitai, *Macromol. Chem. Phys.* **2002**, *11*, 770.
[11] C. Mader, I. Schnöll-Bitai, *Macromol. Chem. Phys.* **2005**, *206*, 649.
[12] R.-S. Cheng, Z.-L. Wang, Y. Zhao, *ACS Symp. Ser.* **1987**, *352*, 281.
[13] J.-P. Busnel, F. Foucault, L. Denis, W. Lee, T. Chang, *J. Chromatogr. A* **2001**, *930*, 61.
[14] N. Aust, M. Parth, K. Lederer, *Int. J. Polym. Anal. Char.* **2001**, *6*, 245.
[15] O. Chiantore, M. Guita, *J. Liquid Chromatogr.* **1982**, *5*, 643.
[16] J.-C. Giddings, Dynamics of Chromatography, Marcel Dekker, New York **1965**.
[17] M. Potschka, *J. Chromatogr.* **1993**, *648*, 41.
[18] I. Schnöll-Bitai, C. Mader, *J. Chromatogr. A* **2006**, *1137*, 198.
[19] A. E. Hamielec, W. H. Ray, *J. Appl. Polym. Sci.* **1969**, *13*, 1319.
[20] A. Kornherr, O. F. Olaj, I. Schnöll-Bitai, G. Zifferer, *Macromolecules* **2003**, *36*, 10021.
[21] A. Kornherr, O. F. Olaj, I. Schnöll-Bitai, G. Zifferer, *Macromol. Theory Simul.* **2004**, *13*, 560.
[22] L. M. Gan, C. H. Chew, I. L. Imae, *Polym. Bull (Berlin)* **1991**, *25*, 193.
[23] The diagrams were drawn with a plot software written by G. Zifferer (Inst. Phys. Chem., University of Vienna, Austria). The program offers several routines like numerical differentiation and smoothing. The smoothing routine is based on low-pass filtering of the data (by use of fast Fourier transformation) as described in W. M. Press, B. P. Flanery, S. A. Teukolsky, W. T. Vetterling, Numerical Recipes, Cambridge University Press **1987** (chapter 13.9.).
[24] O. F. Olaj, M. Zoder, P. Vana, A. Kornherr, I. Schnöll-Bitai, G. Zifferer, *Macromolecules* **2005**, *38*, 1944.
[25] M. Buback, M. Busch, R. Lämmel, *Macromol. Theory Simul.* **1996**, *5*, 845.
[26] J. P. A. Heuts, G. T. Russell, *European Polymer J.* **2006**, *42*(*1*), 3.
[27] P. Vana, L. H. Yee, T. P. Davis, *Macromolecules* **2002**, *35*(*8*), 3008.
[28] A. Kornherr, O. F. Olaj, I. Schnöll-Bitai, G. Zifferer, *Macromol. Theory Simul.* **2006**, *15*, 215.

 

# Propagation Rate Coefficient of Non-ionized Methacrylic Acid Radical Polymerization in Aqueous Solution. The Effect of Monomer Conversion

*Sabine Beuermann,*[1,2] *Michael Buback,*[*1] *Pascal Hesse,*[1] *Silvia Kukučková,*[1,3] *Igor Lacík*[3]

**Summary:** The propagation rate coefficient, $k_p$, of methacrylic acid (MAA) in aqueous solution is strongly dependent on monomer concentration.[1–3] Pulsed laser polymerization (PLP) at 25 °C and ambient pressure in conjunction with polymer analysis via size-exclusion-chromatography (SEC) was used to study whether $k_p$ also depends on monomer conversion. As the applicability of the PLP-SEC method is restricted to polymerization up to a few per cent of monomer conversion, situations of higher monomer-to-polymer conversion were achieved by adding to the MAA solution either (*i*) commercially available high-molecular-weight poly(MAA) or (*ii*) *iso*-butyric acid (IBA), which serves as a model component for an associated polymer with chain length unity. Within these experiments, the overall carboxylic acid concentration has been kept constant at 20 wt.-%. Under these conditions, $k_p$ of MAA turns out to be independent of the relative amounts of MAA and IBA, at least up to MAA:IBA ratios of 1:3, whereas $k_p$ increases by 60 per cent upon replacing half of the MAA content by poly(MAA), which situation corresponds to about 50 per cent monomer conversion in MAA polymerizations with initial MAA contents of 20 wt.-%. This $k_p$ value for 50 per cent conversion is close to the one obtained for PLP-SEC experiments at initial MAA concentrations of 10 wt.-%. The presence of poly(MAA) thus does not affect $k_p$, whereas the IBA content has a similar effect on $k_p$ as has MAA concentration. The behaviour is understood as a consequence of IBA becoming part of the solvent environment at the radical site within the macroradical coil, whereas addition of poly(MAA) does not affect this intra-coil environment. This finding bears important consequences for the modeling of MAA polymerizations carried out at different initial MAA concentrations and up to different degrees of monomer conversion.

**Keywords:** conversion dependence; laser-induced polymerization; methacrylic acid; propagation kinetics; water-soluble polymers

## Introduction

Free-radical polymerization in aqueous solution is of significant industrial importance. To model polymerization processes and product properties, reliable rate coefficients for the individual reaction steps are required. The propagation rate coefficient, $k_p$, may be precisely obtained by the PLP-SEC method, which combines pulsed-laser initiated polymerization with subsequent

[1] Institute of Physical Chemistry, Georg-August-University Göttingen, Tammannstrasse 6, D-37077 Göttingen, Germany
Fax: (+49) 551 393144
E-mail: mbuback@gwdg.de
[2] Present address: University of Potsdam, Institute of Chemistry, Polymer Chemistry, Karl-Liebknecht-Str. 24-25, D-14476 Golm, Germany
[3] Polymer Institute of the Slovak Academy of Sciences, Dúbravská cesta 9, 842 36 Bratislava, Slovakia

analysis of the produced polymer by size-exclusion chromatography.[4] So far, studies into radical polymerizations in aqueous solution resulted in $k_p$ values for non-ionized methacrylic acid (MAA)[1–3] and acrylic acid (AA),[1,5,6] as well as for acrylamide[7] and N-*iso*-propyl acrylamide,[8] but also for ionized AA[9], where the *p*H and hence the degree of ionization was controlled by the addition of sodium hydroxide. As a general trend, $k_p$ of non-ionized monomers dissolved in water was found to decrease toward higher monomer concentration. Association in the aqueous phase,[1] in particular dimerization,[7,8] and local monomer concentrations significantly differing from overall monomer concentration,[6] were proposed as being responsible for the observed behaviour. None of these arguments, however, could provide a satisfactory explanation. MAA polymerization allows for an extended testing of effects on $k_p$. Particular advantages of this system relate to the fact that PLP-SEC measurements in aqueous phase may be carried out over the full concentration range of non-ionized MAA, between 1 wt.-% MAA up to MAA bulk polymerization, and over a wide temperature range, from 20 to 80 °C.[2] Intermolecular interaction of the transition state structure for MAA propagation with the MAA-water solvent environment was shown to be responsible for the strong effects of MAA concentration on $k_p$, e.g., for the reduction in $k_p$ by about one order of magnitude in going from very dilute aqueous solution of non-ionized MAA to bulk MAA polymerization. In view of these large changes in $k_p$ with MAA concentration, the question arises whether and to which extent $k_p$ varies during polymerization to higher conversion, which is also associated with large changes in MAA concentration. PLP-SEC studies are restricted to the initial polymerization period up to a very few per cent conversion.[4] As propagation is considered to be chemically controlled, the low-conversion $k_p$ values from PLP-SEC, are assumed to stay constant up to high conversions and viscosities.[10] Via ESR, this assumption has already been proven for styrene[11] and methyl methacrylate[12,13] polymerization in non-polar solutions. Because of the large changes of $k_p$ in aqueous solution of non-ionized MAA, this assumption can not necessarily be adopted for MAA-water systems.

Our preceding kinetic studies into the aqueous-phase polymerization of AA with propionic acid[6] being present and also into the polymerization of 2-acrylamido-2-methylpropane sulfonic acid (AMPS) up to high degrees of monomer conversion[14] provided some indication that $k_p$ depends on the total concentration of carboxylic groups, which may be part of the monomer, the polymer, or a carboxylic acid co-solvent, rather than only on monomer concentration. The PLP-SEC-derived $k_p$ values for AA were lowered upon increasing the concentration of propionic acid[6] and $k_p$ for AMPS, as obtained from a combination of the single pulse (SP)-PLP technique with chemically initiated polymerization, appeared to be independent of monomer conversion.[14]

In order to deduce PLP-SEC-based information on the dependence of $k_p$ on monomer conversion, the present study addresses $k_p$ measurements for MAA in the presence of poly(MAA) and of *iso*-butyric acid (IBA). The latter component represents the saturated analogue of MAA and thus may be looked upon as the associated ''polymer of chain length unity''. The PLP-SEC experiments have been carried out at 25 °C and ambient pressure on aqueous MAA solutions to which different amounts of poly(MAA) or of IBA have been added. The mixtures were prepared such that the overall concentration of carboxylic acid, irrespective of the COOH groups being part of the monomer, the polymer, or the *iso*-butyric acid, is fixed at 20 wt.-%. Within each PLP-SEC experiment, only a small fraction of the MAA is polymerized, such as to obtain an amount of PLP-induced poly(MAA) which is sufficient for SEC analysis.

 

## Experimental Part

### Materials

Methacrylic acid (MAA) (Fluka, >98% stabilized with 0.025% hydrochinon monomethylether), the photoinitiator 2,2-dimethoxy-2-phenylacetophenone (DMPA, Aldrich, 99%), poly(methacrylic acid) (poly(MAA), Polysciences, lot# 547 827, 5% water) and *iso*-butyric acid (IBA, Fluka, p.a., >99.5%) were used as supplied. Demineralized water was used for preparing the reaction solutions.

### Preparation of Solutions

Solutions with added poly(MAA) were prepared by dissolving poly(MAA) in demineralized water overnight. No such extended pre-mix times were required for addition of IBA. The monomer MAA was added by using a stock solution of DMPA in MAA and pure MAA such as to adjust the DMPA concentration to 2 mmol $\cdot$ L$^{-1}$ for all polymerization reactions. Adding up to 10 wt.-% of poly(MAA) yields homogeneous solutions with viscosities being sufficiently low to allow for easy handling.

### PLP-SEC Conditions

Details of the PLP experiments on aqueous solutions of non-ionized MAA are reported in ref. [2]. The polymerizations were carried out in a in a QS 110 cell (Hellma-Worldwide) of 10 mm path length. The reaction solutions were purged with nitrogen for 4 min and thermostated for 20 min prior to PLP. For each mixture, at least two PLP experiments were performed. To reach monomer conversions up to 5%, between 25 and 300 pulses were applied. Monomer conversion was determined by weighing the polymer after freeze-drying. The polymer molecular weight distribution was determined via aqueous-phase SEC[2] using two injections for each sample.

### Selection of PLP Conditions

The molecular weight distribution (MWD) of the commercial poly(MAA) that was added to the initial solution in some of the PLP experiments is shown in Figure 1. Although the MWD is relatively broad ($M_n = 55\,000$ g $\cdot$ mol$^{-1}$, $M_w = 370\,000$ g $\cdot$ mol$^{-1}$, polydispersity index = 6.7), inflection points of PLP-produced samples may be clearly identified, if they occur at molecular weights below 30 000 g $\cdot$ mol$^{-1}$. According to ref. [2], the molecular weights for the primary inflection points, $M_1$, in aqueous-phase polymerizations at MAA contents of 20 wt.-% should be located at $\sim$20 000 g $\cdot$ mol$^{-1}$ for a pulse repetition rate of 40 Hz. Under such conditions even secondary points of inflection, $M_2$, may be observed. Also on the basis of the experience from ref.[2], the initial DMPA concentration was chosen to be $c_{DMPA} = 2$ mmol $\cdot$ L$^{-1}$. Within the MAA polymerizations in the presence of IBA, a laser pulse repetition rate of 20 Hz was used.

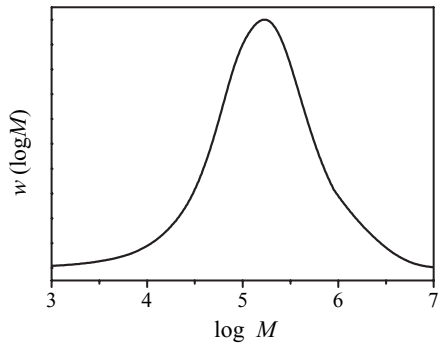


***Figure 1.***
Molecular weight distribution of the commercial poly(methacrylic acid) which was added to some of the aqueous solutions of non-ionized MAA prior to PLP.

## Results and Discussion

The aim of the present work was to study the dependence of the propagation rate coefficient, $k_p$, of MAA in aqueous solution on monomer conversion. As the powerful SEC-PLP method is restricted to experiments at low degrees of monomer conversion, situations occurring during polymerization were simulated by pre-mixing either poly(MAA) to the initial reaction mixture or by adding IBA, which may be considered

 

as a hypothetical ''poly(MAA)'' of chain length unity. Both components have been added such as to reach an overall carboxylic acid concentration of 20 wt.-%. The so-prepared solutions are subjected to pulsed laser polymerization such that MAA conversions of a very few per cents are reached. The $k_p$ values were calculated according to:

$$L_1 = k_p \cdot c_M \cdot t_0 \quad (1)$$

where $L_1$ is the degree of polymerization at the first point of inflection (POI) on the low molecular weight side of the polymer from PLP, $c_M$ is the MAA monomer concentration, and $t_0$ is the dark-time between two successive laser pulses, which is identical to the inverse of laser pulse repetition rate. The occurrence of at least one higher-order inflection point at about twice the chain length of the first point of inflection serves as a consistency criterion for reliable $k_p$ measurement.[15] Monomer concentrations were calculated from density data as detailed in ref.[2]. It was assumed that the densities of poly(MAA) and monomeric MAA are the same and that the temperature dependence of IBA density is identical to that of MAA. The error in $k_p$ estimates due to these assumptions is small as compared to the accuracy of PLP-SEC determinations, which is illustrated by the scatter of the $k_p$ data reported below.

### Aqueous-phase Polymerization of MAA in the Presence of IBA

Table 1 collates the experimental conditions and $k_p$ values obtained for MAA polymerization in aqueous phase with added IBA. The experiments have been carried out at 25 °C and ambient pressure using a laser pulse repetition rate of 20 Hz, an initiator concentration of $c_{DMPA} = 2\ mmol \cdot L^{-1}$ and a constant overall acid concentration of 20 wt.-%. The virtual conversion, $X_{virtual}$, has been estimated under the assumption that the added saturated acid, IBA, has been produced by preceding polymerization of MAA. The PLP-induced conversion, $X_{PLP}$ (in per cent), is always below 6%. To account for changes in MAA concentration during laser pulsing, the relevant monomer concentration in Table 1, $c_{MAA}$, is calculated as the arithmetic mean of MAA concentrations before and after PLP. The virtual conversion, $X_{virtual}$, is determined according to Eq. (2):

$$X_{virtual} = \left(1 - \frac{c_{MAA}}{c_{MAA} + c_{IBA}}\right) \cdot 100\% + \frac{X_{PLP}}{2} \quad (2)$$

The first two entries in Table 1 refer to polymerizations without pre-mixed IBA. The virtual conversion, $X_{virtual}$, thus is given by 50 per cent of the monomer conversion due to laser pulsing, $X_{PLP}$. The ratios of the peak positions of the first and second POI, and thus $M_1/M_2$ in Table 1, are mostly close to 0.5, indicating the reliability of $k_p$ determination. Only at the highest virtual conversion, of about 75%, the $M_1/M_2$ ratio differs by more than 20% from 0.5. Within part of these experiments at high IBA content, no second maximum in the first-derivative curve of the MWD is seen but only a shoulder. The first POI of the MWD is significantly reduced toward increasing $X_{virtual}$, that is toward lower MAA concentration. The $k_p$ values are however more or less independent of virtual conversion.

### Aqueous-phase Polymerization of MAA in the Presence of Poly(MAA)

Within the PLP-SEC experiments on non-ionized MAA in the presence of poly(MAA), the determination of points of inflection, via the maxima in the associated first-derivative curves of the MWD, is complicated by the pre-mixed polymer which obviously can not be removed prior to SEC analysis. Figures 2 and 3 depict MWDs (A) and the associated first-derivative curves (B) of polymer samples obtained by PLP-induced polymerizations of 15 wt.-% MAA dissolved in water containing 5 wt.% of pre-mixed polymer and of 10 wt.-% MAA dissolved in water containing 10 wt.-% of pre-mixed polymer, respectively. The full lines (a) represent the polymer sample after pulsed laser polymerization, whereas the dashed

 

***Table 1.***
Experimental details of pulsed-laser induced polymerizations of methacrylic acid (MAA) in aqueous solution with *iso*-butyric acid (IBA) being added. The IBA content is expressed by a virtual conversion, $X_{virtual}$, which considers the amount of IBA as being produced from MAA by polymerization. The overall concentration of MAA + IBA is 20 wt.-% in all these experiments. Pulsed-laser polymerizations were performed at 25 °C and ambient pressure using a photoinitiator (DMPA) concentration of $c_{DMPA} = 2$ mmol · L$^{-1}$ and a laser pulse repetition rate of 20 Hz. Listed in the columns are the virtual degree of monomer conversion, $X_{virtual}$, the MAA concentration, $c_{MAA}$, (see text), the number of applied laser pulses, the PLP-induced monomer conversion, $X_{PLP}$, the molecular weight at the first point of inflection (POI), $M_1$, the ratio of MWs at the first and second POIs, and the resulting propagation rate coefficient, $k_p$.

| $X_{virtual}$/% | $c_{MAA}$/mol · L$^{-1}$ | *number of laser pulses* | $X_{PLP}$/% | $M_1$/g · mol$^{-1}$ | $M_1/M_2$ | $k_p$/L · mol$^{-1}$ · s$^{-1}$ |
|---|---|---|---|---|---|---|
| 2.6 | 2.29 | 150 | 5.2 | 35 890 | 0.50 | 2 903 |
| 2.6 | 2.29 | 150 | 5.2 | 38 370 | 0.50 | 3 104 |
| 15.7 | 1.99 | 150 | 6.0 | 33 730 | 0.50 | 3 133 |
| 15.7 | 1.99 | 150 | 6.0 | 33 650 | 0.50 | 3 126 |
| 13.6 | 2.04 | 75 | 1.9 | 32 810 | 0.49 | 2 983 |
| 13.6 | 2.04 | 75 | 1.9 | 34 120 | 0.49 | 3 102 |
| 13.5 | 2.04 | 50 | 1.6 | 33 810 | 0.49 | 3 070 |
| 13.5 | 2.04 | 50 | 1.6 | 34 120 | 0.50 | 3 098 |
| 27.5 | 1.73 | 100 | 5.1 | 29 920 | 0.50 | 3 203 |
| 27.5 | 1.73 | 100 | 5.1 | 29 850 | 0.50 | 3 195 |
| 27.4 | 1.73 | 70 | 3.3 | 29 040 | 0.49 | 3 113 |
| 27.4 | 1.73 | 70 | 3.3 | 30 340 | 0.51 | 3 252 |
| 27.1 | 1.73 | 45 | 2.6 | 29 440 | 0.51 | 3 144 |
| 27.1 | 1.73 | 45 | 2.6 | 29 040 | 0.49 | 3 101 |
| 38.3 | 1.46 | 40 | 1.6 | 25 760 | 0.49 | 3 277 |
| 38.3 | 1.46 | 40 | 1.6 | 25 650 | 0.49 | 3 262 |
| 38.1 | 1.46 | 60 | 1.3 | 25 820 | 0.49 | 3 280 |
| 38.1 | 1.46 | 60 | 1.3 | 25 700 | 0.49 | 3 265 |
| 50.6 | 1.17 | 40 | 1.4 | 21 430 | 0.48 | 3 400 |
| 50.6 | 1.17 | 40 | 1.4 | 20 510 | 0.47 | 3 255 |
| 51.1 | 1.16 | 60 | 2.4 | 20 940 | 0.48 | 3 339 |
| 51.1 | 1.16 | 60 | 2.4 | 20 650 | 0.49 | 3 293 |
| 77.6 | 0.57 | 50 | 5.3 | 10 330 | 0.41 | 3 348 |
| 77.6 | 0.57 | 50 | 5.3 | 10 140 | 0.40 | 3 287 |
| 77.2 | 0.57 | 70 | 4.5 | 9 860 | 0.40 | 3 184 |
| 77.2 | 0.57 | 70 | 4.5 | 10 020 | 0.39 | 3 236 |
| 75.9 | 0.59 | 25 | 2.6 | 10 160 | SH | 3 190 |
| 75.9 | 0.59 | 25 | 2.6 | 10 450 | SH | 3 279 |

[SH]The overtone position, $L_2$, only shows up as a shoulder in the first-derivative curve of the MWD.

lines (b) are MWDs measured on the commercial (pre-mix) poly(MAA). Subtraction of MWD (b) from (a), which was carried out via the WinGPC® 7.20 software employed for SEC data acquisition and evaluation, yields polymer trace (c) as the MWD of the PLP-produced sample. The MWD (c) in Figure 2 shows a typical PLP-type structure. Also with the PLP-SEC data depicted in Figure 3, the PLP structure is better seen from curve (c) obtained by the subtraction procedure. The improved detection of PLP-induced structure from MWD curves after applying the subtraction procedure is also evidenced by the first-derivative plots shown in Figures 2B and 3B. In case of 50% virtual conversion (Figure 3), subtraction of the MWD for the pre-mixed polymer is necessary for identification of the POIs.

Table 2 summarizes the experimental results for polymerizations of MAA in the presence of pre-mixed poly(MAA) at 25 °C and ambient pressure, a laser repetition rate of 40 Hz, an initiator concentration of $c_{DMPA} = 2$ mmol · L$^{-1}$, and a constant overall acid concentration of 20 wt.-%. Subtraction of the MWD for the pre-mixed polymer from the overall MWD measured on the sample from PLP allows for precisely detecting the $M_1$ and $M_2$ positions. The propagation rate coefficient clearly

 

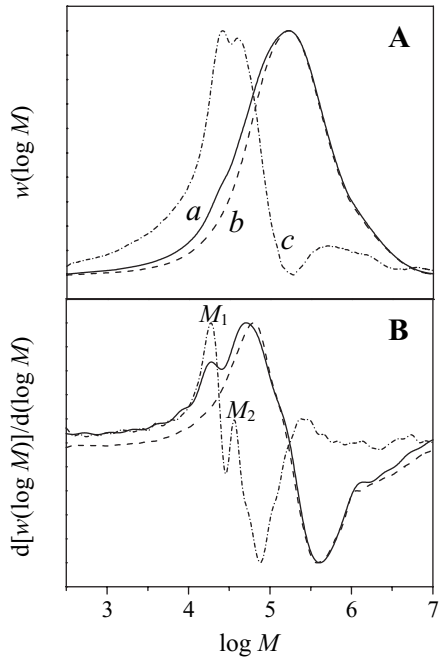


***Figure 2.***
Molecular weight distributions (MWD) **(A)** and associated first-derivative curves **(B)** for samples from PLP-induced polymerization (at 25 °C and 40 Hz) of 15 wt.-% of non-ionized methacrylic acid (MAA) in aqueous solution containing 5 wt.-% poly(MAA). The full line (a) refers to the polymer sample from PLP-SEC, the dashed line (b) represents the pre-mixed poly(MAA), and the dashed-dotted line (c) is obtained by subtracting (b) from (a).

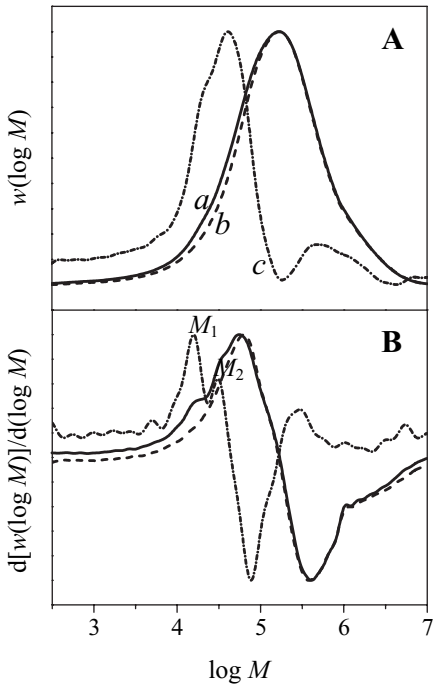


***Figure 3.***
Molecular weight distributions (MWD) **(A)** and associated first-derivative curves **(B)** for samples from PLP-induced polymerization (at 25 °C and 40 Hz) of 10 wt.-% methacrylic acid (MAA) in aqueous solution containing 10 wt.-% poly(MAA). The full line (a) refers to the polymer sample from PLP-SEC, the dashed line (b) represents the pre-mixed poly(MAA), and the dashed-dotted line (c) is obtained by subtracting (b) from (a).

increases toward higher degrees of (virtual) monomer conversion, by about a factor of 1.6 in going from 0 to 10 wt.-% pre-mixed poly(MAA) at constant overall concentration of MAA units. This behavior is in contrast to what has been observed in the experiments with pre-mixed IBA, where no significant change of $k_p$ was seen.

## Discussion

The numbers in Tables 1 and 2 demonstrate that under conditions of constant overall acid concentration (20 wt.-%), which closely corresponds to a constant overall content of (non-ionized) carboxylic acid groups, the replacement of MAA monomer by IBA leaves $k_p$ of MAA constant, whereas the replacement of MAA monomer by poly(MAA) enhances $k_p$. The latter observation is consistent with the finding from PLP-SEC experiments on aqueous MAA solutions (without any added carboxylic acid groups), that lowering the MAA content results in a higher $k_p$.[2] The experimental findings are illustrated in Figure 4, where $k_p$ of MAA is plotted vs. virtual MAA conversion for a constant overall acid concentration of 20 wt.-%. This unusual way of representing $k_p$ solution data requires some further explanation. The $k_p$ data for values of $X_{virtual}$ around 2 to 3 per cent (diamonds) are from experiments on aqueous MAA solutions containing 20 wt.-% MAA, but no added further carboxylic acid groups (as are contained in IBA or in poly(MAA)). The

 

***Table 2.***
Experimental details of pulsed-laser induced polymerizations of methacrylic acid (MAA) in aqueous solution with poly(MAA) being added. The overall concentration of MAA + poly(MAA) is 20 wt.-% in all experiments. Pulsed-laser polymerizations were performed at 25 °C and ambient pressure using a photoinitiator (DMPA) concentration of $c_{DMPA} = 2$ mmol · L$^{-1}$ and a laser pulse repetition rate of 40 Hz. Listed are the virtual degree of monomer conversion, $X_{virtual}$, the MAA concentration, $c_{MAA}$, the number of applied laser pulses, the molecular weight (MW) at the first point of inflection (POI), $M_1$, and the ratio of MWs at the first and second POI. The final column contains the resulting propagation rate coefficients, $k_p$.

| $X_{virtual}$/% | $c_{MAA}$/mol · L$^{-1}$ | *number of laser pulses* | $M_1$/g · mol$^{-1}$ | $M_1/M_2$ | $k_p$/L · mol$^{-1}$ · s$^{-1}$ |
|---|---|---|---|---|---|
| 1.0 | 2.35 | 150 | 19 815 | 0.52 | 3 120 |
| 1.0 | 2.35 | 150 | 20 370 | 0.53 | 3 208 |
| 1.7 | 2.35 | 300 | 20 464 | 0.53 | 3 223 |
| 1.7 | 2.35 | 300 | 20 606 | 0.53 | 3 245 |
| 27.5 | 1.76 | 150 | 18 967 | 0.52 | 3 983 |
| 27.5 | 1.76 | 150 | 19 364 | 0.53 | 4 066 |
| 27.5 | 1.76 | 300 | 18 707 | 0.51 | 3 928 |
| 28.3 | 1.76 | 300 | 18 793 | 0.52 | 3 946 |
| 56.4 | 1.18 | 150 | 16 181 | 0.53 | 5 096 |
| 57.1 | 1.18 | 300 | 15 740 | 0.51 | 4 958 |
| 57.1 | 1.18 | 300 | 16 144 | 0.52 | 5 085 |

associated value of $X_{virtual}$ is thus given by 50 per cent of the MAA conversion brought upon by pulsed laser polymerization.

The triangles refer to PLP-SEC experiments on aqueous MAA solutions with different amounts of added IBA. The $X_{virtual}$ values around 75% refer to experiments on 1:3 mixtures of MAA:IBA at an overall concentration of 20 wt.-% carboxylic acid (MAA + IBA). The virtual conversion thus is made up of a conversion of MAA to an associated "polymer of chain-length unity" plus a small poly(MAA) production by PLP. Toward increasing IBA

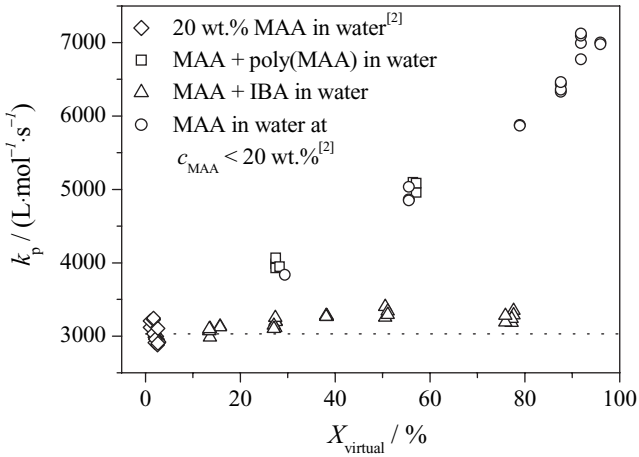


***Figure 4.***
Dependence of $k_p$ on virtual conversion, $X_{virtual}$, for polymerizations of methacrylic acid in water at 25 °C and ambient pressure. The diamond symbols refer to polymerization of MAA (20 wt.-%) in aqueous solution without any added carboxylic acid groups (partially taken from ref.[2]). The squares and the triangles represent aqueous-phase polymerizations of MAA in the presence of poly(MAA) and IBA, respectively, at overall concentration of 20 wt.-% carboxylic acid. The $k_p$ values indicated by the circles are taken from ref.[2]. They refer to polymerization of MAA in aqueous solution at concentrations below 20 wt.-% (for a more detailed explanation see text). The dotted line indicates the mean value of low conversion $k_p$ at 20 wt.-% MAA in aqueous solution (this work and ref.[2]).

 

content, $k_p$ slightly increases. This effect however occurs within the accuracy of PLP-SEC measurements which is estimated to be ±15 per cent for this particular system.

The $k_p$ values of MAA measured in the presence of poly(MAA), indicated by the square symbols, grow significantly with $X_{virtual}$. Within this series of experiments, conversion during an MAA polymerization in aqueous solution of MAA, is simulated by pre-mixing poly(MAA) and by simultaneously lowering MAA monomer concentration of the solution subjected to PLP such that the overall content of MAA units stays at 20 wt.-%.

Also included in Figure 4, as circles, are propagation rate coefficients from ref.[2] for aqueous MAA solutions without added acid. These values are truly virtual in that they are estimated for the hypothetical situation that conversion is only reflected in a reduction of MAA monomer concentration without any polymeric MAA units being produced. Virtual conversion was calculated such that the MAA to water ratio is identical to the one of a reference experiment for an initial monomer concentration of 20 wt.-% in which MAA is actually transformed into polymeric MAA units. Thus the virtual conversion for a PLP-SEC experiments on an aqueous solution containing 10 wt.-% MAA slightly exceeds 50 per cent, as otherwise the MAA monomer to water weight ratio would be 1 : 9 instead of 1 : 8, which is the ratio for a polymerization to 50 per cent conversion starting from an initial concentration of 20 wt.-% MAA. The three types of experiments, indicated by the triangles, squares, and circles, have in common, that identical virtual conversion is associated with the same MAA to water ratio. The circles demonstrate that the reduction in MAA concentration significantly enhances $k_p$.

The close agreement of the MAA $k_p$ values in the presence of poly(MAA) with the ones in aqueous MAA solution of identical monomer concentration (without added carboxylic acid groups, circles in Figure 4) indicates that polymeric MAA units do not contribute to changes of $k_p$. As has been detailed in ref. [2], the propagation rate coefficient of non-ionized MAA in aqueous solution is strongly enhanced toward lower monomer concentration due to weaker intermolecular interactions of the transition state structure with a molecular environment in which carboxylic acid groups are replaced by water molecules. The lower friction of internal rotational motion of the transition state structure in more dilute MAA solution is associated with a higher pre-exponential factor. In an MAA-rich environment, on the other hand, the strong hydrogen-bonded interactions between the carboxylic acid groups lead to significant friction and to a lowering of the pre-exponential factor in the Arrhenius expression for $k_p$. IBA which is structurally rather close to MAA, obviously has a similar effect on $k_p$ of MAA as has MAA itself. Thus replacing MAA by IBA at constant overall acid concentration has no significant effect on MAA $k_p$. That poly(MAA) has not the same effect on MAA $k_p$ as has IBA and, to be more precise, has no detectable effect on MAA $k_p$, indicates that the addition of poly(MAA) is not felt at the reactive site, which is the free-radical functionality of a growing macroradical. The free-radical site is imbedded into the solvent-swollen macroradical coil, which is not or not to a significant extent penetrated by another polymeric coil. Thus the solvent environment of the radical site is not affected by adding polymer. As a consequence, also the effect of solvent friction on the transition structure for propagation remains unchanged. On the other hand, changing the reacting system by adding monomeric carboxylic acid, e.g. MAA or IBA, changes the solvent quality and thus the microscopic environment within the coil. If the two acids are of similar structure, as is the case with MAA and IBA, the $k_p$ value, to a first approximation, depends on overall carboxylic acid concentration, but is insensitive toward the relative amounts of two such acids.

These findings have particularly important consequences for the modeling of

 

polymerization kinetics in aqueous solution, where the concentration dependence of $k_p$ is pronounced. For an estimate of the impact of carboxylic acid concentration on $k_p$ of MAA it needs primarily to be considered whether the carboxylic acid groups (other than of the MAA monomer) are capable of affecting the intra-coil environment of the radical site. Along these lines, $k_p$ of MAA may have a specific chain-length dependence and may be affected by the MWD of produced polymer, in particular by the amount of oligomeric products that may contribute to the intra-coil environment of the growing macroradicals. If an MAA polymerization exclusively produces high molecular weight material, only monomer concentration needs to be taken into account for assessing $k_p$. It appears to be a matter of priority to carry out further PLP-SEC experiments with different types of carboxylic acids being added and to extend the studies to other acid monomers, with particular interest in acrylic acid.

## Conclusion

The propagation rate coefficient, $k_p$, of methacrylic acid (MAA) in aqueous solution is known to strongly depend on MAA concentration. Within the present study, PLP-SEC experiments have been carried out on aqueous solutions of non-ionized MAA to which either *iso*-butyric acid (IBA) or poly(methacrylic acid) have been added. Enhancement of overall acid concentration by adding low molecular weight IBA lowers $k_p$ of MAA, whereas the addition of poly(MAA) has no significant effect on $k_p$. The different impact of low and high molecular weight carboxylic acid species on MAA $k_p$ is understood as being due to IBA becoming part of the solvent environment at the radical site of the growing chain, whereas the addition of poly(MAA), is not reflected in the intra-coil solvent environment. This finding has important consequences for modeling the kinetics of MAA solutions at different initial monomer concentrations and degrees of monomer conversion.

*Acknowledgements:* The authors want to acknowledge financial support by the *Deutsche Forschungsgemeinschaft* within the framework of the European Graduate School ''Microstructural Control in Radical Polymerization'', a fellowship (to P.H.) granted by the *Fonds der Chemischen Industrie*, and support from *BASF AG*.

[1] F.-D. Kuchta, A. M. van Herk, A. L. German, *Macromolecules* **2000**, *33*, 3641.
[2] S. Beuermann, M. Buback, P. Hesse, I. Lacík, *Macromolecules* **2006**, *39*, 184.
[3] S. Beuermann, M. Buback, P. Hesse, F.-D. Kuchta, I. Lacík, A. M. van Herk, *Pure Appl. Chem.* **2006**, accepted for publication.
[4] O. F. Olaj, I. Schnöll-Bitai, F. Hinkelmann, *Makromol. Chem.* **1987**, *188*, 1689.
[5] I. Lacík, S. Beuermann, M. Buback, *Macromolecules* **2001**, *34*, 6224.
[6] I. Lacík, S. Beuermann, M. Buback, *Macromolecules* **2003**, *36*, 9355.
[7] S. A. Seabrook, M. P. Tonge, R. G. Gilbert, *J. Polym. Sci. Part A: Polym. Chem.* **2005**, *43*, 1357.
[8] F. Ganachaud, R. Balic, M. J. Monteiro, R. G. Gilbert, *Macromolecules* **2000**, *33*, 8589.
[9] I. Lacík, S. Beuermann, M. Buback, *Macromol. Chem. Phys.* **2004**, *205*, 1080.
[10] S. Beuermann, M. Buback, *Prog. Polym. Sci.* **2002**, *27*, 191.
[11] H. Yamazoe, P. B. Zetterlund, B. Yamada, D. J. T. Hill, P. J. Pomery, *Macromol. Chem. Phys.* **2001**, *202*, 824.
[12] M. I. Ballard, R. G. Gilbert, D. H. Napper, P. J. Pomery, P. W. O'Sullivan, J. H. O'Donnell, *Macromolecules* **1986**, *19*, 1303.
[13] T. G. Carswell, D. J. T. Hill, D. I. Londero, J. H. O'Donnell, P. J. Pomery, C. L. Winzor, *Polymer* **1992**, *33*, 137.
[14] S. Beuermann, M. Buback, P. Hesse, T. Junkers, I. Lacík, *Macromolecules* **2006**, *39*, 509.
[15] S. Beuermann, M. Buback, T. P. Davis, R. G. Gilbert, R. A. Hutchinson, O. F. Olaj, G. T. Russell, J. Schweer, A. M. van Herk, *Macromol. Chem. Phys.* **1997**, *198*, 1545.

 

 DOI: 10.1002/masy.200750206

# Studying the Fundamentals of Radical Polymerization Using ESR in Combination with Controlled Radical Polymerization Methods

*Atsushi Kajiwara*

**Summary:** Electron spin resonance (ESR) spectroscopy can contribute to understanding both the kinetics and mechanism of radical polymerizations. A series of oligo/poly(meth)acrylates were prepared by atom transfer radical polymerization (ATRP) and purified to provide well defined radical precursors. Model radicals, with given chain lengths, were generated by reaction of the terminal halogens with an organotin compound and the radicals were observed by ESR spectroscopy. This combination of ESR with ATRPs ability to prepare well defined radical precursors provided significant new information on the properties of radicals in radical polymerizations. ESR spectra of the model radicals generated from *tert*-butyl methacrylate precursors, with various chain lengths, showed clear chain length dependent changes and a possibility of differentiating between the chain lengths of observed propagating radicals by ESR. The ESR spectrum of each dimeric, trimeric, tetrameric, and pentameric *tert*-butyl acrylate model radicals, observed at various temperatures, provided clear experimental evidence of a 1,5-hydrogen shift.

**Keywords:** atom transfer radical polymerization (ATRP); ESR/EPR; kinetics (polym.); radical polymerization

## Introduction

Electron Spin Resonance (ESR) spectroscopy can contribute to understanding both the kinetics and the mechanism of radical polymerizations.[1–5] Propagation rate constants ($k_p$) of various kinds of monomers have been estimated using ESR spectroscopy.[1,5] Indeed ESR is one of the most effective methods for estimating values for $k_p$ and it is a mutually complementary method to the Pulsed Laser Polymerization (PLP) method. Usually equation (1), and its integrated form (2), have been used to calculate $k_p$ by ESR.

$$R_p = -\frac{d[M]}{dt} = k_p[P_n^\bullet][M] \quad (1)$$

$$\ln\frac{[M_1]}{[M_2]} = k_p[P_n^\bullet](t_2 - t_1) \quad (2)$$

The advantage of ESR is that the value of $[P_n^\bullet]$ in these equations can be determined from the observed ESR spectra of propagating radicals. Detailed analysis of the spectra provides information, not only on radical concentration, but also on the structure and other physicochemical properties of the radicals. Furthermore, steady state radical concentrations can be confirmed from the spectra. On the other hand, the ESR method makes two important assumptions: one is that we observe the propagating radical with sufficiently long chain length and the other is that we observe real propagating radicals.

Nara University of Education, Takabatake-cho, Nara 630-8528 JAPAN
Fax: (+81) 742 27 9192
E-mail: kajiwara@nara-edu.ac.jp

Atom transfer radical polymerization (ATRP) is one of the most widely applied polymerization techniques in the field of controlled/living radical polymerization.[6,7] The polymers formed in ATRP contain terminal carbon-halogen bonds. Giese *et al.* (Scheme 1)[8] has reported that these bonds can be homolytically cleaved by reaction with organotin compounds. Accordingly, various radicals that model the active end groups in an ATRP can be formed from the corresponding precursors prepared by atom transfer radical addition (ATRA) and ATRP. The generated radicals can be studied by ESR spectroscopy. Systematic variation of the chain length and composition of polymeric radical precursors elucidates the effect of chain length and penultimate units on the ESR spectra of the formed radicals.[9] It was previously reported,[10] that the ESR spectra of propagating *tert*-butyl methacrylate radicals show chain length dependency.

In another study on conventional radical polymerizations of acrylates, large amounts of mid-chain radicals were detected by ESR spectroscopy and it was suggested that the terminal propagating radicals had rearranged to form a mid-chain radical.[2] In that study,[2] and in other reports,[11–16] it was suggested that the formation of mid-chain radicals occurred via a 1,5-hydrogen shift, but no mechanism was proposed and there was no clear experimental evidence for the "1,5-hydrogen shift" reaction. Possibilities of a 1,7-, a 1,9-hydrogen shift, or some other reaction e.g. intermolecular chain transfer remained. This ESR study of model radicals generated from radical precursors prepared by ATRP provided significant information on the rearrangement and allows a conclusion to be reached. Accordingly, ESR spectroscopy in combination with ATRP has given an unambiguous proof of several reactions that are involved in radical polymerization.

In this research work, a series of uniform oligomeric and polymeric radicals, with various chain lengths, were prepared to serve as models of propagating radicals. The model radicals were generated from oligomers prepared by ATRP and purified by column chromatography; each uniform oligomer was a pure compound with an

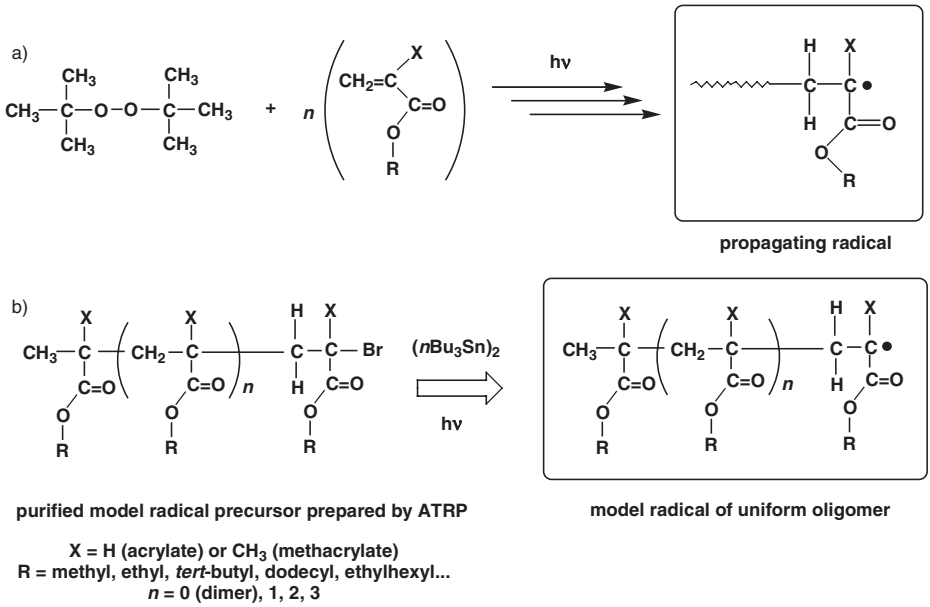


***Scheme 1.***

Generation of propagating radicals (a) and oligomeric model radicals (b). ESR spectra of methacrylate showed chain length dependence. ESR spectra of acrylate radicals show clear proof of a 1,5-hydrogen shift.

 

exact molecular weight. This systematic study using uniform oligomers with various chain lengths would provide a clearer perspective in the study of propagating radicals.

In this article, two examples of the application ESR to conventional radical polymerizations, especially to both kinetics and mechanism, based on materials prepared by controlled/living radical polymerizations will be demonstrated. The first example is the estimation of the effect of chain length on propagating radicals. The second is the detection of chain transfer reactions on propagating radicals in the polymerization of *tert*-butyl acrylate.

## Chain Length Dependence

### *ESR Spectra of Propagating Radicals of tert-Butyl Methacrylate (tBMA)*

When a mixture of a monomer and a radical initiator is heated, or photo-irradiated, in an ESR sample cell, propagating radicals are formed and polymerization proceeds (Scheme 1a, $X = CH_3$). Well-resolved spectra of propagating radicals of *tert*-butyl methacrylate (*t*BMA) have been detected in such polymerization systems at various temperatures; as shown in Figure 1, 16-line spectra were clearly observed. The spectroscopic feature of the spectra showed a clear temperature dependence which can be interpreted by a hindered rotation model of two stable conformations.[2,5,8] The intensity of the inner 8 lines increased with increasing temperature, indicating that there are two exchangeable conformations whose existence have been shown by elucidation of ESR spectra of methacrylates. [2,5,8]

At 150 °C, the intensity of the inner 8 lines increased and the ESR spectrum can be interpreted as a single conformation, indicating that the energy difference between the two conformers is small. The observed ESR spectrum of propagating radicals of *t*BMA at 150 °C is shown in Figure 2a along with the simulated spectrum. The spectrum is completely simulated

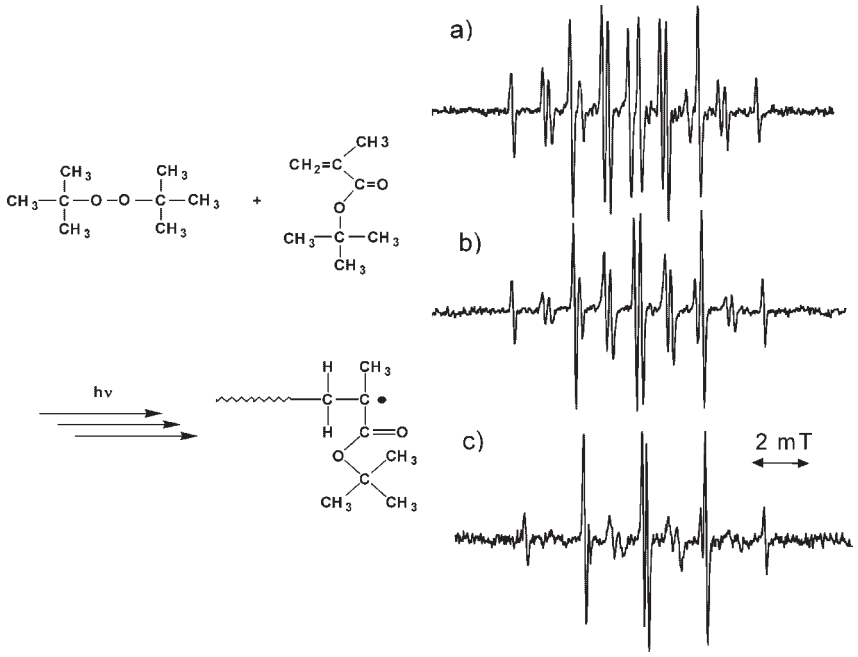


***Figure 1.***
Polymerization scheme and observed ESR spectrum of propagating radical of *t*BMA in radical polymerizations at 150 °C (a), 90 °C (b), and 30 °C (c).

 

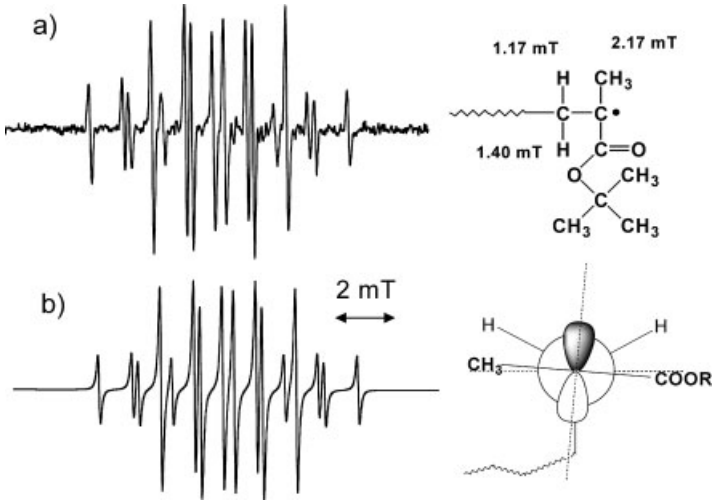


***Figure 2.***
Observed ESR spectrum of propagating radical of *t*BMA in radical polymerizations at 150 °C (a) along with its simulation (b). Values of hyperfine splitting constants are shown in the Figure. A Newman projection of one of stable conformer is also shown.

using hyperfine splitting constants of 1.40 mT for one methylene proton (1:1 doublet), 1.16 mT for the other one proton (1:1 doublet), and 2.17 mT for three equivalent methyl protons (1:3:3:1 quartet) as shown in Figure 2b.

A characteristic result is that different hyperfine splitting constants may be estimated for the two methylene protons. This means that the rate of rotation of the end radical is not fast enough to make the methylene protons equivalent within the time scale of the ESR measurement. Thus, it leads to a 16-line spectrum ($2 \times 2 \times 4$). If the two β-methylene protons were equivalent, the total number of splitting lines would be 12 (4 ($CH_3$–) × 3 (–$CH_2$–)). This suggests the presence of a propagating radical with a long chain that hinders the rotation of the terminal bond to generate the 16-line spectrum and also another oligomeric radical which may show a 12-line spectrum.

If we could observe the ESR spectra of radicals with controlled chain length, chain length dependent phenomena could be precisely examined. In order to clarify the phenomena, model radical precursors were prepared by the ATRP technique. ATRP can provide polymers with controlled molecular weights and low polydispersity, and the resulting polymers have preserved terminal carbon-halogen bonds.[6,7] Model radicals of propagating chains with given chain length could be generated when the carbon-halogen bonds are cleaved homolytically by reaction with organotin compounds, (Scheme 1b, $X = CH_3$).[6,7]

### Differentiating Between Chain Lengths of Observed Radicals

First, a mixture of oligomers containing 2–7 monomer units ($P_n = 2$–7) was prepared by ATRP and the dimeric model radical precursor was isolated and purified from the mixture. Preparation and purification were successful and the dimeric model radical was generated from the precursor. Clear and well-resolved ESR spectra of the model radical were observed at various temperatures. The ESR spectrum of the radicals observed at 150 °C showed a 12-line spectrum, as shown in Figure 3a. The two β-methylene protons are almost equivalent in dimeric radicals at such high temperature. This finding indicates that rotation of the radical chain end is too fast

 

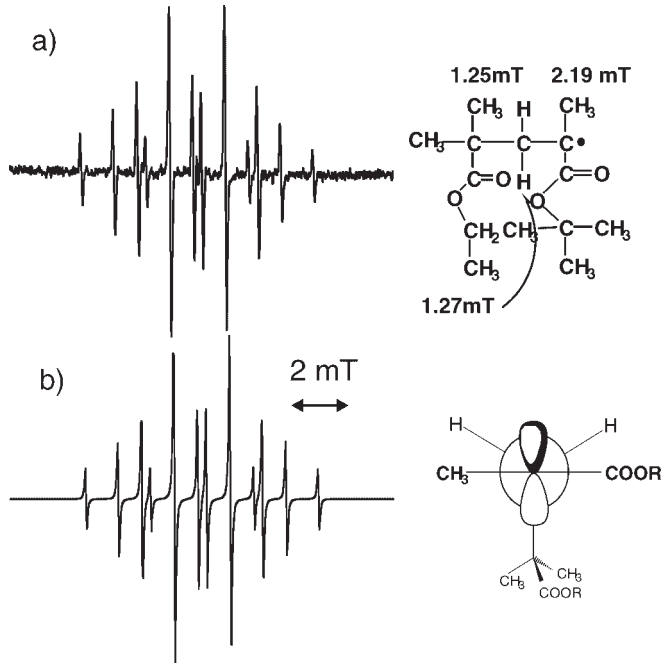


***Figure 3.***
Observed ESR spectrum of dimeric model radical of *t*BMA at 150 °C (a) along with its simulation (b). Values of hyperfine splitting constants are shown in the Figure. A Newman projection of one of the stable conformers is also shown.

to detect differences in methylene protons on the time scale of ESR spectroscopy.

In order to estimate the critical chain length which would show splitting of 16-line spectrum, model radical precursors with degrees of polymerization ($P_n$) of 30, 50, and 100 were prepared by ATRP. Polymers with targeted molecular weights and low polydispersities were obtained. ESR spectra of radicals generated from these precursors were observed at various temperatures. Although the lifetime of the model radicals were very short at 150 °C, clear and well-resolved spectra were observed. These spectra showed similar temperature dependence to that shown in Figure 1. In the case of $P_n = 100$, the intensity of the inner 8 lines increased with increasing temperature, and seems to coalesce into a single line at 150 °C. Similar ESR spectra were observed in radicals from polymeric precursors with $P_n = 50$ and 30. The intensity of the inner 8 lines seems to coalesce more clearly to a single line at 150 °C. The ESR spectra seemed to be 12-line spectrum, but the 4 lines coalesced insufficiently, indicating that the rate of the rotation of the end radical is not sufficiently fast for the methylene protons to be detected as equivalent species on the time scale of the ESR experiment. The inner 4 lines of the 12-line spectrum begin to separate into two lines at $P_n = 30$, and the separation becomes larger with increasing $P_n$ owing to the lowering of the rate of the rotation. The separation was more clearly observed in the propagating radical, indicating that mobility of the chain end radical is restricted.

A comparison of the ESR spectra of the dimeric radical (Fig. 3a), model radicals with $P_n = 100$, and radicals in a polymerization system at 150 °C is shown in Figure 4. The separation of the inner lines, $P_n$ of the propagating radical indicate that the degree of polymerization is higher than 100. When the values of hyperfine splitting constants measured from these spectra, were plotted against chain length, they seemed to show

 

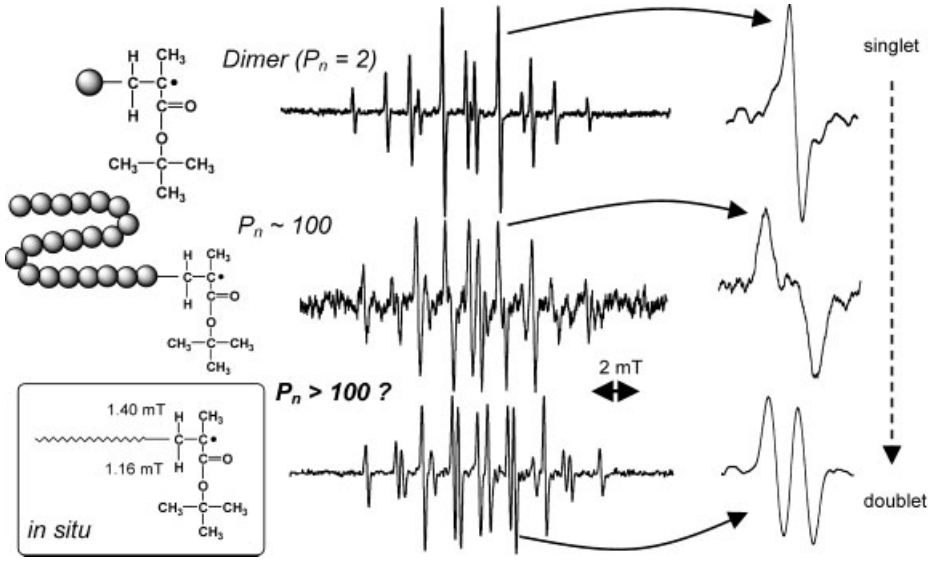


***Figure 4.***
Comparison of ESR spectra of radicals with various chain length at 150 °C. Dimeric model radical, model radical with $P_n = 100$, and radicals in a radical polymerization (propagating radical). Characteristic lines were enlarged on the right hand side.

nearly linear correlation between hyperfine splitting constants and chain lengths in the range up to $P_n = 200$. Molecular weight ($M_n$) of the isolated polymers from polymerization system was determined to be 30000 ($P_n = 210$) by size exclusion chromatography (SEC). The interpretation of the ESR spectra suggests that they correspond to ''long'' propagating radicals, and it is in agreement with SEC. Prior to these experimental results, ESR spectra and overall SEC results did not correlate. However, more experimental results are needed for a more comprehensive correlation of kinetic data with ESR spectra.

We can conclude that the 16-line spectrum in ESR measurements can be ascribed to ''polymeric'' radicals with more than 100 monomer units and that ESR spectroscopy has provided structural information on the propagating radicals at their chain ends.

## Radical Migration during Polymerizations

### *tert-Butyl Acrylate (tBA)*

ESR spectra observed in radical polymerization of acrylates are very different from those for methacrylates, even under almost identical conditions (Fig. 5a). Accordingly, it is difficult to interpret the spectrum to be that of propagating radicals. Spectroscopic changes were observed in ESR spectra during the solution polymerization of *tert*-butyl acrylate (*t*BA) as shown in Figure 5. A 6-line spectrum or a doublet of triplets with narrow line width (Fig. 5c) was observed at −30 °C. This spectrum can be reasonably assigned to a propagating radical with two β-methylene protons (1:2:1 triplet) and one α-proton (1:1 doublet). At 60 °C, a totally different 7-line spectrum with broader line width was observed (Fig. 5a). While it was much easier to observe the latter spectrum than the former one traces of the 6-line spectrum can be seen in the spectrum at 60 °C, but the amount of the species giving rise to the 6-line spectrum is 1000 times lower than that of the source of the high temperature spectrum. At −10 °C, overlapped spectra of the first and latter spectra were observed (Fig. 5b). Signal intensity due to higher temperature spectrum with broader line width increased with time. These results suggest that the spectrum observed at

 

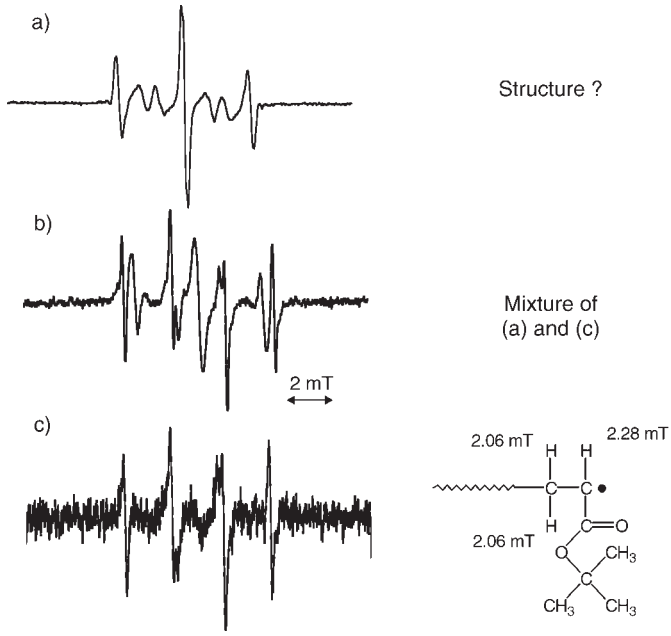


***Figure 5.***
ESR spectra observed in radical polymerization of tBA initiated with tBPO under irradiation at 60 °C (a), −10 °C (b), and −30 °C (c) in toluene.

−30 °C is converted to the spectrum observed at 60 °C. Some reaction should be responsible for such a change. Similar findings were observed for other acrylates, e.g. methyl acrylate, dodecyl acrylate, phenyl acrylate, and others. Two potential explanations for this change had been considered. One is a chain-length dependence of the spectra and the other is chemical transformation (e.g. transfer). These possibilities were examined by analysis of ESR spectra of model radicals with various chain lengths generated from polymeric radical precursors prepared by ATRP.[2–4] The possibility of chain length dependent change was discarded after examination of results from experiments using radical precursors of poly*t*BA with controlled chain lengths (Pn = 15, 50, and 100). The change from low temperature spectrum to the one at higher temperature was clearly observed even in model radical systems with fixed chain lengths. The possibility of chemical transformation remained. The ambiguity was resolved by ESR spectroscopy of several purified oligomeric model radical precursors.

SEC elution diagrams of model radical dimer, trimer, tetramer, and pentamer precursors are shown in Figure 6 along with that of a mixture. As shown in the figure, separation and purification of the oligomers was successful. Model radicals

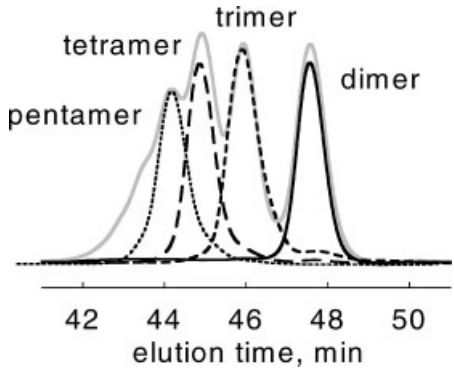


***Figure 6.***
SEC elution diagram of purified dimer, trimer, and tetramer of tBA as uniform radical precursor along with that of mixture of oligomers.

 

with clearly defined structures were generated by the reaction of the corresponding alkyl bromides (H-ethyl acrylate (EA)-*t*BA-Br, H-EA-*t*BA-*t*BA-Br, H-EA-*t*BA-*t*BA-*t*BA-Br, H-EA-*t*BA-*t*BA-*t*BA-*t*BA- Br) with an organotin compound under irradiation.

The resulting radicals had structures of hydrogenated radicals, i.e., H-EA-*t*BA•, H-EA-*t*BA-*t*BA•, H-EA-*t*BA-*t*BA-*t*BA•, and H-EA-*t*BA-*t*BA-*t*BA-*t*BA• respectively. Each of these radicals was investigated by ESR spectroscopy at various temperatures. Clear well-resolved spectra were observed and precise values for hyperfine splitting constants can be determined from the spectra. The ESR spectrum of the dimeric radical (H-EA-*t*BA•) showed a doublet of triplets in each spectrum at various temperatures within the range of −30 to +150 °C. The doublet and triplet were reasonably considered to be due to the splitting from the α- proton and two equivalent β-methylene protons, respectively. Nothing happened to the dimeric radical even at higher temperatures. On the other hand, model trimeric and tetrameric radicals showed a clear irreversible temperature dependent change, as shown below.

In the case of the model trimeric radical (H-EA-*t*BA-*t*BA•), the ESR spectrum observed at −30 °C (Fig. 7a) was very similar to that of the dimeric radical. This spectrum is ascribed to a chain end radical as shown in the figure. ESR spectra were measured every 30 degree as the temperature was increased from −30 °C to 120 °C. As the temperature was raised, the spectrum gradually and irreversibly changed to a different one. Between 0 °C and 60 °C, two overlapping spectra were observed. The change was complete at 120 °C. The resulting spectrum, observed at higher temperatures, was totally different from that at lower temperatures (Fig. 7b). When a 1,5-hydrogen shift occurs, the radical should migrate from one end to the other end of the trimeric model radical as shown in Figure 7. The spectrum can be simulated using hyperfine splitting constants shown in the figure. The most important feature of this simulation is a small triplet (0.11 mT) that appears in each spectroscopic line. When this trimer was prepared by ATRP, ethyl 2-bromo propionate was used as the initiator and the initiator fragment was counted as first monomer unit. So, we only had an ethyl ester group at the other chain end. The presence of a small triplet clearly indicates that the radical is located on the first ethyl acrylate unit. Consequently, we can say that the radical migrated from one end to the other end of the trimer.

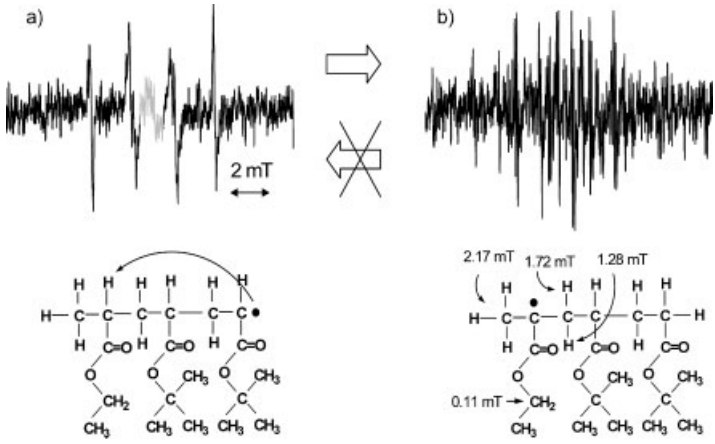


***Figure 7.***
ESR spectra of trimeric model radical (H-EA-*t*BA-*t*BA•) at −30 °C (a) and at +120 °C (b) with their estimated structures. Upon heating, an irreversible spectroscopic change occurred due to hydrogen abstraction.

 

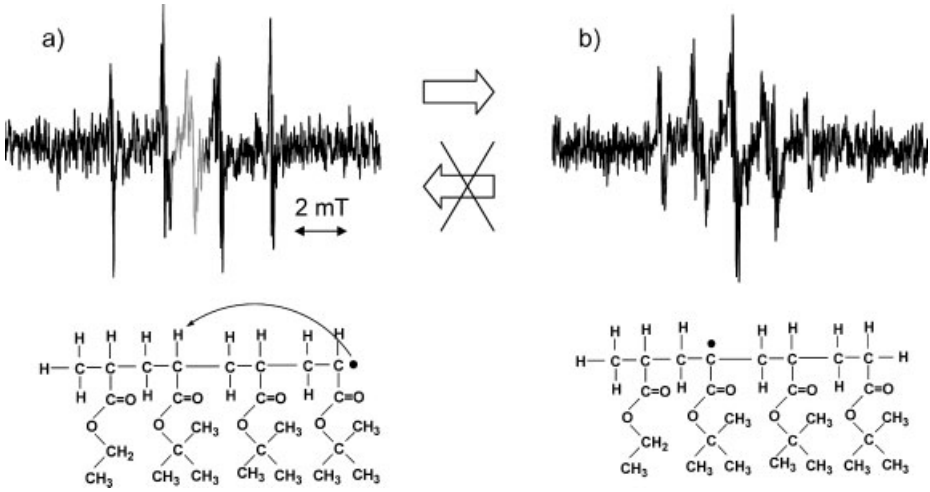


***Figure 8.***
ESR spectra of tetrameric model radical (H-EA-*t*BA-*t*BA-*t*BA•) at −30 °C (a) and at +120 °C (b) with their estimated structures. Upon heating, irreversible spectroscopic change occurred due to hydrogen abstraction.

A similar ESR study was done for the tetrameric model radical (H-EA-*t*BA-*t*BA-*t*BA•). The ESR spectra at −30 °C and 120 °C are shown in Figure 8. The low temperature spectrum, observed at −30 °C, was very similar to those from the dimeric and trimeric model radicals. Similarly to the trimeric model radical, at higher temperatures an irreversible spectroscopic change took place. However the final spectrum was different from that of the trimeric model radical. In the case of a tetrameric model radical, a 1,5-hydrogen shift would cause transfer of a radical from the chain end to the first *t*BA unit, which is located two units away from the other end unit, through a six-membered ring structure (Figure 9).

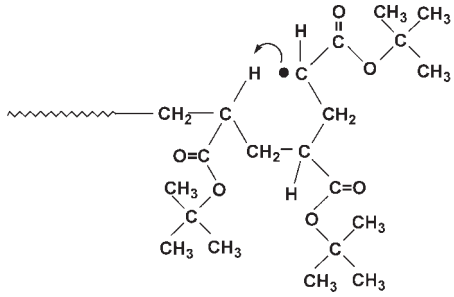

***Figure 9.***
1,5-Hydrogen shift of propagating radical of *t*BA.

The transferred radical should have mid-chain type structure with methylene groups at both sides (H-EA-*t*BA(•)-*t*BA-*t*BA-H). The spectrum of the radical shown in Fig. 8b is attributable to such a mid-chain radical. These findings provide clear experimental evidence of a 1.5-hydrogen shift at the propagating chain end of acrylate radical polymerizations.

A pentameric model radical was also generated and observed by ESR and a similar temperature dependent spectroscopic change to those seen in the case of the trimer and tetramer was observed. The resulting high temperature spectrum is very similar to those observed in polymeric acrylate radicals.

These findings strongly suggest that the mechanism of chain transfer reaction in an acrylate radical polymerization is a 1, 5-hydrogen shift that occurs through a six-member ring structure. Formation of a six- member ring is a kinetically favored process and the transfer occurred from a secondary radical to form a thermodynamically more stable tertiary radical. An additional piece of information can be obtained from the result of the pentamer radical. Actually, the pentamer has one more chance for radical migration, from a

 

mid-chain radical to the other chain end. However, this migration was not observed. The reason for this is unresolved.

Although there may be some minor contribution of intermolecular chain transfer, these systematic studies have provided a clearer perspective of the mechanism of the chain transfer reaction of propagating acrylate radicals. With increasing molecular weight, other factors also are becoming more important like conformation (rigidity), side group bulkiness and statistics. Further investigation will provide decisive proof of the mechanism.

## Conclusion

Electron spin resonance (ESR) of a series of well defined radicals generated from oligomers prepared by atom transfer radical polymerization (ATRP) has provided significant new information on the properties of radicals in radical polymerizations, e. g. effect of chain lengths, dynamics, and reactivity (hydrogen transfer) of propagating radicals. Previously, it had been extremely difficult, even impossible, to obtain such information from ESR spectra during conventional radical polymerizations. Radical precursors of oligo- and poly-(meth)acrylates were prepared by ATRP and purified. Model radicals with given chain lengths were generated by reaction with an organotin compound and the radicals were observed by ESR spectroscopy. Model radicals of *tert*-butyl methacrylate with various chain lengths showed clear chain length dependent ESR spectra. Similar findings were also observed in cases of methyl methacrylate, *n*-butyl methacrylate, and benzyl methacrylate based radicals. These results will provide supporting information on the kinetics of radical polymerization. The ESR spectrum of dimeric, trimeric, tetrameric, and pentameric *tert*-butyl acrylate model radicals observed at various temperatures provided clear experimental evidence for a 1,5-hydrogen shift.

*Acknowledgements:* The author is grateful to Professor Mikiharu Kamachi, Fukui University of Technology, for his kind advice and discussions on ESR study of radical polymerizations. Sincere thanks are also due to Professor Krzysztof Matyjaszewski, Carnegie Mellon University, for his kind suggestions and continuous encouragements. The author wish to thank Dr. James Spanswick for his kind suggestions and help. Financial support from the Japan Society for the Promotion of Science (JSPS) for Japan-U.S. Cooperative Science Program is gratefully acknowledged.

[1] A. Kajiwara, K. Matyjaszewski, M. Kamachi, In "*Controlled/Living Radical Polymerization*", ACS Symposium Series 768; K. Matyjaszewski ed., American Chemical Society, Washington, DC., **2000**; Chapter 5, pp. 68–81.
[2] A. Kajiwara, M. Kamachi, In "*Advances in Controlled/Living Radical Polymerization*", ACS Symposium Series 854; K. Matyjaszewski ed., American Chemical Society, Washington, DC., 2003; Chapter 7, pp. 86–100.
[3] A. Kajiwara, In "*Advances in Controlled/Living Radical Polymerization*", ACS Symposium Series 944; K. Matyjaszewski, ed., American Chemical Society, Washington, DC., **2006**; Chapter 9, pp. 111–124.
[4] A. Kajiwara, K. Matyjaszewski, In "*Advanced ESR Methods in Polymer Research*", Wiley Interscience, N. J. **2006**, Chapter 5, pp. 101–132.
[5] M. Kamachi, *J. Polym. Sci., Part A:. Polym. Chem.*, **2002**, *40*, 269.
[6] V. Coessens, T. Pintauer, K. Matyjaszewski, *Prog. Polym. Sci.*, **2001**, *26*, 337.
[7] K. Matyjaszewski, J. Xia, *Chem. Rev.*, **2001**, *101*, 2921.
[8] B. Giese, W. Damm, F. Wetterich, H.-G. Zeitz, *Tetrahedron Lett.*, **1992**, *33*, 1863.
[9] A. Kajiwra, A. K. Nanda, K. Matyjaszewski, *Macromolecules* **2004**, *37*, 1378.
[10] A. Kajiwara, K. Maeda, N. Kubo, M. Kamachi, *Macromolecules* **2003**, *36*, 526.
[11] R. X. E. Willemse, A. M. van Herk, E. Panchenko, T. Junkers, M. Buback, *Macromolecules* **2005**, *38*, 5098.
[12] D. Britton, F. Heatley, P. A. Lovell, *Macromolecules* **2001**, *34*, 817.
[13] C. Plessis, G. Arzamendi, J. M. Alberdi, M. Agnely, J. R. Leiza, J. M. Asua, *Macromolecules* **2001**, *34*, 6138.
[14] C. Plessis, G. Arzamendi, J. R. Leiza, H. A. S. Schoonbrood, D. Charmot, J. M. Asua, *Macromolecules* **2000**, *33*, 4.
[15] F. Heatley, P. A. Lovell, T. Yamashita, *Macromolecules* **2001**, *34*, 7636.
[16] N. M. Ahmad, F. Heatley, P. A. Lovell, *Macromolecules* **1998**, *31*, 2822.

 

 DOI: 10.1002/masy.200750207

# Competitive Equilibria in Atom Transfer Radical Polymerization

*Nicolay V. Tsarevsky,*[1] *Wade A. Braunecker,*[1] *Alberto Vacca,*[2] *Peter Gans,*[3] *Krzysztof Matyjaszewski**[1]

**Summary:** With the recent development of new initiation techniques in atom transfer radical polymerization (ATRP) that allow catalysts to be employed at unprecedented low concentrations (~10 ppm), a thorough understanding of competitive equilibria that can affect catalyst performance is becoming increasingly important. Such mechanistic considerations are discussed herein, including i) factors affecting the position of the ATRP equilibrium; ii) dissociation of the ATRP catalyst at high dilution and loss of deactivator due to halide dissociation; iii) conditional stability constants as related to competitive monomer, solvent, and reducing agent complexation as well as ligand selection with respect to protonation in acidic media; and iv) competitive equilibria involving electron transfer reactions, including the radical oxidation to carbocations or reduction to carbanions, radical coordination to the metal catalyst, and disproportionation of the $Cu^{I}$-based ATRP activator.

**Keywords:** atom transfer radical polymerization; catalysis; complex stability; competitive complexation; electron transfer

## Introduction

Ten years of research has transformed atom transfer radical polymerization (ATRP) from a technique used to control polymer molecular weights and molecular weight distributions[1] into one where the composition, topology, functionality, and microstructure of a vast array of material products can also be controlled.[2–10] As the full potential of this synthetic technique continues to be realized, much effort is currently focused on making ATRP more viable on an industrial scale,[11] in particular by maximizing the efficiency of catalyst removal or recycling.[12–14] However, with the recent development of two initiation techniques known as activators regenerated by electron transfer (ARGET)[15,16] and initiators for continuous activator regeneration (ICAR),[17] ATRP can now be conducted with dramatically lower catalyst concentrations, where removal of the catalyst from the final product would not be necessary for many applications.

The following discussion highlights facets of the ATRP equilibrium that should be considered when conducting polymerization with the catalyst at very low concentration. After a brief discussion of the factors that determine this equilibrium, particular emphasis is paid to concurrent reactions that may occur during ATRP and will affect the efficiency of the technique, including dissociation of the catalyst, competitive complexation reactions, and equilibria involving electron transfer. Cu-mediated ATRP is described here but most of the concepts can be applied to polymerizations catalyzed by other metal complexes.

### Factors Determining the Activity of the ATRP Catalyst

The ATRP mechanism involves homolytic cleavage of an alkyl halide bond R–X by a

[1] Department of Chemistry, Carnegie Mellon University, 4400 Fifth Avenue, Pittsburgh, Pennsylvania 15213 USA
E-mail: km3b@andrew.cmu.edu
[2] Dipartimento di Chimica, Universita degli Studi di Firenze, Via della Lastruccia 3, I 50019, Sesto Fiorentino, Italy
[3] Protonic Software, Leeds LS15 0HD, U.K.

transition metal complex (typically $Cu^{I}L_m$ where L is a ligand, for example one of those shown in Figure 1) to reversibly generate the corresponding higher oxidation state metal halide complex ($XCu^{II}L_m$) and a propagating alkyl radical $R^{\bullet}$ (Scheme 1).[4,18] Typically, enough Cu catalyst is required (several thousand ppm) to ensure a sufficient concentration of $Cu^{I}$ activator survives, as every act of radical termination results in the irreversible accumulation of $Cu^{II}$ deactivator according to the persistent radical effect.[19–21] However, in ARGET and ICAR ATRP, organic reducing agents and radicals generated from free radical initiators reduce accumulated $Cu^{II}$ back into $Cu^{I}$, effectively regenerating lost activator. This has ultimately allowed ATRP to be successfully conducted with $\leq$10 ppm of Cu catalyst.[17]

For convenience, it has been proposed that the ATRP equilibrium constant (represented in Scheme 1 as $K_{ATRP} = k_{act}/k_{deact}$) is expressed as a combination of four reversible reactions: oxidation of the metal complex, or electron transfer ($K_{ET}$), reduction of a halogen to a halide ion, or electron affinity ($K_{EA}$), alkyl halide bond homolysis ($K_{BH}$), and association of the halide ion to the metal complex, or ''halogenophilicity'' ($K_X$) (Scheme 2).[22]

The relationship between several of these individual reactions and the overall position of the ATRP equilibrium has been clearly demonstrated in several studies. Alkyl halide bond dissociation energies for a series of ATRP monomers/initiators were found to correlate well with measured values of $K_{ATRP}$.[23] Additionally, $K_{ATRP}$ and $E_{1/2}$ for a series of $Cu^{I}$ complexes with different ligands were correlated, which illustrates that catalyst activity is dependent upon the reducing power of the complex.[24,25] These observations further indicate that under ideal conditions, where the predominant reactions in ATRP are those illustrated in Schemes 1 and 2, one can appropriately choose the catalyst/conditions for a given polymerization with a thorough understanding of these reactions. As an example, it is demonstrated herein how appropriate polymerization conditions can be selected in protic media with knowledge of $K_X$.

However, conducting ATRP with the catalyst at very low concentration can present new challenges. In many cases, competitive equilibria that could previously be neglected must now be considered as they may affect the position of the ATRP equilibrium. For example, ligands that are weakly bound to the metal ions may dissociate or be displaced by monomer or solvent, resulting in a new catalyst complex with a different value of $K_{ATRP}$. Such competitive equilibria and their relevance to catalyst selection are now discussed.

## Dissociation of the ATRP Catalyst

### *Dissociation Upon Dilution*

Several factors should be considered when selecting the appropriate ligand for ATRP,

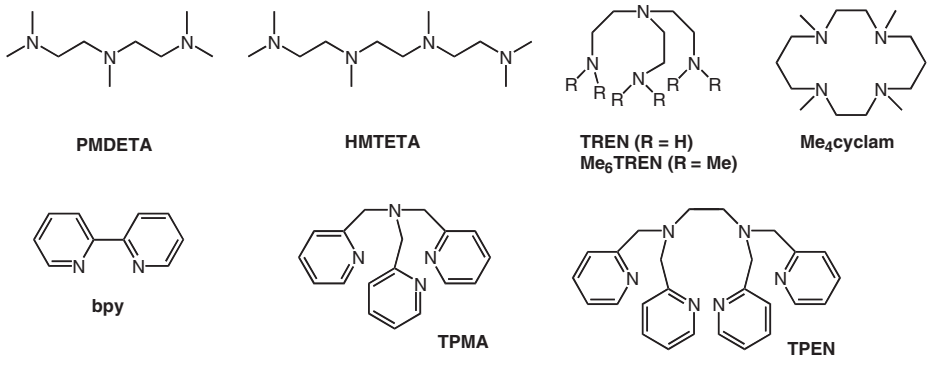


***Figure 1.***
N-based ligands used in ATRP.

 

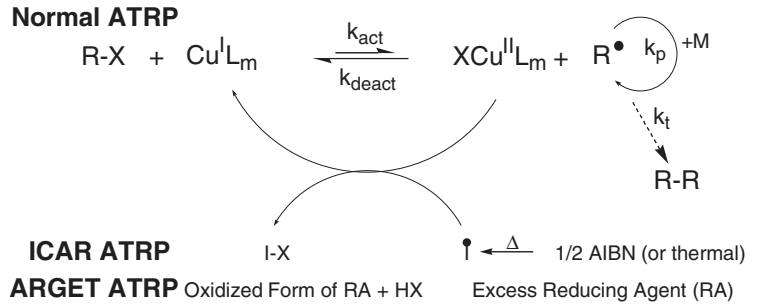


***Scheme 1.***
Representation of ATRP equilibrium.

especially for very dilute systems with respect to the catalyst. First, the catalyst should not dissociate appreciably at the low concentration used in processes such as ARGET or ICAR. The fraction of non-dissociated complex depends upon its stability ($\beta^j$; for definition, *vide infra*, eq (3)) and the dilution. If $[Cu^jL]_0$ ($j$ is the copper oxidation state and L is the ligand) is the initial concentration of catalyst, this fraction is given by eq (1).

$$\frac{[Cu^jL]}{[Cu^jL]_0} = 1 - \frac{\sqrt{1+4\beta^j[Cu^jL]_0}-1}{2\beta^j[Cu^jL]_0} \qquad (1)$$

Figure 2 shows the dependence (1), according to which, if 90% of the catalyst should remain in solution at a total concentration of $10^{-5}$ M (the low limit for ARGET or ICAR), the catalyst should have a stability constant larger than $10^7$. This is true for both the $Cu^I$ and $Cu^{II}$ states of the catalyst. From this point of view, ligands commonly employed under normal ATRP conditions such as PMDETA, where $\beta^I < 10^8$ at room temperature,[26] are not suitable for ARGET or ICAR ATRP.

$$Cu^IL_m \overset{K_{ET}}{\rightleftharpoons} Cu^{II}L_m + e^{\ominus}$$
$$X^\bullet + e^{\ominus} \overset{K_{EA}}{\rightleftharpoons} X^{\ominus}$$
$$R\text{-}X \overset{K_{BH}}{\rightleftharpoons} R^\bullet + X^\bullet$$
$$X^{\ominus} + Cu^{II}L_m \overset{K_X}{\rightleftharpoons} XCu^{II}L_m$$
$$K_{ATRP} = \frac{[R^\bullet][XCu^{II}L_m]}{[RX][Cu^IL_m]} = K_{BH}K_{EA}K_XK_{ET}$$

***Scheme 2.***
Components of the ATRP equilibrium.[22]

Most of the stability constants reported in literature have been determined at room temperature. However, ATRP is often carried out at elevated temperatures, at which the stability of the $Cu^I$ and $Cu^{II}$ complexes decreases, and therefore their dissociation becomes more pronounced. The thermochemistry of polyamine complexes of metal ions, including $Cu^{II}$, has been extensively studied.[27] The enthalpies of formation of $Cu^{II}$ complexes of polyamines in aqueous solution are in the range of $-40$ to $-80$ kJ mol$^{-1}$. A temperature increase from 25 to 110 °C should lead to a decrease in the stability constant by 2–3 orders of magnitude. The dependence of $\beta^{II}$ for the $Cu^{II}$ complexes of PMDETA,[28] TREN,[29] $Me_6$TREN,[28] TPMA,[30,31] and TPEN[30,31] on temperature is presented in Figure 3.

### *Loss of Deactivator*

ATRP reactions in aqueous solvents are usually fast, even at ambient temperature, and the polymerizations are accelerated as the amount of water in the solvent is increased. This could be due to the effect of water or similar protic solvents on $k_p$, $K_{ATRP}$, and/or deactivator concentration $[XCu^{II}L_m]$. The solvent can also change the nature of the catalytic species. Specific solvation of

 

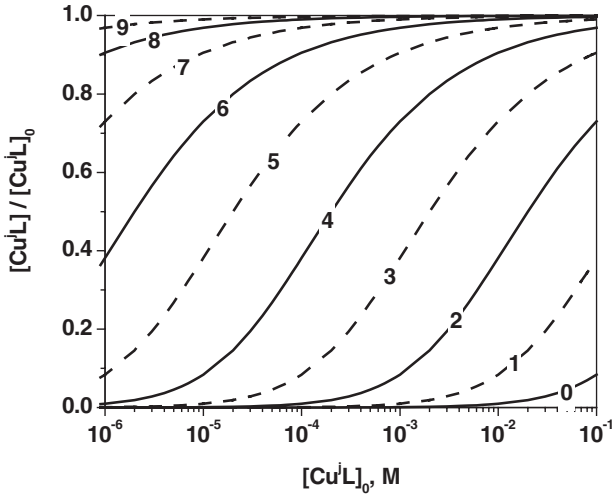


***Figure 2.***
Dependence of remaining, non-dissociated complex as a function of its initial concentration and its stability ($\log\beta^i$ is shown at each curve).

some polar monomers able to form hydrogen bonds with protic solvents does indeed lead to a small increase in $k_p$.[32–34] It was demonstrated[35] that copper-based ATRP deactivators ($XCu^{II}L_m$) are relatively unstable in protic media and tend to dissociate forming the complex $Cu^{II}L_m$ that cannot deactivate radicals. The concentration of deactivator actually present in the system depends upon the value of the halogenophilicity of the $Cu^{II}$ complex, $K_X$, and upon the total concentrations of $Cu^{II}$ complexes and halide ions, according to eq (2) (charges are omitted for simplicity).

$$\left[XCu^{II}L_m\right] = \frac{F - \sqrt{F^2 - 4K_X^2\left[Cu^{II}\right]_{tot}[X]_{tot}}}{2K_X} \quad (F \equiv 1 + K_X\left[Cu^{II}\right]_{tot} + K_X[X]_{tot}) \qquad (2)$$

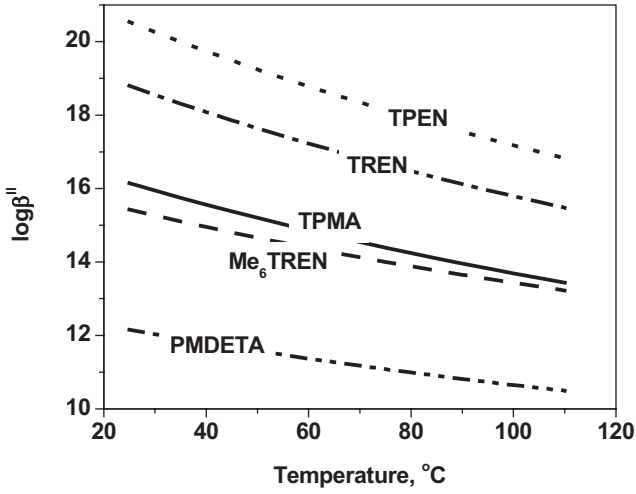


***Figure 3.***
Stability of $Cu^{II}$ complexes with N-based ligands in aqueous solution as a function of temperature.

 

The value of $K_X$ is lower in protic media than in "conventional" solvents. Typical values of $K_X$ in aprotic solvents (hydrocarbons, ethers, ketones, DMF, etc.) are on the order of $10^4$–$10^5$ $M^{-1}$,[36] whereas in protic solvents, these values are two or more orders of magnitude lower (10–$10^3$ $M^{-1}$).[35] Knowledge of the precise values of $K_X$ is crucially important, for it determines both the ATRP catalyst activity (Scheme 2) and the amount of deactivator present in the system (eq (2)) and therefore the degree of polymerization control.[37] The equilibrium constant of halide anion coordination can be measured by spectroscopic means,[38] as described in the literature for bpy-based ATRP deactivators in several protic solvents.[35] The refined values can be easily determined using programs such as Hyperquad.[39] The halogenophilicity of $[Cu^{II}(bpy)_2]^{2+}$ towards both $Br^-$ and $Cl^-$ was studied in various water-containing mixed solvents, and it was shown that in all cases the values of $K_X$ decreased significantly as the amount of water in the mixtures increased (Figure 4).[35,40]

Thus, dissociation of the $XCu^{II}L_m$ complex is very pronounced in protic media, particularly in water-rich solvents, and the lower deactivator concentration leads to increased polydispersity.[41]

There are three general ways to improve the control over polymerization in protic media: i) select ATRP catalysts that possess high values of $K_X$ (this value should depend upon the nature of the ligand L and the metal), ii) employ catalyst containing large initial amounts of deactivator (sometimes up to 80 mol % of the total catalyst), or iii) add extra halide salts to the system. The utility of the last two methods has been demonstrated.[35,42,43]

## Conditional Stability Constants and Catalyst Destabilization by Competitive Complexation

In ATRP, various processes may interfere with the formation of the catalyst, both in the lower and higher oxidation states, resulting in a decrease in the corresponding stability constants. Typical side reactions include formation of additional complexes of the central atom with the solvent, monomer or other reaction components and the protonation of the ligand (especially important when the ligand is a

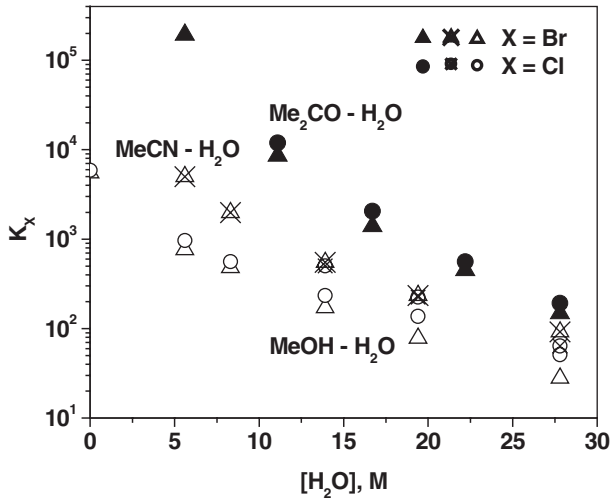


***Figure 4.***
Dependence of halogenophilicity, $K_{Br}$ or $K_{Cl}$, of $[Cu^{II}(bpy)_2]^{2+}$ upon the concentration of water in mixtures of acetone (filled symbols), acetonitrile (crossed symbols), and methanol (open symbols) with water.[40]

 

relatively strong base). The complex formation of interest is now characterized by an apparent or, as Schwarzenbach[44] termed it, *conditional stability constant*, denoted by $K^*$ (stepwise) or $\beta^*$ (overall stability constant). Conditional stability constants have been widely utilized in analytical chemistry and have proven very useful for the understanding of equilibrium reactions in complex systems containing various metal ions and ligands.[44–49]

Consider the formation of the complex CuL (oxidation state is omitted for simplicity) in the presence of acids, which can protonate the ligand L yielding HL, $H_2L, \ldots, H_rL$, and in the presence of another ligand L′. The latter can react with the metal center giving the complexes CuL′, $CuL'_2, \ldots, CuL'_p$. The stability constants of the complexes formed between Cu and the ligand L′ are designated as $\beta_{1,L'}$, $\beta_{2,L'}$, …, $\beta_{p,L'}$ and acidity constants of the protonated ligand L are $K_{a,1}$, $K_{a,2}$, …, $K_{a,r}$:

$$\beta_{k,L'} = \frac{[CuL'_k]}{[Cu][L']^k} \quad (k = 1, 2, \ldots, p) \tag{3}$$

$$K_{a,h} = \frac{[H][H_{r-h}L]}{[H_{r-h+1}L]} \quad (h = 1, 2, \ldots, r) \tag{4}$$

The conditional stability constant of the complex of interest CuL is defined using the concentrations of the metal and ligand in all species except CuL, rather than only the concentrations of free metal and ligand:

$$\begin{aligned}\beta^*(CuL) &= \frac{[CuL]}{([Cu]_{tot} - [CuL])([L]_{tot} - [CuL])} \\ &= \frac{[CuL]}{([Cu] + [CuL'] + \ldots + [CuL'_p])([L] + [HL] + \ldots + [H_rL])}\end{aligned} \tag{5}$$

Schwarzenbach[44] also introduced *alpha-coefficients*, which are related to the extent to which side reactions occur, including the formation of complexes as well as ligand protonation). These coefficients are defined as follows:

$$\begin{aligned}\alpha_{Cu} &\equiv \frac{[Cu]_{tot} - [CuL]}{[Cu]} \\ &= \frac{[Cu] + [CuL'] + \ldots + \left[CuL'_p\right]}{[Cu]} \\ &= 1 + \frac{[CuL']}{[Cu]} + \ldots + \frac{\left[CuL'_p\right]}{[Cu]} \\ &= 1 + \beta_{1,L'}[L'] + \ldots + \beta_{p,L'}[L']^p \\ &= 1 + \sum_{k=1}^{p} \beta_{k,L'}[L']^k\end{aligned} \tag{6}$$

$$\begin{aligned}\alpha_L &\equiv \frac{[L]_{tot} - [MtL]}{[L]} \\ &= \frac{[L] + [HL] + \ldots + [H_rL]}{[L]} \\ &= 1 + \frac{[HL]}{[L]} + \ldots + \frac{[H_rL]}{[L]} \\ &= 1 + \sum_{h=1}^{r} \frac{[H]^h}{\prod_{g=r-h+1}^{r} K_{a,g}}\end{aligned} \tag{7}$$

In the absence of side reactions, the alpha-coefficients are equal to unity, but can become large if side reactions occur, depending on the stability of the complexes CuL′, $CuL'_2, \ldots, CuL'_p$, the strength of the acids HL, $H_2L$, …, $H_rL$, and the concentrations of the ligand L′ and protons. Equation (5) can be rewritten as:

$$\beta^*(CuL) = \frac{[CuL]}{[Cu][L]} \frac{1}{\alpha_{Cu}\alpha_L} = \frac{\beta(CuL)}{\alpha_{Cu}\alpha_L} \tag{8}$$

Organic compounds with double or triple carbon-carbon bonds are known to form complexes with various transition metals, including copper.[50–53] A number of $Cu^I$–olefin complexes have been studied and

 

*Table 1.*
Formation constants of Cu(PMDETA)($\pi$-M)$^+$ complexes[a)] [56]

| Monomer | $K_M$/M$^{-1}$ | $\Delta H^\circ$/kJ mol$^{-1}$ | $\Delta S^\circ$/J mol$^{-1}$ K$^{-1}$ |
|---|---|---|---|
| **MA** | 760 | −30.2 (±2.8) | −46.0 (±9.4) |
| **Sty** | 250 | −22.7 (±0.4) | −30.5 (±1.6) |
| **Oct** | 320 | −26.2 (±0.8) | −40.0 (±2.8) |
| **MMA** | 6 | −25.4 (±0.5) | −70.2 (±1.8) |

a) Thermodynamic information was calculated from formation constants measured over a 40 °C range; $K_M$ is reported at 25 °C.

even structurally characterized, and some of them have considerable stability.[54] The coordination of several monomers such as styrene, 1-octene, methyl acrylate, and methyl methacrylate to the Cu$^{I}$/PMDETA complex with non-coordinating anions was recently reported.[55,56] Formation constants for these complexes (Table 1) were determined from variable temperature $^1$H NMR experiments monitoring the free and complexed vinyl proton resonances. The complexation is comparatively weak relative to halide ions and nitrogen based ligands, but at large monomer concentrations and especially at low catalyst concentration it may lead to a destabilization of the catalyst. These effects are compounded with difunctional monomers such as 4-vinylpyridine, whose coordination to Cu-based ATRP catalysts has been studied by electrochemistry.[57]

In the special case of ATRP of acidic monomers, or in processes where acid is generated throughout the polymerization as in ARGET ATRP,[17] significant ligand protonation may take place, reflected by a large $\alpha_L$ value. Figure 5 shows the dependence of $\beta^{II,*}$ (eq (8)) upon the medium pH for the Cu$^{II}$ complexes of various N-based ligands, for which the protonation constants have been measured, including $Me_4$cyclam,[58] HMTETA,[58] $Me_6$TREN,[58] PMDETA,[26] and TPMA.[59]

The complexes of basic ligands, especially when their stability constants in the absence of protonation are relatively low (e.g., Cu$^{II}$ complex of HMTETA) are very much destabilized in acidic media. The complex of the basic $Me_6$TREN is markedly more destabilized in acidic media than the complex of the less basic ligand TPMA. From this point of view, TPMA is a promising candidate for ARGET and ICAR reactions. The complex of $Me_6$TREN can also be used but in conjunction with excess base (or excess free ligand) that will trap the acid generated during the redox process.[17] In the presence of side reaction, the amount of catalyst actually present in the system

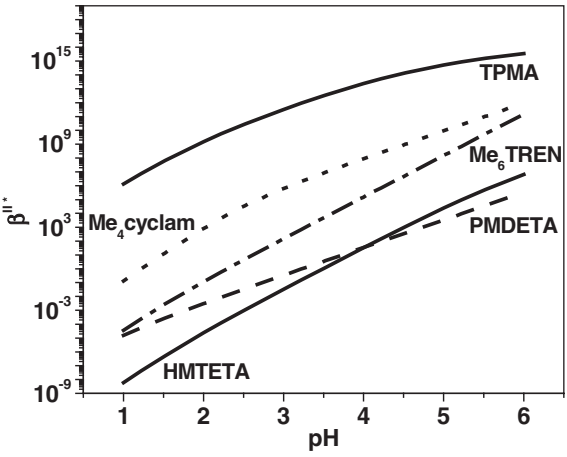


*Figure 5.*
Dependence of the conditional stability constant of Cu$^{II}$L complexes used as ATRP catalysts on pH of the medium.

 

can be calculated using eq (1), but with $\beta^{j,*}$ instead of $\beta^{j}$.

Coordination of alkyl halides to $Cu^{I}$ complexes may also occur;[60,61] the $Cu^{I}(PPh_3)_3Cl$ complex of benzyl iodide was even isolated in the solid state.[61] However, there is not enough evidence that these reactions contribute to the destabilization of the ATRP catalyst.

## Competitive Equilibria Involving Electron Transfer

### *Reduction/Oxidation of Organic Radicals*

Inner sphere electron transfer is generally considered the predominant redox process that occurs in ATRP. However, outer sphere electron transfer (OSET) may also occur between organic radicals and transition metal complexes whereby growing radicals are oxidized to carbocations by $Cu^{II}$ or reduced to carbanions by $Cu^{I}$.[62] The extent to which OSET occurs in ATRP is dictated by the relative redox potentials of the species involved.

The redox potentials of various organic radicals have been measured[63–65] and it is well-established that radicals with α-electron-withdrawing substituents (cyano, carboxy, etc.) are rather electrophilic or oxidizing. In other words, the radicals formed during the ATRP of acrylonitrile or acrylates are likely to oxidize very reducing (i.e., very active) ATRP catalysts. Active catalysts have been observed to reduce electrophilic radicals to their corresponding carbanions, and it is this side reaction that is believed responsible for limiting the attainable conversion and molecular weight of polyacrylonitrile prepared by ATRP.[66–68] Similarly, limited conversions were attained in the ATRP of n-butyl acrylate mediated by an exceptionally active and reducing Cu-based catalyst derived from dimethyl cross-bridged cyclam.[69] Interestingly, the application of ICAR ATRP under high dilution may actually work to minimize OSET between electrophilic radicals and extremely reducing Cu catalysts. The majority of the Cu catalyst under these conditions is present as the higher oxidation state complex, in contrast to normal ATRP, where the majority of the catalyst is in the lower oxidation state. Therefore, under ICAR conditions, very little $Cu^{I}$ would be available to reduce such radicals to carbanions.

The $Cu^{II}$ deactivator can also catalyze electron transfer reactions that result in a loss of halide chain end functionality during the ATRP of styrenic type monomers. HBr can be evolved from alkyl radicals and $Cu^{II}Br_2$/L to give unsaturated chain ends and $Cu^{I}$Br/L.[70–72] This side reaction has thwarted the production of well-defined high molecular weight polystyrene in ATRP, with upper limits between 30,000 and 50,000 g $mol^{-1}$. However, the use of ARGET and ICAR ATRP that minimize Cu concentrations could allow high molecular weight polymers to be produced as side reactions between the chain end and the catalyst should be minimized. Indeed, high molecular weight styrene (co)polymers (200,000 g $mol^{-1}$) with narrow molecular weight distributions ($M_w/M_n < 1.2$) have been synthesized with just 10 ppm of Cu catalyst using these new techniques.[73]

### *Radical Coordination*

One and two electron oxidative addition processes that involve electron transfer between alkyl radicals and transition metal species have been exploited in organic synthesis for many years.[74] These reactions can ultimately result in the formation of stable metal-alkyl complexes. The formation of such organometallic species during ATRP would have several implications on the role of the catalyst. The relative bond dissociation energies of the the Mt–R, Mt–X, and R–X bonds would ultimately dictate whether polymerization would be inhibited by the formation of a Mt–R bond, whether initiation efficiency might just be reduced, or whether the entire polymerization could be mediated through the reversible formation of such a Mt–R bond (as in stable free radical polymerization, or SFRP).[75]

 

While there is currently no experimental evidence that suggests any organometallic $Cu^{II}$–R species are formed during Cu-mediated ATRP,[76] several recent studies have suggested that certain $Mo^{III}$ complexes initiate polymerization from alkyl halide ATRP initiators but then proceed to mediate polymerization through the reversible formation of a $Mo^{IV}$–R species as in SFRP.[77] This is a particularly important mechanistic observation in light of the new ICAR and ARGET processes. As polymerizations mediated by SFRP require a stoichiometric amount of metal species per polymer chain, such a Mo catalyst would not be expected to successfully mediate polymerization under ARGET or ICAR ATRP conditions where sub-stoichiometric amounts of the metal species are employed.

*Disproportionation*

Compounds of $Cu^{I}$ are able to participate in a bimolecular redox process termed *disproportionation*, which yields a $Cu^{II}$ compound and elemental copper according to eq (9).

$$Cu^{I} + Cu^{I} \overset{K_{disp}}{\rightleftharpoons} Cu^{II} + Cu^{0} \qquad (9)$$

While conducting ATRP in aqueous media has both economic and environmental advantages, the equilibrium constant for disproportionation of $Cu^{I}$ is very large in pure water ($K_{disp} = 10^6$), resulting in a loss of the $Cu^{I}$ activator.

However, disproportionation can be suppressed with the choice of appropriate ligands based on knowledge of the overall stability constants of the complexes for the $Cu^{I}$ and $Cu^{II}$ oxidation states ($\beta_j^{I}$ and $\beta_j^{II}$).[14,26,37] The equilibrium constant of disproportionation is changed in the presence of complexing ligands to a new conditional value, $K^*_{disp}$, which is related to the concentration of ligand and its overall stability according to eq (10).

$$K*_{disp} = \frac{1+\sum_{j=1}^{m} \beta_j^{II}[L]^j}{\left(1+\sum_{j=1}^{m} \beta_j^{I}[L]^j\right)^2} K_{disp} \qquad (10)$$

The activity of a catalyst with ligands forming 1:1 complexes with copper ions is proportional to the relative binding constants of the ligand to the higher and lower oxidation state of the metal species ($\beta^{II}/\beta^{I}$).[37] The tendency of a $Cu^{I}$ complex to disproportionate depends on the ratio $\beta^{II}/((\beta^{I})^2[L])$, as expressed in eq 10. Knowledge of these stability constants in aqueous media can therefore be used to screen catalysts that will have both appropriately high activity in ATRP but will also be stable towards disproportionation.[14] For example, knowing the binding constants[78] of the two oxidation states of Cu with bpy,[79] PMDETA,[26] and TPMA,[59] one can predict that while $Cu^{I}$ complexes with bpy would not be very active in ATRP, they would be stable towards disproportionation; $Cu^{I}$(PMDETA) would be more active, but would not be stable towards disproportionation; and $Cu^{I}$(TPMA) would both be active and stable towards disproportionation.

## Conclusions

Several of the side reactions encountered in ATRP, such as catalyst dissociation and competitive monomer complexation, become more pronounced when the catalyst is used at very low concentration. These and other undesirable reactions, such as catalyst disproportionation or radical coordination to the metal center, can often be avoided with the appropriate choice of transition metal and complexing ligands. Still other side reactions, such as electron transfer between alkyl radicals and the metal catalysts, can actually be minimized by using low catalyst concentrations. This work aimed to demonstrate that with a thorough knowledge of the components of the ATRP equilibrium and a general awareness of potential side reactions under certain conditions, ATRP catalysts can be rationally selected and conditions optimized for very diverse polymerization systems.

*Acknowledgements:* The authors thank the members of the ATRP/CRP consortia at Car-

 

negie Mellon University and NSF (grants CHE-0405627 and DMR-0549353) for funding. WAB thanks the Harrison Legacy Dissertation Fellowship for financial support.

[1] J.-S. Wang, K. Matyjaszewski, *J. Am. Chem. Soc.* **1995**, *117*, 5614.
[2] K. Matyjaszewski, Ed., *Controlled Radical Polymerization (ACS Symp. Ser. 685)*; ACS, Washington, DC, 1998.
[3] K. Matyjaszewski, Ed., *Controlled/Living Radical Polymerization. Progress in ATRP, NMP, and RAFT (ACS Symp. Ser. 768)*; ACS, Washington, DC, 2000,
[4] K. Matyjaszewski, J. Xia, *Chem. Rev.* **2001**, *101*, 2921.
[5] V. Coessens, T. Pintauer, K. Matyjaszewski, *Prog. Polym. Sci.* **2001**, *26*, 337.
[6] K. Matyjaszewski, T. P. Davis, Eds., *Handbook of Radical Polymerization*; Wiley, Hoboken, 2002,
[7] K. Matyjaszewski, Ed., *Advances in Controlled/Living Radical Polymerization (ACS Symp. Ser. 854)*; ACS, Washington, DC, 2003,
[8] K. Matyjaszewski, *Macromol. Symp.* **2003**, *195*, 25.
[9] K. Matyjaszewski, *Prog. Polym. Sci.* **2005**, *30*, 858.
[10] K. Matyjaszewski, Ed., *Controlled/Living Radical Polymerization. From Synthesis to Materials (ACS Symp. Ser. 944)*; ACS, Washington, DC, 2006.
[11] K. Matyjaszewski, J. Spanswick, *Mat. Today.* **2005**, *8*(3), 26.
[12] S. C. Hong, H.-J. Paik, K. Matyjaszewski, *Macromolecules.* **2001**, *34*, 5099.
[13] Y. Shen, H. Tang, S. Ding, *Prog. Polym. Sci.* **2004**, *29*, 1053.
[14] N. V. Tsarevsky, K. Matyjaszewski, *J. Polym. Sci.: Part A: Polym. Chem.* **2006**, *44*, 5098.
[15] W. Jakubowski, K. Matyjaszewski, *Angew. Chem., Int. Ed.* **2006**, *45*, 4482.
[16] W. Jakubowski, K. Min, K. Matyjaszewski, *Macromolecules.* **2006**, *39*, 39.
[17] K. Matyjaszewski, W. Jakubowski, K. Min, W. Tang, J. Huang, W. A. Braunecker, N. V. Tsarevsky, *Proc. Natl. Acad. Sci. USA.* **2006**, *103*, 15309.
[18] M. Kamigaito, T. Ando, M. Sawamoto, *Chem. Rev.* **2001**, *101*, 3689.
[19] H. Fischer, *J. Polym. Sci.: Part A: Polym. Chem.* **1999**, *37*, 1885.
[20] H. Fischer, *Chem. Rev.* **2001**, *101*, 3581.
[21] W. Tang, N. V. Tsarevsky, K. Matyjaszewski, *J. Am. Chem. Soc.* **2006**, *128*, 1598.
[22] T. Pintauer, B. McKenzie, K. Matyjaszewski, *ACS Symp. Ser.* **2003**, *854*, 130.
[23] M. B. Gillies, K. Matyjaszewski, P.-O. Norrby, T. Pintauer, R. Poli, P. Richard, *Macromolecules.* **2003**, *36*, 8551.
[24] J. Qiu, K. Matyjaszewski, L. Thouin, C. Amatore, *Macromol. Chem. Phys.* **2000**, *201*, 1625.
[25] K. Matyjaszewski, B. Goebelt, H.-j. Paik, C. P. Horwitz, *Macromolecules.* **2001**, *34*, 430.
[26] N. Navon, G. Golub, H. Cohen, P. Paoletti, B. Valtancoli, A. Bencini, D. Meyerstein, *Inorg. Chem.* **1999**, *38*, 3484.
[27] P. Paoletti, L. Fabbrizzi, R. Barbucci, *Inorg. Chim. Acta Rev.* **1973**, *7*, 43.
[28] P. Paoletti, M. Ciampolini, *Inorg. Chem.* **1967**, *6*, 64.
[29] P. Paoletti, M. Ciampolini, L. Sacconi, *J. Chem. Soc.* **1963**, 3589.
[30] F. Wenk, G. Anderegg, *Chimia.* **1970**, *24*, 427.
[31] G. Anderegg, E. Hubmann, N. G. Podder, F. Wenk, *Helv. Chim. Acta.* **1977**, *60*, 123.
[32] V. F. Gromov, P. M. Khomikovskii, *Russ. Chem. Rev.* **1979**, *48*, 1040.
[33] V. F. Gromov, E. V. Bune, E. N. Teleshov, *Russ. Chem. Rev.* **1994**, *63*, 507.
[34] S. Beuermann, M. Buback, *Prog. Polym. Sci.* **2002**, *27*, 191.
[35] N. V. Tsarevsky, T. Pintauer, K. Matyjaszewski, *Macromolecules.* **2004**, *37*, 9768.
[36] S. Ishiguro, L. Nagy, H. Ohtaki, *Bull. Chem. Soc. Jpn.* **1987**, *60*, 2053.
[37] N. V. Tsarevsky, W. Tang, S. J. Brooks, K. Matyjaszewski, *ACS Symp. Ser.* **2006**, *944*, 56.
[38] W. A. E. McBryde, *Talanta.* **1974**, *21*, 979.
[39] P. Gans, A. Sabatini, A. Vacca, *Talanta.* **1996**, *43*, 1739.
[40] N. V. Tsarevsky, B. McKenzie, W. Tang, K. Matyjaszewski, *Polym. Prepr.* **2005**, *46*(*2*), **482.**
[41] K. Matyjaszewski, C.-H. Lin, *Makromol. Chem., Macromol. Symp.* **1991**, *47*, 221.
[42] S. Perrier, S. P. Armes, X. S. Wang, F. Malet, D. M. Haddleton, *J. Polym. Sci.: Part A: Polym. Chem.* **2001**, *39*, 1696.
[43] D. Paneva, L. Mespouille, N. Manolova, P. Degee, I. Rashkov, P. Dubois, *Macromol. Rapid Commun.* **2006**, *27*, 1489.
[44] G. Schwarzenbach, *Die Komplexometrische Titration*, 2nd ed. Enke, Stuttgart, **1956**,
[45] H. A. Flaschka, *EDTA Titrations*; Wiley, New York, 1959,
[46] A. Ringbom, *Complexation in Analytical Chemistry*; Interscience, New York, 1963,
[47] A. Ringbom, E. Still, *Anal. Chim. Acta.* **1972**, *59*, 143.
[48] A. Ringbom, L. Harju, *Anal. Chim. Acta.* **1972**, *59*, 33.
[49] A. Ringbom, L. Harju, *Anal. Chim. Acta.* **1972**, *59*, 49.
[50] M. A. Bennett, *Chem. Rev.* **1962**, *62*, 611.
[51] R. Jones, *Chem. Rev.* **1968**, *68*, 785.
[52] F. R. Hartley, *Chem. Rev.* **1973**, *73*, 163.
[53] S. D. Ittel, J. A. Ibers, *Adv. Organomet. Chem.* **1976**, *14*, 33.
[54] Q. Ye, X.-S. Wang, H. Zhao, R.-G. Xiong, *Chem. Soc. Rev.* **2005**, *34*, 208.
[55] W. A. Braunecker, T. Pintauer, N. V. Tsarevsky, G. Kickelbick, K. Matyjaszewski, *J. Organometal. Chem.* **2005**, *690*, 916.

 

[56] W. A. Braunecker, N. V. Tsarevsky, T. Pintauer, R. G. Gil, K. Matyjaszewski, *Macromolecules*. **2005**, *38*, 4081.
[57] N. V. Tsarevsky, W. A. Braunecker, S. J. Brooks, K. Matyjaszewski, *Macromolecules*. **2006**, *39*, 6817.
[58] G. Golub, A. Lashaz, H. Cohen, P. Paoletti, A. Bencini, B. Valtancoli, D. Meyerstein, *Inorg. Chim. Acta*. **1997**, *255*, 111.
[59] E. A. Ambundo, M.-V. Deydier, A. J. Grall, N. Aguera-Vega, L. T. Dressel, T. H. Cooper, M. J. Heeg, L. A. Ochrymowycz, D. B. Rorabacher, *Inorg. Chem.* **1999**, *38*, 4233.
[60] W. Z. Peters, *Anorg. Allgem. Chem*. **1914**, *89*, 191.
[61] K. Wada, H. Hashimoto, *Bull. Chem. Soc. Jpn*. **1969**, *42*, 562.
[62] K. Matyjaszewski, *Macromol. Symp*. **1998**, *134*, 105.
[63] D. Griller, D. D. M. Wayner, *Pure & Appl. Chem.* **1989**, *61*, 717.
[64] D. D. M. Wayner, A. Houmam, *Acta Chem. Scand.* **1998**, *52*, 377.
[65] K. Daasbjerg, S. U. Pedersen, H. Lund, In *General Aspects of the Chemistry of Radicals*; Z. B. Alfassi, Ed., Wiley, Chichester, 1999, pp 385–427.
[66] K. Matyjaszewski, S. M. Jo, H.-j. Paik, S. G. Gaynor, *Macromolecules*. **1997**, *30*, 6398.
[67] K. Matyjaszewski, S. M. Jo, H.-j. Paik, D. A. Shipp, *Macromolecules*. **1999**, *32*, 6431.
[68] C. Tang, T. Kowalewski, K. Matyjaszewski, *Macromolecules*. **2003**, *36*, 1465.
[69] N. V. Tsarevsky, W. A. Braunecker, W. Tang, S. J. Brooks, K. Matyjaszewski, G. R. Weisman, E. H. Wong, *J. Mol. Catal. A: Chem*. **2006**, *257*, 132.
[70] J.-F. Lutz, K. Matyjaszewski, *Macromol. Chem. Phys*. **2002**, *203*, 1385.
[71] J.-F. Lutz, K. Matyjaszewski, *J. Polym. Sci.: Part A: Polym. Chem*. **2005**, *43*, 897.
[72] K. Matyjaszewski, K. Davis, T. E. Patten, M. Wei, *Tetrahedron*. **1997**, *53*, 15321.
[73] J. Pietrasik, H. Dong, K. Matyjaszewski, *Macromolecules*. **2006**, *39*, 6384.
[74] A. Fuerstner, N. Shi, *J. Am. Chem. Soc*. **1996**, *118*, 12349.
[75] R. Poli, *Angew. Chem. Int. Ed*. **2006**, *45*, 5058.
[76] K. Matyjaszewski, B. E. Woodworth, *Macromolecules*. **1998**, *31*, 4718.
[77] E. Le Grognec, J. Claverie, R. Poli, *J. Am. Chem. Soc.* **2001**, *123*, 9513.
[78] http://www.acadsoft.co.uk/scdbase/scdbase.htm
[79] *Stability Constants of Metal-Ion Complexes. Supplement No 1. Special Publication No 25*; The Chemical Society, London, 1971.

 

# Kinetic Aspects of RAFT Polymerization

*Philipp Vana*

**Summary:** In this short review, selected experimental approaches for probing the mechanism and kinetics of RAFT polymerization are highlighted. Methods for studying RAFT polymerization via varying reaction conditions, such as pressure, temperature, and solution properties, are reviewed. A technique for the measurement of the RAFT specific addition and fragmentation reaction rates via combination of pulsed-laser-initiated RAFT polymerization and μs-time-resolved electron spin resonance (ESR) spectroscopy is detailed. Mechanistic investigations using mass spectrometry are exemplified on dithiobenzoic-acid-mediated methyl methacrylate polymerization.

**Keywords:** kinetics (polym.); laser-induced polymers; living polymerization; mass spectrometry; reversible addition fragmentation chain transfer (RAFT)

## Introduction

The reversible addition-fragmentation chain transfer (RAFT) polymerization[1] is one of the leading living/controlled radical polymerization methods and allows for the formation of polymers with predefined molecular weights, narrow molecular weight distributions, distinct end-group functionalities, and complex topologies.[2] The RAFT process is highly tolerant of functional groups and can be successfully performed in a broad variety of solvents, including aqueous solutions. Due to this unrivalled versatility, RAFT polymerization becomes an increasingly popular technique for advanced macromolecular design. Besides the rapid development of synthetic applications, a lot of work has been directed toward a profound understanding of the mechanism and kinetics of RAFT polymerization in order to provide essential information for directed RAFT agent design as well as for choosing appropriate reaction conditions.[3] By applying the insights that have been gathered by such fundamental studies, RAFT has made substantial progress during recent times in terms of creating novel polymeric materials.[4] It is the objective of this short review to highlight some of recent experimental approaches performed at the University of Göttingen, by which the kinetics and mechanism of RAFT polymerization were probed, and to detail some key results that were obtained by the presented strategies.!

### The Basic Mechanism of RAFT

RAFT polymerization proceeds via two equilibria (see Scheme 1), which are superimposed on a conventional radical polymerization. During the *pre-equilibrium*, which constitutes the chain initiation of the living process, the initial RAFT agent **1** is consumed. The recurring reversible chain transfer events to the polymeric dithio-compound **3** induce a *main equilibrium* between dormant and living species, which results in living/controlled polymerization behavior. The controlling agents typically are thicarbonyl-thio-compounds, Z–C(=S)S–R, which comprise two characteristic moieties, that is, the reinitiating R-group – also referred to as leaving group – and the Z-group, which stabilizes the

Institut für Physikalische Chemie, Georg-August-Universität Göttingen, Tammannstraße 6, D-37077 Göttingen, Germany
E-mail: pvana@uni-goettingen.de

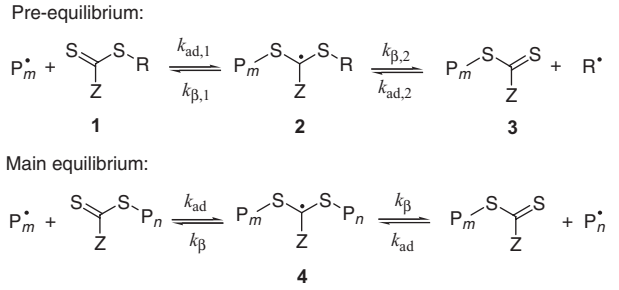


***Scheme 1.***
Basic reaction steps of the RAFT process.

radical center of the intermediate RAFT radical **2** and **4**.

The RAFT reaction rates are described by addition rate coefficients, $k_{ad}$, and fragmentation rate coefficients, $k_{\beta}$ (see Scheme 1). The $k_{ad}$ and $k_{\beta}$ values of the asymmetric pre-equilibrium have to be considered individually and as being different from those of the main equilibrium,[5,6] which is symmetrical apart from small differences in the chain length of the participating macroradicals. It should be noted that for the investigations presented in this article, only systems proceeding in the main equilibrium were considered. The value of $k_{ad}$ mainly determines the efficiency of the overall process and the equilibrium constant $K = k_{ad}/k_{\beta}$ governs the stability of the intermediate radical, which impacts the extent of rate retarding side reactions, such as intermediate radical termination.[3] The primal focus of kinetic studies into RAFT is hence the evaluation of these kinetic parameters. Accompanying mechanistic studies, however, which aim at the identification of alternative reaction pathways that are not accounted for in Scheme 1, are of equal importance, because potential side reactions can have a strong impact on the kinetic results obtained from methods that rely on model assumptions[3] and can influence the observable product spectrum that is used as underpinning for kinetic models.[7]

## Probing RAFT Kinetics by Varying Reaction Conditions

In radical polymerization, a multitude of individual reactions are proceeding in parallel, with each of these reactions having distinct dependencies on characteristic reaction parameters, such as pressure, temperature, and solution properties. Varying these parameters of the polymerization process and observing changes in the overall kinetic characteristics, such as rate of polymerization and molecular weight distributions of the generated polymer, is hence an efficient pathway for obtaining information on the individual reaction steps.

Following this approach, RAFT polymerization kinetics at high pressure up to 2 500 bar was studied.[8] Application of high pressure in radical polymerization is especially advantageous for mechanistic investigations, because of the diverse pressure dependencies of the individual rate coefficients: Chemically controlled bimolecular reactions (e.g., propagation) are typically accelerated at higher pressures, whereas diffusion controlled reactions (e.g., termination) proceed at lower rates. The overall effect of pressure in radical polymerization is an acceleration of the polymerization rate, $R_p$. This effect was also observed in chemically initiated cumyl dithiobenzoate (CDB) mediated styrene RAFT polymerizations at 70 °C.[8] The rate of polymerization was deduced from the time-dependent decrease of monomer concentration, which was monitored via online FT-IR spectroscopy. The pressure-induced relative increase in $R_p$ by a factor of about 3 when going from ambient pressure to 2 500 bar was almost identical for conventional and RAFT polymerization, although a pronounced rate retardation effect[3] was

 

observed in the RAFT system. The experimental rate data was adequately described by Eq. (1),[9] which assumes an irreversible cross-termination of intermediate RAFT radicals with propagating radicals, and provided values for the combined parameter $K \cdot k_{t,cross}/k_t$, which serves as quantification of the rate retardation effect.

$$R_p = R_{p,c}\left(1 + 2\frac{k_{t,cross}}{k_t}K[RAFT]_0\right)^{-0.5} \quad (1)$$

$R_{p,c}$ is the conventional polymerization rate without RAFT agent, $k_{t,cross}$ is the cross-termination rate coefficient, and $[RAFT]_0$ is the initial RAFT agent concentration. Rate retardation, i.e., $K \cdot k_{t,cross}/k_t$ $(=(k_{ad}/k_\beta) \cdot (k_{t,cross}/k_t))$, was essentially independent of pressure, which finding was surprising, as an increased addition rate of macroradicals toward the dithioester groups with increasing pressure (similar to propagation) and a decreased rate of the unimolecular intermediate fragmentation may be anticipated. Possible explanations for the independency of $K \cdot k_{t,cross}/k_t$ on pressure include the scenario that the increase of the equilibrium constant $K$ with pressure is compensated by a decrease of $k_{t,cross}/k_t$, i.e., that the termination of the intermediate is suppressed to a larger extent than the reaction between two macroradicals.[8]

With respect to molecular weight control, application of high pressure is highly advantageous for RAFT polymerizations: Figure 1 shows two molecular weight distributions of polystyrene samples from CDB-mediated polymerization with identical peak molecular weights, generated at ambient pressure and at 2 000 bar, respectively, and with all other reaction parameters kept constant. The molecular weight control is significantly enhanced at high pressure, that is, the chain-length distribution is narrower and polymeric material occurring at the low and high molecular weight slopes of the main peak is reduced. The resulting polydispersity indices, *PDI*, are appreciably lowered (see Figure 1).

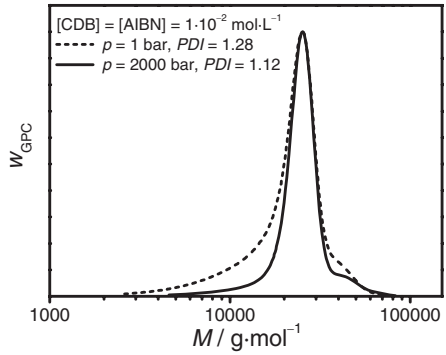


***Figure 1.***
Molecular weight distributions (SEC curves) of polystyrene samples with identical peak molecular weights generated via CDB-mediated styrene bulk polymerization at 70 °C at 1 and 2000 bar, respectively, with all other parameters being kept constant.[8]

Supported by kinetic simulations via PREDICI,[10] this effect could exclusively be attributed to the pressure dependencies of the conventional rate coefficients. Potential pressure dependencies of $k_{ad}$ and $k_\beta$ were found to have only negligible impact on this narrowing. The lowering in polydispersity can mainly be understood in terms of a pronouncedly increased kinetic chain length at high pressure, which is a combined effect of the decreased initiator efficiency and decomposition rate, of the enlarged propagation rate coefficient, and of the decreased termination rate coefficient with increasing pressure. At the beginning of the kinetic chain, that is, at conventional initiation, a small radical is generated, forming a small polymeric RAFT agent **3** after its primary RAFT step. These small species contribute to the broadening on the low molecular weight side of the living polymer peak. At the ending of the kinetic chain, two radicals are terminating, which generates dead polymer that cannot increase its length any longer. In the case of termination by combination, this effect yields polymer at each chain length up to the doubled value of that of the living polymer. It thus becomes evident that with an increase of the kinetic chain length, the beginning and ending events – which both are disturbing the uniform polymer

 

growth – are reduced in their extent relative to propagation events that propel the controlled polymerization.

Further information about the kinetics of the individual RAFT reactions can be obtained via notably changing the reaction temperature. Consequently, the influence of increasing temperature on self-initiated CDB-mediated styrene polymerization between 120 °C and 180 °C was studied by determining full molecular weight distributions of the resulting polymer and by obtaining rate of polymerization data via time-resolved online FT-IR measurement of monomer concentration.[11] In order to compensate for potential side reactions that may broaden the chain-length distribution, high pressure of 1 000 bar was applied, which accelerates the polymerization rate and improves the molecular weight control, as demonstrated above. The increase of average molecular weights with monomer conversion, the shape of the molecular weight distributions, and polydispersity indices well below 1.5 (see Figure 2b on the example of 150 °C) indicated living/controlled behavior even at these high experimental temperatures. The pronounced self-initiation rate at elevated temperatures resulted in the continuous generation of high amounts of chains derived by conventional initiation, which induced a deviation of the linear dependence of number average molecular weight on monomer conversion that is predicted for an ideal living process. In order to probe for livingness in these systems, the peak molecular weights as a good representative for the average molecular weight of the living polymer were evaluated as a function of monomer conversion (see Figure 2a), and adequate linearity for all studied temperatures was found. Neither a substantial decomposition of the dithioester-moieties nor a change in the overall polymerization mechanism, e.g., ionic reactions, was identifiable.[11] The thermal stability of the polymeric RAFT agent is apparently significantly higher than that of the initial low molecular weight dithioesters: Whereas CDB, for instance, is reported to decompose at 120 °C with a half-life time of around 100 min,[12] polymeric RAFT agent is reported to decompose with significant reaction rates only above 180 °C.[13] It should be noted that the overall reaction times for the CDB-mediated self-initiated styrene polymerization at 120 to 180 °C at 1 kbar only took minutes (e.g., 20% monomer conversion after 2 min at 180 °C),[11] that is, the pre-equilibrium period was extremely short and the potentially heat-sensitive RAFT agent was consumed rapidly within seconds.

RAFT polymerization rates were lower than in conventional styrene polymerization at all studied temperatures, signifying a rate retardation effect being operational also at elevated temperature. The extent

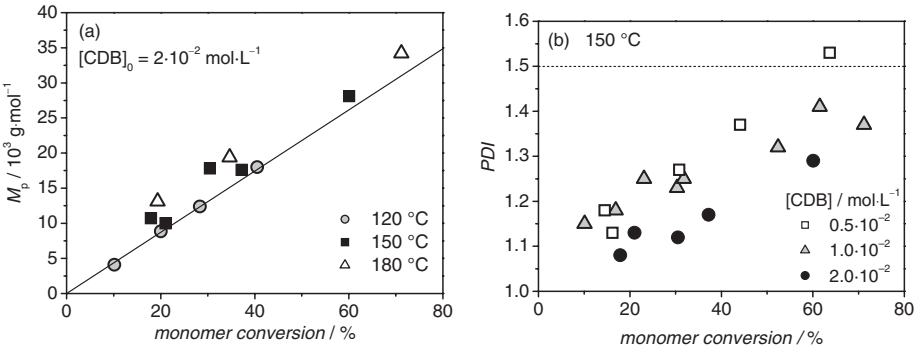


***Figure 2.***
(a) Peak molecular weight, $M_p$, and (b) polydispersity index, *PDI*, vs. monomer conversion for selected CDB-mediated self-initiated styrene bulk polymerizations at elevated temperatures and 1000 bar The straight line in part (a) indicates the theoretical number average molecular weight.[11]

 

of rate retardation, however, is clearly reduced toward higher temperature. Increasing temperature, in principle, favors fragmentation over addition reactions, due to the corresponding entropy term. By applying high temperature the fragmentation of the intermediate RAFT radical may therefore be accelerated compared to the addition reaction, by which the concentration of intermediate radicals is reduced and rate retardation is suppressed.[3] Performing a kinetic analysis using Eq. (1) provided access to the coupled parameter $K \cdot k_{t,cross}/k_t$ as a function of temperature. The resulting overall activation energy of these coupled parameters was estimated to be 40.5 kJ · mol$^{-1}$.[11] As the activation energy of $k_{t,cross}/k_t$ is assumed to be close to zero, because of both kinetic coefficients referring to diffusion-controlled processes, an activation energy of $K$ for the main equilibrium of about 40.5 kJ · mol$^{-1}$ was concluded.[11] This value is significantly lower than the approximately 78 kJ · mol$^{-1}$ expected from *ab initio* calculations for small model species.[14] In conjunction with the pre-exponential factors from transition state theory,[15] the experimentally obtained barrier of 40.5 kJ · mol$^{-1}$ yields $k_\beta = 6 \cdot 10^3$ s$^{-1}$ at 60 °C, which is in excellent agreement with the value of $k_\beta = 10^4$ s$^{-1}$ at 60 °C that was obtained by the combined analysis of polymerization rate and ESR-derived intermediate radical concentrations.[16] The experimental polymerization rate data of CDB-mediated styrene polymerization performed over the wide temperature range between 60 °C and 180 °C can hence be described by the concept of irreversible termination of the intermediate RAFT radical with remarkable internal consistency. In contrast, the data is qualitatively and semi-quantitatively inconsistent with the theory of slow fragmentation of intermediate radicals,[14] which predicts an enormous increase of $k_\beta$ with temperature. E.g., a $k_\beta$ value suggested within the slow fragmentation theory of 0.4 s$^{-1}$ at 30 °C,[14] would increase up to $k_\beta = 1\,200$ s$^{-1}$ at 120 °C, resulting in a decrease of the equilibrium constant $K$ by about 3 orders of magnitude. As a consequence of this lowering in $K$, rate retardation would have disappeared at already 120 °C, as predicted by simulations,[17] which is in clear contradiction to the experimental findings.

The complex interplay of individual reactions occurring in RAFT polymerization can additionally be probed by changing solution properties which selectively impact diffusion controlled reactions. CDB-mediated polymerizations of styrene and methyl acrylate (MA) was thus studied in solution of supercritical carbon dioxide,[18,19] which is known to significantly increase the fluidity of the system. Molecular weight distributions and average molecular weights indicated a successful control of styrene and MA polymerization in solution of around 22 vol.-% of $CO_2$ at 300 bar and 80 °C, with polydispersity indices as low as 1.05. Polymerization rates were retarded depending on the CDB concentration and overall polymerization rates were lowered by replacing the reference solvent toluene by $CO_2$. The latter effect can be attributed to an increased termination reaction rate, due to the enhanced fluidity.[20] Whereas the polymerization rate of CDB-mediated styrene polymerization in bulk or conventional solution can satisfactorily be described by the concept of irreversible cross-termination according to Eq. (1) (see above and Figure 3a), the kinetic situation changes when employing $CO_2$ as the solvent, that is, the polymerization rate can then appropriately be described under the examined conditions by Eq (2)[9] (see Figure 3b), which assumes self-termination between two intermediate RAFT radicals, described by the self-termination rate coefficient, $k_{t,self}$, as the dominant cause of rate retardation.

$$R_p^{-2} = R_{p,c}^{-2}\{1 + (k_{t,self}/k_t)K^2[\mathrm{RAFT}]_0^2\} \quad (2)$$

This kinetic analysis suggests a transition from cross-termination of intermediate radicals with propagating macroradicals in bulk or conventional solution to

 

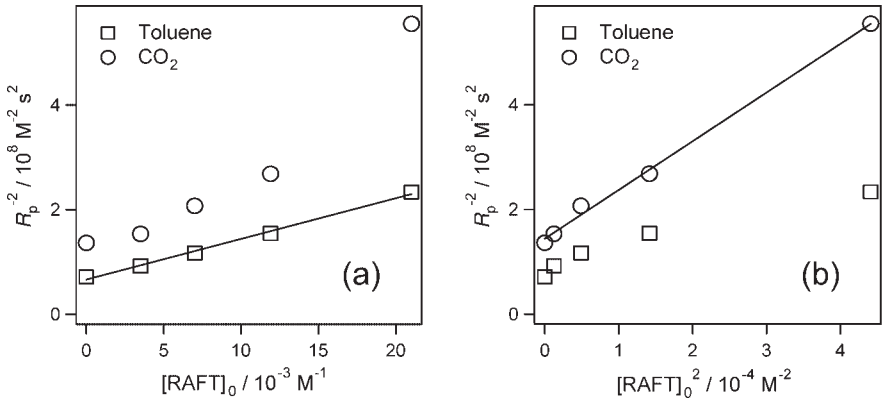


***Figure 3.***
(a) Plot of $R_p^{-2}$ vs. $[RAFT]_0$ according to Eq. (1), and (b) plot of $R_p^{-2}$ vs. $[RAFT]_0^2$ according to Eq. (2) for CDB-mediated styrene polymerizations at 80 °C and 300 bar in solutions of $CO_2$ (circles) and toluene (squares), respectively.[19]

self-termination between intermediate radicals in solution of $CO_2$ being dominant in CDB-mediated styrene polymerization. This effect may be understood by the increased fluidity that enhances the probability of hindered termination reactions, such as self-termination. It should be noted that in the case of CDB-mediated MA polymerization, the rate of polymerization is best described by Eq. (2), independent of the employed solvent. This points toward a high stability, thus high concentration, of the intermediate radical in CDB-mediated MA polymerization, which results in an increased importance of self-termination that scales with the square of the intermediate radical concentration.

## Probing RAFT Kinetics by Pulsed Laser Methods

The numbers reported in the literature for $k_\beta$ of one specific RAFT process differ by several orders of magnitude, depending on the mechanistic assumptions made for the analysis of experiments carried out under continuous thermal initiation. (For a comprehensive description of this issue see reference[3].) In order to improve this situation, a method for the simultaneous determination of $k_{ad}$ and $k_\beta$ from a single experiment was designed,[21] in which the formation and the decay of the intermediate RAFT radical is monitored via μs time-resolved electron spin resonance (ESR) spectroscopy after pulsed-laser initiation in a RAFT polymerization system (see Figure 4). The build-up of the intermediate radical concentration, [Int], directly reflects the addition of radicals toward RAFT species. The decay kinetics of the intermediate species is governed both by the fragmentation rate of the intermediate RAFT radical and by irreversible termination reactions of various radical species. The individual rate coefficients of the RAFT process can be obtained by fitting [Int] vs. time profiles to the following kinetic scheme, which exclusively considers propagating radicals, R, dithioester species, RAFT, and intermediate radicals, Int:

$$\text{(a)}\quad R + RAFT \xrightarrow{k_{ad}} Int$$

$$\text{(b)}\quad Int \xrightarrow{k_\beta} R + RAFT$$

$$\text{(c)}\quad R + R \xrightarrow{k_t} \textit{dead polymer}$$

$$\text{(d)}\quad Int + R \xrightarrow{k_t^{cross}} \textit{dead polymer}$$

$$\text{(e)}\quad Int + Int \xrightarrow{k_t^{self}} \textit{dead polymer}$$

The reactions (a), (b) and (c) are sufficient for modeling the experimental [Int] traces. More detailed estimations are available by using the extended scheme including cross-termination (d) and/or self-

 

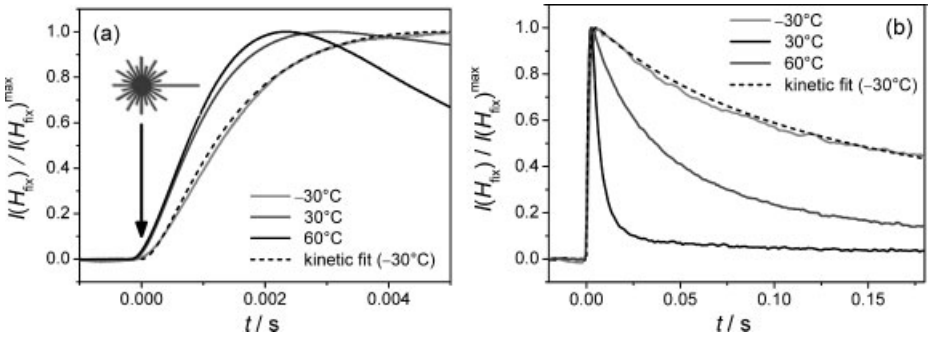


***Figure 4.***
Time evolution ((a) initial time period, (b) extended time regime) of the normalized ESR signal intensity at the field position that corresponds to the peak maximum of the full spectrum after single laser pulse initiation in BMPT-mediated BA polymerizations in toluene ([BMPT] $= 4.1 \cdot 10^{-3}$ mol $\cdot$ L$^{-1}$).[21]

termination (e). The chain length of the participating species needs not to be considered in the modeling, since the radical size is hardly changing during one single-pulse experiment.[22] This feature of single-laser-pulse-initiated RAFT polymerization is also exploited for assessing chain-length dependent termination rate coefficients with unrivaled accuracy, which method is detailed elsewhere.[22–24] The dashed lines in Figure 4 indicate that the simple kinetic model without steps (d) and (e) provides an adequate fit of [Int] vs. time plots measured by ESR spectroscopy during S-S′-bis(methyl-2-propionate)-trithiocarbonate (BMPT) mediated butyl acrylate (BA) polymerizations. The method yields values for, e.g., BMPT-mediated BA polymerization in toluene at $-30\,^{\circ}$C of $k_{ad} = 2 \times 10^5$ mol $\cdot$ L$^{-1} \cdot$ s$^{-1}$ and $k_\beta \approx 1 \times 10^2$ s$^{-1}$.[21] Data for this system obtained at higher temperatures are currently not reliable, as the intermediate radical spectrum overlaps with that of tertiary mid-chain radicals, which readily form in BA polymerization above $-30\,^{\circ}$C.[25] Including cross-termination and/or self-termination gives fits of identical quality as those depicted in Figure 4. Self-termination, however, was not considered in the BMPT system, as this reaction would lead to the formation of six-arm stars, which are unlikely to occur because of steric reasons. Whether or not cross-termination is considered has no effect on $k_{ad}$ – which value agrees excellently with previously reported values for the BMPT system[23] – and influences $k_\beta$ by less than one order of magnitude. This is a largely reduced uncertainty compared to the disparity of several orders of magnitude in $k_\beta$ reported earlier for CDB-mediated polymerizations.[3]

Estimating $k_\beta$ from fitting [Int] vs. time curves is restricted to systems where self-termination of intermediate radicals is not significant. In the case that self-termination is included into the kinetic modeling, the estimated $k_\beta$ values decrease with increasing self-termination rate. When assuming that the intermediate radicals are stable, i.e., $k_\beta = 0$, the experimentally observed decay of [Int] can exclusively be assigned to self-termination. This situation, however, is unreasonable in that no propagating radicals occur in such a system.

As a single-pulse technique, the method can be applied at any time and thus at any monomer conversion during RAFT polymerization. Close inspection of the full ESR spectrum of BMPT-derived intermediate radicals in the early phase of the BA RAFT polymerization indicated that there is an overlap of two singlet lines of different band width and that the contributions of these two species change during the polymerization.[24] Since the BMPT-derived intermediate radical has no proton

 

in the immediate vicinity of the radical center, no hyperfine splitting of the ESR spectrum is anticipated. The observation of two overlapping singlets was hence attributed to the fact that the intermediate RAFT radicals of both the pre- and main equilibrium are observed simultaneously.[24] A third radical species evolved after application of several hundred laser pulses, which could be assigned to the four-line spectrum of the secondary propagating radical in BA polymerization. The change of the concentration ratio between intermediate and propagating radical with progressive polymerization corresponds to a decrease in the equilibrium constant, $K$, by about one order of magnitude. This observation suggests that $k_{ad}$ and $k_{\beta}$ may be different for the pre- and main equilibrium regimes and, additionally, may be chain-length dependent.

### Probing RAFT Kinetics and Mechanism by Mass Spectrometry

During recent times, soft-ionization mass spectrometry have become increasingly important for probing mechanistic features of polymerization processes.[26–28] The detailed structural information of the polymeric product stream, consisting both of major components and of low-concentrated byproducts, may allow for elucidating unidentified reaction pathways in radical polymerization. Especially electrospray ionization (ESI) mass spectrometry (MS) has proven to be a powerful tool for polymer analysis,[29] since it is particularly soft in comparison to other ionization techniques. In an attempt to uncover the reaction mechanism that leads to molecular weight control in radical polymerization in the presence of dithiobenzoic acid, a combined approach of mass spectrometry and kinetic modeling was employed.[30] Dithioic acids, Z–C(=S)–SH, are effective mediating agents that lead to polymers with low polydispersity and increasing molecular weights with progressive monomer conversions.[31] These dithio-compounds are no RAFT agents, because the hydrogen atom is not an appropriate leaving group moiety. The generated polymer, however, is identical in structure to a polymeric RAFT agent as occurring in classical RAFT polymerizations. Based on the fact that dithioic acids are precursors in many RAFT agent syntheses, an in-situ formation of dithioester-type RAFT agent via addition of the dithioic acid to the double bond of the monomer was speculated.[31,32] Such an in-situ formation, however, is not feasible with methyl methacrylate (MMA), which adds to dithioic acids in a Michael-type reaction,[33] which reaction yields an inefficient RAFT agent carrying a primary leaving group. Dithiobenzoic acid (DTBA), however, also imparts living characteristics on MMA polymerization, disproving that this reaction path is the main cause for RAFT agent formation in dithioic acid mediated polymerizations. The DTBA/MMA system was consequently in the center of a mechanistic investigation, in which primarily the product stream being generated in the early reaction phase was probed.[30]

Figure 5a shows a section of the ESI-MS spectrum of poly(MMA) that has been generated in the presence of DTBA at 60 °C during the early reaction period. A repetitive pattern of peaks can be observed, with $m/z$ values that can be assigned to oligomeric poly(MMA) carrying both an initiator derived cyanoisopropyl- and a dithiobenzoate-group as end-groups (see **13** in Scheme 2, e.g., $m/z$ 644.13 for 4-mer). This species constitutes an efficient RAFT agent. In addition, a single, very prominent peak at $m/z$ 529.1 is observed, which can be assigned to a structure consisting of two dithiobenzoate-groups and two monomer units (see species **11** in Scheme 2), which most likely originates from coupling of two unimeric radical species. Comparison of the experimental isotopic structure of the peak at $m/z$ 529.1 with the calculated peak structure for the molecular composition of **11** (see inset in Figure 5a) provides evidence for the correct peak assignment. Increasing the initial concentration of DTBA and enhancing the primary radical flux by raising the temperature resulted in a

 

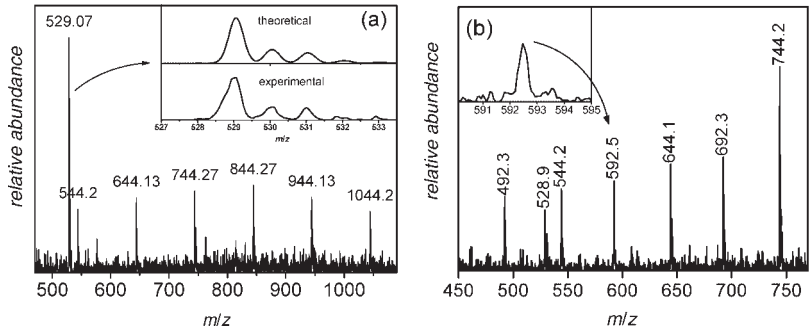


***Figure 5.***
ESI-MS spectrum of $Na^+$-ionized poly(MMA) generated in MMA bulk polymerization mediated by DTBA and using AIBN as the initiator (a) at 60 °C and after 5.0 hours/0.5% monomer conversion, and (b) at 100 °C and after 0.5 hours/1.2% monomer conversion.[30]

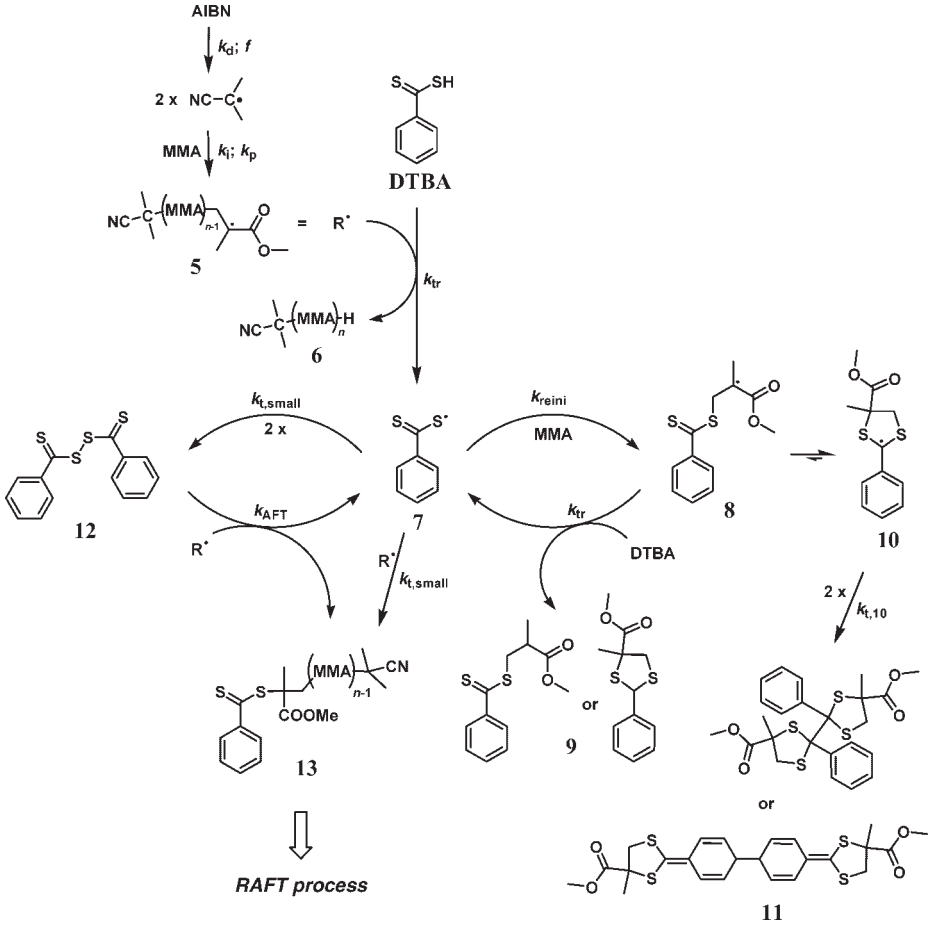


***Scheme 2.***
Proposed reaction scheme for the initial phase of DTBA-mediated MMA polymerization resulting in RAFT-type behavior.[30]

 

more pronounced formation of side products in the early reaction period. Figure 5b shows that in addition to the peaks assigned to the efficient RAFT agent **13**, another peak series occurs, which can be assigned to hydrogen-terminated poly(MMA) (see **6** in Scheme 2, *m*/*z* 592.47 for 5-mer). Closer inspection of the isotopic peak pattern (see inset in Figure 5b) reveals that this peak does not originate from termination via disproportionation, which would give rise to the typical twin-peak shape.[29]

Further mechanistic evidence came from pronounced induction periods observed in DTBA-mediated MMA polymerization, as obvious from Figure 6, and from theoretical molecular weights being pronouncedly higher than expected for DTBA being directly the mediating agent (not shown).[30]

Based on the findings by Bai et al.,[31] on the conceptions presented by Goh et al.,[32] and on our own mass spectrometric, kinetic, and molecular weight data, a mechanism for the RAFT agent formation during the induction period of DTBA-mediated MMA polymerization was formulated and is presented in Scheme 2. The key reaction in Scheme 2 is the abstraction of the sulfur-bound hydrogen from DTBA by propagating radicals, yielding a hydrogen-terminated poly(MMA) **6** – which indeed was found by ESI-MS (see Figure 5b) – and a phenyl-carbonothioylsulfanyl radical **7**. The hydrogen abstraction is assumed to proceed with relatively high rates, due to the resonance stabilization of the generated sulfur-centered alkylsulfanyl radical. This situation suggests that the hydrogen abstraction proceeds even faster than that with alkylthiols.

The sulfur-centered radical **7** may either undergo reinitiation, which reaction path is not leading to the formation of any efficient RAFT agent, but mainly results in the formation of a ring-shaped radical **10** via rapid back-biting. This radical is of high stability, thus occurring in high concentrations, and is therefore expected to undergo pronounced self-termination yielding product **11**, which is in full agreement with the occurrence of the prominent peak at *m*/*z* 529.1 seen in Figure 5. Species **10** (and/or **8**) may also react with the original DTBA to yield back **7**, whereby more than one DTBA molecule is consumed during the kinetic lifetime of a single radical. The alkylsulfanyl radical **7** is also envisaged to terminate with propagating radicals – either directly or via the detour over bis(thiobenzoyl) disulfide **12** – which reaction forms a dithiobenzoate **13** with a tertiary leaving group, i.e., an efficient RAFT agent, which was found via ESI-MS during the induction period.

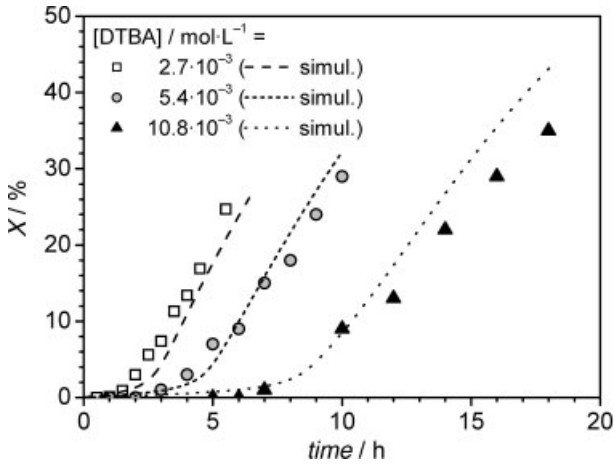


***Figure 6.***
Monomer conversion, *X*, vs. time for MMA bulk polymerizations at 60 °C, mediated by various concentrations of DTBA and using $4.9 \times 10^{-3}$ mol · L$^{-1}$ AIBN as the initiator.[30]

 

The proposed reaction scheme was employed to successfully model the kinetics of the DTBA-mediated MMA polymerization in the early reaction phase via PREDICI simulations (see Figure 6), resulting in a hydrogen abstraction rate coefficient of $k_{tr} = 3.0 \times 10^4\ \mathrm{L \cdot mol^{-1} \cdot s^{-1}}$ and a reinitiation rate of the alkylsulfanyl radical of $k_{reini} = 7.8\ \mathrm{L \cdot mol^{-1} \cdot s^{-1}}$.[30] The finding that all the reactions depicted in Scheme 2 were vital to comprehensively simulate all the kinetic features and to quantitatively predict the experimentally found products lends credit to the plausibility of the postulated mechanism. Based on the mechanistic conclusions, a polymerization protocol using a cocktail of a slowly (1,1′-azobis(cyclohexane-1-carbonitexane-1-carbonitrile) at 100 °C) and rapidly (2,2′-Azobis(*iso*-butyronitrile) at 100 °C) decomposing initiator was developed, which allows for the generation of well-controlled poly(MMA) using DTBA as the mediating agent, but without having the drawback of a pronounced induction period.[30] This novel protocol may be an attractive alternative to classical RAFT polymerizations of MMA, as DTBA is accessible with less effort and at lower costs than dithioesters with tertiary leaving groups.

*Acknowledgements:* Financial support by the *Deutsche Forschungsgemeinschaft* is gratefully acknowledged. The author is indebted to Prof. Michael Buback (University of Göttingen) for continuous support.

[1] J. Chiefari, Y. K. Chong, F. Ercole, J. Krstina, J. Jeffery, T. P. T. Le, R. T. A. Mayadunne, G. F. Meijs, C. L. Moad, G. Moad, E. Rizzardo, S. H. Thang, *Macromolecules* **1998**, *31*, 5559.
[2] G. Moad, E. Rizzardo, S. H. Thang, *Aust. J. Chem.* **2005**, *58*, 379.
[3] C. Barner-Kowollik, M. Buback, B. Charleux, M. L. Coote, M. Drache, T. Fukuda, A. Goto, B. Klumperman, A. B. Lowe, J. B. Mcleary, G. Moad, M. J. Monteiro, R. D. Sanderson, M. P. Tonge, P. Vana, *J. Polym. Sci., Part A: Polym. Chem.* **2006**, *44*, 5809.
[4] S. Perrier, P. Takolpuckdee, *J. Polym. Sci., Part A: Polym. Chem.* **2005**, *43*, 5347.
[5] M. Drache, G. Schmidt-Naake, M. Buback, P. Vana, *Polymer* **2005**, *46*, 8483.
[6] E. I. Izgorodina, M. L. Coote, *Macromol. Theory Simul.* **2006**, *15*, 394.
[7] M. Buback, P. Vana, *Macromol. Rapid Commun.* **2006**, *27*, 1299.
[8] T. Arita, M. Buback, O. Janssen, P. Vana, *Macromol. Rapid Commun.* **2004**, *25*, 1376.
[9] Y. Kwak, A. Goto, T. Fukuda, *Macromolecules* **2004**, *37*, 1219.
[10] M. Wulkow, *Macromol. Theory Simul.* **1996**, *5*, 393.
[11] T. Arita, M. Buback, P. Vana, *Macromolecules* **2005**, *38*, 7935.
[12] Y. Liu, J. P. He, J. T. Xu, D. Q. Fan, W. Tang, Y. L. Yang, *Macromolecules* **2005**, *38*, 10332.
[13] A. Postma, T. P. Davis, G. Moad, M. S. O'Shea, *Macromolecules* **2005**, *38*, 5371.
[14] A. Feldermann, M. L. Coote, M. H. Stenzel, T. P. Davis, C. Barner-Kowollik, *J. Am. Chem. Soc.* **2004**, *126*, 15915.
[15] M. L. Coote, *J. Phys. Chem. A* **2005**, *109*, 1230.
[16] Y. Kwak, A. Goto, Y. Tsujii, Y. Murata, K. Komatsu, T. Fukuda, *Macromolecules* **2002**, *35*, 3026.
[17] P. Vana, T. P. Davis, C. Barner-Kowollik, *Macromol. Theory Simul.* **2002**, *11*, 823.
[18] T. Arita, S. Beuermann, M. Buback, P. Vana, *e-Polymers* **2004**, *003*, 1.
[19] T. Arita, S. Beuermann, M. Buback, P. Vana, *Macromol. Mater. Eng.* **2005**, *290*, 283.
[20] S. Beuermann, M. Buback, C. Isemer, A. Wahl, *Macromol. Rapid Commun.* **1999**, *20*, 26.
[21] M. Buback, P. Hesse, T. Junkers, P. Vana, *Macromol. Rapid Commun.* **2006**, *27*, 182.
[22] M. Buback, T. Junkers, P. Vana, *Macromol. Rapid Commun.* **2005**, *26*, 796.
[23] T. Junkers, A. Theis, M. Buback, T. P. Davis, M. H. Stenzel, P. Vana, C. Barner-Kowollik, *Macromolecules* **2005**, *38*, 9497.
[24] M. Buback, T. Junkers, P. Vana, *ACS Symp. Ser.* **2006**, *944*, 455.
[25] R. X. E. Willemse, A. M. van Herk, E. Panchenko, T. Junkers, M. Buback, *Macromolecules* **2005**, *38*, 5098.
[26] P. Vana, T. P. Davis, C. Barner-Kowollik, *Aust. J. Chem.* **2002**, *55*, 315.
[27] A. Ah Toy, P. Vana, T. P. Davis, C. Barner-Kowollik, *Macromolecules* **2004**, *37*, 744.
[28] C. Barner-Kowollik, T. P. Davis, M. H. Stenzel, *Polymer* **2004**, *45*, 7791.
[29] M. Buback, H. Frauendorf, P. Vana, *J. Polym. Sci., Part A: Polym. Chem.* **2004**, *42*, 4266.
[30] D. H. Nguyen, P. Vana, *Aust. J. Chem.* **2006**, *59*, 549.
[31] R. K. Bai, Y. Z. You, C. Y. Pan, *Polym. Int.* **2000**, *49*, 898.
[32] Y. K. Goh, M. R. Whittaker, M. J. Monteiro, *J. Polym. Sci., Part A: Polym. Chem.* **2005**, *43*, 5232.
[33] S. Oae, T. Okabe, T. Yagihara, *Tetrahedron* **1972**, *28*, 3203.

 

 DOI: 10.1002/masy.200750209

# Scope for Accessing the Chain Length Dependence of the Termination Rate Coefficient for Disparate Length Radicals in Acrylate Free Radical Polymerization

*Tara M. Lovestead, Thomas P. Davis, Martina H. Stenzel, Christopher Barner-Kowollik**

**Summary:** A method that utilizes reversible addition fragmentation chain transfer (RAFT) chemistry is evaluated on a theoretical basis to deduce the termination rate coefficient for disparate length radicals $k_t^{s,l}$ in acrylate free radical polymerization, where *s* and *l* represent the arbitrary yet disparate chain lengths from either a "short" or "long" RAFT distribution. The method is based on a previously developed method for elucidation of $k_t^{s,l}$ for the model monomer system styrene. The method was expanded to account for intramolecular chain transfer (i.e., the formation of mid-chain radicals via backbiting) and the free radical polymerization kinetic parameters of methyl acrylate. Simulations show that the method's predictive capability is sensitive to the polymerization rate's dependence on monomer concentration, i.e., the virtual monomer reaction order, which varies with the termination rate coefficient's value and chain length dependence. However, attaining the virtual monomer reaction order is a facile process and once known the method developed here that accounts for mid-chain radicals and virtual monomer reaction orders other than one seems robust enough to elucidate the chain length dependence of $k_t^{s,l}$ for the more complex acrylate free radical polymerization.

**Keywords:** backbiting; chain length dependent termination (CLDT); kinetics; reversible addition fragmentation chain transfer (RAFT); simulations

## Introduction

Free radical polymerization (FRP) is a facile, cheap and often environmentally friendly process (i.e., one that can occur at room temperature and without solvent addition) that is used to synthesize materials for numerous applications, including adhesives, coatings, contact lenses and dental restorative materials.[1–4] In lieu of the many current applications, market needs continue to demand for more sophisticated materials for highly specific end-use applications. To this end, controlled/living FRP techniques are being developed to generate functional and complex molecular architectures, such as, block copolymers; core-shell nanoparticles; branched structures; and star and graft polymers.[5–13] However, the ability to design novel materials and control the polymerization depends on *a priori* knowledge of the FRP rate coefficients.

Of the three most important reaction steps that constitute FRP, i.e., initiation, propagation and termination, the termination process is the most complex. Much work has been carried out to characterize the termination rate coefficient ($k_t$) and how it depends on the polymerization

Centre for Advanced Macromolecular Design, School of Chemical Sciences and Engineering, The University of New South Wales, Sydney, New South Wales 2052, Australia
E-mail: camd@unsw.edu.au

conditions, e.g., the temperature; pressure; solvent concentration; reaction medium viscosity and the growing radical's size.[14–26] Previously, the dependence of the termination rate coefficient on the radical's size for equal size radicals, i.e., $\alpha$, where $k_t^i \propto i^{-\alpha}$ and $i$ represents the average radical size when only one reversible addition fragmentation chain transfer (RAFT) distribution exists, was ascertained utilizing RAFT chemistry.[19,25,27] This method termed the RAFT chain length dependent termination (RAFT–CLD–T) method extracts the termination rate coefficient as a function of chain length ($k_t^i$) from the on-line determination of the polymerization rate as a function of time, $R_p(t)$, and hence, allows for access to $k_t$'s chain length dependency, i.e., the scaling exponent $\alpha$ when the chain length dependency follows a power law relationship.

The RAFT–CLD–T technique was exemplified on styrene[25,27] and later successfully mapped the chain length dependence of $k_t$ for methyl acrylate (MA),[28] butyl acrylate,[29] dodecyl acrylate[30] and methyl methacrylate.[31] Additionally, the simultaneous dependence of $k_t$ on radical size and monomer conversion was mapped using the RAFT–CLD–T methodology for MA[32] and vinyl acetate.[33] Another accurate and reliable method for accessing the chain length dependence of the termination rate coefficient (i.e., $\alpha$, where $k_t^i \propto i^{-\alpha}$) is the non-stationary single pulse–pulsed laser polymerization–RAFT (SP–PLP–RAFT) technique.[23,34]

Recently, a method for deducing the chain length dependence of the termination rate coefficient for both similar and disparate size radicals, i.e., both $\alpha$ and $\varphi$, where $k_t^{s,l} \propto (sl)^{-\varphi/2}$, was introduced.[35] This method is based on the original RAFT–CLD–T method, which was modified for the parallel polymerization of two RAFT species of disparate average chain lengths, $s$ and $l$. The method was exemplified theoretically using styrene because its kinetic rate coefficients and material properties are well known and its polymerization kinetics exhibit nominal chain transfer and other interfering side reactions. The previously published manuscript details a thorough theoretical assessment of the method and its ability to access $k_t$'s chain length dependence for both similar and disparate size radicals (i.e., both $\alpha$ and $\varphi$) for slowly propagating monomers within reasonable accuracy regardless of the input kinetic parameters and/or the relationship assumed for the termination rate coefficient's chain length dependence.[35]

Acrylates are used extensively in industry and complete characterization of their FRP kinetics would be advantageous as is evident from the numerous investigations of acrylate kinetics found in the literature.[15,21–23,28–30,32,36–44] Testing the method – at least theoretically – to elucidate $k_t^{s,l}$ for fast propagating monomers such as acrylates is an interesting problem. For one, acrylates undergo side reactions such as inter- and intramolecular chain transfer (i.e., chain transfer to polymer and backbiting, respectively), and thus, whether or not these side reactions will impact the method's ability to elucidate the termination kinetic coefficient from only the polymerization rate data needs to be examined.[2,45–49] Additionally, the RAFT–CLD–T method relies on accurate on-line determination of the polymerization rate and – given their rapid polymerization – acrylates seem as an attractive option for experimental validation of this procedure. Thus, the impact of fast propagation, backbiting and mid-chain radical reactions on the method's ability to obtain accurately the chain length dependence of $k_t$ for both similar and disparate size radicals is investigated with the goal of aiding the experimentalist in choosing the optimum polymerization system for validating the recently introduced $k_t^{s,l}$ methodology.

## Model Development

The method presented here builds upon the basic FRP reactions and the reactions that constitute RAFT process, which have been

 

detailed extensively in prior publications and will not be reiterated here.[9,50] The method is based on the direct measurement of the polymerization rate as a function of time, $R_p(t)$, which is given by equation 1.

$$R_p(t) = -\frac{d[M]}{dt} = k_p[M][P\cdot] \quad (1)$$

Here, $t$ is the polymerization time, [M] is the monomer concentration, $k_p$ is the propagation rate coefficient, and [P·] is the propagating radical concentration. $R_p$ relates to the termination rate coefficient, $k_t$, via the well-known classical equations for the initiation and termination rates and the change in the radical concentration with time to provide the following chain-length averaged $k_t$ as a function of time, $\langle k_t \rangle(t)$.[30]

$$\langle k_t \rangle(t) = \frac{2fk_d[I]_0 e^{-k_d t} - \frac{d\left(\frac{R_p(t)}{k_p^*\left([M]_0 - \int_0^t R_p(t)dt\right)^{\omega}}\right)}{dt}}{2\left(\frac{R_p(t)}{k_p^*\left([M]_0 - \int_0^t R_p(t)dt\right)^{\omega}}\right)^2} \quad (2)$$

Here, $k_d$ is the initiator decomposition rate, [I] is the initiator concentration and $f$ is the initiator efficiency. Note that no assumption of a steady state radical concentration is made. Additionally, the non-classical relationship between $R_p$ and the monomer concentration due to the formation of less reactive mid-chain radicals is accounted for using equation 3, which introduces a modified propagation rate coefficient, $k_p^*$, and the possibility of accounting for virtual monomer reaction orders, $\omega$, other than one.[30]

$$k_p^* = k_p[M]_0^{1-\omega} \quad (3)$$

The unique attributes of the RAFT mediated FRP (i.e., a linear increase in the average radical length ($i$) and a nearly monodisperse radical chain length distribution ($i \approx j$) allows for the chain-length averaged $k_t$ to be related directly to the microscopic $k_t^{i,i}$ at any point in time. Thus, the chain length dependence of the termination rate coefficient for equal size radicals, i.e., $\alpha$ (equation 4), is accessible when $R_p$, the molecular weight distribution (MWD) evolution and a value for the termination rate coefficient for two unimers ($k_t^{1,1}$) is assumed.

$$k_t^{i,i} = k_t^{1,1}(i \cdot i)^{-\alpha/2} \quad (4)$$

To elucidate the chain length dependence of the termination rate coefficient for disparate average size radicals, i.e., $\varphi$, where $k_t^{s,l} \propto (sl)^{-\varphi/2}$, two RAFT distributions are generated by simulating the reaction of a system comprised of monomer, initiator, RAFT agent and a macroRAFT species of initial chain length greater than one via implementing two complete RAFT mediated FRP reactions into the kinetic modeling program PREDICI®.[35,51] Chains from different distributions are denoted using the superscript $s$ or $l$ for the "short" or "long" chain species, respectively, for example, $[P_i^{s}\cdot]$ represents a radical concentration of arbitrary chain length $i$ from the distribution of "short" chains $s$. Thus, initiation, propagation, and macroRAFT species generation as well as termination occur for each distribution. In addition, core equilibrium and termination occurs between either the $l$ or $s$ chain macroRAFT species and reactive radical, respectively. Note that within a given RAFT distribution the individual chain lengths are denoted $i$ and $j$ and are assumed to be approximately equivalent and chains belonging to different distributions are denoted $s$ and $l$. Assuming that each RAFT distribution is adequately represented by its average chain length, the average termination rate coefficient is given by equation 5, i.e., the total termination rate divided by the square of the total radical concentration.[35]

$$\langle k_t \rangle = \frac{k_t^{s,s}[P_s\cdot]^2 + 2k_t^{s,l}[P_s\cdot][P_{l'}\cdot] + k_t^{l,l}[P_{l'}\cdot]^2}{([P_s\cdot] + [P_{l'}\cdot])^2} \quad (5)$$

 

Here, $[P_s^{\cdot}]$ and $[P_l^{\cdot}]$ are the concentration of "short" and "long" radicals, respectively, and the total termination rate (the numerator) is equal to the sum of the termination rate for chains of approximately identical size (*ss* or *ll*) and disparate size (*sl* and *ls*). When equal concentrations of reacting species exist (i.e., $[P_s^{\cdot}] = [P_l^{\cdot}]$), equation 5 simplifies to equation 6.

$$\langle k_t \rangle = \frac{1}{4} k_t^{s,s} + \frac{1}{2} k_t^{s,l} + \frac{1}{4} k_t^{l,l} \quad (6)$$

Equal concentrations of reacting species exist when equal concentrations of RAFT agent (for the macroRAFT and initial RAFT species) are employed resulting in a simple relationship for the dependence of $k_t^{s,l}$ on the average termination rate coefficient $k_t$ for equal size radicals (equation 7).

$$k_t^{s,l} = 2\langle k_t \rangle - \frac{1}{2} k_t^{s,s} - \frac{1}{2} k_t^{l,l} \quad (7)$$

To describe the termination rate coefficient's dependence on chain length, the geometric and harmonic means are employed (equations 8 and 9).[35]

$$k_t^{s,l} = k_{t0}(s \cdot l)^{-\varphi/2} \quad (8)$$

$$k_t^{s,l} = k_{t0}\left(\frac{2s \cdot l}{s + l}\right)^{-\varphi} \quad (9)$$

The extent that the termination rate coefficient depends on radical size for similar size macroradicals (*ss* or *ll*), i.e., macroradicals associated with the same macroRAFT distribution, is denoted $\alpha$ and the extent that the termination rate coefficient depends on radical size for disparate size macroradicals (*sl* and *ls*), i.e., macroradicals associated with different macroRAFT distributions, is denoted $\varphi$.

To summarize, the procedure for accessing the extent that the termination rate coefficient depends on disparate length radicals, i.e., $\varphi$, is as follows: (1) use the RAFT-CLD-T method to determine the chain length dependence for equal length radicals terminating (i.e., $\alpha$); (2) obtain a prepolymerized macroRAFT species of chain length greater than one; (3) monitor the polymerization rate for the reaction mixture containing the RAFT agent, initiator, monomer and the prepolymerized macroRAFT species; (4) determine $k_t^{s,l}$ using the above methodology and $\alpha$ and (5) elucidate $\varphi_{out}$ via constructing a double-log plot of equation 8 or 9 and obtaining a best fit to the slope.

## Model Parameters

The material properties and kinetic parameters for methyl acrylate (MA), the initiator 2,2-azobisisobutyronitrile (AIBN) and the RAFT agent methoxycarbonylethyl phenyldithioacetate[32] (MCEPDA) are incorporated into the model (Table 1) including the addition, fragmentation, initiation and the initial termination rate coefficients ($k_{add}$, $k_{frag}$, $k_i$ and $k_{t0}$), along with the initiator decomposition, propagation and reinitiation rate coefficients ($k_d$, $k_p$ and $k_{p,rein}$) and the monomer, RAFT agent and initiator concentrations at time zero. For simplicity, the gel effect is not taken into account. All simulations were carried out using the program package PREDICI®, version 6.36.1, on an Athlon 64 X2 Dual Core Processor 3800+ IBM-compatible computer.

## Results and Discussion

### Accounting for fast propagation-elucidation of $k_t$ for similar and disparate size radicals

First, the impact of fast propagation (neglecting intra-molecular chain transfer) on

*Table 1.*
Input parameters used for the kinetic modelling of the RAFT mediated acrylate FRP initiated with AIBN.[a)]

| $k_{add}$[30] | $k_{frag}/s^{-1}$[30] | $k_i$[30] | $k_{to}$[28] |
|---|---|---|---|
| $1.4 \cdot 10^6$ | $1.0 \cdot 10^5$ | $1.57 \cdot 10^3$ | $1.0 \cdot 10^9$ |
| $k_d/s^{-1}$[28,52] | $k_p$[53][b] | $k_{p,rein}$[28] | $f$[32] |
| $8.4 \cdot 10^{-6}$ | $3.3 \cdot 10^4$ | $3.3 \cdot 10^4$ | 0.7 |
| $[MA]_0$[28,53] | $[MCEPDA]_0$[30] | $[AIBN]_0$[32] | $T/°C$ |
| 10.2 | $3.7 \cdot 10^{-2}$ | $3.0 \cdot 10^{-3}$ | 60 |

a) All rate coefficients are given in L $mol^{-1}$ $s^{-1}$ and all concentrations are given in mol $L^{-1}$ unless otherwise indicated.

b Propagation rate coefficient here is for end chain propagation only.

 

***Table 2.***
$\varphi_{out}$ is presented as determined from the slope of the best linear fit using the geometric mean to the simulated data for the RAFT mediated MA polymerization. Various chain lengths for the macroRAFT species, $i^{prepolymer}$, and input values for the scaling exponent for equal $\alpha$ and disparate $\varphi$ size termination are presented.

| $\alpha_{in}$ | $\varphi_{in}$ | $i^{prepolymer}$ | Slope of best linear fit | $\varphi_{out}$ |
|---|---|---|---|---|
| 0.16 | 0.16 | 32 | −0.0860 | 0.172 |
| 0.16 | 0.16 | 56 | −0.0839 | 0.168 |
| 0.16 | 0.16 | 82 | −0.0873 | 0.175 |
| 0.4 | 0.4 | 32 | −0.194 | 0.388 |
| 0.4 | 0.4 | 56 | −0.160 | 0.320 |
| 0.4 | 0.4 | 82 | −0.133 | 0.266 |
| 0.8 | 0.8 | 32 | −0.372 | 0.744 |
| 0.8 | 0.8 | 56 | −0.205 | 0.410 |
| 0.8 | 0.8 | 82 | +0.165 | −0.330 |

the method's ability to predict the termination rate coefficient's dependence on both similar and disparate size radicals is investigated. To this end, the simultaneous polymerization of two disparate length RAFT distributions is simulated.

Figure 1 shows an example of a double-log plot of equation 8 (i.e., the geometric mean) where the slope yields $-1/2\varphi_{out}$. The value of the slope provides direct feedback as to how accurately the method predicts the chain length dependence of $k_t$ for disparate size radicals since the input $\alpha$ and $\varphi$ values ($\varphi_{in}$) are known. One obvious potential source of error lies in the use of an average (geometric or harmonic) of each distribution's average chain length; however, using RAFT chemistry the polydispersity of the distribution can be minimized. Additionally, this is currently the only proposed method able to address this complex problem of elucidation of the chain length dependence of $k_t$ for both similar and disparate size radicals. The method predicts $\varphi$ more accurately ($\varphi_{in} - \varphi_{out} = \pm 0.012$, where, for the remainder of the manuscript, the subscripts in and out are used to denote the model input parameters and model output values, respectively) when the termination rate coefficient for both equal and disparate length radicals depends less on the chain lengths, i.e., $\alpha_{in}$ and $\varphi_{in}$, respectively, are equal to either 0.16 or 0.4. When a higher extent of chain length dependence is taken into account (i.e., $\alpha_{in}$ and $\varphi_{in}$ are equal to 0.8) the method predicts $\varphi_{out}$ with less accuracy ($\varphi_{in} - \varphi_{out} = 0.056$). Tables 2 and 3 reveal that the method's accuracy decreases when greater extents of chain length dependent termination are assumed. Additionally, when greater extents of chain length dependent termination are assumed,

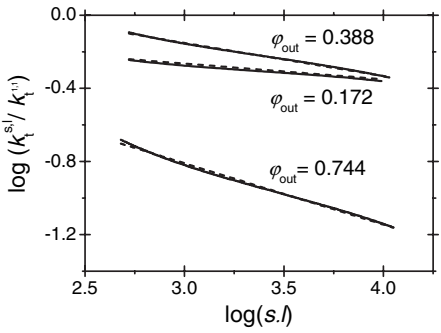


***Figure 1.***
A double-log plot of $k_t^{s,l}$ normalized by $k_t^{1,1}$ vs. the product of the log of each distribution's average chain length ($sl$) is presented for the simulated MA polymerization for $\alpha_{in}$ and $\varphi_{in}$ are equal to 0.16, 0.4, and 0.8. The dashed line is the best linear fit; the slope of which is equal to $-1/2\varphi_{out}$. The macroRAFT species was prepolymerized to an initial average chain length equal to 32. The fit is for ~3% conversion after the macroRAFT species is administered to approximately 85% conversion, which corresponds to the range that the product of the disparate lengths increases linearly with polymerization time.

***Table 3.***
$\varphi_{out}$ is presented as determined from the slope of the best linear fit using the harmonic mean to the simulated data for the RAFT mediated MA polymerization. Various chain lengths for the macroRAFT species, $i^{prepolymer}$, and input values for the scaling exponent for equal $\alpha$ and disparate $\varphi$ size termination are presented.

| $\alpha_{in}$ | $\varphi_{in}$ | $i^{prepolymer}$ | Slope of best linear fit | $\varphi_{out}$ |
|---|---|---|---|---|
| 0.16 | 0.16 | 32 | −0.184 | 0.184 |
| 0.16 | 0.16 | 56 | −0.176 | 0.176 |
| 0.16 | 0.16 | 82 | −0.180 | 0.180 |
| 0.4 | 0.4 | 32 | −0.314 | 0.314 |
| 0.4 | 0.4 | 56 | −0.364 | 0.364 |
| 0.4 | 0.4 | 82 | −0.300 | 0.300 |
| 0.8 | 0.8 | 32 | −0.527 | 0.527 |
| 0.8 | 0.8 | 56 | −0.486 | 0.486 |
| 0.8 | 0.8 | 82 | −0.378 | 0.378 |

 

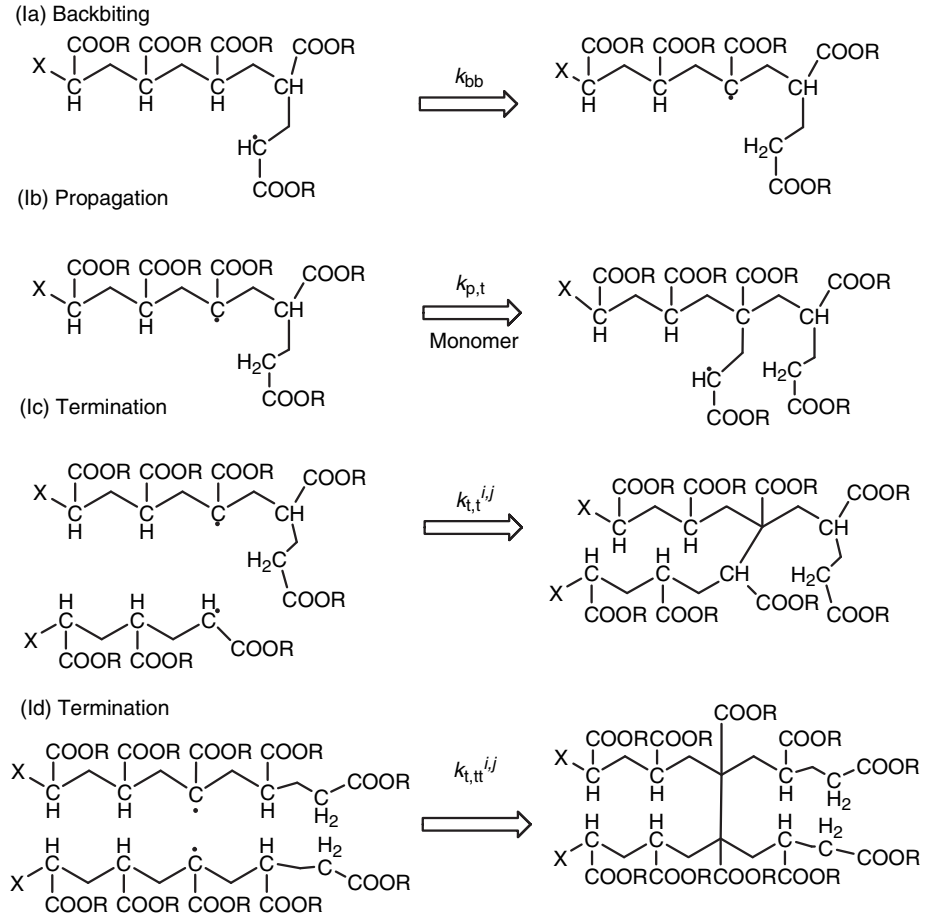


***Scheme 1.***
Tertiary Radical Formation (Backbiting) and Mid-Chain Radical Propagation and Termination.

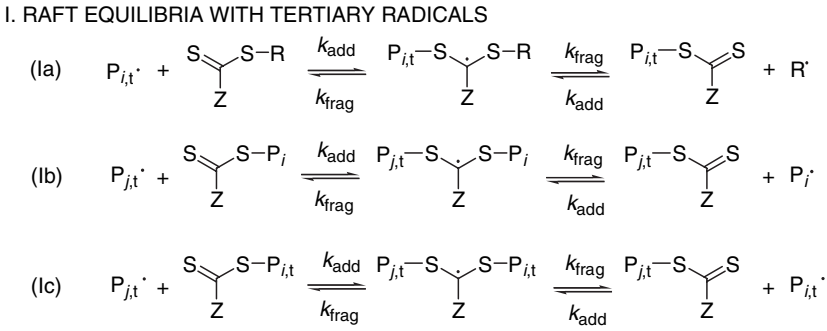


***Scheme 2.***
Basic Reactions for Tertiary Radical Formation (Backbiting) and Mid-Chain Radical Propagation, Termination and RAFT Equilibria.

 

***Table 4.***
Backbiting and tertiary radical formation parameters necessary for the kinetic modelling of the RAFT mediated acrylate FRP initiated with AIBN.[a)]

| $k_{bb}/s^{-1}$[30] | $k_{p,t}$[30] | $k_{t,t}^{i,j}$[30] | $k_{t,tt}^{i,j}$[30] | $k_{add,t}$[30] | $k_{frag,t}/s^{-1}$[30] |
|---|---|---|---|---|---|
| $1.623 \cdot 10^3$ | 55 | $1.0 \cdot 10^8$ | $1.0 \cdot 10^7$ | $1.4 \cdot 10^6$ | $1.0 \cdot 10^5$ |

[a)] All rate coefficients are given in L $mol^{-1}$ $s^{-1}$ and all concentrations are given in mol $L^{-1}$ unless otherwise indicated.

i.e., $\alpha_{in}$ and $\varphi_{in}$ are equal to either 0.4 or 0.8, the method's accuracy also decreases with increasing prepolymer chain length and the harmonic mean is observed to more accurately represents the data.

### Accounting for Backbiting – Elucidation of $k_t$ for Only Similar Size Radicals

To begin backbiting is accounted for via inclusion of the reaction steps for tertiary radical, $P_{i,t}^{\cdot}$, formation (Ia), propagation (Ib) and termination (Ic and Id) into the PREDICI® simulation (see Scheme 1). These reactions depend on the rate coefficients for backbiting, $k_{bb}$, tertiary radical propagation, $k_{p,t}$ and tertiary radical termination, which occurs either between two tertiary radicals, $k_{t,tt}^{i,j}$, or between a mid-chain and an end-chain radical, $k_{t,t}^{i,j}$, where the moiety X represents the continuing chain. Additionally, the model was expanded to account for the reactions for the RAFT equilibria of tertiary radicals (see Scheme 2). The pre-equilibrium of a tertiary radical with the initial RAFT agent (Ia) yields a macroRAFT species that is attached mid-chain. Additionally, the core equilibrium, where the macroRAFT species is formed from an end-chain (Ib) or a mid-chain (Ic) radical, is taken into account. The pre-equilibrium and the core equilibrium are governed by $k_{add,t}$ and $k_{frag,t}$, respectively. All necessary parameters for the kinetic modelling of intramolecular chain transfer are given in Table 4. There are no kinetic parameters to date for how backbiting occurs during the RAFT mediated AIBN initiated methyl acrylate polymerization, thus the kinetic parameters for the RAFT mediated AIBN initiated dodecyl acrylate FRP were used.

Accounting for mid-chain radical formation has been shown to lead to virtual monomer reaction orders (i.e., $\omega$) greater than one.[44] Equation 10 depicts the

***Table 5.***
$\omega$ and $\alpha_{out}$ are presented for various backbiting and termination rate coefficients and $\alpha_{in}$ values as predicted via simulation of the RAFT mediated MA polymerization. $\alpha_{out}$ is determined from the slope of a double-log plot of equation 8 including data from 10 to 40 % conversion. The impact of different $\alpha^t$, $\alpha^{tt}$, $k_{t,t}$ and $k_{t,tt}$ values on $\alpha_{out}$ is shown.[a)]

| $k_{bb}/s^{-1}$[31] | $k_{t,t}$ | $k_{t,tt}$ | $\alpha^t$ | $\alpha^{tt}$ | $\alpha_{in}/\alpha_{out}$ | $\omega$ |
|---|---|---|---|---|---|---|
| 0 | 0 | 0 | 0 | 0 | 0.4/0.39 | 1.0 |
| $1.623 \cdot 10^3$ | $1.0 \cdot 10^9$ | $1.0 \cdot 10^9$ | 0 | 0 | 0.0/0.01 | 2.5 |
| $1.623 \cdot 10^3$ | $1.0 \cdot 10^9$ | $1.0 \cdot 10^9$ | 0 | 0 | 0.4/0.40 | 4.3 |
| $1.623 \cdot 10^3$ | $1.0 \cdot 10^8$ | $1.0 \cdot 10^7$ | 0 | 0 | 0.4/0.40 | 2.2 |
| $1.623 \cdot 10^3$ | $1.0 \cdot 10^9$ | $1.0 \cdot 10^9$ | 0 | 0 | 0.16/0.16 | 3.2 |
| $1.623 \cdot 10^3$ | $1.0 \cdot 10^8$ | $1.0 \cdot 10^7$ | 0 | 0 | 0.16/0.16 | 1.6 |
| $1.623 \cdot 10^3$ | $1.0 \cdot 10^9$ | $1.0 \cdot 10^9$ | 0.4 | 0 | 0.4/0.40 | 3.3 |
| $1.623 \cdot 10^3$ | $1.0 \cdot 10^8$ | $1.0 \cdot 10^7$ | 0.4 | 0 | 0.4/0.41 | 1.3 |
| $1.623 \cdot 10^3$ | $1.0 \cdot 10^9$ | $1.0 \cdot 10^9$ | 0.4 | 0.4 | 0.4/0.37 | 2.6 |
| $1.623 \cdot 10^3$ | $1.0 \cdot 10^8$ | $1.0 \cdot 10^7$ | 0.4 | 0.4 | 0.4/0.41 | 1.3 |

[a)]All rate coefficients are given in L $mol^{-1}$ $s^{-1}$ and all concentrations are given in mol $L^{-1}$ unless otherwise indicated.

 

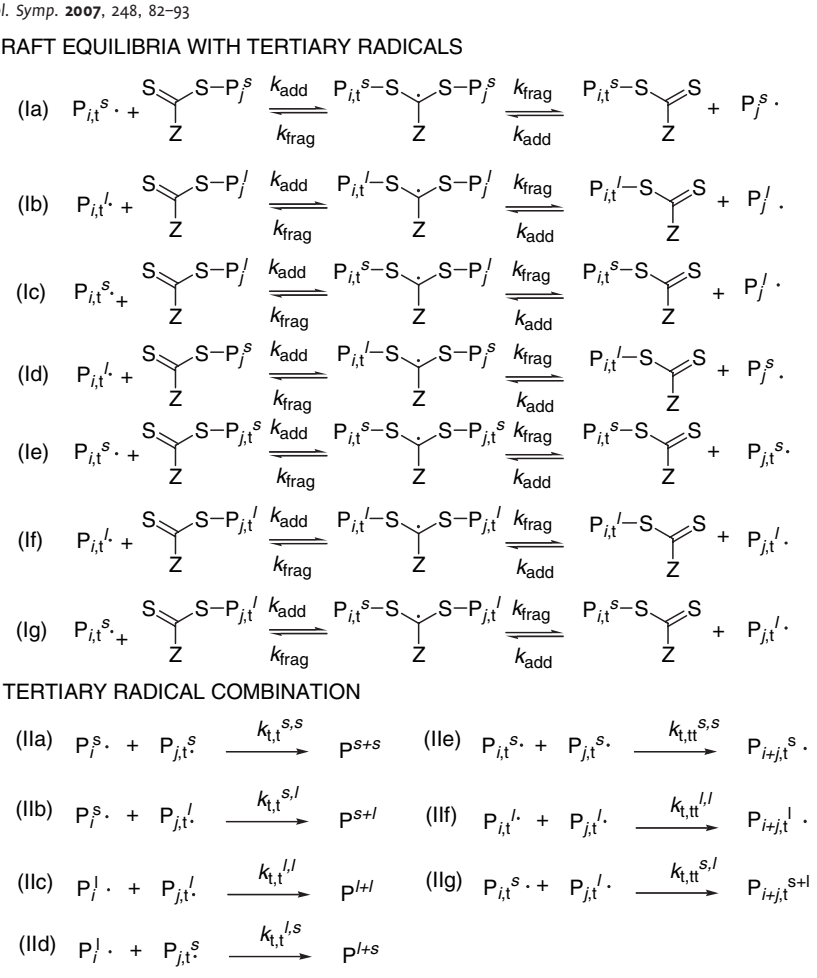


***Scheme 3.***
The Core Equilibrium and Termination Reactions for Two Simultaneous RAFT FRPs when Mid-Chain Radical Formation and Subsequent Reactions are Taken into Account.

important components from the classical polymerization rate equation that are necessary to evaluate the relationship between the polymerization rate, the initiator and monomer concentrations and the termination rate coefficient when the assumption of a steady state radical concentration is made.

$$R_p \approx [M]^{\omega}\left(\frac{[I]}{k_t^{i,i}}\right)^{0.5} \tag{10}$$

Taking the logarithmic form of equation 10 and accounting for the chain length dependence of $k_t$ results in an equation for determination of $\omega$:

$$\log(R_p) - \log([I]^{1/2}) - \log(i^{\alpha/2}) = \omega\log([M]) \tag{11}$$

The impact of the value and chain length dependence of the $k_t$s that are introduced when backbiting and mid-chain radicals are accounted for (i.e., $k_{t,t}^{i,j}$, $k_{t,tt}^{i,j}$, $\alpha^t$ and $\alpha^{tt}$) on the virtual monomer reaction order ($\omega$) was investigated for the case that takes into account only similar size radicals. Table 5 shows that a greater than classical mono-

 

***Table 6.***
$\varphi_{out}$ is presented as determined from the slope of the best linear fit using the geometric mean to the simulated data for the RAFT mediated MA polymerization. Various chain lengths for the macroRAFT species, $i^{prepolymer}$, and input values for the scaling exponent for equal $\alpha$ and disparate $\varphi$ size termination are presented. All termination events involving mid-chain radicals are assumed chain length independent (i.e., $\alpha^{t}$ and $\alpha^{tt} = 0$).

| $\alpha_{in}$ | $\varphi_{in}$ | $i^{prepolymer}$ | $\omega$ | Slope of best linear fit | $\varphi_{out}$ |
|---|---|---|---|---|---|
| 0.16 | 0.16 | 32 | 1.2 | −0.0835 | 0.167 |
| 0.16 | 0.16 | 56 | 1.2 | −0.0807 | 0.161 |
| 0.16 | 0.16 | 82 | 1.2 | −0.0793 | 0.159 |
| 0.4 | 0.4 | 32 | 1.5 | −0.200 | 0.400 |
| 0.4 | 0.4 | 56 | 1.5 | −0.201 | 0.402 |
| 0.4 | 0.4 | 82 | 1.5 | −0.195 | 0.390 |
| 0.8 | 0.8 | 32 | 2.5 | −0.419 | 0.838 |
| 0.8 | 0.8 | 56 | 2.5 | −0.429 | 0.858 |
| 0.8 | 0.8 | 82 | 2.5 | −0.451 | 0.902 |

mer reaction order ($\omega = 1$, classically) is predicted when intramolecular chain transfer is important. Additionally, $\omega$ decreases both when mid-chain radical termination is slower than end-chain radical termination (i.e., $k_{t,tt}^{i,j} < k_{t,t}^{i,j} < k_{t}^{i,j}$ ) and when mid-chain radical termination is chain length dependent (i.e., $\alpha^{t}$ and $\alpha^{tt}$ are greater than zero). Additionally, increasing $\alpha_{in}$ (i.e., from 0.16 to 0.4) increases the polymerization rate's dependence on the monomer concentration ($\omega$). Most importantly, Table 5 clearly shows that when the data is carefully analyzed (i.e., the virtual monomer reaction order is ascertained) that the method predicts accurately the extent that the termination rate coefficient depends on the radical's chain length when backbiting is accounted for. Thus, elucidation of the virtual monomer reaction order eliminates the need to ascertain the adjustable *backbiting* kinetic parameters.

### Accounting for Backbiting - Elucidation of $k_t$ for Disparate Size Radicals

Accessing the chain length dependence of the termination rate coefficient for *disparate* length radicals is a process that is significantly more complex when intramolecular chain transfer occurs. For example, two new termination rate coefficients ($k_{t,t}^{i,j}$ and $k_{t,tt}^{i,j}$) are accounted for that may differ in value and chain length dependence from conventional $k_{t}^{i,j}$. To investigate the impact of backbiting and tertiary radicals on the method's ability to predict the chain length dependence of $k_t$ for disparate length radicals, i.e., $\varphi$, where $k_{t}^{s,l} \propto (sl)^{-\varphi/2}$, the method

***Table 7.***
$\varphi_{out}$ is presented as determined from the slope of the best linear fit using the harmonic mean to the simulated data for the RAFT mediated MA polymerization. Various chain lengths for the macroRAFT species, $i^{prepolymer}$, and input values for the scaling exponent for equal $\alpha$ and disparate $\varphi$ size termination are presented. All termination events involving mid-chain radicals are assumed chain length independent (i.e., $\alpha^{t}$ and $\alpha^{tt} = 0$).

| $\alpha_{in}$ | $\varphi_{in}$ | $i^{prepolymer}$ | $\omega$ | Slope of best linear fit | $\varphi_{out}$ |
|---|---|---|---|---|---|
| 0.16 | 0.16 | 32 | 1.2 | −0.159 | 0.159 |
| 0.16 | 0.16 | 56 | 1.2 | −0.150 | 0.150 |
| 0.16 | 0.16 | 82 | 1.2 | −0.144 | 0.144 |
| 0.4 | 0.4 | 32 | 1.5 | −0.397 | 0.397 |
| 0.4 | 0.4 | 56 | 1.5 | −0.362 | 0.362 |
| 0.4 | 0.4 | 82 | 1.5 | −0.352 | 0.352 |
| 0.8 | 0.8 | 32 | 2.5 | −0.800 | 0.800 |
| 0.8 | 0.8 | 56 | 2.5 | −0.784 | 0.784 |
| 0.8 | 0.8 | 82 | 2.5 | −0.782 | 0.782 |

was expanded to include the necessary reactions for accounting for the core equilibrium and termination events when two RAFT distributions polymerize simultaneously (see Scheme 3). Elucidation of $\varphi_{out}$ when backbiting is important, first requires determination of the virtual monomer reaction order for the specific polymerization condition.

Tables 6 and 7 present $\omega$ as a function of termination and show that $\omega$ increases with increasing chain length dependent termination, i.e., $\omega$ is equal to 1.2, 1.5 and 2.5 when $\alpha_{in}$ and $\varphi_{in}$ are equal to 0.16, 0.4 and 0.8, respectively. Additionally, when backbiting and virtual monomer reaction orders greater than one are accounted for, the method predicts $\varphi_{out}$ better than the method that considers only fast propagation (see Tables 2 and 3).

Since the assumption that equal concentrations of reacting species is guaranteed via employing equal concentrations of RAFT agents (and neglecting a potential CLD of the RAFT equilibrium reactions) the only other assumption that could cause the model to inaccurately predict $\varphi_{out}$ is the assumption that each RAFT distribution is represented adequately by its average chain length. In fact, when backbiting is neglected and fast propagation is accounted for, the model predicts a more polydisperse ''short'' macroRAFT distribution that increases in polydispersity when the termination rate decreases more rapidly (i.e., with increasing chain length dependence, the geometric mean and greater radical size disparity (*s-l*)). When backbiting is accounted for a more monodisperse ''short'' macroRAFT distribution is predicted and consequently the method predicts more accurately $\varphi_{out}$. In this context, it is important to note that the macroRAFT distributions' polydispersity can be controlled via changing the initiation conditions. Thus, when the data is analyzed with extreme care and the reaction thoroughly characterized (i.e., intramolecular chain transfer is accounted for and $\omega$ is determined), determining the extent that the termination rate coefficient depends on disparate size radicals for the acrylate polymerization may be possible using this methodology.

## Conclusions

RAFT chemistry is used to elucidate the extent that $k_t^{s,l}$ depends on disparate length radicals for the fast propagating acrylate free radical polymerization, i.e., $\varphi$. The method builds upon a previously developed method that is able to access $k_t^{s,l}$ for the model monomer system styrene. Application of the method to the methyl acrylate polymerization shows the importance of considering intramolecular chain transfer (backbiting and the subsequent mid-chain radical reactions including RAFT equilibria). Accounting for intramolecular chain transfer reveals that the method's predictive capability is sensitive to the polymerization rate's dependence on monomer concentration, i.e., the virtual monomer reaction order. Simulation is used to illustrate that the virtual monomer reaction order depends on the polymerization conditions such as the termination rate coefficient's value and chain length dependence. Most significantly, knowledge of the virtual monomer reaction order may indeed allow for the accurate determination of the extent that $k_t$ depends on radical size (both $\alpha$ and $\varphi$) for the acrylate FRP. Since the method appears to be robust enough to handle acrylate polymerizations, it is our recommendation that the method be validated experimentally; yet (based on this work) it appears that experimental validation should be carried out initially using a slowly propagating monomer such as styrene to avoid the more complex data analysis necessary for some of the more reactive monomers.

*Acknowledgements:* We thank the Australian Research Council (ARC) for their financial support in the form of a Discovery Grant to C.B.-K. and M.H.S., an Australian Professorial Fellowship to C.B.-K. as well as a Federation

 

Fellowship to T.P.D. Additionally, we recognize Dr. Leonie Barner and Mr. Istvan Jacenyik for their outstanding management of CAMD.

[1] C. Decker, *Eur. Polym. J.* **2005**, *7–8*, 30–32.
[2] A. N. F. Peck, R. A. Hutchinson, *Macromolecules* **2004**, *37*, 5944–5951.
[3] H. Lu, J. A. Carioscia, J. W. Stansbury, C. N. Bowman, *Dent. Mat.* **2005**, *21*, 1129–1136.
[4] J. Ge, M. Trujillo, J. W. Stansbury, *Dental Materials* **2005**, *21*, 1163–1169.
[5] J. Chiefari, Y. K. Chong, F. Ercole, J. Krstina, J. Jeffery, T. P. T. Le, R. T. A. Mayadunne, G. F. Meijs, C. L. Moad, G. Moad, E. Rizzardo, S. H. Thang, *Macromolecules* **1998**, *31*, 5559–5562.
[6] T. Otsu, *Journal of Polymer Science Part A: Polymer Chemistry* **2000**, *38*, 2121–2136.
[7] C. Barner-Kowollik, T. P. Davis, J. P. A. Heuts, M. H. Stenzel, P. Vana, M. Whittaker, *J. Polym. Sci. Part A: Polym. Chem.* **2003**, *41*, 365–375.
[8] G. Chen, D. Huynh, P. L. Felgner, Z. Guan, *J. Am. Chem. Soc.* **2006**, *128*, 4298–4302.
[9] R. T. A. Mayadunne, E. Rizzardo, J. Chiefari, J. Kristina, G. Moad, A. Postma, S. H. Thang, *Macromolecules* **2000**, *33*, 243–245.
[10] C. J. Hawker, A. W. Bosman, E. Harth, *Chem. Rev.* **2001**, *101*, 3661–3688.
[11] Y. K. Chong, T. P. T. Le, G. Moad, E. Rizzardo, S. H. Thang, *Macromolecules* **1999**, *32*, 2071–2074.
[12] M. L. Becker, J. Liu, K. L. Wooley, *Biomacromolecules* **2005**, *6*, 220–228.
[13] H. Gao, K. Matyjaszewski, *Macromolecules* **2006**, *39*, 4960–4965.
[14] P. E. M. Allen, C. R. Patrick, *Makromol. Chem.* **1961**, *47*, 154–167.
[15] M. Buback, A. Kuelpmann, C. Kurz, *Macromol. Chem. Phys.* **2002**, *203*, 1065–1070.
[16] P. G. de Gennes, *J. Chem. Phys.* **1982**, *76*, 3316–3321.
[17] G. I. Litvinenko, V. A. Kaminsky, *Prog. React. Kinetics* **1994**, *19*, 139–193, and references within.
[18] G. T. Russell, *Macromol. Theory Simul.* **1995**, *4*, 497–517.
[19] G. Johnston-Hall, A. Theis, M. J. Monteiro, T. P. Davis, M. H. Stenzel, C. Barner-Kowollik, *Macromol. Chem. Phys.* **2005**, *206*, 2047–2053.
[20] M. Buback, M. Busch, C. Kowollik, *Macromol. Theory Simul.* **2000**, *9*, 442–452.
[21] M. Buback, M. Egorov, R. G. Gilbert, V. A. Kaminsky, O. F. Olaj, F. Oskar, G. T. Russell, *Macromol. Chem. Phys.* **2002**, *203*, 2570–2582.
[22] M. Buback, R. G. Gilbert, G. T. Russell, D. J. T. Hill, G. Moad, K. F. O'Driscoll, J. Shen, M. A. Winnik, *J. Polym. Sci. Part A: Polym. Chem.* **1992**, *30*, 851–863.
[23] M. Buback, E. Mueller, G. T. Russell, *J. Phys. Chem. A* **2006**, *110*, 3222–3230.
[24] G. B. Smith, J. Heuts, G. T. Russell, *Macromol. Symp.* **2005**, *226*, 133–146.
[25] P. Vana, T. P. Davis, C. Barner-Kowollik, *Macromol. Rapid. Commun.* **2002**, *23*, 952–956, and references within.
[26] M. Buback, F. D. Kuchta, *Macromol. Chem. Phys.* **1997**, *198*, 1455–1480.
[27] A. Feldermann, M. H. Stenzel, T. P. Davis, P. Vana, C. Barner-Kowollik, *Macromolecules* **2004**, *37*, 2404–2410.
[28] A. Theis, A. Feldermann, N. Charton, M. H. Stenzel, T. P. Davis, C. Barner-Kowollik, *Macromolecules* **2005**, *38*, 2595–2605.
[29] T. Junkers, A. Theis, M. Buback, T. P. Davis, M. H. Stenzel, P. Vana, C. Barner-Kowollik, *Macromolecules* **2005**, *38*, 9497–9508.
[30] A. Theis, A. Feldermann, N. Charton, T. P. Davis, M. H. Stenzel, C. Barner-Kowollik, *Polymer* **2005**, *46*, 6797–6809.
[31] G. Johnston-Hall, A. Theis, M. J. Monteiro, T. P. Davis, M. H. Stenzel, C. Barner-Kowollik, *Macromol. Chem. Phys.* **2005**, *206*, 2047–2053.
[32] A. Theis, T. P. Davis, M. H. Stenzel, C. Barner-Kowollik, *Macromolecules* **2005**, *38*, 10323–10327.
[33] A. Theis, T. P. Davis, M. H. Stenzel, C. Barner-Kowollik, *Polymer* **2006**, *47*, 999–1010.
[34] M. Buback, T. Junkers, P. Vana, *Macromol. Rapid. Comm.* **2005**, *26*, 796–802.
[35] T. M. Lovestead, A. Theis, T. P. Davis, M. H. Stenzel, C. Barner-Kowollik, *Macromolecules* **2006**, *39*, 4975–4982.
[36] A. Theis, M. H. Stenzel, T. P. Davis, C. Barner-Kowollik, "Obtaining Chain Length Dependent Termination Rate Coefficients via Thermally Initiated RAFT Experiments: Current Status and Future Challanges," in *ACS Symposium Series on Living/Controlled Free Radical Polymerization*, K. Matyjaszewski, Ed. ACS Press: Washington, D.C., **2006**; *944*, 486–500.
[37] M. Buback, M. Egorov, A. Feldermann, *Macromolecules* **2004**, *37*, 1768–1776.
[38] S. Perrier, C. Barner-Kowollik, J. F. Quinn, P. Vana, T. P. Davis, *Macromolecules* **2002**, *35*, 8300–9306.
[39] J. B. McLeary, J. M. McKenzie, M. P. Tonge, R. D. Sanderson, B. Klumperman, *Chem. Commun.* **2004**, 1950–1951.
[40] S. Beuermann, J. Paquet, D.A., J. H. McMinn, R. A. Hutchinson, *Macromolecules* **1996**, *29*, 4206–4215.
[41] K. Tanaka, B. Yamada, C. M. Fellows, R. G. Gilbert, T. P. Davis, L. H. Yee, G. B. Smith, M. T. L. Rees, G. T. Russell, *J. Poly. Sci. Part A: Poly. Chem.* **2001**, *39*, 3902 + 3915.
[42] J. M. Asua, S. Beuermann, M. Buback, P. Castignolles, B. Charleux, R. G. Gilbert, *Macromol. Chem. Phys.* **2004**, *205*, 2151–2160.
[43] M. Busch, M. Muller, *Macromol Symp* **2004**, *206*, 399–418.

 

[44] A. N. Nikitin, R. A. Hutchinson, *Macromolecules* **2005**, *38*, 1581–1590.
[45] E. Chernikova, A. Morozov, E. Leonova, E. Garina, V. Golubev, C. Bui, B. Charleux, *Macromolecules* **2004**, *37*, 6329–6339.
[46] C. Quan, M. Soroush, M. C. Grady, J. E. Hansen, W. J. Simonsick, Jr., *Macromolecules* **2005**, *38*, 7619–7628.
[47] A. Postma, T. P. Davis, G. Li, G. Moad, M. S. O'Shea, *Macromolecules* **2006**, In Press.
[48] E. Sato, T. Emoto, P. B. Zetterlund, B. Yamada, *Macromolecular Chemistry and Physics* **2004**, *205*, 1829–1839.
[49] A. N. Nikitin, P. Castignolles, B. Charleux, J.-P. Vairon, *Macromolecular Rapid Communications* **2003**, *24*, 778–782.
[50] C. Barner-Kowollik, J. F. Quinn, T. L. U. Nguyen, J. P. A. Heuts, T. P. Davis, *Macromolecules* **2001**, *34*, 7849–7857.
[51] M. Wulkow, M. Busch, T. P. Davis, C. Barner-Kowollik, *J. Polym. Sci. Part A: Polym. Chem.* **2004**, *42*, 1441–1448.
[52] N. Charton, A. Feldermann, A. Theis, M. H. Stenzel, T. P. Davis, C. Barner-Kowollik, *J. Polym. Sci. Part A: Polym. Chem.* **2004**, *42*, 5170–5179.
[53] M. Buback, C. H. Kurz, C. Schmaltz, *Macromol. Chem. Phys.* **1998**, *199*, 1721–1727.

 

 DOI: 10.1002/masy.200750210

# Synthesis of Poly(methyl acrylate) Grafted onto Silica Particles by Z-supported RAFT Polymerization

*Youliang Zhao, Sébastien Perrier**

**Summary:** RAFT polymerization of methyl acrylate (MA) mediated by silica-supported 3-(methoxycarbonyl-phenyl-methylsulfanylthiocarbonylsulfanyl) propionic acid (Si-MPPA) and 3-(benzylsulfanylthiocarbonylsulfanyl) propionic acid (Si-BSPA) was investigated. The molecular weight and polydispersity of grafted polymeric chains and the grafted chain transfer agent (CTA) efficiency ($G_e$) were strongly dependent on the types and loading of Si-CTAs and free CTA used in solution. Under similar reaction conditions, the graft polymerization mediated by Si-MPPA was better controlled than that using Si-BSPA. The introduction of a free CTA in solution during Si-MPPA mediated polymerization could significantly decrease the polydispersity of free and grafted polymeric chains and enhance the grafted CTA efficiency, and longer polymeric chains could be grafted onto silica support when Si-MPPA with a higher CTA loading was used to mediate the polymerization. In all cases, the RAFT polymerization using 2-(2-cyanopropyl) dithiobenzoate (CPDB) as a free CTA could afford well-defined grafted PMA and significantly increased $G_e$ value, while the polymerization rate was also decreased.

**Keywords:** graft polymerization; kinetics; poly(methyl acrylate); RAFT polymerization; silica

## Introduction

Reversible addition-fragmentation chain transfer (RAFT) polymerization has become one of the most promising living radical polymerization techniques, due to its tolerance to a wide range of reaction conditions, the straight-forward setup to yield block copolymers, and its versatility towards the range of monomers with variable functionality.[1–5] Meanwhile, the surface modification of inorganic particles and synthetic resins with polymeric chains are of great interest due to their unique properties and potential applications.[6–8] Recently, RAFT graft polymerization has attracted increasing attention due to its ability to afford well-defined polymers with controlled molecular weight, low polydispersity and controlled chain-end functionality,[9–24] and a wide range of polymeric chains have been successfully grafted onto various solid supports using this technique. In general, RAFT graft polymerization based on solid supports can be performed using both (a) the R-group approach where the chain transfer agent (CTA) is attached to the backbone via the leaving and reinitiating R group and (b) the Z-group approach where the CTA is attached to the backbone via the stabilizing Z group, and both methods have advantages and limitations.[3–5] In Z-supported RAFT polymerization, the shielding effect results in relatively low grafting density, but it can produce well-defined grafted polymers with unimodal molecular weight distribution and enable the synthesis of functional block copolymers.[16, 25–28] Until now, reports on Z-supported RAFT polymerization from a solid support are scarce.[14–18]

Department of Colour and Polymer Chemistry, University of Leeds, Leeds LS2 9JT, UK
Fax: +44 113 343 2947
E-mail: s.perrier@leeds.ac.uk

In our previous study, silica-supported 3-(methoxycarbonyl-phenyl-methylsulfanylthio carbonylsulfanyl)propionic acid (Si-MPPA) with a MPPA loading of 0.322 mmol/g was synthesized and applied to RAFT polymerization of methyl acrylate (MA), methyl methacrylate, butyl acrylate and styrene to produce well-defined homopolymer grafted onto silica particles.[16] The Z-supported RAFT polymerization could afford living polymeric chains attached to the solid surface, evident from the highly efficient chain extension polymerization to produce well-defined diblock copolymers. To investigate the effects of types and loading of Si-CTA on graft polymerization, Si-MPPA with a lower MPPA loading and silica supported 3-(benzylsulfanylthiocarbonylsulfanyl)propionic acid (Si-BSPA) were also synthesized in this study, and the RAFT graft polymerization of MA mediated by various Si-CTAs was investigated in detail.

## Experimental Part

### Materials

All solvents, monomers, and other chemicals were of analytical grade. Silica gel particles with particle size of 35–70 μm and a specific surface area of 500 $m^2/g$ were purchased from Aldrich. The benzylchloride functionalized silica (Si–Cl, with a loading of 0.563 mmol/g) and Si-MPPA1 (with a loading of 0.322 mmol/g) were synthesized following previously published methods.[14,16] 3-(Methoxycarbonyl-phenyl-methylsulfanylthiocarbonylsulfanyl) propionic acid (MPPA),[14] 3-(benzylsulfanylthiocarbonylsulfanyl)propionic acid (BSPA)[25] and 2-(2-cyanopropyl) dithiobenzoate (CPDB)[1] were synthesized and purified according to literature methods. MA was passed through a basic alumina (Brockmann I) column to remove the inhibitor before use. Tetrahydrofuran (THF) and toluene were dried over 4 Å molecular sieves. 2,2′-Azobisisobutyronitrile (AIBN, Fisher) was recrystallized twice from ethanol.

### Characterization

The number-average molecular weight ($M_n$) and polydispersity (PDI) of polymer samples were determined by GPC at ambient temperature using a system equipped with a Polymer Laboratories 5.0 μm-bead-size guard column (50 × 7.5 mm) and two PLgel 5.0 μm MIXED-C columns with a differential refractive index detector (shodex, RI-101). THF was used as an eluent at a flow rate of 1.0 mL/min and toluene was used as a flow rate marker. Samples were calibrated with calibrated with PMMA standard samples with $M_n$ value in the range of 1944000-1020 g/mol. $^1H$ NMR spectra were recorded on a Bruker 400 UltraShield spectrometer at 25 °C using $CDCl_3$ as a solvent. Chlorine and sulfur analyses were conducted using the Schoniger Oxygen Flask combustion method followed by the relevant titration. Fourier Transform Infrared (FT-IR) spectra were recorded on a Perkin-Elmer Spectrum One FT-IR spectrometer using a single reflection horizontal ATR accessory. Thermogravimetric analyses (TGA) were carried out using a TA Instrument TGA 2050 Thermogravimetric Analyzer from room temperature to 500 °C at a rate of 10 °C/min under nitrogen.

### Synthesis of Si-CTA

Si-MPPA2 (loading of 0.109 mmol/g) and Si-BSPA (loading of 0.120 mmol/g) were synthesized according to a similar procedure to that of Si-MPPA1 (loading of 0.322 mmol/g).[16] To a round flask was added 15 g (8.45 mmol) of Si–Cl, 1.38 g (10.0 mmol) of potassium carbonate, 2.00 g (6.06 mmol) of MPPA, and 200 mL of THF under nitrogen. After stirring at room temperature for 30 min, 2.90 g (98%, 7.72 mmol) of tetra-n-butyl ammonium iodide was added to the flask. The mixtures were stirred at 60 °C overnight, cooled down, filtered and thoroughly washed with water and organic solvents such as THF and toluene. After drying under vacuum, 15.5 g of Si-MPPA2 was obtained as yellow solid. Elemental analysis: S, 1.05% (loading of 0.109 mmol/g). FT-IR: 1722 (C=O), 1603

 

(C=C), 1556, 1456, 1380 ($CH_3$), 1040 (broad, Si–O, C–O, C=S), 794, 697 $cm^{-1}$.

### RAFT Polymerization of MA Mediated by Si-CTA

In a typical run (see run 3 of Table 1), Si-MPPA1 (0.400 g, 129 μmol), toluene (2.91 mL), CPDB (28.5 mg, 129 μmol), MA (2.78 g, 32.3 mmol), and AIBN (2.11 mg, 12.9 μmol) were added to a Schlenk tube. The tube was subjected to three freeze-pump-thaw cycles to remove oxygen, and then placed into an oil bath preheated to 60 °C. The polymerization was quenched by putting the tube into ice water after 42 h, and small amount of polymerization solution was drawn to do GPC analysis and measure the monomer conversion in solution by $^1$H NMR. The polymer grafted silica was filtered, washed with toluene and THF, and dried under vacuum until constant weight before TGA measurement. GPC analyses: cleaved grafted PMA, $M_n(g) = 4080$, $PDI(g) = 1.08$; free PMA, $M_n(f) = 4360$, $PDI(f) = 1.15$. The total monomer conversion ($C = 39.6\%$) and weight grafting ratio ($G_r = 16.8\%$) of polymeric chains were determined by equations 1 and 2, where $G_r$ means the mass ratio of grafted polymer to solid support, $W\%_{\text{Si-polymer}}$ and $W\%_{\text{Si-CTA}}$ are the percent weight loss between room temperature and 500 °C corresponding to the decomposition of polymer grafted silica (Si-polymer) and Si-CTA, $W_m$, $W_{Si}$ ($W_{Si} = W_{\text{Si-CTA}}(100 - W\%_{\text{Si-CTA}})/100$) and $W_{\text{Si-CTA}}$ are the original weights of monomer, silica gel and Si-CTA, and $C_{m,f}$ is the conversion in solution determined by $^1$H NMR, respectively.

$$G_r = \frac{W\%_{\text{Si-polymer}}}{100 - W\%_{\text{Si-polymer}}} - \frac{W\%_{\text{Si-CTA}}}{100 - W\%_{\text{Si-CTA}}} \quad (1)$$

$$C = \frac{(W_m - W_{Si} \times G_r) \times C_{m,f} + W_{Si} \times G_r}{W_m} \quad (2)$$

### Aminolysis to Cleave the Grafted Polymeric Chains

In a typical experiment, to a glass tube were added 100 mg of PMA grafted silica particles, 5 mL of THF and 2–3 drops of dilute aqueous solution of $Na_2S_2O_4$.[29] The solution was degassed with nitrogen for 10 min, and 0.1 mL of n-hexylamine was

***Table 1.***
Polymerization results for RAFT graft polymerization of MA mediated by Si-MPPA1 (runs 1–3), Si-MPPA2 (runs 4–6) and Si-BSPA (runs 7-11).[a)]

| Run | Free CTA | $r_f$[b)] | $r_m$[c)] | t (h) | C%[d)] | $M_n$(th)[e)] | $M_n$(g)[f)] | PDI(g)[f)] | $M_n$(f)[g)] | PDI(f)[g)] | $G_r$ (%)[h)] | $G_e$ (%)[i)] |
|---|---|---|---|---|---|---|---|---|---|---|---|---|
| 1 | MPPA | 0 | 250 | 21 | 98.4 | 21500 | 18400 | 1.85 | 109000 | 1.96 | 19.4 | 3.26 |
| 2 | MPPA | 1 | 250 | 21 | 97.2 | 10800 | 9800 | 1.18 | 23500 | 1.15 | 25.9 | 8.20 |
| 3 | CPDB | 1 | 250 | 42 | 39.6 | 4480 | 4080 | 1.08 | 4360 | 1.15 | 16.8 | 12.8 |
| 4 | MPPA | 0 | 250 | 21 | 98.0 | 21400 | 31000 | 2.04 | 128500 | 2.34 | 14.9 | 4.41 |
| 5 | MPPA | 1 | 250 | 21 | 95.8 | 10600 | 4560 | 1.20 | 32400 | 1.18 | 11.5 | 23.1 |
| 6 | CPDB | 1 | 250 | 42 | 35.5 | 4040 | 3500 | 1.12 | 4080 | 1.10 | 11.2 | 29.4 |
| 7 | BSPA | 0 | 250 | 21 | 98.4 | 21500 | 27700 | 2.04 | 46200 | 2.12 | 24.7 | 7.43 |
| 8 | BSPA | 1 | 250 | 21 | 98.0 | 10800 | 9400 | 1.56 | 29800 | 2.24 | 15.5 | 13.8 |
| 9 | BSPA | 1 | 350 | 21 | 97.5 | 15000 | 11300 | 1.84 | 49800 | 1.98 | 19.6 | 14.4 |
| 10 | BSPA | 1 | 500 | 21 | 97.2 | 21200 | 15500 | 1.67 | 69700 | 1.39 | 19.2 | 10.3 |
| 11 | CPDB | 1 | 350 | 24 | 32.0 | 5100 | 4100 | 1.18 | 6050 | 1.20 | 15.2 | 30.9 |

a) Polymerization conditions: $[Si\text{-}CTA]_0$:$[AIBN]_0 = 1{:}0.1$, in 50 (v%) of toluene at 60 °C.
b) Molar ratio of free CTA to Si-CTA.
c) Feed ratio of monomer to Si-CTA.
d) Total monomer conversion.
e) $M_n(th) = M_{w,m} \times C\% \times [M]_0/([Si\text{-}CTA]_0 + [\text{free CTA}]_0) + M_{w,CTA}$, where $M_{w,m}$ and $M_{w,CTA}$ are molecular weights of MA and free CTA used in solution.
f) Molecular weight and polydispersity of grafted polymers determined by GPC.
g) Molecular weight and polydispersity of free polymers produced in solution.
h) Weight grafting ratio of PMA grafted silica particles determined by TGA.
i) Apparent grafted CTA efficiency.

 

added. The aminolysis was conducted at room temperature overnight. The solution was filtered and the filtrate was evaporated to remove the volatiles. The cleaved PMA was subjected to GPC analysis.

## Results and Discussion

In this study, two types of silica supported CTAs, Si-MPPA and Si-BSPA, were synthesized by a two-step reaction (Scheme 1): (a) introduction of the benzylchloride functionality on silica surface and (b) attaching MPPA or BSPA to the support by coupling reaction between silica-supported benzylchloride and CTA. The target CTA was successfully attached to silica particles, evident from IR, TGA and elemental analysis. Elemental analysis revealed the loading in active sites of the various Si-CTAs ($G_{Si\text{-}CTA}$) were 0.322 mmol/g (Si-MPPA1), 0.109 mmol/g (Si-MPPA2) and 0.120 mmol/g (Si-BSPA), which was very similar to the value estimated by TGA. TGA analyses of the various Si-CTAs (Figure 1) revealed an amount of physisorbed water around 4%, and the weight loss beyond 120 °C was ascribed to thermal degradation of the grafted CTAs.

RAFT polymerization of MA mediated by different Si-CTAs was conducted in toluene at 60 °C, and the polymerization results are shown in Table 1. It was found that the grafted polymeric chains could be efficiently recovered by aminolysis using n-hexylamine in THF, evident from TGA, IR, GPC and elemental analysis. The weight grafting ratio ($G_r$) of PMA on silica surface was determined by TGA, and the apparent grafted CTA efficiency ($G_e$) was calculated from the equation $G_e = G_r/(G_{Si\text{-}CTA} \cdot M_n(g))$, where $G_e$ is the molar ratio of grafted polymeric chains to the CTA loading on solid support, $G_{Si\text{-}CTA}$ is the loading of CTA grafted onto solid support, and $M_n(g)$ is the molecular weight of grafted PMA determined by GPC. For polymerization mediated by Si-CTA without free CTA in solution (runs 1, 4 and 7 of Table 1), longer polymeric chains could be grafted onto silica particles, but the polydispersity of grafted polymer was very high, and the $G_e$ value was low, suggesting an uncontrolled polymerization system. To better control the polymerization, a free CTA was introduced in the reaction solution. During RAFT polymerization mediated by Si-MPPA in the presence of free MPPA (runs 2 and 5), the polydispersity indices of free and grafted polymers are lowered to less than 1.2, indicating that a better control over the free radical polymerization in solution is obtained by introducing the same CTA in solution. In Z-supported RAFT polymerization, the growing chain radicals always propagate in solution, whilst the polymeric chains attached to the support remain in the dormant state.[14,16] Steric hindrance prevents the addition of the propagating

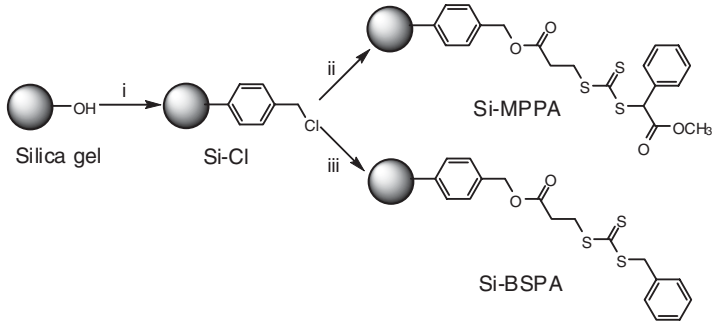


***Scheme 1.***

Synthetic route to Si-MPPA and Si-BSPA. Reaction conditions: (i) 4-(chloromethyl)phenyltrimethoxysilane, toluene, 80 °C, 15 h; (ii) MPPA, $K_2CO_3$, $Bu_4NI$, THF, 60 °C, 18 h; (iii) BSPA, $K_2CO_3$, $Bu_4NI$, THF, 60 °C, 18 h.

 

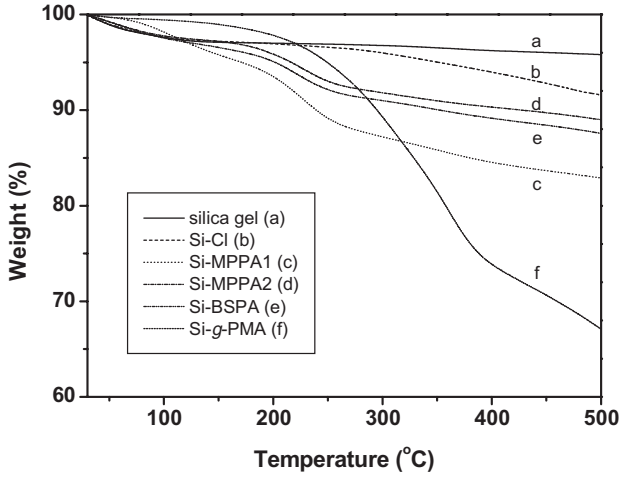


***Figure 1.***
TGA curves of silica gel, Si-Cl, Si-MPPA, Si-BSPA and Si-*g*-PMA.

chains to the Z-supported CTA, thus increasing the number of termination events, and inducing a poor control over molecular weight. Indeed, we observe that the molecular weight values of free polymers were much higher than those of the grafted polymers. Therefore, the introduction of a free CTA should permit to improve the control over polymerization in solution, and favor the addition-fragmentation reactions on solid support.

For RAFT polymerization mediated by Si-BSPA (runs 7–10), the polydispersity of free and grafted polymers was very high even if free BSPA was introduced into the solution, suggesting the RAFT graft polymerization was significantly affected by the type of CTA. To further understand this aspect, polymerization kinetics for RAFT polymerization of MA mediated by MPPA and BSPA in toluene at 60 °C was investigated. From the results shown in Figure 2, it can be seen that first order kinetics were maintained until high conversion in both cases, and the polymerization could indeed afford PMA with well-defined molecular weight and low polydispersity (PDI $< 1.2$) at various conversions. As expected from trithiocarbonates, rates of polymerization are similar, and the only difference is in the presence of an induction time (initialization) for the polymerization mediated by MPPA. A potential explanation to the poor control of a RAFT graft polymerization mediated by Si-BSPA is the poor efficiency of the benzyl group as leaving/reinitiating group. Indeed, RAFT polymerization generally shows an initialization period, during which all the CTAs are consumed, before the polymerization starts. However, in the case of polymerizations mediated by Si-BSPA, the monomer conversion increases immediately, suggesting that polymeric chains start their growth despite the fact that some CTAs have not yet reacted. Slow reaction of the CTA with propagating radicals would lead to polymeric chains starting their growth at different times, therefore leading to broader molecular weight distributions. It is however interesting to note that this effect has a dramatic effect on the control over polymerizations from silica particles, but does not seem to affect the control of the polymerization in solution (see Figure 2, PDI's $< 1.2$).

For RAFT polymerization mediated by Si-MPPA, it was found that the polymerization using Si-MPPA2 (lower CTA loading) could only afford low molecular weight of grafted polymer even at high conversion, indicating that the RAFT graft polymerization is also dependant on the loading of grafted CTA on silica surface. For poly-

 

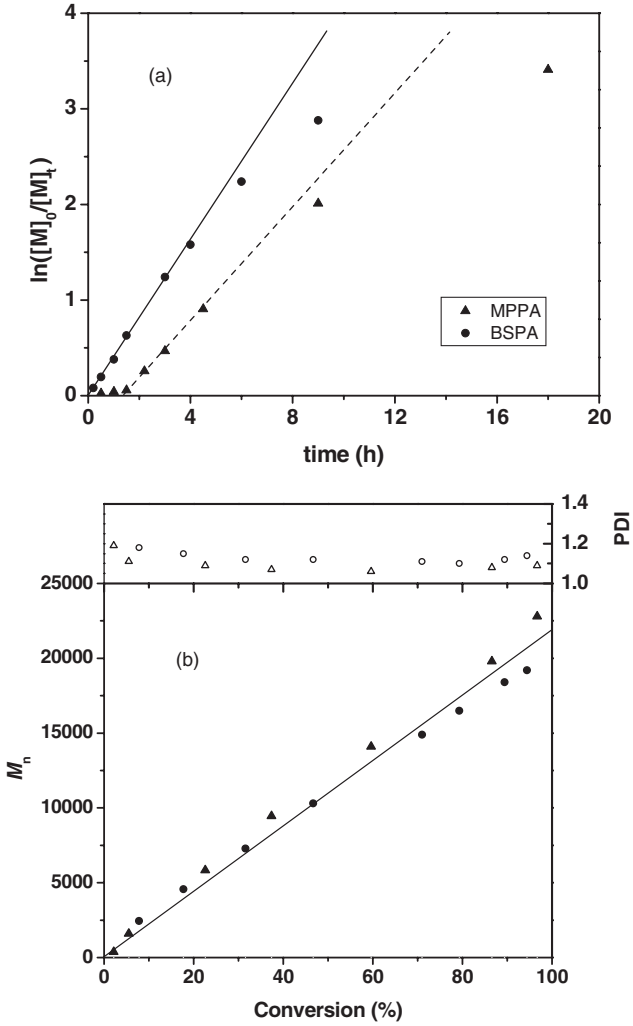


***Figure 2.***
Polymerization kinetic curves (a) and $M_n$ and PDI evolution with conversion (b) for RAFT polymerization of MA mediated by MPPA (triangle) and BSPA (circle): $[MA]_0:[CTA]_0:[AIBN]_0 = 250:1:0.1$, in 50 (v%) of toluene at 60 °C. The line in b means the theoretical molecular weight.

merization mediated by Si-MPPA1 and Si-MPPA2 with different CTA loadings, polymerization kinetics were investigated in order to better understand the relationships between molecular weights and conversion for both free and grafted polymers. When polymerization ($[MA]_0:[Si\text{-}MPPA]_0:[MPPA]_0$: $[AIBN]_0 = 400:1:1:0.1$, $[MA]_0 =$ 3.0 mol/L) was conducted in toluene at 60 °C, the apparent kinetic curves are depicted in Figure 3. It was found that the pseudo-first-order polymerization kinetics was maintained until high conversion up to 80%, while a significant induction period was observed in both cases. Figure 4 indicates the evolution of molecular weight and polydispersity with increasing conversion. For polymerization mediated by Si-MPPA1, the molecular weights of free and grafted polymers were similar at low conversion but tended to differ rapidly with increasing conversion. We attribute this behavior to the increased shielding effect with increasing conversion (Figure 4a).

 

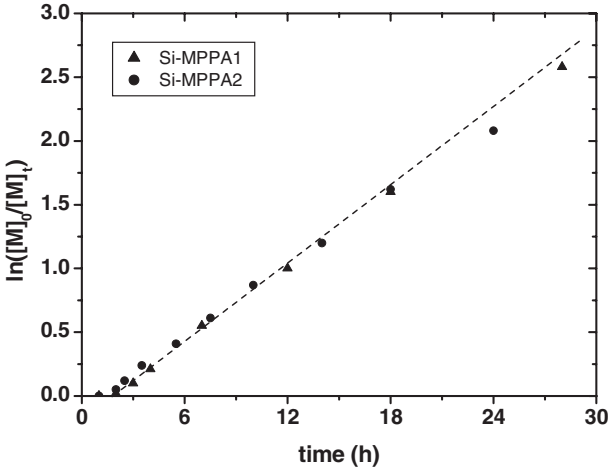


***Figure 3.***
Pseudo-first-order kinetic curves for RAFT polymerization of MA mediated by Si-MPPA in the presence of MPPA. Polymerization conditions: $[MA]_0$:$[Si\text{-}MPPA]_0$:$[MPPA]_0$:$[AIBN]_0 = 400{:}1{:}1{:}0.1$, $[MA]_0 = 3.0$ mol/L, in toluene at 60 °C.

The GPC traces of free and grafted polymers gradually shifted to higher molecular weight sides with increasing time (Figure 5A), indicating the molecular weights could be adjusted by the control of monomer conversion. For polymerization mediated by Si-MPPA2 (Figure 4b), however, only short grafted polymeric chains ($M_n < 5{,}000$ g/mol) could be achieved, and no obvious increase in molecular weight of grafted polymer was observed for monomer conversion higher than 40% (Figure 5B). These results indicate that almost all the reactive sites were hindered from monomer and growing polymeric chain radicals at high conversion. A potential explanation is that most of the CTA functionality at low loading exists in the internal surface of mesopores, and the graft polymerization takes place almost entirely inside the mesopores.[30] As expected, the polydispersity indices of various polymers obtained at different conversions were relatively low ($M_w/M_n < 1.3$), and no obvious shoulders and tailings were observed in the GPC traces of the grafted polymers (Figure 5). This indicates that better-defined polymers without dead polymeric chains could be successfully grafted onto silica support. These results also confirmed the significant effects of loading of Si-CTA on Z-supported RAFT polymerization.

For RAFT graft polymerization, less steric hindrance and similar polymerization rates in solution and on surface are crucial to obtain well-defined free and grafted polymers. To improve control of the graft polymerization, a dithiobenzoate-based CTA, CPDB, was introduced into the polymerization system. Since the polymerization rate for RAFT polymerization mediated by dithiobenzoates (CPDB) is retarded when compared to that using trithiocarbonates (MPPA and BSPA), it is possible to further decrease the polymerization rate in solution. The results as listed in Table 1 (runs 3, 6 and 11) indicated that the polymerization rate in solution was efficiently slowed down. In these cases, the molecular weights of free polymers were very close to those of the corresponding grafted polymers, both were similar to the theoretical values, with PDI less than 1.2. Comparing to similar conversions for the polymerizations in presence of free MPPA, for which the molecular weight of free and grafted polymeric chains differ greatly (Figure 4), it is clear that the introduction of CPDB improves control over molecular weight

 

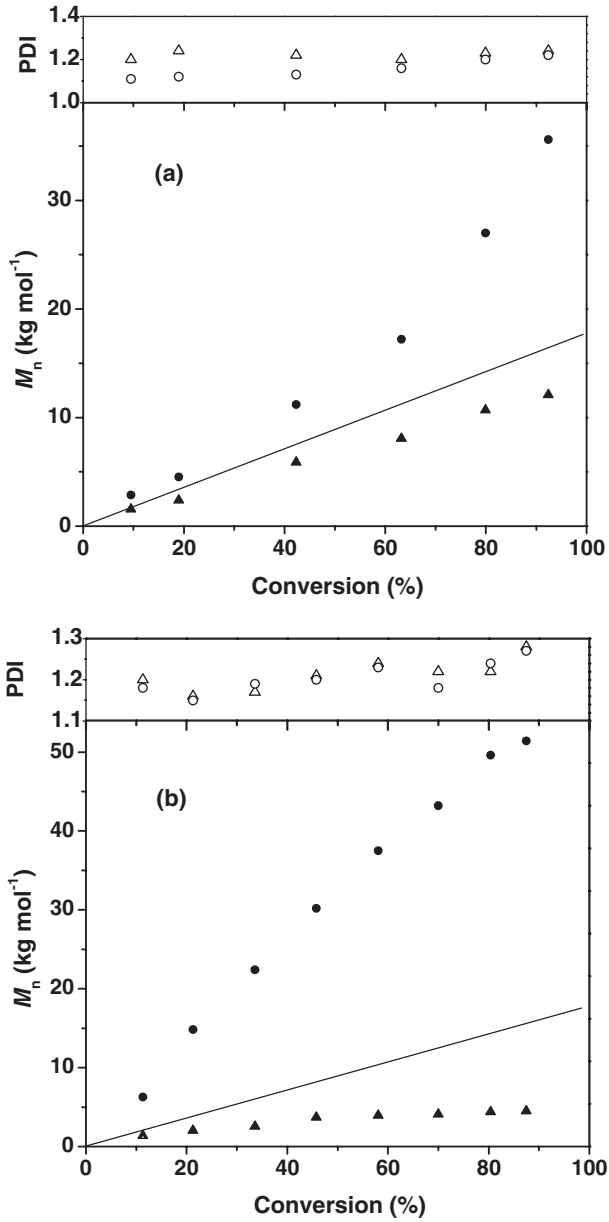


***Figure 4.***
Dependence of $M_n$ and PDI of free (circle) and grafted (triangle) PMAs on conversion for RAFT polymerization of MA mediated by Si-MPPA1 (a) and Si-MPPA2 (b) in the presence of MPPA. See Figure 3 for polymerization conditions.

and PDI. This observation is also supported by a similar study undertaken on different monomers.[16] The above results also demonstrated that the slow propagation of free chains in solution would favor the addition-fragmentation reactions on solid support and result in similar polymerization rate in solution and on surface, therefore affording better-defined grafted polymers than that using the same free CTA.

The results in Table 1 also indicated that the apparent grafted CTA efficiency was affected by the types and loading of

 

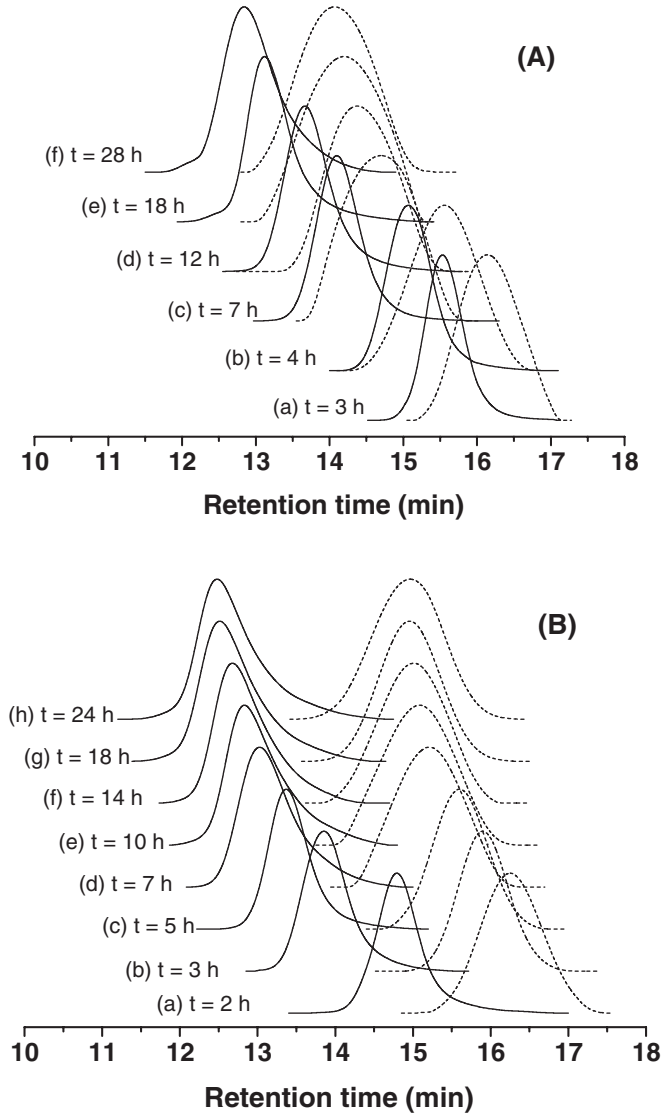


***Figure 5.***
GPC traces of free (solid line) and grafted (dashed line) PMA samples synthesized by RAFT graft polymerization of MA at various times: (A) Si-MPPA1; (B) Si-MPPA2.

Si-CTAs and free CTA in solution. The polymerizations without using a free CTA give low $G_e$ values, maybe due to a poorer control over molecular weights and increased shielding effect resulting from longer propagating polymeric chain radicals. When a free CTA is introduced in the solution, the control over polymerization is improved, and the graft polymerization conducted smoothly, thus favoring the surface graft polymerization and increasing the grafted CTA efficiency. For polymerization mediated by Si-MPPA, higher $G_e$ values are achieved when Si-MPPA2 with a lower CTA loading is used, maybe due to less shielding effect at the early stage of polymerization. In all cases, the graft polymerization using CPDB in reaction system affords very high $G_e$ values, confirming slow propagation of polymeric

 

chain radical in solution favors the graft polymerization and affords more active CTAs on silica surface. The above results indicated that the grafted CTA efficiency depends on the type and loading of Si-CTA, the nature of free CTA used in solution and the grafted polymeric chain length.

## Conclusion

Si-MPPA and Si-BSPA were synthesized and used to mediate the RAFT polymerization of MA. The molecular weight and polydispersity of grafted polymer and the grafted CTA efficiency were affected by the types and loading of Si-CTAs and free CTA in solution. When the same free CTA was introduced into the solution, the polymerization mediated by Si-MPPA was more controlled than that using Si-BSPA. For RAFT polymerization mediated by Si-MPPA, the introduction of a free CTA in solution during polymerization could significantly decrease the polydispersity of free and grafted PMA and enhance the grafted CTA efficiency. Moreover, the RAFT graft polymerization using CPDB as a free CTA afforded well-defined PMA grafted onto silica support and significantly increased $G_e$ value, while the polymerization rate was also decreased.

*Acknowledgements:* Y. L. Zhao acknowledges the financial support from the University of Leeds and EPSRC.

[1] J. Chiefari, Y. K. Chong, F. Ercole, J. Krstina, J. Jeffery, T. P. T. Le, R. T. A. Mayadunne, G. F. Meijs, C. L. Moad, G. Moad, E. Rizzardo, S. H. Thang, *Macromolecules* **1998**, *31*, 5559.
[2] Y. K. Chong, T. P. T. Le, G. Moad, E. Rizzardo, S. H. Thang, *Macromolecules* **1999**, *32*, 2071.
[3] G. Moad, E. Rizzardo, S. H. Thang, *Aust. J. Chem.* **2005**, *58*, 379.
[4] S. Perrier, P. Takolpuckdee, *J. Polym. Sci., Part A: Polym. Chem.* **2005**, *43*, 5347.
[5] A. Favier, M. T. Charreyre, *Macromol. Rapid Commun.* **2006**, *27*, 653.
[6] G. J. de Soler-Illia, C. Sanchez, B. Lebeau, J. Patarin, *Chem. Rev.* **2002**, *102*, 4093.
[7] G. Kickelbick, *Prog. Polym. Sci.* **2003**, *28*, 83.
[8] B. Radhakrishnan, R. Ranjan, W. J. Brittain, *Soft Matter* **2006**, *2*, 386.
[9] Y. Tsujii, M. Ejaz, K. Sato, A. Goto, T. Fukuda, *Macromolecules* **2001**, *34*, 8872.
[10] L. Barner, N. Zwaneveld, S. Perera, Y. Pham, T. P. Davis, *J. Polym. Sci., Part A: Polym. Chem.* **2002**, *40*, 4180.
[11] L. Barner, C. E. Li, X. J. Hao, M. H. Stenzel, C. Barner-Kowollik, T. P. Davis, *J. Polym. Sci., Part A: Polym. Chem.* **2004**, *42*, 5067.
[12] C. Z. Li, B. C. Benicewicz, *Macromolecules* **2005**, *38*, 5929.
[13] C. Z. Li, J. Han, C. Y. Ryu, B. C. Benicewicz, *Macromolecules* **2006**, *39*, 3175.
[14] S. Perrier, P. Takolpuckdee, C. A. Mars, *Macromolecules* **2005**, *38*, 6770.
[15] P. Takolpuckdee, C. A. Mars, S. Perrier, *Org. Lett.* **2005**, *7*, 3449.
[16] Y. L. Zhao, S. Perrier, *Macromolecules* **2006**, *39*, 8603.
[17] M. Hernández-Guerrero, T. P. Davis, C. Barner-Kowollik, M. H. Stenzel, *Eur. Polym. J.* **2005**, *41*, 2264.
[18] M. H. Stenzel, L. Zhang, W. T. S. Huck, *Macromol. Rapid Commun.* **2006**, *27*, 1121.
[19] Q. Peng, D. M. Y. Lai, E. T. Kang, K. G. Neoh, *Macromolecules* **2006**, *39*, 5577.
[20] S. Perrier, P. Takolpuckdee, J. Westwood, D. M. Lewis, *Macromolecules* **2004**, *42*, 2709.
[21] D. Roy, J. T. Guthrie, S. Perrier, *Macromolecules* **2005**, *38*, 10363.
[22] M. Baum, W. J. Brittain, *Macromolecules* **2002**, *35*, 610.
[23] C. Y. Hong, Y. Z. You, C. Y. Pan, *Chem. Mater.* **2005**, *17*, 2247.
[24] C. Y. Hong, Y. Z. You, C. Y. Pan, *J. Polym. Sci., Part A: Polym. Chem.* **2006**, *44*, 2419.
[25] M. H. Stenzel, T. P. Davis, *J. Polym. Sci., Part A: Polym. Chem.* **2002**, *40*, 4498.
[26] X. J. Hao, C. Nilsson, M. Jesberger, M. H. Stenzel, E. Malmström, T. P. Davis, E. Östmark, C. Barner-Kowollik, *J. Polym. Sci., Part A: Polym. Chem.* **2004**, *42*, 5877.
[27] A. Duréault, D. Taton, M. Destarac, F. Leising, Y. Gnanou, *Macromolecules* **2004**, *37*, 5513.
[28] V. Darcos, A. Duréault, D. Taton, Y. Gnanou, P. Marchand, A. M. Caminade, J.-P. Majoral, M. Destarac, F. Leising, *Chem. Commun.* **2004**, 2110.
[29] V. Lima, X. L. Jiang, J. Brokken-Zijp, P. J. Schoenmakers, B. Klumperman, R. van der Linde, *J. Polym. Sci., Part A: Polym. Chem.* **2005**, *43*, 959.
[30] M. Save, G. Granvorka, J. Bernard, B. Charleux, C. Boissière, D. Grosso, C. Sanchez, *Macromol. Rapid Commun.* **2006**, *27*, 393.

 

 DOI: 10.1002/masy.200750211

# RAFT Polymerization: Adding to the Picture

*Ezio Rizzardo,* Ming Chen, Bill Chong, Graeme Moad, Melissa Skidmore, San H. Thang*

**SUMMARY:** Factors affecting the choice of RAFT agent [RSC(Z)=S] for a given polymerization are discussed. For polymerization of methyl methacrylate (MMA), tertiary cyanoalkyl trithiocarbonates provide very good control over molecular weight and distribution and polymerizations show little retardation. The secondary trithiocarbonate RAFT agents with R = CHPh(CN) also gives good control but an inhibition period attributed to slow reinitiation is manifest. Radical induced reduction with hypophosphite salts provides a clean and convenient process for removal of thiocarbonylthio end groups of RAFT-synthesized polymers. Two methods providing simultaneous control over stereochemistry and molecular weight distribution of chains formed by radical polymerization are reported. Polymerization of MMA in the presence of scandium triflate provides a more isotactic PMMA. A similar RAFT polymerization with trithiocarbonate RAFT agents also provides control and avoids issues of RAFT agent instability seen with dithiobenzoate RAFT agents in the presence of Lewis acids. RAFT polymerization of tetramethylammonium methacrylate at 45 °C provides a more syndiotactic PMMA of controlled molecular weight and distribution (after methylation; *mm:mr:rr* 2:21:77 compared to 3:35:62 when formed by bulk polymerization of MMA).

**Keywords:** molecular weight; radical polymerization; RAFT agents; facticity

## Introduction

Control of radical polymerization with the addition of thiocarbonylthio compounds that serve as reversible addition fragmentation chain transfer (RAFT) agents was first reported in 1998.[1,2] Since that time much research carried out in these laboratories and elsewhere has demonstrated that RAFT polymerization is an extremely versatile process.[3–5] It can be applied to form narrow polydispersity polymers or copolymers from most monomers amenable to radical polymerization. It is possible to take RAFT polymerizations to high conversion and achieve commercially acceptable polymerization rates. Polymerizations can be successfully carried out in heterogeneous media (emulsion, miniemulsion, suspension). There is compatibility with a wide range of functionality in monomers, solvents and initiators. Stars, blocks, microgel and hyperbranched structures, supramolecular assemblies and other complex architectures are accessible and can have high purity.

In this paper we add to the picture by describing how to choose RAFT agents for controlling methyl methacrylate polymerization, how to remove the thiocarbonylthio functionality from RAFT-synthesized polymers and how to use RAFT polymerization to achieve simultaneous control over molecular weight, molecular weight distribution and tacticity.

### Choice of RAFT Agents

RAFT polymerization comprises the sequence of addition-fragmentation equilibria shown in Scheme 1.[1] Initiation and radical-radical termination occur as in conventional radical polymerization. In the early

CSIRO Molecular and Health Technologies, Bag 10 Clayton South, Victoria 3169, Australia
E-mail: Ezio.Rizzardo@csiro.au

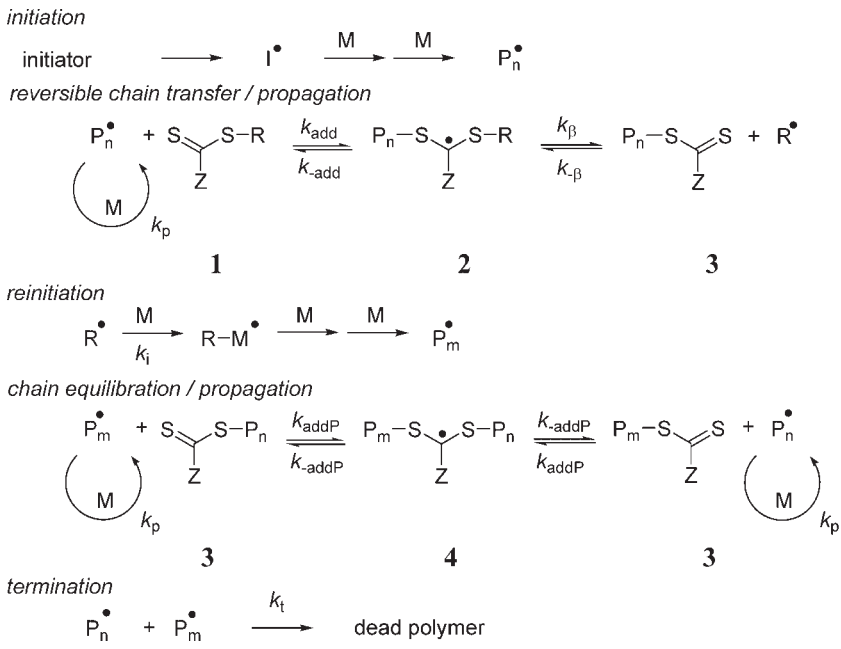


***Scheme 1.***
Mechanism of RAFT polymerization.

stages of the polymerization, addition of a propagating radical ($P_n^\bullet$) to the thiocarbonylthio compound [RSC(Z)=S (**1**)] followed by fragmentation of the intermediate radical provides a polymeric thiocarbonylthio compound [$P_nS(Z)C=S$ (**3**)] and a new radical ($R_\bullet$). Reaction of this radical ($R_\bullet$) with monomer forms a new propagating radical ($P_m^\bullet$). Rapid equilibrium between the active propagating radicals ($P_n^\bullet$ and $P_m^\bullet$) and the dormant polymeric thiocarbonylthio compounds (**3**) provides equal probability for all chains to grow and allows for the production of narrow polydispersity polymers. When the polymerization is complete (or stopped), the vast majority of chains retain the thiocarbonylthio end group and can be isolated as stable materials. The reactions associated with RAFT equilibria shown in Scheme 1 are in addition to those (*i.e.* initiation, propagation and termination) that occur during conventional radical polymerization. In an ideal RAFT process, the RAFT agent should behave as an ideal transfer agent. Thus, as with radical polymerization with conventional chain transfer, the kinetics of polymerization should not be directly influenced beyond those affects attributable to the differing molecular weights of the reacting species. Radical-radical termination is not directly suppressed by the RAFT process. Living characteristics are imparted when the molecular weight of the polymer formed is substantially lower than that which might be formed in the absence of a RAFT agent and the number of polymer molecules with RAFT agent-derived ends far exceeds the number formed as a consequence of termination.

A wide variety of thiocarbonylthio RAFT agents (ZC(=S)SR, **1**) have now been reported. A broad summary of these and the factors which influence choice of RAFT agent for a particular polymerization is presented in recent reviews.[3,6] The effectiveness of the RAFT agent depends on the monomer being polymerized and is determined by the properties of the free radical leaving group R and the group Z which can be chosen to activate or deactivate the thiocarbonyl double bond of the

 

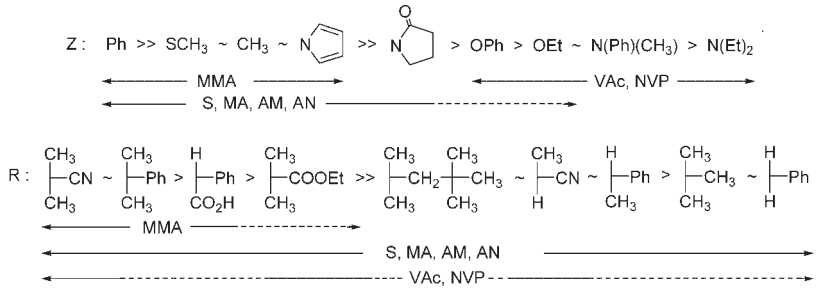


***Figure 1.***
Guidelines for selection of RAFT agents for various polymerizations.[3] For Z, addition rates decrease and fragmentation rates increase from left to right. For R, fragmentation rates decrease from left to right. Dashed line indicates partial control (*i.e.* control of molecular weight but poor polydispersity or substantial retardation in the case of VAc).

RAFT agent (**1**) and modify the stability of the intermediate radicals (**2**) and (**4**).

Figure 1, taken from our recent review,[3] provides a general summary of how to select the appropriate RAFT agent for particular monomers. Note should be made of the dashed lines in the chart. Although some control might be achieved with these monomer RAFT agent combinations, the molecular weight distribution may be broad or there may be substantial retardation or prolonged inhibition.

### Trithiocarbonate RAFT Agents

The utility of trithiocarbonate RAFT agents was disclosed in the first RAFT patent[2] and many papers now describe their application.[3,7–12] Some of the desirable structural features of non-symmetrical trithiocarbonate RAFT agents are summarized below with reference to RAFT agent **5**.

Unsymmetrical primary and secondary trithiocarbonate RAFT agents are readily synthesized from a thiolate anion, carbon disulfide and an alkyl halide.[3]

Radical-induced decomposition of a bis (thioacyl) disulfide (e.g. Scheme 3).[10,13–16] is probably the most used method for the synthesis of RAFT agents requiring tertiary R groups. It is also possible to use this chemistry to generate a RAFT agent *in situ* during polymerization.[13]

Ideally, to avoid odor issues with the RAFT agent and polymer the 'Z', and preferably the 'R(S)' groups, should be based on non-volatile thiols (*e.g.* dodecanethiol for Z in **5**). RAFT agents of this type already described in the literature include

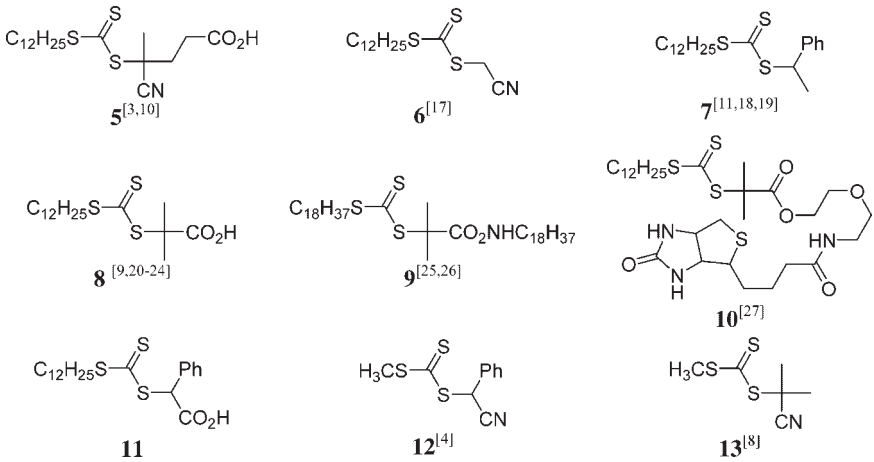


 

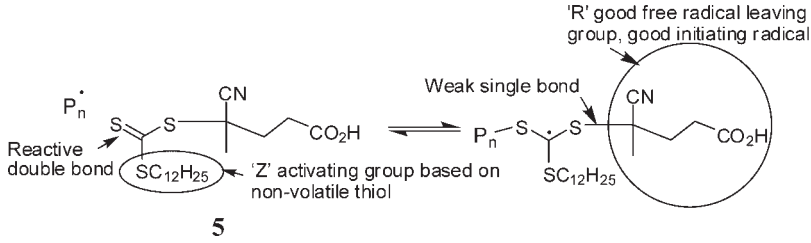


**Scheme 2.**

(**5**–**10**). RAFT agents based on volatile thiols (e.g. **12**, **13**) can be odorous.

Previous work[3] has shown that tertiary (cumyl, cyanoalkyl) dithiobenzoates and trithiocarbonates provide PMMA and other methacrylic polymers with narrow molecular weight distributions. Primary and secondary trithiocarbonates are more readily synthesized but while they may be used to control copolymerization of methacrylic monomers they are not effective in providing living characteristics to their homopolymerization. Recently, secondary aromatic dithioesters with R = –CHPh(CN)[28] or –CHPh($CO_2$alkyl)[29,30] have been reported as RAFT agents for polymerization of methacrylate esters. We have observed that trithiocarbonates with R = –CHPh($CO_2$H) (**11**) or –CHPh(CN) (**12**,[4]**14**) have utility in controlling polymerization of methacrylates. Results of MMA polymerizations at 90 °C with dithiobenzoate (**16**) and dodecyl trithiocarbonates (**5**), (**11**) and (**16**) are compared in Table 1 and Figure 2. The tertiary cyanoalkyl trithiocarbonate (**5**) appears almost as effective as cyanoisopropyl dithiobenzoate (**16**). Trithiocarbonate (**14**) also provides narrow molecular weight distributions (Table 1). However, an inhibition period is observed which is attributed to slow reinitiation by the CHPh(CN) radical. An inhibition period was also reported for with the corresponding dithiobenzoate (**15**) which has the same 'R' group.[28] The Trithiocarbonate (**11**) with secondary R [–CHPh($CO_2$H)] provides a degree of control and no retardation or inhibition period is evident (Table 1). Higher than predicted molecular weights for low monomer

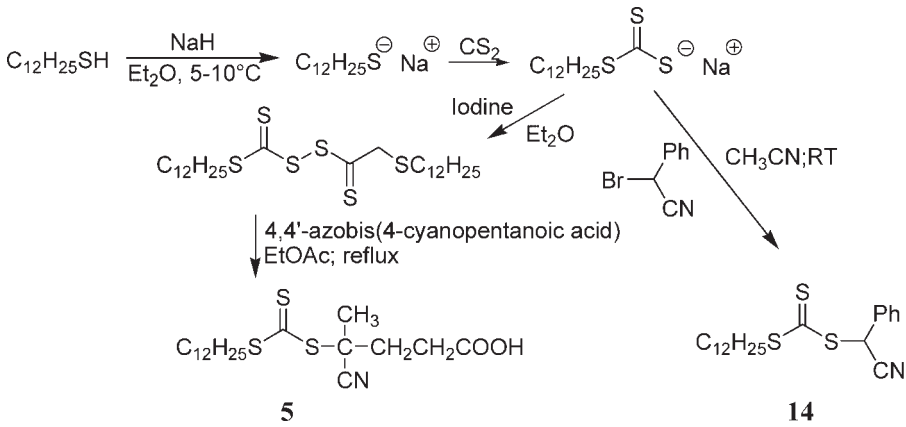


**Scheme 3.**[3]

 

***Table 1.***
Results for RAFT polymerizations of MMA at 90 °C[a)]

| Time (h) | RAFT Agent | | | | | | | | | | | |
|---|---|---|---|---|---|---|---|---|---|---|---|---|
| | **16**[32] | | | **5**[10] | | | **11** | | | **14** | | |
| | Conv (%) | $\overline{M}_n$[b)] g mol$^{-1}$ | $\overline{M}_w/\overline{M}_n$ | Conv (%) | $\overline{M}_n$[b)] g mol$^{-1}$ | $\overline{M}_w/\overline{M}_n$ | Conv (%) | $\overline{M}_n$[b)] g mol$^{-1}$ | $\overline{M}_w/\overline{M}_n$ | Conv (%) | $\overline{M}_n$[b)] g mol$^{-1}$ | $\overline{M}_w/\overline{M}_n$ |
| 1 | 18 | 9400 | 1.28 | 16 | 9400 | 1.42 | 21 | 34000 | 1.70 | 3 | 1600 | 1.44 |
| 2 | 28 | 15900 | 1.15 | 27 | 12800 | 1.24 | 32 | 35100 | 1.65 | 7 | 3500 | 1.44 |
| 4 | 47 | 24200 | 1.11 | 48 | 25300 | 1.13 | 53 | 38100 | 1.56 | 23 | 11000 | 1.20 |
| 16 | 98 | 52500 | 1.09 | 100 | 50300 | 1.09 | 100 | 52900 | 1.33 | 90[c)] | 44300 | 1.06 |

[a)] RAFT polymerizations of MMA (6.55 M in benzene) at 90 °C with RAFT agent (0.011 M) and azobis(cyclohexanenitrile) (0.0018 M) as initiator. Reaction mixtures degassed by three freeze-evacuation-thaw cycles. Polymer isolated by evaporation on monomer.
[b)] GPC Molecular weights in polystyrene equivalents.
[c)] 8 h polymerization time.

conversions is indicative of incomplete usage of RAFT agent and therefore of a low transfer constant.

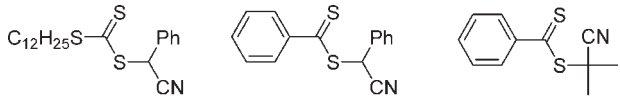


**14** **15**[28] **16**[1,16,31]

## End Group Removal by Radical-Induced Reduction

A key feature of the RAFT process is that the thiocarbonylthio groups, present in the initial RAFT agent, are retained in the polymeric product(s). This makes the process eminently suitable for synthesizing block copolymers and end functional polymers. It means that the polymeric products are themselves RAFT agents. However, in some circumstances, it is also necessary or desirable to deactivate thiocarbonylthio groups because of their reactivity or to

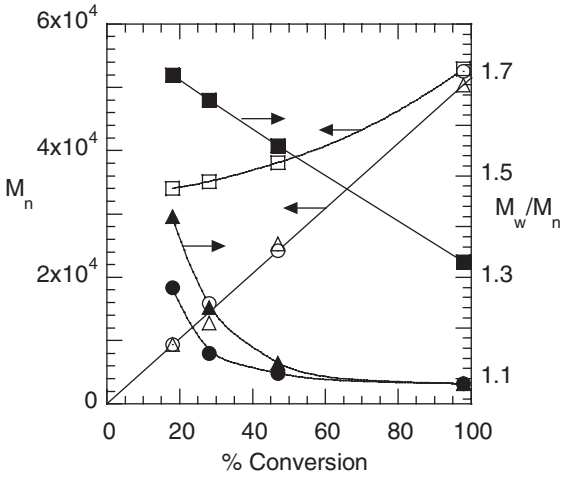


***Figure 2.***
Evolution of number average molecular weight ($\overline{M}_n$) (open symbols) and polydispersity ($\overline{M}_w/\overline{M}_n$) (closed symbols) with conversion for polymerization of methyl methacrylate (6.55 M in benzene) at 90 °C in the presence of dithiobenzoate **16** (●,—), trithiocarbonate **5** (▲,—), and trithiocarbonate **11** (■,—) with RAFT agent (0.011 M) and azobis(cyclohexanenitrile) (0.0018 M). Lines are lines of best fit through data points.

 

transform them for use in subsequent processing.

Thermolysis[10–12,33–35] and radical-induced reactions (such as reduction[10,11,36,37] or termination[11,38]) offer a solution and can provide complete desulfurization. Radical-induced reduction of low molecular weight thiocarbonylthio compounds is well known.[39] Radical-induced reduction of xanthates is the basis of the Barton- McCombie reaction for deoxygenation of secondary alcohols.[40–42] Stannanes are the most efficient reagents for use in this process but are toxic and residual reagent and the devived reaction bydroducts can be difficult to remove. Hypophosphite salts,[43–45] including *N*-ethylpiperidine hypophosphite (**17**),[45] have been recommended as an alternative to stannanes in the radical induced reductions.

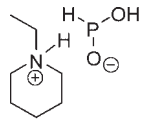

**17**

Radical-induced reduction has also been shown to be applicable to end group removal for RAFT-synthesized polymers.[10,11,36,37] Successful radical-induced reductions with tributylstannane of poly(acenaphthalene)[36,37] or polystyrene[10,11] prepared with dithiobenzoate or trithiocarbonate RAFT agents respectively have been reported. However, residual stannane and derived byproducts can be difficult to remove and the process is unlikely to be industrially acceptable because of the toxicity of tin compounds. The use of less active H-atom donors (*e.g.* isopropanol,[46] silanes[11]) has been reported but these reagents are not always appropriate since coupling of propagating radicals and other side reactions may then compete with H-atom transfer. There is also reference in the patent literature to end group modification by radical-induced processes.[47–49]

We have found that thiocarbonylthio groups of polymers made by RAFT polymerization can be replaced by hydrogen by radical-induced reduction with hypophosphite salts, in particular, *N*-ethylpiperidine hypophosphite.[17,49] Hypophosphite salts are substantially more effective than H-donor solvents such as toluene or isopropanol. The outstanding feature of the hypophosphite salts is that they, and the bydroducts formed in the process, are water soluble and can be removed from the polymer by a simple water wash. GPC traces for poly(butyl acrylate), PMMA and polystyrene prepared with dodecyl trithiocarbonate end groups before/after reduction are shown in Figure 3.

The efficiency of radical induced reduction with the H-donors studied[17] increases in the series toluene $\ll$ isopropanol $<$ triethylsilane $<$ triphenylsilane $\ll$ tris (trimethylsilyl)silane $\sim$*N*-ethylpiperidine hypophosphite $<$ tributylstannane. The end groups of the (meth)acrylic polymers are more readily reduced than those of polystyrene which is in accordance with their known activity in other contexts.[39] Slightly longer reaction times or higher reaction temperatures were required for complete end group removal. The GPC of polystyrene post reduction shows a small high molecular weight shoulder which is attributed to coupling of polystyrene propagating radicals (Figure 3).

### RAFT Polymerization in the Presence of Lewis Acids

Simultaneous control of stereosequence and molecular weight distribution has long been one of the 'holy grails' in the field of radical polymerization. Nitroxide mediated polymerization (NMP), atom transfer radical polymerization (ATRP) and RAFT all offer control over molecular weight distribution. However, polymers produced by these methods show similar tacticity to those obtained by the conventional process. Recently there have been reports of tacticity control of homopolymers[50–53] (which enables the synthesis of stereoblock copolymers[54]) and control of the alternating tendency for copolymerizations[55,56] in ATRP or RAFT polymerization through the use of Lewis acids as additives.

 

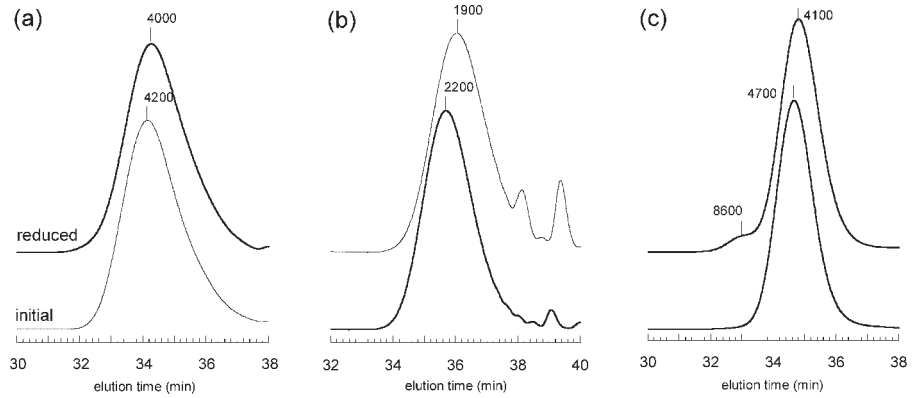


***Figure 3.***
GPC chromatograms for (a) poly(methyl methacrylate) (PMMA), (b) poly(butyl acrylate) (PBA) and (c) polystyrene (PS) prepared with dodecyl trithiocarbonate end groups and the products of their reduction with *N*-ethylpiperidine hypophosphite (**17**) and azobis(cyclohexanenitrile) (ACHN). Peak molecular weights are indicated on the chromatograms.[17] Conditions: (a) [PMMA] 0.05 M, [**17**] 0.25 M, [ACHN] 0.016 M degassed, heated 100 °C/2h; (b) [PBA] 0.05 M, [**17**] 0.42 M, [ACHN] 0.021 M, degassed, heated 100 °C/2h; (c) [PS] 0.05 M, [**17**] 1.0 M, [ACHN] 0.02 M, degassed, heated 110 °C/4h.

However, efforts in this area, particularly those directed towards MMA polymerization, have met with mixed success.

For MMA polymerization, the addition of a Lewis acid, specifically scandium triflate [$Sc(OTf)_3$], is known to increase the fraction of isotactic triads and enhance the rate of polymerization. Similar stereocontrol was observed for RAFT polymerization with cumyl dithiobenzoate and $Sc(OTf)_3$.[57] However, these RAFT polymerizations gave only poor control over molecular weight and polydispersity.[51] Our NMR analyses confirm that the poor results might be attributed to the Lewis acid catalyzed degradation of the dithiobenzoate RAFT agents.[3] It is known from other work that dithiobenzoates are more prone to hydrolysis than, for example, trithiocarbonates or aliphatic dithioesters.[58–60] We have found that trithiocarbonate RAFT agents are also substantially more stable than dithiobenzoates in the presence of Lewis acids. Thus, polymerizations with the trithiocarbonate RAFT agent (**13**) provided polymer with a relatively narrow molecular weight distribution ($\overline{M}_w/\overline{M}_n <$ 1.3 at >95% conversion) as well as the expected enhancement in the fraction of isotactic triads and the rate of polymerization (Table 2). Molecular weights are slightly higher than calculated, the discrepancy increasing at higher $Sc(OTf)_3$ concentrations.

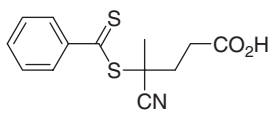


**18**

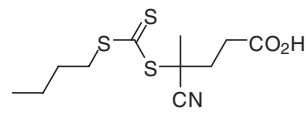


**19**

## RAFT Polymerization of Methacrylate Salts

It has been reported that low temperature photopolymerization of tetraalkylammonium methacrylate salts in water provides a highly syndiotactic polymer.[61]

 

***Table 2.***
Effect of scandium triflate [$Sc(OTf)_3$] concentration on RAFT polymerization of MMA with methyl cyanoisopropyl trithiocarbonate (**13**) and azobis(isobutyronitrile) initiator at 60 °C.[a)]

| [MMA]: [$Sc(OTf)_3$][b)] | time (h)[c)] | conv % | $\overline{M}_n$[d)](g mol$^{-1}$) | $\overline{M}_n$ (theor.) (g mol$^{-1}$) | $\overline{M}_w/\overline{M}_n$ | *mm* | *mr* | *rr* | *m* |
|---|---|---|---|---|---|---|---|---|---|
| Control[e)] | 8 | 50 | 33900 | 33914 | 1.17 | 4 | 33 | 63 | 21 |
| Control[e)] | 16 | 98 | 61000 | 66471 | 1.08 | 4 | 33 | 63 | 21 |
| 34:1 | 4 | 44 | 32000 | 29844 | 1.26 | 5 | 36 | 59 | 23 |
| 34:1 | 8 | 94 | 63600 | 63758 | 1.12 | 6 | 39 | 55 | 26 |
| 16:1 | 2 | 43 | 35000 | 29166 | 1.35 | 7 | 39 | 54 | 27 |
| 16:1 | 6 | 86 | 69000 | 58332 | 1.22 | 7 | 38 | 55 | 26 |
| 8.5:1 | 1 | 26 | 32300 | 17635 | 1.61 | 7 | 38 | 55 | 26 |
| 8.5:1 | 4 | 87 | 78900 | 59010 | 1.31 | 12 | 44 | 44 | 34 |

a) [**13**] = 0.106 M, [AIBN] 0.0061 M.
b) Mole ratio.
c) Reactions times were chosen to provide ~50 and >90% conversion.
d) Molecular weight are in polystyrene equivalents.
e) Control experiment without scandium triflate.

Polymerization of tetramethylammonium methacrylate was carried out in water at 45 °C in the presence of the water soluble dithiobenzoate RAFT agent **18** and with 2,2′-azobis[2-(2-imidazolin-2-yl)propane] dihydrochloride (Wako VA-044) initiator. Methylation of the resultant poly(tetramethylammonium methacrylate) with excess methyl iodide provided PMMA with $\overline{M}_n$ 8200, $\overline{M}_w/\overline{M}_n$ 1.17 and *mm:mr:rr* 2:21:77 compared to poly(methacrylic acid) under similar conditions with *mm:mr:rr* 3:34:63 (this is similar to PMMA obtained by bulk polymerization for which *mm:mr:rr* 3:35:62). Polymerization of salts (Na, K, Cs) methacrylic acid with inorganic counterions also gave a more syndiotactic polymer though the effect appears smaller (Table 3). The enhanced syndiotacticity has been attributed to the mutual repulsion between carboxylate groups favoring alternation in configuration (Figure 5).[61]

## Conclusions

RAFT agents have been compared for their ability to control MMA polymerization. Tertiary cyanoalkyl trithiocarbonates provide very good control over molecular weight and distribution and there is little retardation. The secondary trithiocarbonate RAFT agent with R = –CHPh(CN) also provides good control but a prolonged inhibition period attributed to slow reinitiation is manifest. The trithiocarbonate

***Table 3.***
Molecular weight and tacticity of poly(methyl methacrylate) formed by RAFT polymerization of methacrylic acid and salts.

| Base | RAFT agent | [RAFT]:[MAA] | Conv % | $\overline{M}_n$[a)] g mol$^{-1}$ | $\overline{M}_w/\overline{M}_n$ | *mm* | *mr* | *rr* | *m* |
|---|---|---|---|---|---|---|---|---|---|
| $(CH_3)_4NOH$[b),c)] | **19** | 0.0050 | 97 | 20000 | 1.11 | 1 | 25 | 74 | 14 |
| NaOH[b),c)] | **19** | 0.0050 | 99 | 21200 | 1.11 | 2 | 24 | 75 | 14 |
| KOH[b),c)] | **19** | 0.0050 | 99 | 20000 | 1.09 | 3 | 27 | 69 | 16 |
| CsOH[b),c)] | **19** | 0.0050 | 98 | 20400 | 1.09 | 2 | 26 | 72 | 15 |
| none[b)] | **19** | 0.0050 | 99 | 20600 | 1.07 | 3 | 34 | 63 | 19 |
| none[b)] | none | – | 100 | 745000 | 2.24 | 4 | 33 | 64 | 20 |
| $(CH_3)_4NOH$[d)] | **18** | 0.00724[d)] | 58 | 8200 | 1.17 | 2 | 21 | 77 | 13 |

a) Molecular weight are in polystyrene equivalents.
b) Polymerization of methacrylic acid or salt (33% w/w) in water at 45 °C for 16 h with 2,2′-azobis[2-(2-imidazolin-2-yl)propane] initiator (0.00063% w/w).
c) The salt was formed in situ by neutralization with one molar equivalent of the indicated base (Experimental Part - procedure b).
d) Polymerization of preprepared tetramethylammonium methacrylate (~25% w/v) in water at 45 °C for 16 h (Experimental Part - procedure a).

 

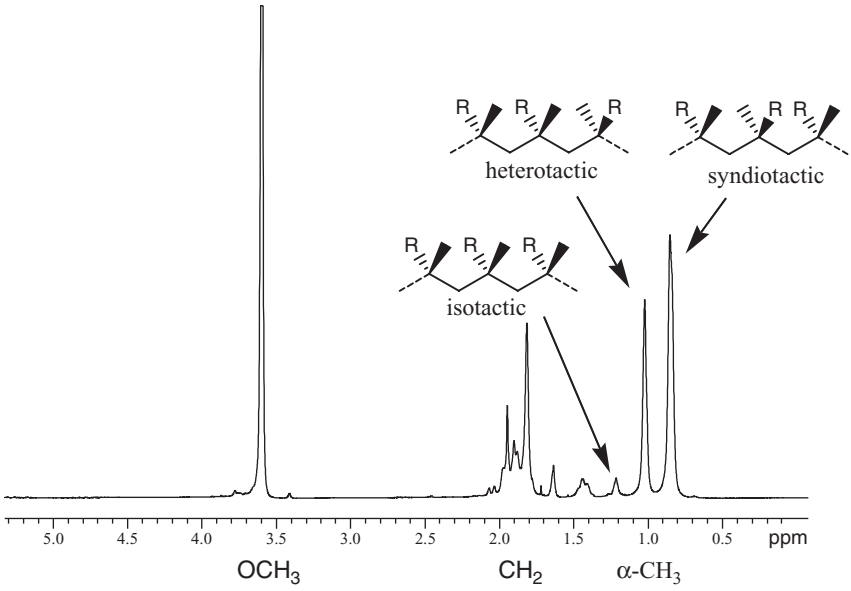


***Figure 4.***
400 MHz $^1$H NMR spectrum of poly(methyl methacrylate) indicating triad assignments for resonances attributable to the hydrogens of the α-methyl group ($R = CO_2CH_3$).

RAFT agents with R = –CHPh($CO_2$H) give poor control and no inhibition period.

Radical induced reduction with hypophosphite salts provides a clean and convenient process for removal of thiocarbonylthio end groups of RAFT-synthesized polymers.

Two methods offering simultaneous control over both molecular weight and polymer chain stereochemistry are reported. RAFT polymerization of MMA with trithiocarbonate RAFT agents and added scandium triflate provides a more isotactic PMMA. RAFT polymerization of tetramethylammonium methacrylate at 45 °C provides a more syndiotactic PMMA.

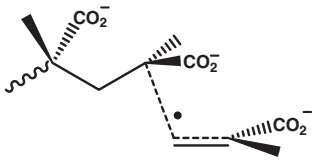


***Figure 5.***
Schematic representation of the transition state for poly(tetramethylammonium methacrylate) propagating radical adding to tetramethylammonium methacrylate leading to a syndiotactic chain (counter ion not shown).

## Experimental Part

Solvents were of AR grade and were distilled before use. Azobisisobutyronitrile (AIBN, Vazo-64) and azobis(cyclohexanenitrile) (ACHN, Vazo-88) were obtained from DuPont and purified by crystallization from chloroform/methanol, 2,2′-azobis[2-(2-imidazolin-2-yl)propane] (Wako VA-044) was used as received. Monomers were purified by filtration through neutral alumina (70–230 mesh) to remove inhibitors and flash distilled immediately prior to use. The syntheses of RAFT agents **5**,[10] **16**[31] and **13**[16] are decribed elsewhere. RAFT agent **19** was synthesized by a procedure analogous to that used for synthesis of **5**.[10] Gel permeation chromatography (GPC) was performed on a Waters Associates liquid chromatograph equipped with differ-

 

ential refractometer and 3 × Mixed C and 1 mixed E PLgel column (each 7.5 mm × 30 mm) from Polymer Laboratories. Tetrahydrofuran (flow rate of 1.0 mL/min) was used as eluent at 22 ± 2 °C and the columns were calibrated with narrow polydispersity polystyrene standards (Polymer Laboratories). Nuclear magnetic resonance spectra (NMR) were obtained with a Bruker AC200 or AC400 spectrometer. Chemical shifts are reported in ppm from external tetramethylsilane.

### 2-(Dodecylthiocarbonothioylthio)-2-phenylacetic Acid (11)

2-Bromo-2-phenylacetic acid (Aldrich, 98%) (2.17 g, 0.01 mol) was added to a stirred suspension of sodium dodecyl trithiocarbonate[10] (3.06 g, 0.01 mol) in diethyl ether (100 mL). The reaction mixture was then stirred at room temperature for 1 h. Water was added and the organic layer separated, extracted twice with water, dried over anhydrous magnesium sulfate and evaporated to leave a residue which was chromatographed on silica gel eluting with 3:7 ethyl acetate:*n*-hexane. The yield of yellow solid (**11**) was 2.9 g (70%) m.p. 60.5–61.5 °C. $^1$H-NMR ($CDCl_3$) δ 0.9 (t, 3H, $CH_3$); 1.3 (br s, 18H); 1.7 (m, 2H, $CH_2$); 3.35 (t, 3H, $CH_2$); 5.9 (s, 1H, CH), 7.3–7.5 (m, 5H, ArH).

### *2-(Dodecylthiocarbonothioylthio)-2-phenylacetonitrile* (*14*)

2-Bromo-2-phenylacetonitrile was prepared by bromination reaction of phenylacetonitrile with *N*-bromosuccinimide in carbon tetrachloride in the presence of AIBN. Thus, *N*-bromosuccinimide (5.3 g, 0.03 mol) and AIBN (100 mg) was added to a stirred solution of phenylacetonitrile (2.9 g, 0.025 mol) in carbon tetrachloride (50 mL) and the resultant solution heated to reflux. After 24 hours, the solution was cooled, filtered to remove the precipitated succinimide and the filtrate concentrated on a rotary evaporator. The residue was purified by silica gel column chromatography with 3:97 ethyl acetate:*n*-hexane as eluent to afford the 2-bromo-2-phenylacetonitrile as a colourless oil (3.1 g, 64%). $^1$H-NMR ($CDCl_3$) δ 5.5 (s, 1H, CH); 7.3–7.6 (m, 5H, ArH).

2-Bromo-2-phenylacetonitrile (1 g, 0.0051 mol) was added to a stirred suspension of sodium dodecyl trithiocarbonate[10] (1.54 g, 0.0051 mol) in acetonitrile (10 mL). The reaction mixture was then stirred at room temperature for 1 h. Water (20 mL) was then added, the mixture extracted with ethyl acetate and the organic layer separated, dried over anhydrous magnesium sulfate and evaporated to leave a residue which was chromatographed on silica gel eluting with 4:96 ethyl acetate:*n*-hexane to provide **14** as a yellow oil that solidified during storage at −15 °C (1.65 g, 82%) $^1$H-NMR ($CDCl_3$) δ 0.9 (t, 3H, $CH_3$); 1.3 (br s, 18H); 1.7 (m, 2H, C**H**$_2$C$H_2$S); 3.4 (t, 3H, $CH_2$S); 6.2 (s, 1H, CH), 7.3-7.6 (m, 5H, ArH).

### RAFT Polymerization of MMA

Procedures for RAFT polymerization have been described previously.[10,32] Conditions used are provided in the footnote to Table 1.

### Radical-Induced Reduction with (17)

A mixture of PMMA ($\overline{M}_n$ 3400, $\overline{M}_w/\overline{M}_n$ 1.18, prepared with RAFT agent **5**, 170 mg), *N*-ethylpiperidine hypophosphite (45 mg) and ACHN (4 mg) in toluene (1 mL) was degassed and heated at 100 °C for 2 hrs. The solution was extracted with water and the toluene removed to give a colorless polymer $\overline{M}_n$ 3380, $\overline{M}_w/\overline{M}_n$ 1.16. The $^1$H NMR spectrum of the product showed that the signals attributable to the dodecyl trithiocarbonate end group were no longer present. A similar procedure was used for other reductions. Details are provided in the legend to Figure 3.

### RAFT Polymerization of MMA in the Presence of Scandium Triflate

The following procedure is typical. Aliquots (0.5 mL) of stock solution comprising MMA (7.5 mL), AIBN (11 mg), *S*-methyl-*S*-cyanoisopropyl trithiocarbonate (0.023 g) and benzene (2.5 mL) from

 

the control experiment were transferred to ampoules containing scandium triflate (0.05g), degassed with three freeze-evacuate-thaw cycles and sealed. The ampoules were heated at $60 \pm 1\,^{\circ}C$ in a thermostatted oil bath for the appropriate time. Conversions were determined by ascertaining the residual MMA in the reaction mixture by $^1H$ NMR. The excess monomer and solvent removed by evaporation at ambient temperature under vacuum and the residues were analyzed directly by GPC. Samples were then further purified by precipitation into methanol before NMR analysis. Triad distributions from $^1H$ NMR analysis are provided in Table 2.

### RAFT Polymerization of Tetramethylammonium Methacrylate

Tetramethylammonium methacrylate is readily prepared by neutralisation of methacrylic acid with tetramethylammonium hydroxide. It is critical not to use an excess of base in this process because of the hydrolytic sensitivity of the RAFT agent. The purity of the tetramethylammonium hydroxide is also important. Polymerizations of other methacrylate salts (Na, K, Cs) were carried out using procedure (b).

#### *(a) Polymerization of Tetramethylammonium Methacrylate*

A stock solution comprising tetramethylammonium methacrylate (5g, 0.0314 mol), 2,2′-azobis(*N,N′*dimethyleneisobutyramidine) dihydrochloride (15mg, $4.64 \times 10^{-5}$ mol) was prepared and made up to 20 mL with water. A reaction vessel was charged with the above stock solution (13.8 mL; 0.0217 mol of tetramethylammonium methacrylate), 4-cyano-4-(thiobenzoyl)sulfanylpentanoic acid (**18**) (43.8 mg, $1.57 \times 10^{-4}$ mol) and methanol (1 mL), degassed by three freeze-evacuate-thaw cycles, sealed and heated under vacuum at 45°C for 44 hours. The vessel was opened, the water and methanol evaporated under vacuum. The residue was dissolved in methanol (15 mL) and an excess of methyl iodide (5 mL) added and the mixture stirred overnight at ambient temperature (~22 °C). Water was then added, the mixture extracted with chloroform and the extract dried over sodium sulfate. Evaporation of the solvent gave PMMA (1.25 g, 58% conversion). $\overline{M}_n$ 8,200; $\overline{M}_w/\overline{M}_n$ 1.17. $^1H$ NMR analysis indicated a triad distribution of *mm:mr:rr* 2:21:77.

#### *(b) Polymerization with in situ Neutralization of Methacrylic Acid*

A mixture of methacrylic acid (1.0g, 0.012 mol), tetramethylammonium hydroxide (2.11g, 0.012 mol), 2,2′-azobis(N, N′dimethyleneisobutyramidine) dihydrochloride (1.9 mg, $5.9 \times 10^{-6}$ mol) , RAFT agent **19** (16.9 mg, $5.8 \times 10^{-5}$ mol) and deionised water (2.0 g) was degassed by three freeze-evacuate- thaw cycles, sealed and heated under vacuum at 45 °C for 16 hours. The vessel was opened and the conversion of the monomer was 97% as determined by $^1H$-NMR. The solution was then acidified by addition of excess aqueous HCl and dried under vacuum. The residue was dis–solved in methanol (15 mL) and an excess of diazomethane in diethyl ether added and the mixture stirred overnight at ambient temperature. Water was then added, the mixture extracted with chloroform and the extract dried over sodium sulphate. Evaporation of the solvent gave PMMA $\overline{M}_n$ 20,000; $\overline{M}_w/\overline{M}_n$ 1.11. $^1H$ NMR analysis indicated a triad distribution of *mm:mr:rr* 1:25:74.

[1] J. Chiefari, Y. K. Chong, F. Ercole, J. Krstina, J. Jeffery, T. P. T. Le, R. T. A. Mayadunne, G. F. Meijs, C. L. Moad, G. Moad, E. Rizzardo, S. H. Thang, *Macromolecules* **1998**, *31*, 5559–5562.
[2] WO 9801478 (**1998**), E. I. Du Pont De Nemours and Co., USA, invs.: T. P. Le, G. Moad, E. Rizzardo, S. H. Thang, *Chem. Abstr. 128*, 115390f.
[3] G. Moad, E. Rizzardo, S. H. Thang, *Aust. J. Chem.* **2005**, *58*, 379–410.
[4] G. Moad, E. Rizzardo, S. H. Thang, *Aust. J. Chem.* **2006**, *59*, 669–692.
[5] G. Moad, *Aust J. Chem.* **2006**, *59*, 661–662.
[6] G. Moad, D. H. Solomon, "*The Chemistry of Radical Polymerization*" 2nd edition, Elsevier, Oxford **2006**.
[7] R. A. Mayadunne, G. Moad, E. Rizzardo, *Tetrahedron Lett.* **2002**, *43*, 6811–6814.

 

[8] R. T. A. Mayadunne, E. Rizzardo, J. Chiefari, J. Krstina, G. Moad, A. Postma, S. H. Thang, *Macromolecules* **2000**, *33*, 243–245.
[9] J. T. Lai, D. Filla, R. Shea, *Macromolecules* **2002**, *35*, 6754–6756.
[10] G. Moad, Y. K. Chong, E. Rizzardo, A. Postma, S. H. Thang, *Polymer* **2005**, *46*, 8458–8468.
[11] A. Postma, T. P. Davis, R. A. Evans, G. Li, G. Moad, M. O'Shea, *Macromolecules* **2006**, *39*, 5293–5306.
[12] A. Postma, T. P. Davis, G. Li, G. Moad, M. O'Shea, *Macromolecules* **2006**, *39*, 5307–5318.
[13] WO 9905099 (**1999**), (Commonwealth Scientific and Industrial Research Organisation, Australia; E. I. Du Pont de Nemours & Co.). invs.: E. Rizzardo, S. H. Thang, G. Moad, *Chem. Abstr. 130*, 154069u
[14] S. H. Thang, Y. K. Chong, R. T. A. Mayadunne, G. Moad, E. Rizzardo, *Tetrahedron Lett.* **1999**, *40*, 2435–2438.
[15] Y. K. Chong, J. Krstina, T. P. T. Le, G. Moad, A. Postma, E. Rizzardo, S. H. Thang, *Macromolecules* **2003**, *36*, 2256–2272.
[16] J. Chiefari, R. T. A. Mayadunne, C. L. Moad, G. Moad, E. Rizzardo, A. Postma, M. A. Skidmore, S. H. Thang, *Macromolecules* **2003**, *36*, 2273–2283.
[17] B. Chong, G. Moad, E. Rizzardo, S. Thang, *Macromolecules* **2006**, submitted.
[18] G. Moad, G. Li, R. Pfaendner, A. Postma, E. Rizzardo, S. Thang, H. Wermter, *ACS Symp. Ser.* **2006**, *944*, 514–532.
[19] G. Moad, K. Dean, L. Edmond, N. Kukaleva, G. Li, R. T. A. Mayadunne, R. Pfaendner, A. Schneider, G. Simon, H. Wermter, *Macromol. Symp.* **2006**, *233*, 170–179.
[20] X. L. Jiang, P. J. Schoenmakers, J. L. J. van Dongen, X. W. Lou, V. Lima, J. Brokken-Zijp, *Anal. Chem.* **2003**, *75*, 5517–5524.
[21] R. Wang, C. L. McCormick, A. B. Lowe, *Macromolecules* **2005**, *38*, 9518–9525.
[22] L. Lu, H. Zhang, N. Yang, Y. Cai, *Macromolecules* **2006**, *39*, 3770–3776.
[23] V. Lima, X. L. Jiang, J. Brokken-Zijp, P. J. Schoenmakers, B. Klumperman, R. Van Der Linde, *J. Polym. Sci., Part A: Polym. Chem.* **2005**, *43*, 959–973.
[24] A. J. Convertine, N. Ayres, C. W. Scales, A. B. Lowe, C. L. McCormick, *Biomacromolecules* **2004**, *5*, 1177–1180.
[25] P. Kujawa, F. Segui, S. Shaban, C. Diab, Y. Okada, F. Tanaka, F. M. Winnik, *Macromolecules* **2006**, *39*, 341–348.
[26] P. Kujawa, H. Watanabe, F. Tanaka, F. M. Winnik, *Eur. Phys. J. E* **2005**, *17*, 129–137.
[27] C. Y. Hong, C. Y. Pan, *Macromolecules* **2006**, *39*, 3517–3524.
[28] C. Z. Li, B. C. Benicewicz, *J. Polym. Sci., Part A, Polym. Chem.* **2005**, *43*, 1535–1543.
[29] J. Bang, S. H. Kim, E. Drockenmuller, M. J. Misner, T. P. Russell, C. J. Hawker, *J. Am. Chem. Soc.* **2006**, *128*, 7622–7629.
[30] S. Perrier, P. Takolpuckdee, *J. Polym. Sci., Part A, Polym. Chem.* **2005**, *43*, 5347–5393.
[31] G. Moad, J. Chiefari, J. Krstina, A. Postma, R. T. A. Mayadunne, E. Rizzardo, S. H. Thang, *Polym. Int.* **2000**, *49*, 993–1001.
[32] M. Benaglia, E. Rizzardo, A. Alberti, M. Guerra, *Macromolecules* **2005**, *38*, 3129–3140.
[33] A. Postma, T. P. Davis, G. Moad, M. S. O'Shea, *Macromolecules* **2005**, *38*, 5371–5374.
[34] J. Xu, J. He, D. Fan, W. Tang, Y. Yang, *Macromolecules* **2006**, *39*, 3753–3759.
[35] B. Chong, G. Moad, E. Rizzardo, M. Skidmore, S. H. Thang, *Aust. J. Chem.* **2006**, *59*, 755–762.
[36] M. Chen, K. P. Ghiggino, T. A. Smith, S. H. Thang, G. J. Wilson, *Aust. J. Chem.* **2004**, *57*, 1175–1177.
[37] M. Chen, K. P. Ghiggino, S. H. Thang, J. White, G. J. Wilson, *J. Org. Chem* **2005**, *70*, 1844–1852.
[38] S. Perrier, P. Takolpuckdee, C. A. Mars, *Macromolecules* **2005**, *38*, 2033–2036.
[39] A. Studer, S. Amrein, *Synthesis-Stuttgart* **2002**, 835–849.
[40] D. H. R. Barton, S. W. McCombie, *J. Chem. Soc., Perkin Trans.* **1975**, *1*, 1574.
[41] M. J. Robins, J. S. Wilson, F. J. Hansske, *J. Am. Chem. Soc.* **1983**, *105*, 4059–4065.
[42] D. H. R. Barton, S. W. McCombie, *J. Chem. Soc., Perkin Trans. 1* **1975**, 1574–1585.
[43] D. H. R. Barton, D. O. Jang, J. C. Jaszberenyi, *Tetrahedron Lett.* **1992**, *33*, 5709–5712.
[44] J. Boivin, R. Jrad, S. Juge, V. T. Nguyen, *Org. Lett.* **2003**, *5*, 1645–1648.
[45] D. O. Jang, D. H. Cho, *Tetrahedron Lett.* **2002**, *43*, 5921–5924.
[46] M. Destarac, C. Kalai, L. Petit, A. Wilczewska, G. Mignani, S. Z. Zard, *Polym. Prepr. (Am. Chem. Soc., Div. Polym. Chem.)* **2005**, *46*(2), 372–373.
[47] WO02090397 (**2002**), Rhodia Chimie, invs.: Z. A. Wilczewska, M. Destarac, S. Zard, C. Kalai, G. Mignani, H. Adam, *Chem. Abstr. 137*, 353541.
[48] US6919409 (**2005**), Symyx Technologies, Inc., invs.: D. Charmot, M. Piotti, *Chem. Abstr. 141*, 350560.
[49] WO2005113612A1 (**2005**), Dupont De Nemours and Company, USA, invs.: W. B. Farnham, M. Fryd, G. Moad, S. H. Thang, E. Rizzardo, *Chem. Abstr. 144*, 23268.
[50] B. Ray, Y. Isobe, K. Matsumoto, S. Habaue, Y. Okamoto, M. Kamigaito, M. Sawamoto, *Macromolecules* **2004**, *37*, 1702–1710.
[51] J. F. Lutz, W. Jakubowski, K. Matyjaszewski, *Macromol. Rapid Commun.* **2004**, *25*, 486–492.
[52] B. Ray, Y. Isobe, K. Morioka, S. Habaue, Y. Okamoto, M. Kamigaito, M. Sawamoto, *Macromolecules* **2003**, *36*, 543–545.
[53] B. Y. K. Chong, G. Moad, M. Rizzardo, M. A. Skidmore, S. Thang, *27th Australian Polymer Symposium*, **2004**, C1/3.
[54] J.-F. Lutz, D. Neugebauer, K. Matyjaszewski, *J. Am. Chem. Soc.* **2003**, *125*, 6986–6993.

 

[55] B. Kirci, J. F. Lutz, K. Matyjaszewski, *Macromolecules* **2002**, *35*, 2448–2451.
[56] J.-F. Lutz, B. Kirci, K. Matyjaszewski, *Macromolecules* **2003**, *36*, 3136–3145.
[57] Y. Isobe, T. Nakano, Y. Okamoto, *J. Polym. Sci., Part A, Polym. Chem.* **2001**, *39*, 1463–1471.
[58] M. Mertoglu, A. Laschewsky, K. Skrabania, C. Wieland, *Macromolecules* **2005**, *38*, 3601–3614.
[59] L. Albertin, M. H. Stenzel, C. Barner-Kowollik, T. P. Davis, *Polymer* **2006**, *47*, 1011–1019.
[60] D. B. Thomas, A. J. Convertine, R. D. Hester, A. B. Lowe, C. L. McCormick, *Macromolecules* **2004**, *37*, 1735–1741.
[61] C. Chovino, P. Gramain, *Macromol. Chem. Phys.* **1996**, *197*, 1411–1418.

 

# Verdazyl-Mediated Polymerization of Styrene

*Steven J. Teertstra,*[1] *Eric Chen,*[1] *Delphine Chan-Seng,*[1] *Peter O. Otieno,*[2] *Robin G. Hicks,**[2] *Michael K. Georges**[1]

**Summary:** Attempted controlled polymerizations of styrene, conducted in the presence of either 1,3,5-triphenyl-6-oxoverdazyl or 1,5-dimethyl-3-phenyl-6-oxoverdazyl radicals initiated with benzoyl peroxide or 1,1′-azobis(cyclohexanecarbonitrile) were universally unsuccessful regardless of the reaction temperature and the initiator/verdazyl molar ratio. No improvement was observed using a verdazyl-terminated styrene initiator adduct prepared by an exchange reaction between a styrene-TEMPO alkoxyamine and a 1,3,5-triphenyl-6-oxoverdazyl radical. However, controlled polymerizations of styrene were achieved at 125 °C using a styrene-verdazyl adduct containing the 1,5-dimethyl-3-phenyl-6-oxoverdazyl radical. Polydispersity indexes remained low throughout the polymerizations and plots of number average molecular weight ($\overline{M}_n$) versus time were linear. However, the actual $\overline{M}_n$ values were considerably lower than theoretical, an unexpected result that is under investigation.

**Keywords:** living-radical polymerization; verdazyl radcials

## Introduction

The use of nitroxides in the stable free radical polymerization (SFRP) process to reversibly terminate the propagating polymer chain enables the controlled polymerization of monomers with activated double bonds. However, while the polymerization of styrene with TEMPO is rather straightforward, the polymerization of acrylates and methacrylates has proven to be more difficult. Two reasons have been advanced for these difficulties. Firstly, the equilibrium constant K for *n*-butyl acrylate polymerization mediated by TEMPO has been reported to be unfavorably small because of a low dissociation rate constant $k_d$ and a high recombination rate constant $k_c$.[1] This prevents a linear increase in molecular weight with increasing monomer conversion and a narrow final molecular weight distribution ($\overline{M}_w/\overline{M}_n$). To address this problem a series of novel nitroxides have been synthesized[2] and applied with good success to the polymerization of acrylates, two of the more successful of these nitroxides being SG1[2f] and TIPNO.[2e] The *K* value for SG1 has been shown to be significantly lower than that for TEMPO.[1]

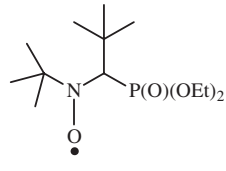

SG1

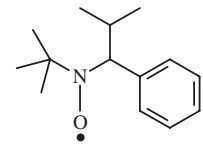

TIPNO

Although the ability of TEMPO to mediate the polymerization of acrylates may be adversely affected by an unfavorable equilibrium constant as compared to other nitroxides, a second, and arguably more serious problem may be the persistence of TEMPO radicals in the polymerization. Unavoidable termination reactions by chain-chain coupling causes accumulation of free nitroxide in the reaction solution.[3] Since acrylates do not exhibit an autopolymerization mechanism that can

[1] Department of Chemical and Physical Sciences, University of Toronto at Mississauga, 3359 Mississauga Rd. N., Mississauga, Ontario, Canada, L5L 1C6
E-mail: mgeorges@utm.utoronto.ca
[2] Department of Chemistry, Univeristy of Victoria, PO Box 3065, Victoria, BC, Canada, V8W 3V6

generate new propagating radicals to consume the excess nitroxide,[4] the accumulation of free nitroxide inhibits further polymerization.[2h–j] To circumvent this problem ene-diol additives have been effectively used to destroy the excess nitroxide and allow the polymerization of acrylates to proceed in a controlled manner in the presence of TEMPO.[5]

Obviously, the use of nitroxides as agents to control polymerizations remains interesting, however, their limitations makes one wonder whether there are other stable radicals which may be superior. Unfortunately, there are a limited number of stable radicals available, and those that have been studied have not been particularly successful. Earlier studies with galvinoxyl radicals[6] have been followed recently with the use of triazolinyl radicals[7] and verdazyl radicals **1**.[8] However, in the only reported use of verdazyl radicals to mediate styrene polymerizations no control was observed with **2**, an adduct of the 1,3,5-triphenylverdazyl radical and the 2-(2-cyano-2-propyl) radical derived from 2,2′-azobisisobutyronitrile (AIBN), at reaction temperatures between 80 °C and 120 °C.[8] In the case of the triazolinyl radicals, a spirotriazolinyl radical controlled the polymerization of styrene reasonably well, but was only moderately effective for methyl methacrylate[7].

many verdazyl radicals are stable enough to be isolated and stored, such as 1,3,5-triphenyl-6-oxoverdazyl, or are stable as a complex, such as 1,5-dimethyl-3-(4-pyridyl)-6-oxoverdazyl with dihydroquinone. Other verdazyl radicals, such as 1,3-diphenyl-5-methyl-6-oxoverdazyl are reported to be too unstable to allow for isolation in a pure state.[9] Interest in verdazyl radicals has led to the study of other similar structured stable radicals, including acyclic and 5-membered analogues, a very comprehensive overview of which is provided by Neugebauer.[10]

Structurally, the verdazyls are allylic radicals, possessing a ring structure with a conformation determined in large part by the substituents at C6. Thus, in the case of **1**, where X is oxygen, the verdazyl ring is nearly planar, whereas when X is sulfur, the ring is in a flat boat conformation. The C6 substituent can also effect the conformation at C1, C3, and C5. In the 1,3,5- triphenyl-6-oxoverdazyl radical, for example, the phenyl groups at C1 and C5 are slightly twisted (about 5 °) out of the plane of the verdazyl ring while the phenyl group at C3 is similarly twisted out of the plane, but to a lesser degree. Alternatively, when X is sulfur the twists of the phenyl groups are much more pronounced.[11b]

Various synthetic approaches to the verdazyl radicals have been reported. All

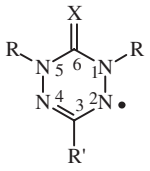

X= $H_2$, O, S
R = alkyl, aryl
R' = alkyl, aryl, H

**1a**- X = O, R = R' = Ph
**1b**- X = O, R= $CH_3$, R' = Ph

**1**

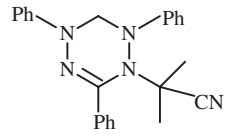

**2**

Despite these results the verdazyl radicals piqued our interest, primarily because they could be synthesized with a variety of substituents, each with the potential to affect the stability of the radical and its steric interactions with a propagating polymer chain. First reported in 1963, the syntheses lead to a tetrazine intermediate **3** (Scheme 1) which can be oxidized to the verdazyl radical by a variety of oxidants, including benzoquinone,[12] lead oxide in acetic acid[9] and potassium ferrocyanate.[11a] Other oxidants include silver carbonate, hydrogen peroxide, thallium oxide

 

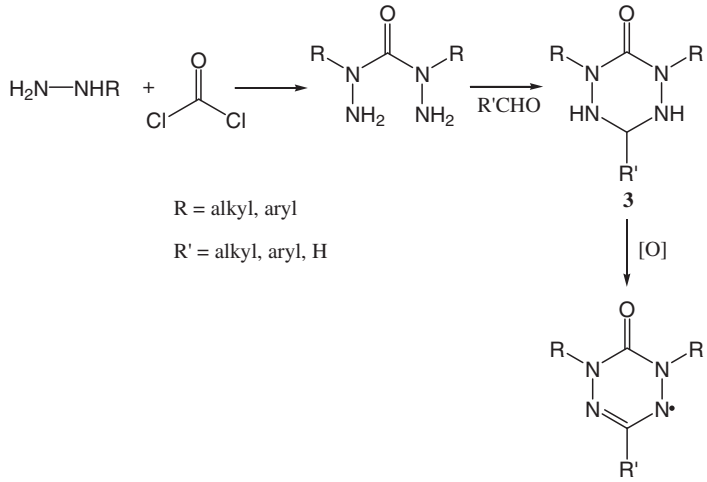


***Scheme 1.***
General synthesis of 6-oxoverdazyl radicals beginning with a monosubstituted hydrazine.

and manganese oxide.[9] The 6-oxoverdazyl radicals, of particular interest to the work presented herein, are synthesized by condensation of a substituted alkyl or aryl hydrazine with phosgene, followed by condensation of the resulting bis-hydrazide with an aldehyde to afford the tetrazine intermediate (Scheme 1).[13] While the use of phosgene is problematic, the reactions proceed in high yield and are relatively simple to execute.

Two other general approaches to the tetrazine **3** have been reported. In one approach a hydrazone is reacted with phosgene to give a 2-chloroformylhydrazone, which is subsequently reacted with hydrazine followed by condensation with an aldehyde to afford **3** in good yield (Scheme 2).[9]

In the second approach the commercially available *tert*-butyl carbazate is condensed with a ketone of choice and the

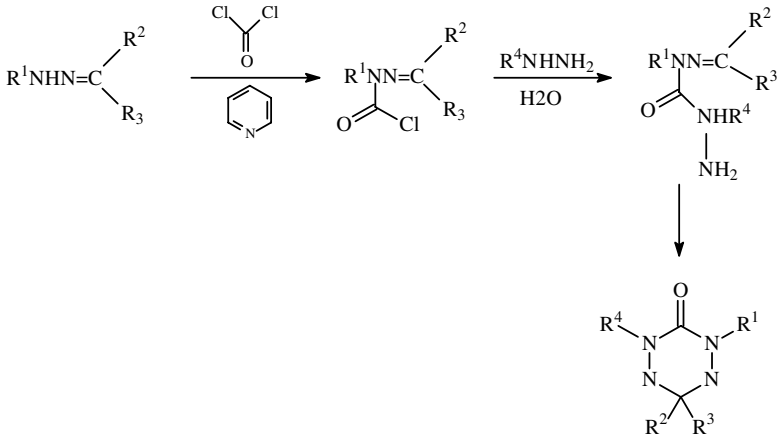


***Scheme 2.***
General synthetic scheme for 6-oxotetrazines beginning with a substituted hydrazone.

 

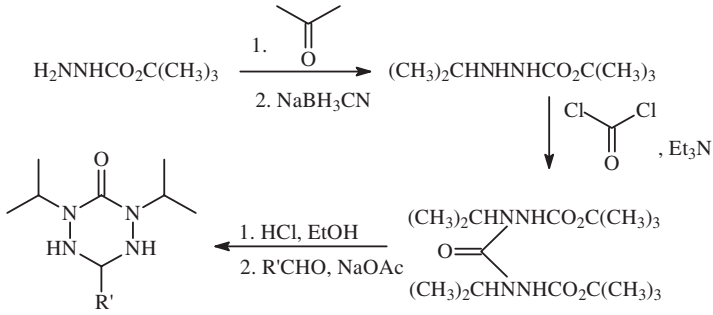


***Scheme 3.***
General synthetic scheme for 6-oxotetrazines beginning with *tert*-butyl carbazate.

resulting hydrazone is reduced to afford the BOC protected alkyl hydrazide. Reaction of the hydrazide with phosgene affords the bis-hydrazide which cyclizes in the presence of acid to yield **3** (Scheme 3).[12b]

The described syntheses offer easy access to a variety of structurally different verdazyl radicals providing the opportunity to extend the initial work of Yamada and coworkers[8] to determine if these stable radicals have the potential to solve some of the problems associated with nitroxides as mediating reagents for living-radical polymerizations.

## Experimental Part

### Styrene Polymerization Using 1a Initiated with Benzoyl Peroxide (BPO)

In a typical experiment, styrene (10 mL, 87 mmol), BPO (28 mg, 0.12 mmol) and 1,3,5-triphenyl-6-oxoverdazyl radical **1a** (86 mg, 0.26 mmol), prepared according to the procedure of Neugebauer[13c], were placed in a 50 mL 3-necked round bottom flask equipped with a thermometer, a condenser equipped with a gas outlet adapter, and a septum, through which argon was introduced and samples were removed via syringe. The reaction solution was purged with argon for 10 min and heated to 110 °C. Samples were withdrawn occasionally beginning after the first 30 min, but typically after every hour beginning with the first. A stream of air was used to remove excess monomer from the samples and the conversion was measured gravimetrically once constant weight was reached. The molecular weights and molecular weight distributions of the remaining polymer were estimated by gel permeation chromatography (GPC) using a Waters 2690 Separations Module equipped with Styragel HR4 ($7.8 \times 300$ mm), Styragel HR2 ($4.6 \times 300$ mm) and Styragel HR1 ($4.6 \times 300$ mm) columns calibrated with polystyrene standards in the range of $\overline{M}_n = 400$–$188{,}000$ g/mol$^{-1}$ and a Waters model 410 differential refractometer (RI) detector. THF was used as eluent at 40 °C and a flow rate of 0.35 mL min$^{-1}$.

### Styrene Polymerization Using 1a Initiated with 1,1′-Azobis(cyclohexanecarbonitrile), (Vazo® 88)

The procedure described in the previous paragraph was repeated with Vazo® 88 (130 mg, 0.53 mmol), 1,3,5-triphenyl-6-oxoverdazyl radical **1a** (203 mg, 1 mmol) in 10 mL styrene at 135 °C.

### BSV Synthesis

In a typical reaction, 2-phenyl-2-(2,2,6,6-tetramethylpiperidin-1-oxy)ethyl benzoate (BST)[14]**4**, (1 molar eq.) and 1,3,5-triphenyl-6-oxoverdazyl radical **1a** (2 molar eq.) were heated in toluene under argon at 110 °C for 3 h. The solvent was evaporated and the resulting oil was passed though a silica gel column with $CH_2Cl_2$ as the eluent to give the 2-phenyl-2-(1,3,5-triphenyl-6-

 

*Table 1.*
Polymerizations of styrene initiated with BPO in the presence of 1,3,5-triphenyl-6-oxoverdazyl radical **1a** at 110 °C. Polymerizations were performed in 10 mL styrene.

| Entry | BPO ($\times 10^{-2}$ M) | **1a**($\times 10^{-2}$ M) | **1a**/BPO | Time (h) | $\overline{M}_n$ g/mol$^{-1}$ | $\overline{M}_w/\overline{M}_n$ | Conv'n (%) |
|---|---|---|---|---|---|---|---|
| 1 | 1.16 | 2.63 | 2.25 | 0.5 | 27700 | 1.6 | 23 |
| | | | | 1 | 28700 | 1.65 | 25 |
| | | | | 2 | 29200 | 1.65 | 26 |
| 2 | 1.16 | 3.12 | 2.7 | 1 | 24500 | 1.7 | 23 |
| | | | | 2 | 24000 | 1.7 | 21 |

oxoverdazyl)ethyl benzoate unimer **5a** in 30–35% yield unimer (BSV **5a**).[15] The 2-phenyl-2-(1,5-dimethyl-3-phenyl-6-oxoverdazyl)ethyl benzoate unimer (BSV **5b**)[15] was prepared in a similar manner.

**Styrene Polymerization Initiated with BSV**
Polymerizations were performed in 10 mL (87.3 mmol) of styrene with 100 mg of BSV **5a** or **5b**, (0.18 to 0.19 mmol, respectively) in a similar manner described for styrene polymerization initiated with BPO.

## Results and Discussion

We began our investigation with a styrene polymerization in the presence of 1,3,5-triphenyl-6-oxoverdazyl radical **1a** initiated with BPO at a reaction temperature of 110 °C, using a verdazyl to BPO molar ratio of 2.25:1. The results of a typical experiment are summarized in Table 1, entry 1. The monomer conversion after 30 min was 23% and did not change in the subsequent 2 h. Only a minimal increase in $\overline{M}_n$ was observed over that time period. The fast initial reaction and high $\overline{M}_w/\overline{M}_n$ values suggested a deficiency of verdazyl radical at the beginning of the polymerization. However, an increase of the verdazyl to BPO ratio to 2.7:1 gave virtually no change in the polymerization results (Table 1, entry 2).

The polymerization of styrene initiated with Vazo® 88 in the presence of 1,5-dimethyl-3-phenyl-6-oxoverdazyl radical **1b** was similarly unsuccessful (Table 2). An initial polymerization attempt with a verdazyl/Vazo® 88 ratio of 2.6 at a reaction temperature of 115 °C gave an 18% monomer conversion after 30 min. However, shortly after 30 min the reaction temperature rose to 119 °C and then slowly decreased to 115 °C.

The reaction mixture quickly became viscous and the conversion after 50 min was 65%. The correlation between the actual and theoretical $\overline{M}_n$ was poor and the higher actual $\overline{M}_n$ suggested the occurrence of some chain termination reactions or a low initiator efficiency. A series of reactions were performed with lower concentrations

*Table 2.*
Polymerizations of styrene initiated with Vazo® 88 (1,1′-azobis(cyclohexanecarbonitrile) in the presence of 1,5-dimethyl-3-phenyl-6-oxoverdazyl radical **1b**. Polymerizations were performed in 10 mL of styrene.

| Entry | Vazo®88 ($\times 10^{-2}$ M) | **1b** ($\times 10^{-2}$ M) | **1b**/ Vazo®88 | Time (h) | $\overline{M}_n$ g/mol$^{-1}$ | $\overline{M}_{nthe}$[a] g/mol$^{-1}$ | $\overline{M}_w/\overline{M}_n$ | Conv'n (%) |
|---|---|---|---|---|---|---|---|---|
| 1[b] | 3.9 | 10.3 | 2.6 | 0.5 | 2000 | – | 2.1 | 18 |
| | | | | 0.9 | 9600 | 7500 | 1.5 | 65 |
| 2[c] | 1.6 | 5.2 | 3.2 | 3 | 1280 | 1700 | 1.5 | 6 |
| | | | | 5 | 15900 | 17900 | 1.5 | 63 |
| | | | | 6 | 18800 | 19600 | 1.4 | 69 |

[a] Reaction temperature 115 °C.
[b] Reaction temperature 105 °C for the first 3h and 110 °C for the last 3h.
[c] Calculation for the theoretical molecular weight: $\overline{M}_{nthe}$ = [(moles monomer ÷ 2× moles of initiator) × MW monomer] × % conversion.

 

***Table 3.***
Characterization results for the polymerization of styrene (10 mL, $8.7 \times 10^{-2}$ mol) at 130 °C initiated with BSV **5a** (0.1 g, $1.8 \times 10^{-4}$ mol).

| Rxn. Time (h) | $\overline{M}_n$ g/mol$^{-1}$ | $\overline{M}_{nthe}$ g/mol$^{-1}$ | $\overline{M}_w/\overline{M}_n$ | Conv'n (%) |
|---|---|---|---|---|
| 0.5 | 17400 | 1000 | 1.7 | 2 |
| 1.5 | 25100 | 4500 | 1.8 | 9 |
| 4 | 30500 | 11100 | 1.7 | 22 |
| 6 | 32700 | 20000 | 1.6 | 39 |

of Vazo® 88 and verdazyl, higher verdazyl/Vazo® 88 ratios, and at lower temperatures to avoid this exotherm, but no improvement was observed. A typical result for these reactions is summarized in Table 2, entry 2. After 3 hours at 105 °C the monomer conversion was 6%. A 5 °C increase in temperature caused a sharp increase in the rate of polymerization resulting in a 63% monomer conversion after 5h. While the $\overline{M}_w/\overline{M}_n$ values of the resulting polystyrene samples are not particularly low, it is interesting to note that the actual and theoretical $\overline{M}_n$ values are in good agreement. However, a high verdazyl/Vazo® 88 molar ratio was required to achieve this result suggesting that the verdazyl radical is not particularly efficient at capping the propagating chain or is not very stable at 110 °C.

reaction mixture with some increase over time, however, there was no correlation between actual and theoretical molecular weights. While the polydispersity values remained low an overlay of the GPC curves showed that there was no livingness associated with these polymerizations (Figure 1). At 0.5 h a significant amount of unimer remained in the reaction mixture, as observed in the GPC analysis, and not until 4 h was most of the unimer consumed. This result clearly shows the dissociation of the triphenylverdazyl-styrene bond in the BSV unimer is quite slow even at 130 °C, accounting for the poor livingness of this polymerization.

Significantly better results were obtained with the BSV unimer **5b**. At 125 °C the polymerization of styrene proceeded with an incremental increase in $\overline{M}_n$

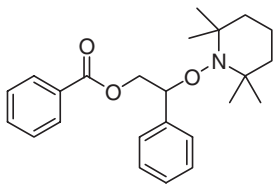

**4**

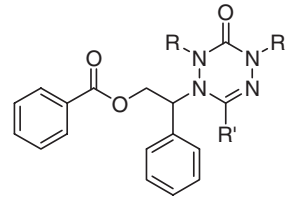

**5a** R, R' = Ph
**5b** R = Me; R' = Ph

With these poor results in hand we turned our attention to using the BSV unimers **5** as the initiating species, prepared by an exchange reaction with BST.[14] The results of a styrene polymerization at 130 °C initiated with unimer **5a** were similar to previous reactions initiated with BPO and mediated with the 1,3,5-triphenyl-6-oxoverdazyl radical (Table 3). High molecular weight was obtained early in the

over time, while the *PDI* remained low (Table 4 and Figure 2). However, while a plot of $\overline{M}_n$ vs conversion is linear (Figure 3), the correlation between the actual and theoretical $\overline{M}_n$ is poor, with the actual $\overline{M}_n$ values considerably lower than expected. There is also a slight upward trend in the $\overline{M}_w/\overline{M}_n$ numbers and observable tailing in the GPC plots at higher conversions. These results would suggest some chain transfer is

 

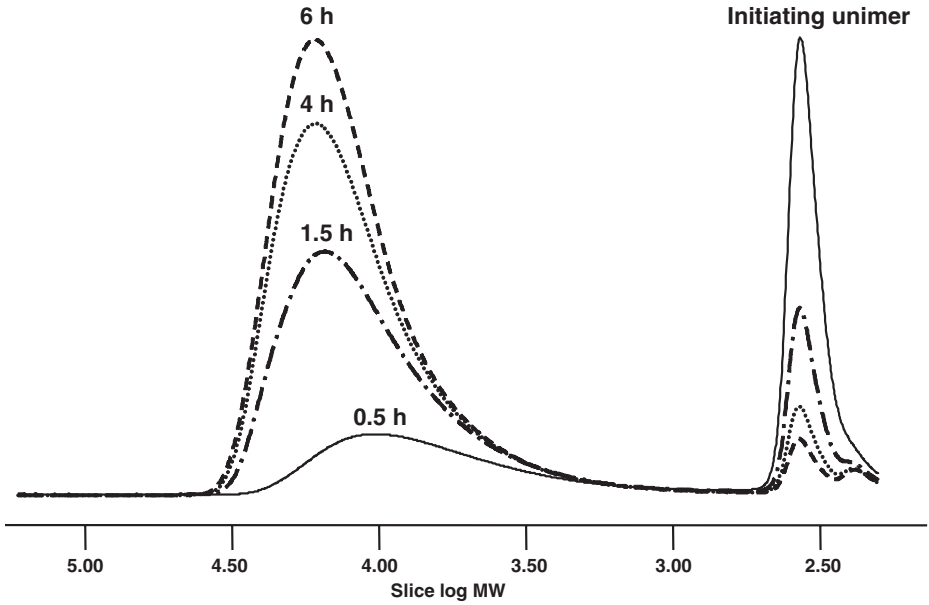


***Figure 1.***
GPC distribution overlap for the polymerization of styrene (10 mL, $8.7 \times 10^{-2}$ mol) at 130 °C initiated with BSV **5a** (0.1 g, $1.8 \times 10^{-4}$ mol). The $\overline{M}_n$ and $\overline{M}_w/\overline{M}_n$ values are listed in Table 3.

occurring and we are presently investigating this possibility.

## Conclusions

While we are not sure at this moment what is causing the discrepancy in the actual and theoretical molecular weights for the 1,5-dimethyl-3-pheny-6-oxoverdazyl radical mediated styrene polymerizations, we are quite encouraged by the fact that there is some degree of livingness associated with the system. As such, we are continuing to synthesize and investigate a series of verdazyl radicals by changing the substituent at C-3. Preliminary results of this investigation have shown that there is clearly a difference in the ability of these various verdazyl radicals to control the radical polymerization of styrene and acrylates, and we are attempting to correlate the stability of the verdazyl radicals to their ability to control radical polymerizations. In addition, we recently reported the use of $^1$H NMR to determine the bond dissociation constants of model alkoxyamines,[16] and we are in the process of extending this methodology to the verdazyl unimers to provide bond dissociation constants for the verdazyl systems.

***Table 4.***
Characterization results for the polymerization of styrene (10 mL, $8.7 \times 10^{-2}$ mol) at 125 °C initiated with BSV **5b** (0.1 g, $1.9 \times 10^{-4}$ mol).

| Rxn. Time (h) | $\overline{M}_n$ g/mol$^{-1}$ | $\overline{M}_{nthe}$ g/mol$^{-1}$ | $\overline{M}_w/\overline{M}_n$ | Conv'n (%) |
|---|---|---|---|---|
| 1 | 4200 | 4600 | 1.13 | 12 |
| 2 | 7700 | 8900 | 1.14 | 23 |
| 3 | 9800 | 11600 | 1.19 | 30 |
| 4 | 11200 | 13500 | 1.22 | 35 |
| 5 | 12100 | 15500 | 1.22 | 40 |

 

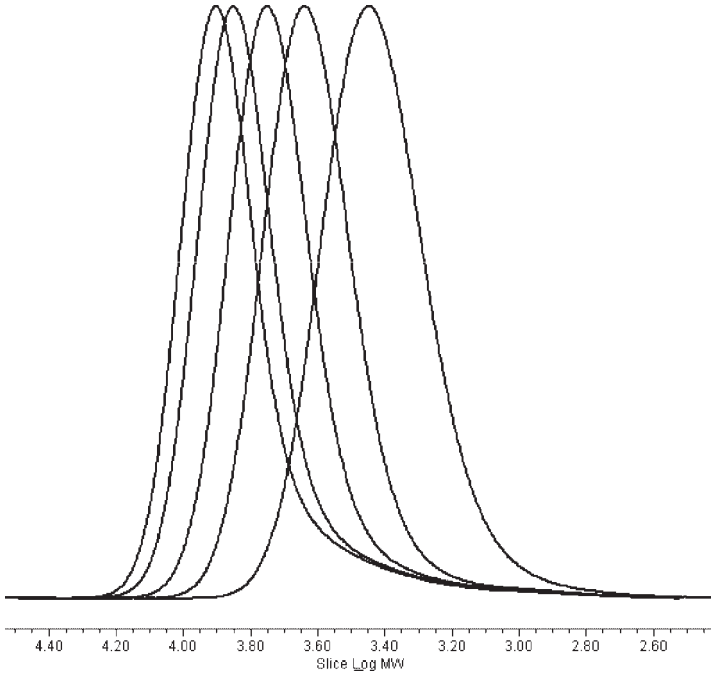


***Figure 2.***
GPC plot for the polymerization of styrene (10 mL, $8.7 \times 10^{-2}$ mol) at 125 °C initiated with BSV **5b** (0.1 g, $1.9 \times 10^{-4}$ mol). Samples were taken from the reaction mixture after each hour for 5 hours. The $\overline{M}_n$ and $\overline{M}_w/\overline{M}_n$ values are listed in Table 4.

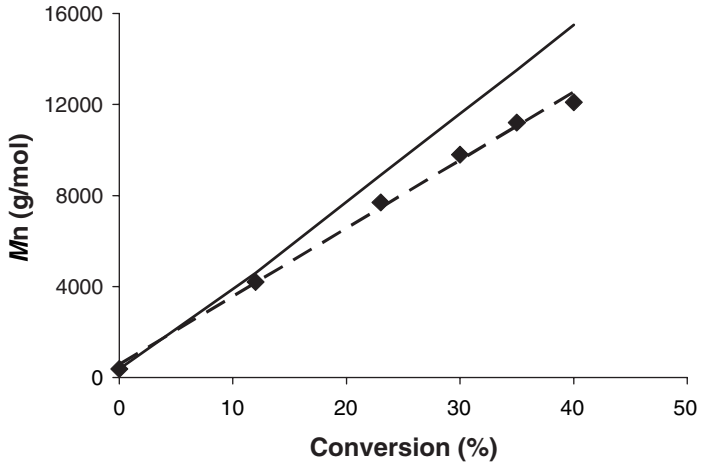


***Figure 3.***
Demonstration of the linear dependence of $\overline{M}_n$ on monomer conversion for styrene at 125 °C initiated by BSV **5b**. The solid line indicates $\overline{M}_{nthe}$, the values listed in Table 4. [styrene]/[BSV **5b**]: $8.7 \times 10^{-2}/1.9 \times 10^{-4}$.

 

[1] J. Sobek, R. Martschke, H. Fischer, *J. Am. Chem. Soc.* **2001**, *123*, 2849–2857.
[2] [2a] P. M. Kazmaier, K. A. Moffat, M. K. Georges, R. P. N. Veregin, G. K. Hamer, *Macromolecules* **1995**, *28*, 1841–1846;[2b] G. Moad, E. Rizzardo, *Macromolecules* **1995**, *28*, 8722–8728;[2c] R. D. Puts, D. Y. Sogah, *Macromolecules* **1996**, *29*, 3323–3325;[2d] Y. K. Chong, F. Ercole, G. Moad, E. Rizzardo, S. H. Thang, *Macromolecules* **1999**, *32*, 6895–6903;[2e] D. Benoit, V. Chaplinski, R. Braslau, C. J. Hawker, *J. Am. Chem. Soc.* **1999**, *121*, 3904–3920;[2f] S. Grimaldi, J. P. Finet, F. Le Moigne, A. Zeghdaoui, P. Tordo, D. Benoit, M. Fontanille, Y. Gnanou, *Macromolecules* **2000**, *33*, 1141–1147; [2g] M. O. Zink, A. Kramer, P. Nesvadba, *Macromolecules* **2000**, *33*, 8106–8108;[2h] D. Benoit, S. Grimaldi, S. Robin, J. P. Finet, P. Tordo, Y. Gnanou, *J. Am. Chem. Soc.* **2000**, *122*, 5929–5939;[2i] C. Wetter, J. Gierlich, C. Knoop, C. Muller, T. Schulte, A. Studer, *Chem. Eur. J.* **2004**, *10*, 1156–1166;[2j] T. Schulte, K. O. Siegenthaller, H. Luftmann, M. Letzel, A. Studer, *Macromolecules* **2005**, *38*, 6833–6833;[2k] K. O. Siegenthaler, A. Studer, *Macromolecules* **2006**, *39*, 1347–1352.
[3] [3a] S. O. Hammouch, J. M. Catala, *Macromol. Rapid Commun.* **1996**, *17*, 149–154;[3b] T. Fukuda, A. Terauchi, K. Goto, K. Ohno, Y. Tsujii, T. Miyamoto, S. Kobatake, B. Yamada, *Macromolecules* **1996**, *29*, 6393–6398;[3c] M. K. Georges, P. G. Odell, N. A. Listigovers, M. H. Quinlan, *ACS Sym. Series 713, Solvent Free Polymerization and Processes*, **1998**, 80–95.
[4] [4a] D. Greszta, K. Matyjaszewski, *Macromolecules*, **1996**, *29*, 7661–7670;[4b] A. Goto, T. Fukuda, *Macromolecules* **1997**, *30*, 4272–4277;[4c] A. Goto, T. Fukuda, *Macromolecules* **1999**, *32*, 618–623.
[5] [5a] M. K. Georges, J. L. Lukkarila, A. R. Szkurhan, *Macromolecules* **2004**, *37*, 1297–1303;[5b] A. Debuigne, T. Radhakrishnan, M. K. Georges, *Macromolecules* **2006**, *39*, 5359–5363.
[6] S. Gaynor, D. Greszta, D. Mardare, M. Teodorescu, K. Matyjaszewski, *J.M.S. Pure Appl. Chem.* **1994**, *A31*(11), 1561–1578.
[7] [7a] D. Colombani, M. Steenbock, M. Klapper, K. Müllen, *Macromol. Rapid Commun.* **1997**, *18*, 243–251;[7b] M. Steenbock, M. Klapper, K. Müllen, C. Bauer, M. Hubrich, *Macromolecules* **1998**, *31*, 5223-5228; [7c] N. S. Khelfallah, M. Peretolchin, M. Klapper, K. Müllen, *Polym. Bull.* **2005**, *53*, 295–304.
[8] [8a] B. Yamada, H. Tanaka, K. Konishi, T. Otsu, *J.M.S. Pure Appl. Chem.* **1994**, *A31*(3), 351–366;[8b] B. Yamada, Y. Nobukane, Y. Miura, *Polym. Bull.* **1998**, *41*, 539–544.
[9] R. Milcent, G. Barbier, *J. Heterocyclic Chem.* **1994**, *31*, 319–324.
[10] F. A. Neugebauer, *Angew. Chem. Int. Ed. Engl.* **1973**, *12*, 455–464.
[11] [11a] F. A. Neugebauer, H. Fischer, R. Seigel, *Chem. Ber.* **1988**, *121*, 815;[11b] F. A. Neugebauer, H. Fischer, C. Krieger, *J. Chem. Soc. Perkin Trans* **1993**, *2*, 535–544.
[12] [12a] C. L. Barr, P. A. Chase, R. G. Hicks, M. T. Lemaire, C. L. Stevens, *J. Org. Chem.* **1999**, *64*, 8893–8897;[12b] E. C. Paré, D. J. Brook, A. Brieger, M. Badik, M. Schinke, *Org. Biomol. Chem.* **2005**, *3*, 4258–4261.
[13] [13a] F. A. Neugebauer, H. Fischer, *Angew. Chem.* **1980**, *92*, 766;[13b] F. A. Kursmitteilung, F. A. Neugebauer, H. Fischer, *Angew. Chem. Int. Ed. Engl.* **1980**, *19*, 724;[13c] F. A. Neugebauer, H. Fischer, R. Seigel, C. Krieger, *Chem. Ber.* **1983**, *116*, 3461–3481.
[14] C. J. Hawker, *J. Am. Chem. Soc.* **1994**, *116*, 11185–11186.
[15] Detailed characterization of this unimer is provided in a paper submission to Macromolecules.
[16] Li. Lichun, G. K. Hamer, M. K. Georges, *Macromolecules*, **2006**, in press.

 

 DOI: 10.1002/masy.200750213

# Germanium- and Tin-Catalyzed Living Radical Polymerizations of Styrene and Methacrylates

*Atsushi Goto, Hirokazu Zushi, Norihiro Hirai, Tsutomu Wakada, Yungwan Kwak, Takeshi Fukuda**

**Summary**: Ge and Sn (non-transition-metal) catalyzed living radical polymerizations were developed. Low-polydispersity ($M_w/M_n \sim 1.1$–$1.3$) polystyrenes, poly(methyl methacrylate)s, poly(glycidyl methacrylate)s, and poly(2-hydroxyethyl methacrylate) with predicted molecular weights were obtained with a fairly high conversion in a fairly short time. The pseudo-first-order activation rate constant $k_{act}$ for the styrene/$GeI_4$ (catalyst) system was large enough, even with a small amount of $GeI_4$, to explain why the system provides low-polydispersity polymers from an early stage of polymerization. The retardation in the polymerization rate observed for the styrene/$GeI_4$ system was kinetically proved to be mainly due to the cross-termination between the propagating radical with $GeI_3^{\bullet}$. Attractive features of the Ge and Sn catalysts include their *high reactivity* hence small amounts (1–5 mM) being required under a mild condition (at 60–80 °C), *high solubility* in organic media without ligands, *insensitivity to air* hence sample preparation being allowed in the air, and *minor color and smell*. The Ge catalysts may also be attractive for their *low toxicity*.

**Keywords:** germanium; iodide; living radical polymerization; non-transition metal; tin

## Introduction

Living radical polymerization (LRP) has attracted much attention as a robust and versatile synthetic route for well-defined polymers.[1] LRP is based on the reversible activation of the dormant species P-X to the propagating radical $P^{\bullet}$ (Scheme 1a). A number of activation-deactivation cycles are requisite for good control of chain length distribution.[2,3] As the capping agent X, halogens have been used mainly in two systems. One is iodide-mediated polymerization, in which P-X (X = I) is activated by $P^{\bullet}$ (degenerative or exchange chain transfer: Scheme 1b).[4] However, due to a low exchange frequency of iodine, the control in polydispersity is limited, in most cases. The other is atom transfer radical polymerization (ATRP), in which P-X (X = Cl, Br) is activated by a transition metal complex (Scheme 1c, where A is an activator, and XA is a deactivator).[5] The addition of the catalyst allows a high activation frequency, yielding low-polydispersity polymers.

We recently developed a new and robust LRP.[6] We added a germanium or tin compound such as $GeI_4$ to the iodide-mediated polymerization. $GeI_4$ works as a deactivator of $P^{\bullet}$, in situ producing $GeI_3^{\bullet}$ (Scheme 2). $GeI_3^{\bullet}$ radical works as an activator for polymer-iodide P-I, producing $P^{\bullet}$ and $GeI_4$. This cycle allows a frequent activation of P-I. This is the first living radical polymerization using a non-transition metal as a catalyst.

In this paper, we will briefly summarize our studies on this new LRP, demonstrating its controllability in molecular weight and molecular weight distribution for styrene (St) and methacrylates and kinetic features regarding the activation process and the polymerization rate for the St/$GeI_4$ system.

Institute for Chemical Research, Kyoto University, Uji, Kyoto 611-0011, Japan
E-mail: fukuda@scl.kyoto-u.ac.jp

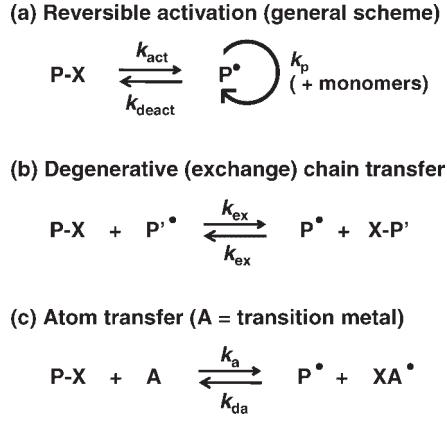


***Scheme 1.***
Reversible activation processes. (a) General Scheme, (b) degenerative (exchange) chain transfer, and (c) atom transfer.

## Control in Molecular Weight and Its Distribution

*Styrene*

We examined the polymerization of St at 80 °C, using 1-phenylethyl iodide (PE-I) as a low-mass alkyl halide initiator, $GeI_4$ as a deactivator, and benzoyl peroxide (BPO) as a conventional radical initiator. In this polymerization, P•, which is originally supplied by BPO, is supposed to react with $GeI_4$, in situ producing the activator $GeI_3^•$ (and P-I). If $GeI_3^•$ effectively abstracts I from PE-I (or P-I) to produce PE• (or P•), a useful sequence of activation and deactivation will be completed.

Table 1 (entries 1-4) and Figure 1 (filled squares) show the results. As shown in Figure 1, $M_n$ linearly increased with conversion and agreed with the theoretical value $M_{n,theo}$. The polydispersity index (PDI or $M_w/M_n$) reached a low value of about 1.2 from an early stage of polymerization, indicating a high frequency of the activation-deactivation cycle. The small amount (2–5 mM) of $GeI_4$ required to control the polydispersity suggests a high reactivity of this catalyst.

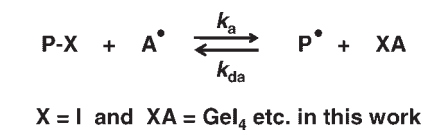


***Scheme 2.***
Catalytic Activation process with the Ge and Sn catalyst.

The activation of P-I occurs not only by the catalytic process (Scheme 2) but also by degenerative chain transfer (Scheme 1b). However, for example, the system with PE-I (80 mM) and BPO (20 mM) but without $GeI_4$ (entry 11: iodide-mediated polymerization) only gave a PDI as large as 1.55 for 4 h at 80 °C, while that with $GeI_4$ (5 mM) (entry 1) achieved a fairly small PDI of 1.17 (with other conditions set the same). This means that the catalytic activation plays a main role in the $GeI_4$ system, with a small contribution of degenerative chain transfer.

Besides $GeI_4$, we also used $GeI_2$, $SnI_4$, and $SnI_2$ as deactivators (entries 5–10 in Table 1 and Figure 1). In all cases, low polydispersity was attained with a small amount (1–5 mM) of the catalyst. The Sn catalysts (entries 7–10) exhibited good polydispersity control at 60 °C, as the Ge catalysts (entries 1–6) did at 80 °C. This suggests that the Sn catalysts are even more active. Both $GeI_2$ and $SnI_2$ were effective catalysts, but the results with them (entries 5, 6, and 10 and Figure 1) were not as good as those with $GeI_4$ and $SnI_4$ (entries 1–4 and 7–9 and Figure 1).

Ge and Sn halides are Lewis acids. $SnCl_4$, which is a strong Lewis acid, can abstract a halogen anion from an alkyl halide to give the alkyl carbocation and is widely used for living cationic polymerizations.[7] On the other hand, Ge and Sn iodides (used in this work) are relatively weak Lewis acids. The tacticities of the produced polymers and the complete inhibition of the polymerization in the presence of 2,2,6,6-tetramethylpiperidinyl-1-oxy (TEMPO) confirmed that the polymerizations in this work proceeded in a radical mechanism.

*Methacrylates*

We examined the polymerization of methyl methacrylate (MMA) with the same low-mass alkyl iodide (PE-I) and catalysts

 

***Table 1.***
Polymerization of St with PE-I in the Presence of Ge and Sn Iodides.

| entry | XA | $[PE\text{-}I]_0/[I^a]_0/[XA]_0$ (mM) | T (°C) | t (h) | conv (%) | $M_n$ ($M_{n,theo}$)[b] | PDI |
|---|---|---|---|---|---|---|---|
| 1 | $GeI_4$ | 80/20/5 | 80 | 4 | 26 | 2500 (2600) | 1.19 |
| | | | | 7 | 37 | 3500 (3700) | 1.16 |
| | | | | 21 | 47 | 4300 (4700) | 1.16 |
| 2 | | 80/20/2 | 80 | 7 | 47 | 4600 (4700) | 1.16 |
| 3 | | 80/40/2 | 80 | 7 | 85 | 8200 (8500) | 1.24 |
| 4 | | 25/10/5 | 80 | 21 | 40 | 11400 (13300) | 1.29 |
| 5 | $GeI_2$ | 80/20/5 | 80 | 21 | 59 | 5700 (5900) | 1.15 |
| 6 | | 80/40/5 | 80 | 25 | 85 | 6800 (8500) | 1.16 |
| 7 | $SnI_4$ | 80/20/5 | 60 | 21 | 36 | 3600 (3600) | 1.13 |
| 8 | | 80/40/5 | | 27 | 72 | 6500 (7200) | 1.21 |
| 9 | | 8/4/1 | 60 | 21 | 24 | 22000 (24000) | 1.18 |
| 10 | $SnI_2$ | 80/20/5 | 60 | 21 | 50 | 4800 (5000) | 1.23 |
| 11 | none | 80/20/0 | 80 | 4 | 41 | 4200 (4100) | 1.55 |

[a] BPO for entries 1–6 and 11 and AIBN for entries 7–10.
[b] Theoretical $M_n$ calculated with [St], [PE-I], and conversion.

($GeI_4$, $GeI_2$, $SnI_4$, and $SnI_2$) as in the styrene system. However, the initiation of PE-I was slow and the polydispersity was not controlled. To increase the initiation rate, we used a tertiary alkyl iodide 2-cyanopropyl iodide (CP-I) instead of the secondary one PE-I, and to increase the activation rate, we used *p*-tolyl germanium triiodide (*p*-$CH_3$-$C_6H_4$-$GeI_3$) ($TGeI_3$)[8] as a catalyst. In this case (entries 1 and 2 in Table 2), low-polydispersity polymers were successfully obtained with a small amount of the catalyst (5 mM) at 70 °C, in which azobis(isobutyronitrile) (AIBN) was used as a conventional radical initiator. Without the catalyst (entry 3 in Table 2), polydispersity was not controlled.

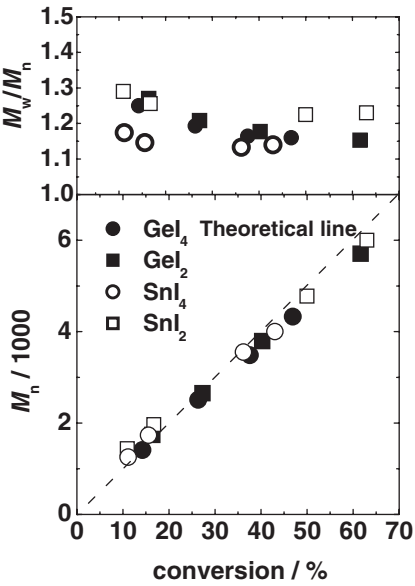


***Figure 1.***
Plot of $M_n$ and PDI vs conversion for the Ge and Sn catalyzed polymerizations of St for entries1, 5, 7, and 10 in Table 1.

We also examined two functional methacrylates (Table 2), i.e., glycidyl methacrylate (GMA) with an epoxide and 2-hydroxyethyl methacrylate (HEMA) with a hydroxy group. For GMA (entry 4), we used $GeI_4$ as a catalyst and BPO as a conventional radical initiator, with other conditions set the same as those for MMA. The $M_n$ well agreed with $M_{n,theo}$, and PDI was about 1.2 from an early stage to a later stage of polymerization, suggesting that the high reactivity of the catalyst retained in GMA. For HEMA (entry 5), $TGeI_3$ and AIBN were used, as in the MMA system. Although a relatively large amount (20 mM) of the catalyst was required, a low-polydispersity polymer was successfully obtained.

### Kinetic Studies for the St/$GeI_4$ System

We made kinetic studies on the activation process and polymerization rate $R_p$ for the St polymerization with a polystyrene iodide (PSt-I) ($M_n = 2000$; PDI = 1.20), BPO, and

 

***Table 2.***
Polymerization of Methacrylates with CP-I in the Presence of Ge Iodides.

| entry | monomer | XA | $[CP\text{-}I]_0/[I^a]_0/[XA]_0$ (mM) | T (°C) | t(h) | conv (%) | $M_n$ ($M_{n,theo}$)[b] | PDI |
|---|---|---|---|---|---|---|---|---|
| 1 | MMA | $TGeI_3$ | 80/20/5 | 70 | 6 | 84 | 6900 (8400) | 1.19 |
| 2 | | | 20/20/5 | 70 | 8 | 60 | 18400 (24000) | 1.28 |
| 3 | | | 40/20/0 | 70 | 4 | 99 | 30300 (20000) | 1.90 |
| 4 | GMA | $GeI_4$ | 40/20/5 | 70 | 0.67 | 20 | 6600 (6300) | 1.14 |
| | | | | | 1.67 | 64 | 21000 (18000) | 1.27 |
| 5 | HEMA[c] | $TGeI_3$ | 80/20/20 | 70 | 2.5 | 85 | 10000 (9700) | 1.35 |

[a] AIBN for entries 1–3 and 5 and BPO for entry 4.
[b] Theoretical $M_n$ calculated with [monomer], [PE-I], and conversion.
[c] In ethanol (50 vol%).

$GeI_4$ at 80 °C. We used the polymeric adduct PSt-I as a starting alkyl iodide to focus on the kinetics of polymer region.

*Reversible Activation*

As mentioned, in the presence of $GeI_4$ (deactivator XA), PSt-I can be activated by degenerative chain transfer (Scheme 1b: rate constant $k_{ex}$) and the catalytic process with $GeI_3^{\bullet}$ (activator $A^{\bullet}$) (Scheme 2: rate constant $k_a$.). Thus, the pseudo-first-order activation rate constant $k_{act}$ is given by

$$k_{act} = k_{ex}[P^{\bullet}] + k_a[A^{\bullet}] \quad (1)$$

In the quasi-equilibrium for the catalytic activation-deactivation process (Scheme 2), Eq. 1 takes the form

$$k_{act} = k_{ex}[P^{\bullet}] + k_{da}[P^{\bullet}]\left(\frac{[XA]}{[P-X]}\right) \quad (2)$$

where $k_{da}$ is the deactivation rate constant with XA (Scheme 2). The equation means that $k_{act}$ increases with the ratio [XA]/[P-X].

By the gel permeation chromatography (GPC) method,[3,9] we determined $k_{act}$ for the PSt-I/$GeI_4$ system with various $[GeI_4]_0/[PSt\text{-}I]_0$ ratios and a (nearly) fixed $[P^{\bullet}]$. As expected from Eq. 2, $k_{act}$ linearly increased with this ratio in the examined range of 0–0.04 (data not shown), suggesting that for the typical case with $[GeI_4]/[PSt\text{-}I] = 5mM/80mM$, $k_{act}$ would be about 12 times larger than in the absence of the catalyst $GeI_4$. This explains why low-polydispersity polymers were obtained from an early stage of polymerization for the $GeI_4$ system.

*Polymerization Rate*

In the presence of Ge and Sn iodides, $R_p$ was somewhat smaller than in their absence (Tables 1 and 2). This is because Ge and Sn radicals ($A^{\bullet}$) undergo irreversible cross-termination with $P^{\bullet}$ (rate constant $k_t'$) and irreversible self-termination between $A^{\bullet}$ (rate constant $k_t''$). This mechanism is analogous to the one for the rate retardation in reversible addition-fragmentation chain transfer (RAFT) polymerization.[10,11]

In the quasi-equilibrium for the catalytic process (Scheme 2) and the stationary-state of radical concentrations ($d[P^{\bullet}]/dt = d[A^{\bullet}]/dt = 0$), $R_p$ is theoretically given by[11]

$$R_p = R_{p,0}\left(1 + 2\left(\frac{k_t'}{k_t K}\right)\frac{[XA]}{[P-X]} + \left(\frac{k_t''}{k_t K^2}\right)\frac{[XA]^2}{[P-X]^2}\right)^{-1/2} \quad (3)$$

where $R_{p,0}$ is the $R_p$ without XA, $K$ is the activation-deactivation equilibrium constant ($K = k_a/k_{da}$ (Scheme 2)), and $k_t$ is the self-termination rate constant for $P^{\bullet}$. This means that $R_p$ decreases with the ratio [XA]/[P-X]. At a small ratio, the last term on the right-hand side for the self-termination of $A^{\bullet}$ may be neglected, and Eq. 3 takes the form

$$R_p = R_{p,0}\left(1 + 2\left(\frac{k_t'}{k_t K}\right)\frac{[XA]}{[P-X]}\right)^{-1/2} \quad (4)$$

The last term in Eq. 3 is also neglected, when the self-termination of $A^{\bullet}$ is reversible and is not a real termination.

 

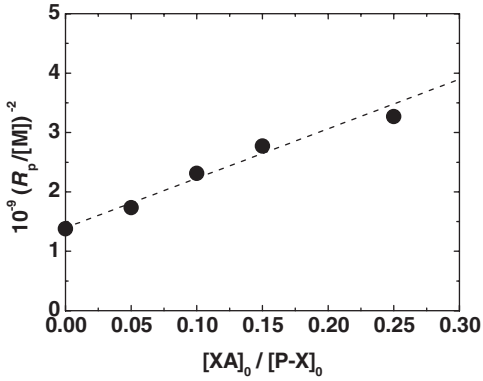


***Figure 2.***
Plot of $(R_p/[M])^{-2}$ vs $[XA]_0/[P\text{-}X]_0$ for the St/PSt-I/BPO/($GeI_4$) system (80 °C): $[PSt\text{-}I]_0 = 20$ mM; $[BPO]_0 = 10$ mM; $[GeI_4]_0 = 0$–5 mM. [M] is the monomer concentration.

We examined the $R_p$ for the St/$GeI_4$ system with various amounts of $GeI_4$ (0–5 mM) and fixed amounts of PSt-I (20 mM) and BPO (10 mM) at 80 °C. We studied an early stage of polymerization (for ≤35 min and at the conversion of ≤7%). The use of the polymer adduct PSt-I instead of the low-mass adduct PE-I minimizes the possible effect of chain length dependence of $k_t$ on $R_p$. The $R_p$ (hence $[P^\bullet]$) was stationary in the studied range of time in all cases, as the theory demands, and decreased with $[XA]_0/[P\text{-}X]_0$. Figure 2 shows the plot of $R_p^{-2}$ vs $[XA]_0/[P\text{-}X]_0$. The plot was linear, confirming the validity of Eq. 4 in the studied range (0–0.25) of the ratio. Thus, for the $GeI_4$ system, at a relatively small ratio, as in entries 1–4 in Table 1 ($[XA]_0/[P\text{-}X]_0 \sim 0.1$), cross-termination is the main cause for the retardation. The cross-termination results in a loss of $GeI_4$, but it is a minor one at an early stage of polymerization. Moreover, the cross-termination products such as PSt-$GeI_3$ (by recombination) are Ge (IV) iodides and would still work as XA, contributing to polydispersity control. From the slope of the line (Figure 2), we had $k_t'/(k_tK) = 3$.

## Conclusions

The Ge and Sn (non-transition-metal) catalyzed LRPs were developed. The molecular weight and its distribution were well controlled for the St, MMA, GMA, and HEMA polymerizations. The $k_{act}$ for the St/$GeI_4$ system was large enough, even with a small amount of $GeI_4$, which explained why low-polydispersity PSts are obtained from an early stage of polymerization. The rate retardation observed for the St/$GeI_4$ system was due to the cross-termination between $P^\bullet$ with $GeI_3^\bullet$. Attractive features of the Ge and Sn catalysts include their *high reactivity* hence small amounts being required under a mild temperature, *high solubility* in organic media without ligands, *insensitivity to air* hence sample preparation being allowed in the air, and *minor color and smell*. The Ge catalysts may also be attractive for their *low toxicity*.

[1] [1a] *Handbook of Radical Polymerization*, K. Matyjaszewski, T. P. Davis Eds., Wiley-Interscience: New York, **2002**. [1b] K. Matyjaszewski Ed. *ACS Symp. Ser.* **1998**, *685*, **2000**, *768*, **2003**, *854*, **2006**, *944*.
[2] For reviews on kinetics: [2a] H. Fischer, *Chem. Rev.* **2001**, *101*, 3581. [2b] A. Goto, T. Fukuda, *Prog. Polym. Sci.* **2004**, *29*, 329.
[3] T. Fukuda, *J. Polym. Sci.: Part A: Polym. Chem.* **2004**, *42*, 4743.
[4] [4a] Y. Yutani, M. Tatemoto, *Eur. Pat. Appl.* 048937OA1, **1991**. [4b] M. Kato, M. Kamigaito, M. Sawamoto, T. Higashimura, *Polym. Prepr., Jpn.* **1994**, *43*, 255. [4c] K. Matyjaszewski, S. Gaynor, J. -S. Wang, *Macromolecules* **1995**, *28*, 2093.
[5] For reviews: [5a] K. Matyjaszewski, J. H. Xia, *Chem. Rev.* **2001**, *101*, 2921. [5b] M. Kamigaito, T. Ando, M. Sawamoto, *Chem. Rev.* **2001**, *101*, 3689.

 

[6] A. Goto, H. Zushi, Y. Kwak, T. Fukuda, *ACS Symp. Ser.* **2006**, *944*, 595.
[7] For reviews: [7a] M. Sawamoto, *Prog. Polym. Sci.* **1991**, *16*, 111. [7b] J. E. Puskas, G. Kaszas, *Prog. Polym. Sci.* **2000**, *25*, 403.
[8] For synthesis: E. A. Flood, *J. Am. Chem. Soc.* **1933**, *55*, 4935.
[9] T. Fukuda, A. Goto, *Macromol. Rapid Commun.* **1997**, *18*, 683: the factor −2 appearing in Eq. 4 is a misprint for C−2.
[10] [10a] H. de Brouwer, M. A. J. Schellekens, B. Klumperman, M. J. Monteiro, A. L. German, *J. Polym. Sci., Part A.: Polym. Chem.* **2000**, *38*, 3596. [10b] Y. Kwak, A. Goto, Y. Tsujii, Y. Murata, K. Komatsu, T. Fukuda, *Macromolecules* **2002**, *35*, 3026. [10c] F. M. Calitz, J. B. McLeary, J. M. Mckenzie, M. P. Tonge, B. Klumperman, R. D. Sanderson, *Macromolecules* **2003**, *36*, 9687. [10d] A. R. Wang, S. Zhu, Y. Kwak, A. Goto, T. Fukuda, M. J. Monteiro, *J. Polym. Sci., Part A.: Polym. Chem.* **2003**, *41*, 2833. [10e] T. Arita, S. Beuermann, M. Buback, P. Vana, *Macromol. Mater. Eng.* **2005**, *290*, 283. [10f] C. Barner-Kowollik, M. Buback, B. Charleux, M. L. Coote, M. Drache, T. Fukuda, A. Goto, B. Klumperman, A. B. Lowe, J. B. Mcleary, G. Moad, M. J. Monteiro, R. D. Sanderson, M. P. Tonge, P. Vana, *J. Polym. Sci.: Part A: Polym. Chem.* **2006**, *44*, 5809.
[11] Y. Kwak, A. Goto, T. Fukuda, *Macromolecules* **2004**, *37*, 1219.

 

 DOI: 10.1002/masy.200750214

# Mechanism and Kinetics of the Induction Period in Nitroxide Mediated Thermal Autopolymerizations. Application to the Spontaneous Copolymerization of Styrene and Maleic Anhydride

*José Bonilla-Cruz,*[1] *Laura Caballero,*[2] *Martha Albores-Velasco,**[2]
*Enrique Saldívar-Guerra,**[1] *Judith Percino,*[3] *Víctor Chapela*[3]

**Summary:** Recently we reported an experimental and theoretical (simulation) investigation on the mechanism of the induction period and the initial polymerization stages in the nitroxide mediated autopolymerization of styrene. In this paper we extend some of the results presented there and perform preliminary induction period experiments for the study of the mechanism and kinetics of the spontaneous copolymerization of styrene (S) and maleic anhydride (MA) in the presence of TEMPO and 4-OH-TEMPO. With even small amounts of MA (2% wt) the induction period is dramatically reduced by a factor of about 20 in comparison with the nitroxide-mediated styrene autopolymerization at 120 °C. Our results suggest that the initiation mechanism involves a first step of reaction between S and MA. We speculate that this reaction is a Diels-Alder cycloaddition followed by hydrogen abstraction through a monomer or TEMPO assisted homolysis to form a radical pair (monomer case) or a single radical (TEMPO case), which either initiates polymerization or is trapped by TEMPO depending on the conditions. Hall and Padias have studied similar electron donor-acceptor co-monomer pairs and favor the formation of a tetramethylene diradical as the initiating species for spontaneous copolymerization. In any case, the rate-limiting step would be the initial reaction of S and MA. These induction experiments allow us to obtain an initial estimate of the order of magnitude for the kinetic constant of the rate-limiting step, as $10^{-6}$ $Lmol^{-1}s^{-1}$.

**Keywords:** autopolymerization; kinetics; styrene – maleic anhydride copolymerization

## Introduction

Various mechanisms have been proposed to explain the initiation mechanism of self initiated copolymerizations of styrene (S) with electron acceptor monomers such as maleic anhydride (MA), acrylonitrile, vinyliden cyanide or dimethyl 1,1-dicianoethane-2-2-dicarboxylate. They have been proposed to be analogous to the self-initiated styrene homopolymerization.

The oldest mechanism for the self-polymerization of styrene was postulated by Flory[1] and involves the formation of a diradical intermediate which leads to the formation of a $2+2$ styrene dimer. The diradical can abstract a hydrogen atom from a hydrogen donor forming a monoradical which reacts with styrene to yield polystyrene.

Another mechanism for polystyrene polymerization (Mayo[2]) involves a regioselective $(4+2)$ Diels Alder adduct which rapidly undergoes hydrogen abstraction (molecular assisted homolysis) by another

[1] Centro de Investigación en Química Aplicada, Blvd. Enrique Reyna 140, 25100, Saltillo, Coahuila México
E-mail: esaldivar@ciqa.mx
[2] Facultad de Química, Universidad Nacional Autónoma de México, Coyoacán CU, México
[3] Laboratorio de Polímeros, Benemérita Universidad Autónoma de Puebla, Puebla, México

monomer unit to form a radical pair. This radical pair can initiate polymerization or can form a trimer. Evidence supporting the Mayo mechanism includes the isolation of the dimer and the trimer from styrene polymerization and the identification of the dimer as an end group in polystyrene using H NMR and UV spectroscopy.[2,3] Buzanowsky[4] studied the polymerization of styrene in the presence of various acid catalysts and the reactive Diels-Alder dimer was quickly aromatized to the inactive dimer, which decreased the rate of initiation and the formation of the trimer. These results were considered as a further support to the Mayo mechanism. This mechanism has been extended to the spontaneous copolymerizations of styrene with maleic anhydride and other electron-acceptor monomers (see Scheme 1, A).[5] Several authors have studied [6–8] the spontaneous polymerization of styrene with acrylonitrile focusing on isolated trimers that are produced presumably as a result of the initiation step; however, the trimer structures do not suffice to differentiate between the Mayo mechanism and the Flory diradical mechanism.

We provide here experimental evidence about the faster rate of spontaneous radical generation of styrene with maleic anhydride than that present in the spontaneous

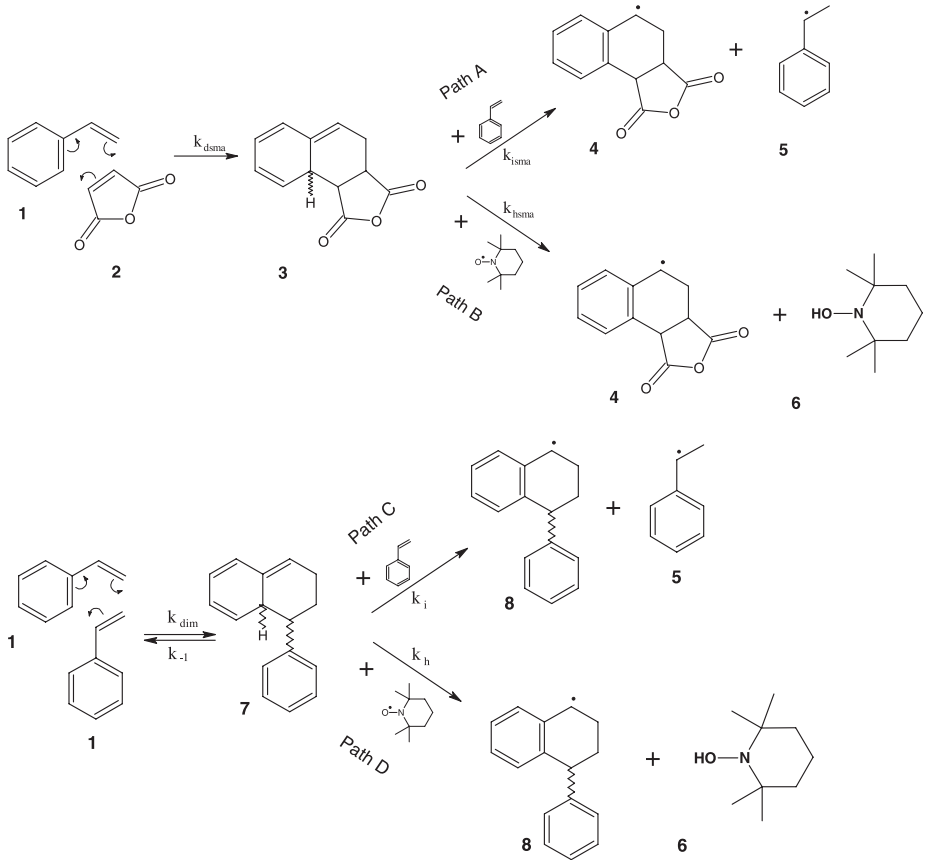


***Scheme 1.***

Paths: A) Mechanism of spontaneous radical formation in styrene-maleic anhydride thermal copolymerization; B) Postulated acceleration of radical generation in styrene-maleic anhydride thermal copolymerization in the presence of TEMPO; C) Accepted mechanism of spontaneous radical formation in styrene thermal polymerization; D) Mechanism of acceleration of radical generation in styrene thermal autopolymerization in the presence of TEMPO.

 

styrene homopolymerization at the same temperature. From this, it is plausible to postulate that there are two parallel and competing mechanisms for radical generation in the copolymerization case: i) the one operating in styrene homopolymerization, ii) an additional mechanism due to the combined presence of styrene and maleic anhydride.

In this communication we give preliminary results aimed at the elucidation of the mechanism and the estimation of the rate of radical generation in the spontaneous copolymerization of styrene and maleic anhydride. First, we show experiments that give order-of-magnitude estimates of the rate of radical generation in the copolymerization system, as compared with the homopolymerization of styrene. Second, we show additional results that give a preliminary estimation of the corresponding kinetic rate constant under some mechanistic assumptions. Notice that this has not been reported in the past due to the difficulty of separating the initiation and propagation steps. Here, by using carefully planned induction-period experiments of copolymerizations in the presence of stable free radicals, it is possible to make a first separation of the initiation and propagation phenomena.

## Radical-Trapping Experiments

Experiments of disappearance of DPPH (2,2′diphenyl-1-picrylhydrazyl radical), which is widely used to test the ability of compounds to act as free radical scavengers or as hydrogen donors at different temperatures, are shown in Figure 1. Fresh distilled styrene or styrene and recently sublimated MA and a solution $10^{-4}$ M of DPPH were put in a vial in the presence OH-TEMPO or without it, and heated at 80 °, 100 ° or 120 °C after oxygen had been

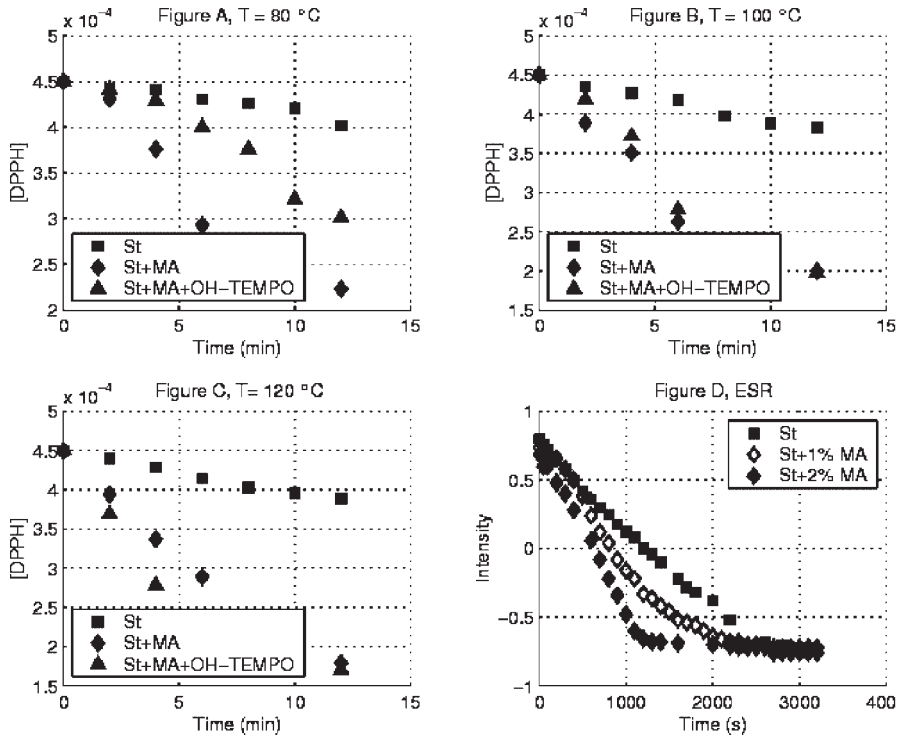


***Figure 1.***
Concentration decay of DPPH in pure styrene, styrene-MA and styrene-MA in presence of OH-TEMPO at 80, 100 and 120 °C (Figures 1A–1C, respectively). Figure 1D shows the concentration decay of OH-TEMPO detected by ESR in thermal autopolymerization of styrene and of styrene-MA at 80 °C.

 

evacuated from the vials. Aliquots of the reactions were taken at different times. The decrement of DPPH was measured by UV spectroscopy to detect the appearance of free radicals. At all the temperatures, it is clear that DPPH disappears faster when MA is added to the reaction, therefore, either radicals or hydrogen donors as the cycloadducts are produced faster. The effect of OH-TEMPO in the reaction was assessed to investigate whether this nitroxide competes with DPPH for the benzylic hydrogen in the Mayo adduct. It can be observed that at 80 °C the disappearance of DPPH is slower in the presence of OH-TEMPO. These results might indicate that radicals react either with DPPH or OH-TEMPO, therefore the rate of DPPH is slower than in the absence of OH-TEMPO. At 100 °C rates of S-MA and S-MA- OH-TEMPO are similar, but at 120 °C, when the self-initiation of styrene participates in the production of radicals through the Mayo adduct, the fastest reaction is the reaction with added OH-TEMPO. We attribute this to the increasing importance with temperature of the thermal autoinitiation due only to styrene. This is not evident in absence of OH-TEMPO because, as discussed in several other references [9,10] and extensively in a recent publication of our group,[11] TEMPO (or its derivatives) considerably enhances the rate of radical generation in the thermal autoinitiation of styrene as long as the TEMPO concentration is far from equilibrium, which occurs during the induction period (see Scheme 1D and discussion below).

ESR (electron spin resonance) experiments of disappearance of OH-TEMPO in reactions of polymerization in which pure styrene or styrene with small amounts of MA (1–2% wt.) are heated at 80 °C in the presence of a small amount of OH-TEMPO ($4.5 \times 10^{-6}$ M), are shown in Figure 1D. These indicate that the nitroxide disappears faster when the concentration of MA increases. The disappearance of the nitroxide would be probably due to the formation of the corresponding alkoxyamine. The possibility of reaction with a free radical might be excluded, since this reversible reaction would produce a constant amount of nitroxide.

### Mechanism and Kinetics

As relevant background for the mechanism that we propose here, we first review the most accepted mechanism (Scheme 1 path C) for spontaneous radical generation in the thermal styrene autopolymerization. In this path, the Mayo dimer is first formed with two styrene molecules, and then radicals are generated at a relatively slow rate via hydrogen abstraction by another styrene molecule from the Mayo dimer. [2,4] This mechanism is modified in inhibition experiments in which styrene is heated in presence of TEMPO. In this case, the most viable mechanism (Scheme 1, path D)[9,10] implies the formation of the Mayo dimer followed by a fast hydrogen abstraction by TEMPO from the Mayo dimer, generating the dimeric radical **8** and the hydroxylamine **6**. In these cases an induction period whose length is proportional to the initial TEMPO concentration is first experimentally observed, followed by polymerization at the rate of styrene autopolymerization. During the induction period the radicals generated are trapped by TEMPO until this reaches its equilibrium concentration with the dormant species; at this point the induction period is over and the polymerization proceeds in a controlled fashion. Also, during induction, hydrogen abstraction from the Mayo dimer assisted by TEMPO is faster than that assisted by monomer as in the traditional Mayo mechanism (path C), and this leads to two consequences: i) the rate of radical generation is much faster in presence of TEMPO than without it during the induction period (when free TEMPO concentration is relatively high and far from equilibrium) and, ii) apparently, during the induction period in presence of TEMPO, the dimer concentration reaches a quasi-stationary state (QSS) that does not occur in the thermal styrene polymerization in absence of TEMPO.[11,12] This last fact allowed Kothe and Fischer[12] to measure

 

the rate of dimer formation by following the TEMPO consumption with ESR. We recently reviewed in detail the path D by simulation and estimated the kinetic coefficient for the hydrogen abstraction from the Mayo dimer by TEMPO ($k_h$) as 0.5–1 L mol$^{-1}$ s$^{-1}$.[11]

By analogy with the mechanisms of spontaneous thermal radical generation for styrene in absence and in presence of TEMPO, and given the stronger donor-acceptor character of the pair S-MA as compared to a pair of styrene molecules, we believe that the radical generation in this spontaneous copolymerization proceeds by the mechanism in Scheme 1 path A (without TEMPO) and path B (in presence of TEMPO). We postulate that an adduct styrene-maleic anhydride (analogous to the Mayo dimer) can be formed in a first step either in a concerted way or via radicals, and this can further react with more monomer to form initiating radicals in the absence of TEMPO (Scheme 1 path A, analogous to the Mayo mechanism), or it can undergo faster hydrogen abstraction by a TEMPO molecule (Scheme 1 path B). Simultaneously, the analogous mechanisms for the spontaneous autopolymerization of styrene would be present generating additional radicals (Schemes 1 paths C and D). Inhibition experiments heating the pair S-MA in presence of TEMPO will likely lead to a QSS concentration of the S-MA adduct, allowing one in principle to measure its rate of formation by monitoring the disappearance of free TEMPO (or the length of the induction period), in a way similar to that used by Kothe and Fischer in the styrene case. A key point here is to select experimental conditions in which the contribution of styrene-styrene radical generation can be minimized and/or substracted from the S-MA contribution. Shorter periods of induction in the copolymerization case as shown in Figure 1D are consistent with a faster dimerization reaction.

Before discussing the kinetics of these mechanisms we provide evidence and theoretical justification for the proposed mechanism. It has been a long controversy on the styrene copolymerization with electron acceptor monomers. In a survey of many experimental data, Hall and Padias[13] have suggested that a tetramethylene biradical initiates the copolymerization of electron rich and electron poor olefins, although there are also evidences that in certain cases, [4 + 2] cycloadditions compete with the tetramethylene type reactions.

Hakko-Hukki[14] and Wagner-Jauregg[15] were able to synthesize styrene-maleic anhydride adducts whose structure was demonstrated by chemical methods and Sato et al.[16] studied the initiation mechanism of the alternating copolymerization of styrene with some electro-accepting monomers in the presence of zinc chloride by the spin trapping technique and showed that the nitroxide obtained in the system styrene-acrylonitrile derived from 1-cyanotetraline-4 radical, produced by the hydrogen abstraction from the Diels Alder adduct. The adduct of styrene-maleic anhydride was also detected by Sato et al.[17] by spin trapping, although they also detected radicals from a charge transfer mechanism in this reaction.

There is no doubt that a cycloadduct can be obtained in the self-initiation of styrene-maleic anhydride, although this is not necessarily a concerted reaction. A semi empirical calculus comparing the energy difference between reactants (styrene and maleic anhydride) and their cycloaduct and between two styrene molecules and their cycloadduct was carried out with the PM3 semi- empirical method provided by the Hyperchem program.[18] Molecular geometries were calculated initially by molecular mechanics and afterwards by the PM3 calculation, at 0.01 convergence limits. The results were $\Delta E = 31.7$ Kcal/mol for the S-MA cycloadduct and $\Delta E = 122.8$ Kcal/mol for the Mayo styrene cycloadduct. However, the formation of the biradical of styrene requires 11.7 Kcal/mol and that of S-MA requires only 5.5 kcal/mol. The resonance stabilization of the biradical would easily produce the cycloadduct.

 

These data seem to indicate that the cycloadduct can be formed, although a biradical intermediate is possible. The isolation of a Styrene-MA oligomer, obtained by heating a solution of 2.5% MA in styrene during 30 minutes at 80 °C allowed the identification in the $^1$H NMR spectra (Figure 2) of a signal as a doublet at 4.1 ppm which may be assigned to the benzylic hydrogen which is also alpha to a carbonyl group and beta to other carbonyl group of the maleic anhydride (2.85 ppm for the alpha hydrogen of 1,2,3,4-tetahydronaphtalene + 1.35 ppm from the influence of two carbonyl groups in the alpha and beta positions).[19] The isolation and purification of this oligomer is difficult since at this temperature there is a certain amount of styrene oligomer as a result of the thermal styrene autoinitiation, besides maleic anhydride and styrene in the reaction mixture. Due to the oligomer solubility in dichloromethane, its precipitation is not easy, and the detection of the hydrogen at 4.1 ppm is not always possible. Kothe and Fischer measured the dimer formation rate in the case of styrene autopolymerization in presence of TEMPO. They showed that at *[TEMPO]* >0.05 M it is safe to assume that the dimer concentration is at quasi-steady state (QSS), which implies that the rate controlling step for radical generation is the dimer formation. They measured the rate of consumption of TEMPO, and correlated it with the rate of radical generation. Presumably, the rate limiting step for radical generation in the reaction of S and MA in presence of TEMPO-like nitroxide (*N*) is the formation of the Diels Alder adduct **3**. This adduct rapidly reacts with *N* reaching quasi-steady state. The length of the induction period can be correlated with the initial *N* concentration and the rate constants of the dimerization reactions.

Considering the presence of an *N* radical in the thermal auto-copolymerization of S-MA, and assuming that: i) path A is negligible with respect to path B, ii) path C

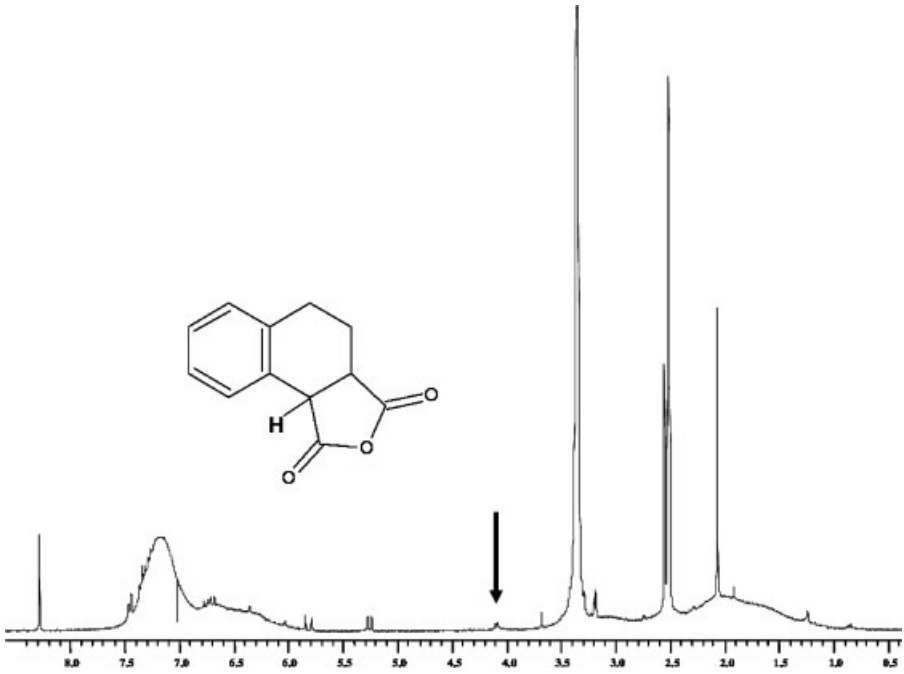


***Figure 2.***
NMR spectra of S-MA oligomer, evidence of dimer presence.

 

is negligible with respect to path D, and iii) **3** and **7** are at quasi steady state, then the rate of consumption of *N* radicals is given by the following equation:

$$\frac{d[N]}{dt} = -2k_{dsma}[S][MA] - 2k_{\mathrm{dim}}[S]^2 \qquad (1)$$

Where [S] and [MA] are the concentrations of styrene and maleic anhydride respectively, which can be considered constant during the induction period. Assuming also that at the end of the induction period [*N*] is negligible and integrating eq (1), results in:

$$[N]_0 = (2k_{dsma}[S]_0[MA]_0 + 2k_{\mathrm{dim}}[S]_0^2)T \qquad (2)$$

Where the sub-index *0* indicates initial conditions and *T* is the induction period. $k_{\mathrm{dim}}$ in equation 1 has been measured with precision by Kothe and Fischer as $k_{\mathrm{dim}} = 2.51 \times 10^4 \exp(-93{,}500/(RT))$ $\mathrm{L \cdot mol^{-1} \cdot s^{-1}}$ with R in $\mathrm{J \cdot mol^{-1} \cdot {}^{\circ}K^{-1}}$ and T, the temperature, in °K. In order to obtain initial estimates of the value of $k_{\mathrm{dsma}}$ we performed reactions for the system S-MA in presence of OH-TEMPO (*[N]*) in a capillary dilatometer in order to measure the induction period and the conversion – time curve after induction. Different compositions of the pair S-MA and of the nitroxide mixture increased its volume by thermal expansion until thermal equilibrium was established. At that point zero time was marked and the volume contraction of the reaction mixture with time was correlated with conversion via standard calculations that use the density of the monomer mixture and the polymer.[20] Table 1 contains a summary of the results and Figure 3 shows conversion – time curves for some of the experiments performed.

The fifth column in Table 1 shows an estimation of the percentage of MA consumed at the end of the induction period in the initiation reaction; this quantity is relevant since the calculation of $k_{\mathrm{dsma}}$ assumes constant MA concentration. This estimation is based on the assumption of 1 molecule of MA consumed for each two molecules of nitroxide, since the radical **4** is trapped by a second nitroxide molecule during the induction period. Experiments **4** and **5** are not analyzed in this table because their consumption of MA does not justify to approximate constant concentration of this monomer during the induction period. A second source of deviation for the assumption of constant MA concentration is the fact that some of the reactions show an induction period which is not ''clean''; that is, they exhibit some limited conversion before the polymerization starts at full rate. Such a behavior is rather a retardation period in which inhibition presumably competes with limited propagation. This phenomenon especially affects experiment 6 and, to a lesser extent, experiment 1. Since the conversion at the end of the retardation period is known from the experimental data, it is possible to estimate the total amount of MA that was copolymerized during the retardation period if the composition of the copolymer formed is also known. From measurements of the polymer composition by $^1$H NMR under different reaction conditions and monomer composition, we consistently obtained copolymer of 50% molar composition of MA, as long as the MA was not completely consumed. This

***Table 1.***
Experimental conditions and kinetic coefficient estimated for the rate limiting step in S-MA autoinitiation. All the reactions were run in bulk in a capillary dilatometer at 125 °C.

| Experiment | [% 4-oxo-TEMPO], M | % MA wt. | Induction time, min | % MA consumed | $k_{\mathrm{dsma}}$ L mol$^{-1}$ s$^{-1}$ |
|---|---|---|---|---|---|
| 1 | $5.2 \times 10^{-4}$ | 0.1 | 27 | 2.8 | $2.6 \times 10^{-6}$ |
| 2 | $5.2 \times 10^{-4}$ | 1 | 7 | 0.3 | $0.9 \times 10^{-6}$ |
| 3 | $5.2 \times 10^{-4}$ | 5 | 2.5 | 0.06 | $0.6 \times 10^{-6}$ |
| 6 | $5.2 \times 10^{-2}$ | 5 | 41 | 11.2 | $2.9–5.3 \times 10^{-6}$ |

 

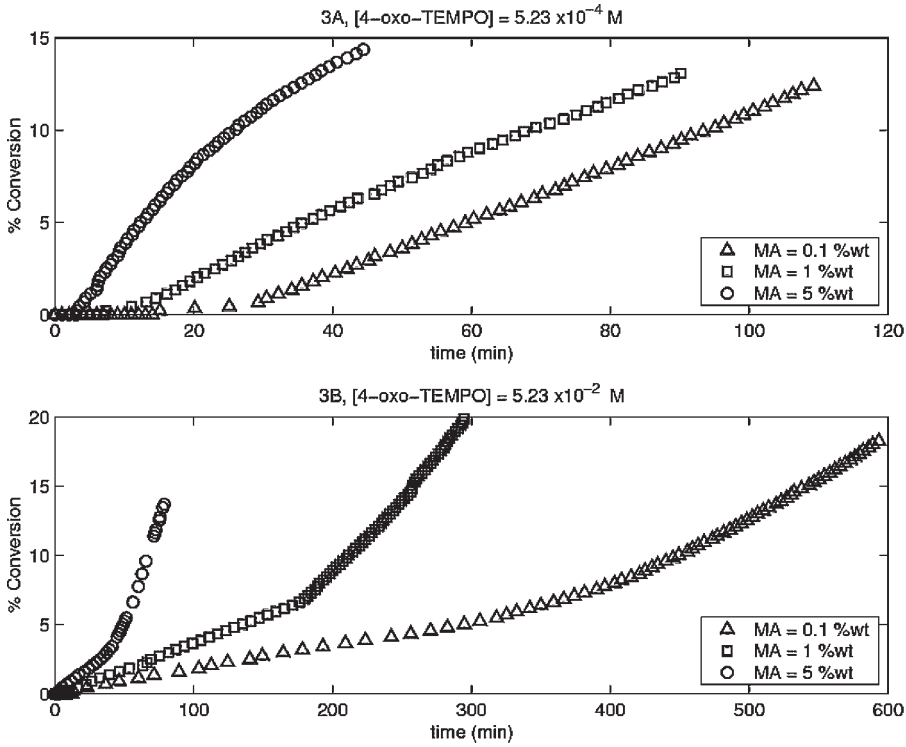


***Figure 3.***
Conversion vs time data by capillary dilatometry for the system S-MA in bulk at 125 °C.

is consistent with the formation of alternate copolymer of S-MA, that has been widely reported in the literature for copolymerizations performed at lower temperatures. Taking into consideration these two sources of consumption of MA for experiment 6, it is possible to estimate a lower and upper bound for the value of $k_{dsma}$ assuming constant concentration of MA at its initial or final value, respectively (the final value is about 55% of the initial value for experiment 6). In experiments with low oxo-TEMPO concentration (1 to 3) we neglect the second term in the parenthesis of the right hand side of eq (2) for the estimation of the kinetic constant in Table 1. Its contribution must be negligible since it has been reported that path D requires a nitroxide concentration of the order of 0.01 M or above in order to be significant;[13] however, we assume that, due to the presumed higher reactivity of MA with styrene, path B is significant even at this low nitroxide concentration.

Although the variation of the estimated $k_{dsma}$ in Table 1 is relatively large (average value of $2.1 \times 10^{-6}$ L mol$^{-1}$ s$^{-1}$) it gives a first order of magnitude estimation of this constant of $10^{-6}$ L mol$^{-1}$ s$^{-1}$. This value is considerably larger than that of styrene dimerization at 125 °C, $1.3 \times 10^{-8}$ L mol$^{-1}$ s$^{-1}$. Even if the mechanism that we propose here is not the only one operating in this copolymerization, and the initiation via a diradical species, as that suggested by Flory and supported by Hall and Padias, is also contributing initiating radicals, it is still reasonable to assume that the rate limiting step is the reaction between one molecule of each of the two monomers. If both mechanisms have significant contributions, the kinetic constant estimated here is an

 

effective one. In a future publication we will explore a much broader set of experimental conditions in order to have a better estimation of the initiation rate and a stricter test of the validity of the assumptions and kinetic laws proposed.

## Conclusions

In this paper we give evidence showing that the rate radical generation in the spontaneous copolymerization of styrene with MA is faster than the corresponding to the spontaneous polymerization of styrene at comparable conditions. We propose that the mechanism of radical generation in the copolymerization case is in good part due to the formation of a Diels-Alder adduct of S and MA, either in a concerted way or via a biradical. Semiempirical calculations and spectroscopic evidence of the adduct support the proposed mechanism. Finally, by inhibition experiments, we make a first order-of-magnitude estimate of the rate constant for the dimerization of S and MA, which results about 2 orders of magnitude larger than that of styrene dimerization at 125 °C.

*Acknowledgements:* Thanks are due to Dr. Carlos Rius Alonso for the semiempirical calculus of ΔHs of the formation of free radicals and adducts. J Bonilla and E. Saldívar-Guerra also thank CONACYT-México for the granting of a generous doctoral scholarship for J. Bonilla and for grant 46048-2004 supporting this research.

[1] P. J. Flory, *J. Am. Chem. Soc.* **1937**, *59*, 241.
[2] F. R. Mayo, *J. Am. Chem. Soc.* **1953**. *75*, 6133.
[3] R. R. Hiatt, P. D. Bartlett, *J. Am. Chem. Soc.* **1959**, *81*, 1149.
[4] W. C. Buzanowsky, J. D., Graham, D. B., Priddy, E. Shero, *Polymer* **1992**, *33*, 3055.
[5] G. Moad, D. H. Solomon, "*The Chemistry of Free Radical Polymerization*", Elsevier Science, New York 1995, p. 95.
[6] K. Kichner, H. Schlapkohol, *Makromol Chem.* **1976**, *177*, 2031.
[7] D. L. Hasha, D. B. Priddy, P. R. Rudolf, E. J. Stark, M. De Pooter, F. Van Damme, *Macromolecules* **1992**, *25*, 3046.
[8] D. Liu, A. B. Padias, H. K. Hall, *Macromolecules* **1995**, *28*, 622.
[9] G. Moad, E. Rizzardo, D. H. Solomon, *Polym. Bull.* **1982**, *6*, 589.
[10] B. Boutevin, D. Bertin, *Eur. Polym. J.* **1999**, *35*, 815.
[11] E. Saldívar-Guerra, J. Bonilla, G. Zacahua, M. Albores-Velasco, *J. Polym. Sci., A. Polym. Chem.* **2006**, *44*, 6962.
[12] T. Kothe, H. Fischer, *J. Polym. Sci. A: Polym. Chem.* **2001**, *39*, 4009.
[13] H. K. Hall, A. B. Padias, *J. Polym. Sci., A. Polym. Chem.* **2001**, *39*, 2069.
[14] Jakko-Hukki, *Acta Chimica Scandinavica* **1951**, *5*, 31.
[15] Th. Wagner-Jauregg, *Ann.* **1931**, *491*, 1.
[16] T. Sato, K. Hibino, T. Otsu, *J., Macromol Sci. Chem.* **1975**, *A9*(7), 1165.
[17] T. Sato, M. Abe, T. Otsu, *Makromol. Chem.* **1977**, *178*, 1061.
[18] Hyperchem 5.01 for Windows. Molecular Model System. Hypercube, Inc.Gainesville, Florida.
[19] E. Pretsch, T. Clerc, J. Seibl, W. Simon, "*Tablas para la elucidación estructural de compuestos orgánicos por métodos espectroscópicos*". 1st Spanish Edition, 1980. Editorial Alambra, S.A.
[20] M. J. Percino, V. M. Chapela, A. Jiménez, *J. Appl. Polym. Sci.* **2004**, *94*, 1662.

 

# NMR Spectroscopy in the Optimization and Evaluation of RAFT Agents

*Bert Klumperman,*[*1,2] *James B. McLeary,*[2] *Eric T.A. van den Dungen,*[2] *Gwenaelle Pound*[2]

**Summary:** The selection of a suitable mediating agent in Reversible Addition-Fragmentation Chain Transfer (RAFT) mediated polymerization is crucial to the degree of control that can be achieved. An overview of work from the Stellenbosch group is presented in which the use of NMR spectroscopy as a tool for evaluating RAFT-agents is highlighted. The occurrence of selective initialization, *i.e.* the selective conversion of a RAFT-agent into its single monomer adduct is discussed for various classes of monomers, as well as for copolymerization. One of the general rules for living polymerization is that chains should start growing early in the polymerization reaction. Selective initialization is claimed to be the extreme case where all chains have begun growing after the conversion of only one monomer equivalent per RAFT-agent.

**Keywords:** dithiobenzoates; dithioesters; initialization; NMR Spectroscopy; RAFT-mediated polymerization; xanthates

## Introduction

Reversible Addition-Fragmentation Chain Transfer (RAFT) mediated polymerization is among the most versatile living/controlled radical polymerization techniques.[1] It allows for the controlled polymerization of virtually any monomer that can be polymerized via conventional radical polymerization. However, the selection of a suitable RAFT-agent is of extreme importance in order to obtain a high degree of control. The inventors of RAFT-mediated polymerization at CSIRO (Australia) have drawn up a scheme of so-called leaving (R) groups, and activating (Z) groups that are expected and/or found to be suitable for various classes of monomers.[1] In general one can say that an R-group should be a good homolytic leaving group and a good re-initiating radical for a particular monomer. The Z-group should activate the C=S bond sufficiently to obtain a high addition rate of propagating radicals to the C=S bond. It should also stabilize the intermediate radical that is formed upon addition of the propagating radical to the RAFT-agent. In the present publication we will summarize some of our findings and discuss the results in terms of the mechanism underlying the phenomenon of initialization.

## Results and Discussion

It was shown previously that some monomer – RAFT-agent combinations lead to induction periods and retardation phenomena.[3] A lively discussion in the literature has resulted on the origin of these observations. This discussion largely focused on the retardation phenomena. A few years ago the Stellenbosch group started to use *in situ* $^1$H-NMR spectroscopy to investigate the

[1] Eindhoven University of Technology, Lab of Polymer Chemistry, P.O. Box 513, 5600MB Eindhoven, The Netherlands
Fax: (+31) 040 246 3966
E-mail: L.Klumperman@tue.nl
[2] University of Stellenbosch, Dept. of Chemistry and Polymer Science, Private Bag X1, 7602 Matieland, South Africa

induction period during the early stages of dithiobenzoate-mediated polymerizations of styrene (STY).[2] After assignment of the signals, concentration profiles of the relevant species can be recorded as a function of time. In doing so, it was found that the RAFT-agent is selectively converted into the so-called single monomer adduct, a process for which the name *initialization* was coined. In the cyanoisopropyl dithiobenzoate (CiPDB) mediated polymerization of styrene at 70 °C with [STY]:[CiPDB]:[AIBN] = 5:1:0.1 [mol] an initialization period of circa 40 minutes was observed (see Figure 1). Recently, these results were modeled in two independent publications. Coote and co-workers used *ab initio* quantum chemical calculations to predict equilibrium constants for the various equilibriums involved in the early stages of the polymerization.[4] They were able to show a fairly good agreement between experimental and predicted data, without using any adjustable parameters. In a publication from the Stellenbosch group, it was shown that both, the slow fragmentation model and the intermediate radical termination model are able to provide a good fit with the experimental data.[5] A similar experiment in which the CiPDB was replaced by cumyl dithiobenzoate (CDB) showed an initialization period of circa 240 minutes (see Figure 2).[6] On the basis of the close to linear conversion of the RAFT-agent as a function of time in the CiPDB experiment (see Figure 1) a mechanistic interpretation was proposed. It was concluded that the RAFT-agent cannot be involved in the rate-determining step, or otherwise the observed pseudo-zero order kinetics would not be observed. In other words, if the RAFT-agent would were involved in the rate-determining step, a first order decay of the RAFT-agent concentration should be observed. Hence, a curved RAFT-agent concentration *versus* time profile would be obtained. The fragmentation reaction cannot be rate-determining either, since this would lead to unrealistically high intermediate radical concentrations. Hence, the only remaining explanation is that the rate-determining step is the addition of the primary radical (or leaving group radical) to the first monomer unit. This explanation is in contradiction with the slow fragmentation model, and the *ab initio* quantum chemical calculations by Coote and co-workers.[4] A simple model, in which primary radical addition as the rate-

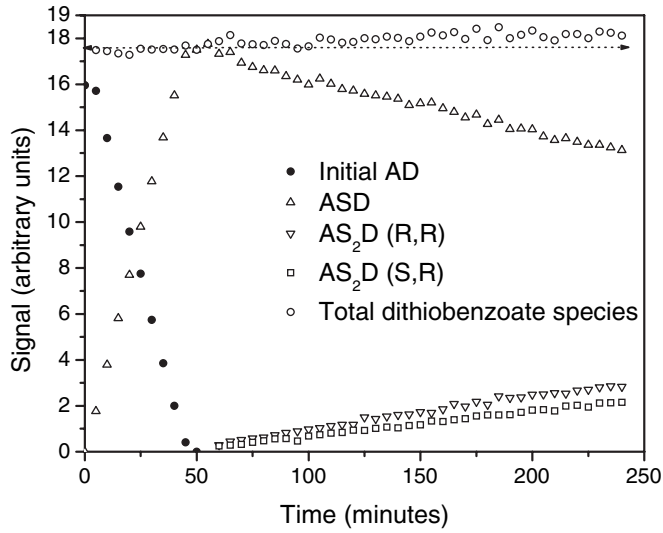


***Figure 1.***
Relative concentrations of relevant species as a function of time determined via *in situ* $^1$H-NMR spectroscopy during the CiPDB-mediated polymerization of styrene at 70 °C, where A = CiP fragment, S = styrene, D = dithiobenzoate. [STY]:[CiPDB]:[AIBN] = 5:1:0.1 [mol].[2]

 

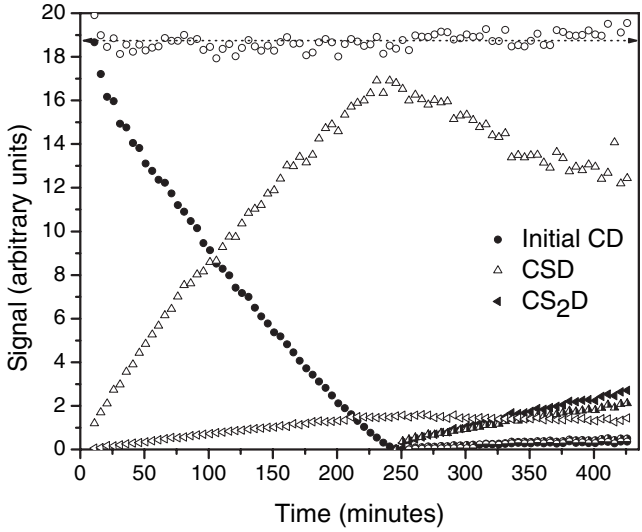


***Figure 2.***
Relative concentrations of relevant species as a function of time determined via *in situ* $^1$H-NMR spectroscopy during the CDB-mediated polymerization of styrene at 70 °C, where C = cumyl fragment, S = styrene, D = dithiobenzoate. The non-assigned symbols are CiP-initiated chains as indicated in the CiPDB study (see Figure 1). [STY]:[CDB]:[AIBN] = 6.7:1:0.2 [mol].[6]

determining step is implemented, shows a good fit of the concentration profile of the RAFT-agent concentration for the CiPDB and CDB experiments. This observation points at a significant difference in addition rate constant of the cyanoisopropyl radical to styrene compared to the cumyl radical to styrene or the bimolecular combination rates of the respective radicals. These rate constants have been calculated[7] based on Arrhenius parameters that were determined independently.[8,9] The differences observed in initialization behavior between the CiPDB and CDB case have been discussed using these previously reported rate constants.[6] In a qualitative sense the results were in agreement, and a more quantitative assessment was hampered by the inaccuracies in the rate constants due to extrapolations over large temperature intervals.

The same experimental approach was chosen for the investigation of methyl acrylate (MA) polymerization, mediated by CDB and by cumyl phenyl dithioacetate (CPDA)[10]. The purpose was to check the degree to which selective *initialization* is a general phenomenon. Figure 3 shows the concentration profiles of RAFT-agent and monomer. It is immediately evident that there is a large difference in initialization behavior between CDB and CPDA as the mediating agent. It is noteworthy to point at the great similarity in experimental data between the work presented here, and that of Vana and co-workers on CDB-mediated MA polymerization.[11] They explain the occurrence of initialization by a combination of intermediate radical termination and equilibrium constants that differ between pre-equilibrium and main equilibrium.

CPDA mediated polymerization of MA behaves in a fashion somewhat similar to the situation of styrene polymerization mediated by dithiobenzoates as shown in Figure 1 and 2. The decrease of the RAFT-agent concentration with time is nearly linear, and growth of the polymer chains beyond single monomer adduct formation only commences after all RAFT-agent is converted. On the other hand, in the case of CDB-mediated polymerization

 

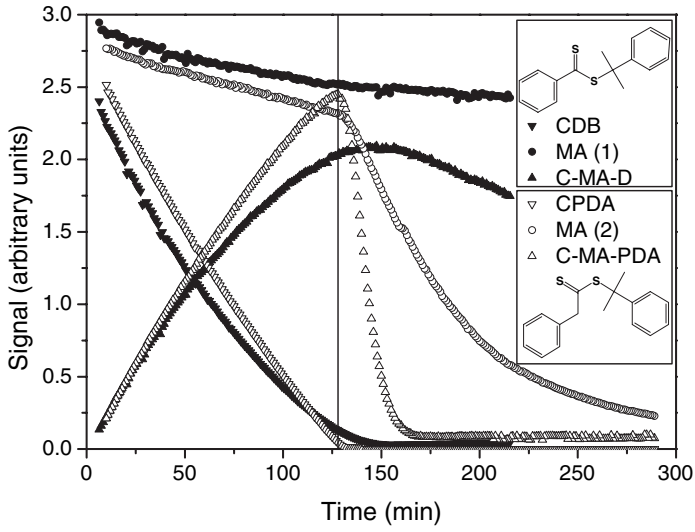


***Figure 3.***
Relative concentrations of relevant species as a function of time determined via *in situ* $^1$H-NMR spectroscopy during the polymerization of methyl acylate mediated by CDB and by CPDA $[MA]_0/[RAFT\text{-}agent]_0 = 7.5$ at 70 °C.[10]

of MA, significant curvature of the RAFT-agent conversion as a function of time is observed. The curvature is due to the buildup of intermediate radical species within the reaction system, due to the formation of longer lived intermediate radicals derived from MA and the concomitant rate retardation that occurs. In other words, CDB-mediated polymerization of MA does not show as clean an initialization behavior as observed in the earlier discussed situations. *In situ* ESR measurements with similar time resolution as in the NMR studies are presently being investigated by different groups in order to confirm the abovementioned buildup of intermediate radical species. At this point it is good to comment on the statistical nature of the process. The whole process of RAFT-mediated polymerization is governed by probabilities, as is conventional radical polymerization. This means that very reactive radicals, *i.e.* radicals that exhibit a high propagation rate constant, may experience competition between addition to the RAFT agent providing selective initialization and addition to monomer providing chain growth at an earlier stage than the less reactive ones. The radical addition to the RAFT agent is inherently dependent on the RAFT-agent and the susceptibility of the specific thio-carbonyl thiol moiety to radical addition, which means that a selective initialization can only be obtained if the RAFT-agent is properly designed for the specific monomer. This will be further exemplified below.

For further insight into the initialization process, the focus is shifted to a copolymerization system. The copolymerization of styrene and maleic anhydride (MAh) was investigated using CDB and CiPDB as the RAFT-agents.[12] This provides an excellent opportunity to investigate the effect of an electron-deficient comonomer on the initialization behavior of styrene as an electron-rich monomer. As indicated above, under certain conditions, the initialization time for the CiPDB-mediated polymerization of styrene is approximately 40 minutes. An experiment was conducted under comparable conditions, where styrene is now replaced by a 1:1 [mol] mixture of styrene and maleic anhydride. Despite

 

the slightly different reactant concentrations it is interesting to notice that the initialization time is virtually identical to the styrene homopolymerization case. Closer inspection of monomer conversion and the nature of the single monomer adducts reveals that the cyanoisopropyl radical adds almost exclusively to styrene. This is not too surprising as the cyano-isopropyl radical is electron-deficient, which leads to a higher affinity for an electron-rich monomer (styrene). Figure 4 shows the concentration profiles of the relevant species. Since the majority of CiP radicals add to styrene it is logical that the initialization time quite closely resembles that of styrene homopolymerization.

Figure 5 shows the concentration profiles of the relevant species in the CDB-mediated copolymerization of styrene and maleic anhydride. This experiment was conducted at 70 °C, in the same fashion as the previously discussed experiments. The initialization in this experiment was extremely fast in comparison to the homopolymerization of styrene. Where the initialization period for a CDB-mediated styrene homopolymerization was 240 minutes, here the initialization period is less than 5 minutes, again with slightly different reactant concentrations. In the first NMR spectrum acquired, which was recorded after 5 minutes, no CDB remained. Assignment of the peaks indicates that the single maleic anhydride adduct is formed virtually exclusively. Again, this is no surprise if one considers the electron-rich nature of the cumyl radical, and the electron-deficient nature of maleic anhydride. However, the overwhelming increase in conversion rate of the RAFT-agent of more than 50 times is surprising. The finding confirms the hypothesis that the addition of the leaving group radical to the monomer is rate-determining during the initialization process.

Interesting phenomena are observed in this copolymerization if one looks beyond the initialization period. In the case of cumyl as the leaving group, exclusive addition to maleic anhydride takes place. Maleic anhydride does not undergo homopropagation, which means that after initialization styrene consumption starts, whereas the maleic anhydride consumption rate reduces to virtually zero. The behaviour visually resembles a second initialization, but the

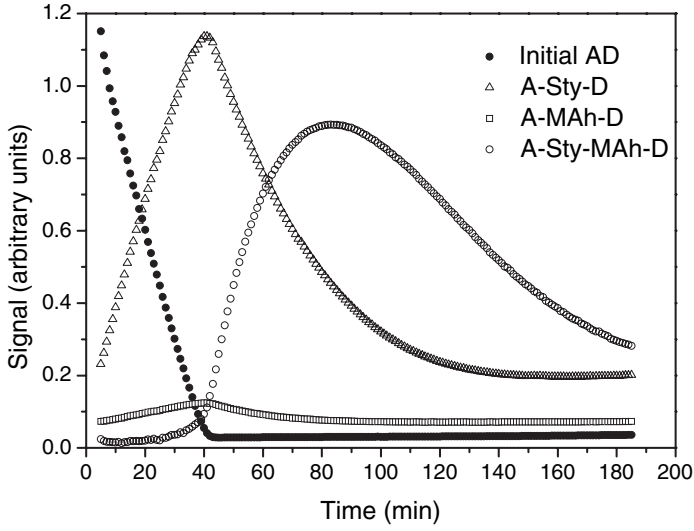


***Figure 4.***
Relative concentrations of relevant species as a function of time determined via *in situ* $^1$H-NMR spectroscopy during the CiPDB-mediated copolymerization of styrene and maleic anhydride at 70 °C. [STY]:[MAh]:[CiPDB]:[AIBN] = 4.1:3.8:1:0.20 [mol].[12]

 

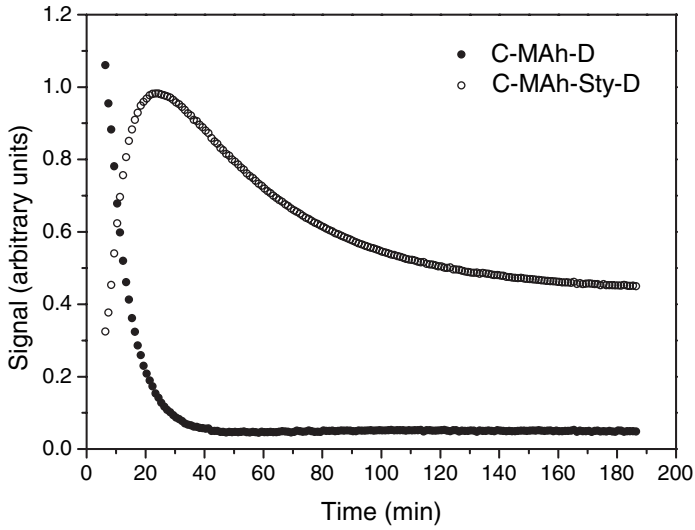


***Figure 5.***
Relative concentrations of relevant species as a function of time determined via *in situ* $^1$H-NMR spectroscopy during the CDB-mediated copolymerization of styrene and maleic anhydride at 70 °C. [STY]:[MAh]:[CDB]:[AIBN] = 3.6:3.6:1:0.2 [mol].[12]

specificity is lower in this case. In additional experiments (not shown), temperature was decreased to 60 °C, which reduces the rate of initialization sufficiently to be monitored accurately by NMR spectroscopy.

Until recently only stabilized monomers, carrying an electron-withdrawing substituent, were investigated in terms of initialization behavior. In order to explore the general applicability of the concept, poorly

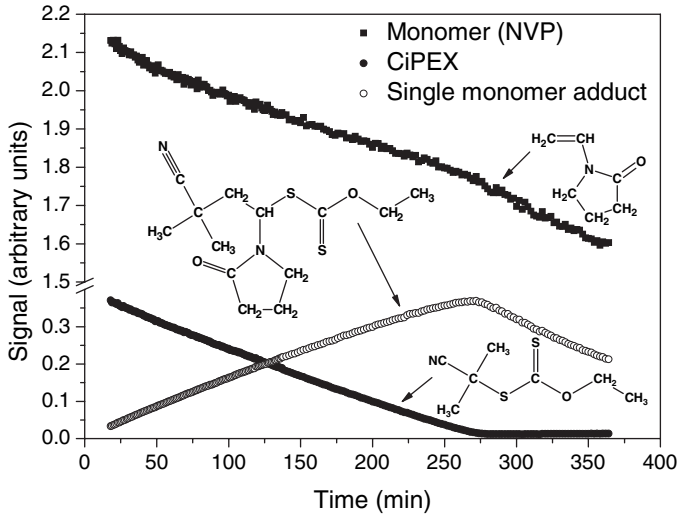


***Figure 6.***
Relative concentrations of relevant species as a function of time determined via *in situ* $^1$H-NMR spectroscopy during the CiPEX-mediated polymerization of *N*-vinyl pyrrolidone at 70 °C in $C_6D_6$, $[Monomer]_0/[Xanthate]_0 = 5$.[13]

 

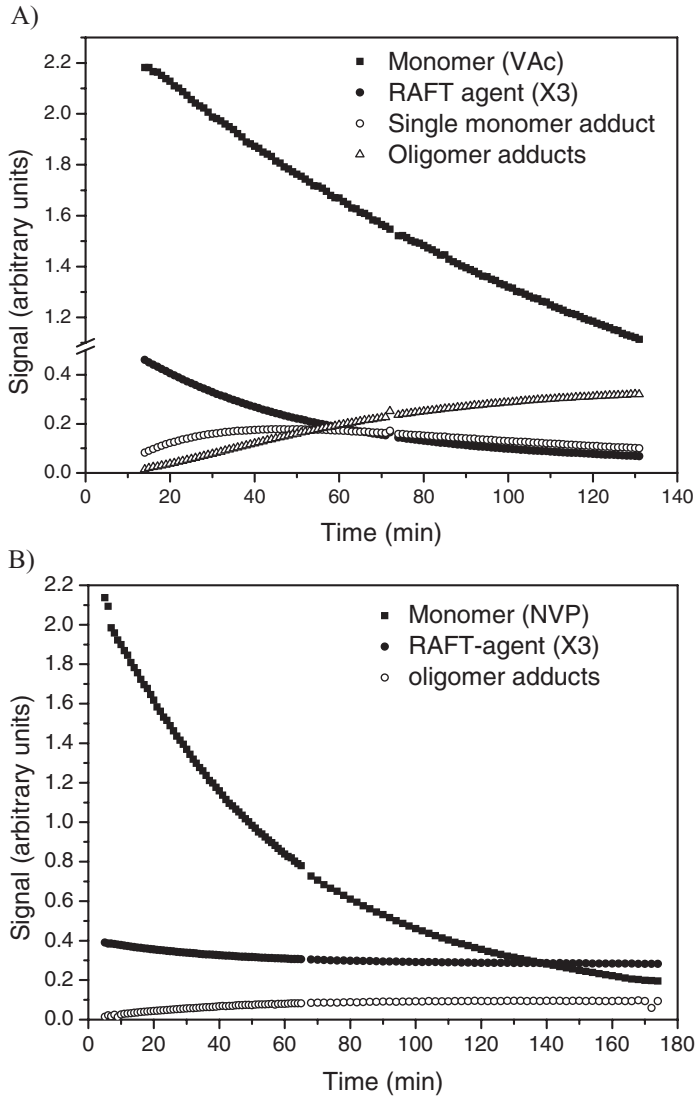


***Figure 7.***
A and 7B. Relative concentrations of relevant species as a function of time determined via *in situ* $^1$H-NMR spectroscopy during the *tert*-butyl ethyl xanthate (X3)-mediated polymerization of vinyl acetate (A) and of *N*-vinyl pyrrolidone (B) at 70 °C in $C_6D_6$, $[Monomer]_0/[Xanthate]_0 = 5$.[13]

stabilized monomers were recently subjected to *in situ* NMR studies. *N*-vinyl pyrrolidone (NVP) and vinyl acetate (VAc) were investigated in RAFT-mediated polymerization. It is reasonably well-documented that dithiocarbamates and xanthates are the RAFT-agents of choice for the controlled polymerization of these classes of monomers.[14–16] After preliminary experiments that will not be detailed here, it was decided to implement *O*-ethyl xanthates as the RAFT-agents to control NVP and VAc polymerization.[13] The leaving groups were varied in order to judge their effect on the initialization behavior. Figure 6 shows the concentration profiles of relevant species for the cyanoisopropyl *O*-ethyl xanthate (CiPEX)

 

mediated polymerization of NVP. It is clearly visible that an initialization process takes place that is not too dissimilar from what was observed for styrene and MA. In the first 270 minutes of the reaction exclusively the single monomer adduct of CiPEX and NVP is formed. Only after complete conversion of CiPEX, does further polymerization commence in a similar fashion as previously observed for styrene and MA. The initialization process in the case of CiPEX-mediated polymerization of NVP is fairly slow, which is expected to be due to the low rate constant of addition of the CiP radical to NVP. However, if the same experiment is repeated with VAc, it is observed that initialization is even much slower than in the case of NVP. It looks as if initialization is highly selective, but the estimate of the length of the initialization period is around 22 hours extrapolated from the first 3 hours of the reaction. Despite the fact that VAc and NVP are often considered as similar monomers in terms of their reactivity, this seems to point at a large difference in the rate coefficient of CiP radical addition. A leaving group that shows very selective initialization behavior for VAc appeared to be 2-propionic acid (results not shown). The initialization time for the 2-propionic acid ethyl xanthate-mediated polymerization of VAc is only 20 minutes under comparable conditions as the abovementioned systems.

Inspection of the scheme of leaving groups for the various monomer classes as mentioned above reveals that *tert*-butyl should be an appropriate leaving group for VAc.[1] For this reason, *tert*-butyl ethyl xanthate (X3)-mediated polymerizations of VAc and of NVP were investigated. Figures 7A and 7B show the concentration profiles of the relevant species of VAc and of NVP polymerizations respectively. It is immediately clear that neither of these two systems undergoes selective initialization. After 130 minutes close to 50% VAc conversion is observed, while there is still a significant fraction of the original RAFT-agent present. In the case of NVP, after 170 minutes some 90% monomer conversion has taken place, where only approximately 25% of the RAFT-agent is converted. Both results point at a poor leaving group quality, *i.e.* the asymmetrical intermediate radical that carries an oligomeric fragment on one side and the original leaving group on the other side fragment preferentially on the oligomeric side. Note that this is a different scenario from the slow re-initiating leaving group radical as was observed for the CiPEX-mediated polymerization of VAc, where the fragmentation rate was appropriate, but the reinitiation rate was extremely slow. The two different modes of failure for appropriate initialization point at the subtle optimization of RAFT-agents suitable for a specific monomer system.

## Conclusions

Initialization is frequently observed in RAFT-mediated polymerization. The selective transformation of the initial RAFT-agent into its single monomer adduct is commonly observed for RAFT-agents that possess a good leaving group that also yields an effective re-initiating radical. The process of initialization is observed for homopolymerizations of various monomers including poorly stabilized monomers such as vinyl acetate and *N*-vinyl pyrrolidone. It is also observed in copolymerizations, where the specificity of the formation of the single monomer adduct is directly related to the addition rate constants of the leaving group radical to the two monomers.

NMR spectroscopy is an efficient tool to monitor the quality of the R-group as a leaving group, and as a reinitiating fragment. As such it can be used for the selection and optimization of RAFT-agents for specific monomer systems.

[1] G. Moad, E. Rizzardo, S. H. Thang, *Aust. J. Chem.* **2005**, *58*, 379–410.
[2] J. B. McLeary, F. M. Calitz, J. M. McKenzie, M. P. Tonge, R. D. Sanderson, B. Klumperman, *Macromolecules* **2004**, *37*, 2383–2394.

 

[3] C Barner-Kowollik, M Buback, B. Charleux, M. L. Coote, M. Drache, T. Fukuda, A. Goto, B. Klumperman, A. B. Lowe, J. B. McLeary, G. Moad, M. J. Monteiro, R. D. Sanderson, M. P. Tonge, P. Vana, *J. Polym. Sci. Part A: Polym. Chem.* **2006**, *44*, 5809–5831.
[4] M. L. Coote, E. I. Izgorodina, E. H. Krenske, M. Busch, C. Barner-Kowollik, *Macromol. Rapid Commun.* **2006**, *27*, 1015–1022.
[5] J. B. McLeary, M. P. Tonge, B. Klumperman, *Macromol. Rapid. Commun.* **2006**, *27*, 1233–1240.
[6] J. B. McLeary, F. M. Calitz, J. M. McKenzie, M. P. Tonge, R. D. Sanderson, B. Klumperman, *Macromolecules* **2005**, *38*, 3151–3161.
[7] Y. K. B. Chong, J. Krstina, T. P. T. Le, G. Moad, A. Postma, E. Rizzardo, S. H. Thang, *Macromolecules* **2003**, *36*, 2256–2272.
[8] K. Herberger, H. Fischer, *Int. J. Chem. Kinet.* **1993**, *25*, 249–263.
[9] M. Walbiner, J. Q. Wu, H. Fischer, *Helv. Chim. Acta* **1995**, *78*, 910–924.
[10] J. B. McLeary, J. M. McKenzie, M. P. Tonge, R. D. Sanderson, B. Klumperman, *Chem. Comm.* **2004**, *17*, 1950–1951.
[11] M. Drache, G. Schmidt-Naake, M. Buback, P. Vana, *Polymer* **2005**, *46*, 8483–8493.
[12] E. T. A. Van den Dungen, J. Rinquest, N. O. Pretorius, J. M. McKenzie, J. B. McLeary, R. D. Sanderson, B. Klumperman, *Aust. J. Chem.* **2006**, *59*, 742–748.
[13] G. Pound, J. B. McLeary, J. M. McKenzie, R. F. M. Lange, B. Klumperman, *Macromolecules* **2006**, *39*, 7796–7797.
[14] M. Destarac, patent application PCT Int. Appl. (2002), WO 2002022688 A2.
[15] R. T. A. Mayadunne, E. Rizzardo, J. Chiefari, Y. K. Chong, G. Moad, S. H. Thang, *Macromolecules* **1999**, *32*, 6977–6980.
[16] M. H. Stenzel, L. Cummins, G. E. Roberts, T. P. Davis, P. Vana, C. Barner-Kowollik, *Macromol. Chem. Phys.* **2003**, *204*, 1160–1168.

 

 DOI: 10.1002/masy.200750216

# Reverse Iodine Transfer Polymerization (RITP) in Emulsion

*Patrick Lacroix-Desmazes,* Jeff Tonnar, Bernard Boutevin*

**Summary:** Reverse iodine transfer polymerization (RITP) is a new controlled radical polymerization technique based on the use of molecular iodine $I_2$ as control agent. This paper aims at presenting the basics of RITP and the strategy that we have followed for the development of this process in the past three years, from the validation in homogeneous solution polymerization up to recent results in heterogeneous aqueous polymerization processes. Typical examples of RITP of butyl acrylate in emulsion and RITP of styrene in miniemulsion are discussed.

**Keywords:** emulsion polymerization; miniemulsion polymerization; reverse iodine transfer polymerization

## Introduction

The area of radical polymerization has seen a real breakthrough with the invention of controlled/''living'' radical polymerization techniques (CRP).[1] These techniques make it possible to design copolymers with unusual chain microstructures (e.g. gradient copolymers, well-defined graft copolymers), copolymers of complex architectures that were only accessible by other specific methods such as living ionic polymerizations (e.g. block copolymers, star polymers, ...), copolymers with functional groups (e.g. homo- or hetero-telechelic polymers, macromonomers, functional star polymers, ...), and composites (e.g. polymer brushes from modified surfaces). The CRP techniques rely on a reversible activation-deactivation of the polymer chains, i.e. an equilibrium between a reservoir of dormant chains (capped polymer chains) and a tiny population of active chains (propagating chains) (Figure 1). Two main strategies have been used so far: the first one deals with a reversible termination mechanism and the quality of the control is then essentially based on the persistent radical effect (i.e. an accumulation of the persistent species $[X\text{-}(Y)] \gg [P^\bullet]$ leading to a favored cross-coupling rather than self-termination $R_c = k_c\ [X\text{-}(Y)][P^\bullet] \gg R_t = k_t\ [P^\bullet]^2$), the second one deals with a reversible chain transfer mechanism and the quality of the control is then essentially based on the high probability of reversible transfer reactions in comparison with termination (i.e. domination of degenerative chain transfer $R_{ex} = k_{ex}\ [P^\bullet][P\text{-}X(+Y)] \gg R_t = k_t\ [P^\bullet]^2$)[2] Sometimes, the two processes (reversible termination and reversible transfer) can operate simultaneously (example: living radical polymerizations mediated by organocobalt porphyrin complexes reported by Wayland et al.[3,4]). Several CRP techniques have been developed in the past thirty years, but their implementation at an industrial scale, especially in heterogeneous aqueous processes which are of major importance nowadays, remains a challenge.[5,6] In this paper, we report our strategy to set up a new CRP technique based on simple, readily available and economical chemicals and our attempts to control the polymerization in aqueous emulsion polymerizations. Experimental details are given elsewhere.[7–11]

Institut Charles Gerhardt UMR 5253 – CNRS, Ingénierie et Architectures Macromoléculaires, Ecole Nationale Supérieure de Chimie de Montpellier, 8 rue de l'Ecole Normale, 34296 Montpellier Cedex 5, France
Fax: (+33) 4 67 14 72 20
E-mail: patrick.lacroix-desmazes@enscm.fr

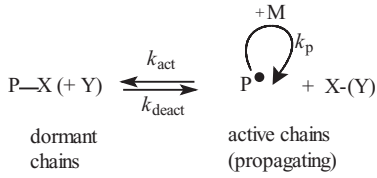


***Figure 1.***
General scheme of reversible activation in controlled radical polymerization.

## Strategy

The first CRP techniques were developed as early as in the late seventies (iodine transfer polymerization, ITP)[12] and early eighties (photo-INIFERTERS)[13] (nitroxide-mediated polymerization, NMP).[14] In the nineties, the CRP mechanisms were rationalized thanks to an intensive research particularly based on kinetics, and other CRP techniques have been proposed (atom transfer radical polymerization, ATRP)[15] (reversible addition-fragmentation chain transfer, RAFT).[16] Since then, new CRP techniques are still appearing (e.g. based on cobalt, tellurium,...) and the subtleties of the CRP mechanisms are often still subject to debate (example: side reactions with the radical intermediate in RAFT[17]). It is interesting to note that each CRP technique can be applied according to at least two important alternatives: a) on the one hand a R-X(+Y) can be directly used (e.g. an alkoxyamine R-ON$R_1R_2$ in the case of NMP), b) on the other hand a X-(Y) can be used together with a source of radicals to form in situ the R-X(+Y) compound (e.g. a nitroxide $R_1R_2NO\bullet$ in the presence of an azo initiator R-N=N-R in the case of NMP). It is also interesting to note that in the second case a powerful radical scavenger is required (the nitroxide $R_1R_2NO\bullet$ is the radical scavenger for the case mentioned above) to limit the propagation during the initialization period.[18] A last observation is that ITP is an attractive CRP technique because it does not require complicated chemicals and it has already led to commercial products,[12] but the second variant was not reported yet in the literature although molecular iodine $I_2$ is known to be a powerful radical scavenger.[19] We have decided to fill this gap by developing the reverse iodine transfer polymerization (RITP) technique, based on the use of molecular iodine $I_2$ as a control agent.[7,20–22]

## Validation of the Concept in Solution Polymerization

The concept of RITP was first checked in solution polymerization.[7,8,20] The basic mechanism of RITP is presented in Figure 2. It was shown that the use of molecular iodine $I_2$ allowed the controlled polymerization of a wide range of monomers such as acrylates, alpha-fluoro acrylates, styrenics, vinylidene halides, and methacrylates. A typical result is given in Table 1 (run 1) for RITP of butyl acrylate in butyl acetate at 85 °C with 2,2′-azobis-(isobutyronitrile) AIBN as the initiator.[7]

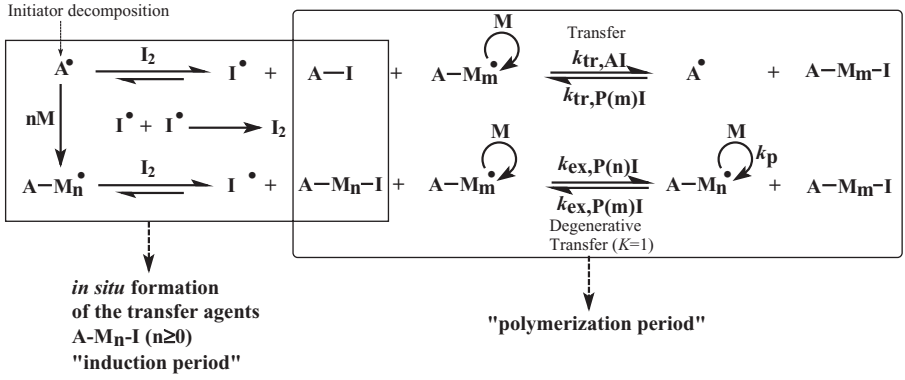


***Figure 2.***
Basic mechanism of reverse iodine transfer polymerization.

 

***Table 1.***
Reverse iodine transfer polymerization in solution, emulsion and miniemulsion.[a)]

| Run | Solvent | Monomer | Additive | Time (h) | Conv. (%) | $M_{n,th}$[b)] ($g \cdot mol^{-1}$) | $M_{n,SEC}$ ($g \cdot mol^{-1}$) | $M_w/M_n$ | pH | $d_p$[c)] (nm) |
|---|---|---|---|---|---|---|---|---|---|---|
| 1 | Butyl acetate | Butyl acrylate | No | 5 | 95 | 9 500 | 9 700 | 1.83 | n.a. | n.a.[d)] |
| 2 | Water (emulsion) | Butyl acrylate | No | 7 | 99 | 10 300 | 31 000 | 1.98 | 5.2 | 106 |
| 3 | Water (emulsion) (surfactant-free) | Butyl acrylate | No | 15 | 83 | 8 700 | 22 000 | 1.88 | 5.1 | 443 |
| 4 | Water (miniemulsion) | Styrene | No | 16 | 72 | 7 500 | 13 900 | 1.73 | 2.4 | 334 |
| 5 | Water (miniemulsion) | Styrene | $H_2O_2$/HCl | 16 | 78 | 7 900 | 7 900 | 1.46 | 3.4 | 316 |

a) Run 1: polymerization of *n*-butyl acrylate at 80% w/v versus butyl acetate as solvent ([BuA] = 3.30 M) in the presence of 2,2′-azobisisobutyronitrile as initiator with $[AIBN]/[I_2] = 1.9$, $T = 85\ ^\circ C$. Run 2: polymerization of BuA in emulsion at $T = 85\ ^\circ C$ ($[ACPA]/[I_2] = 1.7$, $[SDS] = 0.15 \times CMC$, $M_{n,targeted} = 10\,400\ g \cdot mol^{-1}$). Run 3: polymerization of BuA in emulsion at $T = 85\ ^\circ C$ ($[ACPA]/[I_2] = 1.6$, no SDS, $M_{n,targeted} = 10\,100\ g \cdot mol^{-1}$). Run 4: polymerization of styrene in miniemulsion at $T = 60\ ^\circ C$ in the presence of Perkadox 16S as initiator, $[Perkadox]/[I_2] = 1.99$. Run 5: polymerization of styrene in miniemulsion at $T = 60\ ^\circ C$ in the presence of Perkadox 16S as initiator, $[Perkadox]/[I_2] = 2.44$. BuA: *n*-butyl acrylate; ACPA: 4,4′-azobis(4-cyanopentanoic acid); AIBN: 2,2′-azobisisobutyronitrile; SDS: sodium dodecyl sulfate; *CMC*: critical micelle concentration; Perkadox 16S: bis(4-tert-butylcyclohexyl) peroxydicarbonate.

b) Calculated by $M_{n,theoretical} = (\text{mass of monomer}) \times \text{Conversion}/(2 \times (\text{moles of } I_2)) + M_{A\text{-}I}$ in which $M_{A\text{-}I}$ is the molecular weight of the chain ends.

c) Particle diameter.

d) Not applicable.

The kinetic analysis in the case of RITP of methyl acrylate at 70 °C showed the existence of an initialization period during which iodine is consumed to form short A-$M_n$-I telomers which can further act as reversible transfer agents (reversible chain transfer) (Figure 3). For high monomer to iodine $[M]/[I_2]$ ratio, the monomer conversion during this period is negligible: this is the reason why in most cases this period can be called ''inhibition period'' or ''induction period''. This favored reaction of radicals

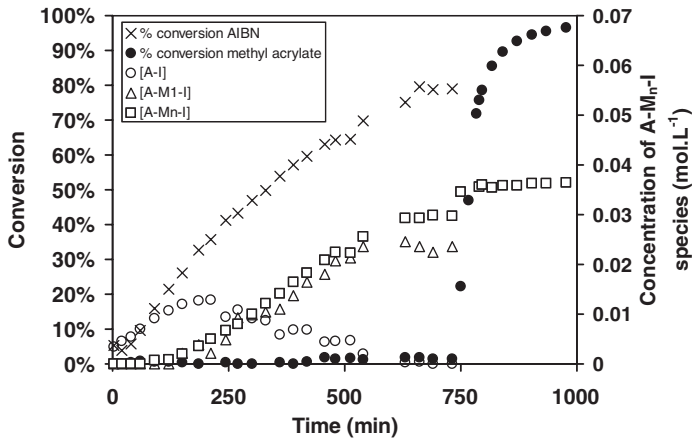


***Figure 3.***
Typical evolution of monomer conversion, initiator conversion, and concentrations of A-$M_n$-I species in reverse iodine transfer polymerization of methyl acrylate at 70 °C in deuterated benzene (determined by $^1$H-NMR analyses) ([methyl acrylate] = 5.47 M, $[C_6D_6] = 5.70$ M, $[2,2'\text{-azobis(isobutyronitrile)}] = 3.78 \times 10^{-2}$ M, and $[I_2] = 2.22 \times 10^{-2}$ M).

 

with iodine is due to the high reactivity of iodine.[23,24] Indeed, the scavenging of alkyl radicals by iodine $I_2$ is nearly a diffusion-controlled reaction (typically in the range $10^9$–$10^{10}\ M^{-1} \cdot s^{-1}$) and it was reported that there are certainly no spin effects in the scavenging of alkyl radicals by iodine and that steric effects can be expected to be small.[24] Furthermore, iodine radicals $I_\bullet$ produced by the scavenging reaction can recombine to form $I_2$ and this reaction is again a very fast nearly diffusion-controlled reaction (in the range $10^9$– $10^{10}\ M^{-1} \cdot s^{-1}$).[24,25] Actually, the observed rate constants for the scavenging of alkyl radicals by iodine $R_\bullet + I_2$ and for the recombination of iodine radicals $I_\bullet + I_\bullet$ were not found to be completely proportional to the inverse of the viscosity of the media, indicating that they are not solely diffusion rate-controlled, but they could be described with a combination of a diffusion-controlled rate constant and an activation-controlled rate constant.[24]

After the induction period, the polymerization takes place and is dominated by the degenerative chain transfer mechanism. A typical evolution of the molecular weight and polydispersity index with conversion is given in Figure 4 in the case of RITP of methyl methacrylate in toluene.[8] The experimental data are in relatively good agreement with the theoretical evolutions of the molecular weight $M_n$ (Eq. 1) and polydisersity index *PDI* (Eq. 2).[12]

$$M_n = (p[M]_0 M_{monomer})/\{2[I_2]_0 \times [1-(1-p)^{Cex}]\} \quad (1)$$

$$PDI = \{1 + ([M]_0/(2[I_2]_0)) \times [2 + (2-p)(1-C_{ex})/C_{ex}]\}/\{p[M]_0/(2[I_2]_0[1-(1-p)^{Cex}])\} \quad (2)$$

in which $p$ is the fractional monomer conversion, $M_{monomer}$ is the molecular weight of the monomer, $[I_2]_0$ is the initial concentration of iodine, and $C_{ex}$ is the degenerative chain transfer constant.

In the case of poly(methyl acrylate) where the polymers chain-ends are stable enough to survive during a Maldi-Tof analysis (in addition to $^1$H-NMR, $^{13}$C-NMR, and SEC characterizations), the expected structure A-$M_n$-I was confirmed, supporting the proposed mechanism of RITP.[7]

### Ab Initio Emulsion Polymerization

Ab initio emulsion polymerization is one of the most used heterogeneous processes in

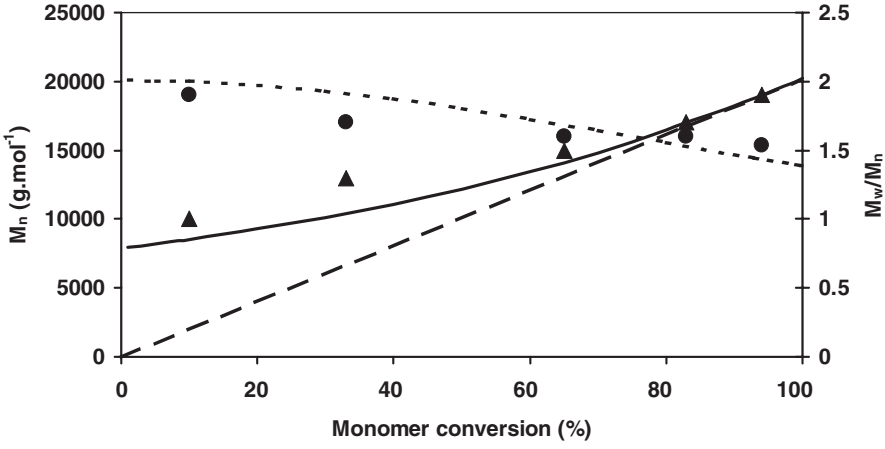


*Figure 4.*
Evolution of molecular weight $M_n$ (▲) and polydispersity index $M_w/M_n$ (●) with monomer conversion in reverse iodine transfer polymerization of methyl methacrylate in toluene at 80 °C in the presence of AIBN as initiator with $[AIBN]/[I_2] = 1.7$ ($M_{n,targeted} = 20\,200\ g \cdot mol^{-1}$). Theoretical evolutions are given by Eq. 1 (—) and Eq. 2 (- - -) with $C_{ex} = 2.6$. The ideal behavior of $M_n$ assuming a high $C_{ex}$ is also given for comparison (– – –).

 

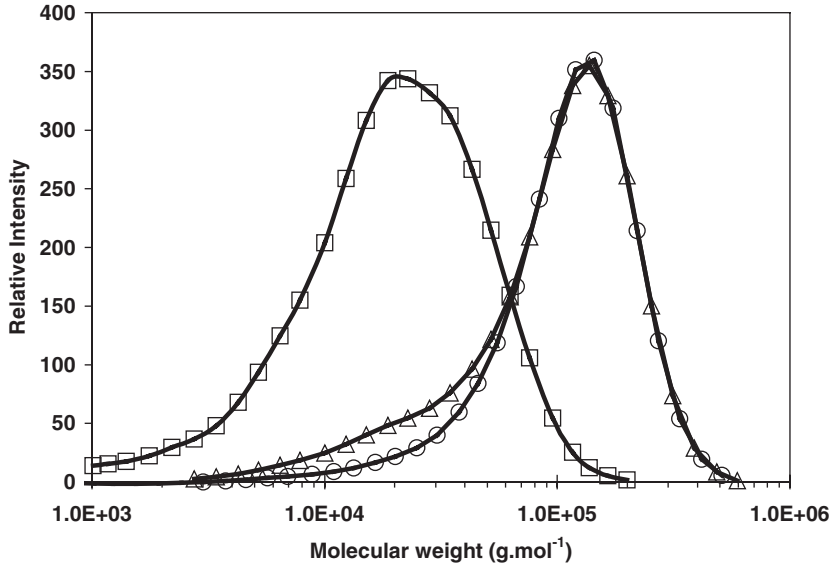


***Figure 5.***
Molecular weight distributions of the seed poly(BuA) latex ($M_{n,SEC} = 15\,900\ g \cdot mol^{-1}$) prepared by RITP and of the block copolymer latex poly(butyl acrylate)-bock-poly(styrene-*co*-butyl acrylate) ($M_{n,SEC} = 53\,400\ g \cdot mol^{-1}$) prepared by seeded emulsion polymerization at 85 °C: (□) refractive index detector (seed latex), (○) UV detector at 254 nm (copolymer latex), (△) refractive index detector (copolymer latex). Seed: [ACPA]/[$I_2$] = 1.6, [SDS] = 0.15 × *CMC*, targeted $M_n = 2\,500\ g \cdot mol^{-1}$, conversion = 40%, particle diameter = 127 nm; Block copolymer: second monomer = styrene; $Monomer_{Feed}/Monomer_{Seed}$ = 4.7 w/w, conversion = 32%, particle diameter = 203 nm.

the industry.[26] It initially involves two phases: a monomer phase dispersed in an aqueous phase containing a hydrosoluble radical initiator and a surfactant. The polymerization creates a new phase of polymer particles (nucleation). The nucleation step is very important since it will determine the number of particles (and so the final latex particle size) which in turn will partly determine the kinetics of the polymerization.[27] Most CRP techniques tested so far failed in ab initio emulsion polymerization because they encountered difficulties related to the nucleation step (e.g. instability of the latex, slow diffusion of hydrophobic control agents,...)[5,6,28] and only a few works gave promising results.[29] In our first attempts, we tested ab initio emulsion RITP of *n*-butyl acrylate, using 4,4′-azobis(4-cyanopentanoic acid) (ACPA) neutralized with sodium hydroxide as initiator and sodium dodecyl sulfate (SDS) as surfactant.[9] It was possible to obtain a stable and uncolored (white) monodisperse

$$I_{2,aq} + H_2O \rightleftharpoons I^- + H^+ + HOI \quad (1)$$

$$3HOI \rightleftharpoons IO_3^- + 2I^- + 3H^+ \quad (2)$$

$$3\,I_{2,aq} + 3\,H_2O \rightleftharpoons IO_3^- + 5\,I^- + 6\,H^+ \quad (3)$$

$$I_{2,aq} + I^- \rightleftharpoons I_3^- \quad (4)$$

***Figure 6.***
Some important reactions of iodine $I_2$ in the aqueous phase: hydrolytic disproportionation of iodine $I_2$ and triiodide $I_3^-$ formation.

 

$$H_2O_2 + 2H^+ + 2I^- \rightleftharpoons I_2 + 2H_2O$$

***Figure 7.***
Oxydation of iodide by hydrogen peroxide.

latex with high monomer conversion (Table 1, run 2). The potentially surface-active iodinated transfer agents synthesized in situ during the process (A-$M_n$-I oligomers in which A is a hydrophilic moiety from the radical initiator) can take part in the nucleation step and contribute to the electrostatic stabilization of the latex, as indicated by a successful surfactant-free RITP experiment in emulsion (Table 1, run 3). It was checked that the molecular weight of the latex could be tuned by varying the initial concentration of iodine $[I_2]$. Furthermore, the successful preparation of a block copolymer latex poly(butyl acrylate)-block-poly(styrene-*co*-butyl acrylate) proved that the polymer chains could be reactivated (living character) (Figure 5). Nevertheless, it was also noticed that the molecular weights of the latexes prepared by RITP were much higher than the theoretical values, as shown in Table 1 runs 2-3. In order to account for this upward deviation of the molecular weights, the peculiarities of emulsion polymerization (partitioning of the reactants between the different phases) and the chemistry of iodine in water must be considered (Figure 6).[10] Indeed, although the partitioning of iodine is in favor of the butyl acrylate monomer phase ($K = [I_2]_{aq}/[I_2]_{BuA} = 2.03 \times 10^{-3}$ at 25 °C), the disproportionation of iodine in water plays a serious deleterious role in the control of the polymerization. By following the evolution of the concentration of iodide $[I^-]$ by a selective electrode for the experiment of Table 1 run 2, it was shown that the side reaction of hydrolysis

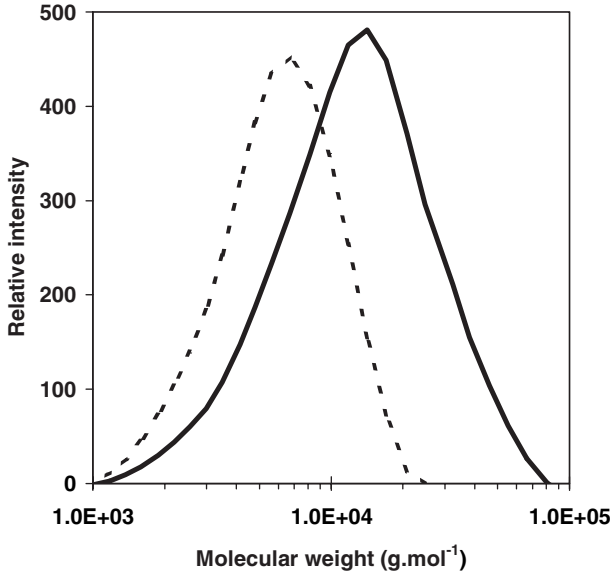


***Figure 8.***
Molecular weight distributions of the seed polystyrene latex prepared by reverse iodine transfer polymerization in miniemulsion ($M_{n,SEC} = 4\,900$ g·mol$^{-1}$, $M_w/M_n = 1.48$, $M_{n,th} = 4\,100$ g·mol$^{-1}$, – – – –) and the final polystyrene latex prepared by iodine transfer polymerization of styrene in seeded emulsion polymerization ($M_{n,SEC} = 8\,900$ g·mol$^{-1}$, $M_{n,th} = 9\,800$ g·mol$^{-1}$, —). Seed latex (miniemulsion polymerization at $T = 60$ °C): water (150 g), $I_2$ (0.3833 g, 1.51 mmol), n-hexadecane (0.45 g, 1.99 mmol), styrene (15 g, 144 mmol), Perkadox 16S (1.495 g, 3.75 mmol), dodecyl sulfate sodium salt (0.4 g, 1.39 mmol) and addition of hydrogen peroxide (0.7 g $H_2O_2$ 30% wt. solution in water, 6.23 mmol) in 15 g of water during 3 hours; Chain extension (seeded emulsion polymerization at 75 °C): seed PS-I latex (42.5 g, $M_n = 4\,900$ g·mol$^{-1}$, 0.54 mmol), α,α′-azobisisobutyronitrile (0.0233 g, 0.142 mmol), styrene (3.01 g, 28.9 mmol).

 

was actually very important and that only 33% of the initial iodine was effectively consumed through the RITP mechanism ($\alpha = n_{I2,effective}/n_{I2,initial} = 33\%$). Based on this value of 33%, the experimental molecular weight now matches the corrected targeted value ($M_{n,targeted\ (corrected)} = (mass\ of\ monomer)/(2 \times \alpha \times n_{I2,initial}) + M_{A\text{-}I} = 31\,000\ g \cdot mol^{-1}$). The identification of the side reactions was a key step toward the development of improved RITP procedures in heterogeneous aqueous processes as described below.

### Miniemulsion Polymerization

In order to counterbalance the hydrolytic disproportionation of iodine in water, a modified RITP procedure was developed. The new procedure is based on the use of an oxidant to regenerate iodine $I_2$ by oxidation of iodide $I^-$. In this section, this new concept is illustrated in the case of miniemulsion polymerization of styrene by RITP initiated by bis(4-tert-butylcyclohexyl) peroxydicarbonate (Perkadox 16S) at $T = 60\,^{\circ}C$ with dodecyl sulfate sodium salt as surfactant and hexadecane as hydrophobe.[11] The continuous addition of hydrogen peroxide (as oxidant) in acidic conditions leads to the oxidation of iodide $I^-$ to form iodine $I_2$ and water (Figure 7). This new concept allowed us to prepare a stable polystyrene latex with a much better agreement between theoretical and experimental molecular weight (Table 1, run 5) than the corresponding RITP in the absence of hydrogen peroxide (Table 1, run 4). Furthermore, the successful chain-extension (resuming the polymerization with a new shot of styrene and AIBN) indicates that the living character of the RITP polymerization is maintained with this new procedure (Figure 8).

## Conclusion

The RITP process has been invented few years ago and it has rapidly led to promising results in heterogeneous aqueous processes. Stable and uncolored (white) monodisperse poly(butyl acrylate) latex could be obtained by RITP in emulsion. However, a large deviation of the molecular weights from the theoretical values was observed in the early attempts of RITP in emulsion: hydrolytic disproportionation of iodine has been identified as a serious deleterious side reaction. Based on this knowledge, an improved RITP procedure has been set up that is based on the use of an oxidant to regenerate iodine. For instance, RITP of styrene in miniemulsion has been successfully performed with a continuous addition of hydrogen peroxide as oxidant. Thanks to this new concept, in addition to the living character of the latex, a good correlation between theoretical and experimental molecular weights can now be obtained, reinforcing the interest of RITP for the industrial development of controlled radical polymerization in dispersed aqueous processes. Our current efforts focus on the application of this new concept to a wide range of experimental conditions to test its robustness.

*Acknowledgements:* Vincent Bodart and Christophe Fringant (Solvay) are acknowledged for their constant interest in the RITP process.

[1] K. Matyjaszewski, *ACS Symp. Ser.* **2003**, *854*, 2.
[2] A. Goto, T. Fukuda, *Prog. Polym. Sci.* **2004**, *29*, 329.
[3] Z. Lu, M. Fryd, B. B. Wayland, *Macromolecules* **2004**, *37*, 2686.
[4] B. B. Wayland, C.H. Peng, X. Fu, Z. Lu, M. Fryd, *Macromolecules* **2006**, *39*, 8219.
[5] M. F. Cunningham, *Prog. Polym. Sci.* **2002**, *27*, 1039.
[6] J. Qiu, B. Charleux, K. Matyjaszewski, *Polimery (Warsaw, Poland)* **2001**, *46*, 663.
[7] P. Lacroix-Desmazes, R. Severac, B. Boutevin, *Macromolecules* **2005**, *38*, 6299.
[8] C. Boyer, P. Lacroix-Desmazes, J.-J. Robin, B. Boutevin, *Macromolecules* **2006**, *39*, 4044.
[9] J. Tonnar, P. Lacroix-Desmazes, B. Boutevin, *ACS Symp. Ser.* **2006**, *944 Chapter41*, 604.
[10] J. Tonnar, P. Lacroix-Desmazes, B. Boutevin, *Macromol. Rapid Commun.* **2006**, *27*, 1733.
[11] J. Tonnar, P. Lacroix-Desmazes, B. Boutevin, *Macromolecules* **2007**, in press.
[12] G. David, C. Boyer, J. Tonnar, B. Ameduri, P. Lacroix-Desmazes, B. Boutevin, *Chem. Rev.* **2006**, *106*, 3936.

 

[13] T. Otsu, *J. Polym. Sci., Part A: Polym. Chem.* **2000**, *38*, 2121.
[14] C. J. Hawker, A. W. Bosman, E. Harth, *Chemical Reviews (Washington, D. C.)* **2001**, *101*, 3661.
[15] K. Matyjaszewski, J. Xia, *Chemical Reviews (Washington, D. C.)* **2001**, *101*, 2921.
[16] R. T. A. Mayadunne, E. Rizzardo in "*Living and Controlled Polymerization: Synthesis, Characterization and Properties of the Respective Polymers and Copolymers*", J. Jagur-Grodzinski, Ed, Nova Science Publisher Inc., New York, **2006**, 65.
[17] C. Barner-Kowollik, M. Buback, B. Charleux, M. L. Coote, M. Drache, T. Fukuda, A. Goto, B. Klumperman, A. B. Lowe, J. B. McLeary, G. Moad, M. J. Monteiro, R. D. Sanderson, M. P. Tonge, P. Vana, *J. Polym. Sci., Part A: Polym. Chem.* **2006**, *44*, 5809.
[18] C. Le Mercier, J. F. Lutz, S. Marque, F. Le Moigne, P. Tordo, P. Lacroix-Desmazes, B. Boutevin, J. L. Couturier, O. Guerret, R. Martschke, J. Sobek, H. Fischer, *ACS Symp. Ser.* **2000**, *768*, 108.
[19] E. A. Lissi, J. Aljaro, *J. Polym. Sci., Polym. Lett. Ed.* **1976**, *14*, 499.
[20] P. Lacroix-Desmazes, R. Severac, B. Otazaghine, B. Boutevin, *Polym. Prepr. (Am. Chem. Soc., Div. Polym. Chem.)* **2003**, *44*, 683.
[21] Fr 2839724, (Solvay SA, Belg.). P. Lacroix-Desmazes, R. Severac, B. Boutevin, V. Bodart, V. Kurowsky, **2003**.
[22] Wo 2004094356, (Solvay Societe Anonyme, Belg.). P. Lacroix-Desmazes, R. Severac, B. Boutevin, V. Bodart, V. Kurowski. **2004**.
[23] G. Foldiak, R. H. Schuler, *J. Phys. Chem.* **1978**, *82*, 2756.
[24] J. A. LaVerne, L. Wojnarovits, *J. Phys. Chem.* **1994**, *98*, 12635.
[25] H. Rosman, R. M. Noyes, *J. Am. Chem. Soc.* **1958**, *80*, 2410.
[26] J.-C. Daniel, C. Pichot, *Les latex synthétiques: élaboration et applications;* Tec&Doc-Lavoisier: Paris, **2006**.
[27] R. G. Gilbert, *Emulsion polymerization : a mechanistic approach;* Academic Press, 1995.
[28] S. W. Prescott, M. J. Ballard, E. Rizzardo, R. G. Gilbert, *Aust. J. Chem.* **2002**, *55*, 415.
[29] M. J. Monteiro, M. M. Adamy, B. J. Leeuwen, A. M. van Herk, M. Destarac, *Macromolecules* **2005**, *38*, 1538.

 

 DOI: 10.1002/masy.200750217

# A Missing Reaction Step in Dithiobenzoate-Mediated RAFT Polymerization

*Michael Buback,* Olaf Janssen, Rainer Oswald, Stefan Schmatz, Philipp Vana*

**Summary:** The debate on the mechanism of dithiobenzoate-mediated RAFT polymerization may be overcome by taking the so-called "missing step" reaction between a highly reactive propagating radical and the three-arm star-shaped product of the combination reaction of an intermediate RAFT radical and a propagating radical into account. The "missing step" reaction transforms a propagating radical and a not overly stable three-arm star species into a resonance-stabilized RAFT intermediate radical and a stable polymer molecule. The enormous driving force behind the "missing step" reaction is estimated via DFT calculations of reaction enthalpies and reaction free enthalpies.

**Keywords:** kinetics (polym.); living polymerization; quantum chemistry; reaction mechanism; reversible addition fragmentation chain transfer (RAFT)

## Introduction

Despite the enormous success of RAFT polymerization[1] for producing polymer of controlled architecture and well-defined molecular weight, the RAFT mechanism is not yet fully understood, which is particularly true for reactions with dithiobenzoates, $C_6H_5$–C(=S)S–R, being the RAFT agent.[2] With these systems extended induction periods with virtually no polymerization are observed as well as significant rate retardations in comparison to conventional free-radical polymerizations (without RAFT agent) under otherwise identical conditions. Two divergent mechanisms have been proposed for interpreting rate retardation: (*i*) The intermediate RAFT radical produced by fast addition of a propagating radical to the RAFT species undergoes *irreversible termination* with an other radical species (cross-termination) or with itself (self-termination), which processes are associated with radical loss and thus result in rate retardation.[3–5] (*ii*) The second mechanism assigns rate retardation to *slow fragmentation* of the intermediate RAFT radical, but neglects participation of intermediate RAFT radicals in irreversible termination reactions.[6–8] Monomer conversion-vs.-time curves which have been measured for a range of dithiobenzoate-mediated RAFT polymerizations are not capable of distinguishing between these two limiting mechanisms, as the experimental data may be fitted equally well by the *irreversible termination* and the *slow fragmentation* models, although with the fragmentation rate coefficients for the intermediate RAFT radical differing by orders of magnitude.[5,7] Electron-spin-resonance (ESR) experiments on dithiobenzoate-mediated polymerizations are in conflict with the *slow fragmentation* model because the measured concentration of intermediate RAFT radicals is far below the one predicted by this model.[4,9,10] The *irreversible termination* model, on the other hand, can account for such low concentrations of intermediate RAFT radicals, but the three-arm star products of irreversible termination,[11] are not found in the product mixture of dithiobenzoate-mediated acrylate RAFT polymerizations, although

Institut für Physikalische Chemie, Georg-August-Universität Göttingen, Tammannstraße 6, D-37077 Göttingen, Germany
E-mail: mbuback@uni-goettingen.de

these reactions exhibit significant rate retardation.[12,13] For styrenic systems such three-arm star species were demonstrated to be stable at typical polymerization temperatures.[14]

Even more complex models, which include reversible termination into the slow fragmentation scheme,[15,16] or consider both irreversible termination and slow fragmentation of RAFT intermediate radicals,[17] or assume different kinetics under RAFT pre-equilibrium and main-equilibrium conditions. The kinetic scheme is presented in Eq. (1), where **1** refers to the propagating radical, **2** to the polymeric dithiobenzoate, and **3** to the intermediate RAFT radical. Because of their close similarity, the macroradicals $P_i^\bullet$ and $P_j^\bullet$ are both indicated by **1** and the two polyRAFT agents in Eq. (1) by **2**. Also represented by identical notations are the two addition and the two fragmentation rate coefficients, $k_{ad}$ and $k_\beta$, respectively.

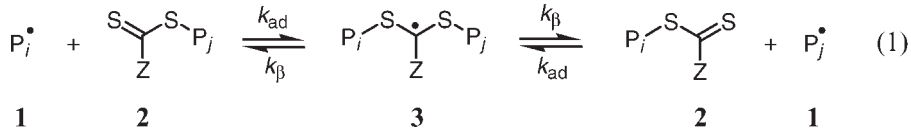


(1)

equilibrium conditions,[10,17] provide no satisfactory mechanistic description of dithiobenzoate-mediated RAFT polymerization. Within a recent paper from our group,[18] arguments have been put forward for an important kinetic step having not yet been included into the RAFT schemes discussed so far. This so-called ''missing step'' occurs between a highly reactive propagating radical and the star-shaped product from irreversible (or reversible) termination of a propagating radical and an intermediate RAFT radical. This step definitely needs to be considered in RAFT polymerizations of acrylate monomers. In the present contribution, the arguments for the relevance of this ''missing step'' are briefly summarized and the driving force behind this reaction is estimated via DFT calculations of reaction enthalpies and reaction free enthalpies.

## Results and Discussion

The subsequent discussion will focus on RAFT polymerizations under main-

RAFT polymerizations mediated by dithiobenzoates experience significant rate retardation due to resonance stabilization of **3**. Delocalization of the radical functionality, as is illustrated in Scheme 1, affords resonance structures with significantly reduced steric hindrance for radical-radical combination (or disproportionation) reactions.[16]

The consequences of resonance stabilization of **3** may be summarized: (*i*) the reaction of **1** + **2** to **3**, in which a resonance-stabilized radical **3** is produced from a reactive radical **1**, should be very fast which is indeed reported;[19] (*ii*) the resonance stabilization of **3** disfavors fragmentation; (*iii*) delocalization of the radical functionality, e.g., into the para position, reduces problems for radical reactions of **3** due to steric hindrance, which may be severe in the case that the radical functionality is localized exclusively at the carbon atom between the sulfur atoms; (*iv*) radical reactions of **3** are favored, as the resonance-stabilized species **3** occurs in significantly larger concentrations than, e.g., in situations where the

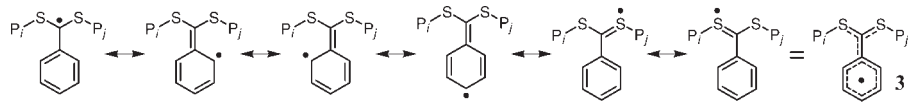


***Scheme 1.***
Resonance structures of the intermediate radical occurring in dithiobenzoate-mediated RAFT polymerizations.

 

Z-group of the RAFT agent is benzyl rather than phenyl; ($v$) even at significant concentrations of **3**, propagation reactions starting from this intermediate RAFT radical are unlikely because of the resonance stabilization of **3**.

By combination of the radicals **1** and **3**, the cross-combination product **4**, $P_k$–Int, is formed:

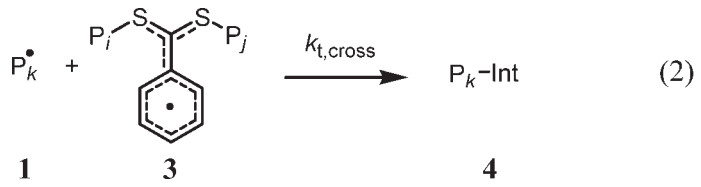


As is illustrated in Scheme 2, **4** will actually be a mixture of several regioisomers. The relative amounts to which isomers such as **4a** to **4f** are produced from **1** and **3** may be rather different.

tion. As has been pointed out in our previous paper,[18] the puzzling kinetic behavior of finding neither significant concentrations of three-arm star components **4** nor of intermediate radicals **3** in dithiobenzoate-mediated acrylate polymerizations may be explained by including, as an additional step, the reaction between **4** and a highly reactive acrylate propagating radical **1**. An example of this so-called "missing step" reaction of **1** + **4d** to yield, **3** + dead polymer **5** is illustrated in Eq. (3):

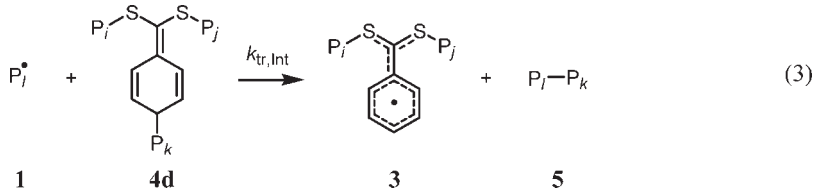


It needs to be noted that the reaction depicted in Eq. (3) is just one example out of several processes, which the different regioisomers of **4** may undergo. The reactions of **1** + **4a**, of **1** + **4b**, and of **1** + **4e** are illustrated in Eqs. (4) to (6), respectively.

Implementing the individual steps presented in Eqs. (1) and (2) into the kinetic treatment is not sufficient for adequately describing all essential features of dithiobenzoate-mediated RAFT polymerization of acrylates. Even including reversibility of the combination step in Eq. (2) or taking both irreversible termination of **1** and **3** and slow fragmentation of **3** into account, does not provide a fully consistent kinetic description.

The variety of **1** + **4** reactions may be even larger, as for a given regioisomer **4** radical attack of **1** may occur in different ways. As has been noted in Ref.[18], the driving force of the **1** + **4** reaction should be sufficiently high to also give rise to

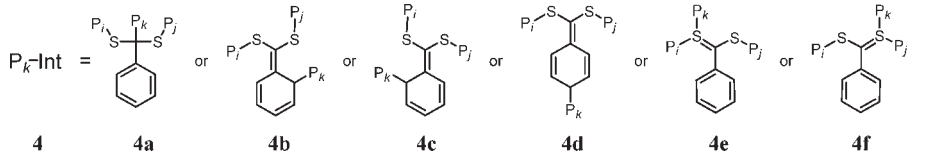


***Scheme 2.***

Structures of regioisomers **4** produced by combination of a propagating radical **1** with the intermediate RAFT radical **3**.

 

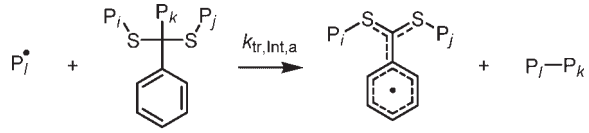


**1** **4a** **3** **5**

(4)

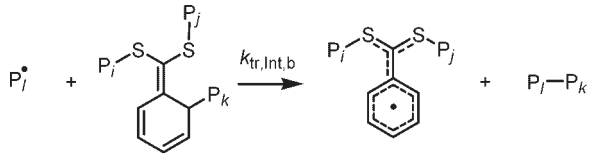


**1** **4b** **3** **5**

(5)

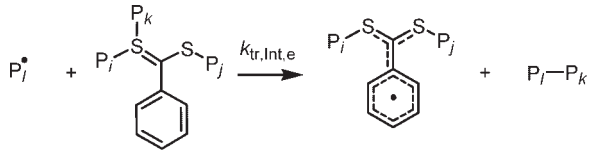


**1** **4e** **3** **5**

(6)

hydrogen abstraction from **4**. As an example, hydrogen abstraction is illustrated for the **1**+**4d** reaction in Eq. (7):

molecule, such as **5** or **7**. Each of these reactions is associated with a strong driving force and is thus expected to be very fast.

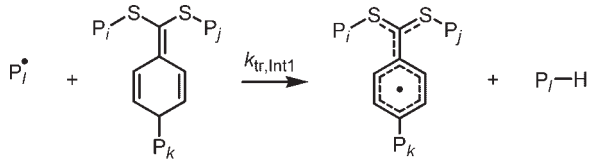


**1** **4d** **6** **7**

(7)

Irrespective of the particular regioisomer that undergoes the **1**+**4** reaction and of the reaction pathway, which may either proceed via radical abstraction according to Eqs. (3) to (6) or via hydrogen abstraction according to Eq. (7), all **1**+**4** ''missing step'' reactions have an important feature in common: A reactive propagating radical **1** and a weakly bound star-shaped molecule **4** are transformed into a resonance-stabilized radical, such as **3** or **6**, and a very stable polymeric (or oligomeric)

The value of the rate coefficient of the ''missing step'' reaction in Eq. (3), $k_{tr,Int}$, may come close to or even exceed that of $k_{ad}$, which is the **1**+**2** addition rate coefficient (see Eq. (1)), because within both reactions, at least in the case of acrylate polymerizations, a highly reactive propagating radical is transformed into a resonance-stabilized one. PREDICI simulations including the reactions presented in Eqs. (2) and (3) have been carried out for dithiobenzoate-mediated methyl

 

acrylate polymerizations under main-equilibrium conditions assuming $k_{tr,Int}$ and $k_{ad}$ to be of identical size.[18] The concentration-vs.-time correlations for both the acrylate monomer and the intermediate radical **3** turned out to be almost insensitive toward the ''missing step'' reaction, whereas the concentration of the three-arm star combination product **4** becomes negligibly small when the **1** + **4** reaction is included. This result is in full agreement with the experimental finding that noticeable amounts of **4** may not be detected in the product mixture from dithiobenzoate-mediated acrylate polymerizations.[12,13]

The essence of the RAFT mechanism with the ''missing step'' being included is visualized in Figure 1. Starting from the intermediate RAFT radical **3**, two successive irreversible reactions occur. The first one, with rate coefficient $k_{t,cross}$, yields the combination product **4**, and the subsequent one, with rate coefficient $k_{tr,Int}$, yields **3** back again. In both steps, a propagating radical is involved. In the second step, the radical $P_l^\bullet$ picks up the $P_k$ species from **4** to yield **5**, which component is identical to the combination product of two propagating radicals. The reaction sequence resembles a catalytic cycle in which two propagation radicals, $P_l^\bullet$ and $P_k^\bullet$, via the dithiobenzoate components **3** and **4**, are transformed into a polymer molecule $P_l$–$P_k$. It should be stressed that the concentration of **3** remains unchanged, which may explain the excellent control of dithiobenzoate-mediated RAFT polymerizations even under conditions of irreversible termination. Figure 1 does not apply to situations where the reaction presented in Eq. (7) plays a major role, although even in this case retardation due to irreversible radical termination does occur.

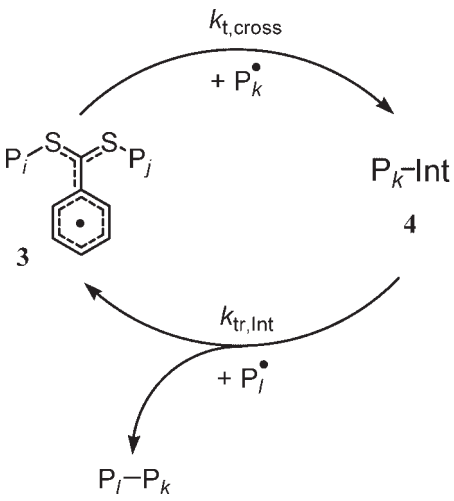


***Figure 1.***
The lower part of the figure illustrates the ''missing step'' reaction according to Eq. (3) for dithiobenzoate-mediated polymerizations. This reaction needs to be considered in RAFT polymerizations with highly reactive propagating radicals. The dithiobenzoate compounds **3** and **4** assist the termination of the two radicals, $P_l^\bullet$ and $P_k^\bullet$.

The mechanism of the ''missing step'' reaction has not yet been investigated in any detail. Because of the multitude of regioisomers **4**, a considerable number of **1** + **4** transition state structures needs to be analyzed. Moreover, several reaction channels may be relevant for a given regioisomer, as is illustrated for the **1** + **4d** reaction in Figure 2. According to the upper reaction pathway in Figure 2, the propagating radical, ($P_l^\bullet$ = **1**) picks up the $P_k$ moiety from the six-membered ring. The second pathway, which is illustrated in the lower part of Figure 2, suggests that $P_l^\bullet$ first adds to one of the double bonds of the six-membered ring and the polymer molecule $P_l$–$P_k$ is released after bond rearrangement.

According to the high reactivity of the ''missing step'' reaction, the kinetics of the **1** + **4** step is not easily accessed by experimental methods. The star-shaped component **4** needs to be prepared by a non-radical route, that is, without highly reactive radicals **1** being present. For styrenic species, a model experiment for producing **4** has been designed and successfully carried out by the Fukuda group.[11] Several three-arm star products **4** were obtained by reacting polystyrene-dithiobenzoate and polystyrene bromide (with well defined, very similar lengths of the polystyryl moieties) in solution of *tert*-butyl benzene and in the presence of a CuBr/

 

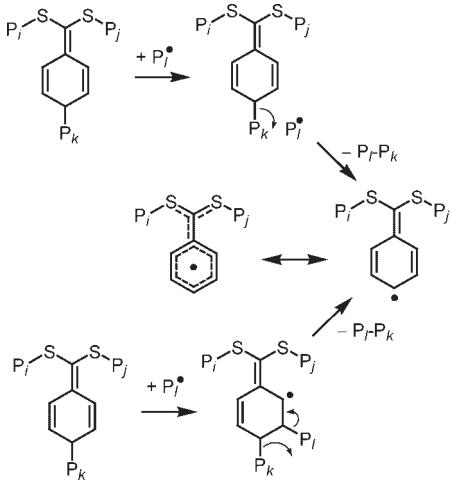

***Figure 2.***
Two suggestions for mechanisms of the **1** + **4d** → **3** + **5** "missing step" reaction.

$Me_6$TREN complex. Applying a corresponding strategy toward an acrylate system did not yield convincing evidence for the production of three-arm star cross-combination product **4**.[20] The results of the latter experiments may even be interpreted in such a way that a significant amount of **5**, the radical–radical combination product $P_l$–$P_k$, is formed. Adopting this interpretation would provide another experimental indication of the "missing step" reaction being relevant for acrylate systems. The capability of adequately representing the experimental observations made for dithiobenzoate-mediated acrylate polymerizations, however, constitutes the most striking evidence for the validity of the extended RAFT kinetic scheme that includes "missing step" reactions, such as the ones shown in Eqs.(3) to (7).

To deduce further information on the "missing step" reaction, density functional theory (DFT) calculations have been applied toward estimating reaction enthalpies, $\Delta H_R$, and reaction free enthalpies, $\Delta G_R$, at 298.15K for several of the **1** + **4** processes. The $\Delta G_R$ value provides a measure of the driving force behind the individual reaction channels. Although such calculations for small molecules are closer to conditions as are met in the pre-equilibrium period of RAFT polymerizations, it appears rewarding to use this quantum-chemical tool for some general analysis of the "missing step" reaction. The program package Gaussian03[21] was used for the quantum-chemical calculations. The structures of all species involved were fully optimized employing the DFT variant UB3LYP in conjunction with the 6-31G(d,p) basis set (333 contracted Gaussian-type orbitals for the **1** + **4** reactions). The B3LYP hybrid method[22] combines the Becke three-parameter exchange functional[23] with the Lee, Yang and Parr[24] correlation functional. The full conformational space of the system was scanned to find the lowest energy conformation of each species. To establish the existence of true minima on the potential energy surface, the Hessian matrices at the stationary points were determined. The calculated harmonic vibrational frequencies and equilibrium rotational constants were used to estimate the thermal contribution to thermodynamic quantities within the harmonic-oscillator-rigid-rotor model.

DFT estimates of $\Delta H_R$ and of $\Delta G_R$ have been made for the two reaction steps of the cyclic pathway, **1** + **3** → **4** and **1** + **4** → **3** + **5** (Figure 1). The P moieties in the compounds **3**, **4**, and **5** have been chosen to be ethyl and **1** is an ethyl radical. The calculations have been performed for reactions via the four characteristic types of the 3-arm star combination products: **4a**, **4b**, **4d**, and **4e** (see Scheme 2). The so-obtained reaction enthalpies and reaction free enthalpies for 298.15K are summarized in rows [3] to [6] of Table 1 with $\Delta H_{R,C}$ and $\Delta G_{R,C}$ referring to the **1** + **3** → **4** combination reactions and $\Delta H_{R,MS}$ and $\Delta G_{R,MS}$ referring to the **1** + **4** → **3** + **5** missing step reactions. Presented in row [7] is the reaction enthalpy for the "missing step" reaction of **4d** proceeding via hydrogen-abstraction, i.e., the reaction shown in Eq. (7). Listed in the first row of Table 1 are the DFT-estimated enthalpies for the **1** + **2** → **3** addition reaction. Given in row [2] are the enthalpies for the **1** + **1** → *n*-butane combination reaction.

 

***Table 1.***
Reaction enthalpies, $\Delta H_R$, and reaction free enthalpies, $\Delta G_R$, at 298.15 K estimated via DFT calculations (UB3LYP, 6-31G(d,p)) for the addition of an ethyl radical to ethyl dithiobenzoate, for several radical-radical combination reactions, and for the "missing step" reactions of the four cross-combination products (**4a**, **4b**, **4d**, and **4e**) with an ethyl radical **1**. The reaction enthalpy and reaction free enthalpy values are given in units of $kJ \cdot mol^{-1}$.

| Reaction | $\Delta H_{R,ad}$ | $\Delta G_{R,ad}$ | | |
|---|---|---|---|---|
| [1] **1** + **2** → **3** | −80.4 | −33.5 | | |
| Reaction | $\Delta H_{R,C}$ | $\Delta G_{R,C}$ | $\Delta H_{R,MS}$ | $\Delta G_{R,MS}$ |
| [2] **1** + **1** → *n*-butane | −344.4 | −282.9 | | |
| [3] **1** + **3** → **4a**; | −237.1 | −170.5 | | |
| **1** + **4a** → **3** + **5** | | | −107.3 | −112.4 |
| [4] **1** + **3** → **4b**; | −134.4 | −73.1 | | |
| **1** + **4b** → **3** + **5** | | | −210.0 | −209.8 |
| [5] **1** + **3** → **4d**; | −152.2 | −90.4 | | |
| **1** + **4d** → **3** + **5** | | | −192.2 | −192.5 |
| [6] **1** + **3** → **4e**; | −47.3 | 17.6 | | |
| **1** + **4e** → **3** + **5** | | | −297.1 | −300.3 |
| [7] **1** + **4d** → **6** + **7** | | | −203.7 | −200.3 |

The data in rows [1] and [2] essentially serve the purpose of validating the DFT procedure. The enthalpy for the ethyl + ethyl dithiobenzoate reaction given in row [1], $\Delta H_{R,ad} = -80.4\ kJ \cdot mol^{-1}$, is close to the value from quantum-chemical calculations reported by Coote and Radom[25] for the related addition of a methyl radical to methyl dithiobenzoate: $\Delta H_{R,ad} = -95.2\ kJ \cdot mol^{-1}$. The slightly larger exothermicity for the methyl system results from the higher reactivity of the methyl radical as compared to the ethyl radical. The comparison of the two numbers indicates that the DFT-derived enthalpy for the **1** + **2** → **3** reaction is of reasonable size, which suggests that the DFT procedure used within the present study should be capable of providing reliable $\Delta H_R$ values. The entry in row [2] of Table 1 supports this conclusion, as the absolute value of the combination enthalpy of two ethyl radicals **1**, $\Delta H_{R,C} = -344.4\ kJ \cdot mol^{-1}$, is relatively close to the reported value for the dissociation enthalpy of *n*-butane into two ethyl radicals, $\Delta H_{R,diss} = 367.7\ kJ \cdot mol^{-1}$.[26] On the basis of the satisfying match with literature data of our DFT-derived $\Delta H_R$ values (entries [1] and [2]) it is assumed that the other reaction enthalpies (and the reaction free-enthalpies) in Table 1, for which no reference data is available, are also reliable.

The sum of the reaction enthalpies of associated **1** + **3** → **4** and **1** + **4** → **3** + **5** reactions (entries [3] to [6] in Table 1) adds up to $-344.4\ kJ \cdot mol^{-1}$, as the net reaction of each of the cyclic processes, via **4a**, **4b**, **4d**, or **4e**, is the combination of two ethyl radicals to produce *n*-butane. Thus, in cases where the first step is poorly exothermic, such as with the cross-combination of **1** + **3** → **4e**, where the ethyl radical adds to one of the sulfur atoms, the second step, **1** + **4** → **3** + **5**, is highly exothermic. A different type of behavior is seen with the **4a** regioisomer, where the first step is highly exothermic, as a carbon-carbon bond is formed without any accompanying reduction of aromatic delocalization of the phenyl moiety. The associated missing step reaction, **1** + **4a** → **3** + **5**, has a significantly lower reaction enthalpy than, e.g., the **1** + **4e** reaction, but even this lower value exceeds the enthalpy of the **1** + **2** → **3** reaction. With the two other regioisomers, **4b** and **4d**, the (negative) reaction enthalpies of the "combination step" and the "missing step" are both well above the enthalpy of the **1** + **2** → **3** reaction. In both cases the "missing step" has a higher exothermicity than the associated combination step. For the **4d** regioisomer entry [7] in Table 1 allows for a comparison of the reaction enthalpies for hydrogen abstraction and ethyl abstraction reactions,

 

i.e., for the **1** + **4d** → **6** + **7** vs. the **1** + **4d** → **3** + **5** steps. The two reaction enthalpies differ by no more than about 5%.

Rough information about the driving force of the ''missing step'' reaction may be deduced from an inspection of the reaction free enthalpies, $\Delta G_{R,MS}$. As with the reaction enthalpies, the sum of the reaction free enthalpies of associated **1** + **3** → **4** and **1** + **4** → **3** + **5** reactions (see rows [3] to [6] in Table 1) adds up to the same value: $\Delta G_{R,C} + \Delta G_{R,MS} = -282.9\ kJ \cdot mol^{-1}$, which is the reaction free enthalpy for the net reaction of each of the cyclic processes, via **4a**, **4b**, **4d**, or **4e**, that is the combination of two ethyl radicals to produce *n*-butane. The $\Delta G_{R,MS}$ values are rather close to the associated $\Delta H_{R,MS}$ values. Thus the arguments put forward for $\Delta H_{R,MS}$ also apply to $\Delta G_{R,MS}$. The highest driving force is expected for the ''missing step'' reaction of **4e** + **1**. This reaction may however not take place to a significant extent, as the $\Delta G_{R,MS}$ value for the **1** + **3** → **4e** reaction indicates that the production of **4e** is not favored. The reaction of **4a** + **1** should exhibit the lowest driving force among the ''missing step'' processes. Even this slower reaction, however, has a larger negative $\Delta G_{R,MS}$ than the **1** + **2** → **3** reaction, which is generally considered to be a fast process in well controlled RAFT polymerizations. The $\Delta G_{R,MS}$ data in Table 1 thus suggests that the missing step reactions according to the entries in rows [3] to [7] are relatively fast reactions in the case of **1** being a reactive radical, such as ethyl. The difference in the $\Delta G_{R,MS}$ values for the ''missing step'' channels according to rows [5] and [7] is too small as to allow for deducing any firm conclusions about the relative weight of these two reaction channels.

For obtaining such detailed information, high-level quantum-chemical calculations of activation energies and pre-exponential factors are required, which are not easily obtained for large species, such as **2**, **3**, **4**, and **6**. Thus further reactions in conjunction with detailed product analyses, as in ref.[20], need to be carried out in order to identify the contribution of ''missing step'' reactions occurring via hydrogen abstraction. If cross combination of **1** + **3** yields **4a** and **4e**, hydrogen abstraction is not expected to play a significant role.

Although the arguments on the ''missing step'' reaction have essentially been made on the basis of reaction free enthalpies rather than on reaction barriers or activation energies, the results strongly indicate that the missing step should be a very fast in the case of reactive propagating radicals, as in acrylate polymerization. It is highly recommendable, if not mandatory, to consider this step in the kinetic modeling of dithiobenzoate-mediated acrylate polymerizations. Including the ''missing step'' into the kinetic scheme allows for the first time to consistently represent the entire body of experimental observations made under main-equilibrium conditions during dithiobenzoate-mediated acrylate polymerizations.

It goes without saying that further reaction steps may be added to the overall kinetic scheme. A star-star coupling reaction of **3** + **3** and follow-up processes of products from this reaction may be included, as should be chain-length and conversion dependent rate coefficients for the diffusion-controlled processes. Such modifications are useful for fine-tuning of dithiobenzoate-mediated RAFT kinetics.

Analysis of RAFT polymerizations via the kinetic scheme that contains the ''missing step'' reaction is not restricted to dithiobenzoate-mediated polymerizations, but should be generally used with RAFT-mediated polymerizations, even in situations where **3** is high in energy and the fragmentation rate is very fast. Under such conditions, the reactions presented in Eq. (2) and, in particular, the one in Eq. (3) will however be of minor importance.

It appears to be a matter of priority to carry out DFT estimates for reactions in which the ethyl radical and ethyl moieties are replaced by styryl or by acrylate-type units. The results of such DFT calculations should indicate to which extent the ''missing step'' reaction contributes to dithio-

 

benzoate-mediated polymerizations of different types of monomers under main-equilibrium conditions. The existence of three-arm star cross-combination products in styrenic systems suggests that the ''missing step'' is less important in case of lower-energy propagating radicals. An obvious reason for such different behavior is seen in lower reaction free enthalpies. As the free enthalpy of combination of two styryl radicals, which is identical to the sum of the free enthalpies for the $\mathbf{1}+\mathbf{3}\rightarrow\mathbf{4}$ and $\mathbf{1}+\mathbf{4}\rightarrow\mathbf{3}+\mathbf{5}$ reaction steps, is significantly lower than the one of combination of two ethyl radicals, also the individual free enthalpies, including $\Delta G_{R,MS}$, should be much smaller in styrenic systems. Moreover, the activation barriers may be higher for these systems. The quantitative analysis of the ''missing step'' kinetics for a range of monomers will largely benefit from DFT estimates of transition-state structures. Such calculations are currently underway in our laboratory.

## Conclusions

Introducing the reaction of propagating radicals, **1**, with the cross-combination product from irreversible termination, **4**, resolves the major problem encountered in kinetic analyses of dithiobenzoate-mediated acrylate polymerizations via the *irreversible termination* model. The reaction of $\mathbf{1}+\mathbf{4}$ to yield $\mathbf{3}+\mathbf{5}$ or $\mathbf{6}+\mathbf{7}$ which has been overlooked so far, can fully account for the loss of the three-arm star product **4**. Without introducing any new species, the extended kinetic scheme adequately represents all essential observations made for the main-equilibrium period of dithiobenzoate-mediated RAFT polymerizations. The novel reaction is expected to be very fast, due to the enormous driving force associated with transforming a highly reactive propagating radical **1** and a loosely bound star-shaped molecule **4** into a resonance-stabilized radical **3** and a very stable dead polymer molecule **5**. The ''missing step'' reaction applies irrespective of cross-termination being reversible or irreversible. It seems advisable to generally use the extended kinetic scheme for analysis of reactivity and selectivity in RAFT polymerizations, although reaction $\mathbf{1}+\mathbf{4}\rightarrow\mathbf{3}+\mathbf{5}$ is less important in the case that the intermediate RAFT radical **3** is not significantly stabilized or the propagating radical is of lower reactivity.

*Acknowledgements:* The authors gratefully acknowledge the scientific interaction with several members of the *IUPAC Subcommittee* on ''Modeling of Polymerization Kinetics and Processes'' and of the *European Graduate School* ''Microstructural Control in Radical Polymerization''. Financial support provided by the *Fonds der Chemischen Industrie* and by the *Deutsche Forschungsgemeinschaft* is gratefully acknowledged.

[1] J. Chiefari, Y. K. Chong, F. Ercole, J. Krstina, J. Jeffery, T. P. T. Le, R. T. A. Mayadunne, G. F. Meijs, C. L. Moad, G. Moad, E. Rizzardo, S. H. Thang, *Macromolecules* **1998**, *31*, 5559.
[2] G. Moad, E. Rizzardo, S. H. Thang, *Aust. J. Chem.* **2005**, *58*, 379.
[3] M. J. Monteiro, H. de Brouwer, *Macromolecules* **2001**, *34*, 349.
[4] Y. Kwak, A. Goto, Y. Tsujii, Y. Murata, K. Komatsu, T. Fukuda, *Macromolecules* **2002**, *35*, 3026.
[5] A. R. Wang, S. Zhu, Y. Kwak, A. Goto, T. Fukuda, M. S. Monteiro, *J. Polym. Sci., Part A: Polym. Chem.* **2003**, *41*, 2833.
[6] C. Barner-Kowollik, J. F. Quinn, D. R. Morsley, T. P. Davis, *J. Polym. Sci., Part A: Polym. Chem.* **2001**, *39*, 1353.
[7] T. P. Davis, C. Barner-Kowollik, T. L. U. Nguyen, M. H. Stenzel, J. F. Quinn, P. Vana, *ACS Symp. Ser.* **2003**, *854*, 551.
[8] A. Feldermann, M. L. Coote, M. H. Stenzel, T. P. Davis, C. Barner-Kowollik, *J. Am. Chem. Soc.* **2004**, *126*, 15915.
[9] E. Chernikova, A. Morozov, E. Leonova, E. Garina, V. Golubev, C. Bui, B. Charleux, *Macromolecules* **2004**, *37*, 6329.
[10] M. Drache, G. Schmidt-Naake, M. Buback, P. Vana, *Polymer* **2005**, *46*, 8483.
[11] Y. Kwak, A. Goto, K. Komatsu, Y. Sugiura, T. Fukuda, *Macromolecules* **2004**, *37*, 4434.
[12] A. Ah Toy, P. Vana, T. P. Davis, C. Barner-Kowollik, *Macromolecules* **2004**, *37*, 744.
[13] A. Feldermann, A. A. Toy, T. P. Davis, M. H. Stenzel, C. Bamer-Kowollik, *Polymer* **2005**, *46*, 8448.
[14] Y. Kwak, A. Goto, T. Fukuda, *Macromolecules* **2004**, *37*, 1219.

 

[15] C. Barner-Kowollik, J. F. Quinn, T. L. U. Nguyen, J. P. A. Heuts, T. P. Davis, *Macromolecules* **2001**, *34*, 7849.
[16] M. J. Monteiro, R. Bussels, S. Beuermann, M. Buback, *Aust. J. Chem.* **2002**, *55*, 433.
[17] C. Barner-Kowollik, M. Buback, B. Charleux, M. L. Coote, M. Drache, T. Fukuda, A. Goto, B. Klumperman, A. B. Lowe, J. B. Mcleary, G. Moad, M. J. Monteiro, R. D. Sanderson, M. P. Tonge, P. Vana, *J. Polym. Sci., Part A: Polym. Chem.* **2006**, *44*, 5809.
[18] M. Buback, P. Vana, *Macromol. Rapid Commun.* **2006**, *27*, 1299.
[19] A. Goto, K. Sato, Y. Tsujii, T. Fukuda, G. Moad, E. Rizzardo, S. H. Thang, *Macromolecules* **2001**, *34*, 402.
[20] R. Venkatesh, B. B. P. Staal, B. Klumperman, M. J. Monteiro, *Macromolecules* **2004**, *37*, 7906.
[21] M. J. Frisch, G. W. Trucks, H. B. Schlegel, G. E. Scuseria, M. A. Robb, J. R. Cheeseman, J. Montgomery, J. A., T. Vreven, K. N. Kudin, J. C. Burant, J. M. Millam, S. S. Iyengar, J. Tomasi, V. Barone, B. Mennucci, M. Cossi, G. Scalmani, N. Rega, G. A. Petersson, H. Nakatsuji, M. Hada, M. Ehara, K. Toyota, R. Fukuda, J. Hasegawa, M. Ishida, T. Nakajima, Y. Honda, O. Kitao, H. Nakai, M. Klene, X. Li, J. E. Knox, H. P. Hratchian, J. B. Cross, V. Bakken, C. Adamo, J. Jaramillo, R. Gomperts, R. E. Stratmann, O. Yazyev, A. J. Austin, R. Cammi, C. Pomelli, J. W. Ochterski, P. Y. Ayala, K. Morokuma, G. A. Voth, P. Salvador, J. J. Dannenberg, V. G. Zakrzewski, S. Dapprich, A. D. Daniels, M. C. Strain, O. Farkas, D. K. Malick, A. D. Rabuck, K. Raghavachari, J. B. Foresman, J. V. Ortiz, Q. Cui, A. G. Baboul, S. Clifford, J. Cioslowski, B. B. Stefanov, G. Liu, A. Liashenko, P. Piskorz, I. Komaromi, R. L. Martin, D. J. Fox, T. Keith, M. A. Al-Laham, C. Y. Peng, A. Nanayakkara, M. Challacombe, P. M. W. Gill, B. Johnson, W. Chen, M. W. Wong, C. Gonzalez, J. A. Pople, Gaussian, Inc., Wallingford CT **2004**.
[22] P. J. Stephens, F. J. Devlin, C. F. Chabalowski, M. J. Frisch, *J. Phys. Chem.* **1994**, *98*, 11623.
[23] A. D. Becke, *J. Chem. Phys.* **1993**, *98*, 5648.
[24] C. T. Lee, W. T. Yang, R. G. Parr, *Physical Review B* **1988**, *37*, 785.
[25] M. L. Coote, L. Radom, *J. Am. Chem. Soc.* **2003**, *125*, 1490.
[26] D. L. Baulch, C. T. Bowman, C. J. Cobos, R. A. Cox, T. Just, J. A. Kerr, M. J. Pilling, D. Stocker, J. Troe, W. Tsang, R. W. Walker, J. Warnatz, *J. Phys. Chem. Ref. Data* **2005**, *34*, 757.

 

 DOI: 10.1002/masy.200750218

# RAFT Polymerization in Bulk and Emulsion

*Alessandro Buttè, A. David Peklak, Giuseppe Storti, Massimo Morbidelli*

**Summary:** Detailed models of the RAFT polymerization in both non-segregated (bulk) and segregated (seeded emulsion) systems are presented. It is shown that satisfactory agreements between experiments and models can be achieved, and that effects such as inhibition and retardation, or the polymerization behavior at high conversions can be readily explained. In all cases the model parameter fitting has been minimized, being mostly limited to the rate coefficients of the addition/fragmentation reactions in the RAFT polymerization. Therefore, such models are believed to be invaluable tools towards a deeper understanding of the main phenomena underlying RAFT polymerization.

## Introduction

Among the different techniques presented in the literature to carry out a living free-radical polymerization (LRP), reversible addition–fragmentation chain transfer (RAFT) polymerization has attracted particular attention.[1] Two main reasons can be identified for its success: (1) the large versatility of the process and (2) its peculiar chemistry. The latter is illustrated in Figure 1: a polymer chain capped e.g. by a dithiocarbonyl group (RAFT group), also called a dormant chain, $D_m$, and a radical chain, $R_n^\bullet$, undergo first an addition reaction to form an intermediate radical, $T_{n,m}^\bullet$, in which both chains are attached to the RAFT group. Because this intermediate radical is unstable, it breaks either giving back the original chains, or resulting in the exchange of the RAFT group between the two chains. Since the rate of fragmentation is typically much faster than that of addition, the RAFT reaction is often approximated as transfer reaction of the RAFT group and it is then supposed not to affect the overall radical concentration. As a consequence, the same kinetics of monomer consumption as in conventional free-radical polymerization processes is expected.

Despite this ideal description, it became soon evident that the true kinetics of RAFT polymerization is more complex. Experimental observations as (i) long inhibition times at the beginning of the reaction,[2] (ii) polymerization rates slower than the corresponding non-living processes (retardation),[3] and (iii) a less pronounced gel effect at high conversion values[4a] have been often reported.

To approach truly living conditions in free radical polymerization, the extent of the termination reactions has to be reduced as much as possible. The natural way to establish such conditions is the reduction of the concentration of active chains, which, in turn, results in the decrease of polymer productivity. To contrast such decrease, the segregation of the radical chains, which is present in heterogeneous processes such as emulsion polymerization, can be exploited. This allows reducing terminations while preserving the overall concentration of radical chains. However, the application of RAFT mediated polymerizations to emulsion systems has also been rather problematic, mainly with respect to the transport of RAFT agent through the aqueous phase. Attempts to carry out RAFT polymerizations in *ab-initio* emulsion processes

Institute for Chemical and Bioengineering, Department of Chemistry and Applied Biosciences, ETH Zurich, 8093 Zurich, Switzerland
E-mail: alessandro.butte@chem.ethz.ch

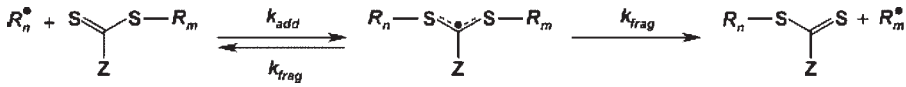

*Figure 1.*
Schematic representation of the RAFT reaction. $R_n^\bullet$ represents a polymer radical chain; $R_m - S - C(-Z) = S$ a dormant chain ($D_m$); and $R_m - S - C^\bullet(-Z) - S - R_n$ an intermediate radical ($T_{n,m}^\bullet$).

typically led to the formation of coagulum and to unfeasibly low reaction rates.[5] To overcome such inconveniences, either the transport of the RAFT agent through the aqueous phase has to be enhanced, e.g., through the use of cyclodextrines,[6] or different approaches to establish segregation have to be employed, such as miniemulsion.[7,8] Recently, the successful application of RAFT polymerization to seeded emulsion systems by distributing the RAFT agent in the emulsion seed prior to the actual polymerization with an acetone transport technique has been reported.[9] Experimental results suggest that the kinetics of such polymerizations is significantly different from that of conventional seeded emulsion polymerization. In particular, considerable inhibition times before the onset of monomer consumption, as well as reduced reaction rates (retardation) in comparison to the equivalent nonliving reactions have been observed.

While most of the research activity referred above was focused on the kinetic analysis of the first part of the polymerization, the reaction behavior at high conversion has been investigated much less.[4] Nonetheless, this problem deserves special attention because the chemistry of the RAFT reaction involves a direct reaction of two polymer chains and, therefore, can be strongly affected by diffusion limitations. Wang and Zhu analyzed the effects of diffusion limitations and chain-length dependent rate constants through model calculations.[10] They demonstrated that the polymerization kinetics is controlled by diffusion limitations at high conversions only and that the same limitations slow down the RAFT mechanism, thus making the control of the polymer growth more difficult.

In this work, the previous two issues, namely the behavior of the polymerization at very low and very high conversion values, will be addressed. In the first case, it will be shown that, in spite of the fact that both non-segregated and segregated systems exhibit inhibition and retardation, the cause for these two effects is different in the two systems. In the case of non-segregated systems, this analysis will be supported by a simple analytical solution. The issue of the system behavior at high conversion values will be addressed for non-segregated systems only, since in these systems the change in behavior due to diffusion limitations is most pronounced. In particular, it will be shown that a complete description of the chain length distribution (CLD) is of paramount importance to accurately predict the system behavior.

## Inhibition and Retardation in Non-Segregated Systems

A typical kinetic scheme for homogeneous systems is considered, which includes radical initiation ($k_i$), monomer propagation ($k_p$), bimolecular termination by radical combination ($k_t$), and RAFT reaction, i.e., addition reaction to a dormant chain ($k_{add}$) and fragmentation of the radical intermediate ($k_{frag}$). In addition, bimolecular termination by combination of radicals with the radical intermediates ($k_{it}$) has been included. The methodology first proposed by Fischer[11] to study the persistent radical effect in NMLP is used to find an analytical solution for the mass balances on the different species (radicals, $R^\bullet$, intermediate radicals, $T^\bullet$, and dormant chains, $D$). In particular, by plotting the solution in a log-log scale, it has been shown[12] that it becomes possible to identify distinct time intervals or regions where the different

 

dimensionless concentrations follow a power law like $c = a\tau^b$, where $c(\tau)$ is the generic dimensionless concentration, while $a$ and $b$ are constants. Moreover, the same balances can be expressed into a non-dimensional form, where the concentration of the radicals ($R^\bullet$ and $T^\bullet$) are made dimensionless using the stationary expression of the radical concentration in non-living bulk polymerization ($R_s^\bullet = \sqrt{R_i/k_t}$), the dormant and dead chains using the initial concentration of dormant chains ($D^{(0)}$), and the time using the process characteristic time $[1/(k_p R_s^\bullet)]$, so to obtain the quantities $r$, $q$, $d$ and $\tau$, respectively (cf Figures 2 to 4). As a result, it is possible to identify a set of dimensionless parameters which can be used to predict the polymerization behavior. Among them, the parameter $\alpha$ is of particular importance, defined as follows:

$$\alpha = k_{add} D^{(0)} / k_{frag} \tag{1}$$

This parameter represents the ratio between the frequency at which one radical reacts with a dormant chain and the frequency at which an intermediate radical fragments. Therefore, it is directly related to the accumulation of intermediate radicals. Another relevant quantity is the parameter $\varepsilon_r$, defined as:

$$\varepsilon_r = k_{ti}/k_t \tag{2}$$

Such quantity is the ratio between radical-intermediate and radical-radical termination rate constants.

Let us analyze the system behavior in terms of dimensionless concentrations at different values of such key parameters. In Figure 2, the log-log plot of the dimensionless concentrations of radicals ($r$) and intermediate radicals ($q$) versus the non-dimensional reaction time ($\tau$) is shown for the case $\alpha < 1$ and in the absence of intermediate radical termination ($\varepsilon_r = 0$). Looking at the radical concentration, two well-distinct regions can be identified: in the first one, the radical concentration grows with slope one; while in the second one a steady-state value is established. This takes place at dimensional time $t_2 = 1/(k_t R_s^\bullet)$ (corresponding to $\tau_2$ of Figure 1), which corresponds to the characteristic time of the termination reactions. It can be easily proved that such a behavior is equal to that of a non-living polymeriza-

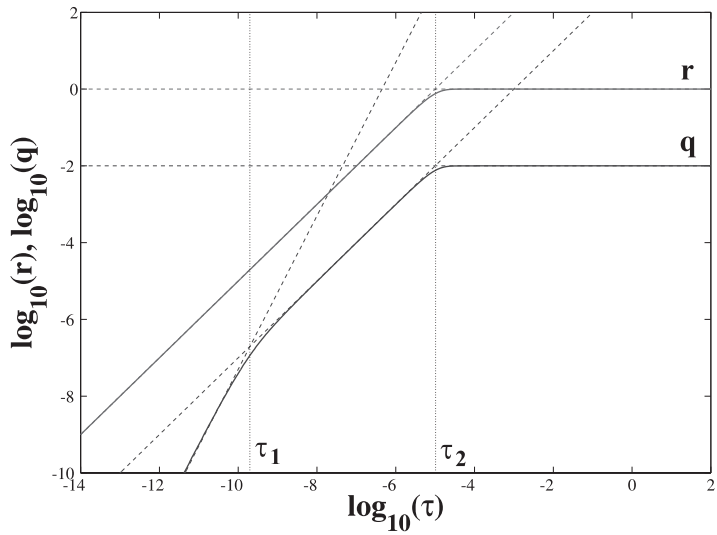


***Figure 2.***
Logarithmic dimensionless concentration of intermediate radicals (q) and radicals (r) versus non-dimensional polymerization time ($\tau$) for $\alpha = 10^{-2}$ in the absence of intermediate termination ($\varepsilon_r = 0$). More details in Ref. 12, Figure 2.

 

tion: therefore, the same concentration profile is expected in the two cases at low conversion values. The same analysis can be repeated for the concentration of the intermediate radicals. When large enough concentration of intermediate radicals is built up, the rate of addition equilibrates the rate of fragmentation. The time needed to build up this concentration corresponds to the characteristic time of the fragmentation reaction, $t_1 = 2/k_{frag}$ (corresponding to $\tau_1$ of Figure 1). At this point, the concentration of the intermediates reaches a quasi-steady state (QSS) value and the same QSS concentration is maintained when the radical concentration reaches the steady-state behavior. Note that $\alpha$ represents the steady state concentration of the intermediate radicals.

The case $\alpha > 1$, i.e., the case where the frequency of fragmentation is smaller than that of addition, is shown in Figure 3. The radical concentration, $r$, is initially growing due to radical initiation as in Figure 2, while the intermediate radicals accumulate due to addition to the dormant chains. At $\tau = \tau_1$, which corresponds to the characteristic time of the addition reaction, the production of new radicals by initiation is equilibrated by the rate of addition [i.e., $k_{add}DR^{\bullet} = R_i$]. This temporary solution is valid as long as the concentration of the intermediates is small enough. At $\tau = \tau_3$, which corresponds to the characteristic time of fragmentation, the production of radicals by fragmentation becomes predominant: fragmentation and addition proceed with the same reaction rate and the radical concentration reaches a QSS value with respect to the intermediate concentration. This situation lasts until both material balances reach the steady-state at $\tau = \tau_4$. By comparison of Figures 2 and 3, it can be noticed that the radical concentration profile follows two different paths depending on the value of $\alpha$: for $\alpha < 1$, the radical concentration follows the path A-B-C, while for $\alpha > 1$ it follows the path A-D-C. Accordingly, it can be said that the segment AD = BC represents the delay introduced in the reaction due to the slower fragmentation rate. In other words, the inhibition time can be roughly estimated as $t_{inhib} = t_C - t_B \approx t_C = \alpha/(k_t R_s^{\bullet})$. It can be therefore concluded that, in the case of slow fragmentation, an inhibition time is

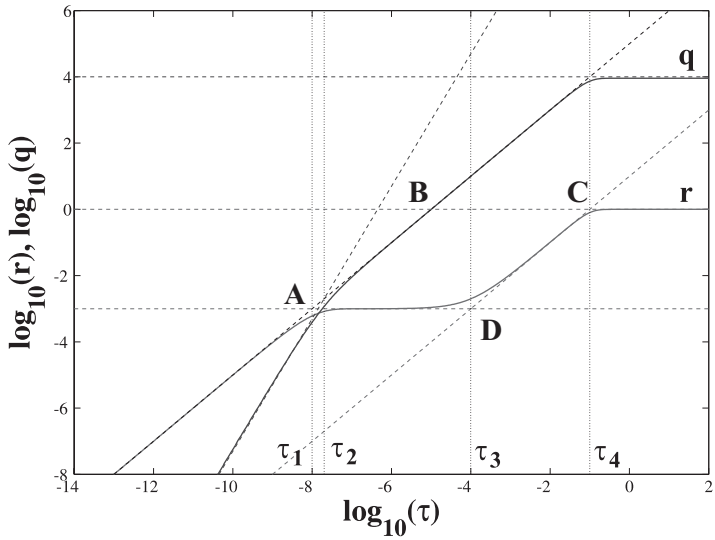


***Figure 3.***
Logarithmic dimensionless concentration of intermediate radicals (q) and radicals (r) versus non-dimensional polymerization time ($\tau$) for $\alpha = 10^4$ in the absence of intermediate termination ($\varepsilon_r = 0$). More details in Ref. 12, Figure 5.

 

expected at the beginning of the polymerization. On the other hand, it should be also observed that, since $\alpha$ corresponds to the dimensionless steady state concentration of intermediate radicals, this analysis is valid as long as this value is much smaller than the initial concentration of dormant chains. It can be shown that, as a result, the ratio between the maximum inhibition time and the process time is $t_{inhib}^{max}/t_{proc} = 1/(2\gamma)$, where $\gamma$ represents the ratio between the dead chains and the dormant chains at the characteristic process time. Accordingly, when the targeted livingness of the process is very large ($\gamma \ll 1$), large inhibition times can be actually observed.

It is now interesting to analyze the latter case in the presence of the intermediate termination ($0 < \varepsilon_r < 1$). This is shown in Figure 4, where again the radical concentrations are plotted versus the dimensionless time. An additional plateau appeared in the evolution of the radical concentration, $r$, at time $\tau = \tau_3$, while for shorter times the solution is identical to that in Figure 3. At $\tau = \tau_3$, an equilibrium is reached between the rates of radical initiation and bimolecular termination. However, due to the simultaneous termination of the radicals with the intermediate radicals, the overall rate of termination is larger compared to the cases in Figure 2 and 3 and, thus, a smaller QSS value is reached. On the other hand, every time an intermediate radical is consumed, a RAFT agent is subtracted from the activation/deactivation equilibrium. This leads to a faster consumption of the RAFT agent, so that, at $\tau = \tau_4$, no more dormant chains are available in the system and the reaction continues as a non-living one. As a side effect, the value of $r$ reaches its final steady-state, since the intermediate termination rate also drops to zero. Accordingly, in the presence of intermediate termination, a lower steady state value of the radical concentration is achieved [$r^2 = 1/(1 + 2\alpha\varepsilon_r d)$], thus explaining the occurrence of retardation in some experimental observations. It should be noted that recently a different intermediate termination mechanism has been proposed, which not involved the consumption of the RAFT agent.[13] In this case, the analysis remains valid up to the final decay in the dormant chain concentration.

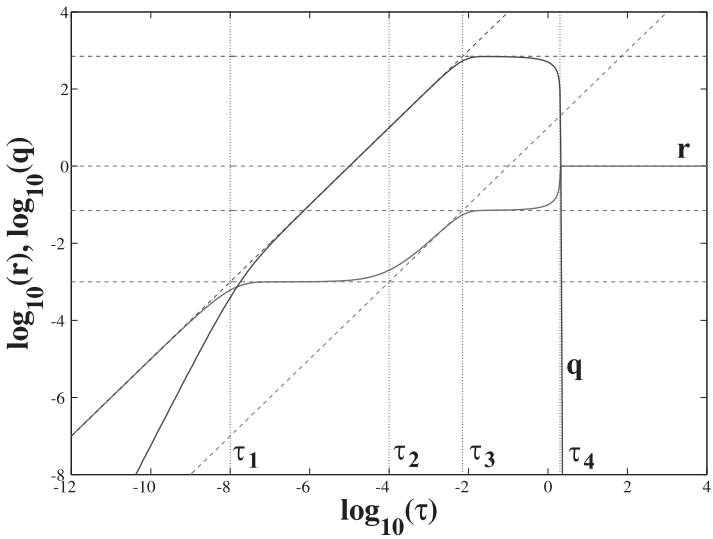


***Figure 4.***
Logarithmic dimensionless concentration of intermediate radicals (q) and radicals (r) versus non-dimensional polymerization time ($\tau$) for $\alpha = 10^4$ in the presence of intermediate termination ($\varepsilon_r = 10^{-2}$). More details in Ref. 12, Figure 8.

 

### Inhibition and Retardation in Segregated Systems

Living seeded emulsion polymerizations, using cumyl dithiobenzoate as RAFT agent, were performed at different levels of initiator and RAFT agent, as shown in Figure 5.[14] With respect to the central experiment, having an initial RAFT agent concentration equal to 8.41 mM and an initiator concentration of 1.7 mM, two more sets of experiments have been carried out to check the sensitivity on conversion to both RAFT agent and initiator concentration. It can be noticed that both inhibition time and slope of the conversion curve depend on the initiator as well as on the RAFT agent concentration. Whereas an increase of initiator concentration promotes larger reaction rates and shorter inhibition times, the opposite is true for the RAFT agent concentration: here, an increase leads to increased inhibition time and decreased reaction rate. Notably, the reaction rate is much more sensitive to RAFT agent than to initiator concentration.

To understand the changes in inhibition time and retardation, it is useful to analyze in detail the model results of the central experiment (Run 3 of Table 1) at two times during the reaction: (i) at the very beginning, when the polymerization rate is extremely small, so as to investigate the inhibition, and (ii) at the time where steady state is reached, so as to investigate the retardation. Figure 6 visualizes the situation at the beginning of the polymerization. The absorption of a short radical in $N_0$ particles (with frequency $a$) changes the particle state to $N_1$(short), where this notation indicates a particle with one ''short'' radical, i.e. a radical able to desorb. In the $N_1$(short) population, desorption dominates over all other mechanisms. However, the radical can also propagate and this changes the particle state to $N_1$(long), i.e. a radical which cannot desorb is formed. In this state, RAFT exchange with the RAFT agent dominates and leads to the formation of a RAFT leaving group radical. This brings the particle state back to $N_1$(short), since the RAFT leaving group is typically short and can be easily extracted by the aqueous phase. Since in $N_1$(short) the most likely fate of this radical is desorption, it can

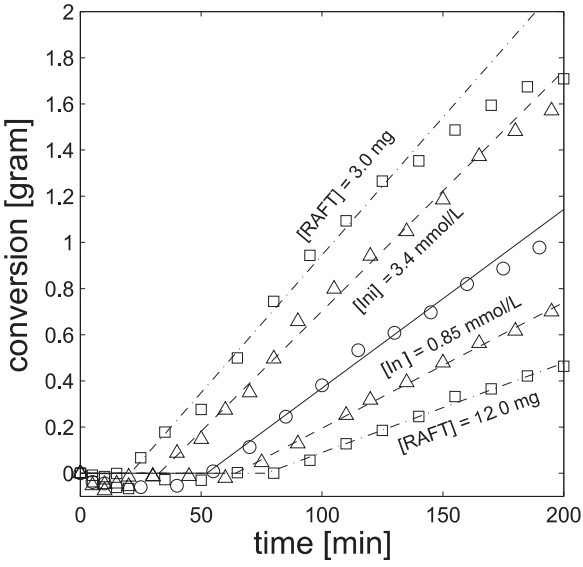


***Figure 5.***
Experimental conversion versus time curves for the living experiments in seeded emulsion. In the same figure, the effect of different initiator [Ini] and dormant chain [RAFT] concentration is plotted. More details in Ref. 13, Figure 2.

 

***Table 1.***
Comparison between the measured and the simulated values of inhibition time and polymerization rate at different initial concentrations of initiator and RAFT agent. For details refer to Table 5 in Ref. 13.

| Run | 1 | 2 | 3 | 4 | 5 |
|---|---|---|---|---|---|
| Initiator [mg] | 1.7 | 1.7 | 1.7 | 0.85 | 3.4 |
| RAFT Agent [mg] | 3 | 6 | 12 | 6 | 6 |
| Inhibition Time [min] (model/experiment) | 15/29 | 47/47 | 71/78 | 49/68 | 28/32 |
| Polymerization Rate [mg/min] (model/experiment) | 11.9/11.7 | 7.8/7.8 | 3.9/5.2 | 5.5/7.4 | 10.4/8.2 |

be concluded that in the presence of RAFT agent, all the kinetic events favor fast desorption. As a result, the reaction does not proceed, causing inhibition.

As the reaction proceeds, the amount of RAFT agent inside the particles slowly decreases and so does the frequency of exchange from $N_1$(long) to $N_1$(short). This corresponds to a reduction of the rate of desorption and, thus, to an increase in the polymerization rate, which takes place until all the RAFT agent is consumed and steady state is reached. This is depicted in Figure 7. At this point, the particles contain predominantly long dormant chains. Since upon RAFT exchange long radical chains are produced leaving unchanged the particle state, the situation is expected to be equal to that of a non-living polymerization. However, as shown in Figure 7, upon absorption of a short radical into a particle $N_0$, there are two pathways to change the particle state from $N_1$(short) to $N_1$(long):- the radical can either propagate, as typical of non-living reactions, or it can undergo a RAFT exchange with a long dormant chain. Notably, this exchange is typically faster than propagation and leads to the formation of short dormant chains. In other words, by radical entry a small but significant amount of short dormant chains accumulates in the particles. Once activated, these short dormant chains are producing short radicals which can promptly desorb, thus depressing the polymerization rate and causing the phenomenon of retardation. Thus concluding, both inhibition and retardation in segregated systems can be justified by accounting for the desorption of short radicals originated by the presence of short dormant chains. In other words, it is not necessary to account for the presence of radical intermediates, as in non-segregated systems, to explain inhibition and retardation.

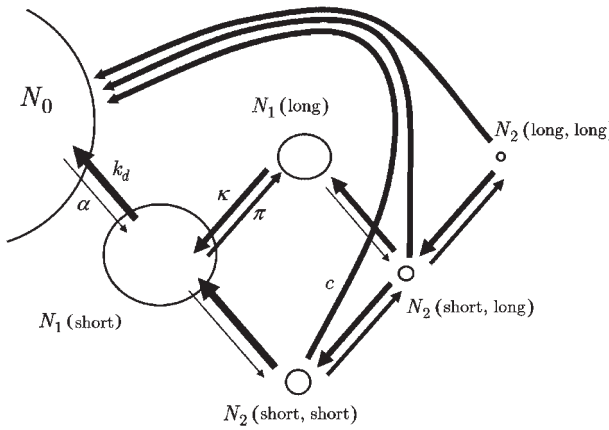


***Figure 6.***
Visualization of the particle population at the beginning of the living reactions (inhibition period). More details in Ref. 13, Scheme 3.

 

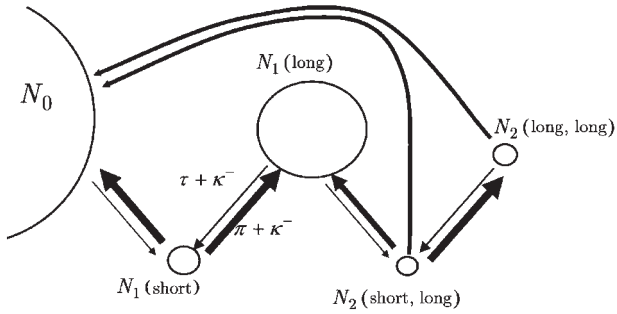


***Figure 7.***
Visualization of the particle population of the living reactions just after the system has reached steady state conditions (retardation). More details in Ref. 13, Scheme 4.

**Gel Effect in Non-Segregated Systems**

Recently, a model to evaluate the CLD and the polymerization rate in RAFT polymerizations in bulk at high conversion has been developed.[4] In the model, the presence of intermediate radicals and diffusion limitations for all involved reactions have been accounted for. Then, not only the rate constant of bimolecular termination but also that of RAFT addition are supposed to be conversion and chain-length-dependent. In particular, the kinetic rate constants of these two bimolecular reactions have been evaluated according to the following general expression:

$$\frac{1}{k_{eff}} = \frac{1}{k_0} + \frac{1}{4\pi r_{AB} \mathrm{D}_{AB} N_A} \qquad (3)$$

where $k_{eff}$ is the effective rate constant, $k_0$ the kinetic rate constant of the reaction in the absence of diffusion limitations, $r_{AB}$ and $\mathrm{D}_{AB}$ the radius of interaction and the mutual rate of diffusion between the chains A and B, respectively, and $N_A$ the Avogadro's number. The diffusion coefficient, $\mathrm{D}_{AB}$, is a function of both chain length of the polymers and monomer conversion. The complex resulting set of PBEs has been solved numerically with the discretization method originally proposed by Kumar and Ramkrishna.[15]

Model validation has been carried out by performing several experimental runs, operated under both living and nonliving conditions, in which the effects of the initial concentrations of initiator and RAFT agent on both the conversion and CLD as a function of time have been investigated. The diffusion limitations on the reaction rate constants have been estimated using the free volume theory of diffusion,[16] with all the involved parameters taken from independent literature sources. The only exception is represented by the chain diffusion coefficient, for which the exponential dependence on the chain length has been reduced by about 20% with respect to the original one. This change is needed to compensate for the fact that viscosity in non-living systems is smaller than that in the corresponding living systems at the same conversion, due to the fact that the polymer chains are generally shorter. The values of the reaction rate constants have also been taken from independent literature sources, with the only exception of the RAFT exchange ones, which have been fitted to the experimental data.

On the whole, the agreement of the model results with the experimental data is satisfactory. This agreement can be appreciated in Figure 8, where the comparison between the experimental data (open symbols) and the model simulation (solid curves) is shown for two sets of living reactions at different amounts of initiator (left figure) and RAFT agent (right figure), respectively. The model correctly predicts the system behavior at high conversion values, at which the effect of diffusion limitations on the reaction rate constants becomes important. In particular, it can be

 

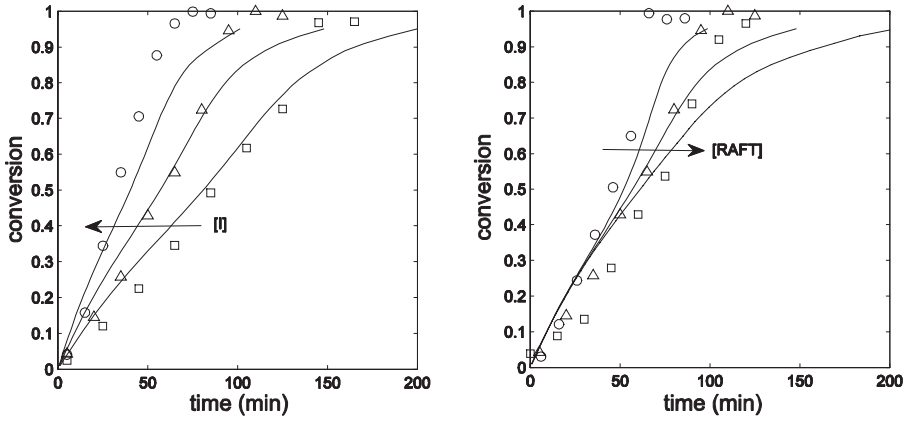


*Figure 8.*
Experimental conversion versus time for a living polymerization in bulk with different initial initiator concentrations (left figure) and RAFT agent concentrations (right figure). Open symbols: experimenal points; solid curves: model predictions. More details in Ref. 4(a), Figures 6 and 7.

shown that the effect of the RAFT reaction rate constants on the conversion curves is negligible, whereas the diffusion rate constant of the monomer as a function of the conversion plays a fundamental role. On the contrary, the knowledge of the rate of addition in the RAFT reaction is fundamental in the prediction of the evolution of the polymer chain distribution.

These effects have been analyzed in more detailed in a separate work.[4b] In particular, it was carried out a comparison between a model accounting for the complete CLD and a simplified model in which the different rate constants are function of the average degree of polymerization (DP), evaluated by the method of moments. Even though it was expected that for living polymerizations the results of the two models would be almost equal due to the typically small polydispersity of the CLD, it was found that the differences between the two models can actually be significant.

In order to provide a general criterion to determine a priori whether the CLD-dependent model has to be used, a critical chain length, $DP_{crit}$, at which the rate of the diffusion step of a bimolecular reaction equals the rate of the chemical step, i.e. where the two terms in the right hand side of Eq (3) become equal, has been defined. The so defined critical DP is shown in Figure 9 for both the bimolecular termination (dashed curve) and the RAFT addition (dash-dotted curve) reactions. In the same figure, the evolution of the average degree of polymerization of the radical chains for three different polymerizations is shown: non-living (NL), living (L) and so-called ''long''-living (LL) polymerization, where the target degree of polymerization is very large and comparable to that of the non-living case. It has been found that the two models give different results shortly after the DP of the system reaches its critical value. As far as termination rate and conversion are concerned (open circles in Figure 9), this happened below 40% conversion in all the investigated case studies.

Above this point, the conversion curves obtained with the two models differed significantly from each other, as shown in Figure 10, where the conversion plots as a function of time are reported for the three cases. Two important effects can be observed: when the critical degree of polymerization is reached (open circles), the conversion rate accelerates as a result of the diffusion limitations. At the same time, the conversion curves predicted by the complete model (dashed curves) start differing significantly from the simplified model (solid curves), where the CLD

 

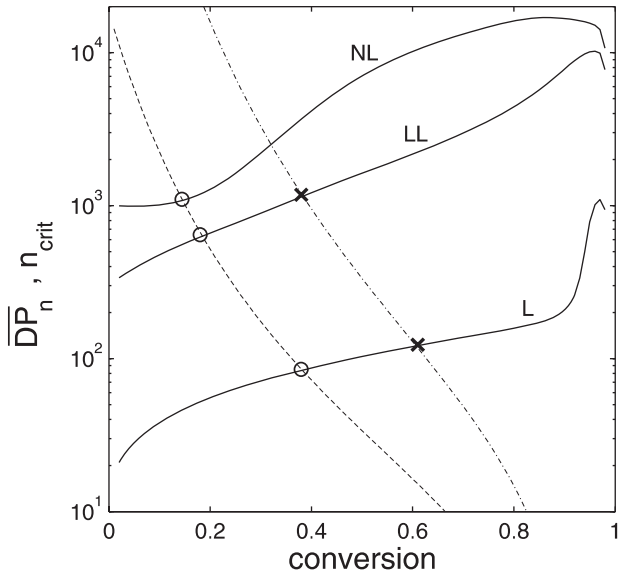


***Figure 9.***
Critical DP for termination (dashed curve) and RAFT addition (dash-dotted curve) as a function of conversion. Solid curves: DP for three model polymerizations. More details in Ref. 4(b), Figure 5(a).

moments only are accounted for. This difference is very pronounced even in the case of living polymerizations, in spite of the narrow chain length distribution of the radical chains observed in this case. In particular, the kinetics predicted by the simplified model is always faster than that predicted by the complete model. In fact,

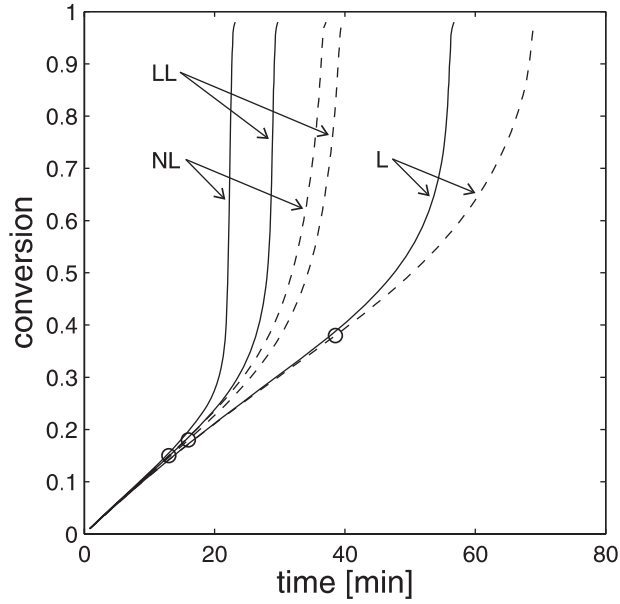


***Figure 10.***
Conversion curves for the model polymerizations of Figure 9. Solid curve: simplified model; dashed curves: full model; circles: conversion at which the critical DP is reached. More details in Ref. 4(b), Figure 1.

 

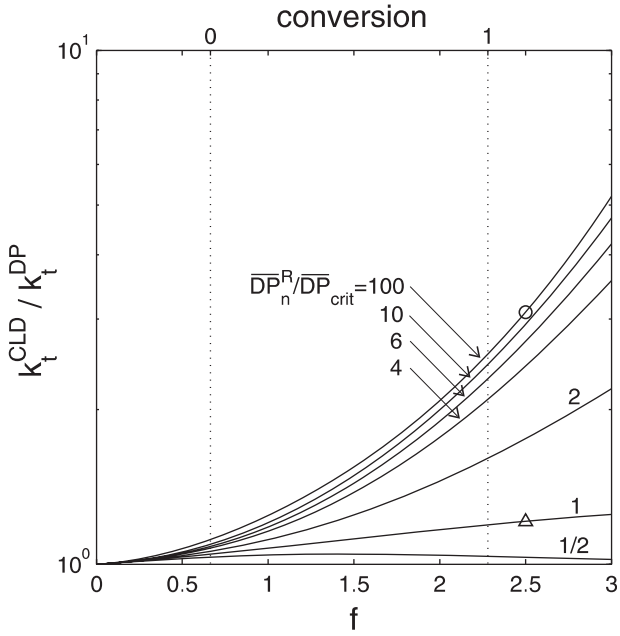


***Figure 11.***
Ratio between the termination rate constant computed by the complete ($k_t^{CLD}$) and the simplified model ($k_t^{DP}$) for a model distribution of radical chains with $P_d = 1.2$. See the text for the definition of f. More details in Ref. 4(b), Figure 8(a).

the role played by the short radical chains is neglected in the simplified model and the diffusion limitations are overestimated. The extent of this effect is quantified in Figure 11 for a model distribution having a relatively narrow polydispersity of the CLD equal to 1.2. In this figure, the quantity f on the abscissa is linearly proportional to conversion, as indicated by the top axis, and it represents the dependence of the diffusion coefficient of a polymer chain, $D_p$, upon its chain length, $n$ ($D_p \propto n^{-f}$). It should be noticed that the value of f generally ranges between about 0.5 and 2.5 for null and full conversions, respectively (the case in Figure 11 refers to PMMA). In the same figure it can be observed that, the kinetic rate constant predicted by the complete model strongly differs from that predicted by the simplified model, especially at high conversions. This effect becomes even more pronounced when broader distributions are analyzed, for which the difference can be of several orders of magnitude. It is also worth noting that the same difference can be observed on the prediction of the CLD of the dormant chains. In Figure 12, the polydispersity predicted by the two models is compared. It

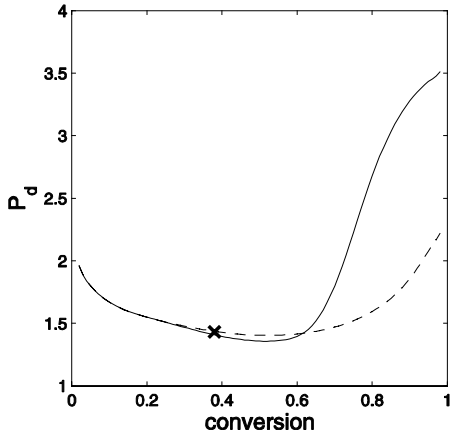


***Figure 12.***
Polydispersity versus conversion for the model polymerization LL of Figure 9. Solid curve: simplified model; dashed curves: complete model; cross: conversion at which the critical DP is reached. More details in Ref. 4(b), Figure 4(b).

 

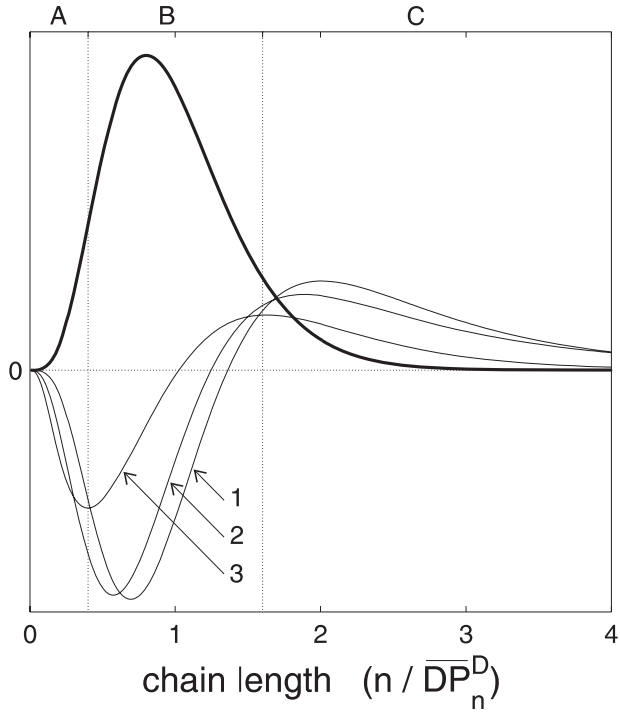


***Figure 13.***
Full solid curve: starting model dormant CLD; solid curves: change in the CLD ($dD_n/dt$) for three levels of diffusion limitations. More details in Ref. 4(b), Figure 9(c).

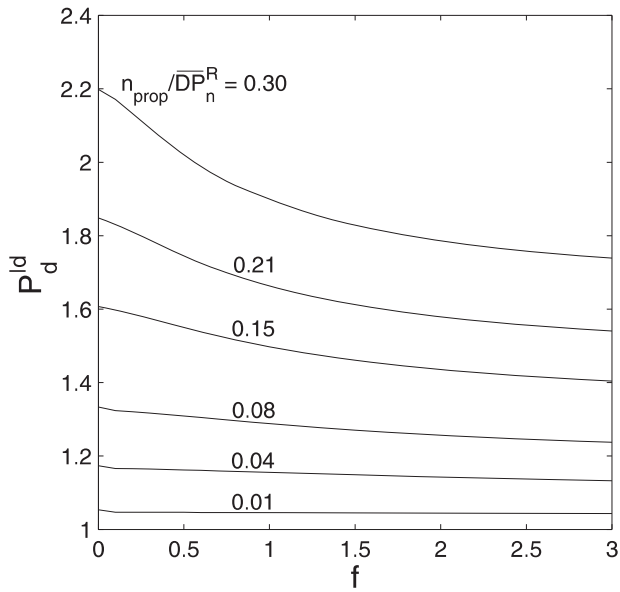


***Figure 14.***
Ideal polydispersity value for different intensities of the diffusion limitations (f) and different number of propagations steps per active step. See the text for the definition of f. More details in Ref. 4(b), Figure 10.

 

can be observed that, as soon as the critical degree of polymerization for the RAFT addition is reached (cross), the prediction of the two models starts to significantly deviate from each others.

It was also verified that diffusion limitations are favoring the production of narrower dormant chain length distributions. This effect can be observed in Figure 13, where for a model dormant CLD (bold solid curve), the change in time of the CLD has been computed for three different levels of diffusion limitations. In Case 3 (strongest diffusion limitations), the number of short dormant chains consumed is larger than in the case without diffusion limitations (Case 1), while, at the same time, the number of long dormant chains produced is smaller, thus resulting in narrower CLD. In order to quantify this effect, the concept of *ideal polydispersity* was introduced: it is the polydispersity value approached by the system when evolving under constant conditions. Two parameters are mainly affecting this value: the ratio between the average chain length and the average number of propagation steps in between two RAFT additions ($n_{prop}/DP_n^R$), and the intensity of diffusion limitations, quantified by the parameter $f$ in Figure 14. It can be observed that smaller polydispersity values of the dormant CLD are obtained for both large diffusion limitations and small number of monomer additions per active period. All these important effects can be captured only if a numerical model accounting for the complete CLD is used.

## Concluding Remarks

In this work, the importance of using detailed models to describe the RAFT polymerization kinetics is shown. In particular, it is shown how such models can successfully account for unexpected behaviors such as inhibition, retardation and diffusion limitations in both non-segregated (bulk) and segregated (emulsion) systems. With respect to the first two phenomena, it is important to notice that the same behavior can have very different origins. In the case of non-segregated systems, inhibition and retardation can be explained only by accounting for the complete RAFT kinetics and, in particular, by accounting for the fundamental role played by the intermediate radicals. On the other hand, it is not strictly necessary to account for these radicals to explain the same experimental evidence in segregated systems. As a matter of fact, in this case inhibition and retardation are mainly caused by radical segregation and, in particular, by desorption of radical chains caused by the activation of short dormant chains. Clearly, the same mechanisms discussed for non-segregated systems remain operative and they could partly contribute to determine the final behavior of the reaction. Future work is then needed to determine to which extent intermediate radicals can contribute to inhibition and retardation in the presence of radical segregation.

*Acknowledgements:* This work was financially supported by Suisse National Science Foundation (Grant No. 200020-101714).

[1] J. Chiefari, Y. K. Chong, F. Ercole, J. Krstina, J. Jeffery, T. P. T. Le, R. T. A. Mayadunne, G. F. Meijs, C. L. Moad, G. Moad, E. Rizzardo, S. H. Thang, *Macromolecules* **1998**, *31*, 5559.
[2] G. Moad, J. Chiefari, Y. K. Chong, J. Krstina, R. T. A. Mayadunne, A. Postma, E. Rizzardo, S. H. Thang, *Polym. Int.* **2000**, *49*, 993.
[3] M. Monteiro, H. de Brouwer, *Macromolecules* **2001**, *34*, 349.
[4] [4a] A. D. Peklak, A. Butté, G. Storti, M. Morbidelli, *J. Polym. Sci. Part A: Polym. Chem.* **2006**, *44*, 1071. [4b] A. D. Peklak, A. Butté, *Macromol. Theory Simul.* **2006**, *15*, 546.
[5] M. J. Monteiro, M. Hodgson, H. De Brouwer, *J. Polym. Sci. Part A: Polym. Chem.* **2000**, *38*, 3864.
[6] B. Apostolovic, F. Quattrini, A. Butté, G. Storti, M. Morbidelli, *Helv. Chim. Acta* **2006**, *89*, 1641.
[7] [7a] A. Butté, G. Storti, M. Morbidelli, *Macromolecules* **2001**, *34*, 5885; [7b] A. Butté, G. Storti, M. Morbidelli, *Macromolecules* **2000**, *33*, 3485.
[8] W. W. Smulders, C. W. Jones, F. J. Schork, *Macromolecules* **2004**, *37*, 9345.
[9] S. W. Prescott, M. J. Ballard, E. Rizzardo, R. G. Gilbert, *Macromolecules* **2002**, *35*, 5417.

 

[10] A. R. Wang, S. Zhu, *Macromol. Theory Simul.* **2003**, *12*, 196.
[11] H. Fischer, *Macromolecules* **1997**, *30*, 5666.
[12] A. Butté, A. D. Peklak, *Macromol. Theory. Simul.* **2006**, *15*, 285.
[13] A. D. Peklak, A. Butté, *J. Polym. Sci. Part A: Polym. Chem.* **2006**, *44*, 6144.
[14] M. Buback, P. Vana, *Macromol. Rapid Commun.* **2006**, *27*, 1299.
[15] [15a] S. Kumar, D. Ramkrishna, *Chem. Eng. Sci.* **1996**, *51*, 1311; [15b] A. Butté, G. Storti, M. Morbidelli, *Macromol. Theory Simul.* **2002**, *11*, 22.
[16] P. A. Müller, G. Storti, M. Morbidelli, *Chem. Eng. Sci.* **2005**, *60*, 377.

 

 DOI: 10.1002/masy.200750219

# Reaction Calorimetry for the Development of Ultrasound-Induced Polymerization Processes in $CO_2$-Expanded Fluids

*Maartje F. Kemmere,*[*1,2] *Martijn W.A. Kuijpers,*[1] *Jos T.F. Keurentjes*[1]

**Summary:** A strong viscosity increase upon polymerization hinders radical formation during an ultrasound-induced bulk polymerization. Since $CO_2$ acts as a strong anti-solvent for most polymers, it can be used to reduce the viscosity of the reaction mixture. In this work, a process for the ultrasound-induced polymerization in $CO_2$-expanded fluids has been developed. Temperature oscillation calorimetry has been applied to study the influence of $CO_2$ on the viscosity during the ultrasound-induced polymerization. In contrast to polymerizations in bulk, the results show that a low viscosity is maintained during polymerization reactions in $CO_2$-expanded methyl methacrylate (MMA). As a consequence, a constant or even increasing polymerization rate is observed when pressurized $CO_2$ is applied. Moreover, the ultrasound-induced polymer scission in $CO_2$-expanded MMA is demonstrated, which appears to be a highly controlled process. Finally, a preliminary sustainable process design is presented for the production of 10 kg/hour pure PMMA (specialty product) in $CO_2$-expanded MMA by ultrasound-induced initiation.

**Keywords:** cavitation; molecular weight distribution; pressurized carbon dioxide; radical polymerization; ultrasound

## Introduction

The chemical effects of ultrasound arise from cavitation, i.e. the collapse of microscopic bubbles in a liquid. Upon implosion of a cavity, locally extreme conditions in the bubble occur (5000 K and 200 bar)[1] and high strain rates are generated outside the bubble ($10^7$ $s^{-1}$).[2] Monomer molecules are dissociated by the high temperatures inside the hot-spot, whereas polymer chains are fractured by the high strain rates outside the cavitation bubble.[3–5] Since the radicals are generated in-situ by ultrasound, no initiator or catalyst is required to perform an ultrasound-induced polymerization. An additional advantage of this technique is the intrinsic safe operation, because turning off the electrical power supply will immediately stop the radical formation and consequently the polymerization reaction.

Viscosity is an important factor during ultrasound-induced bulk polymerizations as the long polymer chains formed upon reaction cause a drastic increase in the viscosity of the reaction mixture,[6] thereby hindering cavitation and consequently reducing the production rate of radicals.[7] Precipitation polymerization forms a potential solution to this problem, because a constant viscosity and hence a constant radical formation rate can be maintained. In this perspective, high-pressure carbon dioxide is an interesting medium as most monomers have a high solubility in $CO_2$, whereas it exhibits an anti-solvent effect for most polymers.[8]

[1] Process Development Group, Department of Chemical Engineering & Chemistry, Eindhoven University of Technology, P.O. Box 513, 5600 MB, The Netherlands
Tel: +31-40-2473673; Fax: +31-40-2446104
E-mail: M.F.Kemmere@tue.nl
[2] Current address: Friesland Foods Corporate Research, P.O. Box 87, 7400 AB Deventer, The Netherlands,
Tel: +31-570-695981; Fax: +31-570-695918
E-mail: maartje.kemmere@frieslandfoods.com

Up till now ultrasound is rarely studied at higher pressures, because in most cases a high static pressure hampers the growth of cavities. Recently, we have shown that cavitation is possible in pressurized $CO_2$.[9] Unlike ordinary liquids, carbon dioxide has a high vapor pressure, which counteracts the static pressure.[10] Cavitation is possible if the difference between the static and vapor pressure is smaller than the maximum acoustic pressure that can be applied.[11] Dense-phase fluids (with a strong emphasis on $CO_2$) provide possibilities for the development of sustainable polymer processes.[12,13] Additionally, ultrasound combined with high-pressure carbon dioxide allows the development of clean routes to produce polymers with specific properties, since no organic anti-solvents are required.

In this work, a process for the ultrasound-induced polymerization in $CO_2$-expanded MMA has been developed. For this purpose, ultrasound-induced polymerization and scission experiments have been performed in a RC1e HP60 reactor (Mettler-Toledo GmbH, Switzerland) extended with a Sonics and Materials VC-750 ultrasonic generator. Moreover, a preliminary process design of an ultrasound-induced polymerization process is presented for a 10 kg/h industrial plant to produce specialty PMMA.

## Ultrasound-Induced Polymerization

In ultrasound-induced polymerization reactions, the viscosity has a large influence on the radical formation rate. Therefore, it is important to monitor the viscosity during these reactions. By coupling the overall heat transfer coefficient $U$ to the viscosity of the reaction mixture, the influence of the $CO_2$-concentration on the viscosity of polymer solutions has been determined.[14,15]

$$\frac{1}{U} = \frac{1}{h_i} + \frac{D_i}{2k_w}\ln\frac{D_0}{D_i} + \frac{1}{h_0}\frac{D_i}{D_0} \quad (1)$$

In Equation 1 the heat transfer coefficient is based on the inside area of the reactor, for which $h_i$ and $h_o$ represent the partial heat transfer coefficients in the vessel and in the jacket, respectively; $k_w$ stands for the thermal conductivity coefficient of the wall; $D_i$ and $D_o$ are the inner and outer diameter of the vessel.

The last two terms of Equation 1 remain constant during a polymerization reaction, because the properties of the reactor wall and cooling liquid will not change during the experiments. This is only true for low polymer concentrations present in the reaction mixture, as used for these experiment. If reactor fouling would occur at higher polymer concentration, obviously the assumption of constant properties of the reactor wall are no longer valid. However, when no fouling occurs and the last two terms of Equation 1 remain constant, $U$ is an indirect measure of the viscosity of the reaction mixture, since the empirical relation for the Nusselt number ($Nu$) as a function of the Reynolds ($Re$) and Prandtl number ($Pr$) can be applied to couple $h_i$ to the viscosity. Equation 5, which is derived from Equations 2, 3 and 4, shows the influence of the viscosity on the overall heat-transfer coefficient. An increase in the viscosity ($\mu$) thus results in a decrease of the overall heat transfer coefficient.

$$Nu = \frac{h_i D_i}{k_i} = 0.75\,\mathrm{Re}^{2/3}\,\mathrm{Pr}^{1/3} \quad (2)$$

Where the Reynolds and the Prandtl number stand for:

$$\mathrm{Re} = \frac{\rho N D^2}{\mu} \quad (3)$$

$$\mathrm{Pr} = \frac{\mu C_p}{k_i} \quad (4)$$

$$\frac{1}{U} \sim \sqrt[3]{\mu} + \mathrm{Constant} \quad (5)$$

First some calibration experiments have been performed to determine the overall heat transfer coefficient $U$ for polymer solutions in which no polymerization occurs. Figure 1A shows the influence of the polymer concentration ($Cpol$) and $CO_2$ fraction on U and consequently on the liquid viscosity. The plotted difference ($\Delta U$) is calculated by subtracting U of the system with polymer present ($U(Cpol)$) from $U$

 

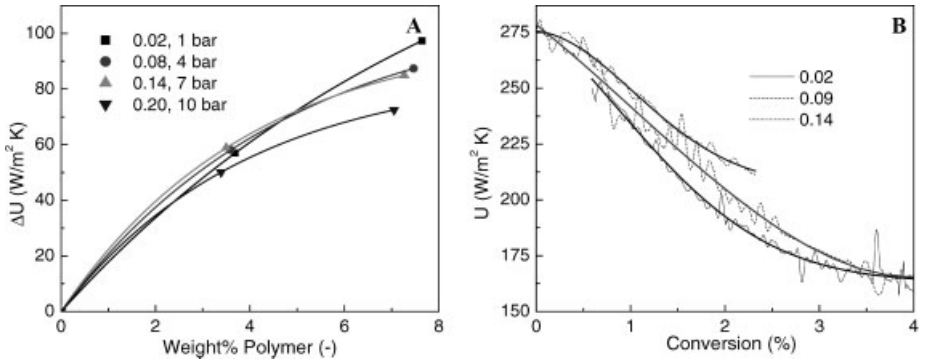


***Figure 1.***
**A** Heat transfer coefficient difference $\Delta U$ as a function of the polymer weight percentage at different $CO_2$ fractions. **B** Development of the overall heat transfer coefficient $U$ during the polymerization reactions at three different $CO_2$ fractions.

without polymer ($U(0)$) at a given $CO_2$ fraction (Equation 6). The curves in Figure 1 give the trend of the heat transfer decrease and consequently the viscosity increase (Equation 5).

$$\Delta U = U(0) - U(C_{pol}) \quad (6)$$

According to Figure 1A, at polymer concentrations above 4 weight percent, a distinct difference between the overall heat transfer coefficients at different $CO_2$ fractions is obtained. This is a clear evidence for the anti-solvent effect of $CO_2$, since at higher $CO_2$ fractions $\Delta U$ is lower due to a smaller increase in viscosity. The smaller viscosity enhancement is caused by a stronger anti-solvent effect, which forces the polymer coils to be less extended in the reaction mixture.[8] It is not a dilution effect, resulting from the expansion of MMA by $CO_2$, as this is taken into account by the calculation of the polymer concentration. It should be noted that the anti-solvent effect in Figure 1A is most clearly visible by comparing $CO_2$-fractions 0.02 and 0.20 at the highest polymer concentration measured, respectively.

Figure 1B shows the development of $U$ upon polymerization, which is determined by temperature oscillation calorimetry.[16,17] It can clearly be seen that the decrease in $U$ is smaller and hence the increase in viscosity is lower for higher $CO_2$ fractions during polymerization. This is a result of the smaller gyration radius of the polymer coils due to the anti-solvent effect.[8] No precipitated polymer has been observed at the final conversion.

In Figure 2, the ultrasound-induced bulk polymerization with argon, added to saturate the cavitation bubbles, is compared to the set of polymerization reactions pressurized with $CO_2$ (i.e. $CO_2$-fraction 0.02 versus $CO_2$-fractions 0.08, 0.14 and 0.20, respectively). In this comparison, it is obvious from both the conversion-time history as well as the polymerization rate curves that during the ultrasound-induced bulk polymerization the reaction rate is declining, whereas the polymerization rate remains constant or even increases when pressurized $CO_2$ is used. The variation in calculated reaction rates for the $CO_2$-fractions 0.08, 0.14 and 0.20, is simply caused by the inaccuracy of determining the derivative of the conversion-time history curves. Still, Figure 2A already shows the significant difference between the decrease in polymerization rate of the experiment with $CO_2$-fraction 0.02 versus the maintained reaction rate for the polymerizations with $CO_2$-fractions 0.08, 0.14 and 0.20, respectively.

Typically, in ultrasound-induced bulk polymerizations a maximum conversion of approximately 15% can be achieved.[7] At this conversion the collapse of cavitation

 

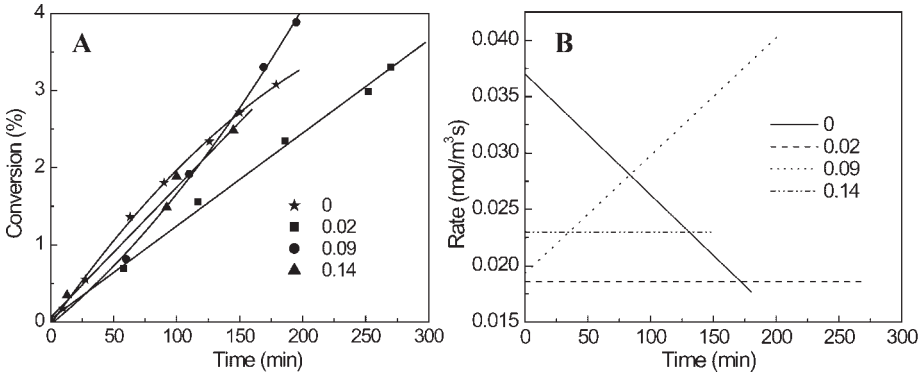


***Figure 2.***
Ultrasound-induced polymerizations in $CO_2$-expanded MMA at various $CO_2$ fractions. **A** Conversion-time history. **B** Reaction rates. Note that in the experiment without $CO_2$ present, argon has been added to saturate the cavitation bubbles.

bubbles is no longer sufficiently strong to generate radicals by ultrasound, due to the high viscosity. The decrease in viscosity by the $CO_2$ anti-solvent effect indicates that higher conversions in $CO_2$-expanded MMA as compared to bulk MMA would be possible. Moreover, at higher conversions the polymer will precipitate in the presence of an anti-solvent, due to which a constant viscosity is maintained and even higher conversions are expected.

### Ultrasound-Induced Polymer Scission

Besides polymerization, ultrasound-induced polymer scission reactions have been investigated. Ultrasound-induced polymer scission is a well-controlled process, as fracture occurs approximately in the middle of the chain, see Figure 3. A mechanism is proposed for this non-random fracture behavior,[18] from which it can be concluded that complete stretching of the polymer chains is required before breakage can occur. The developed model, which is a combination of strain rate and drag force calculations, predicts a limiting molecular weight and a quadratic dependence of the polymer molecular weight on the scission rate, which have experimentally been confirmed. The developed degradation model is also capable to describe the effects of various process variables on cavitation-induced polymer scission, such as the lower scission rate at a higher liquid viscosity.

At increasing polymer concentration, the scission process becomes less effective and eventually stops. This is a drawback for the development of a scission process based on ultrasound, because concentrated polymer systems are favored in industry. The addition of an anti-solvent for the polymer can prevent the increase in viscosity at higher polymer concentrations. To determine the influence of $CO_2$ as an anti-solvent on the ultrasound-induced scission rate,

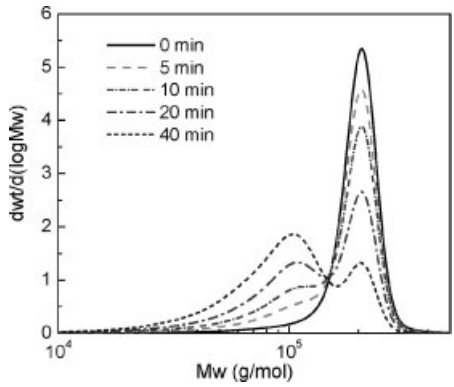


***Figure 3.***
Highly controlled ultrasound-induced polymer scission of 0.1 wt% PMMA in MMA in the presence of the radical scavenger 1,1-diphenyl-2-picrylhydrazyl (DPPH) to prevent further polymerization of the formed macro-radicals.

 

ultrasonic scission experiments of PMMA have been performed in bulk MMA as well as in $CO_2$-expanded MMA. Modeling the experimental time-dependent molecular weight distributions (MWD) has revealed the scission kinetics at different polymer concentrations and $CO_2$ fractions.[19] The model is composed of a dynamic bubble simulation and a bead-rod model. The dynamic cavitation calculations predict that total stretching of a polymer chain is possible during explosive growth and collapse of a cavitation bubble in microseconds. This is a prerequisite for scission at the polymer chain center. With the bead-rod model a limiting molecular weight of $6^{*}10^{4}$ g/mol is calculated for PMMA dissolved in MMA, which has been experimentally confirmed. An almost squared dependence of the molecular weight on the scission rate is obtained from the measured time-dependent molecular weight distributions. Moreover, the general degradation model is capable to describe the effects of various process variables on cavitation-induced polymer scission.

## Preliminary Process Design

Applications of ultrasound in processing and synthesis are widespread on laboratory scale. However, no industrial plant in which ultrasound initiates a polymerization reaction has been built so far. This is a consequence of the relatively low energy efficiency ($10^{-5}$ J/J) for the generation of radicals in the ultrasound process,[20] which results in a high electrical power consumption. For the development of an economically feasible bulk process (larger than 5000 kg/h), the energy conversion still needs to be improved. For specialty products, however, it is expected that an ultrasound-based process can be viable. A product with a high-added value has thus to be produced, e.g. polymers for biomedical applications. These types of polymers have stringent demands concerning impurities, such as catalyst and initiator traces, residual monomer and organic solvents. With the ultrasound-induced polymerization process in $CO_2$, no initiators and organic solvents are required. In this work, a preliminary process design has been developed to produce 10 kg/hour pure PMMA (specialty product) in $CO_2$-expanded MMA by ultrasound-induced initiation, which has resulted in the clean, closed-loop process shown in Figure 4.[21]

The MMA fed to the reactor is converted to PMMA till a conversion of 15%. The product stream (2) consisting of PMMA, MMA and $CO_2$, is sprayed into the extraction column, in which it is contacted with supercritical $CO_2$ counter currently. The PMMA precipitates and the MMA dissolves in the supercritical phase. This extraction process is better known as the Supercritical Anti-Solvent process

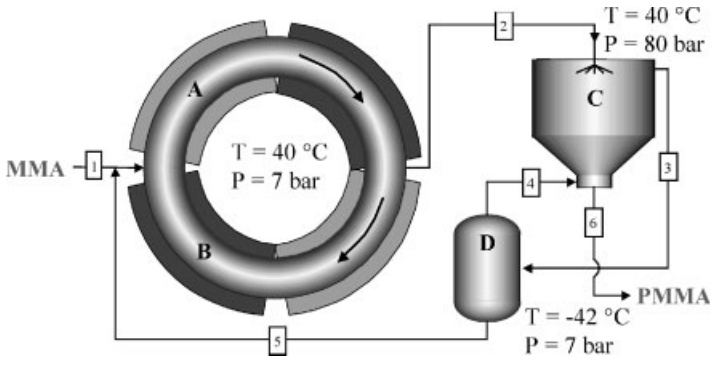


***Figure 4.***
Process flow diagram of the ultrasound-induced polymerization of MMA in $CO_2$-expanded MMA; with cavitation (A) and cooling areas (B) in a loop reactor, an extraction column (C) and a separation unit (D).

 

(SAS).[22] Typically, residual monomer concentration in the final product can go down to 10 ppm,[23] because of the significant extraction capacity of $CO_2$ for MMA. However, in literature no references have been found that describe the extraction of large amounts of MMA from PMMA. Therefore, it is assumed that 20 times (molar basis) the amount of $CO_2$ is required to produce pure PMMA. The resulting MMA/$CO_2$-stream from the SAS-column (3) is separated in a flash-drum (D) into almost pure $CO_2$ (4) and MMA (5). The flash-drum is operated adiabatically at 7 bar, resulting in an operation temperature of −42 °C. The cold $CO_2$ stream has to be recompressed to 80 bar before it can be reintroduced into the extraction column, which requires a compressor of 24 kW. By compression, the $CO_2$ is heated to 180 °C, which has to be cooled down to 40 °C. The cold MMA stream (5) can be added directly at multiple places into the loop reactor, which already results in a cooling capacity of approximately 30 kW.

## Conclusions and Outlook to the Future

In this study, the potentials and challenges of ultrasound-induced polymerization and scission reactions in high-pressure fluids have been explored. It can be concluded that ultrasound allows producing well-defined polymers in $CO_2$-expanded fluids without using additional chemicals. Still, the energy consumption and the relatively low polymerization rates make it a relatively expensive way to produce polymers. An improved energy efficiency and polymerization rate would enable a larger application potential for ultrasound-induced polymerization processes than specialty polymers only. Although no large-scale industrial polymerization processes based on ultrasound exist yet, commercial applications in other fields such as ultrasound cleaning and sterilization prove that ultrasound is a readily available technique. Nevertheless, the application of ultrasound for polymerization purposes requires a thorough multidisciplinary understanding of ultrasound parameters, liquid properties and polymerization kinetics, for which reaction calorimetry has proven to be a indispensable tool.

### Notation

| | |
|---|---|
| $\mu$ | Viscosity (Pa s) |
| $\rho$ | Density (kg/m$^3$) |
| $C_p$ | Specific heat capacity (J/kg K) |
| D | Impeller diameter (m) |
| $D_0$ | Outer diameter of reactor (m) |
| $D_i$ | Inner diameter of reactor (m) |
| $h_i$ | Partial heat transfer coefficient reactor (W/m$^2$ K) |
| $h_0$ | Partial heat transfer coefficient jacket (W/m$^2$ K) |
| $k_i$ | Conductivity of liquid inside reactor (W/m K) |
| $k_0$ | Conductivity of liquid inside jacket (W/m K) |
| $k_w$ | Conductivity of reactor wall (W/m K) |
| N | Stirrer speed (s$^{-1}$) |
| Nu | Nusselt number (−) |
| Pr | Prandtl number (−) |
| Re | Reynolds number (−) |
| U | Overall heat transfer coefficient (W/m$^2$ K) |

[1] Y. T. Didenko, W. B. Mcnamara III, K. S. Suslick, *Nature*, **2000**, *407*, 877.
[2] T. Q. Nguyen, Q. Z. Liang, H.-H. Kausch, *Polymer*, **1997**, *38*, 3783.
[3] P. Kruus, *Ultrasonics*, **1987**, *25*, 20.
[4] G. J. Price, P. J. West, P. F. Smith, *Ultrason. Sonochem.*, **1994**, *1*, S51.
[5] M. W. A. Kuijpers, M. F. Kemmere, J. T. F. Keurentjes, "Ultrasound-induced radical polymerization." In: "*Encyclopedia of Polymer Science and Technology*.", John Wiley & Sons, New York, **2004**.
[6] J. M. Pestman, J. B. F. N. Engberts, F. de Jong, *Recl. Trav. Chim. Pays-Bas*, **1994**, *113*, 533.
[7] G. J. Price, *Ultrasonics Sonochemistry*, **1996**, *3*, S229.
[8] D. A. Canelas, J. M. DeSimone, *Adv. Pol. Sci.*, **1997**, *133*, 103.
[9] M. W. A. Kuijpers, D. van Eck, M. F. Kemmere, J. T. F. Keurentjes, *Science*, **2002**, *298*, 1969.
[10] M. W. A. Kuijpers, M. F. Kemmere, J. T. F. Keurentjes, *Ultrasonics Sonochemistry*, **2006**, accepted.
[11] T. J. Leighton, "*The Acoustic Bubble*", Academic Press, London, 1994.

 

[12] P. G. Jessop, W. Leitner, "*Chemical Synthesis using Supercritical Fluids*", Wiley-VCH, Weinheim, 1999.
[13] M. A. Abraham, L. Moens, "*Clean Solvents, Alternative Media for Chemical Reactions and Processing*", ACS Symposium Series 819, Washington, 2002.
[14] M. F. Kemmere, J. Meuldijk, A. A. H. Drinkenburg, A. L. German, *Polymer Reaction Engineering*, **2000**, *8*, 271.
[15] M. W. A. Kuijpers, L. J. M. Jacobs, M. F. Kemmere, J. T. F. Keurentjes, *AIChE J.*, **2005**, *51*, 1726.
[16] R. Carloff, A. Proβ, K.-H. Reichert, *Chem. Eng. Tech.*, **1994**, *17*, 406.
[17] A. Tietze, A. Proβ, K.-H. Reichert, *DECHEMA Monogr.*, **1995**, *131*, 673.
[18] M. W. A. Kuijpers, P. D. Iedema, M. F. Kemmere, J. T. F. Keurentjes, *Polymer*, **2004**, *45*, 6461.
[19] M. W. A. Kuijpers, R. M. H. Prickaerts, M. F. Kemmere, J. T. F. Keurentjes, *Macromolecules*, **2005**, *38*, 1493.
[20] M. W. A. Kuijpers, M. F. Kemmere, J. T. F. Keurentjes, *Ultrasonics*, **2002**, *40*, 675.
[21] M. F. Kemmere, M. W. A. Kuijpers, R. M. H. Prickaerts, J. T. F. Keurentjes, *Macromol. Mater. Eng.*, **2005**, *290*, 302.
[22] L. Dan, L. Zhimin, Y. Guanying, H. Buzxing, Y. Haike, *Polymer*, **2000**, *41*, 5707.
[23] M. F. Kemmere, M. H. W. Cleven, M. A. van Schilt, J. T. F. Keurentjes, *Chem. Eng. Sci.*, **2002**, *57*, 3929.

 

# Size-Exclusion Effect and Protein Repellency of Concentrated Polymer Brushes Prepared by Surface-Initiated Living Radical Polymerization

*Chiaki Yoshikawa,*[1] *Atsushi Goto,*[1] *Norio Ishizuka,*[2] *Kazuki Nakanishi,*[3] *Akio Kishida,*[4] *Yoshinobu Tsujii,*[1] *Takeshi Fukuda**[1]

**Summary:** The adsorption of proteins on poly(2-hydroxyethyl methacrylate) (PHEMA) brushes was systematically investigated from the viewpoint of the size-exclusion effect of the concentrated brushes. By use of surface-initiated atom transfer radical polymerization, well-defined, concentrated PHEMA brushes were successfully grafted on the inner surface of the silica monolithic column with meso pores of ca. 80 nm as well as a silicon wafer and a quartz crystal microbalance (QCM) chip. By eluting low-polydispersity pullulans with different molecular weight through the modified monolithic column, the concentrated PHEMA brush was characterized and demonstrated to sharply exclude solute molecules with the critical molecular size (size-exclusion limit) comparable to the distance between the nearest-neighboring graft points *d*. The elution behaviors of proteins with different sizes were studied with this PHEMA-grafted column: the protein sufficiently larger than the critical size was perfectly excluded from the brush layer and separated only in the size-exclusion mode by the meso pores without affinity interaction with the brush surface. Then, the irreversible adsorption of proteins on PHEMA brushes was investigated using QCM by varying graft densities ($\sigma = 0.007$, 0.06, and 0.7 chains/nm$^2$) and protein sizes (effective diameter = 2–13 nm). A good correlation between the protein size and the graft density was observed: proteins larger than *d* caused no significant irreversible adsorption on the PHEMA brushes. Thus, we experimentally substantiated the postulated size-exclusion effect of the concentrated brushes and confirmed that this effect plays an important role for suppressing protein adsorption.

**Keywords:** biocompatibility; biointerface; living radical polymerization; polymer brush; protein; size exclusion

## Introduction

Surface-initiated living radical polymerization (LRP) has been explored to yield well-defined polymer brushes with dramatically high graft densities.[1–9] The graft density $\sigma$ reached as large as 0.7 chains/nm$^2$ for common polymers like poly(methyl methacrylate) (PMMA) and polystyrene (PS).[9] This density was more than 1 order of magnitude higher than those of typical ''semi-dilute'' brushes, going deep into the ''concentrated brush'' regime which had been little explored systematically because of the unavailability of such brush samples. Our recent studies revealed that these concentrated brushes have structure and properties quite different and even

[1] Institute for Chemical Research, Kyoto University, Uji, Kyoto 611-0011, Japan
E-mail: fukuda@scl.kyoto-u.ac.jp
[2] Emaus Kyoto, Shimotsubayashi, Nishikyo-ku, Kyoto 615-8035, Japan
[3] Graduate School of Science, Kyoto University, Sakyo-ku, Kyoto 606-8502, Japan
[4] Institute of Biomaterials and Bioengineering, Tokyo Medical and Dental University, Chiyoda, Tokyo 101-0062, Japan

unpredictable from those of semi-dilute brushes:[9] most strikingly, the PMMA concentrated brushes swollen in a good solvent (toluene) exhibited an equilibrium film thickness as large as 80–90% of the contour length of the graft chains, indicating that the chains are extended to a similarly high degree.[9,10] Reflecting these characteristic features of graft chain conformation, swollen concentrated brushes brought about unique properties such as extremely strong repulsion against compression and ultra-low friction.[9–13]

As one of the most interesting potential applications of concentrated polymer brushes, attention has been directed toward biointerfaces to tune interactions of solid surfaces with biologically important materials. For example, proteins will adsorb on surfaces through non-specific interactions, often triggering a bio-fouling, e.g., the deposition of biological cells, bacteria, and so on. Attempts have been made to modify surfaces with polymer brushes to prevent protein adsorption. To understand the process of protein adsorption, the interactions between proteins and brush-coated surfaces can be modeled by the three generic modes illustrated in Scheme 1 (after Curie et al.[14] with some modifications). One is the primary adsorption, in which a protein diffuses into the brush and adsorbs on the substrate surface. The secondary adsorption is the one occurring at the outermost surface of the swollen brush film. The last one is the tertiary adsorption, which is caused by the interaction of protein with the polymer segments within the brush layer. For relatively small proteins, the primary and tertiary adsorptions would be particularly important, but they should become less important with increasing protein size and increasing graft density, since a larger protein would be more difficult to diffuse against the concentration gradient formed by the polymer brush, and this gradient, clearly, is a function of graft density. However, the size and density dependence of protein adsorption would manifest itself much more clearly for concentrated brushes due to a different mechanism. As already noted, the graft chains in a concentrated brush are highly extended and hence highly oriented so that the entire brush layer, from the substrate surface to the outermost surface throughout, could have a size-exclusion effect. By the terms ''size exclusion'', we stress the *physical* aspect of the phenomenon, meaning that the protein (or probe molecule) is excluded from the brush layer to avoid the large (mainly conformational) entropy loss caused on the highly extended chains by the entrance of the large molecule, as illustrated in Scheme 2a. Since the degree of chain extension is much less significant in semi-dilute brushes, this effect should be minor for them, and thus even a larger protein will partly diffuse into the brush layer depending on its size (Scheme 2b). Thus concentrated brushes are expected to have a protein repellency effect by this new mechanism of size exclusion and hence much better biocompatibility. This strategy has little been discussed explicitly, although surface-initiated LRP has already been applied for creating novel biointerfaces.

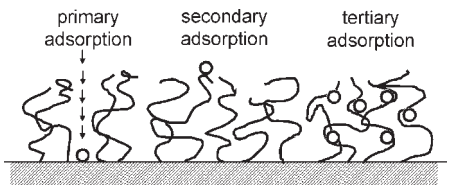


***Scheme 1.***
Schematic illustration of possible interactions of probe molecules with a polymer brush.

In this work, we will discuss the characteristic size-exclusion effect and excellent protein repellency of concentrated brushes on the basis of our experimental data previously reported with poly(2-hydroxyethyl methacrylate) (PHEMA) brushes.[15,16] PHEMA is a hydrophilic, biocompatible polymer,[17] but the biocompatibility of PHEMA cast film is reported to be not as good as e.g., poly(2-methacryloxyethyl-phosphorylcholine)[18,19] and poly(2-methoxyethylacrylate) cast films.[20,21] Hence any favorable results on the PHEMA brushes could be ascribed more to the structural,

 

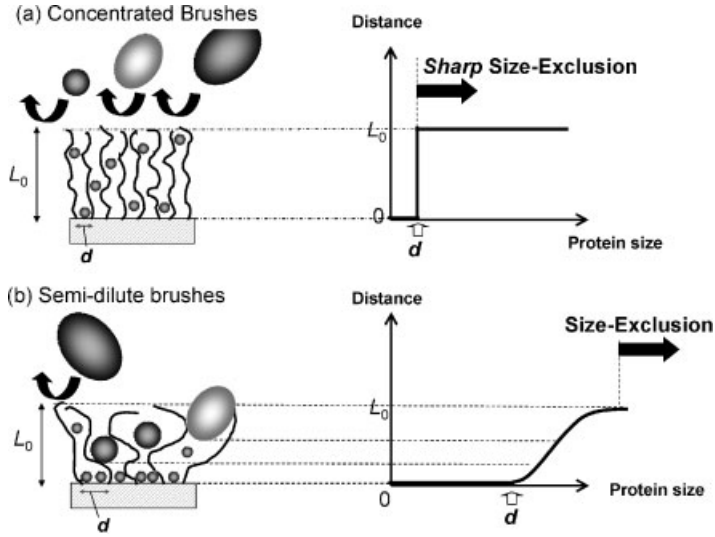


***Scheme 2.***
Schematic illustration of a size-exclusion effect for (a) concentrated brush and (b) semi-dilute brush. $L_0$ is the swollen brush thickness and $d$ is the average distance between the nearest-neighbor graft points. The vertical and horizontal axes show the distance from the substrate and the protein size, respectively.

rather than thermodynamic, properties of the system.

## Experimental Part

### Materials

2-Hydroxyethyl methacrylate (HEMA) (99%, Nacalai Tesque, Japan) was purified according to the literature.[22] An immobilizable ATRP-initiator, 6-(2-bromo-2-isobutyloxy)hexyltriethoxysilane (BHE), was synthesized as previously reported.[23] Bovine serum aprotinin (Aprotinin), bovine serum albumin (BSA), bovine serum immunoglobulin G (IgG), bovine serum thyroglobulin (Thyroglobulin), and horse heart myoglobin (Myoglobin) were purchased from Sigma Co. Ltd. (Osaka, Japan) and used without further purification. All other chemicals were commercially available and used as received.

The monolithic silica material in a rod shape (diameter = 0.5 cm) was prepared and encased according to the literature.[24–26] The pore structure of the monolith was characterized by mercury porosimetry (PORESIZER-9320, Micrometrics, USA). It had meso pores of ca. 80 nm in mean size and surface area of 21 $m^2/g$.

Silicon wafers were cleaned by ultrasonication in $CHCl_3$ and ultraviolet (UV)/ozone treatment. QCM chips (optically polished square-shaped AT-cut quartz crystals ($1 \times 1$ $cm^2$) with gold electrodes) (Seiko EG&G, Seiko Instruments Inc.) were similarly cleaned. On the cleaned chip, Cr and then $SiO_2$ were deposited in vacuum with the thicknesses of 5 and 40 nm, respectively.

### Preparation of PHEMA Brushes

A high-density (concentrated) PHEMA brush was grafted on the inner surface of the silica monolithic column by the immobilization of BHE and subsequent atom transfer radical polymerization (ATRP) of HEMA[27,28] in an on-line (on-column) process using a high-performance liquid chromatography (HPLC) system (see Scheme 3). The BHE-immobilization was conducted by injecting a tetrahydrofuran (THF) solution of BHE (1 wt.-%) and $NH_3$ (1 wt.-%) at room temperature, and ATRP was conducted by injecting a degassed methanol solution of HEMA (4.5 M),

 

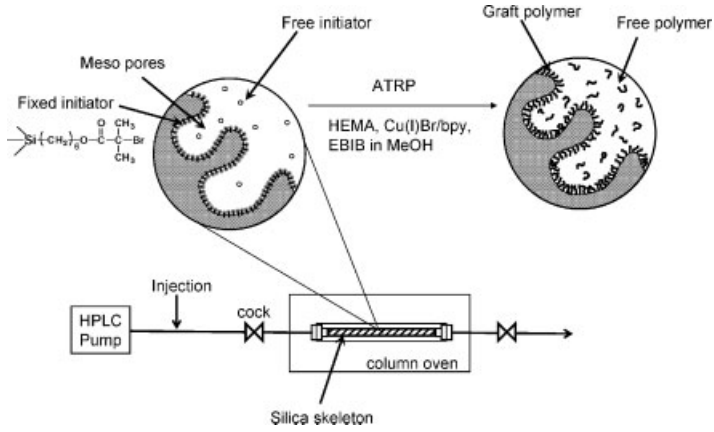


***Scheme 3.***
Schematic illustration of surface-initiated ATRP by on-line (on-column) process using a HPLC system.

Cu(I)Br (25 mM), bpy (63 mM), and EBIB at 30 °C. The detailed procedure was described elsewhere.[15,16] After the polymerization, the monolithic column was washed by elution of methanol for 24 h to remove free polymers and impurities. The eluted free polymer was analyzed by GPC and used as a good measure in molecular characteristics of the graft polymer. The amount of the grafted PHEMA was determined by elemental analysis.

A high-density (concentrated) PHEMA brush was also prepared on a silicon wafer and a $SiO_2$-deposited QCM chip by the surface-initiated ATRP.[15] The experimental conditions were the same as those for the on-line (on-column) experiment. The BHE-immobilized substrate was immersed in a degassed polymerization solution, sealed under vacuum in a glass tube, and heated at 30 °C for a prescribed time. After polymerization, the substrate was rinsed in a Soxhlet apparatus with methanol for 5 h to remove physisorbed free polymers and impurities. Lower-density PHEMA brushes were prepared on these substrates by a grafting-to method. Namely, PHEMA chains with an alkoxysilyl group at one chain end were immobilized on a substrate in solution. We prepared two end-functionalized PHEMAs with different chain lengths:[15] the shorter one had $M_n = 1.5 \times 10^4$ and $M_w/M_n = 1.2$, and the longer one had $M_n = 1.2 \times 10^5$ and $M_w/M_n = 1.2$. The immobilization of these polymers yielded a middle- and a low-density brush ($\sigma = 0.06$ and 0.007 chains/nm$^2$, respectively).

## Measurements

The GPC analysis for PHEMA was made on a Tosoh CCP&8020-series high-speed liquid chromatograph (Tokyo, Japan) equipped with two Shodex gel columns LF804 (300 × 80 mm; bead size = 6 μm; pore size = 20-3000 Å) (Tokyo). DMF was used as eluent with a flow rate of 0.8 mL/min (40 °C). The column system was calibrated with Tosoh standard polyethyleneglycols (PEGs). As an absolute number-average molecular weight $M_n$ of PHEMA, the theoretical value $M_{n,theo}$ calculated with the monomer-to-initiator molar ratio and the conversion was used (for selected samples, the validity of this assumption was confirmed by GPC with a multiangle laser light-scattering (MALLS) detector). The following discussion will be based on $M_{n,theo}$ for absolute $M_n$ and $M_{w,PEG}/M_{n,PEG}$ for absolute polydispersity index.

For the GPC analysis of proteins, the above-noted chromatograph equipped with a Shodex gel columns KW804 (300 × 80 mm; bead size = 7 μm; pore size = 300 Å) (Tokyo) was calibrated with

 

Shodex standard pullulans. PBS was used as eluent with a flow rate of 0.8 mL/min (30 °C).

Chromatograms of pullulans and proteins through the monolithic columns were recorded on a JASCO HPLC system (Jasco co. Ltd., Tokyo, Japan) using PBS as eluent at room temperature. The flow rate was 0.2 ml/min.

QCM analysis was made on a quartz crystal analyzer 917 (Seiko EG&G) driving a 9-MHz QCM chip at 25 °C. The QCM chip was mounted in a thermostated home-made QCM-cell by means of O-ring seals, which allowed only one face of the chip to come in contact with the solution. The Sauerbrey's equation[29] was applied to estimate the adsorbed amount (we confirmed using the QCMs with different fundamental frequencies that the energy dissipation reducing the applicability of this equation was negligibly small in the studied cases).

The dry thicknesses of the PHEMA layers grafted or spin-cast on a silicon wafer or a QCM chip were determined by a spectroscopic ellipsometer (M-2000U$^{TM}$, J. A. Woolam, NE, USA). The graft density $\sigma$ was estimated from the dry thickness of graft layer, the $M_n$ value, and the bulk density of PHEMA (1.15 g/cm$^3$).

Contact angles ($\theta$) were measured at room temperature with a contact angle meter CA-X (Kyowa Interface Science, Saitama, Japan).

## Results and Discussions

### Size-Exclusion Effect of Concentrated PHEMA Brush

In order to investigate the interaction of the concentrated brush with proteins, we attempted a chromatographic test using a silica monolithic column modified with a well-defined, concentrated PHEMA brush. The chromatographic technique generally provides useful information on the interactions between the analytes and the stationary phase (the brush layer) with a high sensitivity if the stationary phase has a sufficiently large surface area (and volume). The silica monolith with its macro pores of μm size and meso pores of tens of nm size has an extremely large surface area accessible by large molecules like proteins and is ideally suited for our purpose. The on-column surface-initiated ATRP successfully afforded a concentrated PHEMA brush ($M_{n,theo} = 10700$, $M_{w,PEG}/M_{n,PEG} = 1.3$, $\sigma = 0.38$ chains/nm$^2$) uniformly grafted on the inner surface of the silica monolithic column with ca. 80-nm mesopores.[16] The $M_{n,theo}$ and $M_{w,PEG}/M_{n,PEG}$ values are those for the free polymer with nearly the same molecular characteristics as the graft polymer, and the $\sigma$ value was estimated from the $M_{n,theo}$ and the amount of grafted PHEMA, which was determined by elemental analysis after all the chromatographic experiments.

A series of low-polydispersity standard pullulans were eluted using PBS as eluent through the PHEMA-grafted monolithic column, and the molecular weight $M$ of pullulans was plotted against elution volume $v$ by the closed squares in Figure 1. The arrowhead on the abscissa in the figure indicates the position of the so-called ''ghost peak'', which is believed to come from low-mass impurities dissolved in the sample solution and correspond to the mobile phase volume $v_o$. The pullulan-elution curve through the PHEMA-modified column suggests the existence of two modes of size exclusion designated by regions (a) and (b). The region (a) was ascribed to the size exclusion by the meso pores from the similarity with the elution curve for the monolithic column without brushes (data not shown). More interestingly, the $v$ value was sharply shifted in a rather small interval of $M$ in region (b), which was ascribed to the size exclusion by the brush phase for the following reasons. The $v$ value approaches the ghost peak in a low-$M$ region, suggesting that such probe (pullulan) molecules are accessible to the solvent phase even in the brush layer. The horizontal difference corresponding to region (b) is close to the volume of solvent in the brush layer (the

 

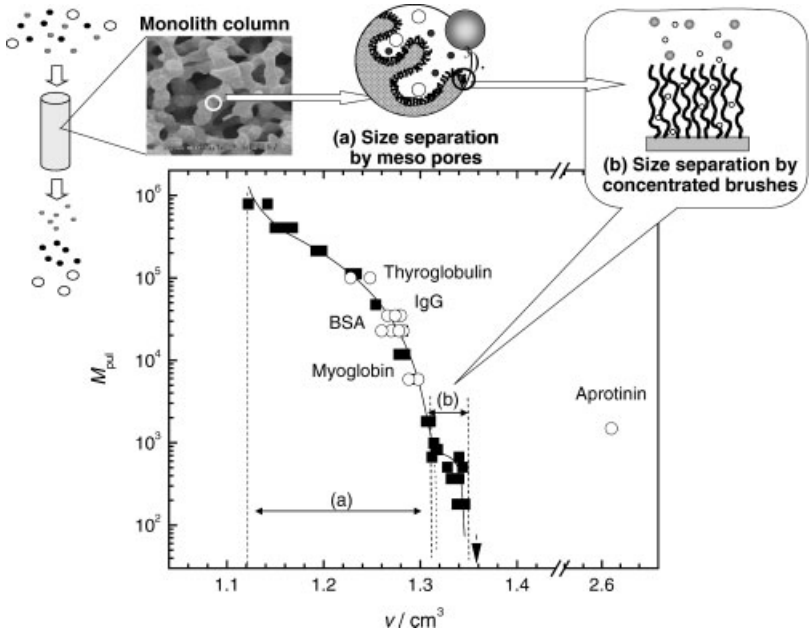


***Figure 1.***
Plot of molecular weight $M_{pul}$ vs elution volume $v$ for pullulans (filled squares and solid curve) and proteins (open circles) eluted through the PHEMA-grafted monolithic column. The molecular weights of the proteins are the reduced values independently determined by pullulan-calibrated GPC. The arrow head shows the so-called ghost peak of the eluent. The flow rate was 0.2 ml/min with PBS as eluent at room temperature. The inset shows a cartoon illustrating two size-exclusion modes of the brush-modified monolith.

swelling ratio of the PHEMA brush in PBS was estimated to be about 1.5 on a silicon wafer by ellipsometry). This means that almost the whole brush layer is unavailable for the molecules with an $M$ larger than the critical molecular weight about 1000. Here, we calculated the size of pullulan $2R_g$ at $M = 1000$ to be about 1.6 nm, where $R_g$ is the radius of gyration evaluated by using the known relation between the $R_g$ and molecular weight of pullulan.[30,31] It should be noted that this $2R_g$ value is close to the average distance between the nearest-neighbor graft points, $d\,(=\sigma^{-1/2} =$ 1.6 nm). This size exclusion effect must be characteristic of concentrated brushes, in which the graft chains are highly extended and highly oriented so that solutes larger than the distance between the nearest-neighbor graft points $d$ are *sharply* excluded from the entire brush layer, as expected in Scheme 2a.

**Interaction of Concentrated PHEMA Brush with Proteins**

Then we investigated the elution behavior of proteins with different molecular weights (Thyroglobulin, IgG, BSA, Myoglobin, and Aprotinin) through the PHEMA-grafted column. In order to discuss the interaction of the proteins with the brush, we determined the pullulan-reduced molecular weight $M_{pul}$ of proteins using the conventional GPC columns calibrated with pullulans. Table 1 lists the molecular weight $M$ and the $M_{Pul}$ of proteins as well as the $2R_g$ value evaluated from $M_{Pul}$. The values of $2R_g$ may be good indices for the protein size (these values of Myoglobin and BSA well agreed with the crystallographically-detemined dimensions).

When these proteins were injected into the BHE-immobilized column (without PHEMA brush), no elution peak was observed. On the other hand, all the proteins injected into the PHEMA-grafted

 

***Table 1.***
Absolute and Pullulan-Calibrated Molecular Weights, Crystallographic Dimensions, and $2R_g$ for Studied Proteins.

| Protein | Molecular weight $M$ | Pullulan-calibrated $M_{Pul}$ | Crystallographic dimension/nm | $2R_g$[a)]/nm |
|---|---|---|---|---|
| Aprotinin | 6500 | 1500 | | 2.0 |
| Myoglobin | 17000 | 5900 | $3 \times 4 \times 4$[32] | 4.5 |
| BSA | 67000 | 22800 | $3 \times 8 \times 9$[32–35] | 9.9 |
| IgG | 146000 | 35000 | | 12.7 |
| Thyroglobulin | 669000 | 100000 | | 23.4 |

[a)] Calculated from the known relation between $R_g$ and molecular weight of pullulan.

column were quantitatively recovered as a sharp elution peak. This means that the PHEMA-grafted column caused no such adsorbing interaction with the protein as the BHE-immobilized column did. The $M_{pul}$ value is plotted against the elution volume $v$ for each protein by open circles in Figure 1 (a few elution tests were made for each protein to check reproducibility). The data for the largest four proteins fell on the pullulan-elution curve, suggesting no affinity or adsorbing interaction with the PHEMA-grafted column. More specifically, *those large proteins were perfectly excluded from the brush layer*, separated only in the size-exclusion mode by the meso pores *without affinity interaction with the brush surface*. Reason(s) for this inertness of the brush surface in the interaction with proteins remain to be clarified in terms of static, dynamic, or other properties of solvent-swollen concentrated brushes.

The smallest protein, Aprotinin, was eluted much behind the pullulan of the equivalent size, suggesting a strong affinity interaction with the brush. By analogy of the larger proteins, Aprotinin is also expected to have little affinity interaction with the outermost surface of the brush. Therefore, such interaction may be caused within the brush layer. Here, the question arises as to why Aprotinin can get in the brush, although its molecular weight ($M_{pul} = 1500$) is larger than the above-mentioned size-exclusion limit of the brush layer ($M \approx 1000$). One possible answer to this question may be the difference in shape between Aprotinin and pullulan. Since many proteins are anisotropic (ellipsoidal) in shape, they would get more easily in the brush by an end-on approach, i.e., by setting their long axis normal to the brush surface, than more symmetrical molecules of the same $R_g$. Another issue to be considered is a local structure of the brush. Generally speaking, even a concentrated brush must have a local distribution in graft density on the substrate surface. Moreover, the effective graft density on the outermost surface of the brush cannot be the same as that on the substrate surface and should be locally fluctuated with time and position. For this reason, even molecules larger than the critical size will also get in the brush layer and stay in there for a certain time.

### Irreversible Adsorption of Proteins on PHEMA Brushes with Different Graft Densities

By using QCM, we systematically investigated the irreversible adsorption of proteins on PHEMA brushes by varying graft densities ($\sigma = 0.007$, 0.06, and 0.7 chains/nm$^2$) and protein sizes (Aprotinin, Myoglobin, BSA, and IgG). The characteristics of the studied surfaces are listed in Table 2. The high-density brush was prepared by surface-initiated ATRP. The middle- and low-density brushes were prepared by the grafting-to method. The hydrophilicities of PHEMA brushes are almost equal to that of the PHEMA cast films independent of their graft densities and thicknesses. This means that the substrate surfaces were perfectly coated with PHEMA. The adsorption of proteins was in-situ monitored by the QCM. For example, BSA was readily (within 10 min) adsorbed, from the PBS solution of BSA (1 g/L), on the low-density brush as well as the BHE

 

***Table 2.***
Characteristics of Studied PHEMA Brushes on Substrates.

| Surface[a] | $M_{n,theo}$[b] | $M_{n,PEG}$[c] | $M_{w,PEG}/M_{n,PEG}$[c] | $L$[d]/nm | $\sigma$[e]/chain nm$^{-2}$ | $d$[f]/nm | $\theta$[g]/degree |
|---|---|---|---|---|---|---|---|
| high-density brush | $1.7 \times 10^3$ | $3.5 \times 10^3$ | 1.21 | 2 | 0.7 | 1.2 | 29 |
| high-density brush | $9.7 \times 10^3$ | $8.0 \times 10^3$ | 1.26 | 10 | 0.7 | 1.2 | – |
| high-density brush | $16.8 \times 10^3$ | $12.3 \times 10^3$ | 1.30 | 15 | 0.7 | 1.2 | 29 |
| middle-density brush | $19.0 \times 10^3$ | $15.3 \times 10^3$ | 1.27 | 2 | 0.06 | 4.1 | 27 |
| low-density brush | $1.8 \times 10^5$[i] | $1.2 \times 10^5$ | 1.24 | 2 | 0.007 | 11.9 | 29 |

[a] Characteristics of brushes were almost identical on silicon wafers and QCM chips, and typical values on silicon wafers are listed.
[b] Calculated according to $M_{n,theo} = [HEMA]_0/[EBIB]_0 \times MW \times C/100$, where $[HEMA]_0$ and $[EBIB]_0$ are the feed concentration of HEMA and EBIB, respectively, $MW$ is the molecular weight of HEMA, and $C$ is the monomer conversion in %.
[c] Estimated by PEG-calibrated GPC.
[d] Film thickness in the dry state, the error is within 10%.
[e] Graft density calculated with $L$ and $M_{n,theo}$.
[f] Average distance between the nearest-neighbor graft points, calculated according to $d = \sigma^{-1/2}$.
[g] Contact angle, the error is within 2 degrees.
[i] Estimated by GPC with a multiangle laser light-scattering detector.

surface and not desorbed by washing with PBS, indicating an irreversible adsorption. For other proteins, the adsorbed amount, if any, reached almost constant within 1 h. Thus, the amount of adsorbed protein was determined after 1 h of soaking followed by washing with PBS. The PBS washing was expected to remove any weakly/reversibly

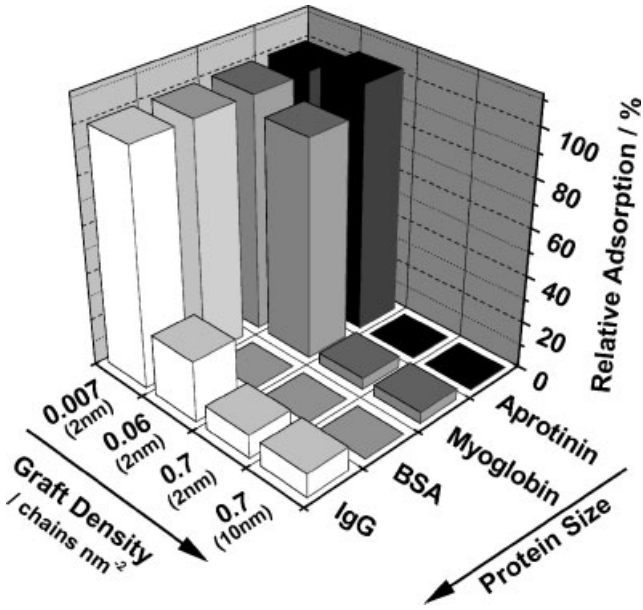


***Figure 2.***
Irreversible adsorption of proteins onto PHEMA brush surfaces with different graft densities after 1 h of soaking at 25 °C. The protein concentration was 1.0 g/L in all cases. The vertical axis shows the adsorption amount normalized by that adsorbed on the low-density brush ($\sigma = 0.007$ chains/nm$^2$) for each protein. The values in parentheses along the axis of graft density are the dry thicknesses $L$.

 

adsorbed proteins. Figure 2 shows the relative amount of proteins irreversibly adsorbed on PHEMA brushes: the amount of adsorbed proteins was normalized by that adsorbed on the low-density brush for each protein. The low-density brush adsorbed all the proteins, the middle-density one adsorbed only Aprotinin and Myoglobin, and the high-density one, none. These data clearly shows a good correlation between the protein size ($2R_g$: see Table 1) and the graft density, namely, no significant irreversible adsorption of proteins takes place on PHEMA brushes when the brush $d$ was smaller than $2R_g$. All these results confirm that the size-exclusion effect of concentrated brushes plays an important role in the biocompatibility of brush-modified surfaces. We demonstrated by fluorescence microscopy that BSA diffuses deeply into the bulk of the PHEMA-cast film, resulting in an irreversible adsorption mainly by the tertiary adsorption with minor contributions of the primary and secondary ones.

It should be noted that Approtinin caused an affinity interaction with the high-density PHEMA brush (by chromatographic test) but little irreversible adsorption on it (by QCM experiment). This may be due to the difference in graft density: even though these high-density brushes were prepared under the same polymerization conditions, the graft density ($\sigma = 0.38$ chains/nm$^2$) on the inner surface of the monolith was lower than that ($\sigma = 0.7$ chains/nm$^2$) on the flat substrate for unclear reason. Aprotinin must be *perfectly* excluded from the brush layer with $\sigma = 0.7$ chains/nm$^2$ ($d = \sigma^{-1/2} = 1.2$ nm). Another possibility is the fact that the affinity interaction is too weak to cause irreversible adsorption.

We also examined the protein adsorption on the high-density brush with different graft thicknesses $L = 2$ and 10 nm. The high-density brushes with different graft thickness were all free from protein adsorption. This means that a thick brush has a size-exclusion effect from its bottom to the outer surfaces through out. This is the very feature expected for a concentrated brush, as shown in Scheme 2a.

## Conclusions

We experimentally verified the idea of protein repellency of concentrated brushes based on their size-exclusion effect: namely when the protein is large enough to perfectly suppress its permeation into the brush layer, no protein adsorption occurs, while when protein is small enough to diffuse into the brush layer, protein adsorption takes place. Furthermore we confirmed the interaction of the concentrated PHEMA brush with proteins is very low at the outermost surface but significant inside. These results strongly indicate that the size exclusion plays an important role in biocompatibility. With other unique properties of concentrated polymer brushes along with a range of possibility to design chain architecture by LRP, PHEMA concentrated brushes will find a wide variety of applications as a novel biointerface, such as biochips, biosensors, bioseparators, and medical body implants.

*Acknowledgements:* We thank Japan Analytical Industry (Tokyo) for the fractionation of PHEMA by preparative GPC. This work was supported by Grant-in-Aids for Scientific Research, the Ministry of Education, Culture, Sports, Science and Technology, Japan (Grant-in-Aids 17002007 and 17205022).

[1] M. Ejaz, S. Yamamoto, K. Ohno, Y. Tsujii, T. Fukuda, *Macromolecules* **1998**, *31*, 5934.
[2] X. Huang, M. J. Wirth, *Macromolecules* **1999**, *32*, 1694.
[3] K. Matyjaszewski, P. J. Miller, N. Shukla, B. Immaraporn, A. Gelman, B. B. Luokala, T. M. Siclovan, G. Kickelbick, T. Vallant, H. Hoffmann, T. Pakula, *Macromolecules* **1999**, *32*, 8716.
[4] M. Husseman, E. E. Malmstrom, M. McNamara, M. Mate, D. Mecerreyes, D. G. Benoit, J. L. Hedrick, P. Mansky, E. Huang, T. P. Russell, C. J. Hawker, *Macromolecules* **1999**, *32*, 1424.
[5] J.-B. Kim, M. L. Bruening, G. L. Baker, *J. Am. Chem. Soc.* **2000**, *122*, 7616.
[6] B. Zhao, W. J. Brittain, *Prog. Polym. Sci.* **2000**, *25*, 677.
[7] J. Pyun, Y. Kowalewski, K. Matyjaszewski, *Macromol. Rapid. Commun.* **2003**, *24*, 1043.
[8] S. Edmonsdon, V. L. Osborne, W. T. S. Huck, *Chem. Soc. Rev.* **2004**, *33*, 14.
[9] Y. Tsujii, K. Ohno, S. Yamamoto, A. Goto, T. Fukuda, *Adv. Polym. Sci.*, **2006**, *197*, 1.

 

[10] [10a] S. Yamamoto, M. Ejaz, Y. Tsujii, M. Matsumoto, T. Fukuda, *Macromolecules* **2000**, *33*, 5602. [10b] S. Yamamoto, M. Ejaz, Y. Tsujii, T. Fukuda, *Macromolecules* **2000**, *33*, 5608.
[11] S. Yamamoto, M. Ejaz, Y. Tsujii, T. Fukuda, *Macromolecules* **2002**, *35*, 6077.
[12] K. Urayama, S. Yamamoto, Y. Tsujii, T. Fukuda, D. Neher, *Macromolecules* **2000**, *35*, 9459.
[13] S. Yamamoto, Y. Tsujii, T. Fukuda, N. Torikai, M. Takeda, *KENS Report* **2001–2002**, *14*, 204.
[14] E. P. K. Currie, W. Norde, M. A. Cohen Stuart, *Adv. Collide Interface Sci.* **2003**, *100-102*, 205.
[15] C. Yoshikawa, A. Goto, Y. Tsujii, T. Fukuda, K. Kimura, K. Yamamoto, A. Kishida, *Macromolecules* **2006**, *39*, 2284.
[16] C. Yoshikawa, A. Goto, Y. Tsujii, T. Fukuda, K. Kimura, K. Yamamoto, A. Kishida, *Polym. Prepr., Jpn. (Soc. Polym. Sci., Jpn.)* **2005**, *54*, 5151.
[17] J. P. Montheard, M. Chatzopoulos, D. Chappard, *J. M. S-Rev. Macromol. Chem. Phys.* **1992**, *C32*, 1.
[18] [18a] K. Ishihara, R. Aragaki, T. Ueda, A. Watanabe, N. Nakabayashi, *J. Biomed. Mater. Res.* **1990**, *24*, 1069. [18b] K. Ishihara, N. P. Ziats, B. P. Tierney, N. Nakabayashi, J. M. Anderson, *J.Biomed. Mater. Res.* **1991**, *25*, 1397.
[19] S. Sawada, S. Sakaki, Y. Iwasaki, N. Nakabayashi, K. Ishihara, *J. Biomde. Mater. Res.* **2003**, *3*, 411.
[20] M. Tanaka, T. Motomura, M. Kawada, T. Anzai, Y. Kasori, T. Shiroya, K. Shimura, M. Onishi, A. Mochizuki, *Biomaterials* **2000**, *21*, 1471.
[21] M. Tanaka, A. Mochizuki, T. Motomura, K. Shimura, M. Onishi, Y. Okahata, *Coll. Surf. A Physcicochem. Eng. Aspects* **2001**, *193*, 145.
[22] L. K. Beers, S. Boo, S.G. Gaynor, K. Matyjaszewski, *Macromolecules* **1999**, *32*, 5772.
[23] K. Ohno, T. Morinaga, K. Koh, Y. Tsujii, T. Fukuda, *Macromolecules* **2005**, *38*, 2137.
[24] K. Nakanishi, *J. Porous Materials* **1997**, *4*, 67.
[25] H. Minakuchi, K. Nakanishi, N. Soga, N. Ishizuka, N. Tanaka, *Anal. Chem.* **1996**, *68*, 3498.
[26] N. Ishizuka, H. Minakuchi, K. Nakanishi, K. Hirao, N. Tanaka, *Colloids and Surfaces A: Physicochem. Eng. Aspects* **2001**, *187*, 273.
[27] J.-S. Wang, K. Matyjaszewski, *J. Am. Chem. Soc.* **1995**, *117*, 5614.
[28] M. Kato, M. Kamigaito, M. Sawamoto, T. Higashimura, *Macromolecules* **1995**, *28*, 1721.
[29] G. Z. Sauerbrey, *Phys.* **1959**, *155*, 206.
[30] U. Asolphi, W.-M. Kulicke, *Polymer* **1997**, *38*, 1513.
[31] J. H.-Y. Liy, D. A. Brant, S. Kitamura, K. Kajiwara, M. Mimura, *Macromolecules* **1999**, *32*, 8611.
[32] A. Baszkin, D. J. Lyman, *J. Bio. Mater. Res.* **1980**, *14*, 393.
[33] P. Suttiprasit, V. Krisdhasima, J. Mcguire, *J. Colloid Interface Sci.* **1992**, *154*, 316.
[34] D. C. Carter, X.-M. He, *Science* **1990**, *249*, 302.
[35] F. Hook, M. Rodahl, P. Brzezinski, B. Kasemo, *Langmuir* **1998**, *14*, 729.

 

# Synthesis of Rod-Coil Block Copolymers using Two Controlled Polymerization Techniques

*Simone Steig,*[1] *Frauke Cornelius,*[1] *Andreas Heise,*[2] *Rutger J. I. Knoop,*[2] *Gijs J. M. Habraken,*[2] *Cor E. Koning,*[2] *Henning Menzel**[1]

**Summary:** A double-headed initiator was synthesized yielding two functional groups for the initiation of the nickel mediated ring-opening polymerization of γ-benzyl-L-glutamate-*N*-carboxyanhydride and controlled radical polymerization of vinyl monomers via ATRP or NMP. Well-defined block copolymers combining polypeptides and synthetic polymers were obtained.

**Keywords:** atom transfer radical polymerization; living polymerization; polypeptides; ring-opening polymerization; rod-coil diblock copolymers

## Introduction

The combination of bio-inspired structure elements and classical polymer chemistry provides promising opportunities to design polymeric materials with unique solution and solid state properties. Examples are rod-coil type polymers comprising helical polypeptide and flexible vinyl polymer blocks. Block copolymers of this architecture are of interest from both functional and structural points of view. Compared to ''simple'' coil-coil block copolymers the self-assembling of the rod-coil block copolymers is not only controlled by the microphase separation, but also by the tendency to form anisotropic supramolecular assemblies. These competitive processes can lead to morphologies which are different from those commonly observed for block copolymers.[1–5]

We introduced a new synthetic route for well defined pure polypeptide based rod-coil block copolymers combining the controlled ring-opening polymerization of *N*-carboxyanhydrides (NCA) with the controlled radical polymerization techniques via a double-headed initiator (Scheme 1).[6] This combination opens a wide range of possibilities for the controlled synthesis of rod-coil block copolymers by avoiding polymer end group modification. We have chosen a nickel mediated NCA polymerization[7] because this method has proven its potential in the polymerization of a variety of amino acid NCA's.[8] Atom transfer radical polymerization (ATRP) on the other hand, was used for the synthesis of the flexible block due to its robustness and efficiency in macroinitiation. Also the nitroxide mediated polymerization (NMP) was chosen for the combination via a double-headed initiator to show the universal applicability of this method.

## Experimental Part

### Materials

All solvents were dried and distilled using standard procedures[9] and if necessary degassed by freeze-pump-thaw procedure. Methylmethacrylate (90% Acros) and styrene (Acros) were destilled from $CaH_2$ under reduced pressure and were stored under nitrogen atmosphere at −30 °C. Cu(I)Br (98% Fluka) was purified according to the published procedure[9]. Hexamethyltriethyltetraamine (HMTETA,

[1] Institute for Technical Chemistry, Braunschweig University of Technology, Hans-Sommer-Straße 10, 38106 Braunschweig, Germany
E-mail: h.menzel@tu-bs.de
[2] Laboratory of Polymer Chemistry, Eindhoven University of Technology, Den Dolech 2, P.O. Box 513, 5600 MB Eindhoven, The Netherlands

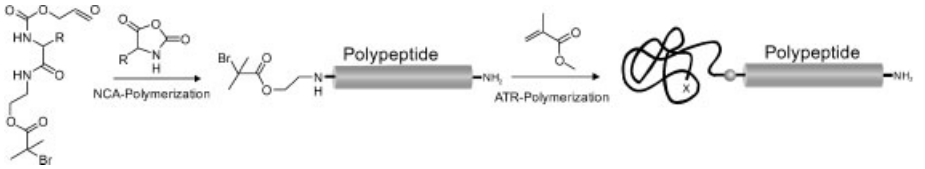


***Scheme 1.***
Strategy for the combination of two controlled polymerization techniques with a double-headed initiator.

97%, Aldrich) was destilled under reduced pressure and stored under nitrogen, γ-Benzyl-L-glutamic acid-*N*-carboxyanhydride (BLG-NCA) was synthesized[10] and PBLG was polymerized[8] according to the literature.

*Combination of NCA Polymerization with ATRP*
The synthesis of alloc-L-leucine-*N*-hydroxysuccinimidyl ester **1** and its use for preparation of alloc amides is described in.[8,11] The preparation of the double-headed initiator **4** and the synthesis of PBLG macro-initiator were described before.[6]

Block copolymerization (PBLG-b-PMMA): In a dry round bottomed flask charged Cu(I)Br and macro-initiator were dissolved in DMF (abs.), the solution was degassed by bubbling with nitrogen for 15 minutes. The ligand (HMTETA), MMA and anisole as internal standard were added. The polymerization was done at 80 °C. After the desired polymerization time the catalyst was removes by an alox column and the polymer was precipitated into methanol, isolated and reprecipitated two times.

*Combination of NCA polymerization with NMP*
The nitroxide **5** with the spacer $X_1$ (**5a**: 2,2,5 Trimethyl-3-(1-p-6-aminohexanoic acid methylphenylethoxy)-4-phenyl-3-azahexan) and $X_2$ (**5b**: 2,2,5 Trimethyl-3-(1-p-aminomethylphenylethoxy)-4-phenyl-3-azahexane) were prepared according to literature[12,13] and converted with alloc-L-leucine-*N*-hydroxysuccinimidyl ester **1** following the same procedure as described for the combination of NCA polymerization with ATRP.[6]

The synthesis of the double-headed initiator **(phen)Ni(amido-amidate)-NMP complex 7** was performed following a procedure similar to the method published by DEMING:[8] 86 mg (0.477 mmol) 1, 10 phenanthroline (phen) (dissolved in 4 mL DMF (abs.)) were added under a nitrogen atmosphere to 136 mg (0.494 mmol) $Ni(COD)_2$ suspended in 10 ml DMF (abs.). The mixture was stirred at room temperature for two hours to form a (phen)Ni(COD) solution and subsequently 269 mg (0.487 mmol) Alloc-L-leucin-NMP **6** (dissolved in 4 mL DMF (abs.)) were added. The mixture was allowed to react over night at room temperature. The product was isolated by precipitation into 50 mL diethyl ether (abs.). After drying in vacuum the solid product was obtained (**7a**: it was not possible to determine the yield due to a very low conversion; **7b**: 0.43 g (0.061 mmol), 12% yield). **IR** (KBr pellet, in $cm^{-1}$): 3385 (N–H, valence), 3051 (C–H-valence, aromatic), 2961 (C–H, valence aliphatic), 1715 (C=O, ester), 1655 (amide I, C=O-valence), 1516 (amide II, C=O-valence)

Synthesis of NMP macro-initiator: Polymerization of **γ-benzylglutamate-*N*-carboxyanhydride** (macro-initiator). γ-BLG-NCA was dissolved in DMF (abs.) and transferred with a syringe to the initiator **7** (dissolved in (DMF (abs.)) under nitrogen atmosphere. The mixture was stirred for 16 hours at room temperature. The polymer solution was precipitated with cool methanol (0 °C) with a small concentration of HCl (4 mM HCl) to destroy the nickel complex. The polymer was isolated and reprecipitated two times from THF with methanol.

 

Block copolymerization (PBLG-b-PS): A dry round bottomed flask was charged with the macro-initiator. It was dissolved in DMF (abs.) and styrene was added. The polymerization by heating the mixture to 130 °C. After the desired polymerization time the polymer was precipitated with methanol, isolated and reprecipitated two times.

### Characterization

Polymer conversions were determined by investigation of monomer consumption by gas chromatography. Molecular weights and molecular weight distributions were measured by SEC/MALLS combination in DMF (membrane filtered and degassed) containing LiBr (0.1 mol%) on two PL-gel 5μm mixed-C columns (Polymer Laboratories) at 80 °C and a flow rate of 0.5 mL/min. Detection was performed with a Melz LCD201 differential refractive-index detector (set at 35 °C), a Thermo Separation Products UV150 Spectraseries UV-visible light detector set at 270nm, and a TriStar MiniDawn light scattering detector from Wyatt Technology (angles at 30, 90, and 120 °).

## Results and Discussion

### Combination of Nickel Mediated NCA Polymerization with ATRP

The synthesis of the double-headed initiator **4** (Scheme 2) for the combination of nickel mediated NCA polymerization with ATRP has already been described.[6] It was synthesized as depicted in Scheme 2 with an overall yield of 23%. First alloc-L-leucin-*N*-hydroxysuccinimidyl ester **1**[14] was reacted with aminoethanol to yield alloc-L-leucin-(2-hydroxyethyl)amide **2**. Subsequently the ATRP initiator moiety α-bromoisobutyrate was introduced by esterification of the hydroxyl group with acid bromide. Converting **3** with nickel cyclooctadien complex ($Ni(COD)_2$) and phenanthroline as ligand the initiating complex **4** was received. **4** can be isolated and stored under nitrogen.

Both polymerization mechanisms include transition metal complexes, and Nickel complexes are used for ATR-polymerizations, too.[15] Thus one question was whether or not the ATRP initiator is stable under the conditions of the last step in the initiator synthesis and the polymerization of the NCA itself.

Previous approaches towards peptide containing rod-coil block copolymers all used the coil polymer as macro-initiator for the NCA polymerization.[1–5] The double-headed initiator can be used for both sequences – peptide first or vinyl polymer first. In the later case it is necessary to perform the ATR-polymerization with the initiator in the alloc-amide form, thus before the activation with $Ni(COD)_2$ (see scheme 2). The activation step then has to be done after the polymerization, thus this sequence requires polymer end group modification. On the other hand if the NCA polymerization is done first no end group modifications are necessary and the peptide block is used as macro-initiator.

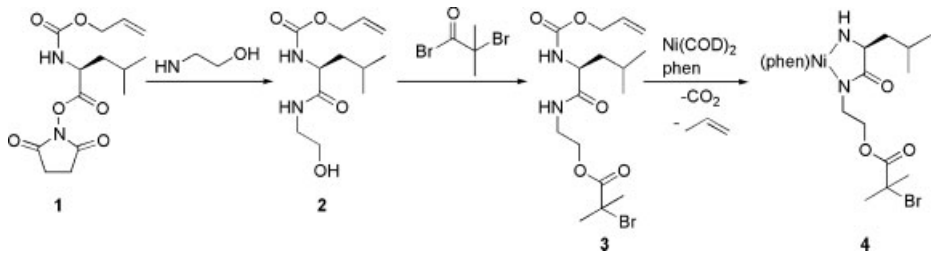


***Scheme 2.***
Synthesis of the double-headed initiator for combination of Nickel mediated NCA polymerization with ATRP.[6]

 

The NCA polymerization of γ-benzyl-L-glutamate N-carboxyanhydride (γ–BLG-NCA) was carried out in DMF as solvent with initiator **4**. The monomer to initiator ratio was varied and different initiator batches were used. The results of these experiments reveal a reasonably linear increase of the molecular weight with the monomer to initiator ratio for each individual initiator batch as determined by size exclusion chromatography with light scattering detector (SEC/MALLS).[6] The variations of the experimental molecular weight obtained from every individual initiator batch resulted from inactive impurities which were found in the initiator.[6] Similar effects have been reported by Deming for nickel amido-amidate initiators.[16] The polymerization is well controlled and poly(γ-benzyl-L-glutamate) (PBLG) with a narrow molecular weight distribution can be obtained (polydispersity 1.2–1.4). Taking into account the effect due to the inactive impurities, it is possible to get well controlled polymers with adjusted molecular weight.

These polymers all have an intact bromo isobutyrate end group as evidenced by MALDI-TOF investigation.[6] Thus the treatment with $Ni(COD)_2$ and the NCA polymerization did not destroy the ATRP initiator and well defined macro-initiators were obtained.

These PBLG macro-initiators were used in the ATRP of MMA. Due to the low solubility of polypeptides in conventional ATRP solvents, suitable polymerization conditions (catalyst, ligand, temperature, concentration, etc.) had to be identified. Cu(I)/HMTETA in DMF at 80 °C was found to be an appropriate system for the ATRP of MMA with the PBLG macro-initiator.[6] In addition, the influence of the PBLG as macro-initator on the kinetics of the ATR-polymerization was investigated. As shown in Figure 1 the reaction follows a first order kinetics under the macro-initiation conditions. After three days a conversion of 90% was reached. However, if α-bromo isobutyric acid ethyl ester was used as initiator instead of the PBLG macro-initiator the reaction starts very fast, but stops after a short time (approximately 1 h). Thus under these conditions only low conversion can be reached. It can be speculated, that the catalyst system in DMF is too active and thus the radical concentration too high resulting in termination reactions. The addition of PBLG without a functional end group has a big influence to the monomer conversion, too. The polymerization starts fast but after a

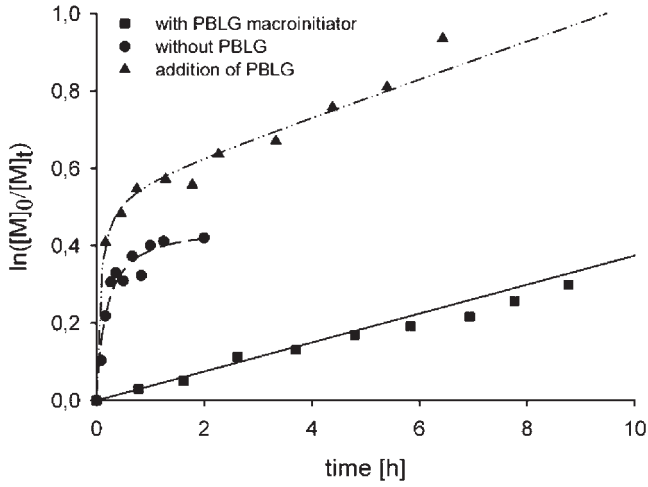


***Figure 1.***
$\ln([M]_0/[M]_t)$ as a function of time with macro-initiator, without macro-initiator and with addition of PBLG, ATRP of MMA at 80 °C with Cu(I)Br, HMTETA, DMF as solvent and anisole as internal standard.

 

short time $\ln[M]_0/[M]_t$ becomes linear. The linear part is almost parallel to the curve obtained for the polymerisation employing the macro-initiator (see Figure 1). It is supposed that the polyamide backbone of the peptide shows interactions with the Cu-catalyst system and thus influences the equilibration of the ATRP.[17] Probably the the complexation of the Cu with PBLG reduces the activity of the initiating complex. The results are evidence that it is not possible to simply transfer the conditions used for low molecular weight initiators to a polymerization of the same monomer with the PBLG macro-initiators, but a screening for suitable reaction conditions is necessary.

The rod-coil block copolymers obtained by the controlled nickel mediated NCA polymerization and subsequent ATRP (PBLG-b-PMMA) were investigated by XRD measurements and AFM after storage in THF vapour. The XRD measurements (not shown) reveal that before treatment with THF vapour there were peaks attributed to both α-helical and β-sheet material. After the treatment only peaks resulting from α-helical material were observed. The AFM pictures reveal a lamellar structure of the block copolymer (Figure 2).

### Combination of Nickel Mediated NCA Polymerisation with NMP

For many vinyl monomers, especially for styrene, the nitroxide mediated polymerization (NMP) is an alternative technique for a controlled radical polymerization which is less sensitive to variations in parameters like solvent polarity, concentration etc.

Therefore the possibility of combining NMP and nickel mediated NCA polymerization was investigated by synthesizing the double headed initiator **7** with an amido-amidate group and a nitroxide group (Scheme 3). A nitroxide **5** (synthesis according to literature[18]) was converted with alloc-L-leucine-*N*-hydroxysuccinimidyl

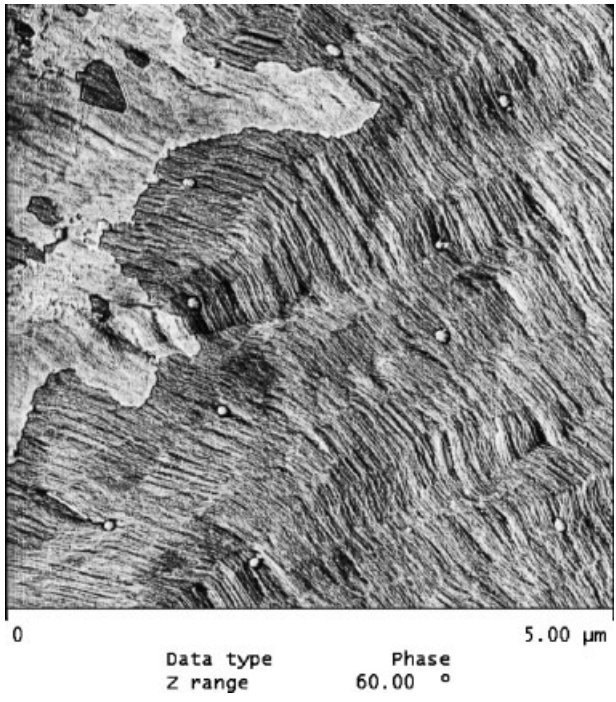


***Figure 2.***
AFM picture of PBLG-b-PMMA block copolymer ($M_n$ of PBLG block 85000 g/mol, $M_n$ of PMMA block 50500 g/mol) after storage in THF vapour.

 

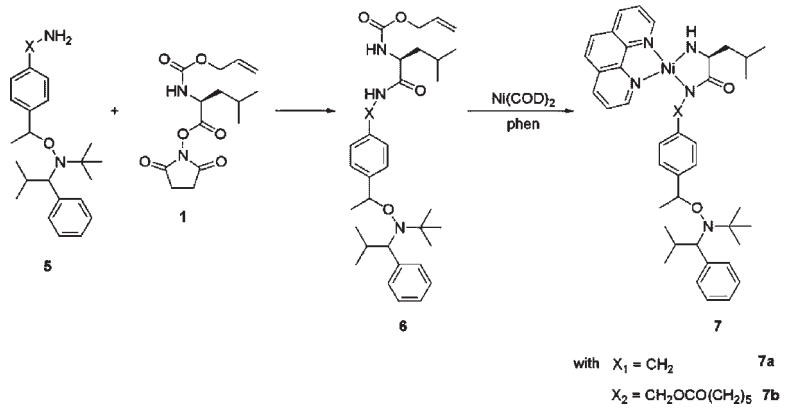


***Scheme 3.***
Synthesis of double-headed initiators **7** for combination of NCA polymerization with NMP.

ester **1** into the corresponding ester **6** and reacted with $Ni(COD)_2$ and phenanthroline to yield the double-headed initiator **7**(yield 12%). We used two different spacers (group X) between the amido-amidate group and the nitroxide.

Both initiators **7a** and **7b** were used to initiate the polymerization of γ–BLG-NCA. PBLGs were obtained having a molecular weight of $M_n = 42\,000$ g/mol (PBLG-$X_1$) and 23 000 g/mol (PBLG-$X_2$) and a polydispersity of 1.5 and 1.4 respectively. The presence of the nitroxide end group in the PBLG macroinitiator was confirmed by MALDI-ToF measurements. These PBLGs macro-initiators with nitroxide end groups were used in the NMP of styrene in DMF under reaction conditions as described in reference.[13] The results of the block copolymerizations are summarized in Table 1.

For the block copolymers obtained with PBLG-$X_1$ as macro-initiator (Table 1/entry 1 and 2) a shoulder in the SEC chromatogram (Figure 3) was observed. This shoulder is supposed to be due to PS-homopolymer resulting from the styrene autopolymerization. The investigation of the polymerizations kinetics via GC (see Figure 4) shows a

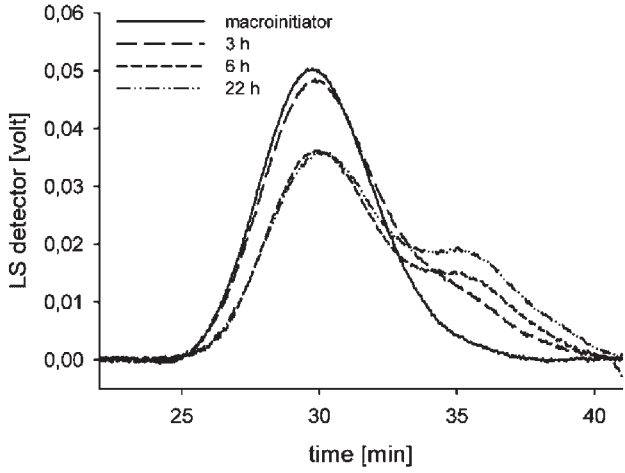


***Figure 3.***
SEC-MALLS chromatogram of PBLG-PS block copolymers prepared by NMP with the PBLG-$X_1$ macro-initiator (Table 1/entry 2).

 

***Table 1.***
Molecular weight of PBLG-b-PS block copolymers.

| Entry | macroinitiator | $PG^{b)} = \frac{[M]_0}{[I]_0}$ | block copolymer $M_n$ [g/mol]$^{c)}$ | PD$^{c)}$ | PS block $M_n$ [g/mol]$^{c)}$ |
|---|---|---|---|---|---|
| 1$^{a)}$ | PBLG-$X_1$ | 815 | 150 000 | 1.2 | 108 000 |
| 2$^{a)}$ | PBLG-$X_1$ | 870 | 130 000 | 1.2 | 88 000 |
| 3$^{a)}$ | PBLG-$X_2$ | 960 | 73 000 | 1.5 | 50 000 |

a) polymerization at 130 °C in DMF.
b) calculated.
c) Measured by SEC-MALLS (eluent DMF/LiBr)

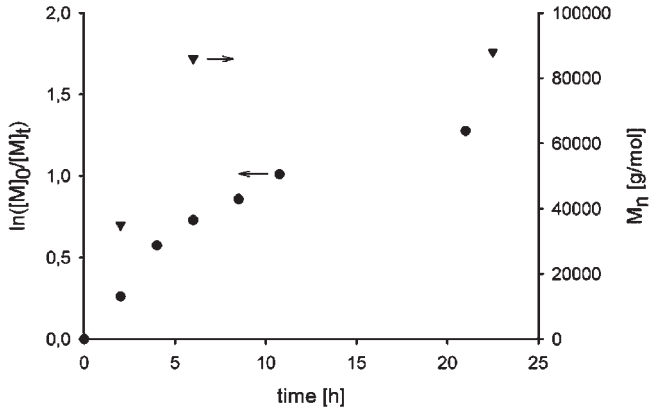


***Figure 4.***
Kinetics of the NMP of styrene with PBLG-$X_1$ (Table 1/entry 2) and evolution of the molecular weight.

linear increase of the conversion and the molecular weight only for approximately the first 8 hours. After this time the polymerization kinetics is no longer first order and the molecular weight does not increase with the conversion anymore.

On the other hand for the macro-initiator PBLG-$X_2$ having only a small spacer between the two functional groups of the double-headed initiator (Table 1/entry 3) the formation of PS homopolymer during the polymerisation was not observed. The

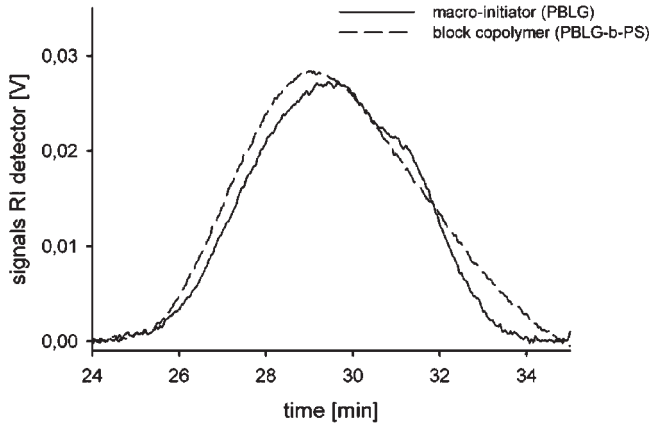


***Figure 5.***
SEC-MALLS chromatogram of PBLG-PS block copolymers prepared by NMP with PBLG-$X_2$ macro-initiators (Table 1/enrty 3).

 

SEC chromatogram (Figure 5) shows a shift of the block copolymer to higher molecular weights upon styrene polymerization without the formation of an additional shoulder. Further investigations copolymerisation of the BLG-NCA and styrene using double-headed initiators with amido-amidate and NMP groups are necessary.

## Conclusion

Synthesis of well defined polypeptide based rod-coil block copolymers is possible via the combination of the ring-opening polymerization of *N*-carboxyanhydrides and controlled radical polymerization employing doubled-headed initiators. Two bifunctional initiators were synthesized having a nickel amido-amidate group for NCA polymerization and an ATRP group or an NMP group respectively. The nickel-amido-amidate group was in both cases used to initiate the polymerization of benzyl-L-glutamate-NCA, yielding macro-initiators for the controlled radical polymerization. Subsequent ARTP of MMA yielded well defined block copolymers. However, the ATRP requires fine tuning of the reaction conditions for each monomer, in order to adjust the reactivity of the chains and to ensure control. NMP using PBLG macro-initiators seems to be less sensitive.

*Acknowledgements:* The authors thank the Deutsche *Forschungsgemeinschaft (DFG)* and the *Netherlands Organisation for Scientific Research (NWO)* for financial support and Dr. Ralf Kleppinger (DSM) for the XRD and AFM measurements. This project is associated with the European Graduate School ''Microstructural Control in Free-Radical Polymerization''.

[1] H. A. Klok, J. F. Langenwalter, S. Lecommandoux, *Macromolecules* **2000**, *33*, 7819.
[2] R. Yoda, S. Komatsuzaki, E. Nakanishi, T. Hayashi, *Eur. Polym. J.* **1995**, *31*, 335.
[3] H. Schlaad, B. Smarsly, M. Losik, *Macromolecules* **2004**, *37*, 2210.
[4] M. Losik, S. Kubowicz, B. Smarsly, H. Schlaad, *Eur. Phys. J. E.* **2004**, *15*, 407.
[5] H. A. Klok, S. Lecommandoux, *Adv. Mater.* **2001**, *13*, 1217.
[6] S. Steig, F. Cornelius, P. Witte, B. B. P. Staal, C. E. Koning, A. Heise, H. Menzel, *Chem. Comm.* **2005**, 5420.
[7] T. J. Deming, *J. Polym. Sci., Part A: Polym. Chem.* **2000**, *38*, 3011.
[8] S. A. Curtin, T. J. Deming, *J. Am. Chem. Soc.* **1999**, *121*, 7427.
[9] W. L. F. Armarego, D. D. Perrin, *Purification of Laboratory Chemicals*, 4th ed.,Butterworth-Heinemann, Oxford, **1996**.
[10] W. D. Fuller, M. S. Verlander, M. Goodman, *Biopolymers* **1976**, *15*, 1869.
[11] K. R. Brzezinska, T. J. Deming, *Macromolecules* **2001**, *34*, 4348.
[12] J. Dao, D. Benoit, C. J. Hawker, *J. Polym. Sci. A* **1998**, *36*, 2161.
[13] A. W. Bosman, R. Vestberg, A. Heumann, J. M. J. Frechet, C. J. Hawker, *J. Am. Chem. Soc* **2003**, *125*, 715.
[14] K. R. Brzezinska, T. J. Deming, *Macromol. Biosci.* **2004**, *4*, 566.
[15] M. Kamigaito, T. Ando, M. Sawamoto, *Chem. Rev.* **2001**, *101*, 3689.
[16] T. J. Deming, S. A. Curtin, *J. Am. Chem. Soc.* **2000**, *122*, 5710.
[17] H. Rettig, E. Krause, H. G. Börner, *Macromol. Rapid Commun.* **2004**, *25*, 1251.

 

# Production of Polyacrylic Acid Homo- and Copolymer Films by Electrochemically Induced Free-Radical Polymerization: Preparation and Swelling Behavior

*Johanna Bünsow, Diethelm Johannsmann**

**Summary:** Films of polyacrylic acid hydrogels were produced on a conducting substrate by means of electrochemically initiated polymerization (EIP). An electrochemical quartz crystal microbalance was used to monitor film growth in situ. Homopolymer and copolymer films of polyacrylic acid and poly-*N*-isopropylacrylamide were characterized by FTIR spectroscopy. The degree of swelling of these films could be tuned via the pH.

**Keywords:** electrochemically initiated polymerization; hydrogels; polyelectrolytes; stimuli-sensitive polymers; surfaces

## Introduction

The preparation of hydrogels at solid surfaces has attracted much scientific interest in recent years. Surface-attached gels strongly modify the surface, affecting properties such as hydrophilicity and biocompatibility of the substrate. Thin films of hydrogels are also extensively used in sensing,[1,2] microfluidics,[3] drug release,[4,5] and tissue engineering.[4,6]

There are numerous ways of attaching polymers to a solid surface. Examples are photo cross-linking of pre-formed polymer chains,[7] in-situ atom transfer radical polymerization (ATRP),[8] electron beam irradiation,[9] and plasma polymerization.[10] Electrochemical techniques are particularly suited for conducting substrates. For example, Palacin et al. have grafted vinylic monomers from anhydrous solutions.[11,12] This technique is mainly based on an anionic polymerization and leads to a covalent link between the polymer and the metal. Schuhmann et al. produced coatings by electrochemically induced precipitation of polyelectrolytes.[13]

Our work employs electrochemically initiated polymerization (EIP) which is an easy and flexible method to produce surface coatings of various kinds.[14–17] The technique makes use of the decomposition of an electro-active initiator at an electrode to start a free-radical polymerization. The polymer is formed directly at the electrode surface. As a consequence, the films adhere tightly to the surface. Adhesion is based on physisorption of the hydrogel to the metal. Note in this context that EIP is different from electrografting of conductive polymers. In EIP, the initiator is the electro-active species, rather than the monomer. Recently, we reported on the formation of thermoresponsive poly-*N*-isopropylacrylamide (pNIPAm) hydrogel coatings on gold surfaces based on this approach.[18]

In this work we use electrochemically initiated polymerization to produce coatings of polyacrylic acid (pAA) and copolymer coatings consisting of pAA and pNIPAm[19] on gold surfaces. The films were characterized by Fourier transform infrared (FTIR) spectroscopy. Swelling and deswelling were measured as a function of

Institute of Physical Chemistry, Clausthal University of Technology, Arnold-Sommerfeld-Strasse 4, D-38678 Clausthal-Zellerfeld, Germany
E-mail: johannsmann@pc.tu-clausthal.de

pH using a quartz crystal microbalance (QCM).

The literature contains a few reports on EIP of pAA containing copolymers. Teng and Mahalingam deposited such a copolymer of pAA and polyacrylonitrile (pAN) by EIP in aqueous sulfuric acid.[20] Kolzunova et al. studied the EIP of AA and AN in aqueous ammonium persulfate solutions.[21]

Polyacrylic acid is a pH-sensitive polymer. At low pH, the carboxylic acid groups of pAA are protonated and therefore uncharged. When increasing the pH, the side groups become charged and render the polymer more hydrophilic. Copolymerization with hydrophobic monomers diminishes this effect. When using NIPAm as comonomer, the film thickness becomes sensitive to temperature changes in addition to its pH sensitivity.[22]

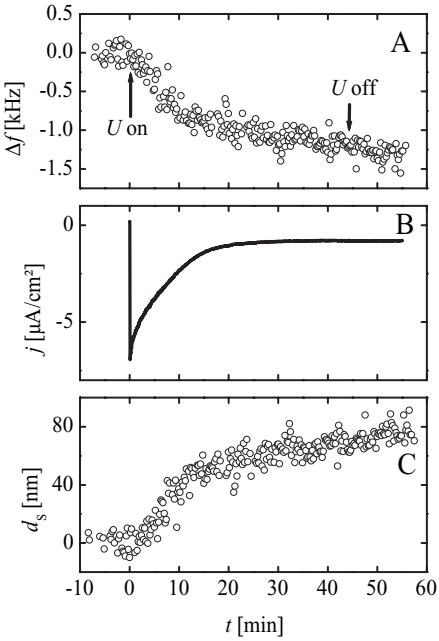


***Figure 1.***
A: Frequency shift $\Delta f$ on the 5th overtone (25 MHz), B: current density $j$, and C: Sauerbrey thickness $d_S$ measured when depositing polyacrylic acid on the front electrode of a quartz crystal. A voltage $U$ of $-0.8$ V was applied for 45 minutes, as indicated by the arrows. The resulting film had a Sauerbrey thickness of about 75 nm in the reactant solution.

**Production of Hydrogel Films**

Films of polyacrylic acid were produced in an aqueous solution containing 0.3 mol/L acrylic acid, 0.4 mol/L potassium sulfate as supporting electrolyte, 6 mmol/L *N,N′*-methylenebisacrylamide as cross-linker, and 10 mmol/L potassium persulfate as electro-active initiator. A voltage of $-0.8$ V vs. saturated calomel electrode (SCE) was applied for 45 minutes. The deposition was performed at room temperature. For further experimental details see ref. 18. The deposition process was investigated in situ with an electrochemical quartz crystal microbalance (EQCM).[23] Figure 1 shows the frequency shift $\Delta f$ of the quartz crystal (panel A), the current density $j$ (panel B), and the Sauerbrey thickness $d_S$ (panel C). The frequency shows a significant decrease. This decrease is correlated to an increase of mass on the front electrode of the quartz crystal. The Sauerbrey Equation (1) allows for the determination of film thickness of a laterally homogeneous, rigid film:[24]

$$\Delta f = -\frac{2nf_f^2}{Z_q} m_S = -\frac{2nf_f^2}{Z_q} \rho_f d_S, \qquad (1)$$

where $n$ is the overtone order, $f_f$ is the fundamental frequency, $m_S$ is the mass per unit area of the film, $Z_q = 8.8 \times 10^6$ kg m$^{-2}$ s$^{-1}$ is the acoustic impedance of AT-cut quartz, $\rho_f \approx 1$ g/cm$^3$ is the density of the film, and $d_S$ is the film thickness in the Sauerbrey sense, also called ''Sauerbrey thickness''. The Sauerbrey thickness of a pAA film in dependence on polymerization time is displayed in panel C. The final film thickness was about 75 nm in the reactant solution. Presumably, some free polymer is generated during EIP as well. However, the solution remained clear and there was no precipitate at the bottom of the flask.

Panel B shows the current density which results from the reduction of initiator according to Equation (2). After reduction, most of the radical anions take up another electron from the gold surface (3). Only a few radicals initiate the polymerization

 

according to Equation (4).[25,26]

$$S_2O_8^{2-} + e^- \rightarrow SO_4^{\bullet -} + SO_4^{2-} \quad (2)$$

$$SO_4^{\bullet -} + e^- \rightarrow SO_4^{2-} \quad (3)$$

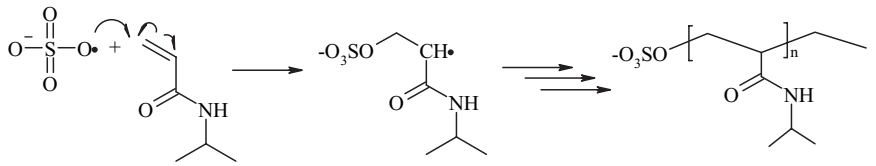

(4)

In the current trace shown in Figure 1B, there is an initial peak, followed by a plateau. The reactivity of the surface drops quickly after the polymerization has started. The reduced reactivity may be either due to poisoning of the active sites or to a reduced initiator diffusion coefficient inside the newly formed gel. Note, however, that the current is not necessarily an indicator of polymer growth, but rather an indicator of initiator decomposition.

Usually, the films show good adhesion to the gold surface. Delamination of the films did not appear in water or salt solutions at room temperature, even over months. The films were heated in water up to 40°C and they remained stable.

An FTIR spectrum taken in reflection on a gold electrode covered with pAA is displayed in Figure 2. It shows all the characteristic bands of the polymer and clearly proves that pAA was deposited on the surface.

Copolymer films were deposited from a reactant solution with a monomer concentration of 0.2 mol/L AA and 0.2 mol/L NIPAm. The film growth was performed in a similar way as described above. The FTIR spectrum (Figure 3) proves that both monomer units are present in the film. Both homopolymers show distinct bands. The band at 1726 $cm^{-1}$ stems from a vibrational motion of the pAA acid groups. The amide group of the pNIPAm homopolymer causes a characteristic peak at 1540 $cm^{-1}$.

The FTIR spectra do not allow to distinguish between copolymers and a mixture of homopolymers. We have indirect evidence in favor of the formation of copolymers (or at least a very intimate mixture), which is based on the fact that the

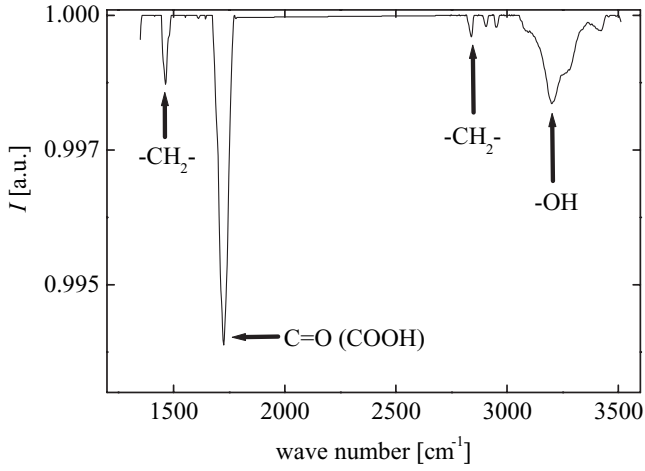


***Figure 2.***
FTIR spectrum taken on a gold electrode covered with polyacrylic acid – it shows the typical pAA bands.

 

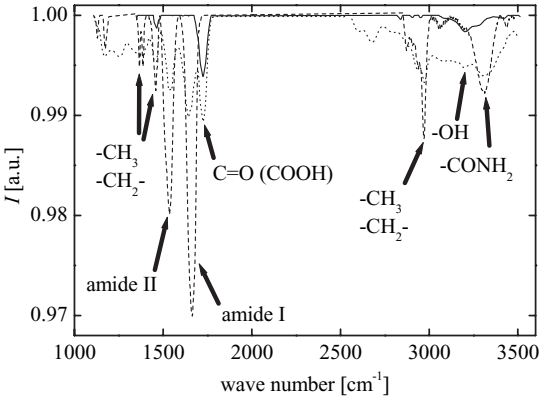


***Figure 3.***
FTIR spectra of a pAA film (—), of a pNIPAm film (- - -), and of a pAA-co-pNIPAm film (· · · ·) taken on the gold surface in reflection – the spectra demonstrate that EIP is useful to produce pAA and pNIPAm homopolymer films as well as the corresponding copolymer films.

films do not display a temperature driven swelling transition. Had we produced segregated domains of pAA and pNIPAm, the pNIPAm domains would collapse at the lower critical solution temperature (LCST) of 32 °C. It is known that copolymerization of pNIPAm with pAA increases the LCST. Should we have produced copolymers with an LCST above 45 °C (which was our instrumental limit) this would explain the experimental findings. For practical application, the question of whether or not copolymers were produced is of minor importance, as long as the material shows uniform properties.

### Swelling Behavior of the Films

The swelling of the films in dependence on the solution pH was investigated. For this purpose, we used aqueous solutions of 0.025 M sulphuric acid and 0.05 M potassium hydroxide at room temperature. The pH was varied by addition of the acid to the base. Figure 4 shows the results obtained with a pure pAA hydrogel film. The frequency shift $\Delta f$ was measured during pH induced swelling (see panel A). After addition of an aliquot of acid, the quartz was allowed to equilibrate.

The increase of the frequency shift with decreasing pH is caused by water leaving the network when the polymer becomes uncharged. Both the frequency shift and the shift of half bandwidth at half maximum (bandwidth, for short) of the resonance curve were determined by impedance

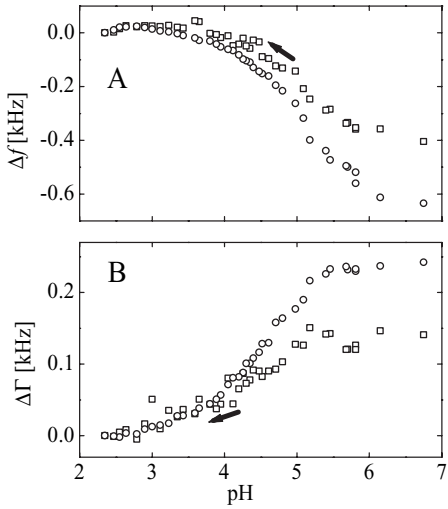


***Figure 4.***
A: Frequency shift $\Delta f$ and B: bandwidth shift $\Delta\Gamma$ on the third (□, 15 MHz) and 5th overtone (○, 25 MHz) overtone during the pH dependent swelling of a pAA film deposited on the front electrode of a quartz crystal. The pH was high in the beginning of the experiment and was lowered by addition of acid (as indicated by the arrows). The film collapsed at low pH. This becomes evident by the low mass (low amount of water) and by the high stiffness at low pH. At high pH, the hydrogel is swollen and softer.

 

analysis. The bandwidth is an indicator of the film's softness. At high pH, the film was soft and the bandwidth was large (right-hand-side in panel B). When decreasing the pH, the film deswelled and became stiffer, resulting in a decreased bandwidth. We observed reswelling when subsequently varying the pH from low to high, but the behaviour was not entirely reversible. Part of the irreversibility may be caused by the fact that the ionic strength of the solution increased during the experiment.

Figure 5 displays the results obtained when using a pAA-co-pNIPAm film. The frequency shift decreases slightly with increasing pH. The shift is much smaller than the one observed when swelling the homopolymer film. We attribute this observation to the fact that the copolymer contains less pH sensitive groups than the homopolymer. A response of the copolymer sets in at around pH 4.5. The homopolymer of pAA shows the first shift at around pH 3. This off-set of the copolymer response indicates that the comonomer influences the $pK_A$ of the hydrogel.

In future experiments, the influence of the ionic strength on the swelling should be investigated. Monomer ratio in the feed as well as cross-linker and initiator concentration should be varied. The method may then open up an easy route to coat sensors with *multi*-stimuli responsive hydrogels.

## Conclusions

We demonstrated that electrochemically initiated polymerization is suited to produce polyacrylic acid coatings on gold. The film thickness was about 75 nm after a polymerization time of 45 min. FTIR spectroscopy proved that polyacrylic acid films and films consisting of polyacrylic

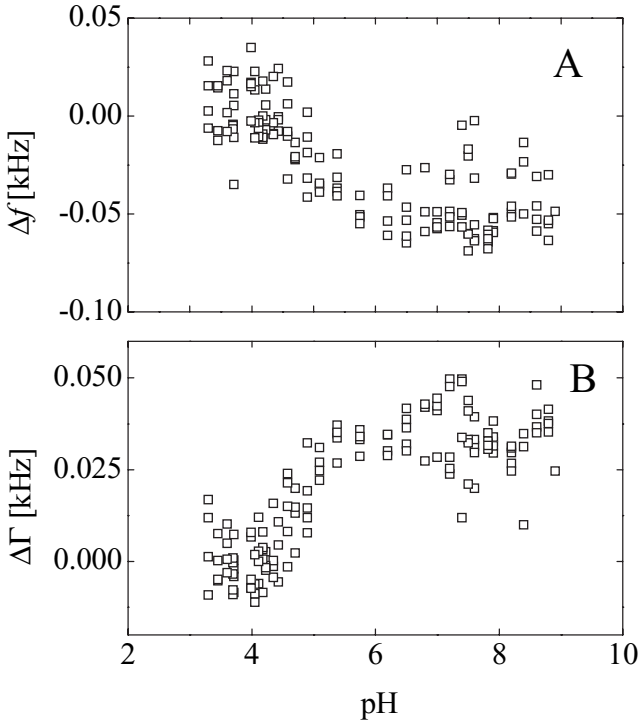


***Figure 5.***
A: Frequency shift $\Delta f$ and B: bandwidth shift $\Delta\Gamma$ of a quartz crystal covered with a pAA-co-pNIPAm film as a function of pH – a small shift when increasing the pH proves that the copolymer is sensitive to pH. The response is much smaller as compared to the pAA homopolymer (see Figure 4).

 

acid and poly-*N*-isopropylacrylamide were formed on the gold surface. The investigation of the LCST behavior indicates the formation of a copolymer. The swelling of the films as a function of pH was investigated with a quartz crystal microbalance. The pAA homopolymer showed a strong response at $pH > 3$. The swelling ratio decreased strongly when incorporating NIPAm as comonomer. In addition, the copolymerization influenced the pH at which the first conformational variations appeared. The method is useful to produce smart hydrogel films of defined properties.

*Acknowledgements:* We thank W. Oppermann for stimulating discussions and J. Vogel and W. Daum for the FTIR spectra.

[1] J. Heo, R. M. Crooks, *Anal. Chem.* **2005**, *77*, 6843.
[2] J. Kim, N. Singh, L. A. Lyon, *Angew. Chem. Int. Ed.* **2006**, *45*, 1446.
[3] M. E. Harmon, M. Tang, C. W. Frank, *Polymer* **2003**, *44*, 4547.
[4] N. A. Peppas, J. Z. Hilt, A. Khademhosseini, R. Langer, *Adv. Mater.* **2006**, *18*, 1345.
[5] Y. Qiu, K. Park, *Adv. Drug. Deliver. Rev.* **2001**, *53*, 321.
[6] A. Kikuchi, T. Okano, J. Control. *Release* **2005**, *101*, 69.
[7] O. Prucker, C. A. Naumann, J. Rühe, W. Knoll, C. W. Frank, *J. Am. Chem. Soc.* **1999**, *121*, 8766.
[8] X. Kong, T. Kawai, K. Abe, T. Iyoda, *Macromolecules* **2001**, *34*, 1837.
[9] N. Yamada, T. Okano, H. Sakai, F. Karikusa, Y. Sawasaki, Y. Sakurai, *Makromol. Chem. Rapid Commun.* **1990**, *11*, 571.
[10] Y. V. Pan, R. A. Wesley, R. Luginbuhl, D. D. Denton, B. D. Ratner, *Biomacromolecules* **2001**, *2*, 32.
[11] S. Palacin, C. Bureau, J. Charlier, G. Deniau, B. Mouanda, P. Viel, *Chem. Phys. Chem.* **2004**, *5*, 1468.
[12] G. Deniau, J. Charlier, B. Alvado, S. Palacin, P. Aplincourt, C. Bauvais, *J. Electroanal. Chem.* **2006**, *586*, 62.
[13] C. Kurzawa, A. Hengstenberg, W. Schuhmann, *Anal. Chem.* **2002**, *74*, 355.
[14] N. Baute, C. Jérôme, L. Martinot, M. Mertens, V. M. Geskin, R. Lazzaroni, J.-L. Brédas, R. Jérôme, *Eur. J. Inorg. Chem.* **2001**, 1097.
[15] G. Yildiz, H. Çatalgil-Giz, F. Kadirgan, *J. Appl. Electrochem.* **2000**, *30*, 71.
[16] C. S. Lee, J. P. Bell, *J. Mater. Sci.* **1995**, *30*, 3827.
[17] S. L. Cram, G. M. Spinks, G. G. Wallace, H. R. Brown, *J. Appl. Polym. Sci.* **2003**, *87*, 765.
[18] J. Reuber, H. Reinhardt, D. Johannsmann, *Langmuir* **2006**, *22*, 3362.
[19] F. Xia, L. Feng, S. Wang, T. Sun, W. Song, W. Jiang, L. Jiang, *Adv. Mater.* **2006**, *18*, 432.
[20] F. S. Teng, R. Mahalingam, *J. Appl. Polym. Sci.* **1979**, *23*, 101.
[21] L. G. Kolzunova, N. Y. Kovarsky, A. S. Inberg, *Russ. Chem. Bull.* **1994**, *43*, 227.
[22] M. J. Serpe, L. A. Lyon, *Chem. Mater.* **2004**, *16*, 4373.
[23] D. A. Buttry, M. D. Ward, *Chem. Rev.* **1992**, *92*, 1355.
[24] G. Sauerbrey, *Z. Phys.* **1959**, *155*, 206.
[25] A. N. Frumkin, N. V. Nikolaevafedoro, N. P. Berezina, K. E. Keis, *J. Electroanal. Chem.* **1975**, *58*, 189.
[26] Z. Samec, K. Doblhofer, *J. Electroanal. Chem.* **1994**, *367*, 141.

 

# Designing Organic/Inorganic Colloids by Heterophase Polymerization

*Elodie Bourgeat-Lami,*[*1] *Norma Negrete Herrera,*[1] *Jean-Luc Putaux,*[2] *Adeline Perro,*[3] *Stéphane Reculusa,*[3] *Serge Ravaine,*[3] *Etienne Duguet*[4]

**Summary:** Polymer/silica and polymer/Laponite nanocomposite colloids with various morphologies have been elaborated through emulsion polymerization using a polymerizable organosilane (route I) and a methyl methacrylate-terminated macromonomer (route II) as coupling agents. Depending on the synthetic strategy and on the nature of the mineral particles, either core-shell, raspberry-like, multipod-like, currant bun or inverted core-shell morphologies (the mineral forming the shell) were achieved. Beyond the control of particle shape, we have demonstrated that some of the polymerizations exhibited particular kinetics behaviors which could be correlated to the mechanism of formation of the composite particles. Interestingly, conversion versus time curves of a series of soap free polymerizations performed in the presence of the macromonomer showed a significant increase in the polymerization rate with increasing the inorganic particles concentration. Characterization of the composite latexes by transmission electron microscopy showed that the mineral was located at the surface of the latex spheres and participated therefore to their stabilization. The higher the amount of inorganic particles, the lower the particles size and the higher the polymerization rate.

**Keywords:** emulsion polymerization; kinetics; laponite; nanocomposite colloids; silica

## Introduction

The combination of organic and inorganic components into composite colloids is attracting increasing interest as it enables to create new nanostructured materials with unsual shapes, compositions and properties originating from their starting components.[1–6] Among the various techniques, *in situ* polymerization offers many advantages compared to physical approaches as it allows controlling the nature and the chemical composition of the polymer. *In situ* polymerization generally involves polymerizing in the presence of mineral particles which have been previously functionalized in order to promote polymer chain growth on their surface.[1] Once performed in dispersed media, this strategy allows designing organic/inorganic colloids with completely original shapes and morphologies (core-shell, multicores, raspberry-like, dumbell-like, currant bun, etc.) which cannot be achieved by simply mixing organic and inorganic particles. These colloids can additionnaly be used as building blocks to fabricate nano or microstructured materials with tailored textural, optical or mechanical properties. During the last ten years, we and others have developped various routes to such nanostructured colloids by heterophase polymerization including suspension,[7] dispersion,[8,9] miniemulsion[10–12] and emulsion polymerizations.[13–27] Although there have

[1] Laboratoire de Chimie et Procédés de Polymérisation - CNRS-CPE Lyon - Bâtiment 308 F, 43, boulevard du 11 novembre 1918 - BP 2077 - 69616 Villeurbanne Cedex, France
[2] Centre de Recherches sur les Macromolécules Végétales, ICMG/CNRS, BP 53, F-38041 Grenoble Cedex 9, France
[3] Centre de Recherche Paul Pascal – CNRS, 115, avenue du Dr Schweitzer - 33600 Pessac, France
[4] Institut de Chimie de la Matière Condensée de Bordeaux – CNRS - 87, avenue du Dr Schweitzer - 33608 Pessac Cedex, France

been immense efforts to synthesise well defined organic/inorganic particles in multiphase media, much less attention has been paid to the mechanistic aspects of the polymerization reaction in such complex systems. In this article, we report recent results along this line on the elaboration of organic/inorganic colloids through emulsion polymerization following two routes. In a first method, organic modification of the mineral particles was performed by grafting organosilane molecules bearing a reactive methacrylate functionality (Structures 1 and 2) while in the second method, the organic modification was performed by adsorption of a methyl methacrylate-terminated polyethylene glycol macromonomer (PEG-MA, Structure 3). The article is divided in two parts. The first part is devoted to the synthesis of silica/polystyrene composite particles while the second part reports the elaboration of clay-based composite particles using organically-modified anisotropic Laponite platelets as seeds. The paper describes the surface modification of the mineral particles and addresses the effect of the experimental parameters on the composite particles morphology, polymerization kinetics and mechanism.

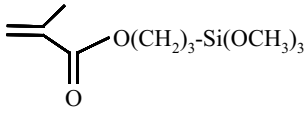


**Structure 1 :** MPS

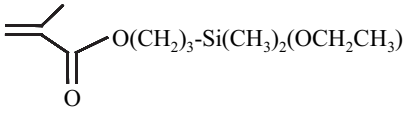


**Structure 2 :** MPDES

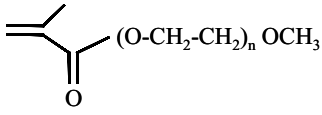


**Structure 3 :** PEG-MA

## Experimental Part

### Materials

Commercial silica sols with diameters of 13 and 80 nm and a solid content of around 30% (Klebosol 30N12 and Klebosol 30N50, respectively) were kindly supplied by Clariant. The 30N50 silica sol was used as received meanwhile 30N12 was dialyzed against desionized water until the obtention of a neutral *pH* before use. Suspensions of silica particles in a mixture of ethanol and water, with diameters of 500 nm and 1 μm, respectively, were prepared according to the procedure of Stöber et al. as described previously.[21] They were evaporated in order to remove part of ammonia and ethanol and to reduce the volume of the suspension. The latter was then dialyzed against water until *pH* 7. Its final concentration was determined gravimetrically and adjusted to the desired value before use. Laponite RD with a cation exchange capacity of 0.75 $meq \cdot g^{-1}$ was supplied from Laporte Industries and used without further purification.

γ-Methacryloyloxypropyl trimethoxysilane (MPS, $M_w = 248.3\ g \cdot mol^{-1}$, Aldrich), and γ-methacryloyloxypropyl dimethylethoxysilane (MPDES, $M_w = 230.3\ g \cdot mol^{-1}$, Gelest), were used as supplied. The macromonomer, poly(ethylene glycol) 1000 monomethylether methacrylate (PEG-MA) was obtained from Polysciences. The peptizing agent: tetrasodium pyrophosphate ($Na_4P_2O_7$, Aldrich), the monomers: styrene (Sty, Aldrich), methyl methacrylate (MMA, Aldrich) and butyl acrylate (BuA, Aldrich) and the initiators: potassium persulfate (KPS, Acros Organics) and azo-bis cyano pentanoic acid (ACPA, Wako Chemicals) were used as received. The anionic surfactant, sodium dodecyl sulfate (SDS, $M_w = 288.4\ g \cdot mol^{-1}$, Acros Organics) and the nonylphenol poly(oxyethylenic) nonionic surfactant (Remcopal $NP_{30}$, $M_w = 1540\ g \cdot mol^{-1}$, a gift from CECA S.A, Paris), were of analytical grade and used as supplied. Deionized water was purified by a Milli-Q Academic system (Millipore Cooperation).

 

## Organic Modification Procedures

### Silica

Grafting of the commercial Klebosol 30N50 silica sol was performed by introducing known amounts of MPS into 100 mL of a 10 $g \cdot L^{-1}$ stock silica suspension containing 1 $g \cdot L^{-1}$ of SDS. The dispersions were stirred magnetically at ambient temperature and allowed to equilibrate for 19 hours. They were next centrifuged and the supernatant solutions were analyzed by UV spectroscopy. The amount of grafted MPS, $Q_{MPS}$ ($\mu mol \cdot m^{-2}$), was determined by difference between the total amount and the free amount of MPS using a predetermined calibration curve established on silica-free suspensions of identical composition as reported elsewhere.[23] Macromonomer adsorption was performed by adding a known amount of a calibrated PEG-methacrylate solution to a known amount of the aqueous silica suspension in a capped glass vessel. The dispersion was shaken magnetically at ambient temperature and allowed to equilibrate for 24 hours.

### Laponite

Grafting of the MPS and MPDES molecules on the Laponite clay edges was performed as follows. 1 g of Laponite was suspended into 100 mL of toluene and a known amount of the coupling agent (comprised between 0.75 and 7 mmoles) was introduced in the reaction flask and allowed to react for 21 days at room temperature. The grafted Laponites were filtered, extensively washed with toluene in order to remove the excess of functional alkoxysilane, and dried overnight in a vacuum oven at 40 °C before characterization. The grafted amount, expressed in mmoles of grafted silane per g of bare laponite, was determined from the difference $\Delta C$(wt%) of carbon content after and before grafting as described elsewhere.[28]

## Emulsion Polymerization

### Silica/Polystyrene Nanocomposite Particles

The polymerization reactions were carried out in batch at 70 °C for up to 24 hours under nitrogen atmosphere. The 300 mL glass reactor fitted with a condenser was charged with the organically-modified silica suspension and the surfactant. Degassing was carried out for 30 minutes under gentle stirring before increasing the temperature up to 70 °C. Then, the required amounts of KPS, dissolved in 10 mL of de-ionized water, and of monomer were added at once to start polymerization. A typical recipe involving MPS as coupling agent is as follows: MPS-functionalized silica, 1 g; water, 100 g; styrene, 10 g; KPS, 0.1 g and SDS, 0.1 g · Polymerizations performed in the presence of PEG-MA were conducted as follows. Typically, the silica suspension (10 $g \cdot L^{-1}$) containing predetermined amounts of macromonomer (1.5$\mu mol/m^2$ silica) and surfactant ($NP_{30}$, 3 $g \cdot L^{-1}$) was charged into the reactor. After degassing at 70 °C, the monomer (styrene, 100 $g \cdot L^{-1}$) was introduced at once under stirring followed by the initiator (KPS, 1 $g \cdot L^{-1}$). A series of soap-free emulsion polymerizations of styrene and MMA were performed in the presence of the Klebosol 30N12 silica as follows. A known quantity of the macromonomer (2.5 wt%, respect to silica) was introduced into the silica suspension (concentration comprised between 10 and 80 $g \cdot L^{-1}$) and the mixture was allowed to equilibrate for one night. The suspension was next introduced into the reactor and purged with nitrogen at 70 °C. Then, after degassing, the monomers (styrene: 160 $g \cdot L^{-1}$ and MMA: 40 $g \cdot L^{-1}$) were added at once under strong agitation and the polymerization was initiated by the addition of the initiator (KPS, 1 $g \cdot L^{-1}$).

### Clay-based Nanocomposite Particles

Emulsion polymerization was carried out at 70 °C in a 250 mL three-necked double wall reactor equipped with a condenser, a nitrogen inlet tube and a stirrer. A typical recipe for MPDES-grafted Laponites is as follows. The reactor was charged with 100 g of the aqueous MPDES-grafted Laponite suspension (10 $g \cdot L^{-1}$) containing the surfactant (SDS, 2 $g \cdot L^{-1}$) and the peptizing agent ($Na_4P_2O_7$, 1 $g \cdot L^{-1}$). After degassing,

 

the monomers, a mixture of styrene (3 g) and butyl acrylate (7 g), and the initiator (ACPA, 0.1 g) were successively introduced at 70 °C under stirring. Polymerizations performed using the PEG-MA/clay complexes involved slighlty different experimental conditions. In a typical run, Laponite (3 g) was first suspended in water (150 g) and magnetically stirred for 1 h to totally exfoliate the clay tactoïds. Then, the macromonomer (0.15 g) and the peptizing agent (0.3 g) were introduced in the clay suspension and the mixture was fed to the reactor followed by the monomer (styrene, 30 g). The polymerization was initiated by introducing 0.15 g of ACPA dissolved into 3 mL of water.

### Characterizations

UV analysis was performed using an UV/VIS spectrophotometer and quartz cells. The measurements were carried out at the wavelength of 205 nm. A JEOL JCXA 733 electron microprobe analyzer was used to determine the carbon content of the bare and organically-modified Laponite samples. The monomer-to-polymer conversions were determined gravimetrically. Typically, 3–7 g of the latex suspension was placed in an aluminium dish and dried to constant weight at 70 °C. Particle size was determined by dynamic light scattering (DLS). The morphology of the nanocomposite particles was characterized by ''conventional'' transmission electron microscopy (TEM) and cryogenic transmission electron microscopy (cryo-TEM). Specimens for TEM were prepared by evaporating one drop of dilute latex ($10^{-3}$/$10^{-6}$ $g \cdot cm^{-3}$) on a 200 mesh formvar-coated copper electron microscope grid. The grids were placed in the vacuum chamber of a Philips CM120 electron microscope operating at 80 kV and observed under low illumination dose. The diameters of the polymer particles were measured directly from the electron micrographs. A minimum of 100 particles were counted for each batch. The number average diameter, $D_n$, was calculated using Equation 1 where *ni* designates the number of particles of diameter *Di*.

$$Dn = \frac{\sum niDi}{\sum ni} \quad (1)$$

The weight average diameter, $D_w$, was calculated from:

$$Dw = \frac{\sum niD_i^4}{\sum niD_i^3} \quad (2)$$

and the polydispersity index (*PDI*) was given by:

$$PDI = \frac{Dw}{Dn} \quad (3)$$

Following procedures described elsewhere,[9,29,30] specimens for cryo-TEM analysis were prepared by quench-freezing thin films of the latex suspensions in liquid ethane. They were then mounted in a Gatan 626 cryo-holder, transferred in a Philips CM200 'Cryo' electron microscope operating at 80 kV, and observed at low temperature (−180 °C) under low dose illumination. Images were recorded on Kodak SO163 films. The particle number per unit volume of water (*Np/L*) was calculated by the following equation:

$$Np/L = \frac{\frac{M}{\rho}}{\frac{\pi}{6}Dn^3 \cdot V} \times 10^{19} \quad (4)$$

where *M* (g) is the total mass of solid, $\rho$ ($g \cdot cm^{-3}$) is the density of the particles, *Dn* (nm) is the number average particles diameter determined either from the TEM micrographs or by DLS, and *V* (in liter) is the total volume of water.

## Results and Discussion

### Silica/Polystyrene Composite Particles

#### *Grafting of γ-methacryloyloxypropyl trimethoxysilane*

The grafting was carried out at $pH = 9.5$ by direct addition of MPS to the aqueous colloidal suspension of the Klebosol 30N50 silica particles containing 1 $g \cdot L^{-1}$ of the anionic SDS surfactant. The role of the surfactant is to help disperse the MPS

 

molecules in water and achieve high grafting densities. Controlling the MPS grafting density is essential as the growing polystyryl radicals are expected to copolymerize with the double bonds of silica, and thus promote the formation of composite particles. The amount of chemisorbed MPS was determined by UV titration of the supernatant solutions recovered by centrifugation of the suspension medium according to the so-called depletion method. This method allowed accurate determination of the MPS grafting density even for low initial concentrations. The MPS grafting densities are indicated in Table 1 as a function of the MPS concentration. The higher the silane concentration, the higher the MPS grafting density in agreement with previous works reported in the literature for related systems.[31]

In order to investigate the effect of the amount of double bonds on the composite particles morphology, a series of polymerization experiments were performed in the presence of the MPS-grafted silica suspensions under otherwise identical conditions in order to analyse the effect of the MPS grafting density only. Figure 1 shows the TEM images obtained for grafting densities of 0,0.95 and 1.9 $\mu mol \cdot m^{-2}$, respectively. For the sake of clarity, micrographs were recorded at low and high magnification to better visualize the particles shape. It can be seen from Figure 1 that the polymerization performed in the presence of non-grafted silica particles gave rise to separate populations of silica beads and polymer latexes with no apparent interaction between them. For all the other experiments, the latex spheres showed more or less affinity for the silica surface indicating that the organic modification is essential in order to yield nanocomposite particle morphologies. For very low MPS grafting densities (typically below $0.5 \mu mole \cdot m^{-2}$), irregular daisy-shaped morphologies were produced with only a few colloids surrounding the silica spheres in an irregular fashion. When the MPS grafting density increases and reaches a value close to e.g., $1 \mu mole \cdot m^{-2}$, most of the polymer latexes are located around the silica particles in more regular flower-like morphologies, each particle being surrounded in average by eight polystyrene petals, as determined by the ratio of the number of polymer particles to the number of silica particles. With increasing further the MPS grafting density, core-shell particles were obtained as shown in Figure 1c. It is also noticeable on these TEM pictures that the diameter of the polystyrene particles is not constant in the different experiments, and hence is the overall particle number and overall surface area.

Table 1 summarizes the particle size and size distribution of the polystyrene latexes directly determined from the TEM micrographs as a function of the MPS grafting density. It can be seen that the number of polystyrene latex particles increases with increasing the MPS grafting density and then decreases for larger MPS concentrations to reach a value which is identical to that determined in the absence of silica particles. This result suggests that for low

***Table 1.***
Number average particle diameters, weight average particle diameters and polydispersity indexes of polystyrene latex particles synthesized in the presence of MPS-grafted 30N50 silica particles with increasing MPS grafting densities.

| [MPS] ($\mu mol \cdot m^{-2}$) | $Q_{MPS}$ ($\mu mol \cdot m^{-2}$) | Conversion (%) | $D_n$ (nm) | $D_w$ (nm) | $D_w/D_n$ | $Np/L$ |
|---|---|---|---|---|---|---|
| 0 | 0 | 100 | 197.2 | 201.1 | 1.02 | $2.5\ 10^{16}$ |
| 0.1 | 0.1 | 96 | 129.5 | 143.4 | 1.11 | $8.4\ 10^{16}$ |
| 0.2 | 0.2 | 95 | 113.9 | 128.3 | 1.13 | $1.2\ 10^{17}$ |
| 0.5 | 0.35 | 86 | 92.8 | 113.6 | 1.22 | $2.1\ 10^{17}$ |
| 1 | 0.65 | 96.2 | 110.5 | 122.6 | 1.11 | $1.4\ 10^{17}$ |
| 2 | 0.95 | 99.6 | 113.0 | 116.9 | 1.03 | $1.3\ 10^{17}$ |
| 10 | 1.9 | 98.5 | 190.5 | 194.3 | 1.02 | $2.5\ 10^{16}$ |

$[SiO_2] = 10\ g \cdot L^{-1}$, $[SDS] = 1\ g \cdot L^{-1}$, [Styrene] = $100\ g \cdot L^{-1}$, KPS = 0.5 wt% relative to styrene.

 

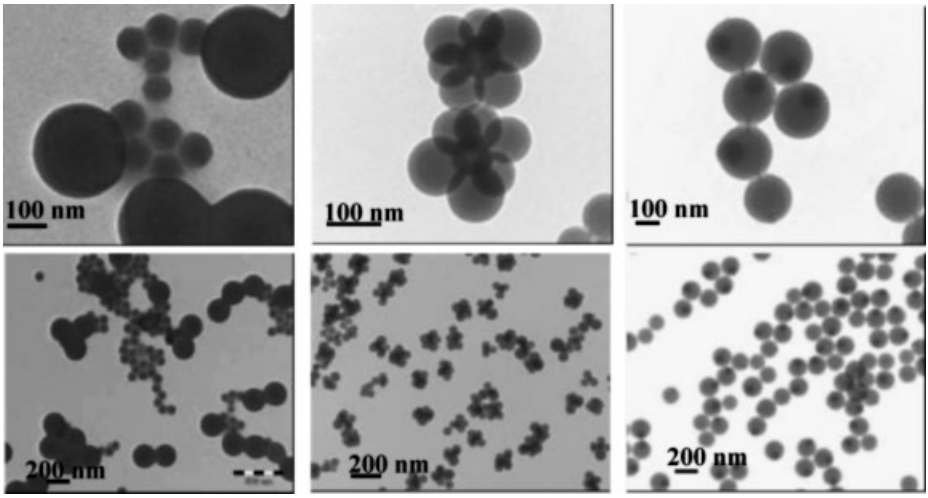


***Figure 1.***
TEM images of Klebosol 30N50 silica/polystyrene composite particles obtained for different MPS grafting densities. (a) without MPS, (b) $Q_{MPS} = 0.95\ \mu mol \cdot m^{-2}$, and (c) $Q_{MPS} = 1.9\ \mu mol \cdot m^{-2}$. The images were recorded at low (bottom) and high magnifications (top).

MPS grafting densities, the silica particles are able to stabilize the growing polymer spheres and generate a greater latex particle number than when SDS is used as surfactant alone. This is presumably due to the presence of negative charges on the silica surface that enable electrostatic stabilization of the growing polystyrene nodules. However, when the MPS grafting density increases, the polymer spheres no longer phase-segregate on the silica surface and the diameter of the resulting core-shell composite particles increases to reach the value corresponding to pure polymer particles stabilized by surfactant only. As it is known that the rate in emulsion polymerization is proportional to the particle number, one can expect the polymerization kinetics to be influenced by the MPS grafting density (which in turn leads to different polystyrene particles size). The results shown in Figure 2 indicate that, as predicted, the polymerization rate increases with increasing the MPS grafting density and then decreases in agreement with the particles size evolution.

The mechanism of formation of the silica/polystyrene composite particles using MPS as coupling agent can be explained as follows. First, persulfate initiator starts to decompose in the water phase giving rise to the formation of radicals. These radicals will propagate with aqueous phase monomers until they undergo one of the following fates: i) aqueous phase termination or ii) entry into a micelle or precipitation (depending on the surfactant concentration), creating somehow a new particle. Aqueous-phase oligomers of all degree of polymerization can also undergo frequent collision with the surface of the silica seed particles, and have therefore a high probability to copolymerize with the double bonds at the silica surface, thus generating chemisorbed polymer chains in the early stages of polymerization. These discrete loci of adsorption are preferred to adsorb monomer or radicals compared with the bare seed surface. As a result, these discrete loci of adsorption become discrete loci of polymerization. The higher the MPS grafting density, the higher the probability of free radicals capture by silica and therefore the higher the affinity of the growing polymer for the surface. The nucleated polystyrene nodules can thus coalesce and

 

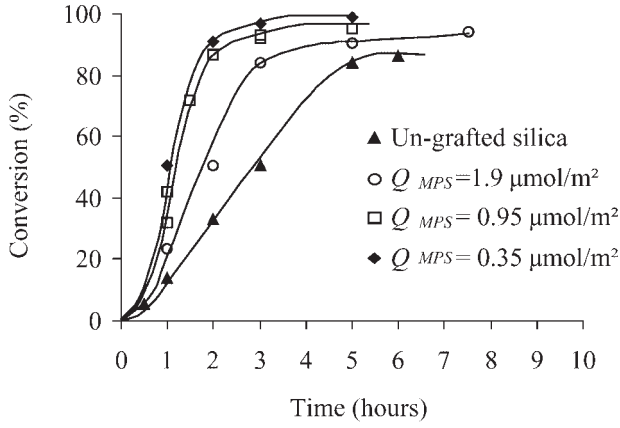


***Figure 2.***
Conversion versus time curves for polymerization of styrene performed in the presence of Klebosol 30N50 silica particles with increasing amounts of MPS on their surface. $Q_{MPS}$ indicates the actual MPS grafting density as determined by UV analysis using the depletion method.

form a homogeneous coating around the silica seed particles with no change in the overall surface area (i.e., the particles number is kept constant) whereas for low MPS grafting densities, the hydrophilic nature of the surface promotes phase segregation of the growing polymer spheres, the later being presumably stabilized by the negative charges of silica together with adsorbed surfactant molecules. Therefore, the number of polymer particles increased by one order of magnitude which had a significant influence on the polymerization kinetics as shown above.

### *Adsorption of a Polyethylene Glycol-based Macromonomer*

Apart from the use of a polymerizable alkoxysilane, silica/polystyrene composite particles with a raspberry-like morphology have been elaborated in the presence of a methyl methacrylate-terminated polyethylene glycol macromonomer. This macromonomer is mainly hydrophilic due to the presence of ethylene oxide repeat units ($n \sim 23$), which are able to form hydrogen bonds with the silanol groups of silica and adsorb on its surface.[32] In addition, this molecule contains a methacrylate functionality able to copolymerize with styrene thus promoting *in situ* formation of composite particles. As a part of this work, we indeed demonstrated that polymerizations performed in the absence of the macromonomer did not give rise to composite colloids and produced instead separate populations of silica beads and latex spheres. In contrast, when the polymerization was carried out in the presence of micron-size silica beads and a tinny amount of the macromonomer ($1.5\mu mol/m^2$ of silica), hybrid particles with a raspberry-like morphology were successfully obtained (Figure 3). It must be mentioned that free polymer spheres were also present at the end of polymerization but due to the large difference between silica and polystyrene densities, they could be separated from the composite particles by centrifugation which enabled us to observe the morphology of the hybrid particles alone. To investigate the effect of the silica particles size on particles morphology, we synthesized silica spheres of various diameters using a procedure inspired from the literature[33,34] and compared them to very small silica particles of commercial origin. Figure 3 shows the TEM micrographs of the resulting composite particles obtained for silica particles with diameters of 1000, 500 and 13 nm, respectively. In these pictures,

 

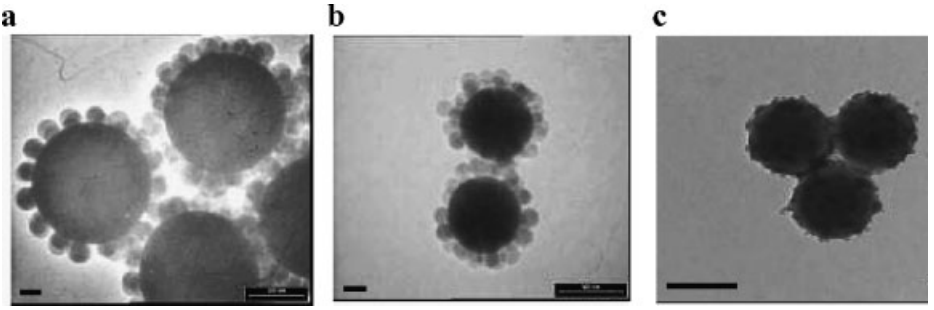


***Figure 3.***
TEM images of silica/polystyrene composite particles based on 1000 nm (a), 530 nm (b) and 13 nm (c) silica particles. (a, b) polymerization performed using $NP_{30}$ as surfactant and (c) soap-free polymerization. $[SiO_2] = 10$ $g \cdot L^{-1}$ (a, b) and 20 $g \cdot L^{-1}$ (c). Scale bar = 200 nm.

the silica beads can be identified by their size and their contrast. While the largest silica spheres (in dark, Figures 3a and 3b) appear to be regularly surrounded by polystyrene nodules (in grey) forming raspberry-like colloids, the very small silica particles appear to be mainly situated at the surface of the copolymer latex spheres (Figure 3c) although it is hard to conclude from this TEM image whether or not there are also some embedded silica particles. Moreover, it is noteworthy to mention that there is no free silica particles nor free latex spheres in this system which suggests a strong affinity of the growing polymer for the silica particles which are present in large amounts.

The mechanism of composite particles formation can be explained as follows. During the early steps of the polymerization, free molecules of monomer and PEG-MA react to form copolymers. These copolymers will continue to grow until they reach a critical size and become nuclei. Due to the presence of ethylene oxide groups in the structure of the macromonomer, and also because of the presence of the surfactant, these nuclei can become steady and evolve as mature polymer particles.[35] This scenario also holds for the macromonomer adsorbed on the silica surface. In that case, the growing copolymers are expected to strongly attach on silica via the anchored PEG derivative. Free PEG molecules are also initially present in the suspension medium but it can be anticipated that the particles or at least the copolymers they form with styrene will also have a strong tendency to adsorb on silica. In summary, we can briefly describe our system as a self-stabilized copolymerization between the PEG macromonomer and styrene. When very small silica particles are involved in the process, the polymerization is expected to proceed in a similar way except that the primary particles, made of individual silica nanoparticles and polymer chains adsorbed on their surface by means of the macromonomer molecules, coagulate to decrease the overall surface area and become stable mature particles. Due to the hydrophilicity of silica, the later are thrown out of the particle during nucleation and accumulate on the surface of the colloid which situation is presumably the most favorable one from a thermodynamic point of view. If the silica particles really participate to nucleation, we should have an influence of the silica concentration on particles size and polymerization kinetics. Figure 4 shows the evolution of the conversion versus time and of particles size for a series of soap-free polymerizations performed in the presence of silica particles with concentrations comprised between 10 and 80 $g \cdot L^{-1}$.

As predicted, the data in Figure 4 show that the higher the amount of silica, the lower the particles size and the higher the polymerization rate. However, it seems that a minimum silica concentration is required to efficiently stabilize the composite latexes as the polymerization performed with only

 

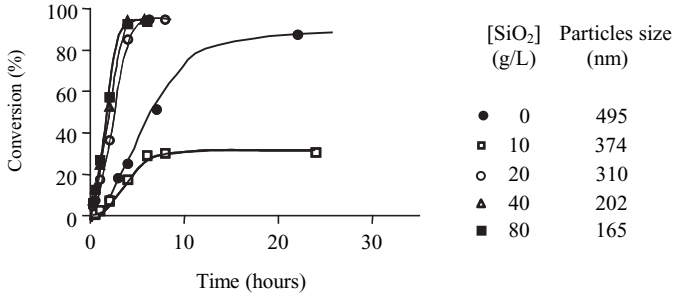


***Figure 4.***
Conversion versus time curves for a series of soap-free emulsion polymerizations of styrene performed in the presence of macromonomer (2.5 wt% respect to silica) and nanometer sized silica particles. [KPS] = 1 g · L$^{-1}$. [MMA] = 40 g · L$^{-1}$. [Styrene] = 160 g · L$^{-1}$.

10 g/L of silica led to relatively large particles and low conversions.

## Laponite/Polymer Composite Particles

### *Clay Structure*

Laponite RD is a fully synthetic clay similar in structure and composition to natural hectorite of the smectite group (Scheme 1). Each layer is composed of three sheets: two outer tetrahedral silica sheets and a central octahedral magnesia sheet. Isomorphous substitution of magnesium with lithium in the central sheet creates a net negative charge compensated by intralayer sodium ions located between adjacent layers in a stack. The cation exchange capacity of Laponite is 0.75 meq · g$^{-1}$.[36] The dimensions of the elementary platelets are the following: diameter 30 nm and thickness 0.9 nm. In the dry state or in organic solvents, the platelets are piled up into tactoïds of around 2–3 layers thick held together by long-range attractive forces. Reactive silanols, corresponding to structural defects, are located at the broken edges of these stacks while Mg-OH groups are contained into the internal space of the individual clay sheets. Figure 5a is a cryo–TEM image of a suspension of raw Laponite platelets. As mentioned in a previous work,[28] only the crystallites with their basal plane parallel to the observation direction can be clearly seen as dark ''filaments'', as they exhibit a strong diffraction contrast in this orientation. Platelets in other orientations, showing poor absorption contrast, are difficult to detect.

### *Grafting of the MPS and MPDES Molecules*

Grafting of the functional alkoxysilanes was performed in toluene by adding

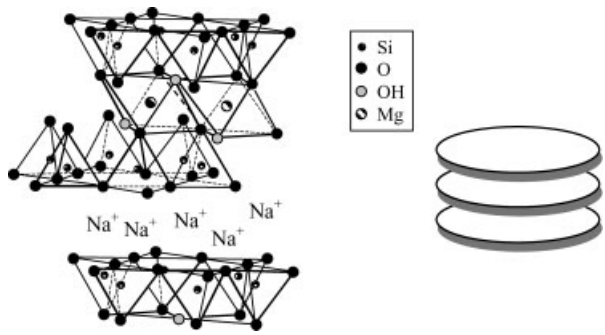


***Scheme 1.***
Laponite clay structure.

 

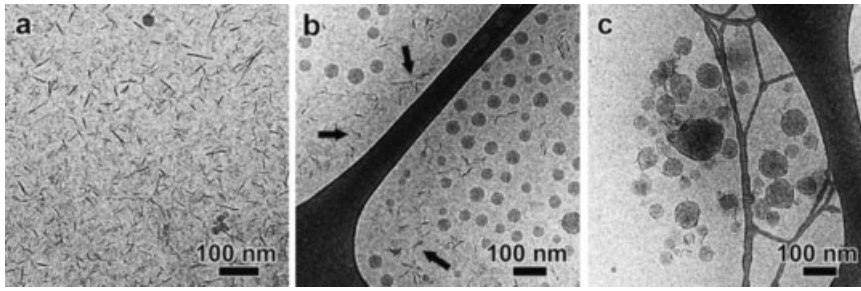


***Figure 5.***
Cryo-TEM images of: a) a suspension of Laponite platelets (the dark filaments are clay particles seen edge-on); b,c) "hybrid latexes" synthesized by seeded emulsion polymerization of styrene and butyl acrylate in the presence of raw Laponite (b) and 10 wt% of MPDES-functionalized Laponite clay platelets (c). In b, the arrows indicate the presence of Laponite aggregates.

increasing amounts of the coupling agents to the clay suspension. The grafting was qualitatively evidenced by FTIR, $^{29}Si$ and $^{13}C$ solid state NMR while the grafted amount was determined by carbon elemental analysis. FTIR indicates successful reaction of the organosilane molecules with the clay edges ($\nu_{C=O}$, 1700 $cm^{-1}$; $\nu_{CH}$, 2850, 2920 and 2980 $cm^{-1}$ and $\delta_{CH}$, 1380 $cm^{-1}$). More in depth examination of the carbonyl region showed that both the MPS and the MPDES coupling agents formed hydrogen bonds with the clay surface as the signal of the carbonyl group, which can be detected at 1720 $cm^{-1}$ in the original grafted molecules, was shifted to a lower wavenumber. However, in case of the trialkoysilane MPS coupling agent, a shoulder at 1720 $cm^{-1}$, which can be assigned to free carbonyl groups, appeared for high grafting densities suggesting the formation of a multilayer coverage. Indeed, MPS molecules can undergo self-condensation in the presence of water giving rise to the formation of polysiloxane oligomers that are attached to the clay edges. These oligomers can also link together the individual platelets and neighbouring clay stacks.

Contrary to the trialkoxysilane, the MPDES coupling agent, cannot condense in solution and forms a monolayer coverage lying flat on the border of the clay plates. Synthesis of the nanocomposite latexes in the presence of grafted Laponite was carried out using 1 g of the organically-modified Laponite suspended into 100 g of water in the presence of SDS and of a peptizing agent. Commercially, peptizers are added to raw Laponite powders in order to retard clay aggregation when the latter is suspended in water (giving rise to the so-called "sol grade"). These molecules are generally multivalent ion salts that bind specifically to the edges of the Laponite platelets. In the case of tetrasodium pyrophosphate ($Na_4P_2O_7$), which was the peptizer used in our study, this tetravalent negatively charged ion adsorbs onto the positively charged rims and thereby effectively screens the rim charge. Under such conditions, satisfactory clay suspensions were obtained in case of the MPDES-grafted Laponite whereas we did not succeed in redispersing the MPS-grafted clay. We presume that this is due to the fact that the clay platelets are irreversibly locked together by siloxane bridges bonding the clay edges as mentioned above. Therefore, in the following, only clay particles modified with the MPDES coupling agent will be involved in the polymerization reaction. Figure 5c shows a cryo-TEM image of c.a. 120 nm copolymer/Laponite nanocomposite particles obtained using MPDES-grafted Laponite as the seed while the micrograph in Figure 5b corresponds to a sample prepared by emulsion polymerization in the presence of raw Laponite. The polymer particles appear as gray spheres and some Laponite crystallites are seen as dark filaments. As

 

expected, no particular interaction was observed between the clay platelets and the latex particles in Figure 5b. Moreover, some clay aggregates can be clearly seen in between the latex spheres. In contrast, when the monofunctional silane molecule was used as coupling agent, a nanocomposite structure was obtained, the clay platelets constituting a ''shell'' around the polymer latex particles (Figure 5c). Moreover, it is worth noticing that the particles are slightly polygonal as the natural rigidity of Laponite crystals generates a faceting of the surface. It must be underlined that noticeable differences in colloidal stability were observed when bare Laponite was introduced in the polymerization reaction. Although the latexes were stable just after polymerization, they showed only a limited stability with time and coagulation was systematically observed upon storage. This is presumably related to the fact that as the clay platelets were not incorporated within the latex particles, they could form a gel in a similar way as they do in pure water solutions, a mechanism which is additionally promoted by the high ionic strength of the suspension medium. In contrast, successful incorporation of the clay sheets within the polymer particles allowed to achieve a better long term stability of the suspension medium as there were no ''free'' clay plates present in the surrounding aqueous solution.

### *Adsorption of a Polyethylene Glycol Based Macromonomer*

As before for silica, the PEG macromonomer was introduced in the clay suspension to promote *in situ* interactions of the growing radicals with the inorganic surface and generate composite latexes. The interaction of clays with PEO is well known and has been extensively studied in the past.[37–39] Polyethylene oxide polymers have been shown to interact with clay surfaces through ion-dipole interactions between ethylene oxide units and clay ions.[40] Qualitative evidence of the presence of the macromonomer on the clay surface was provided by FTIR spectroscopy after clay separation by precipitation in methanol. Based on our experience on silica, a series of soap-free emulsion polymerization reactions was carried out in the presence of the macromonomer and various concentrations of Laponite in order to establish whether the so-formed clay/macromonomer complexes were able to stabilize the growing latex spheres and influence consequently the polymerization rates and average particle diameters. As expected, polymerizations performed in the presence of the macromonomer but without Laponite gave rise to the formation of big latex spheres (Table 2) and slow polymerization kinetics (Figure 6). In contrast, polymerizations performed in the presence of both the macromonomer and Laponite gave rise to much smaller particles and higher polymerization rates (Figure 6). In addition, the higher the Laponite concentration, the faster was the polymerization reaction as could be expected with regards to the concomittant decrease in particles size with increasing the Laponite concentration (Table 2).

As before for silica, the kinetic data thus suggest that the clay platelets are capable to

***Table 2.***
Recipe, monomer conversion, particles size and particles number for a series of soap-free emulsion polymerizations of styrene in the presence of macromonomer and increasing concentrations of Laponite.

| Runs | Laponite (g/L) | PEG-MA (g/L) | $Na_4P_2O_7$ (g/L) | Conversion[a] (%) | *Dp* (nm) | *Np/L* |
|---|---|---|---|---|---|---|
| 1 | 0 | 1 | 2 | 17 | 456 | $6.8\ 10^{14}$ |
| 2 | 20 | 1 | 2 | 88 | 205 | $3.9\ 10^{16}$ |
| 3 | 30 | 1.5 | 3 | 96 | 199 | $4.7\ 10^{16}$ |
| 4 | 40 | 2 | 4 | 98 | 167 | $8.0\ 10^{16}$ |
| 5 | 60 | 3 | 6 | 99 | 167 | $8.1\ 10^{16}$ |

[Styrene] = 200 $g \cdot L^{-1}$, ACPA = 0.5 wt% relative to styrene, 70 °C, batch.
[a] Reaction time = 5 hours.

 

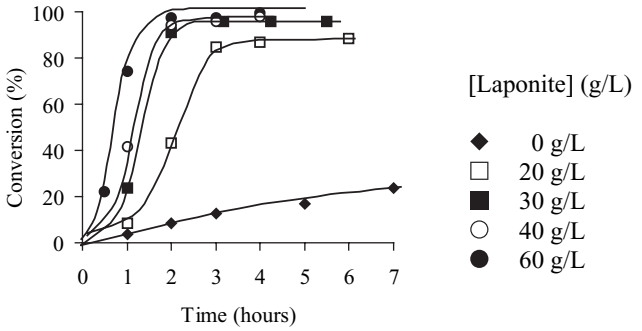


***Figure 6.***
Conversion versus time curves for a series of soap-free emulsion polymerizations of styrene performed in the presence of the macromonomer but without Laponite (◆) and polymerizations performed in the presence of the macromonomer and increasing Laponite concentrations (□, ■, ○, ●).

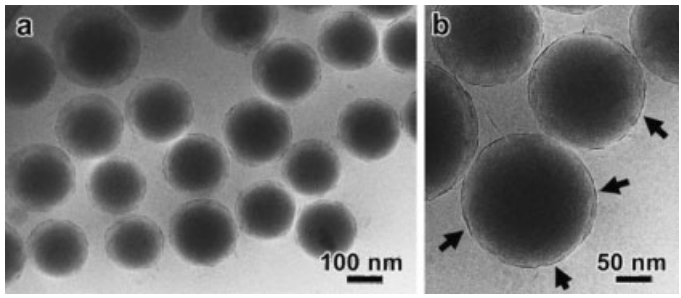


***Figure 7.***
Cryo-TEM images of spherical polystyrene latex particles stabilized by 10 wt% Laponite crystallites (run 2 in Table 2). In b, the arrows point to a few Laponite platelets seen edge-on on the surface of the polystyrene particle.

stabilize the polymer spheres by accumulating on their surface. To confirm this hypothesis, we analyzed the particles morphology. Figure 7 shows the cryo-TEM image of polystyrene/Laponite composite particles prepared using 10 wt% of the PEG-MA-Laponite complex (run 2 in Table 2). Regular spherical particles with a diameter of around 200 nm are observed. As seen from the distribution of dark ''filaments'' which correspond to the Laponite platelets (see Figure 7a), they are surrounded by clay particles which form a protecting, negatively charged shell structure around the polymer core. The ability of layered silicates to stabilize emulsions or miniemulsions has been reported in several articles.[41–43] The present work gives further evidence that synthetic clay platelets as Laponite can also be used to provide pickering stabilization to polymer latexes produced by emulsion polymerization.

## Conclusion

Nanocomposite latexes based on silica and Laponite clay platelets were synthesized through emulsion polymerization using two different strategies which both aimed at to overcome the intrinsic hydrophilic character of the inorganic colloids and promote the growth of polymer on their surface. The mineral particles were modified either by grafting a polymerizable organoalkoxysilane or by the adsorption of a PEG-based macromonomer carrying a terminal MMA group. As far as silica is concerned, we have shown that the morphology of the nanocomposite colloids can be finely tuned by

 

varying the surface density of the reactive double bonds. Either multipod-like or core-shell morphologies were obtained depending on the silane grafting density. All the results reported in this article support the idea that the nucleation takes place through the capture of the growing radicals by the silica particles. As the latter carry negative charges on their surface, they are able to stabilize the growing latex spheres which number is much larger than in the absence of silica. As the rate in emulsion polymerization is proportional to the particle number, the kinetics of polymerization was strongly accelerated under these conditions. In the second route, double bonds on the silica surface are provided by the adsorption of the PEG macromonomer derivative. The growing polymer nodules are only physisorbed on the mineral surface and homogeneously distributed around the particles forming raspberry-like colloids. The morphology also depends on the silica particle diameter and evolves from raspberry to currant bun with decreasing the silica particles size. In the situation where the polymerization is performed in the presence of very small silica particles and without surfactant, the conversion versus time curves have show that the silica particles participate to the stabilization of the polymer latex spheres giving rise to smaller particles and thus to higher polymerization rates.

In the second part of this article, polymer latexes surrounded by anisotropic Laponite platelets have been successfully obtained by the two routes. It was demonstrated that the clay particles play the role of a pickering stabilizer and are capable to stabilize the composite particles whose diameter depends on the amount of Laponite initially introduced into the reactor. The higher the clay concentration, the larger the composite particle number and, therefore, the higher the polymerization rate as predicted from the emulsion polymerization theory.

*Acknowledgements:* The authors thank Christian Novat and Nicolas Tissier (LCPP, Villeurbanne) for their great help in TEM analysis. The gift of a sample of Laponite RD by Rockwood Additives is greatly acknowledged.

[1] C. H. M. Hofman-Caris, *New J. Chem.* **1994**, *18*, 1087.
[2] A. D. Pomogalio, *Russ. Chem. Rev.* **2000**, *69*, 53.
[3] G. Kickelbick, *Prog. Polym. Sci.* **2002**, *28*, 83.
[4] V. Castelvetro, C. De Vita, *Adv. Coll. Interf. Sci.* **2004**, *108-109*, 167.
[5] E. Bourgeat-Lami, in "*Encyclopedia of Nanoscience and Nanotechnology*", H. S. Nalwa, Ed., American Scientific Publishers, Los Angeles, **2004**, Vol. 8, pp. 305–332.
[6] E. Bourgeat-Lami, *J. Nanosci. Nanotechnol.* **2002**, *2*, 1.
[7] M. Abboud, L. Casaubieilh, F. Morvan, M. Fontanille, E. Duguet, *J. Biomed. Mater. Res. (Appl. Biomater.)* **2000**, *53*, 728.
[8] E. Bourgeat-Lami, J. Lang, *J. Colloid Interf. Sci.* **1999**, *210*, 281.
[9] S. Chalaye, E. Bourgeat-Lami, J. L. Putaux, J. Lang. *Macromol. Symp.* **2001**, *169*, 89.
[10] D. Hoffmann, K. Landfester, M. Antonietti, *Magnetohydrodyn.* **2001**, *37*, 221.
[11] B. Erdem, D. Sudol, V. L. Dimonie and M. El-Aasser, *J. Polym. Sci., Part A: Polym. Chem.* **2000**, *38*, 4441.
[12] F. Tiarks, K. Lanfester, M. Antonietti, *Langmuir* **2001**, *17*, 5775.
[13] Th. Batzilla, A. Tulke, *J. Coat. Technol.* **1998**, *70*, 77.
[14] C. Barthet, A. J. Hickey, D. B. Cairns, S. P. Armes, *Adv. Mater.* **1999**, *11*, 408.
[15] M. J. Percy, C. Barthet, J. C. Lobb, M. A. Khan, S. F. Lascelles, M. Vamvakaki, S. P. Armes, *Langmuir* **2000**, *16*, 6913–6920.
[16] M. J. Percy, S. P. Armes, *Langmuir* **2002**, *18*, 4562.
[17] M. J. Percy, J. I. Amalvy, D. P. Randall, S. P. Armes, S. J. Greaves, J. F. Watts, *Langmuir* **2004**, *20*, 2184.
[18] J. L. Luna-Xavier, A. Guyot, E. Bourgeat-Lami, *J. Colloid Interf. Sci.* **2001**, *250*, 82.
[19] J. L. Luna-Xavier, A. Guyot, E. Bourgeat-Lami, *Polym. Int.* **2004**, *53*, 609.
[20] J. Zhang, N. Coombs, E. Kumacheva, *J. Am. Chem. Soc.* **2002**, *124*, 14512.
[21] S. Reculusa, C. Poncet-Legrand, S. Ravaine, C. Mingotaud, E. Duguet, E. Bourgeat-Lami, *Chem. Mater.* **2002**, *14*, 2354.
[22] S. Reculusa, C. Mingotaud, E. Bourgeat-Lami, E. Duguet, S. Ravaine, *Nano Letters* **2004**, *4*, 1677.
[23] E. Bourgeat-Lami, M. Insulaire, S. Reculusa, A. Perro, S. Ravaine, E. Duguet, *J. Nanosci. Nanotechnol.* **2006**, *6*, 432.
[24] K. Zhang, H. Chen, X. Chen, Z. Chen, Z. Cui, B. Yang, *Macromol. Mater. Eng.* **2003**, *288*, 380.
[25] N. Negrete-Herrera, J.-M. Letoffe, J.-L. Putaux, L. David, E. Bourgeat-Lami, *Langmuir* **2004**, *20*(5), 564.
[26] N. Negrete-Herrera, S. Persoz, J-L. Putaux, L. David, E. Bourgeat-Lami, *J. Nanosci. Nanotechnol.* **2006**, *6*, 421.

 

[27] M. Schappacher, A. Deffieux, J.-L. Putaux, P. Viville, R. Lazzaroni. *Macromol.* **2003**, *36(15), 5776.*
[28] N. Negrete-Herrera, J.-M. Letoffe, J.-P. Reymond, E. Bourgeat-Lami, *J. Mater. Chem.* **2005**, *15*, 863.
[29] M. Schappacher, A. Deffieux, J.-L. Putaux, P. Viville, R. Lazzaroni. *Macromolecules* **2003**, *36*(15), 5776
[30] V. Durrieu, A. Gandini, M. N. Belcacem, A. Blayo, G. Eiselé, J.-L. Putaux. *J. Appl. Polym. Sci.* **2004**, *94*(2), 700.
[31] E. Bourgeat-Lami, P. Espiard, A. Guyot, *Polymer* **1995**, *36*, 4385.
[32] D. N. Furlong, J. R. Aston, *Colloids Surf.* **1982**, *4*, 121.
[33] W. Stöber, A. Fink, E. Bohn, *J. Colloid Interf. Sci.* **1968**, *26*, 62.
[34] S. Kang, S. I. Hong, C. R. Choe, M. Park, S. Rim, J. Kim, *Polymer* **2001**, *42*, 879.
[35] R. H. Ottewill, R. Satgurunathan, *Colloid Polym. Sci.* **1995**, *273*, 379.
[36] See for instance: [36a] M. Morvan, D. Espinat, J. Lambard, T. Zemb, *Colloids Surf. Pt. A* **1994**, *82*, 193; [36b] B. S. Neumann, K. G. Sanson, *Israel J. Chem.* **1970**, *8*, 315; [36c] J. D. F. Ramsay, S. W. Swanton, J. Bunce, *J. Chem. Soc. Faraday Trans.* **1990**, *86*, 3919.
[37] R. A. Vaia, S. Vasudevan, X. Krawiec, L. G. Scanlon, E. P. Giannelis, *Adv. Mater.* **1995**, *7*, 154.
[38] P. Arranda, Y. Mosqueda, E. Perez-Cappe, E. Ruiz-Hitzky, *J. Polym. Sci. B: Polym. Phys.* **2003**, *41*, 3249.
[39] E. Loizou, P. Butler, L. Porcar, G. Schmidt, *Macromol.* **2006**, *39*, 1614.
[40] Z. Shen, G. P. Simon, Y. Cheng, *Polymer* **2002**, *43*, 4251.
[41] N. P. Ashby, B. P. Binks, *Phys. Chem. Chem. Phys.* **2000**, *2*, 5640.
[42] S. Cauvin, P. J. Cauvin, S. A. F. Bon, *Macromol.* **2005**, *38*, 7887.
[43] D. K. Voorn, W. Ming, A. M. van Herk, *Macromol.* **2006**, *39*, 2137.

 

# Unusual Kinetics in Aqueous Heterophase Polymerizations

*Klaus Tauer,* Muyassar Mukhamedjanova, Christian Holtze, Pantea Nazaran, Jeongwoo Lee*

**Summary:** The heterogeneous nature of aqueous heterophase polymerizations is the base for an easy route to unique block copolymers, for the development of new and more effective polymerization strategies, and the abilities to unique studies of radical polymerization kinetics. Thermo-sensitive double hydrophilic block copolymers and micro- or nano-gel particles of poly(N-isopropyl acrylamide) as thermo-responsible block and charged or uncharged hydrophilic polymers can easily be prepared if the polymerization of N-isopropyl acrylamide is started with the corresponding polymeric radicals. The application of extremely fast microwave heating allows the development of highly effective pulsed thermal polymerization strategies and the production of polymers with desired molecular weight distributions over wide ranges. 2,2′-azobisisobutyronitrile simultaneously initiates the polymerization in both the monomer and the aqueous phase and leads, even under surfactant-free conditions, to stable latex particles.

**Keywords:** 2,2′-azobisisobutyronitrile; block copolymers; heterophase polymerization; microwave heating; particle nucleation

## Introduction

Aqueous heterophase polymerization is not only an industrially important radical polymerization technique but also scientifically challenging as well as offering unique possibilities for basic scientific studies. All advantages as well as all kinetic peculiarities of heterophase polymerizations are grounded on the heterogeneous nature of the reaction system creating at least two, extremely different reaction loci. The potential ability to produce amphiphilic block copolymers via a simple radical polymerization mechanism under such circumstances was recognized already 1952.[1]

This paper emphasizes the utilization of unusual kinetic effects in aqueous heterophase polymerizations regarding (1) the comparably facile synthesis of block copolymers, (2) the advantages of the use of microwave heating, and (3) the abilities to study radical polymerization reactions taking place simultaneously in both the monomer and the continuous aqueous phase if monomer soluble initiators are employed mainly during the particle nucleation period.

Max Plank Institute of Colloids and Interfaces, Am Mühlenberg, D 14476 Golm, Germany
E-mail: klaus.Tauer@mpikg.mpg.de

## Experimental Part

### Block Copolymer Formation

All polymerization experiments were carried out at 70 °C in 100 ml all - glass reactors. The precursor polymers were synthesized with the following recipe: 100 g of water, 20 g of monomer, 0.32 g of 2,2-azobis(2-methyl-N-(2-hydroxyethyl)propionamide) (VA-086 from Wako) as initiator. The recipe for the production of the linear and cross-linked block copolymers with N-isopropyl acrylamide (NIPAm) was 100 g of water, 2 g of the corresponding precursor polymer as reductant, 4 g of NIPAm, 0.4 g of ceric

ammonium nitrate dissolved in 5 ml of concentrated nitric acid as oxidant, and 0.1 g of N,N′-methylenebis(acrylamide) ylenebis(acrylamide) (MBAm), respectively. After polymerization all polymers were cleaned by ultrafiltration through DIAFLO membranes with a molecular weight cut-off of $10^4$ g/mol (type YM 10 from Amicon, Inc., USA) as long as the amount of original water was replaced ten times. Then, the polymers were isolated by freeze drying. The molecular weight distributions of the precursor polymers with hydroxymethyl terminal groups were analyzed by analytical ultracentrifugation according to standard procedures.[2,3] The particle size ($D_i$, intensity weighted average particle size) in solution or in dispersion was measured using a NICOMP particle sizer (model 370). Additionally some samples were investigated with transmission electron microscopy (TEM) with a Zeiss EM 912 Omega microscope.

### Pulsed Thermal Polymerizations with Microwave Heating

The experimental and analytical procedures are described in great detail elsewhere.[4] Miniemulsions were prepared according to standard procedures from an organic phase that consisted of 6 g of styrene and 250 mg of hexadecane (hydrophobe) and an aqueous phase that consisted of 24 g of water (continuous phase) and 74 mg of SDS (surfactant). After pre-emulsification for 1 h homogenization was carried out by ultrasonicating the macroemulsion with a sonicatortip (Branson sonifier W450 Digital) under ice cooling for 2 min. Oil-soluble radical initiators were added to the organic phase before homogenization, and water-soluble radical initiators were added to the miniemulsion after homogenization.

### Investigations of Particle Nucleation with 2,2′-Azobisisobutyronitrile

These investigations were carried out at 70 °C in an experimental setup allowing on-line measurement of optical transmission and conductivity of the aqueous phase as described in.[5] First, the reactor was filled with 400 g of de-ionized and degassed water from a Seral purification system (PURELAB Plus) with a conductivity of 0.06 μS/cm. Then, styrene was placed on top of the water confined in a glass funnel maintaining a constant monomer – water interface of 31 $cm^2$ throughout the experiment (the remaining water – air interface is 80 $cm^2$). 120 minutes after styrene addition the polymerizations were started by adding 76 mg of 2,2′-azobisisobutyronitrile (AIBN) dissolved in 1.2 g of styrene. The total amount of styrene for all experiments was 3.7 g. The AIBN in styrene solution was added either to the monomer reservoir in the glass funnel or directly into the aqueous phase. At the end of the polymerizations the monomer phase was separated from the aqueous phase and the polymers formed in both phases were characterized regarding their molecular weight distributions by means of SEC. Additionally, the latex particles were imaged by TEM.

### Block Copolymer Formation

The production of block copolymers via radical polymerization premises at least a much shorter radical formation period compared with the duration of the propagation reaction, a negligible probability of radical termination throughout the whole polymerization process, and a sequential monomer addition. The latter requirement is the easiest to fulfill. In contrast, the realization of the two other points strongly requests much more efforts. To block the radical termination means to restrict the probability of radical encounters which is possible by either decreasing the number density of radicals per unit volume or by the generation of high molecular weight radicals. A low number density of growing radicals per unit volume is successfully realized by the various controlled or living radical polymerization techniques.[6] The creation of a situation where only high molecular weight radicals grow during the entire polymerization reaction is possible by the application of polymeric initiators.[7–9] Under such conditions block copolymer formation is the more effective

 

the higher the molecular weight of the initiating radicals as radical termination decreases according to a power law with increasing molecular weight.[10] In general, the requirement of timely separated radical formation and propagation can be realized in different ways. Any kind of radiation-induced radical formation allows controlling the duration of the period of initiation of growing chains. For the first synthetic block copolymers ever described BOLLAND & MELVILLE used UV-light.[11] These authors reported as early as 1939 the formation of poly(methyl methacrylate)-*b*-polychloroprene-*b*-poly(methyl methacrylate) triblock copolymers by radical gas phase polymerization. After switching off the UV-light growing radicals deposited at the reactor walls survived quite a long time and continued to grow after addition of new monomer. Another remarkable example how heterophase conditions can be used to make block copolymers by conventional radical polymerization is the application of a special initiating system in emulsion polymerization.[12] HORIE & MIKULASOVA used a polymeric redox-initiator system. Though, the initiator system was removed after 30 minutes the polymerization in the latex continued until complete styrene conversion and moreover, after the addition of methyl methacrylate block copolymer formation was proven. Obviously, growing radicals can easily survive inside latex particles as it was also proven by electron spin resonance investigations of MMA emulsion polymerization. [13] The continuation of a radical polymerization reaction after ending primaryradical formation is known as 'post-effect' and is characterized by non-steady state free radical polymerization kinetics.[14] O'SHAUGHNESSY & YU have demonstrated that the 'infinite' lifetime in the post-effect situation emerges directly from principles of polymer physics after the onset of entanglements under homogeneous reaction conditions.[14,15]

These considerations allow the conclusion that under the conditions of emulsion polymerization initiated with polymeric radicals a latex particle is the perfect place for polymeric radicals to survive not only in the glassy but also in the swollen state which is a high concentrated polymer in monomer solution (about 50 weight-%). Consequently, an optimum reaction system for producing block copolymers by ordinary radical polymerization is a heterophase polymerization with the generation of polymeric radicals. It was experimentally proven that a redox initiator system with $Ce^{4+}$ as oxidant and a hydrophilic polymer with hydroxymethyl end groups as reductant leads to the formation of single polymeric radicals at the terminal carbon atom (cf. Figure 1).

For monomethoxy terminated poly(ethylene glycol) as reductant it was shown that during the polymerization of N-isopropyl acrylamide (NIPAm) the formation of primary poly(ethylene glycol) radicals stops after about five minutes whereas the growing poly(ethylene glycol)-*b*-PNIPAm radicals survive many hours.

The polymerization could be restarted many times after the addition of new batches of monomer.[16] In these experiments the survival of radicals was observed even after the aggregation of the growing poly(ethylene glycol)-*b*-PNIPAm chains to

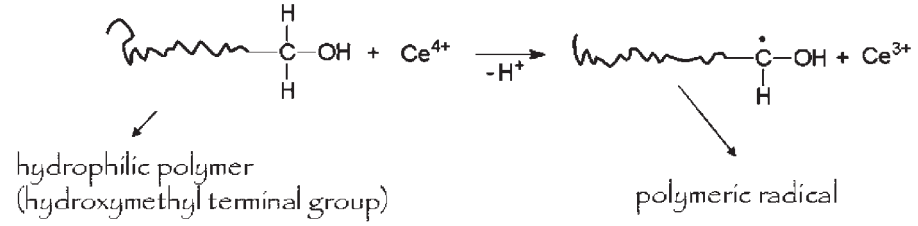


***Figure 1.***
Illustration of the formation of poly-meric radicals.

 

latex particles as the polymerization temperature was above the critical solution temperature of PNIPAm. This experimental fact was utilized to produce a huge variety of amphiphilic block copolymers by adding, after the polymerization of the first batch of NIPAm was completed, other hydrophobic monomers which swell the PNIPAm core of the latex particles.[17,18]

Hydrophilic precursor polymers with hydroxymethyl end groups can easily be prepared by polymerization in aqueous solution with corresponding initiators such as 2,2-azobis(2-methyl-N-(2-hydroxyethyl)-propionamide) or symmetrical poly(ethylene glycol)-azo initiators.[7] Apparently, the average molecular weight and the molecular weight distribution (MWD) of the precursor polymers is not crucial as poly(ethylene glycols) with a molecular weight of 5000 g/mol and the hydrophilic polymers mentioned in Table 1 with much higher average molecular weights and much broader MWD have been successfully employed as polymeric reductants in NIPAm polymerization.

These precursor polymers lead to hydrophilic thermo-sensitive block copolymers, which form at room temperature (RT) transparent solutions which convert during heating into electrosterically stabilized PSS-PNIPAm, PAA-PNIPAm, PDADMAC-PNIPAm, and PDEAMEMA-PNIPAm block copolymer particles.

For the PSS-PNIPAm, PDADMAC-PNIPAm, and PDEAEMA-PNIPAm block copolymers the average particle size of the aggregates decreases with increasing temperature up to 35 °C and remains constant at higher temperatures (cf. Figure 2). The size of the aggregates at temperatures below the critical solution temperature of the PNIPAm–block depends strongly on the nature of the other block. The observed order PSS > PDADMAC > PDEAEMA indicates both an influence of the electrical nature and the chain length. The PNIPAm-block possesses a quite strong aggregation power as not only the uncharged PDEAEMA chains but also the polyelectrolyte chains are brought into much closer contact in the aggregated state. Interestingly, the thermal behavior of the PAA-PNIPAM block copolymers is the opposite as the aggregate size increases with increasing temperature over the whole range. This indicates a specific acid – base interaction and hence, a partly ampholytic nature of this block copolymer causing colloidal destabilization.

Thermo-sensitive micro- or nano-gel particles can be obtained if the block copolymer formation is carried out in the presence of MBAm as a cross-linker.

Expectedly, the thermo-sensitivity of the gels is much lower that that of the uncross-linked counterparts as $D_i$ decrease during heating by only 100 nm. TEM images of the block copolymer gel particles reveal an interesting effect of the nature of the hydrophilic block on the morphology (Figure 3). The anionic PSS and PAA – blocks collapse on the PNIPAm cores but the cationic PDADMAC blocks remain stretched on the sample grids and reveal nicely the core shell morphology of the block copolymer gel particles.

***Table 1.***
Precursor polymers with hydroxymethyl end groups.

| Precursor polymer | Range of the MWD |
|---|---|
| Poly(styrene sulfonate) (PSS) | $1.0 \cdot 10^5$–$1.6 \cdot 10^6$ |
| Poly(diallyldimethylammonium chloride) (PDADMAC) | $1.0 \cdot 10^4$–$2.0 \cdot 10^5$ |
| Poly(acrylic acid) (PAA) | $5.0 \cdot 10^5$–$3.0 \cdot 10^6$ |
| Poly(diethylaminoethyl methacrylate) (PDEAEMA) | $1.0 \cdot 10^5$–$2.5 \cdot 10^6$ |

## Microwave Heating

Aqueous heterophase polymerizations may be carried out in microwave ovens because the polar nature of the continuous phase allows for efficient microwave coupling. This dielectric heating is extremely fast as the reaction mixture can be warmed up within about 12 seconds from room temperature to >90 °C. Comparable with radiation induced polymerization pulsed thermal polymerizations (PTP) with alternating 'hot' and 'cold' stages as illustrated in Figure 4 give rise to

 

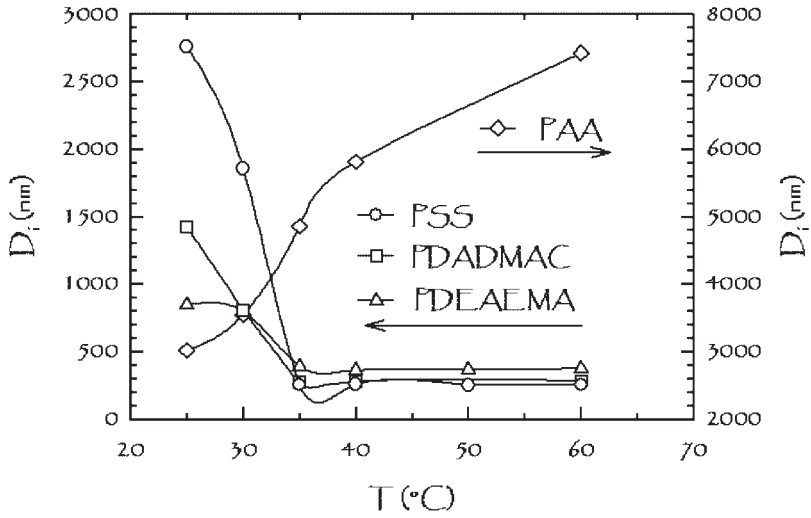


***Figure 2.***
Average aggregate size ($D_i$) in dependence of the temperature (T) for PNIPAm block copolymers with various hydrophilic blocks.

conditions, in which the cold stages are perfect post-effect situations in the above sense.

In a comprehensive study about the initiator influence during PTP of styrene in miniemulsions it turned out that medium hydrophobic initiators such as AIBN and PEGA200 lead to largely enhanced conversion (Table 2) compared to the much more hydrophilic potassium peroxodisulfate (KPS) or the much more hydrophobic 2,2′-azobis(2-methyl-butyronitrile) (V59).[4]

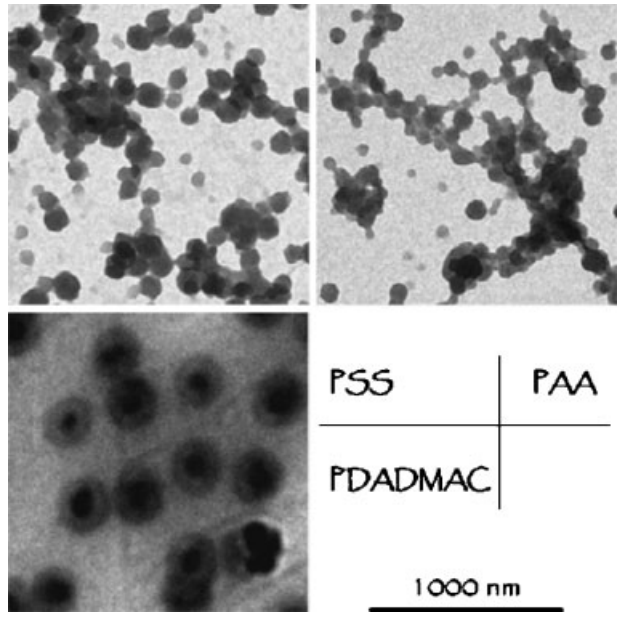


***Figure 3.***
TEM images of PNIPAm block copolymer gel particles with various hydrophilic blocks.

 

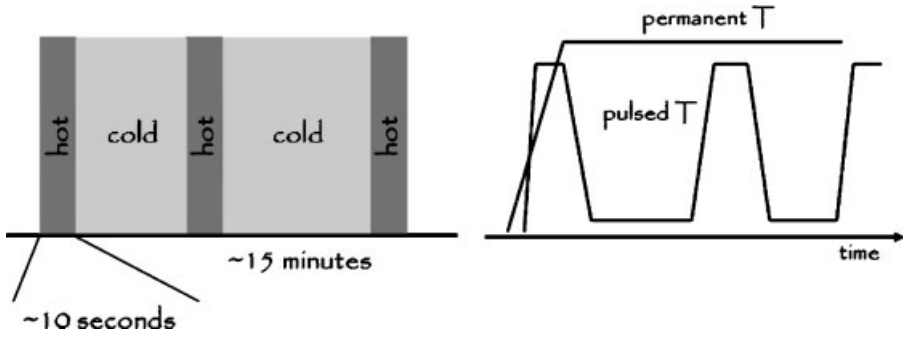


***Figure 4.***
Illustration of the pulsed thermal polymerization (PTP) procedure (left) with cycles of alternating hot and cold stages and the temperature profiles during polymerizations with pulsed and permanent heating (right).

***Table 2.***
Conversion during PTP of styrene miniemulsions after 4 pulses of 1kW power and an initiator concentration of 450 μmol except V59, where 900 μmol were used.

| Initiator | V59 | AIBN | PEGA200 | KPS |
|---|---|---|---|---|
| Conversion | 39.8% | 88.4% | 80.4% | 39.0% |
| Water solubility | <1 mM | 2.44 mM[19] | 4.58 mM[7] | 18.5 mM[20] |

The temperature profile during the polymerization has no influence on the achievable conversion for a given initiator concentration but a strong influence on the average molecular weight (cf. Figure 5). The PTP results in polymers with much higher molecular weights than the polymerizations with permanent microwave heating.

The MWD changes during PTP in a very specific way in dependence on both the initiator concentration and the number of pulses as exemplarily shown for AIBN in

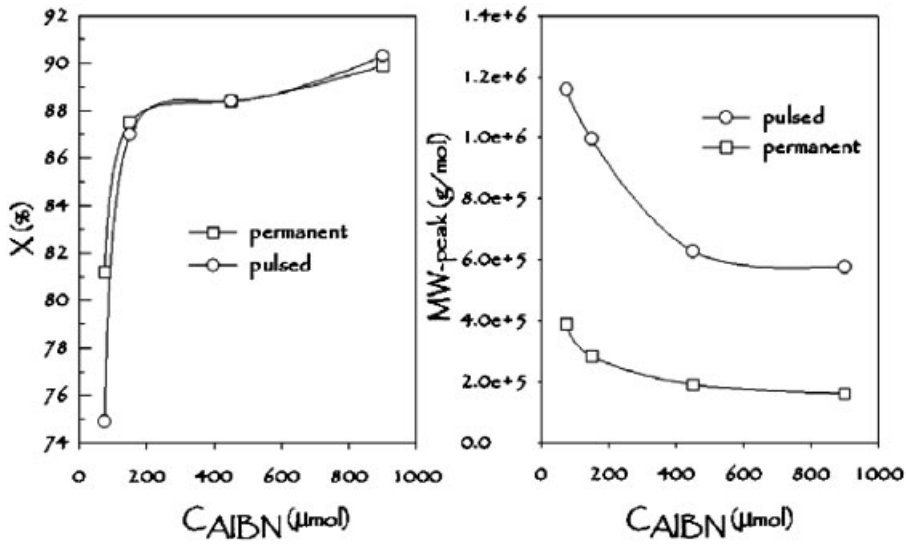


***Figure 5.***
Dependence of the monomer conversion and the peak molecular weight (MW-peak) on the AIBN concentration and the temperature profile obtained in styrene miniemulsion polymerization with microwave heating.

 

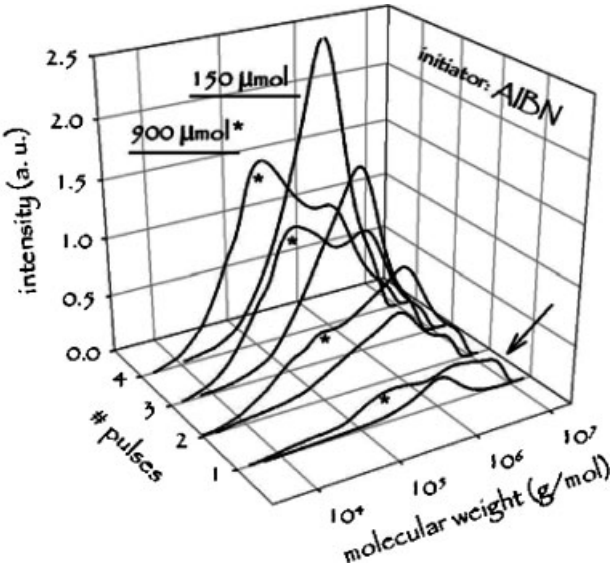


***Figure 6.***
Development of the MWD during the PTP of styrene miniemulsions at low and high initiator concentration (AIBN) after an increasing number of microwave pulses; the target temperature during the microwave pulse was 92 °C.

Figure 6. This graph contains conversion weighted MWD in which the area under the SEC traces is directly proportional to the monomer conversion. This kind of presentation makes it easy to see how much polymer in a certain molecular weight range has been formed in a given conversion range or microwave pulse.

The monomer conversion for the polymerizations of Figure 6 after each cycle at the end of the 'cold period' obeys common experience. It is the higher the higher the initiator concentration and after 4 temperature pulses it reaches 87 and 90% for 150 and 900 μmol of AIBN, respectively. But the MWD's as depicted elucidate the peculiarities of PTP.

In the range of the MWD below $10^6$ g/mol the expected influence of the AIBN concentration is observed as higher amounts of initiator cause the formation of higher portions of polymer chains in the low molecular weight region. But also in the high molecular weight region, close to the exclusion limit of the SEC apparatus, a large portion of polymer chains is present especially for the high AIBN concentration (indicated by the arrow in Figure 6). Particularly, after the first two cycles the maximum in the MWD is in the high molecular weight region above $10^6$ g/mol. This is an unusual but interesting feature of PTP and illustrates the possibilities to realize high rates and high molecular weights simultaneously.

Another unusual result of PTP is illustrated in Figure 7. These data show for both the mass average molecular weight ($M_w$) and the conversion a clear tendency to decrease with increasing energy input during the radiation period.

The parallel change of conversion and average molecular weight with increasing energy input is not clear at a glance as it apparently contradicts the 'normal' expectation of radical kinetics. However, an explanation is possible considering the peculiarities of both the pulsed thermal polymerization procedure and the heterophase conditions.

During the hot stage of the cycle the rate of radical formation is high and the huge number of low molecular weight radicals favors bimolecular termination as it scales

 

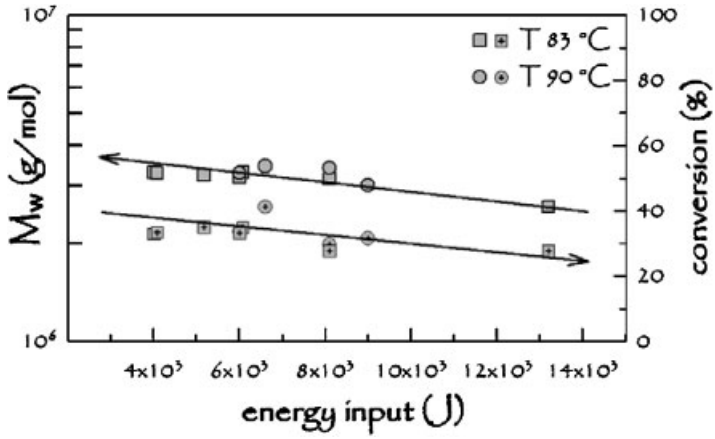


***Figure 7.***
Change of conversion and mass average molecular weight ($M_w$) after the first cycle with the energy input (microwave power times duration of the pulse) for two different target temperatures; one single pulse, initiator: 450 μmol PEGA200.

with the radical concentration squared. However, a few radicals survive and continue to grow during the cold stage where no radicals are generated. The heterophase nature of the reaction system supports the surviving of some radicals due to the compartmentalization and the high viscosity inside the particles. The chain transfer limit of the average molecular weight for radical styrene polymerization at 0 °C can be estimated to be about $10^7$ g/mol.[21–23] The following model calculation elucidates the importance of the cold stage for the PTP. An average miniemulsion droplet with a diameter of 100 nm contains about $3 \cdot 10^6$ styrene molecules. Assuming 40% monomer conversion after the first cycle (that is the highest value obtained so far) and chain growth until the transfer limit means that a single radical per particle has to generate about 12 chains or 11 times to do radical transfer to monomer. This scenario would require at most a duration of the cold stage of about $12 \cdot (10^5/k_p[M]) =$ 4400 s if a propagation frequency at 0 °C of $k_p[M] = 270.6$ 1/s is assumed. [24] These estimations – though quite rough – seem to be not unrealistic as the gap between two pulses is at least 900 s and the temperature has to decrease from 90 °C to zero within this time. Moreover, as the propagation frequency at 90 °C is only 30 times of that at 0 °C most of the monomer conversion is generated by the surviving radicals during the cold stage.

An increasing rate of primary radical formation (higher initiator concentration or energy input) increases the number of surviving radicals. However, if this number is above a critical value and if there is more than one growing radical per particle the small radical formed after chain transfer to monomer can cause termination. This might explain the dependence of the conversion and the average molecular weight on the energy input.

In conclusion of this section, the extremely fast heating capabilities of microwaves can be used to tailor the MWD during aqueous heterophase polymerizations only by physical means. The PTP scenario or the generation of alternating sequences of steady state and non-steady state conditions regarding the concentration of growing radicals allows a certain control over the MWD. Broad MWD are accessible, which might be of interest for practical applications as they combine easy processibility with good mechanical properties.

 

## Particle Nucleation in the Case of Monomer Soluble Initiators

Thermodynamics requires in any heterophase system an exchange of matter between all phases. It will take place as soon as it is kinetically possible. This is important for any kind of heterophase polymerization and is one reason that aqueous phase kinetics plays a crucial role even if hydrophobic initiators are employed.[25–27] As shown in the former section medium hydrophobic initiators such as AIBN are very useful carrying out PTP of styrene miniemulsions and hence, an interesting question might be what happens in surfactant–free polymerizations? Is it possible to get latex particle if the polymerization is started with AIBN, which is predominantly dissolved in the monomer phase? What differences exist between the polymerization inside the monomer and the water phase? In order to investigate these points a procedure as depicted in Figure 8 was employed.[5]

The polymerization was started by adding an AIBN in styrene solution 120 minutes after placing the styrene monomer in the funnel on top of the aqueous phase. The initiator was injected either into the monomer phase (mode 1) or into the water phase (mode 2). At the end of the polymerization the monomer phase was separated from the aqueous phases and the products formed in any phase were analyzed. Surprisingly, polymerization was observed in both phases. Besides the expected bulk polymer in the monomer phase also latex particles were obtained (cf. Figure 9).

The reactions in the aqueous phase lead initially to a change in the conductivity and subsequently to the formation of latex particles accompanied by the drop in the transmission (cf. Figure 10). Moreover, the shape of the conductivity curve is qualitatively the same as observed for surfactant-free emulsion polymerizations initiated with potassium peroxodisulfate.[5,28] The bend of the conductivity curves marks the onset of particle nucleation as conducting species are captured in the diffuse electrical double layer of the particles. These results clearly prove that side reactions of carbon radicals in water lead to conducting species. The zeta-potential of the particles is pH-dependent and negative at pH >4. First hints that such radicals can attack water molecules have been obtained by NMR investigations of polymers made by 'normal' emulsion polymerization (i.e. in the presence of surfactants) initiated with azo-initiators.[29] Ongoing studies try to clarify the reaction mechanisms.

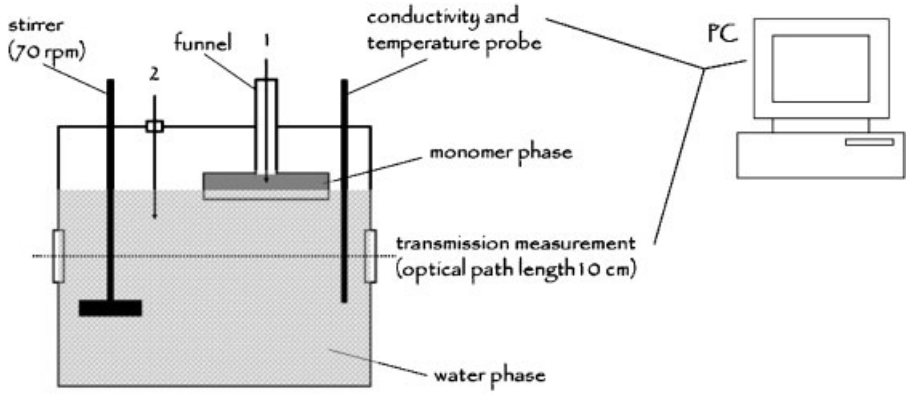


***Figure 8.***
Illustration of the reactor and the methodology to investigate the initial period of heterophase polymerizations with on-line monitoring of transmission and conductivity (not to scale); 1 and 2 denote possibilities to inject AIBN; the stirrer speed is just enough to avoid concentration gradients in the continuous phase and does not cause the formation of monomer droplets.

 

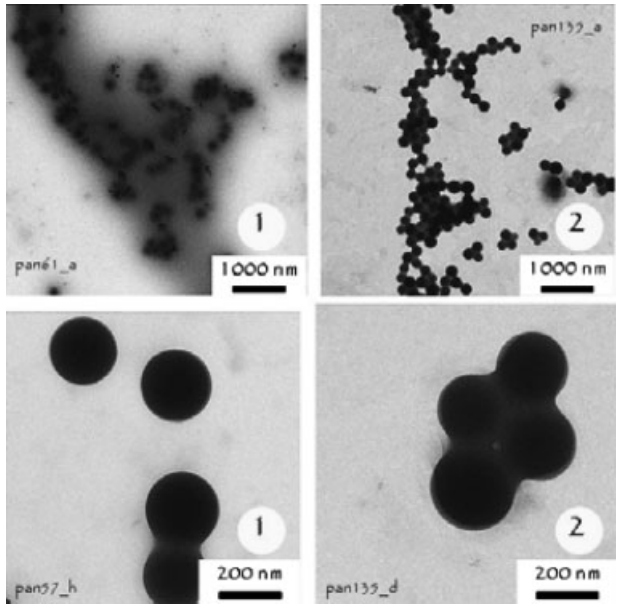


***Figure 9.***
TEM images of latex particles obtained during surfactant-free emulsion polymerization of styrene initiated with AIBN; 1,2 – AIBN injection modes.

The differences in the averaged curves between both injection modes are only marginal. The higher is the amount of AIBN in the bulk monomer phase (mode 1 vs. mode 2) the lower the initial slope of the conductivity – time curve, the longer the pre-nucleation period, and the later the transmission starts to drop.

Interestingly, after the bend (i.e. after particle nucleation) the slopes of both

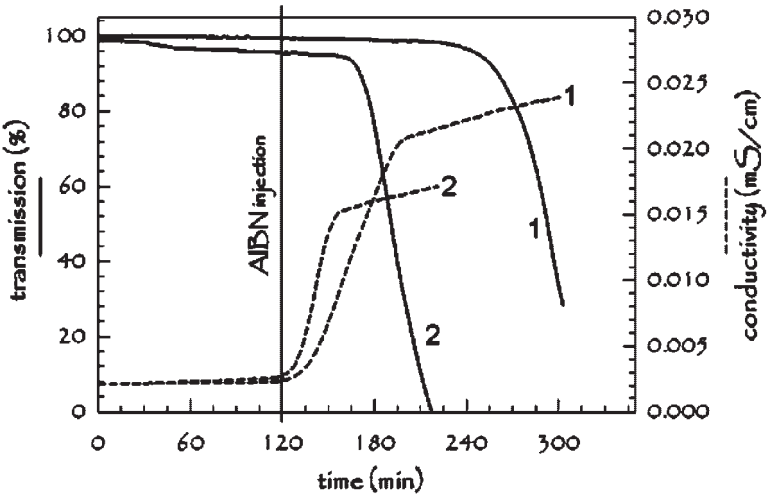


***Figure 10.***
On-line record of the changes in transmission (solid lines) and conductivity (dashed lines) during AIBN-initiated surfactant-free styre-ne heterophase polymerize-tion; the curves represent averages of 5 repeats; 1, 2 AIBN addition into the monomer and the water phase, respectively.

 

conductivity curves are almost identical and thus, indicating the same overall surface area of the nucleated particles. This conclusion is confirmed by the average size of the particles which is almost the same ($D_i$ of 190 and 184 nm for mode 1 and 2, respectively, cf. also Figure 9). Note, the initiator addition mode 2 leads to a thin monomer layer at the water air interface, which obviously facilitates AIBN diffusion into the water phase compared to mode 1, which favors a higher AIBN concentration in the thicker bulk monomer phase possessing a smaller interface to the water phase.

The average molecular weight of the polymer depends on both the AIBN addition mode and the reaction locus (cf. Table 3). The molecular weight data scatter a lot, especially those obtained for the polymer formed in the latex particles after AIBN addition to the monomer phase (mode 1). Despite the scatter, which might be due to a post-effect situation in the latex particles before isolating the polymer, the order of the molecular weights can be explained as follows. The polymerization to high molecular weight polymers starts in the monomer phase soon after initiator addition. Whereas the formation of polymers in the latex can start only after nucleation, which is 30 (for mode 2) or 70 minutes (for mode 1) after initiation (cf. Figure 10). The polymer formed during this pre-nucleation period inside the monomer phases retains the monomer and reduces swelling of the particles with monomer. Thus, the polymerization inside the monomer phase prevents the formation of high molecular weight polymers inside the latex particles.

In conclusion, the formation of latex particles in surfactant-free emulsion polymerization of styrene initiated with AIBN obeys the same rules of aggregative nucleation as verified for KPS.[5,28] The latex particles are electrostatically stabilized by ionic or ionizable groups which are formed by side reactions of carbon radicals under participation of water.

***Table 3.***
Number average molecular weight (g/mol) of the polymer formed during surfactant-free emulsion polymerization of styrene in dependence on the AIBN addition mode and the polymerization locus; average values and standard deviation of 6 repeats.

| | Latex | Bulk |
|---|---|---|
| Initiation mode 1 | 11200 ± 11000 | 31400 ± 4100 |
| Initiation mode 2 | 1900 ± 190 | 21200 ± 6500 |

*Acknowledgements:* The authors thank the Max Planck Society for financial support and the director of the colloid chemistry department of the Max Planck Institute of Colloids and Interfaces, Markus Antonietti, for many encouraging and fruitful discussions. M.M. gratefully acknowledges a fellowship from the DAAD (German Academic Exchange Service) and J.L. a joint fellowship from the Korea Science and Engineering Foundation (KOSEF) and the DAAD. The authors are indebted for the analytical ultracentrifugation to Mrs. A. Völkel and for the electron microscopy images to Mrs. R. Pitschke and Mrs. H. Runge.

[1] A. S. Dunn, H. W. Melville, *Nature* **1952**, *169*, 699.
[2] P. H. Brown, P. Schuck, *Biophys. J.* **2006**, *90*, 4651.
[3] P. Schuck, P. Rossmanith, *Biopolymers* **2000**, *54*, 328.
[4] C. Holtze, M. Antonietti, K. Tauer, *Macromolecules* **2006**, *39*, 5720.
[5] I. Kuehn, K. Tauer, *Macromolecules* **1995**, *28*, 8122.
[6] K. Matyjaszewski, " *Controlled Living Radical Polymerization. Progress in ATRP, NMP, and RAFT*", ACS, Washington D.C. 2000.
[7] K. Tauer, M. Antonietti, L. Rosengarten, H. Mueller, *Macromolecular Chemistry and Physics* **1998**, *199*, 897.
[8] R. Walz, B. Bomer, W. Heitz, *Makromol. Chem.* **1977**, *178*, 2527.
[9] R. Walz, W. Heitz, *J. Polym. Sci., Part A, Polym Chem.* **1978**, *16*, 1807.
[10] G. T. Russell, *Aus. J. Chem.* **2002**, *55*, 399.
[11] J. L. Bolland, H. W. Melville, *Oester. Chem. Z.* **1939**, *42*, 201.
[12] K. Horie, Mikulaso. D, *Makromol. Chem.* **1974**, *175*, 2091.
[13] H. Y. Parker, D. G. Westmoreland, H. R. Chang, *Macromolecules* **1996**, *29*, 5119.
[14] B. O'Shaughnessy, J. Yu, *Phys. Rev. Lett.* **1998**, *80*, 2957.
[15] B. O'Shaughnessy, J. Yu, *Macromolecules* **1998**, *31*, 5240.
[16] M. D. C. Topp, I. H. Leunen, P. J. Dijkstra, K. Tauer, C. Schellenberg, J. Feijen, *Macromolecules* **2000**, *33*, 4986.
[17] K. Tauer, V. Khrenov, N. Shirshova, N. Nassif, *Macromol. Symp.* **2005**, *226*, 187.
[18] K. Tauer, V. Khrenov, *Macromol. Symp.* **2002**, *179*, 27.
[19] R. A. Smiley, " *Nitriles*", Wiley-Interscience, New York 1981, p.888.

 

[20] R. Blachnik, S. Koritnig, D. Steinmeier, A. Wilke, A. Feltz, H. Reuter, E. Stieber, "*D'ans Lax Taschenbuch für Chemiker und Physiker*", Springer, Berlin 1998, p.522.
[21] T. E. Ferington, A. V. Tobolsky, *J. Amer. Chem. Soc.* **1955**, *77*, 4510.
[22] G. M. Burnett, *Quat. Rev.* **1950**, *4*, 292.
[23] C. H. Bamford, M. J. S. Dewar, *Proc. Royal Soc., London, Ser. A* **1948**, *192*, 309.
[24] R. X. E. Willemse, B. B. P. Staal, A. M. van Herk, S. C. J. Pierik, B. Klumperman, *Macromolecules* **2003**, *36*, 9797.
[25] M. Nomura, K. Suzuki, *Ind. Eng. Chem.* **2005**, *44*, 2561.
[26] J. M. Asua, V. S. Rodriguez, E. D. Sudol, M. S. El-Aasser, *J. Polym. Chem., Part A, Polym. Chem.* **1989**, *27*, 3567.
[27] J. W. Breitenbach, H. Edelhauser, *Makromol. Chem.* **1961**, *44-46*, 196.
[28] K. Tauer, K. Padtberg, C. Dessy, *ACS Symp. Ser.* **2002**, *801*, 93.
[29] K. Tauer, *Polym. Adv. Technol.* **1995**, *6*, 435.

 

# Surface – Functionalized Inorganic Nanoparticles in Miniemulsion Polymerization

*Oliver Töpfer, Gudrun Schmidt-Naake**

**Summary:** Two inorganic cores, consisting of silica and titania, have been prepared via basic Stoeber synthesis. Those cores have been functionalized, using trimethoxysilyl propylmethacrylate (MPTMS) and introduced into a miniemulsion copolymerization system. The miniemulsion consisted of styrene (S) and 2-hydroxyethyl methacrylate (HEMA), styrene sulfonic acid (SSA) or aminoethyl methacrylate hydrochloride (AEMA) as comonomer in varying compositions. The morphology of the products has been investigated by SEM and dynamic light scattering (DLS) measurements. The composition of the products has been investigated by photoacoustic FTIR (PA-FTIR) spectroscopy and elemental analysis. Thermal properties have been determined by TGA and DSC analysis.

**Keywords:** functional precursors; miniemulsion; nanoparticles; polymer composites; reactive fillers

## Introduction

In recent years, the combination of polymers and inorganic materials to polymer composites comes to steadily growing interest. Synergetic aspects such as chemical resistance or elasticity of the organic compounds and hardness, stability or interesting electrical and optical properties of the inorganic compounds offer an immense potential for new materials or applications. Hofman-Caris presented a detailed review about particle formation procedures as well as chemical coupling procedures that form core shell structures prior to 1994.[1]

A wide range of inorganics has been used as components in polymer composites. However, silica offers a broad and interesting variety of structural modifications such as layered silicates like montmorillonite, colloidal nanoparticles like Stoeber synthesis products or highly ordered architectures like siloxane or silsequioxane structures.[2,3]

A major problem is always the organic inorganic interface which does not interact per se and would lead to phase separation. While montmorillonite forms, depending on the reaction conditions, either intercalated or exfoliated composites with clearly separated phases, a phase separation in the composites with silica nanoparticles or siloxanes respectively silsesquioxanes is unrequested.[4,5]

Although first attempts used inorganic particles as fillers or additives without any covalent bonding, soon further development led into the covalent attachment of polymers onto sub-micrometer size particles.[6]

Therefore, miniemulsion polymerization turned out to be a suitable technique to produce polymer composites with an inorganic core and an organic shell.[7,8]

A following step was the copolymerization, using a second monomer, which enables the introduction of a secondary functionality into the emulsion bead. This leads to reactive fillers, which can be varied in composition and concentration of accessible functional groups at the particle

Institut für Technische Chemie, Technische Universität Clausthal, Erzstr. 18, 38678 Clausthal-Zellerfeld, Germany
Tel: (+49) 05323 722036 Fax: (+49) 05323 723655
E-mail: Gudrun.Schmidt@TU-Clausthal.de

surface. In recent publications, Landfester et al. reported about the synthesis and the uptake of fluorescent labelled poly(styrene-*co*-acrylic acid) core shell systems containing an magnetic iron oxide core for biomedical applications such as stem cell research.[9,10]

Few approaches have been done, using S in combination with Glycidyl methacrylate (GMA), HEMA or ω-amino alkyl methacrylates as functional comonomers.[11–13]

Besides the mentioned comonomers, SSA as well as AEMA has been used as comonomer in a miniemulsion copolymerization with styrene in our workgroup.[14]

Two different inorganic cores have been synthesized via basic Stoeber synthesis.[15,16] Both inorganic cores, the $SiO_2$ core as well as the $TiO_2$ core, have been functionalized with trimethoxysilyl propylmethacrylate (MPTMS) under condensation conditions. Scheme 1 shows a condensation and functionalization process exemplarily given on tetraethoxysilane (TEOS).

Those cores have been copolymerized under miniemulsion conditions using sodium dodecyl sulphate (SDS) as surfactant and potassium persulphate (KPS) as initiator with styrene as matrix monomer and HEMA, SSA and AEMA as comonomer. Apart from diffusion controlled effects in a swollen polymer shell, only those functional groups that are situated on the surface of the core shell particle are accessible for further reactions. To increase the specific surface area as well as the structural integrity of the core shell particle, the acrylate based crosslinker tetraethylene glycol diacrylate (TEGDA) has been introduced.

With this versatile reaction method we established an easy preparation scheme for reactive fillers with a broad variety of functionalities in adjustable concentration on the particle surface.

## Experimental Part

### Preparation and Functionalization of Silica Nanoparticles

Tetraethoxysilane (TEOS, 0.73 mol) is dissolved in absolute ethanol (1 000 mL) and is stirred at ambient temperatures. Via a syringe gaseous ammonia is added over a period of 30 minutes. After addition of ammonia, the dispersion is kept still for 6 hours.

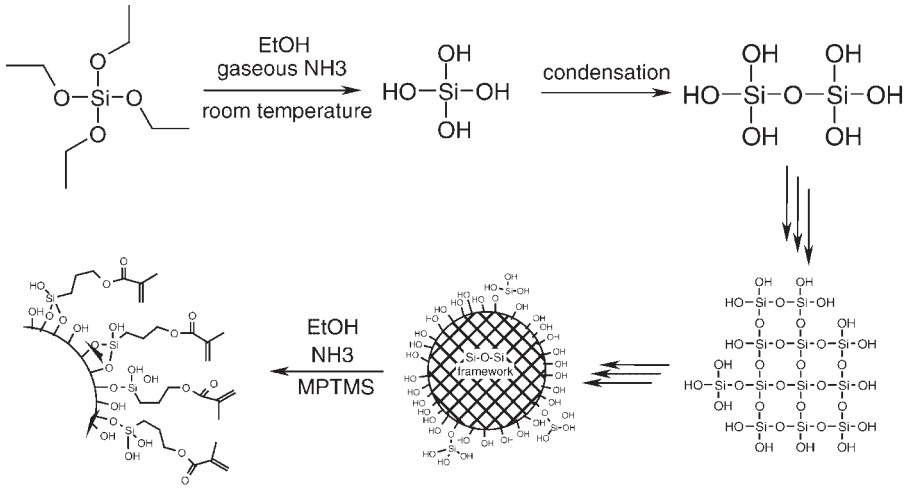


***Scheme 1.***
Condensation and functionalization process exemplarily shown on silica, using MPTMS for in-situ functionalization.

 

For functionalization the dispersion is stirred and MPTMS (4.0 mmol dissolved in 2 mL Ethanol) is added. The mixture is stirred for 12 hours. The solid content reaches 6 wt.-%.

### Preparation and Functionalization of Titania Nanoparticles

The preparation and functionalization of $TiO_2$ follows the procedure given above, using Tetraethoxytitanate instead of TEOS for the condensation process.

### Miniemulsion Polymerization Setup

1.9 wt.-% of SDS is dissolved into a dispersion of 1 g inorganic compound (corresponds to 0.47 mmol functional groups) in ethanol. The monomer mixture of S/functional monomer/TEGDA is added. The system is diluted with ethanol to an overall volume of 95 mL. The collective monomer concentration is set to 0.3 mol/L. The mixture is emulsified by ultrasonification (90 sec.) and transferred into a double mantle heating reactor, equipped with a mechanical stirrer and a nitrogen inlet. The emulsion is heated to 70 °C. KPS (0.5 wt.-% resp. the amount of monomer) is dissolved in 5 mL deionized water and added to the preheated emulsion. Reaction time is set to 60 minutes.

### Analytical Equipment

Photoacoustic-FTIR has been done, using the FTS 7000 series machine from DIGILAB, equipped with a photoacoustic detector model 300 from MTEC. Helium was used as purge gas and the software Win-IR-Pro was used for data analysis.

Dynamic light scattering measurement has been done, using the Photon Cross-correlation Spectroscopy (PCCS) machine NANOPHOX provided by SYMPATEC. Data analysis has been done, using the system software Windox 5.2.2.0 from SYMPATEC.

Elemental analysis has been done on a Vario EL2 machine from ELEMENTAR. The elements C, H, N, S has been detected with a thermal conductivity detector. Oxygen has been detected with an infrared detector. Sulfanilic acid and benzoic acid have been used for calibration.

Thermogravimetrical measurements have been done on a TGA 850 from METTLER TOLEDO. Temperature range was 25 °C to 850 °C with a temperature ramp of 20 K/min.

Scanning Electron Microscopy has been done on a Gemini 982 from ZEISS. For high magnification, Cr has been used as sputter medium.

## Results

### Inorganic Particle Formation and Functionalization

The particle formation follows the well known Stoeber synthesis in basic ethanol. A time resolved nanoparticle formation has been observed in the case of silica. The result is given in Figure 1 as particle size versus condensation time curve.

The fitted curves in Figure 1 show that the particle growth process reaches a limit at 180 minutes. To ensure a full conversion, a reaction time of 6 hours seems to be sufficient for particle formation.

The nanoparticle functionalization using MPTMS follows in situ. Figure 2 shows the particle size distribution of silica and titania nanoparticles before and after functionalization. The mentioned polydispersity index (PDI) represents the quotient of $X_{90}$ divided by $X_{50}$.

The average particle size increases in both cases by a few nm due to the attached methacryloyl groups. However, no aggregation is observed during particle formation or functionalization. Thermogravimetrical analysis of the washed and dried product indicates 9 wt.-% of organic compound covalently bond onto the particle surface which can be calculated to a number of 200,000 methacryloyl groups on the surface of a particle with a diameter of 100 nm or 0.47 mmol methacryloyl groups per gram inorganic compound.

The successful attachment of MPTMS to silica or titania can be shown in the infrared spectra of the washed and dried silica and titania, given in Figure 3.

 

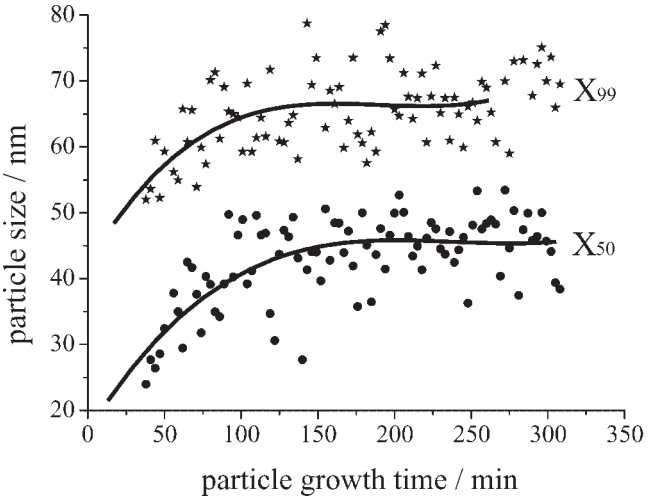


***Figure 1.***
Particle size as a function of time given for the condensation of TEOS in basic ethanol. $X_{50}$ value represents maximum particle size, which 50% of the particles underrun; $X_{99}$ represents maximum particle size, which 99% of the particles underrun.

The attached methacryloyl group can be seen at the cumulative vibrations of the ester group at 1 295 $cm^{-1}$ and 1 460 $cm^{-1}$ as well as the double bond stretching at 1 721 $cm^{-1}$. Furthermore, significant framework vibrations are visible, for silica in the range of 750 $cm^{-1}$ to 1 250 $cm^{-1}$ and for titania below 1 000 $cm^{-1}$ as broad signals.

**Polymer Composite Properties**

The functionalized nanoparticles were copolymerized in a miniemulsion system of S and a variety of functional comonomers.

The miniemulsion polymerization products were washed with acetone to remove soluble components from the polymer composite. Spectroscopic characterization of the dried products was done using PA-FTIR spectroscopy. This method allows a convenient and fast spectroscopic analysis.

Figure 4 shows the PA-FTIR spectra of poly(S-*co*-HEMA) polymer composite of functionalized silica with increasing HEMA concentration.

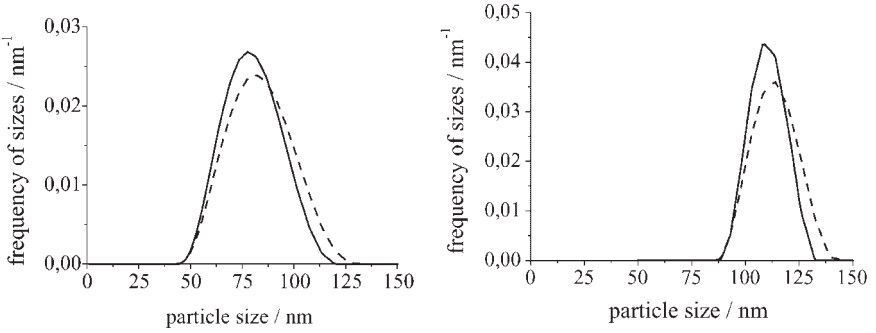


***Figure 2.***
left: Particle size distribution of non modified silica (solid line) with an average particle size of 77 nm (PDI 1.2) and MPTMS modified silica (dashed line) with an average particle size of 79 nm (PDI 1.4).; right: Particle size distribution of non modified titania (solid line) with an average particle size of 112 nm (PDI 1.1) and MPTMS modified titania (dashed line) with an average particle size of 115 nm (PDI 1.4).

 

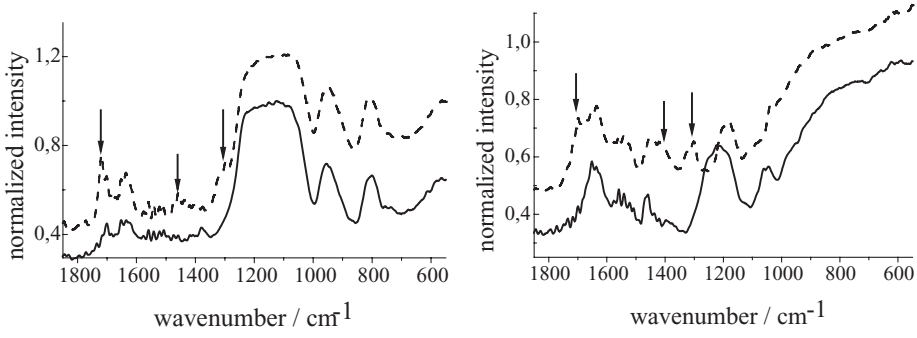


***Figure 3.***
left: Photoacoustic infrared spectra of non modified silica (solid line) and MPTMS modified silica (dashed line).; right: Photoacoustic infrared spectra of non modified titania (solid line) and MPTMS modified titania (dashed line).

The variation of the functional monomer concentration is reflected in the PA-FTIR spectra of the miniemulsion products. An increasing of the HEMA content in the polymer composite can be seen at the significant carbonyl stretching band at 1 600 $cm^{-1}$ which increased in the spectra from product 1 to product 3 with increasing of the HEMA content in the monomer composition. Nevertheless, next to the typical copolymer bands for poly(S-*co*-HEMA), significant silica core bands are visible in all spectra. The monomer composition as well as the product composition after copolymerization is given in Table 1.

The polymer composition has been calculated using the copolymerization parameters of HEMA and S ($r_S = 0.44$ and $r_{HEMA} = 0.54$).[17] The influence of the crosslinker TEGDA has been neglected in both cases, the preparation of the copolymer and of the polymer composite. Nevertheless, a good agreement within the error margin has been found for the typical copolymerization with HEMA contents below 20 mol% in the monomer

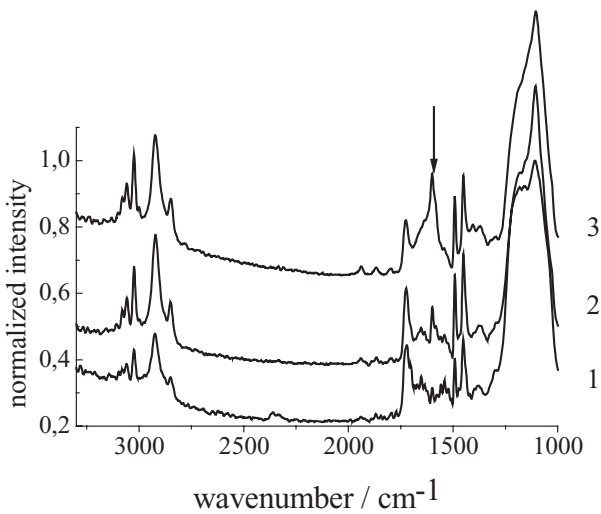


***Figure 4.***
PA-FTIR spectra of S-*co*-HEMA polymer composite of functionalized silica with increasing HEMA content in the product. 1: HEMA content 7.1 mol%; 2: HEMA content 11.1 mol%; 3: HEMA content 19.8 mol%.

 

***Table 1.***
Data of monomer and polymer composition as well as particle size and polydispersity index (PDI) of the particle size distribution.

| | monomer system | feed composition [mol%] | polymer composition [mol%] | Conversion [%] | Particle size $X_{50}$ [nm] | PDI ($X_{90}/X_{50}$) |
|---|---|---|---|---|---|---|
| $SiO_2$ | S/SSA/TEGDA | 93,5/**4,9**/1,6 | 95,6/**2,6**/1,8 | 90 | 113 | 1,2 |
| | | 88,5/**9,8**/1,6 | 86,5/**12,2**/1,3 | 95 | 151 | 1,4 |
| | | 78,7/**19,7**/1,6 | 80,2/**17,6**/1,8 | 97 | 175 | 1,2 |
| | S/AEMA/TEGDA | 93,5/**4,9**/1,6 | 84,9/**13,2**/1,8 | 96 | 112 | 1,6 |
| | | 88,5/**9,8**/1,6 | 80,1/**18,1**/1,8 | 98 | 124 | 1,3 |
| | | 78,7/**19,7**/1,6 | 68,5/**29,6**/1,9 | 97 | 135 | 1,2 |
| | S/HEMA/TEGDA | 93,5/**4,9**/1,6 | 91,1/**7,1**/1,8 | 80 | 96 | 1,4 |
| | | 88,5/**9,8**/1,6 | 87/**11,1**/1,8 | 76 | - | - |
| | | 78,7/**19,7**/1,6 | 78,4/**19,8**/1,9 | 70 | 149 | 1,2 |
| - | S/SSA/TEGDA | 93,5/**4,9**/1,6 | 95,8/**2,6**/1,6 | 95 | - | - |
| | | 88,5/**9,8**/1,6 | 90,8/**8,1**/1,1 | 97 | 143 | 1,2 |
| | | 78,7/**19,7**/1,6 | 79,6/**19,2**/1,2 | 94 | 173 | 1,3 |
| - | S/AEMA/TEGDA | 93,5/**4,9**/1,6 | 96,7/**1,6**/1,8 | 96 | 123 | 1,2 |
| | | 88,5/**9,8**/1,6 | 93,3/**4,9**/1,8 | 92 | 125 | 1,2 |
| | | 78,7/**19,7**/1,6 | - | 97 | 139 | 1,3 |
| - | S/HEMA/TEGDA | 93,5/**4,9**/1,6 | 87/**11,4**/1,6 | 78 | 196 | 1,3 |
| | | 88,5/**9,8**/1,6 | 81,7/**16,8**/1,5 | 80 | 216 | 1,3 |
| | | 78,7/**19,7**/1,6 | 74,2/**24,1**/1,7 | 75 | 191 | 1,2 |
| $TiO_2$ | S/SSA/TEGDA | 93,5/**4,9**/1,6 | 90,7/**9,1**/0,2 | 92 | 494 | 1,8 |
| | | 88,5/**9,8**/1,6 | 85,7/**14,1**/0,2 | 90 | 317 | 1,7 |
| | | 78,7/**19,7**/1,6 | 77,4/**22,3**/0,3 | 86 | 357 | 1,6 |
| | S/AEMA/TEGDA | 93,5/**4,9**/1,6 | 93,5/**4,9**/1,6 | 98 | 141 | 1,5 |
| | | 88,5/**9,8**/1,6 | 88,5/**9,8**/1,6 | 98 | 146 | 1,7 |
| | | 78,7/**19,7**/1,6 | 78,7/**19,7**/1,6 | 97 | 158 | 1,5 |

feed composition (Figure 5). Contrary to the copolymerization, the formation of the polymer composite does not follow the predicted copolymerization diagram. Especially for higher HEMA contents, the polymer composition deviates from the predicted copolymerization behaviour.

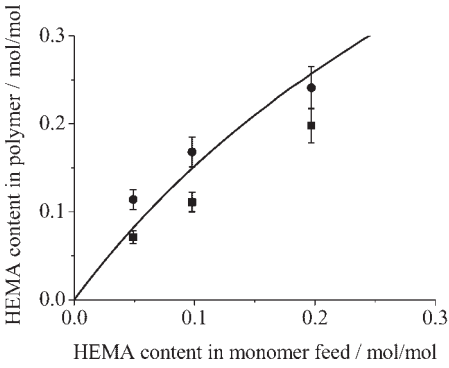


***Figure 5.***
HEMA content in the polymer composite (squares) and HEMA content in the copolymer (dots) as function of the HEMA content in the monomer feed. The copolymer composition calculated from $r_S = 0.44$ and $r_{HEMA} = 0.54$ is given as reference (solid curve).

This leads to the assumption, that the inorganic nanoparticle influences the copolymerization in the emulsion droplet. Besides the functional methacryloyl groups, each nanoparticle provides many hydroxyl groups at the surface. Those hydroxyl groups at the surface could interact with the hydroxyl groups of the added monomer in a way of repulsion. Therefore, the monomer composition in the emulsion droplet changes which could lead to a different polymer composition in the organic inorganic copolymerization product.

Due to the fact that HEMA as a component in the copolymerization decreases the thermal stability, the decreasing of the thermal degradation temperature for both, the polymer composite and the copolymer, with an increasing HEMA content is understandable. Nevertheless, the inorganic core in the polymer composite seems to influence the thermal stability positively. An increase of 15 K in the thermal stability of the polymer composite is observed (Figure 6).

 

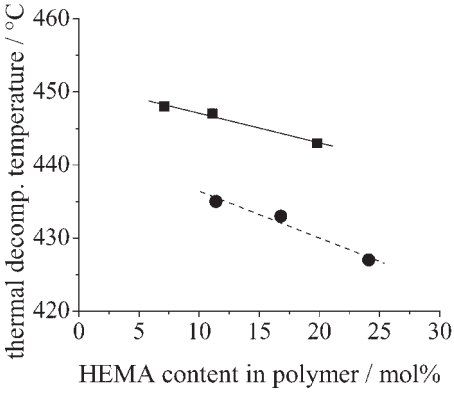


***Figure 6.***
Thermal decomposition temperature of the polymer composite (squares, solid line) and the copolymer (dots, dashed line) as function of the HEMA content in the product.

The morphology of the S-*co*-HEMA polymer composite exhibits a typical miniemulsion product of spherical particles with a narrow particle size distribution (Figure 7).

Figure 8 shows the PA-FTIR spectra of the poly(S-*co*-AEMA) polymer composite with functionalized silica at increasing AEMA concentration.

The conversion of the 2-aminoethyl methacrylate hydrochloride monomer to the free amino group in the polymer composite has been conducted completely which is clearly visible at the shift of the amino-hydrochloride band (spectrum 4; broad at 2 700 $cm^{-1}$ to 2 900 $cm^{-1}$) to the free amino group vibration band (spectra 1 to 3; broad at 3 200 $cm^{-1}$ to 3 500 $cm^{-1}$). The increasing band intensities of the amino group vibration as well as the carbonyl group (weak, sharp at 1 650 $cm^{-1}$) indicate the growing incorporation of the functional monomer into the polymer composite compound.

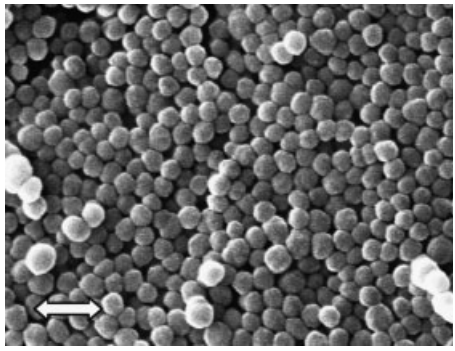

***Figure 7.***
SEM image of S-*co*-HEMA polymer composite (HEMA content 19.8 mol%) with an average particle size of 150 nm. Arrow size is 500 nm.

Figure 9 shows the concentration of the functional monomer, HEMA and AEMA, in the polymer composite as a function of the functional monomer content in the feed.

Significantly more AEMA is integrated into the polymer composite than HEMA is integrated in the composite. Furthermore, more AEMA is integrated into the polymer composite than it is provided in the monomer feed. However, a tailoring of compositions with up to 30 mol% AEMA content or up to 20 mol% HEMA content in the polymer composite is possible and easily accessible.

The average particle size as well as the particle size distribution of the prepared lattices was investigated under reaction state concentration using a novel dynamic light scattering method.[18,19] Table 1 summarizes relevant data of the prepared products. Furthermore, the composition of the monomer feed as well as the composition of the polymer is given in Table 1. The polymer composition has been calculated from elemental analysis data.

The particle sizes of the minimeulsion product increase in all samples compared to the silica and titania precursors. Furthermore a low PDI is found which indicates an extensive incorporation of the silica and titania cores into the miniemulsion droplet.

The incorporation of functionalized titania into a S/SSA system follows equal schemes, given above.

Figure 10 shows the PA-FTIR spectra of the polymer composite with increasing SSA content in the product indicated at the vibrations of the sulfonic acid group at 1 650 $cm^{-1}$ (medium, sharp) and at 3 450 $cm^{-1}$ (medium, broad)

 

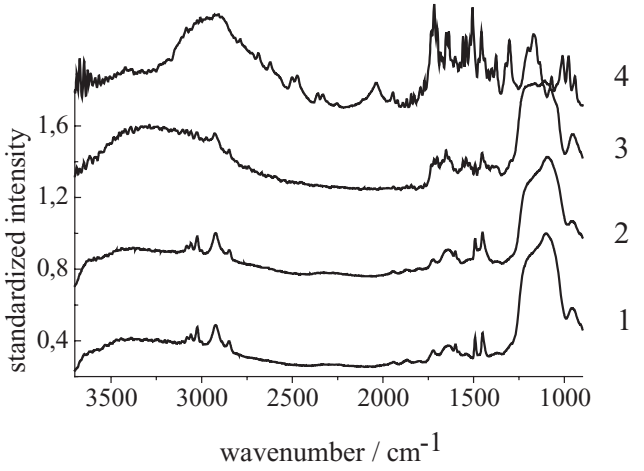


***Figure 8.***
S-*co*-AEMA polymer composite with functionalized silica and increasing AEMA content in the product. 1: AEMA content 13.2 mol%; 2: AEMA content 18.1 mol%; 3: AEMA content 29.6 mol%; 4: 2-Aminoethyl methacrylate hydrochloride monomer.

The SEM image of the miniemulsion product (Figure 11) shows spherical particles with a narrow particle size distribution and an average particle size of 150 nm. This confirms the results from the dynamic light scattering measurements.

The thermal stability of the prepared poly(S-*co*-SSA) polymer composites with silica and titania decreases with increasing SSA content. However, the prepared copolymers of poly(S-*co*-SSA) show significant higher decomposition temperatures which are not affected by the increasing SSA content in the product. Figure 12 shows the thermal decomposition temperature as a function of the SSA content in the miniemulsion polymerization product.

The polymer composites show a decreased thermal stability compared to the S-*co*-SSA copolymer. This might be an effect of different thermal conductivities at the organic – inorganic interface which interferes with the polymer matrix. Furthermore, monomer –specific interactions between the inorganic surface and the

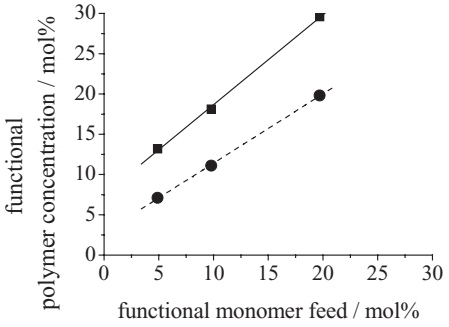


***Figure 9.***
Functional monomer concentration of HEMA (dots, dashed line) and AEMA (squares, solid line) in the polymer composite versus functional monomer concentration in the monomer feed.

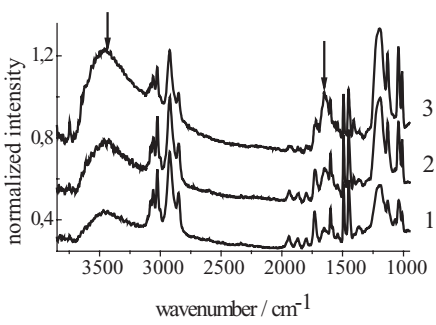


***Figure 10.***
S-*co*-SSA polymer composite with functionalized titania and increasing SSA content in the product. 1: SSA content: 9.1 mol%; 2: SSA content: 14.1 mol%; 3: SSA content: 22.3 mol%.

 

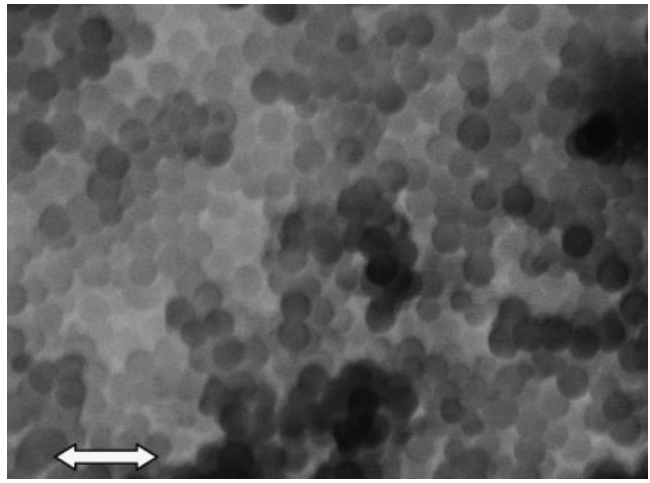

***Figure 11.***
SEM image of S-*co*-SSA polymer composite of functionalized silica (SSA content 12.2 mol%) with an average particle size of 150 nm. Arrow size is 500 nm.

copolymer might cause the different thermal behaviour with an increasing SSA content in the composite.

The ion exchange capacity (IEC) of the polymer composite containing SSA has been determined. Figure 13 gives the theoretical IEC and the obtained IEC as function of the SSA content in the polymer composite with silica.

It is clearly visible, that the IEC is increasing with increasing SSA content in the polymer composite. The theoretical IEC represents the maximum IEC if all SSA groups are accessible. Hence, a reduced IEC for the real accessible SSA groups is expected. Nevertheless, at least 75% of the SSA groups are accessible (sample with 17.6 mol% SSA content). Due to the effect that the TEGDA increases the specific surface area and produces highly porous particles, this high amount of available SSA groups can be achieved.

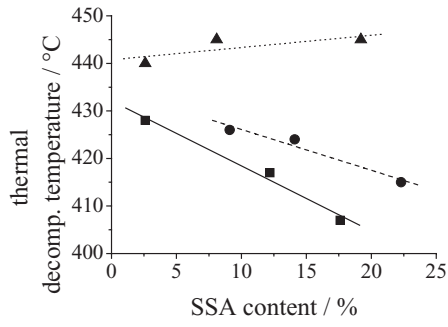


***Figure 12.***
Thermal stability of S-*co*-SSA polymer composite with silica (squares, solid line), titania (dots, dashed line) and S-*co*-SSA polymer (triangles, dotted line) for comparison.

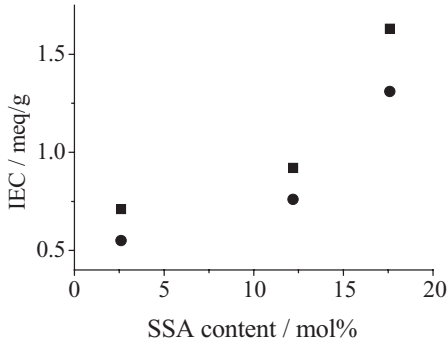


***Figure 13.***
Ion exchange capacity (IEC) of S-*co*-SSA polymer composite with silica. Expected IEC from EA composition calculation (squares) and obtained IEC from equivalence titration (dots).

 

## Conclusion

It has been shown that the preparation of functionalized organic/inorganic polymer composites, consisting of silica or titania cores and an organic copolymer shell was successful. Therefore, the inorganic cores have been prepared by basic Stoeber synthesis, functionalized using MPTMS and embedded into a miniemulsion copolymerization system. The used monomers for copolymerization were S and HEMA or AEMA and SSA in a variation of 5 mol% over 10 mol% to 20 mol% functional monomer related to S.

In the case of poly(S-*co*-HEMA) polymer composites with silica, the HEMA content could be varied from 8 mol% to 20 mol% which could be adjusted in the monomer feed. However, higher incorporation rates than poly(S-*co*-HEMA) polymer composites could be achieved in the poly(S-*co*-AEMA) system with either silica or titania.

Dynamic light scattering measurements of the miniemulsion lattices prove the successful incorporation of the inorganic cores into the miniemulsion droplet. All silica based polymer composites show particle sizes between 120 nm and 150 nm with a low PDI, whereas the silica precursor itself showed an average particle size of 79 nm. Hence, all silica nanoparticles have been incorporated into the emulsion droplet and each droplet contains only one silica particle. This can be proved by the SEM image of the composite.

In the case of the titania based polymer composites, the samples with poly(S-*co*-AEMA) show average particle sizes of 140 nm to 160 nm. Here, the polymer shell has been formed around one nanoparticle in the emulsion droplet.

The titania based polymer composites with poly(S-*co*-SSA) show rather large particles with particle sizes of 300 nm to 500 nm. In this case, it is possible that two or more titania particles could have entered the emulsion droplet. Still the product remains stable and no aggregation has been observed. However the IEC measurements confirm the integration of SSA into the polymer composite. The accessible SSA groups reach up to 75% of the calculated maximum due to the fact that the added crosslinker TEGDA increases the specific surface area by forming porous and highly swellable shells around the inorganic core of this system.

The presented three step method of inorganic particle preparation, consequent functionalization and finally embedding into a miniemulsion copolymerization system offers an easy way to prepare core shell particles with a wide range of functionalities at the surface. Those products inherit a high potential as reactive filler materials in advanced polymers composites.

[1] C. H. M. Hofman-Caris, *New J. Chem.*, **1994**, *18*, 1087.
[2] A. Shimojima, K. Kuroda, *Chem. Lett.*, **2000**, 1310–1311.
[3] J. Wen, G. L. Wilkes, *Chem. Mater.*, **1996**, *8*, 1667–1681.
[4] M. Biswas, S. S. Ray, in: New Polymerization Techniques and Synthetic Methodologies, Vol. 155 of Advances in Polymer Science, Springer Verlag 2001, p. 167–234.
[5] M. Biswas, S. S. Ray, *Polymer*, **1998**, *39*, 6423–6428.
[6] E. Bourgeat-Lami, *J. Nanosci.Nanotech.*, **2002**, *2*, 1–24.
[7] E. Bourgeat-Lami, *Polymer*, **1995**, *36*, 4385–4389.
[8] P. Espiard, A. Guyot, *Polymer*, **1995**, *36*, 4391–4395.
[9] V. Holzapfel, M. Lorenz, C.-K. Weiss, H. Schrezenmeier, K. Landfester, V. Mailander, *J. Phys. Cond. Matter*, **2006**, 18(38), 2581–2594.
[10] M. Lorenz, V. Holzapfel, A. Musyanovych, K. Nothelfer, P. Walther, H. Frank, K. Landfester, H. Schrezenmeier, V. Mailander, *Biomaterials*, **2006**, *27*(14), 2820–2828.
[11] E. Bourgeat-Lami, J. Lang, *Macromol. Symp.* **2001**, *169*, 89–91.
[12] P. Innocenzi, T. Kidchob, T. Yoko, *J. Sol-Gel Sci. And Technol.*, **2005**, *35*, 225–235.
[13] Z. Zeng, J. Yu, Z.-X. Guo, *J. Polym. Sci. Part A*, **2004**, *42*, 2253–2262.
[14] I. Grabs, G. Schmidt-Naake, *publication in progress*.
[15] W. Stöber, A. Fink, E. Bohn, *J. Coll. Int. Sci.*, **1968**, *26*, 62–69.
[16] P. Philipse, A. Vrij, *J. Coll. Int. Sci.*, **1989**, *128*, 121–136.
[17] J. Brandrup, E. H. Immergut, in: Polymer Handbook, 3rd Edition, Wiley-Interscience Publication, p. II–251; New York, Brisbane, Chichester, Toronto, Singapore.
[18] W. Witt, L. Aberle, H. Geers, *Particlulate System Analysis*, **2003**, Harrogate.
[19] W. Witt, L. Aberle, H. Geers, Partec, **2004**.

 

# Reversible Addition Fragmentation Chain Transfer Mediated Dispersion Polymerization of Styrene

*Prakash J. Saikia, Jung Min Lee, Byung H. Lee, Soonja Choe**

**Summary:** Polystyrene microspheres have been synthesized by the reversible addition-fragmentation chain transfer (RAFT) mediated dispersion polymerization in an alcoholic media in the presence of poly(*N*-vinylpyrrolidone) as stabilizer and 2,2′-azobisisobutyronitrile as a conventional radical initiator. In order to obtain monodisperse polystyrene particles with controlled architecture, the post–addition of RAFT agent was employed to replace the weak point from the pre-addition of RAFT. The feature of preaddition and postaddition of RAFT agent was studied on the polymerization kinetics, particle size and its distribution and on the particle stability. The living polymerization behavior as well as the particle stability was observed only in the postaddition of RAFT. The effects of different concentration on the postaddition of RAFT agent were investigated in terms of molecular weight, molecular weight distribution, particle size and its distribution. The final polydispersity index (PDI) value, particle size and the stability of the dispersion system were found to be greatly influenced by the RAFT agent. This result showed that the postaddition of RAFT agent in the dispersion polymerization not only controls the molecular weight and PDI but also produces stable monodisperse polymer particles.

**Keywords:** living radical dispersion polymerization; nucleation; particle size distribution; RAFT; stability

## Introduction

Reversible addition-fragmentation chain transfer (RAFT)[1,2] polymerization has been one of the most promising recent advances in the controlled free radical polymerization (CRP) technique for both the homogeneous and heterogeneous system.[3,4] The mechanism of the RAFT has been established by a dynamic equilibrium between the active and the dormant species.[1,2] Although RAFT polymerizations were well developed in the heterogeneous media via emulsion,[2,5,6] miniemulsion[2,7,8] and *ab initio* emulsion[9] polymerization, RAFT emulsion polymerization was unsuccessful due to the slow polymerization rate, poor molecular weight control and high levels of coagulum and formation of thick red layers.[9,10] However, good control and colloidal stability were achieved only under limited conditions or by using different polymerization techniques.[5,8,11] In the *ab initio* RAFT emulsion polymerization, Gilbert et al.[12,13] reported the living character of polymers with controlled molecular weights and polydispersities without the loss of colloidal stability.

Living radical dispersion polymerization techniques have been explored to provide polymer dispersions with controlled morphology in contrary to the traditional free radical dispersion polymerization. Although living radical dispersion polymerization gives both the controlled molar mass and particle morphology, only a few studies have been reported with broad

Department of Chemical Engineering, Inha University, 253 Yonghyundong, Namgu, Incheon, Republic of Korea 402-751
Tel.: +82-32-860-7467; Fax: +82-32-876-7467
E-mail: sjchoe@inha.ac.kr

particle size distributions.[14–16] Mülhaupt et al.[14] carried out the 2,2,6,6-tetramethyl-1-piperidinyloxy (TEMPO) mediated dispersion polymerization of styrene in *n*-decane at 135 °C in presence of polystyrene-*block*-poly(ethene-*alt*-propene) ''Kraton'' block copolymers as a steric stabilizer, where a very broad particle size distribution ranging from 50 nm ~ 10 μm was reported. The synthesis of polystyrene (PS) latex via living free-radical dispersion polymerization with TEMPO in both the alcoholic and aqueous alcoholic media using poly(*N*-vinylpyrrolidone) (PVP) at 112–130 °C was reported.[15] In a recent study, Winnik et al.[17] reported living/controlled radical dispersion polymerization of styrene in the presence of perfluorohexyl iodide as a degenerative chain transfer (DCT) agent and 1-cyano-1-methylpropyl dithiobenzoate as a RAFT agent in ethanol and in ethanol-water mixtures. They obtained the characteristics of a living/controlled radical polymerization on the delayed addition of the chain transfer agents (DCT or RAFT) i.e. until the completion of the nucleation stage which they named as two-stage living radical dispersion polymerization.[17] In this methodology, they were able to obtain monodisperse micron-sized PS particles consisting of chain extendible low molar mass polymer. So, with the advantages of CRP techniques, the preparation of polymer particles in the dispersion polymerization has an important goal as monodisperse polymer particles have many important applications.[18] Here, we report the effect of RAFT agent on the dispersion polymerization of styrene to control not only the molecular weight and molecular weight distribution but also the uniformity of the PS particles. In the dispersion polymerization of styrene in an ethanol medium, the *tert*-butyl dithiobenzoate (*t*-BDB) was used as a chain transfer agent (CTA) and 2, 2′-azobisisobutyronitrile (AIBN) as a radical initiator in the presence of a steric stabilizer PVP. The CTA, *t*-BDB contains a better leaving group that resulted the faster fragmentation of the corresponding intermediate radical due to a better *tert*-butyl radical stability and to steric factors.[2,7,19] Initially, in the presence of a RAFT agent, the experimental condition was optimized for the formation of polymer particles and then the effect of concentration of the RAFT agent on molecular weight, particle size and their distributions were studied in the dispersion polymerization.

## Experimental Part

### Materials

S-(Thiobenzoyl) thioglycolic acid (Aldrich, 99% purity) and 2-methyl-2-propanethiol (Aldrich, 99%) were used as received for the preparation of the RAFT agent. Anhydrous diethyl ether and HPLC grade tetrahydrofuran (THF) were purchased from J. T. Baker Co. (USA) and distilled. Styrene (Junsei Chemicals, Japan) was purified using an inhibitor removal column and stored at −5 °C prior to use. AIBN (Junsei Chemicals, Japan) was purified by recrystallization in ethanol and dried *in vacuo*. PVP (weight-average molecular weight = 40,000; Sigma Chemical Co.) was used as a stabilizer. Ethanol (Samchun Chemical Co., Korea) was used as a reaction medium.

### Synthesis of RAFT Agent

*t*-BDB was synthesized as reported earlier.[7]

### Dispersion Polymerization

The dispersion polymerization was carried out in a capped 50-mL scintillation vial with magnetic stirring under nitrogen atmosphere. Ethanol was first poured into the vial, and 0.69 mol $L^{-1}$ of styrene was charged. The amount of AIBN was fixed at 0.002 mol $L^{-1}$ and the concentration of the RAFT agent was varied from 0.0017 to 0.0068 mol $L^{-1}$. The polymerization temperature in the oil bath was fixed at 70 °C. The amount of PVP concentration was fixed at 0.0002 mol $L^{-1}$ throughout the experiments. The general procedure was as follows: Ethanol, AIBN and styrene were charged into the vial and degassed with

 

bubbling nitrogen gas at room temperature for 30 min. Then, the RAFT agent dissolved in ethanol was introduced into the vial which was then placed in an oil bath at the desired temperature for a given time. During the polymerization, aliquots of the sample were periodically withdrawn through a degassed syringe for further characterization of the polymerization progress. After the completion of the polymerization, the resulting latex particles were centrifuged and redispersed in methanol. These centrifugation and redispersion cleanup cycles were repeated many times to ensure the removal of any excess stabilizer and unreacted styrene monomer.

### Characterization

The chemical structure of the synthesized RAFT agent was confirmed with a Varian 400-Mhz $^{1}H$ NMR and $^{13}C$ NMR with $CDCl_3$ as the solvent. The monomer conversion to polymer was determined gravimetrically. The molecular weights and the polydispersity index (PDI) were measured using a Waters GPC (gel permeation chromatography) equipped with a 510 differential refractometer and Viscotek T50 differential viscometer. High resolution of $10^5$-, $10^3$-, and $10^2$-Å μ-Styragel packed columns were employed. A universal calibration curve was obtained with 10 polystyrene (PS) standard samples (Polymer Laboratories, UK) with molecular weights ranging from 7,500,000 to 580 g/mol. The flow rate of the PS solution dissolved in THF was 1.0 mL/min. Scanning electron microscopy (SEM; S-4300, Hitachi) was used to study the morphology of the synthesized PS particles. The number- and weight-average diameters ($D_n$ and $D_w$, respectively), uniformity ($D_w/D_n$) and the coefficient of variation (CV) were obtained using Scion Image Analyzer software (Scion Corp., Frederick, MD) by the counting 100 individuals particles from the SEM photographs.[16] The CV is calculated from the following equation:

$$CV = \frac{(\sum(d_i - (\sum n_i d_i / \sum n_i))^2 / \sum n_i)^{1/2}}{(\sum n_i d_i / \sum n_i)} \times 100$$

where $n_i$ is the number of particles with a diameter of $d_i$.

## Results and Discussion

### RAFT Behavior in the Dispersion Polymerization

Figure 1(a) and 1(b) show the SEM photographs of the PS particles prepared for 24 h in the presence of pre-addition and postaddition of 0.0034 mol $L^{-1}$ of the RAFT agent. In general, in the dispersion polymerization, all reaction ingredients are dissolved in the medium, in which particles are generated from the oligomeric species and microspheres subsequently grown by the adsorption of oligomers and monomers

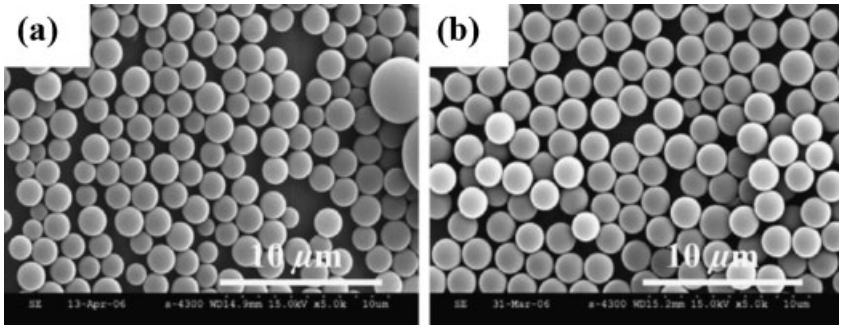


*Figure 1.*
PS microspheres prepared in the presence of 0.0034 mol $L^{-1}$ of RAFT agent in the dispersion polymerization of styrene at 70 °C in an ethanol medium for 24 h; (a) pre-addition of RAFT (b) post-addition of RAFT.

 

from the medium. The process of dispersion polymerization is separated into two stages, nucleation and particle growing stage where the former is short, but complex and sensitive, whereas the latter is relatively long, simple and robust.[18] Herein, the pre-addition of RAFT is defined as the addition of RAFT agent at the beginning of the dispersion polymerization along with all the other ingredients whereas postaddition refers to the addition of RAFT agent after the completion of the sensitive nucleation stage. For the PS particle prepared in the pre-addition of RAFT at 24 h, as seen in the Figure 1(a), the final $D_w$, $D_w/D_n$ and CV are 1.97 μm, 1.31 and 23.12% respectively. In this case, the nucleation period was much longer than to the nucleation period of normal dispersion polymerization and a pink coagulant at the bottom of the reactor was observed until the end of the reaction. This indicated no completion of the polymerization due to the phase separation and this could be one of the reasons for observing polydisperse PS particles at the end of the polymerization reaction in the preaddition of RAFT. In the seeded emulsion polymerization of styrene, the formation of the red layer was reported to be observed in the presence of a RAFT agent and explained it as due to the slow transportation of the RAFT agent into the particles.[10] However, in the postaddition of RAFT, monodisperse PS particles were obtained from the very beginning of the polymerization without any pink layer of precipitation. The particle instability in the early stage of the polymerization with preaddition of RAFT would be overcome with the postaddition of RAFT. The final $D_w$, $D_w/D_n$ and CV of PS particle obtained in the postaddition of RAFT were 1.75 μm, 1.01 and 5.76% respectively. Thus, the postaddition of the RAFT agent controls the particle size and its distribution without changing the particle morphology. It is obvious that the particle numbers and its distribution are determined by the nucleation stage if no secondary particles or coagulum are formed during the particle growth.[18]

Figure 2 shows the kinetics of the dispersion polymerization for both the preaddition and postaddition of RAFT in an ethanol medium at 70 °C. The linear correlations between $\ln([M]_o/[M])$ and the polymerization time indicate that the polymerization is a first order reaction with respect to the monomer and that the number of radicals remains constant throughout the dispersion polymerization. It implies that the chain transfer agent influences the kinetics of the dispersion polymerization i.e. on the propagating species concentration. The rate of polymerization for the pre-addition and

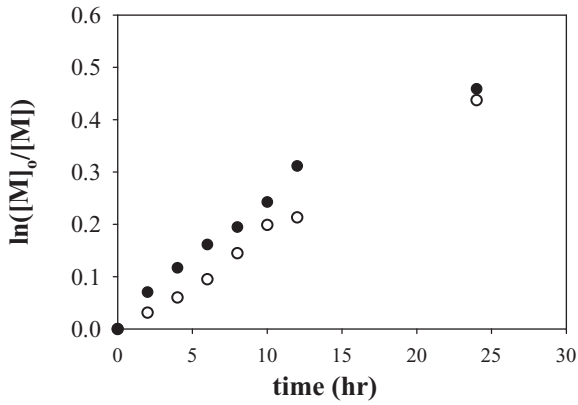


***Figure 2.***
Polymerization kinetics for the dispersion polymerization of styrene in the (○) preaddition and (●) postaddition addition of 0.0034 mol $L^{-1}$ of RAFT at 70 °C in an ethanol medium.

 

postaddition of RAFT are similar to each other, though the polymerization in the postaddition of RAFT is slightly faster than that of preaddition of RAFT. More detailed kinetic data are needed to determine whether there is any significant effect of the RAFT concentration on the dispersion polymerization rate. The evolution of the number-average molecular weight ($M_n$) and PDI with the monomer conversion in the preaddition and postaddition of RAFT agent has been depicted in Figure 3(a) and 3(b), respectively.

The theoretical $M_n$ was calculated with the following equation

$$M_{n(theo)} = ([Sty]_o/[CTA]_o)X_m M_m + M_{CTA}$$

where $X_m$ is the fractional conversion, $M_m$ is the molecular weight of the monomer and $M_{CTA}$ is the molecular weight of the chain transfer agent.

An important aspect of living polymerization is the linear increase in the molecular weight with conversion. As seen in Figure 3(a), the $M_n$ increased linearly with increased conversion and theoretical $M_n$ values were in good agreement with the experimental one, indicating the ''living'' polymerization nature for both the preaddition and postaddition of RAFT. In the postaddition of RAFT, it was observed that the initial experimental $M_n$ values were slightly higher than those of the theoretical $M_n$. This was due to the chemical

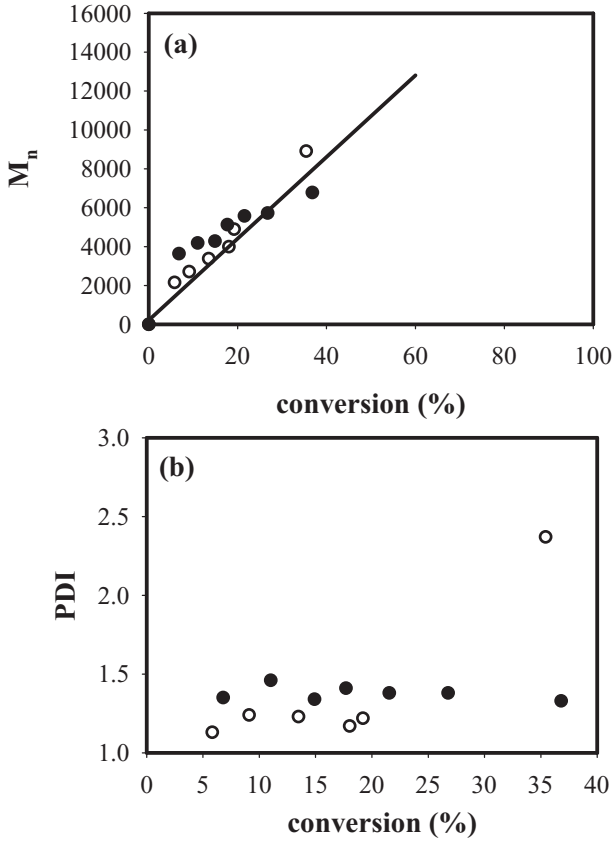


***Figure 3.***
(a) $M_n$ and (b) *PDI* as functions of the conversion of PS microspheres prepared by living radical dispersion polymerization in the (○) preaddition and (●) postaddition of 0.0034 mol $L^{-1}$ of RAFT in an ethanol medium at 70 °C. Solid line represents the theoretical $M_n$.

 

attachment of PVP on the polymer molecules, which significantly increased the molecular weight of PS, causing the deviation from the origin.[16] In the TEMPO-mediated dispersion polymerization of styrene, it also reported that the stabilizer, PVP, was not located exclusively on the outside of the PS latex particles, a significant proportion of the PVP was also located inside of the latex.[15] This might also be due to the non-controlled character of the polymer chains formed initially in the absence of chain transfer agent. However, in the preaddition of RAFT, as we see, the experimental $M_n$ values have a good correlation to the theoretical one. In this case, turbidity was not observed for 4 h of reaction and no stable PS particles were obtained until the 8 h of polymerization. So, we assumed that initially at least, only solution polymerization occurred.[15] Although the stability improved with the preaddition of RAFT for 24 h, but broad particle size distribution was observed (Figure 1(b)). As soon as the stabilized PS particles were obtained for the pre-addition of RAFT, the final $M_n$ value dramatically increased and deviated from the theoretical $M_n$ value. It might be due to the chemical attachment of PVP to the PS particles, as unstable particles observed at the beginning of the reaction, with the results that the initial PVP-PS graft could be a poor stabilizer. A short nucleation period and an uniform growth of the primary particles are necessary for monodisperse polymer particles.[20] Thus, the broadening of the particle size distribution could be due to the prolonged nucleation time in the pre-addition of RAFT.[15]

The PDI of the PS microspheres prepared in the RAFT mediated dispersion polymerization in ethanol is shown in Figure 3(b). Fairly narrow PDI values are observed in the postaddition of RAFT which decreases to 1.33 with the final conversion. The sudden increased of PDI value to 2.37 with the higher conversion observed in the pre-addition of RAFT which might be due to the longer nucleation period. In fact, the initial low PDI values for the preaddition of RAFT reflects that the solution polymerization took place at the early stage while the dispersion polymerization occurred in the later stage.[15] Figure 4 shows the GPC traces of the final PS latex in the dispersion polymerization of styrene in preaddition and postaddition of RAFT. In the preaddition of RAFT, a bimodal distribution curve was observed

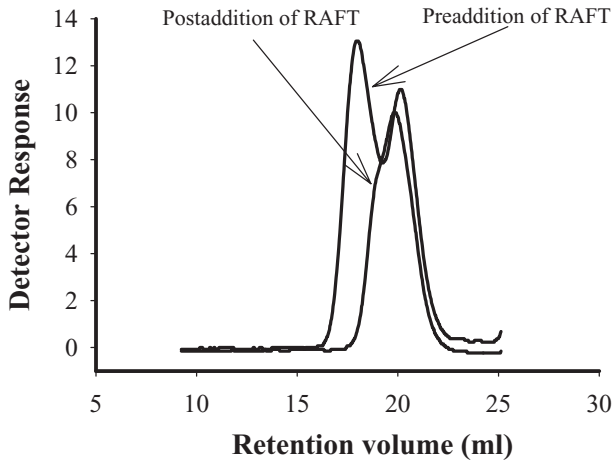


***Figure 4.***
GPC chromatograms of PS microspheres prepared by living radical dispersion polymerization of styrene in presence of preaddition and postaddition of 0.0034 mol $L^{-1}$ of RAFT at 70 °C in an ethanol medium for 24 h.

 

which could be due to the nonhomogeneous distribution of the active species among the particles. It might also be due to the delayed nucleation that results in the broad distribution of particle size (Figure 1(a)). However, a narrow molecular weight distribution curve is observed with the postaddition of RAFT (Figure 4). In the RAFT miniemulsion polymerization of styrene, Luo et al.[21] also obtained a bimodal distribution for the final PS latex. They reported the formation of two kinds of particles in the polymer chains i.e. polymer particles and oligomer particles. Oligomer particles were larger in size and lower in molecular weight, leading to a bimodal distribution of both particle size and molecular weight. However, they reported to obtain narrow particle size and molecular weight distributions in the postaddition of surfactant in RAFT miniemulsion polymerization. So, the living behavior with controlled molecular weight, particle size and its distribution can only be obtained in the postaddition of RAFT agent in the dispersion polymerization.

### Effect of the Post Addition of RAFT in the Dispersion Polymerization

To study the effect of the postaddition of RAFT in the dispersion polymerization, three experimental runs were designed for the synthesized of PS particles. Figure 5 shows the SEM photographs of PS microspheres prepared at three different concentrations of postaddition of RAFT with 0.0002 mol $L^{-1}$ of PVP stabilizer. Table 1 summarized the results obtained with the postaddition of RAFT on conversion, $M_n$, $M_w/M_n$, $D_w$ and CV. It is observed that PS particle are in spherical morphology with a good monodispersity (Figure 5).

The final $D_w$ and $D_w/D_n$ of the PS with respect to the RAFT concentrations are plotted in Figure 6. The particle size decreases with the increased concentration of the RAFT agent and good particle size uniformity was obtained in the presence of

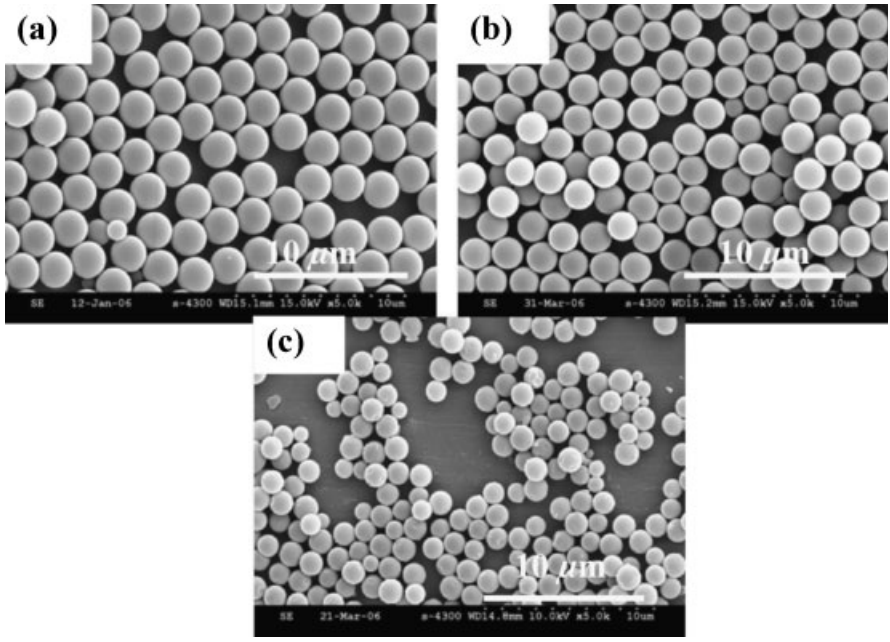


*Figure 5.*
SEM images of the PS microspheres prepared by living radical dispersion polymerization in an ethanol medium at 70 °C for 24 h in the presence of different concentrations of postaddition of RAFT: (a) 0.0017; (b) 0.0034; and (c) 0.0068 mol $L^{-1}$.

 

***Table 1.***
Properties of the PS microspheres prepared in the dispersion polymerization of styrene with various concentration of postaddition of RAFT.

| RAFT (mol $L^{-1}$) | Time (h) | $M_n$ (theo) (g/mol) | $M_n$ (GPC) (g/mol) | $M_w/M_n$ (GPC) | Conversion (%) | $D_w$ (μm) | CV (%) |
|---|---|---|---|---|---|---|---|
| 0 | 24 | | 27800 | 3.47 | 71.13 | 2.22 | 30.17 |
| 0.0017 | 4 | 6752 | 7600 | 1.44 | 15.06 | 1.48 | 3.82 |
| | 6 | 9355 | 7900 | 1.43 | 21.65 | | |
| | 10 | 14171 | 8600 | 1.68 | 33.05 | | |
| | 12 | 16186 | 14100 | 2.21 | 37.82 | 1.77 | 5.64 |
| | 24 | 23722 | 15600 | 3.34 | 55.6 | 2.04 | 8.43 |
| 0.0034 | 4 | 2522 | 4100 | 1.46 | 11.01 | 0.46 | 4.22 |
| | 6 | 3339 | 4300 | 1.34 | 14.90 | | |
| | 10 | 4733 | 5500 | 1.38 | 21.54 | | |
| | 12 | 5829 | 5700 | 1.37 | 26.76 | 1.32 | 4.61 |
| | 24 | 7937 | 6800 | 1.33 | 36.79 | 1.75 | 5.76 |
| 0.0068 | 12 | 1452 | 3600 | 1.35 | 11.83 | | |
| | 24 | 2563 | 4200 | 1.28 | 22.40 | 1.24 | 4.79 |

RAFT agent. The growing radicals produced from the fragmentation of the RAFT agent exit the particles and reenter into the continuous phase to form new particles before the precipitation of the existing particles, thus increased the exit rate coefficient with RAFT concentration.[5] This induces the retardation of the polymerization due to the transfer of the RAFT agent to the particles and so the particle size decreases with the RAFT concentration. In the emulsion polymerization of styrene, the particle diameter decreased and the size distribution became narrower with the RAFT concentration.[9] However, a partial destabilization of the final latexes has been observed at 0.0068 mol $L^{-1}$ concentration of RAFT (Figure 5(c)).

The molecular weight of the resulting polymer increased with the conversion but decreased with the increasing RAFT concentration (Table 1). At low concentration of RAFT (0.0017 mol $L^{-1}$), there was a marked deviation between the experimental and theoretical $M_n$. This could be due to the formation of dead polymeric materials via conventional termination that usually observed at lower concentrations of the RAFT.[22] With the increased RAFT concentration, $M_n$ values were fairly close to

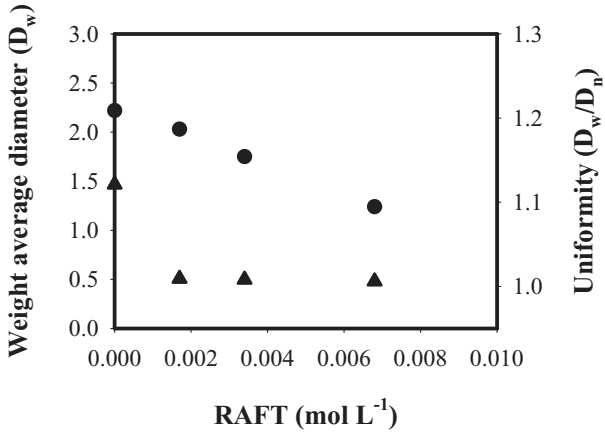


***Figure 6.***
Effect of postaddition of RAFT concentration on the weightaverage diameter ($D_w$; ●) and uniformity ($D_w/D_n$; ▲) of PS microspheres prepared in the dispersion polymerization of styrene in an ethanol medium at 70 °C for 24 h.

 

the theoretical ones. A deviation from the theoretical $M_n$ was due to the polymeric stabilizer, which is not only physically adsorbed but also chemically bonded with the monomer. Stabilizer is not easily removal from the polymer particles since the nucleation starts on PVP molecules by abstraction of labile hydrogen.[15,16,23]

Regarding on the PDI, the initial value of PDI decreased to 1.43, and again increased to 3.34 with the conversion at 0.0017mol $L^{-1}$ concentration of RAFT. This implies that the less amount of RAFT is insufficient to control the PDI in the dispersion polymerization of styrene. With the increased concentration of the RAFT, the PDI value decreased to 1.28, which is fairly narrow PDI value in the dispersion polymerization as compared to the homogeneous living radical polymerization in solution or bulk in presence of RAFT.[2,14]

Due to the presence of stabilizer PVP, slightly broad PDI values were obtained as narrow PDI value was obtained in the TEMPO-mediated dispersion polymerization of styrene without the use of PVP stabilizer.[15] From the obtained results it can be concluded that the addition of the RAFT agent in the dispersion polymerization not only controls the molecular weight and PDI but also produces stable polymer particles.

## Conclusion

Living free radical dispersion polymerization has been successfully carried out using the RAFT agent *tert*-butyl dithiobenzoate. The strategy of preaddition and postaddition of RAFT agent in the dispersion polymerization was carried out and established that the postaddition of RAFT showed living polymerization behavior along with controlled particle size and its distribution. The concentration of the RAFT agent proved to be an important variable to control the molecular weight, particle size and distribution as well as its stability in the dispersion polymerization. Polymerization occurred in an uncontrolled manner in the presence of less amount of RAFT while particle destabilization observed with more amount of RAFT concentration. The effect of the RAFT agent on the particle size is currently poorly understood and needs further investigation. Finally, it can be concluded that the right tuning between the nucleation rate and concentration of the RAFT agent is essential to obtain the stable monodisperse polymer particles with controlled architecture in the living radical dispersion polymerization.

*Acknowledgements:* It is acknowledged that this work has been supported by the National Research Laboratory of the Ministry of Science and Technology in Korea, by a grant number M10203000026-02J0000-01410, in the years of 2002-2007.

[1] J. Chiefari, B. Y. K. Chong, F. Ercole, J. Krstina, J. Jeffery, T. P. T. Le, R. T. A. Mayadunne, G. F Meijs, C. L. Moad, G. Moad, E. Rizzardo, S. H. Thang, *Macromolecules* **1998**, *31*, 5559.
[2] G. Moad, J. Chiefari, J. Krstina, R. T. A. Mayadunne, E. Rizzardo, A. Postma, S. H. Thang, *Polym. Int.* **2000**, *49*, 993.
[3] J. Qiu, B. Charleux, K. Matyjaszewski, *Prog. Polym. Sci.* **2001**, *26*, 2083.
[4] M. F. Cunningham, *Prog. Polym. Sci.* **2002**, *27*, 1039.
[5] S. W. Prescott, M. J. Ballard, E. Rizzardo, R. G. Gilbert, *Macromolecules* **2002**, *35*, 5417.
[6] S. E. Shim, Y. Shin, J. W. Jun, K. Lee, H. Jung, S. Choe, *Macromolecules* **2003**, *36*, 7994.
[7] A. Butté, G. Storti, M. Morbidelli, *Macromolecules* **2001**, *34*, 5885.
[8] L. Yang, Y. Luo, B. Li, *Polymer* **2006**, *47*, 751.
[9] M. J. Monteiro, J. de Barbeyrac, *Macromolecules* **2001**, *34*, 4416.
[10] M. J. Monteiro, M. Hodgson, H. de Brouwer, *J. Polym. Sci. Part A: Polym. Chem.* **2000**, *38*, 3864.
[11] M. Manguian, M. Save, B. Charleux, *Macromol. Rapid Commun.* **2006**, *27*, 399.
[12] C. J. Ferguson, R. J. Hughes, B. T. T. Pham, B. S. Hawkett, R. G. Gilbert, A. K. Serelis, C. H. Such, *Macromolecules* **2002**, *35*, 9243.
[13] C. J. Ferguson, R. J. Hughes, D. Nguyen, B. T. T. Pham, R. G. Gilbert, A. K. Serelis, C. H. Such, B. S. Hawkett, *Macromolecules* **2005**, *38*, 2191.
[14] M. Hölderle, M. Baumet, R. Mülhaupt, *Macromolecules* **1997**, *30*, 3420.
[15] L. I. Gabaston, R. A. Jackson, S. P. Armes, *Macromolecules* **1998**, *31*, 3883.

 

[16] S. E. Shim, H. Jung, H. Lee, J. Biswas, S. Choe, *Polymer* **2003**, *44*, 5563.
[17] J.-S. Song, M. A. Winnik, *Macromolecules* **2006**, *39*, 8318.
[18] J.-S. Song, F. Tronc, M. A. Winnik, *J. Am. Chem. Soc.* **2004**, *126*, 6562.
[19] A. Favier, M.-T. Charreye, P. Chaumont, C. Pichot, *Macromolecules* **2002**, *35*, 8271.
[20] S. Shen, E. Sudol, M. S. El-Aasser, *J. Polym. Sci. Part A: Polym. Chem.* **1993**, *31*, 1393.
[21] L. Yang, Y. Luo, B. Li, *J. Polym. Sci. Part A: Polym. Chem.* **2006**, *44*, 2293.
[22] T. Arita, M. Buback, P. Vana, *Macromolecules* **2005**, *38*, 7935.
[23] S. Oh, K. Kim, B. H. Lee, S. E. Shim, S. Choe, *J. Polym. Sci. Part A: Polym. Chem.* **2006**, *44*, 62.

 